Agronomy Research

Established in 2003 by the Faculty of Agronomy, Estonian Agricultural University

Aims and Scope:

Agronomy Research is a peer-reviewed international Journal intended for publication of broad-spectrum original articles, reviews and short communications on actual problems of modern biosystems engineering incl. crop and animal science, genetics, economics, farm- and production engineering, environmental aspects, agro-ecology, renewable energy and bioenergy etc. in the temperate regions of the world.

Copyright:

Copyright 2009 by Estonian University of Life Sciences, Latvia University of Life Sciences and Technologies, Vytautas Magnus University Agriculture Academy, Lithuanian Research Centre for Agriculture and Forestry. No part of this publication may be reproduced or transmitted in any form, or by any means, electronic or mechanical, incl. photocopying, electronic recording, or otherwise without the prior written permission from the Estonian University of Life Sciences, Latvia University of Life Sciences and Technologies, Vytautas Magnus University Agriculture Academy, Lithuanian Research Centre for Agriculture and Forestry.

Agronomy Research online:

Agronomy Research is available online at: http://agronomy.emu.ee/

Acknowledgement to Referees:

The Editors of *Agronomy Research* would like to thank the many scientists who gave so generously of their time and expertise to referee papers submitted to the Journal.

Abstracted and indexed:

SCOPUS, EBSCO, CABI Full Paper and Thompson Scientific database: (Zoological Records, Biological Abstracts and Biosis Previews, AGRIS, ISPI, CAB Abstracts, AGRICOLA (NAL; USA), VINITI, INIST-PASCAL).

Subscription information:

Institute of Technology, EULS
St. Kreutzwaldi 56, 51014 Tartu, ESTONIA
E-mail: timo.kikas@emu.ee

Journal Policies:

Estonian University of Life Sciences, Latvia University of Life Sciences and Technologies, Vytautas Magnus University Agriculture Academy, Lithuanian Research Centre for Agriculture and Forestry, and Editors of *Agronomy Research* assume no responsibility for views, statements and opinions expressed by contributors. Any reference to a pesticide, fertiliser, cultivar or other commercial or proprietary product does not constitute a recommendation or an endorsement of its use by the author(s), their institution or any person connected with preparation, publication or distribution of this Journal.

ISSN 1406-894X

CONTENTS

Agronomy Research **17**(2), 313–321, 2019
https://doi.org/10.15159/AR.19.027

The environmental noise level in the rejuvenation pruning on centuries-old olive tree

L.M. Abenavoli*, G. Zimbalatti, A. De Rossi, S. Papandrea and A.R. Proto

University of the *Mediterranea* of Reggio Calabria - Department of AGRARIA, Feo di Vito, IT89123 Reggio Calabria, Italy
*Correspondence: laben@unirc.it

Abstract. In the Italian agricultural economy, olive cultivation plays a fundamental role, and this is especially true for the southern regions where almost all cultivation is spread. In Calabria, in particular, olive cultivation has seen over the last few decades significantly improve the quality of production also as a result of investments aimed at the creation of new mechanizable plants and/or the modernization of existing ones; today some areas have got both PDO and PGI certification.
In the 'Piana di Gioia Tauro', located north-west of the Reggio Calabria metropolitan area, olive growing extends over 20,000 hectares and the presence of centuries-old olive tree is still widespread. The olive varieties mainly belong to the local cultivars of 'Sinopolese' and 'Ottobratica', characterized by a remarkable rusticity and high development, perhaps unique in the world; they reach 20–25 meters high, forming what is called a 'forest of olive trees'.
The pruning operations are carried out by means of chainsaws of different power and size whereby, in addition to the previously described difficulties, operators are exposed to prolonged periods of noise levels. The purpose of this study is precisely to assess the exposure of operators to this particular olive grove. The aim is to identify the acoustic levels generated by the two pruning and cross-cutting activities, the risk thresholds and the exposure to which the individual workers of the two work sites are subjected, giving indications on the appropriate safety distances to maintain (according to current regulations) compared to noise sources.

Key words: mechanized pruning, chainsaw, safety, dB, phonometer.

INTRODUCTION

The cultivation of the olive tree (*Olea europaea L.*) plays a fundamental role in the Italian agricultural economy, this is especially true in the southern regions where the highest share of olive oil production is concentrated.

Italy, in the world, is in second place among the producing and exporting countries of olive oil, after Spain, and the employed in the sector determine a commitment of about 30 million working days (CO.RE.R.A.S, 2007).

The olive tree is one of the most important crops in the Mediterranean region, where 97% of the world's olive oil is produced (IOOC, 2013). Calabria, in southern Italy, is the second region for olive production in Italy (ISTAT, 2016). The economic sustainability of olive groves necessarily implies the reduction of production costs

especially those relating to manual harvesting, which accounts for approximately 40% of the total (Abenavoli & Proto, 2015; Abenavoli et al, 2016; Sorgonà et al., 2018).

Olive cultivation is therefore very widespread in the Calabrian territory and over the last few decades has seen a considerable improvement in the quality of olive oil production, following the introduction of new investments aimed at the implementation of agricultural mechanization. Therefore, new and more modern systems have been made or, where possible, existing ones have been modernized. Currently, some of these areas particularly suited, have had from European systems the recognition of the trademarks 'PDO' (Protected Designations of Origin) and 'PGI' (Protected Geographical Indications). Fruit picking and harvesting systems play an important role in the quality of drupes and olive oil (Mele et al., 2018).

Recent studies were conducted on olive and olive oil quality in Calabria in which the effects of cultivar, harvest date and harvest year on biometrics of fruits and on physico-chemical parameters of oil were evaluated (Abenavoli & Proto, 2015; Giuffrè, 2017; Giuffrè, 2018). In the territory of the 'Plain of Gioia Tauro', wide and fairly homogeneous area, composed of 33 municipalities and located in the North-West of the Reggio Calabria metropolitan area, where the olive growing covers over 20,000 hectares, still today, is widespread the presence of traditional planted trees, where the densities of planting varies from 50 to 80 plants ha^{-1} in the plains from 100 to 140 plants ha^{-1} in the hilly areas (Cavazzani & Sivini, 2001) and the distance between the plants, often irregular (due to the soil conditions), on average between 7–12 meters (Fig. 1).

The olive trees present, mostly centuries-old, belong mainly to the local 'Sinopolese' and 'Ottobratica' cultivars, which here assume a notable growth, perhaps unique in the world, with trees that reach 20–25 meters in height and that form a real 'forest of olive trees' (Fardella, 1995). Even if we find ourselves in a suggestive landscape, due to the majesty of these trees, the management of these plants is really problematic and not very rational due to the work overload that they require as well as the economic effort necessary for their maintenance (Proto & Zimbalatti, 2010; Abenavoli & Marcianò, 2013; Proto & Zimbalatti, 2015).

The farms of the district are mainly small or medium-sized and therefore have a low investment capacity and, at the same time, a high need for labor due to low levels of mechanization. In these conditions all the cultivation operations are more complex, but in particular the pruning of the trees, as the operators, as real 'climbers', with the only help of ropes must climb to make the cuts of the branches at high height. So this operation, which in other places and conditions falls within the normal routine of agricultural management, in the 'Plain of Gioia Tauro', due to the particular conditions of danger in which it is performed and its high cost, takes on an extraordinary character, so it is averaged every 7-8 years (Abenavoli & Marcianò, 2013).

The extraordinary pruning, depending on the purpose that is proposed, is distinguished in: pruning of rejuvenation, reform, transformation, rehabilitation and preparation for grafting. They are all based on a common principle, the ease with which the olive tree emits the suckers in every part of the tree, whatever its age (Morettini, 1972).

As a result, pruning in the 'Plain of Gioia Tauro' is particularly complex and involves the removal of large masses of wood, because the cuts are made on large diameter branches (Morettini, 1972).

At a later time, other operators making the sawing of the branches, left on the ground from the previous yard, up to the preparation of logs and their transport to different destinations based on their use (Abenavoli & Marcianò, 2013). While pruning residues and cuttings, which were previously left on the ground today, given the high calorific power they possess, are reduced to pellets and used as a source of energy or, alternatively, they can be transformed into high quality biochars, such as they have shown recent studies (Abenavoli et al., 2016).

To perform this type of pruning mechanical cutting equipment (chainsaws) of different powers and sizes are used and the operators, in addition to dealing with the difficulties described above, are also exposed to high and prolonged noise levels.

The purpose of the work was precisely to evaluate the exposure to noise of operators, who work in this particular Italian olive growing area. Moreover, we have proposed to identify the acoustic levels generated by the two activities (pruning and cross-cutting), the risk thresholds and the exposure to which the individual workers of the two work sites are subject, giving the indications (according to current regulations) on the appropriate safety distances to be maintained with respect to noise sources (Proto et al., 2016).

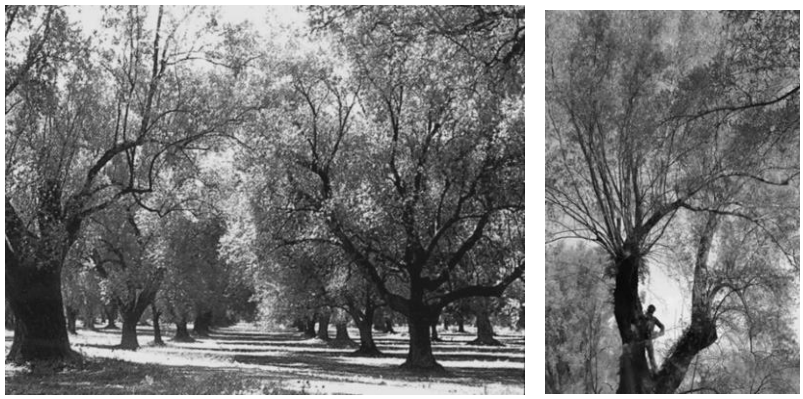

Figure 1. Typical olive-grove in 'Plain of Gioia Tauro' and an example of traditional pruning.

Noise is a relevant risk factor to be taken into account in evaluating health and safety of workers in agriculture (Vallone et al., 2017). Many studies have demonstrated that noise has serious effects (psychological and physiological) on humans, such as loss of concentration, difficulties to speak, loss of reflexes, reduced speech intelligibility, irritation, permanent hearing loss to permanent deafness, among others (Türker et al., 2011; De Souza et al., 2012; Proto et al., 2016; Grigolato et al., 2018). In particular, the process of mechanization in agricultural sector has led to an increase of the noise sources and, as a result, of an increase of the percentage of workers exposed to this risk. This study focuses on the assessment of workers' exposure to noise and was tested in compliance with the Italian legislation. The objective of this study was to evaluate the daily personal noise exposure of the underserved workers during pruning operations.

MATERIAL AND METHODS

The legislation reference

In Italy, Law Decree 81/2008 defined the requirements for assessing and managing noise risk, identifying a series of procedures to be adopted at different noise levels to limit workers exposure. Excessive noise, in fact, is a global occupational health hazard with considerable social and physiological impacts, including noise induced hearing loss (NIHL) (Deborah et al., 2005). The Italian Occupational Safety and Health legislation, in agreement with the EU Directive and ISO standard, establishes that both the worker's exposure time and instantaneous peak exposure must be considered, defining both the peak sound pressure level (L_p,C_{peak}), that is, the highest instantaneous sound pressure weighted through the 'C' ponderation curve, and the daily A-weighted noise exposure level, $LE_{X,8h}$, that is, the average value, time-weighted, of all the noise levels at work concerning an eight-hour working day (Pascuzzi & Santoro, 2017).

Instrumentation and test parameters

The noise exposure assessment during the pruning phase has been done with the use of integrator phonometer Class 1, by which were recorded sound pressure levels at ear of exposed workers and using 26 sound level data logger Class 2 (IEC 61672-1) to recorded acoustic levels located in a geometric scheme to assess the noise propagation in the area test. Before and after each series of measurements a field calibration with appropriate adjustment has been performed using a sound calibrator.

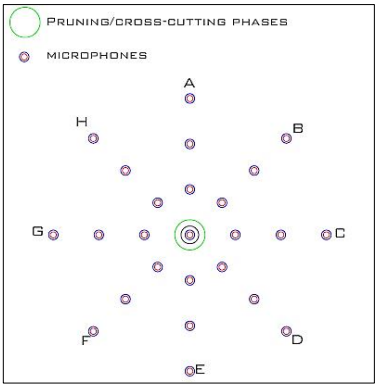

Figure 2. Locations of the sound level data logger for the noise measurements.

Figure 3. Sound level data logger for the noise measurements.

In order to measure the sound level at the ear level of the operator, the microphone was properly attached on a helmet and the operator was told to look continuously at the direction of movement during the measurements. Each data logger was mounted at 2 meters above the ground and positioned at 3, 6 and 9 meters away from the operator; the area was subdivided into 8 cardinal directions (Fig. 2). The measurements were taken in an open field using a properly set measurement system without any obstacle that might have caused sound reflection. During the sound level measurements the relative humidity and temperature of the experiment environment was measured by electronic thermo-hygrometer. During the noise measurements the environmental noise were

ignored when the difference between the chainsaw sound levels and environmental noise levels were more than 10 dB (Brüel & Kjaer, 2001). Nine measurement periods were considered at each of the measuring points and these observations pointed out that the stated time interval T (measurement duration).

The collected data were processed in order to calculate the levels of personal noise exposure of workers involved in the pruning and cross-cutting operations.

The A-weighted equivalent continuous sound pressure level, $L_{p,A,eqT}$ was calculated by the following equation (ISO, 2013; Pascuzzi & Santoro, 2017):

$$L_{p,A,eqT} = 10lg\left[\frac{\frac{1}{T}\int_{t1}^{t2} p_A^2(t)dt}{p_0^2}\right] \text{ dB} \quad (1)$$

where p_a is the A-weighted sound pressure during the stated time interval T starting at t_1 and ending at t_2; p_0 is the reference pressure value (20 μPa).

On the other hand, the C-weighted peak sound pressure level, $L_{p,Cpeak}$ was calculated by the following equation (ISO, 2013; Pascuzzi & Santoro, 2017):

$$L_{p,Cpeak} = 10lg\frac{p_{Cpeak}^2}{p_0^2} \text{ dB} \quad (2)$$

where p_0 is the reference pressure value (20 μPa).

Work sites

The trials were conducted in the municipality of Cosoleto, metropolitan area of Reggio Calabria (Calabria region, Italy), typical olives-oil district. Two workers were monitored during the pruning phase and cross-cutting operations conducted on centuries-old olive trees. The plant density was very low and the average diameters of the crown was 14 m (Fig. 3), with a planting density of 73 plants for hectare (Table 1).

Table 1. Characteristics of the olive grove that has been subject to pruning (pre-intervention)

Biometric data	***Mean***	***SD***
Tree density (trees ha^{-1})	73.0	4.0
Tree height (m)	18.6	0.4
Crown diameter (m)	14.0	0.5
Trunk diameter (cm)	80.9	5.5

In the studied farms the pruning is usually done every ten years, so the cuts made are necessarily very drastic, and the wood mass removed is very significant. The first worker used a chainsaw Stihl, Ms-261C-BM model, for pruning operations and an assistant operator helped during this phase. The assistant was engaged like work place cleaning, accessories carrying, moving the branches away after delimbing, producing and stacking of fuel wood, etc. The second chainsaw operator used a Jonsered, CS-2188 model, and another operator was an assistant. The chainsaws' weight, guide bar length, and chain type are shown in Table 2.

Table 2. Description of the chainsaws

Sites	*Pruning*	*Cross-Cutting*
Chainsaw Type	Jonsered	Stihl
Model	CS 2188	Ms-261C-BM
Displacement (cm³)	87.9	50.2
Power (kW)	4.8	4.1
Weight (Kg)	7.1	5.0
Guide bar (cm)	60.0	45.0
Specific power (kW kg^{-1})	1.8	1.4

RESULTS AND DISCUSSION

Daily exposure values were also calculated with the maximum daily time and each measurement was added with the uncertainty (ε) related to the level of daily personal exposure, to define if a specific limit of exposure is, or can be exceeded. In particular, uncertainties are a quantitative indication of the reliability of the result. In the case of environmental acoustic noise measurements, exceeding thresholds may cause health risks for the public and then it becomes essential to find the relationship between measurement uncertainty and acceptable risk (Russo, 2015). Analysis of noise levels are exceeded in first 6 meters from the area of operations (Fig. 4). In no station the value of L_{peak}(C) came out higher to135 dB(C), so the verification of the respect of the action values and the exposure limits has been carried out exclusively on the base of the values of the daily personal exposure $L_{EX,8h}$. Values in this case varied from 92.8 and 91.0 dB(A) during pruning phase while the operator is exposed at an equivalent noise pressure levels between 92.0 and 89.6 for cross-cutting operation. Another important factor to considered is the different daily personal exposure; in fact during the pruning phase the operator typically used a chainsaw for less time respect the cross-cutting. In the Tables 4 and 5 are reported the daily personal exposure in a period of eight hours, distinct for phase and distances. This confirms that a chainsaw is one of the most critical machines in terms of noise level (Proto et al., 2016; Grigolato et al., 2018).

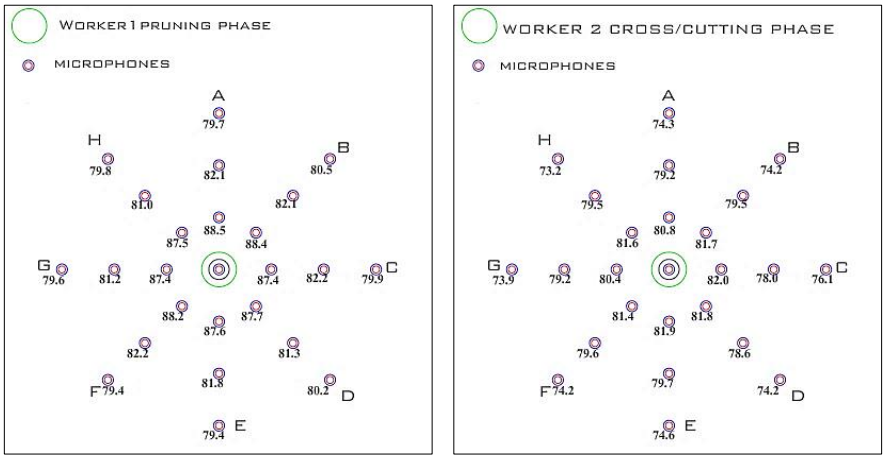

Figure 4. Noise levels – dB(A) – at the studied operations following the eight directions (A – H): during pruning phase (left) and cross-cutting phase (right).

This management of work tasks exposes all workers to acoustic levels, which are always higher than the maximum exposure limit, and obliges them, in the same way, to the use of PPE, that are however appropriate to reduce these levels. The second worker, assistant for each phase monitored, at the level of the ear, the equivalent continuous sound levels of the machines used, were measured between 81.6 and 79.6 dB(A) for the pruning operation, and between 73.8 and 71.2 dB(A) for the cross-cutting operation, with an average level varied from the 5 measurements carried out for both operations of 80.8 and 72.6 dB(A), respectively.

Table 4. Acoustic levels of pruning phase

	Worker 1	**Assistant 1**	**Distance 3 m**	**Distance 6 m**	**Distance 9 m**
	$L_{eq,i}$ (ε)	$L_{eq,i}$ (ε)	$L_{eq,i}$ (ε)	$L_{eq,i}$ (ε)	$L_{eq,i}$ (ε)
Test 1	92.8 (± 0.2)	81.0 (± 0.4)	87.4 (± 0.5)	85.2 (± 0.3)	79.0 (± 0.6)
Test 2	91.9 (± 0.4)	79.6 (± 0.2)	86.6 (± 0.3)	84.2 (± 0.4)	78.2 (± 0.3)
Test 3	92.6 (± 0.2)	81.4 (± 0.5)	87.3 (± 0.6)	85.1 (± 0.6)	79.6 (± 0.4)
Test 4	92.9 (± 0.3)	81.6 (± 0.3)	87.6 (± 0.2)	85.4 (± 0.5)	79.8 (± 0.2)
Test 5	91.0 (± 0.5)	80.2 (± 0.6)	86.4 (± 0.4)	84.6 (± 0.2)	78.1 (± 0.5)
Mean	92.3 (± 0.6)	80.8 (± 0.4)	87.0 (± 0.2)	84.9 (± 0.4)	78.9 (± 0.2)

Table 5. Acoustic levels of Cross-Cutting phase

	Worker 2	**Assistant 2**	**Distance 3 m**	**Distance 6 m**	**Distance 9 m**
	$L_{eq,i}$ (ε)	$L_{eq,i}$ (ε)	$L_{eq,i}$ (ε)	$L_{eq,i}$ (ε)	$L_{eq,i}$ (ε)
Test 1	90.9 (± 0.6)	73.8 (± 0.3)	81.7 (± 0.4)	79.6 (± 0.5)	74.7 (± 0.2)
Test 2	91.3 (± 0.3)	72.9 (± 0.6)	80.7 (± 0.6)	79.6 (± 0.2)	74.7 (± 0.4)
Test 3	90.4 (± 0.6)	73.5 (± 0.5)	80.9 (± 0.2)	79.2 (± 0.4)	73.6 (± 0.6)
Test 4	92.0 (± 0.3)	71.2 (± 0.6)	80.6 (± 0.5)	78.2 (± 0.6)	73.4 (± 0.3)
Test 5	89.6 (± 0.4)	71.4 (± 0.2)	80.7 (± 0.3)	78.3 (± 0.3)	74.0 (± 0.2)
Mean	90.8 (± 0.2)	72.6 (± 0.4)	80.9 (± 0.4)	79.0 (± 0.5)	74.1 (± 0.6)

In relation to the equivalent continuous sound levels in the work environment, the measurements monitored during the pruning operation with sound data logger, positioned at 2 3, 6 and 9 meters respectively from the operator number 1, reported levels between: 86.4 and 87.6 dB(A), 84.2 and 85.4 dB(A), 78.1 and 79.8 dB(A) with averages of 87.0 dB(A), 84.9 dB(A) and 78.9 dB(A). Instead the measurements carried out, during the cross-cutting operation, with microphones positioned at same distances from the operator number 1, reported levels between: 81.7 and 80.6 dB(A), 78.2 and 79.6 dB(A), 73.4 and 74.7 dB(A), with averages of 80.9 dB(A), 79.0 dB(A) and 74.1 dB(A) respectively. The differences were observed in the acoustic levels both at the operator's ear level and at the work environment level, depending on the type of chainsaw used, the speed of the equipment's progress and the diameter of the trunks.

CONCLUSIONS

This study has enabled to widen our understanding of the general picture whose many criticalities in terms of work safety have not only been highlighted and observed, but also analyzed. During the use of chainsaw with an equivalent acoustic level higher than 85.0 dB(A), it would be important to adopt specific balancing measures or precautionary interventions, and limit the access only to the employers with appropriate personal protective equipment, as well (earphones or auricular insets) (Zimbalatti et al., 2008). The phonometric data processing has enabled to outline a typical representation, even though approximate, of the acoustic conditions during the rejuvenation pruning on centuries-old olive tree. Unfortunately, it has turned out that the non-reception and non-application of the present legislation endangers the safety of workers, who, in most cases, are unaware of the risks they run. In the work stations where there is an equivalent acoustic level higher than 85 dB(A), the results of this work should be interpreted as being indicative as they only account for a descriptive case study which can prove its utility and replicability in similar conditions (Cheta et al., 2018). The noise reduction, at

the source or on the run, should be one of the main management programs of this risk factor. This activity must take into account both the facilities and planning, as well as maintenance to control acoustic pollution. In the future new measurement sessions will be conducted to study the reduction of the noise levels and to define possible interventions with low technical and economic impacts.

REFERENCES

Abenavoli, L.M., Longo, L., Proto, A.R., Gallucci, F., Ghignoli, A., Zimbalatti, G., Russo, D. & Colantoni, A. 2016. *Characterization of biochar obtained from olive and hazelnut prunings and comparison with the standards of European Biochar Certificate* (EBC). Procedia: Social & Behavioral Sciences, vol. **223**, pp. 698–705 doi: 10.1016/j.sbspro.2016.05.244

Abenavoli, L.M. & Marcianò, C. 2013. Technical and economic analysis of alternative pruning systems in high dimensions olive trees in Calabria. *Agronomy Research* **11**(1), 7–12.

Abenavoli, L.M. & Proto, A.R. 2015. Effects of the divers olive harvesting systems on oil quality. *Agronomy Research* **13**(1), 7–16.

Brüel & Kjaer. 2001. *Environmental Noise*. Brüel & Kjaer. Sound & Vibration Measurement A/S, Denmark.

Cavazzani, A. & Sivini, G. 2001. *L'olivicoltura Italiana e Spagnola in Europa*. (Italian and Spanish olive growing in Europe). Rubbettino, Soveria Mannelli, Italy, 396 pp.

Cheta, M., Marcu, V. & Borz, A.S. 2018. Workload, exposure to noise, and risk of musculoskeletal disorders: a case study of motor-manual tree feeling and processing in poplar clear cuts. *Forests* **9**, 300. doi:10.3390/f9060300

CO.RE.R.A.S. 2007. *La filiera olivicolo-olearia in Sicilia*. Ricerche nell'ambito delle attività istituzionali dell'Osservatorio sul Sistema dell'Economia Agroalimentare della Sicilia (OSEAAS). Catania, Italy, 89 pp.

Deborah, I.N., Robert, Y.N., Marison, C.B. & Marilyn, F. 2005. The global burden of occupational noise induced hearing loss. *Am. J. Ind. Med*. **48**(6), 446–458.

De Souza, A.P., Minette, L.J., Sanches, A.L.P., da Silva, E.P., Rodrigues, V.A.J., de Oliveira, L.A. 2012. Ergonomic factors and production target evaluation in eucalyptus timber harvesting operations in mountainous terrains. IEA 2012: *18th World congress on Ergonomics – Designing a sustainable future*. doi: 10.3233/WOR-2012-0038-4957

Fardella, G.G. 1995. Profilo economico dell'olivicoltura calabrese. (Economic profile of Calabrian olive growing). *Proceedings of the Conference of Accademia Nazionale dell'Ulivo of Spoleto, II Tornata in Calabria* (II Round to Calabria), Reggio Calabria, Italy.

Giuffrè, A.M. 2017. Biometric evaluation of twelve olive cultivars under rainfed conditions in the region of Calabria, South Italy. Emir. *J. Food Agric*. **29**, 696–709. doi: 10.9755/ejfa.2017.v29.i9.110

Giuffrè, A.M. 2018. The evolution of free acidity and oxidation related parameters in olive oil during olive ripening from cultivars grown in the region of Calabria, South Italy. *Emir. J. Food Agric.* **30**, 539–548. doi: 10.9755/ejfa.2018.v30.i7.1737

Grigolato, S., Mologni, O., Proto, A.R., Zimbalatti, G., Cavalli, R. 2018. Assessment of noise level and noise propagation generated by light-lift helicopters in mountain natural environments. *Environmental Monitoring and Assessment* **190**(88). doi.org/10.1007/s10661-018-6464-2

International Olive Council – IOOC (2013) – *www.internationaloliveoil.org*

International Organization for Standardization. *Acoustics—Estimation of Noise-Induced Hearing Loss*; ISO 1999:2013; International Organization for Standardization: Geneva, Switzerland, 2013.

Mele, M.A., Islam, M.Z., Kang, H.M. & Giuffrè, A.M. 2018. Pre-and post-harvest factors and their impact on oil composition and quality of olive fruit. Emir. *J. Food Agric*. **30**, 592–603. doi: 10.9755/ejfa.2018.v30.i7.1742.

Morettini, A. 1972. *Trattati di Agricoltura. Olivicoltura.* (Treaties of Agriculture. Olive Growing). Ramo editoriale degli agricoltori Roma, Italy, 522 pp.

Pascuzzi, S. & Santoro, F. 2017. Analysis of Possible Noise Reduction Arrangements inside Olive Oil Mills: A Case Study. *Agriculture* **7**, 88. doi: 10.3390/agriculture7100088

Proto, A.R., Grigolato, S., Mologni, O., Macrì, G., Zimbalatti, G. & Cavalli, R. 2016. *Modelling noise propagation generated by forest operations: a case study in Southern Italy*. Procedia Social and Behavioral Sciences **223**, pp. 841–848.

Proto, A.R. & Zimbalatti, G. 2010. Risk assessment of repetitive movements in the citrus fruit industry. *Journal of Agricultural Safety and Health - Ed. American Society of Agricultural and Biological Engineers* (ASABE) **16**(4), 219–228.

Proto, A.R. & Zimbalatti, G. 2015. Risk assessment of repetitive movements in olive growing: analysis of annual exposure level assessment models with the ocra checklist. Journal of Agricultural Safety and Health - Ed. *American Society of Agricultural and Biological Engineers* (ASABE) **21**(4), 241–253; doi.org/10.13031/jash.21.10884

Russo, D. 2015. *Innovative procedure for measurement uncertainty evaluation of environmental noise accounting for sound pressure variability*. Ph.D. Thesis in Industrial Engineering (XV Cycle-New Series, XXIX Cycle).

Sorgonà, A., Proto, A.R, Abenavoli, L. & Di Iorio, A. 2018. *Spatial distribution of coarse root biomass and carbon in a high-density olive orchard: effects of mechanical harvesting methods*. *Trees-Structure and Function* **32**(4), 919–931. https://doi.org/10.1007/s00468-018-1686-z

Türker, S., Bülent, C., Cengiz, Ö. & Fazilet, N.A. 2011. Vibration and noise characteristics of hook type olive harvesters. *African Journal of Biotechnology* **10**(41), 8074–8081, 3 August, 2011 DOI: 10.5897/AJB10.2482

Vallone, M., Morello, G. & Catania, P. 2017. *Noise Risk Assessment in a Modern Olive Oil Mill*. The Italian Association of Chemical Engineering. vol. 58, 2017. ISBN 978-88-95608-52-5; ISSN 2283-9216

Zimbalatti, G., Proto, A.R. & Morabito, S. 2008. Acoustic levels in the manufacture of wood chairs. *Proceedings of International Conference Innovation Technology to Empower Safety, Health and Welfare in Agriculture and Agro-food Systems*, Ragusa, Italy.

Agronomy Research **17**(2), 322–332, 2019
https://doi.org/10.15159/AR.19.081

Model for ammonia emissions' assessment and comparison of various dairy cattle farming systems and technologies

A. Aboltins[1], L. Melece[2,*] and J. Priekulis[1]

[1]Latvia University of Life Sciences and Technologies, Institute of Agricultural Machinery, Cakstes blvd.5, LV-3001 Jelgava, Latvia
[2]Institute of Agricultural Resources and Economics, Department of Economics, Struktoru str. 14, LV-1039 Riga, Latvia
[*]Correspondence: ligita.melece@arei.lv

Abstract. A dairy cattle farming is an important source of ammonia emissions, particularly in Latvia. Models using a wide range in level of detail have been developed to represent or predict these emissions. Besides, models are useful for improving the understanding of various farm processes and their interacting effects on ammonia emissions. The model for ammonia emissions' assessing or representing, predicting and comparing for manure management chain of dairy cattle was created. The model provides a tool for evaluating mitigation and management strategies, abatement measures and techniques to reduce of ammonia emissions and improve the sustainability of dairy production systems both on the dairy farm and at the national level. It could be used as a supplement tool for officials and experts. The model estimates those ammonia abatement measures and techniques that have the highest emission reduction potential and opportunities for implementation on Latvia's dairy farms. The simulation model assesses the ammonia emissions into each stage of the farming: animal housing, manure management - manure handling and storage, and manure application. An important stage in reducing ammonia emissions is manure storage. It should be noted that the main task of the model was to compare the impact of the ammonia emission reduction options. When entering the number of animals, the average nitrogen quantity per animal, the percentage distribution of manure quantities, the first three levels of the program can be used to estimate the amount of nitrogen to be incorporated into the soil and, as the difference; and the amount of ammonia emissions.

Key words: model, ammonia emissions, mitigation, dairy cattle.

INTRODUCTION

Agriculture is the main source of ammonia emissions, contributing more than 90% of overall emissions. Moreover, emissions mainly occur during the housing of animals, storage and application of animal manures. In most countries, dairy cattle is the largest source of ammonia (NH_3) emissions (EEA, 2016). In 2016 the management of dairy cattle manure was responsible for 54.2% of total ammonia emissions emitted by the manure management of all livestock species and categories in Latvia (Eionet, 2018). Moreover, manure management of dairy cattle generates 23% of total ammonia emissions in Latvia.

The Directive 2016/2284/EU was adopted by EU respecting the revised Gothenburg Protocol of the UN Convention on Long-range Transboundary Air Pollution (EC, 2016). This Directive sets obligations for each EU Member State to reduce ammonia emissions from 2020 to 2029 and from 2030 onwards. Besides, the Directive requires each member state to adopt, implement and regularly update a national program for the reduction of air pollution, particularly ammonia emissions. The adoption of techniques to reduce ammonia emissions needs to be taken into account when estimating national emissions (EEA, 2017). Information will also be needed on the proportions of livestock housed in reduced-emission buildings, the proportion of manures stored under cover and the proportion of manures applied by reduced-emission techniques.

On an EU level it is stressed that thirteen Member States, including Latvia, should make the greatest effort to reduce ammonia emissions, because reported projected emissions are above their agreed commitments (EEA, 2018).

Therefore, for more successful evaluation, assessment and comparing, as well as prioritization of most appropriate ammonia abatement measures for Latvia's dairy cattle farming, the new tool should be developed. The overall purpose for developing models is to provide information for supporting decisions and policies (Jones et al., 2017). A widely used approach for modelling various agricultural systems can be classified as dynamic system simulation models. In contrast to the statistical approach, these models have functions that describe the changes in systems states in response to external drivers (e.g., weather and management practices), and how those changes are affected by other components in the system (Wallach & Thorburn, 2014). This approach is used for all types of models, including crop, livestock, and farming system models, with model outputs being the values of model state variables over time (e.g., typically daily outputs for crop and pasture models). These dynamic models can be used to simulate multiple responses for the specific time and variables as needed (Bjerg et al., 2013; Wallach & Thorburn, 2014), and thus can compare effects of alternative decisions or policies on trade-offs among those various responses.

The models have been developed and applied world-wide to quantify emissions and to test mitigation strategies (Del Prado et al., 2013). A large number of approaches and computational techniques exist to support decision-making under deep uncertainty (Haasnoot et al., 2013). It is not possible that developing a model all factors affecting the agricultural system can be taken into consideration (Antle et al., 2017). Accordingly, models are based on a logical structure in which some factors determined by the model developer or model user.

The purpose of the study was to develop the simulation model assesses the ammonia emissions into each stage of the dairy cattle farming, particularly manure management. The model should provide a tool for evaluating mitigation and management strategies, abatement measures and techniques to reduce of ammonia emissions.

MATERIALS AND METHODS

Principle of program construction

The model is designed for comparative studies/ calculations of ammonia emission as result of implementation of various abatement measures. The specialized software is designed for convenient review of ammonia emissions in the form of a tree structure.

Ammonia emission review programs are built on the .NET Framework, which is supported by default on all Microsoft operating systems. The software screen is shown in the Fig. 1.

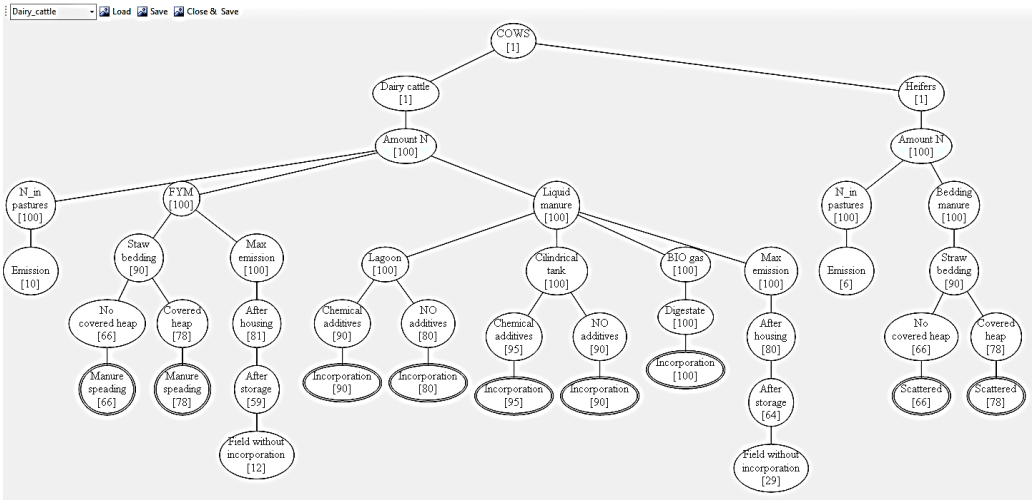

Figure 1. Software screen, where numbers in brackets indicate the output of nitrogen (N) units per animal via excreta.

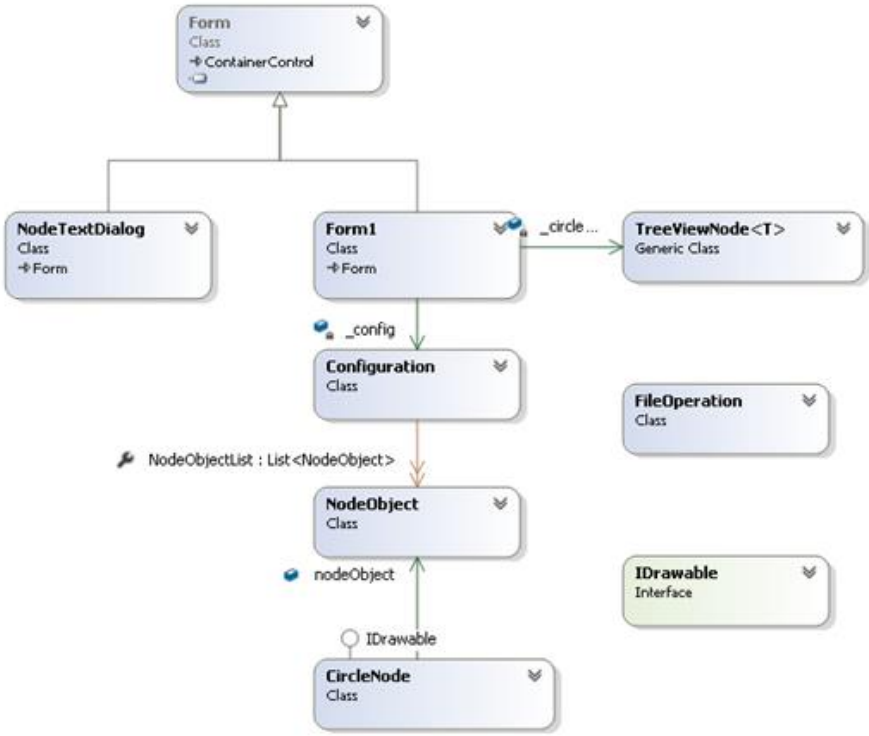

Figure 2. Program Class Diagram.

The program has two dialogue windows that are inherited from the 'Form' class (Fig. 2):

– '*NodeTekstDialog*' is implemented to enter the tree branch parameters of the model.

– '*Form1*' is a representation of a tree structure.

The '*TreeViewNode*' class, which is the '*IDrawable*' interface, is used to create the tree structure of the main window '*Form1*'. This class reconstructs a tree structure that is curiously constructed. With these classes, the tree structure is recursively shaped.

For the maintenance of the parameters of the tree branches, a '*Configuration*' class has been created, in which a list of parameters of each tree branch with the properties of the class '*NodeObject*' is realized. These characteristics are presented in Fig. 3.

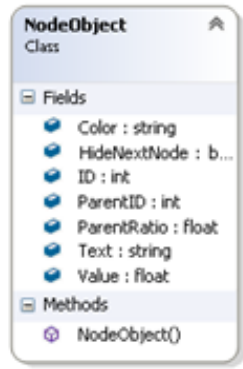

Figure 3. Properties of '*NodeObject*'.

The program consists of files such as '*Aep.exe*' - an executable file and files with a launcher '* .*pig*'. The file '* .*pig*' stores all parameters related to the developed calculation model. When the '*Aep.exe*' software has been started, the algorithm searches for all files that have the extension '* .*pig*' and retrieves all attributes of the file in the selection window of calculation model (Fig. 4). Selecting a particular model will activate the '*Load*' button. By pressing the '*Load*' button, the program will create a tree after the selected model. In this selection window, the model branch actions could be selected: '*Add Child*' - add a new sub-branch under the selected branch; '*Edit Child*' - edit the parameters of the selected branch; '*Copy*' - copy the selected branches of the selected branch; '*Paste*' - to create sub-branches of '*Copy*' branch on selected branch; '*Delete Node*' – to delete selected branch. If there are sub-branches of the selected branch, they will also be deleted; '*Refresh - Restore*' - the model view; '*Save'* - to save the model.

The retention of these properties in the file is accomplished with the class '*FileOperation*', which implements *XML* serialization and deserialization. The model structure is stored in a file with the extension '*pig*'. The file model is stored in *XML* file language structure. The name can be changed in the '*<text>* </ *text>*' label. This text will appear in the select models window.

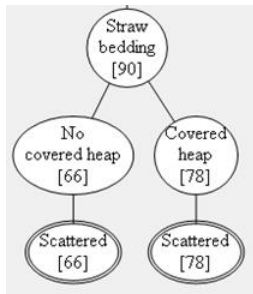

Figure 4. Branch display of tree structure.

The model consists of branches of a tree structure depicted in the form of a bubble. The bubble consists of an oval ring. Inside the ring are the name of the branch and the value of that branch in brackets (Fig. 4).

The values in brackets are indicated the amount of the total N quantity lost in emissions at each of the manure management stages without the use of ammonia emission reducing measures.

To make the model easier to review, the sub-branches of branch have the ability to hide in the program. Hiding the branches can be done by sliding the cursor over the selected branch bubble and by double-clicking the left mouse button. After the button double-clicks the sub-branches of the selected branch will not be displayed and the branch bubble will be displayed with a double line (Fig. 4).

RESULTS AND DISCUSSION

The program design principle with applications was described below. The created model aimsto determine the effectiveness of ammonia abatement measures, in which ammonia emission factors (EFs) are used for calculations. Emission factor (EF) methods have long been utilized for quantifying NH_3 emissions from individual category of livestock (e.g., dairy cow) or specific manure handling processes (Deng et al., 2015). Emissions from livestock, i.e., dairy cattle, farming occur during different stages in the manure management chain. The practical options to reduce ammonia emissions from manure management can be implemented during the individual stages of manure management, i.e., during grazing, from animal housing, manure storage and manure application (Amann et al., 2017).

The model traces the chain of N changes from animal manure occurring to application/ incorporation. Ammonia emissions are quantified using a nitrogen (N) flow approach, in which the NH_3 emission is calculated from the N flows and NH_3 emission factors (EFs) (Velthof et al., 2012).

The primary module of the simulation system evaluates ammonia emissions at each stage of the manure management chain and manure application: animal housing (barns, sheds or pastures/ grazing), manure treatment and storage and application or disposal of manure (Fig. 5). Despite that an application of inorganic N-fertilizers is also a significant source of ammonia emissions, it is not included in model, because does not apply directly to dairy farming.

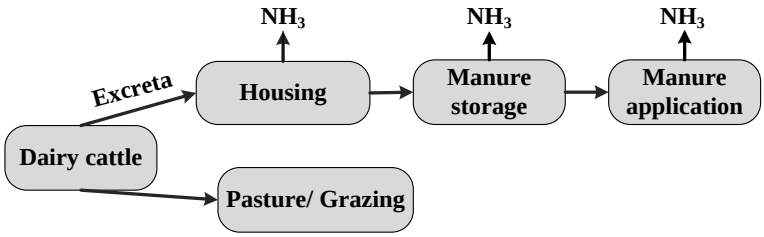

Figure 5. Schematic representation of ammonia emissions model.

Depending on the number and category of animals, stalls, ventilation and manure collection methods, ammonia emissions can be determined at the housing stage. An important stage in reducing ammonia emissions is the storage of both types of manure – liquid manure or slurry (hereinafter referred as – liquid/ slurry) and solid manure. It consists of environmental conditions (temperature, humidity and wind direction and

speed), storage type and storage technologies. The manure application time, depth of incorporation and application technology also reduces or increases ammonia emissions (EEA, 2016).

The ammonia abatement options that have the highest emission reduction potential and that have possibility to implement in Latvia's dairy farming were selected for model calculations (Table 1). The choice of measures to reduce ammonia emissions was based on the results of the research carried out by Melece et al. (2017). Differences in agricultural practices, such as housing and manure management, and differences in climate have significant impacts on emissions.

Table 1. Ammonia abatement or mitigation measures and reduction potential for dairy cattle farming

Abatement measure		NH_3 reduction	
		%	coefficient
Housing facilities			
Adsorption by bedding, e.g., straw		50%	0.50
Farmyard or solid manure storage			
Plastic sheeting (floating cover)		50%	0.50
Liquid manure or slurry storage			
'Tight' lid, roof or tent structure		70%	0.70
Replacement of lagoon, etc., with covered tank or tall open tanks		50%	0.50
Application of solid manure			
Incorporation of surface applied manure:	Immediately	90%	0.90
	In 4 hours	50%	0.50
	In 24 hours	30%	0.30
Application of slurry			
Injection 10-30 cm		90%	0.90
Injection 4-6 cm		75%	0.75
Acidification of liquid manure		50%	0.50
Trailing shoe		50%	0.50
Direct incorporation following surface application:	Immediately	75%	0.75
	In 4 hours	50%	0.50
	In 24 hours	30%	0.30

Source: Melece et al., 2017.

For this purpose, it was formally considered that at the beginning of manure management or first stage (i.e., housing, grazing) output of each animal via excreta is 100 units of nitrogen (N). The reduction coefficient of implementing measure (Table 1) and emission factors (EFs) of ammonia emissions (Table 2), were used for estimating the changes of the N quantity at the each stage manure management, as well as through the manure management chain, for every ammonia abatement option or measure (i.e., technique). Remaining nitrogen (N) was estimated by Eq. (1):

$$N_r = [1 - (EF \times R_c)] \cdot 100 \quad (1)$$

where N_r – remaining nitrogen units; EF – emission factor; R_c – emissions reduction coefficient.

The model calculations were performed using the Tier 2 emission factors (EFs) or values (Table 2) (EEA, 2017).

The default Tier 2 emission factors (EFs) from manure management of dairy cattle (Table 2) are from EMEP/EEA air pollutant emission inventory Guidebook 2016 (EEA, 2016) part 3B Manure management, which are updated in 2017 (EEA, 2017). Tier 2 uses a mass-flow approach based on the concept of a flow of TAN through the manure management system (EEA, 2017). It should be noted that the calculations of a mass-flow approach must be carried out on the basis of kg of N.

Table 2. Emission factors (EFs) used for calculation of the ammonia emissions from manure management of dairy cattle

Livestock	Manure type	EF housing	EF storage	EF spreading	EF grazing
Dairy cattle	Slurry/ liquid	0.20	0.20	0.55	0.10
	Solid	0.19	0.27	0.79	

Source: EEA, 2017.

Despite ammonia emission factors (EFs) in the livestock and manure management has been planned to review in 2019 by UNECE (2018), there is no restrictions in our model to replace the current EFs values with new ones.

Because the model is dynamic not static, it allows to make various changes and additions, for example, to delete some of NH_3 abatement measures (i.e., techniques) or to add new ones, as well as to change reduction coefficient. All ammonia abatement options or measures (i.e., techniques) in dairy cattle farming, which are presented in the Table 1, were evaluated using the created model.

Due to the limited length of the paper some examples of the model are presented below.

The calculation results, using the equation (1), for example, for the straw bedding in dairy cattle stalls, which reduces ammonia emissions (expressed as N units) by 50% or coefficient is 0.50 (Table 1), and emission factor – EF = 0.19 (Table 2), show that after housing 90 N units remain in manure and then reach the manure storage (Fig. 6):

$$N_{r\ straw} = \lfloor 1 - (0.19 \cdot 0.5) \rfloor \cdot 100 = 91 \quad (2)$$

where $N_{r\ straw}$ – remaining N units, using straw bedding.

Without use of straw bedding in the dairy cattle stalls, after housing less N – 81 units remain in manure and then reach the manure storage (Fig. 6):

$$N_r = (1 - 0.19) \cdot 100 = 81 \quad (3)$$

where N_r – remaining N units.

Ammonia emissions' reduction expressed as N units in the first stage (housing) and partially second stage (storage) of dairy cattle manure management before the application is shown in Fig. 6.

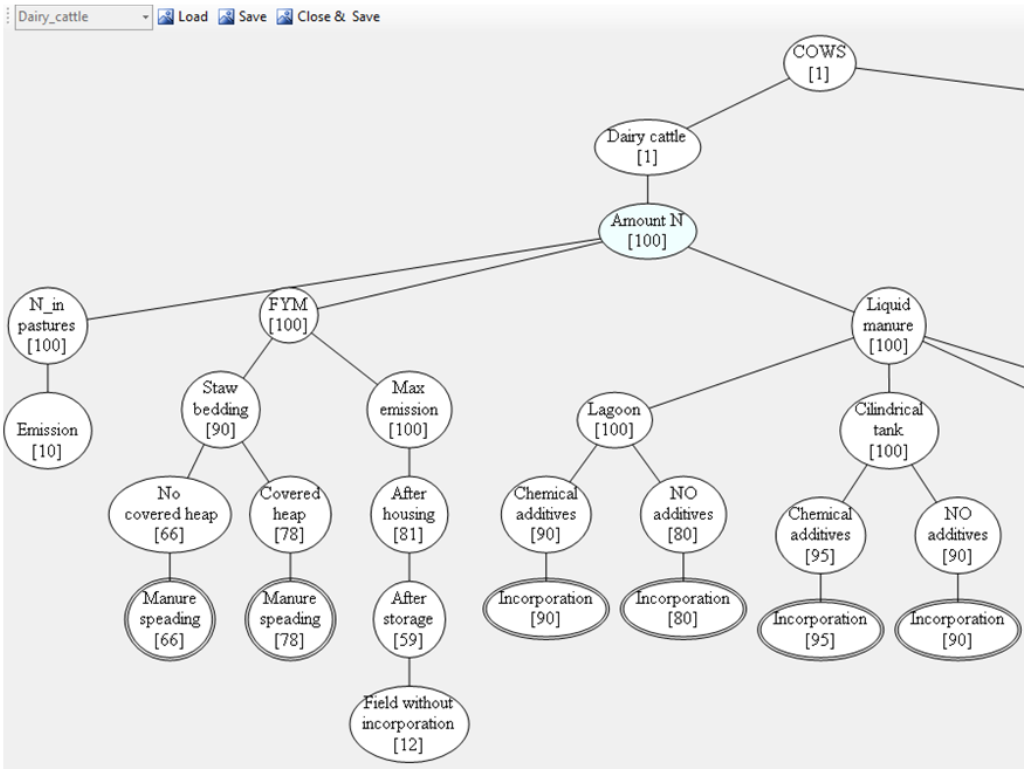

Figure 6. Values of remaining nitrogen units via the dairy cattle housing, storage, treatment and application.

An example showing the N remaining values for solid manure storage (covered heaps or non-covered heaps) in the tied-stall dairy cattle housing type, using straw bedding, as well as for various manure application and incorporation options is given in Fig. 7 (part of the model screen).

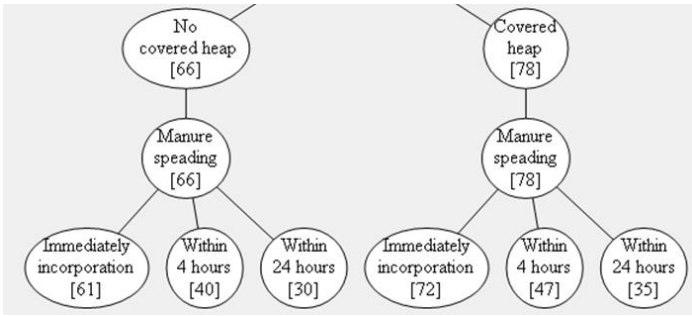

Figure 7. Part of model screen: storage and application/ incorporation of solid manure of dairy cattle with straw bedding.

Whereas, N remaining values via the dairy cattle liquid/ slurry storage in lagoon, manure treatment and application/ incorporation techniques are presented as part of the model screen (Fig. 8).

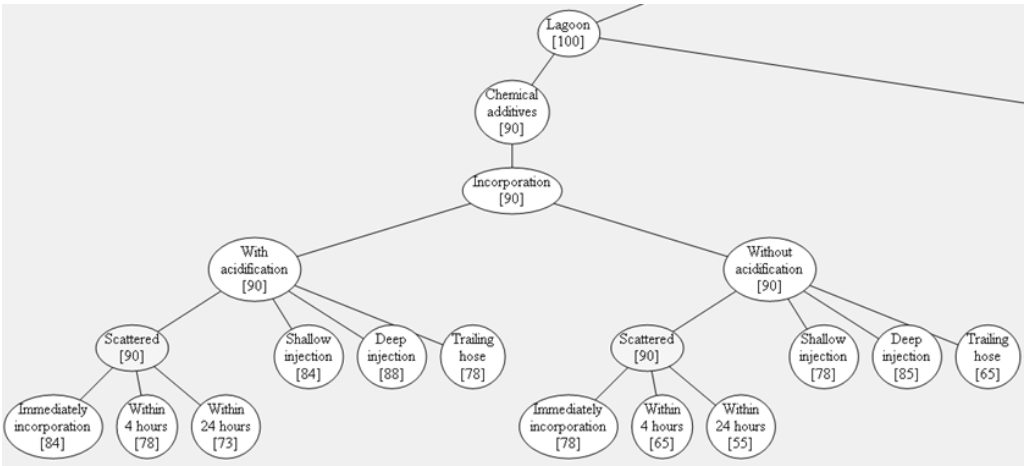

Figure 8. Part of model screen: storage, treatment and application/ incorporation of slurry or liquid manure of dairy cattle.

Acidification of livestock manure can reduce emission of the ammonia (NH_3), as well as greenhouse gases such as methane (CH_4) and nitrous oxide (N_2O) (Sommer et al., 2017). A number of the slurry acidifying additives have been considered, i.e., in Latvia, that may reduce the ammonia emissions from liquid manure or slurry, but they are not strongly recommended as abatement measure due to the following considerations: (i) safety issues (i.e., risk to workers, animals and the environment) by adding sulphuric acid to manure at any stage of the farm operation; (ii) adding additives other than acids to slurry, has not proven to be effective in reducing emissions or presents practical problems limiting their use (UNECE, 2015; Loyon et al., 2016).

Notwithstanding the need to develop integrated approach, in which interactions between ammonia and greenhouse gases emissions should be explored, are proposed by scholars and experts (i.e., EC, 2016; Hendriks et al., 2016; Sajeev et al., 2018), the purpose of using the model, term of its development and amount of financing was determined by the funder.

CONCLUSIONS

The developed model provides an opportunity to assess the impact of each individual ammonia abatement or mitigation measure (i.e., technique) both at a given stage of dairy cattle manure management and throughout the all manure management chain.

The model is applicable both on the dairy farm and at the national level to predict and estimate the effectiveness of the specific reduction measure. The model also can be used in developing ammonia abatement strategies by the policy-makers, as well as in the

decision-making process on state support to farms for the implementation of investment-intensive, but more effective measures for ammonia emissions reduction.

Ammonia emissions of manure management, and the mitigation potential of individual and combined measures to prevent emissions, are calculated for dairy cattle with an emissions factor approach. However, a more precise determination of ammonia emissions requires a model that accounts for the complex interactions between C and N transformations at each stage of the manure management chain.

Further research is required to provide evidence of the effectiveness and practicability of liquid manure or slurry acidification, as well as to clarify the application stage in manure management chain.

ACKNOWLEDGEMENTS. The paper was partially supported by the Ministry of Agriculture of Republic of Latvia, project No 10.9.1-11/17/886); and project 'INTERFRAME-LV' (No VPP-IZM-2018/1-0005) within the National Research Program 'Challenges and Solutions of the Latvian State and Public in the International Context'.

REFERENCES

Amann, M., Gomez-Sanabria, A., Klimont, Z., Maas, R. & Winiwarter, W. 2017. *Measures to Address Air Pollution from Agricultural Sources*. Laxenburg, Austria, International Institute for Applied Systems Analysis (IIASA). 40 pp.

Antle, J.M., Basso, B., Conant, R.T., Godfray, H.C.J., Jones, J.W., Herrero, M. & Tittonell, P. 2017. Towards a new generation of agricultural system data, models and knowledge products: Design and improvement. *Agricultural systems* **155**, 255–268.

Bjerg, B., Norton, T., Banhazi, T., Zhang, G., Bartzanas, T., Liberati, P. & Marucci, A. 2013. Modelling of ammonia emissions from naturally ventilated livestock buildings. Part 1: Ammonia release modelling. *Biosystems Engineering* **116**(3), 232–245.

Del Prado, A., Crosson, P., Olesen, J.E. & Rotz, C.A. 2013. Whole-farm models to quantify greenhouse gas emissions and their potential use for linking climate change mitigation and adaptation in temperate grassland ruminant-based farming systems. *Animal* **7**(s2), 373–385.

Deng, J., Li, C. & Wang, Y. 2015. Modelling ammonia emissions from dairy production systems in the United States. *Atmospheric Environment* **114**, 8–18.

EC 2016. Directive (EU) 2016/2284 on the reduction of national emissions of certain atmospheric pollutants, amending Directive 2003/35/EC and repealing Directive 2001/81/EC. *OJ* L **344**, 1–31.

EEA 2016. EMEP/EEA air pollutant emission inventory guidebook 2016 - 3.B Manure management 2016. *https://www.eea.europa.eu/publications/emep-eea-guidebook-2016.* Accessed 11.12.2018.

EEA 2017. Emission factors. *http://efdb.apps.eea.europa.eu.* Accessed 9.12.2018.

EEA 2018. NEC Directive reporting status 2018. *ttps://www.eea.europa.eu/themes/air/national-emission-ceilings/nec-directive-reporting-status-2018.* Accessed 11.01.2019.

Eionet 2018. Central Data Repository, Latvia, National emission inventories (CLRTAP). *http://cdr.eionet.europa.eu/lv/un/clrtap/inventories*. Accessed 12.01.2019.

Haasnoot, M., Kwakkel, J.H., Walker, W.E. & ter Maat, J. 2013. Dynamic adaptive policy pathways: A method for crafting robust decisions for a deeply uncertain world. *Global environmental change* **23**(2), 485–498.

Hendriks, C., Kranenburg, R., Kuenen, J.J.P., Van den Bril, B., Verguts, V. & Schaap, M. 2016. Ammonia emission time profiles based on manure transport data improve ammonia modelling across north western Europe. *Atmospheric Environment* **131**, 83–96.

Jones, J.W., Antle, J.M., Basso, B., Boote, K.J., Conant, R.T., Foster, I. & Keating, B.A. 2017. Brief history of agricultural systems modelling. *Agricultural Systems* **155**, 240–254.

Loyon, L., Burton, C.H., Misselbrook, T., Webb, J., Philippe, F.X., Aguilar, M. & Bonmati, A. 2016. Best available technology for European livestock farms: Availability, effectiveness and uptake. *Journal of Environmental Management*, **166**, 1–11.

Melece, L., Priekulis, J., Āboltiņš, A., Jonkus, D., Laurs, A., Krieviņa, A., Pecka, A. & Hāzners, J. 2017. *The selection and assessment of effectiveness of ammonia emissions mitigation and reduction measures in agriculture*, Report of 2nd stage of MoA project No 10.9.1-11/17/886. Riga, AREI. 79 pp. (In Latvian).

Sajeev, M., Purath, E., Winiwarter, W. & Amon, B. 2018. Greenhouse gas and ammonia emissions from different stages of liquid manure management chains: abatement options and emission interactions. *Journal of Environmental Quality* **47**(1), 30–41.

Sommer, S.G., Clough, T.J., Balaine, N., Hafner, S.D. & Cameron, K.C. 2017. Transformation of organic matter and the emissions of methane and ammonia during storage of liquid manure as affected by acidification. *Journal of Environmental Quality* **46**(3), 514–521.

UNECE 2015. Framework Code for Good Agricultural Practice for Reducing Ammonia Emissions. *http://www.unece.org*. Accessed 7.02.2018.

UNECE 2018. Addendum - 2018–2019 workplan for the implementation of the Convention. ECE/EB.AIR/140/Add.1. *https://www.unece.org*. Accessed 9.12.2018.

Velthof, G.L., Van Bruggen, C., Groenestein, C.M., De Haan, B.J., Hoogeveen, M.W. & Huijsmans, J.F.M. 2012. A model for inventory of ammonia emissions from agriculture in the Netherlands. *Atmospheric environment* **46**, 248–255.

Wallach, D. & Thorburn, P.J. 2014. The error in agricultural systems model prediction depends on the variable being predicted. *Environmental Modelling & Software* **62**, 487–494.

Agronomy Research **17**(2), 333–342, 2019
https://doi.org/10.15159/AR.19.092

Special tractor driving wheels with two modification of spikes inclination angle

R. Abrahám[1,*], R. Majdan[1] and R. Drlička[2]

[1]Department of handling and transport machinery, Faculty of Engineering, Slovak University of Agriculture in Nitra, Tr.A. Hlinku 2, SK949 76 Nitra, Slovak Republic
[2]Department of Quality and Engineering Technologies, Faculty of Engineering, Slovak University of Agriculture in Nitra, Tr.A. Hlinku 2, SK949 76 Nitra, Slovak
[*]Correspondence: rudolf.abraham@uniag.sk

Abstract The paper presents a research on an improvement of tractor drawbar properties using special driving wheels. Two modifications of the special driving wheels were designed and tested under field conditions. The results were compared with standard tyres. The special driving wheels consists of the tyres with a modified tyre-tread pattern and equips with the spike segments. The special driving wheels allow to activate or deactivate the spike segments to improve a drawbar pull at worse adhesive conditions of the ground or transport on roads with standard tyres. The first modification activates all 8 spike segments at spike inclination angle 90° and the second one 4 at angle 90°and 4 at 30°. The measurements were realised in October 2017 in an area of the Slovak Agricultural Museum in Nitra. The drawbar properties of the special driving wheels were evaluated based on drawbar pull of the test tractor Mini 070 type connected with a load tractor MT8-065 type. Using the test tractor in 1st and 2nd gear, the measurements were realized at 100% wheels slip and repeated 4 times. The results show the statistically significant differences in the drawbar pull of the test tractor with different driving wheels on a grass plot. The highest increase in drawbar pull reached the value 25.56% (2nd gear) and 19.98% (1st gear) in case of the special driving wheels with 4 spike segments at 90° and 4 at 30°. In case of the special driving wheels with 8 spike segments at 90°, increase in the drawbar pull reached the value 10.09% (1st gear) and 15.21% (2nd gear) in comparation with the standard tyres.

Key words: tyres, drawbar pull, force sensor, wheels slip.

INTRODUCTION

At present, agricultural tractors as manufactured are characterised by high rates of standardisation and feature a range of additional attachments which allow the wider use of each tractor and greatly facilitate its operation (Kosiba et al., 2012). The need for tractors and agricultural machinery to be tested from the point of view of their suitability to agricultural use will grow continuously because these machines directly affect agricultural production (Hujo et al., 2012; Hujo et al., 2017).

Driving wheels are significant part of a tractor construction because they transmit power to a ground. Therefore, tractor wheels affect a total energy efficiency, a fuel consumption (Uhrinová et al., 2012; Uhrinová et al., 2013), and a soil compaction (Rataj et al. 2009; Hrubý et al., 2013; Malý & Kučera 2014; Malý et al., 2015).

Agricultural tractor loses a lot of energy by a driving wheels slip. To reduce the wheels slip, an additional ballast load loads the tractors. This solution improves a drawbar property of the tractors but on the other hand increases the soil compaction and tyres wear on a hard surface (Semetko et al., 2002; Semetko et al., 2004).

The drawbar efficiency affects the fuel consumption and an emission production. The wheels slip reduction improves the fuel consumption, reduces the emission production and so improves an economy and an ecology of a tractor operation.

Many authors (Dickson et al. 1983; Nadykto et al., 2015; Adamchuk et al., 2016; Kučera et al., 2016) researched an impact of driving wheels on the tractor drawbar properties and an environment. This paper is aimed at a research on a new type of the special driving wheels to improve the tractor drawbar pull without a need for the addition ballast load.

MATERIALS AND METHODS

Special driving wheels with spike segments

The special driving wheels (Fig. 1) consists of the spike segments (1) which are placed in special grows (2) in the tire-tread pattern. The tyre-tread pattern of a standard tractor tyre was cut to make eight special grows around the wheel circumference.

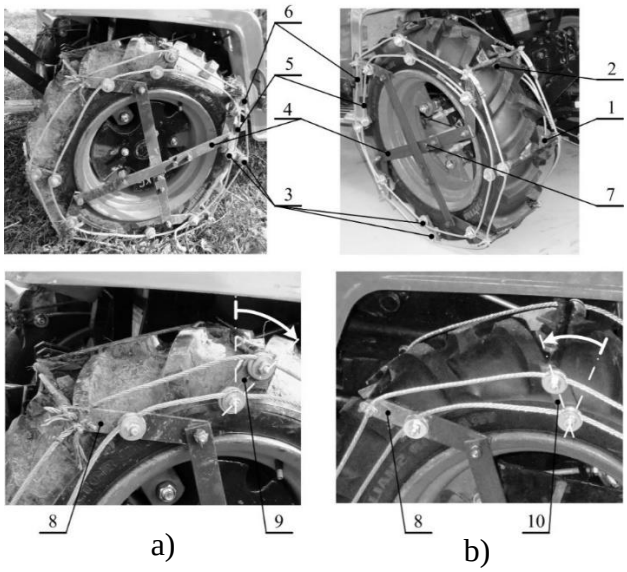

Figure 1. The special driving wheels: a) 8 spike segments at 90° inclination angle under test operation, b) 4 spike segments at 90° inclination angle and 4 at 30° inclination angle: 1 – spike segments; 2 – grow in tyre-tread pattern; 3 – pins; 4 – control levers; 5 – control steel rope; 6 – supporting steel rope; 7 – safety screw; 8 – spike segments at 90°; 9 – position of the lever of spike segments at 90°; 10 – position of the lever of spike segments at 30°.

The grows are parallel with rear wheels axle. Every spike segment consists of two spikes. Therefore, the special driving wheels can use 16 spikes to improve the tractor drawbar properties. The shape and dimensions of the spikes are adopted to the tyre-tread pattern

to allow active or inactive position. The spike segments can turn to the active position when the spikes overhang the wheels diameter and help to generate the drawbar pull. To transport of tractor on the roads, the spike segments turn to the inactive position when the spikes do not contact the ground. Abrahám et al. (2018) and Majdan et al. (2018) detailly describe the construction of the special driving wheels with the spike segments. This article presents the modification of the special driving wheels to compare the system with different inclination angles of spikes. The first one with all 8 spike segments at 90° inclination angle (Fig. 2, a) and second one with 4 spike segments at 90° and 4 at 30° inclination angle (Fig. 2, b). In both cases, the spike segments (8) connected with control levers (4) can be activated only at 90° while others spike segments can be activated at 90° (9) or 30° (10) depending on two possible lever position. White arrow sign (Fig. 1) shows the difference position of the lever allowing the 90° or 30° inclination angle of spikes.

Two experiments were realized. The first one (Fig. 2, a) uses the special driving wheels with all 8 spike segments at 90° inclination angle (3). The second one (Fig. 2, b) with 4 spike segments at 30° inclination angle (2) and 4 at 90° inclination angle (3). Construction of the special driving wheels uses the tractor tyre (1) and allows to modify the angle of every other spike segments which are not connected with lever mechanism (Fig. 1, position 6).

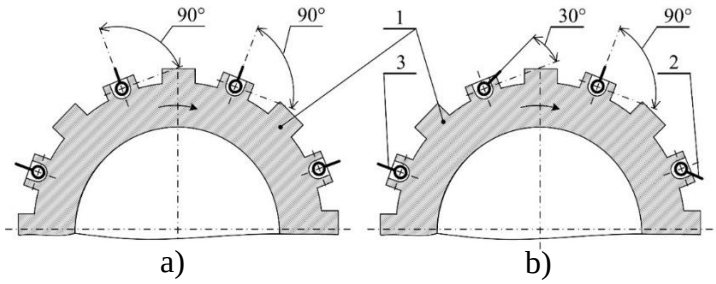

Figure 2. Position of spike segments: a) all 8 spike segments at 90°; b) 4 spike segments at 90° and 4 at 30°.

Measurement system

The properties of the special driving wheels with the spike segments were tested according to drawbar pull of the test tractor Mini 070 type (Agrozet, Czech Republic) which was equipped with different driving wheels. The force sensor 150 EMS type (Emsyst spol. s. r. o., Slovak Republic) measured the drawbar pull of the test tractor at 100% of driving wheels slip. Parameters of the force sensor EMS 150 type are listed in the Table 3.

Table 3. Specification of force sensor EMS 150 type

Parameter		Unit	Value
Accuracy class			0.5
Rated		N	10,000
Capacities			
Rated Output	Voltage	V	0–10
	Current	mA	4–20
Non-linearity		%	0.1 of full
Hysteresis			scale
Temperature	Compensated	°C	0–50
range	Operating		-20–50

A portable record device HMG 3010 (Hydac GmbH, Germany) recorded the measured data at sampling frequency 50 Hz. Tulík et al. (2013) and Tkáč et al. (2014) detailly describe the technical specification of device HMG 3010 type. The steel chain connected the test tractor with load tractor MT8-065 type (Agrozet, Czech Republic) to stop the first one and reach the 100% of driving wheels slip (Fig. 3). Novák et al. (2014) Procházka et al. (2015) and Porteš et al. (2013) also used the connection of the test and load tractor under field conditions.

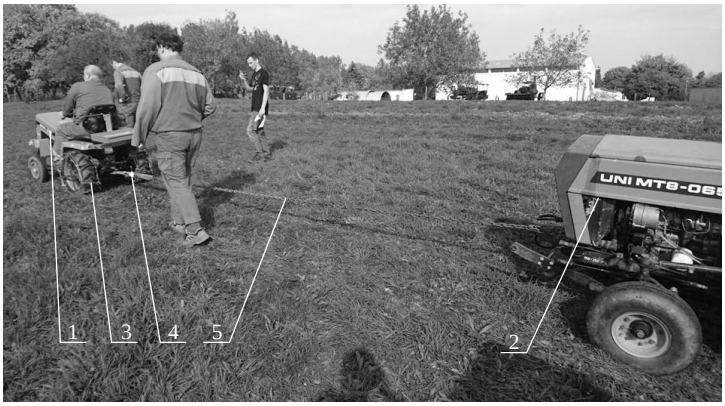

Figure 3. Measurement of drawbar pull of the tractor with special driving wheels: 1 – test tractor Mini 070 type; 2 – load tractor MT8-0652 type; 3 – special driving wheels; 4 – force sensor EMS 150 type; 5 – steel chain.

The weight of the load tractor MT8-065 type (970 kg) is approximately three times higher than the test tractor Mini 070 type (310 kg) to generate adequate braking force to stop the test tractor. The relatively low tractor weight together with a power (8 kW at 3,600 rpm) of a gasoline engine of the test tractor continually generates the drawbar pull at 100% of driving wheels slip.

Experiment conditions

The paper presents results of two experiments. The first one evaluates the drawbar pull of the test tractor with the special driving wheels with all 8 spike elements at 90° (Fig. 1a and Fig. 2a) and the second one with 4 spike segments at 90° and 4 at 30°. Two versions of the special driving wheels were compared with the standard tractor tyres TS-02 6.5/75-14 4PR TT type, (Mitas, a. s., Czech Republic).

The measurements of the test tractor drawbar pulls were four times repeated to eliminate the measurements errors. The results were verified by two measurements of the drawbar pull of the test tractor in 1st and 2nd gear.

All experiments were realized on the grass plot (Chernozem soil type) of the Slovak Agricultural Museum in Nitra (Slovak Republic). We used plain grass plot area in October 2017.

Statement of soil moisture and bulk weight

The bulk weight of soil was stated according to standard STN 72 1010 using Kopecky rollers as follows:

$$\rho_w = \frac{m_1 - m_2}{V_s}, \text{ g cm}^{-3} \quad (1)$$

where m_1 – weight of soil volume and Kopecky roller, g; m_2 – weight of empty Kopecky roller, g; V_s – volume of Kopecky roller, cm^3.

The soil moisture was stated according to standard STN 72 1012 after drying at temperature 105 °C as follows:

$$w = \frac{m_1 - m_3}{m_3 - m_2} \cdot 100, \% \quad (2)$$

Where m_3 – weight of soil volume after drying and Kopecky roller, g.

Average value of drawbar pull

The drawbar pull measurements of the test tractor with different driving wheels were repeated four times to eliminate the measurements errors. To compare the different driving wheels types, average values of the drawbar pulls (F_{DP}) were calculated.

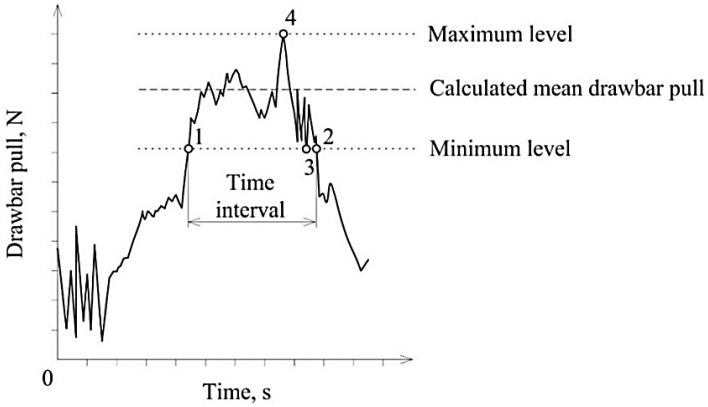

Figure 4. Example of one measurement of the drawbar pull and statement of the average value.

During the drawbar pull measurement the values (y_i) oscillate around the average value (x) mainly due to the shape of the tire-tread pattern and the spikes of the special driving wheels. Therefore, the drawbar pull of the test tractor is not constant. Fig. 4 shows an example of one measurement of the drawbar pull to state mean values x_1, x_2, x_3 and x_4. A begin (point 1) and an end (point 2) of a time interval must be stated to identify a data set for average value calculation. These points are cross-sections of dotted line (minimum level) with solid line (measured course of the drawbar pull). The position of the dotted line (minimum level) is determined by the lowest value (point 3) of the data set. Therefore, the data set contains the values from minimum (point 3) to maximum (point 4) level.

RESULTS AND DISCUSSION

Fig. 5 shows the test tractor equipped with the special driving wheels during the drawbar pull measurement under field measurement conditions. The measurements were realised on a grass plot in October 2017. The soil moisture 19.45% was calculated according Eq. 2 and bulk weight of soil 1.24 g cm^{-3} according to Eq. (1).

Tables 4 and 5 show the results of four measurement repetitions of drawbar pull of the test tractor with two versions of the special driving wheels in comparison with standard tyres. Using the Microsoft Excel, the drawbar pulls F_{DP} and a confidence interval (95%) were calculated to state if the differences between the various driving wheels are statistically significant. Švenková et al. (2010) and Kozelková et al. (2018) present, that the 95% confidence interval is adequate for experiments in agricultural praxis.

Figure 5. The test tractor Mini 070 type equipped with the special driving wheels.

Table 4. The measured values of the drawbar pull of the test tractor in 1st gear

Parameter	Type of driving wheels		
	8 spike segments at 90°	4 spike segments at 90° and 4 at 45°	Standard tyres
	Drawbar pull, N		
x_1	3,530.1	4,074.4	3,123.1
x_2	3,570.8	3,917.5	3,268.0
x_3	3,620.2	4,006.3	3,187.6
x_4	3,488.2	3,968.5	3,196.6
F_{DP}	3,552.3	3,991.7	3,193.8
Confidence	3,462.5	3,886.5	3,099.5
interval (95%)	3,642.1	4,096.8	3,288.2

Table 5. The measured values of the drawbar pull of the test tractor in 2nd gear

Parameter	Type of driving wheels		
	8 spike segments at 90°	4 spike segments at 90° and 4 at 45°	Standard tyres
	Drawbar pull, N		
x_1	3,654.2	4,207.3	3,061.0
x_2	3,612.0	4,258.4	2,994.7
x_3	3,635.6	4,217.0	3,204.6
x_4	3,814.3	4,100.4	3,217.3
F_{DP}	3,679.0	4,195.8	3,119.4
Confidence	3,532.9	4088.6	2,945.6
interval (95%)	3,825.2	4,302.9	3,293.2

Fig. 6 and 8 show the comparison of various driving wheels based on the drawbar pull F_{DP} with the confidence interval (95%). The measured and statistically processed results show the statistically significant differences between all driving wheels versions in case of 1st and 2nd gear. The special driving wheels with 4 spikes segments at 90° and 4 at 30° shows the best improvement of the drawbar properties of the test tractor in comparison with the second one and the standard tyres. Higher differences were reached in case of 2nd gear because the test tractor can generate a higher power.

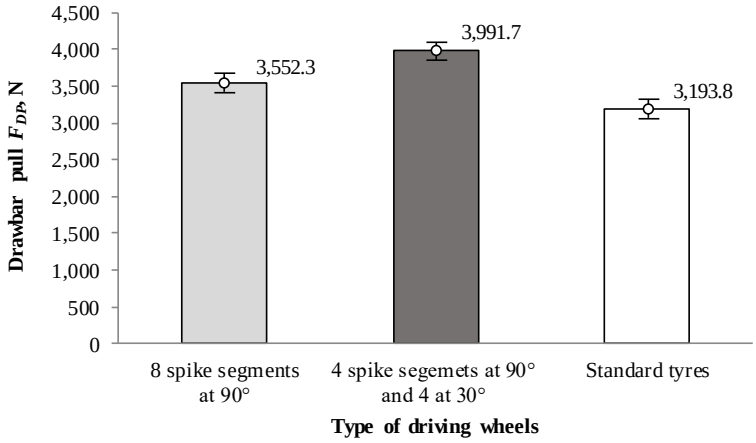

Figure 6. Comparison of the drawbar pulls of the test tractor in 1st gear.

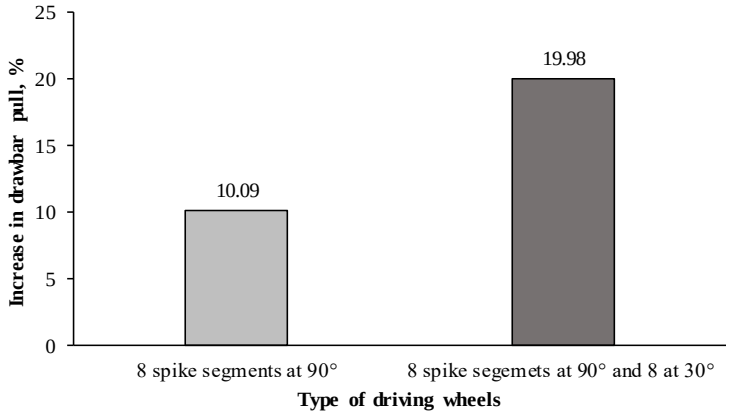

Figure 7. Percentage increase in drawbar pulls compared with the standard tyre (1st gear).

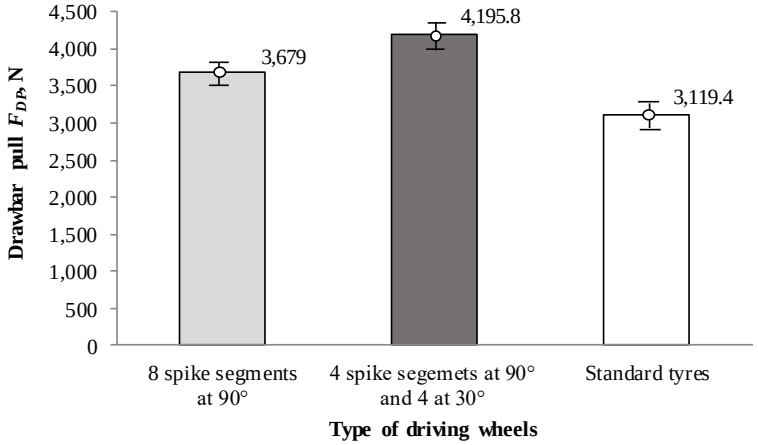

Figure 8. Comparison of the drawbar pulls of the test tractor in 2nd gear.

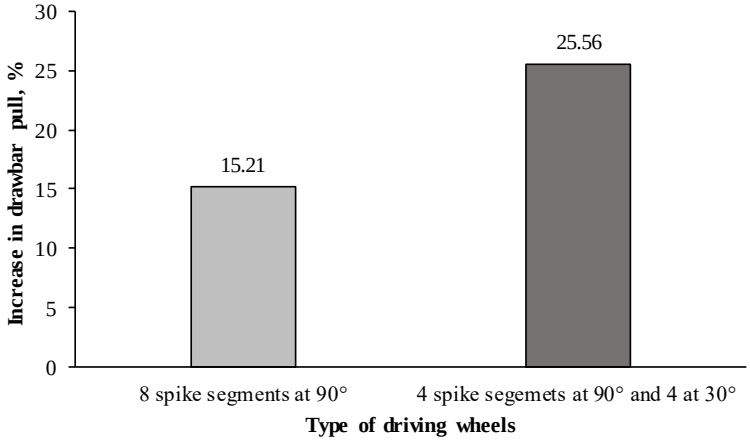

Figure 9. Percentage increase in drawbar pulls compared with the standard tyre (2nd gear).

Hermawan et al. (1996) and Hermawan et al. (1997) realised experiments with single movable lug to state the influence of the lug inclination angle on the pull force. The flat movable lug with 45° lug inclination angle generated a slightly higher peak of pull force than those with 30° and 60° lug inclination angles. Therefore, the authors demonstrated the significant differences between pull forces resulting in lug inclination angle. Fajardo et al., (2014) reached the higher performance index and tractive efficiency in case of wheel with 13° lug inclination angle in comparison of 0°. Statistical analyses of this results showed that draft, axle power, drawbar power, performance index and tractive efficiency were significantly affected by the lug angle, number of pass, shaft speed, and the combination of lug angle and shaft speed. Yang et al., (2014) researched force interaction between the lug and soil at various inclination angles. They measured normal and tangential forces acting on a single lug as functions of inclination angle, moving direction angle, sinkage length, horizontal displacement, and traveling speed. The authors experimentally confirmed the effect of lug inclination angle on lug-soil forces. The special driving wheels allow to change the inclination angle of the spikes. The experiment with 4 spike segments at 90° and 4 at 30° showed the better drawbar properties of the test tractor than with all 8 spike segments at 90°. In the first case, the increase in the drawbar pull of the test tractor in 1st gear reached the value19.98% (Fig. 7) and in 2nd gear 25.56% (Fig. 9). In the second case the increase in the drawbar pull reached lower values, namely 10.09% (Fig. 7) when the test tractor was in 1st gear and 15.21% (Fig. 9) in 2nd gear. Therefore, we experimentally confirmed the fact that the spike inclination angle affect the drawbar pull of the tractor with the special driving wheels.

CONCLUSIONS

The design of the special driving wheels allows to use two versions of the inclination angles of the spike segments. The first one uses all 8 spike segments at 90° and the second one 4 spike segments at 90° and 4 at 30°. It allows to compare the drawbar pull of the test tractor with two versions of the special driving wheels and standard tyres. The drawbar properties of the test tractor were improved by both versions of the special driving wheels. The drawbar pull of the test tractor were measured at 100% driving

wheels slip when the tractor was stopped. The standard tyres started to slip at the lowest drawbar pull. The special driving wheels with all 8 spike segments at 90° reached 10.09% increase in the drawbar pull (1st gear) and 15.21% (2nd gear). The highest increase in the drawbar pull 19.98% (1st gear) and 25.56% (2nd gear) reached the test tractor with the special driving wheels with 4 spike segments at 90° and 4 at 30°. We can conclude that the spike inclination angle of the special driving wheels affects the tractor drawbar pull. In the future research, the special driving wheels will be modified to reach the best improvement of the drawbar properties at optimum inclination angle of the spikes.

ACKNOWLEDGEMENTS. VEGA 1/0155/18 'Applied research of the use of environmentally friendly of energy sources in the agricultural, forestry and transport technology'.

REFERENCES

Abrahám, R., Majdan, R. & Drlička, R. 2018. Comparison of consumption of tractor at three different driving wheels on grass surface. *Agronomy Research* **16**, 621–633.

Adamchuk, V., Bulgakov, V., Nadykto, V., Ihnatiev, Y. & Olt, J. 2016. Theoretical research into the power and energy performance of agricultural tractors. *Agronomy Research* **14**, 1511–1518.

Dickson, D.J.W., Campbell, J.K. & Henshall, A. 1983. An assessment of seedbed compaction by open, flat-lugged, steel tractor wheels. *Journal of Agricultural Engineering Research* **28**, 45–60.

Fajardo, A.L., Delfin, C.S., Engelbert, K.P., Pepito, M.B. & Eduardo, P. 2014. Paningbatan, Force and puddling characteristics of the tilling wheel of float-assisted tillers at different lug angle and shaft speed, *Soil and Tillage Research* **140**, 118–125.

Hermawan, W.H., Oida, A. & Yamazaki, M. 1997. The characteristics of soil reaction forces on a single movable lug. *Journal of Terramechanics* **34**, 23–35.

Hermawan, W.H., Oida, A. & Yamazaki, M. 1996. Measurement of soil reaction forces on a single movable lug. *Journal of Terramechanics* **33**, 91–101.

Hrubý, D., Bajla, J., Olejár, M., Cviklovič, V. & Tóth, L. 2013. New generation portable vertical penetrometer design. In *Trends in agricultural engineering 2013*. Prague, pp. 223–227 (in Czech).

Hujo, Ľ., Tkáč, Z., Jablonický, J., Uhrinová, D. & Halenár, M. 2017. The action of force measurement for the three-point hitch of a tractor. *Agronomy Research* **15**, 162–169.

Hujo, Ľ., Kosiba, J., Jablonický, J. & Drabant, Š. 2012a. Theoretical design of a laboratory test device for the testing of tractor hydraulics. *Technics in Agrissector Technologies.* Nitra, pp. 68–73 (in Slovak).

Kosiba, J., Varga, F., Mojžiš, M & Bureš, Ľ. 2012. The load characteristics of tractor Fendt 926 Vario for simulation on test device. *Acta Facultatis Technicae* **17**, 63–72.

Kozelková, D., Országhová, D., Matejková, E., Fikselová, M., Horská, E., Ďurdíková, D. & Matysik-Pejas, R. 2018. Eggs and their consumption affected by the different factors of purchase. *Slovak Journal of Food Sciences* **12**, 570–577.

Kučera, M., Helexa, M. & Molenda, M. 2016. Selected tire characteristics and their relation to its radial stiffness. *MM Science Journal* **12**, 1524–1530.

Majdan, R., Abrahám, R., Tkáč, Z. & Mojžiš, M. 2018. Drawbar parameters of tractor with prototypes of driving wheels and standard tyres. *Acta technologica agriculturae* **21**, 63–68.

Malý, V., Tóth, F., Mareček, J. & Krčálová, E. 2015. Laboratory test of the soil compaction. *Acta Universitatis Agriculturae et Silviculturae Mendelianae Brunensis* **63**, 77–85.

Malý, V. & Kučera, M. 2014. Determination of mechanical properties of soil under laboratory conditions. *Research in agricultural engineering* **60**, 66–69.

Nadykto, V., Arak, M. & Olt, J. 2015. Theoretical research into the frictional slipping of wheel-type undercarriage taking into account the limitation of their impact on the soil. *Agronomy Research* **13**, 48–157.

Novák, P., Chyba, J., Kumhála, F. & Procházka, P. 2014. The measurement of stubble cultivator draught force under different soil conditions. *Agronomy Research* **12**, 135–142.

Porteš, P., Bauer, F. & Čupera, J. 2013. Laboratory-experimental verification of calculation of force effects in tractor's three-point hitch acting on driving wheels. *Soil and Tillage Research* **128**, 81–90.

Procházka, P., Novák, P., Chyba, J. & Kumhála, F. 2015 Evaluation of measuring frame for soil tillage machines draught force measurement. *Agronomy Research* **13**, 186–191.

Rataj, V., Galambošová, J. & Macák, M. 2009. Experiences with Implementing of CTF System in Slovakia. *GPS autopiloty v zemědělství*. Prague, pp. 34–38 (in Czech).

Semetko, J., Janoško, I. & Pernis, P. 2002. Determination of driving force of tractor and trailer wheels. *Acta technologica agriculturae* **5**, 1–4.

Semetko, J., Janoško, I. & Pernis, P. 2004. Determination of power of multidrive vehicles. *Acta technologica agriculturae* **7**, 20–23.

STN 72 1012 Laboratory determination of moisture content of soils. 1989.

Švenková, J., Dědina, M. & Matejková, E. 2010. Verifying ammonia emissions factors currently valid in breeding of livestock. *Acta technologica agriculturae* **13**, 29–32.

STN 72 1010. The statement of soil bulk density. 1989.

Tkáč, Z., Kosiba, J., Hujo, Ľ., Štulajter, I. & Jánošová, M. 2014. Operating test of hydraulic pump of tractor with use of ecologic fluid. *Riadenie tekutinových systémov 2014*. 8–15.

Tulík, J., Kosiba, J., Hujo, Ľ., Jablonický, J. & Šinský, V. 2013. The durability of a tractor gear-hydraulic circuit. *Trends in agricultural engineering.* Prague, pp. 617–621 (in Czech).

Uhrinová, D., Jablonický, J., Hujo, Ľ., Kosiba, J., Tkáč, Z., Králik, M. & Chrastina, J. 2013. Research of limited and unlimited emission effect on the environment during the burning of alternative fuels in agricultural tractors. *Journal of Central European Agriculture* **14**, 1402–1414.

Uhrinová, D., Jablonický, J., Hujo, Ľ., Tkáč, Z., Kučera, M. & Kosiba, J. 2012. Measurement of operating parameters and emissions of tractor with diesel ol and biofuel. In *TEAM* **4**, 299–302.

Yang Yang, Y.S., Shugen, M. & Ryohei, Y. 2014. Characteristics of normal and tangential forces acting on a single lug during translational motion in sandy soil. *Journal of Terramechanics* **55**, 47–59.

Agronomy Research **17**(2), 343–348, 2019
https://doi.org/10.15159/AR.19.085

Comparison of lycopene and β-carotene content in tomatoes determined with chemical and non-destructive methods

I. Alsina[1,*], L. Dubova[1], M. Duma[2], I. Erdberga[1], A. Avotiņš[3] and S. Rakutko[4]

[1]Latvia University of Agriculture, Faculty of Agriculture, Institute of Plant and Soil Science, Liela street 2, LV-3001 Jelgava, Latvia
[2]Latvia University of Agriculture, Faculty of Food Technology, Department of Chemistry, Liela street 2, LV-3001 Jelgava, Latvia
[3]Riga Technical University, Faculty of Power and Electrical Engineering, Kalku street 1, LV-1658 Riga, Latvia
[4]Institute for Engineering and Environmental Problems in Agricultural Production, Tyarlevo, Pushkinsky distr., RU196625 St. Petersburg, Russia
[*]Correspondence: ina.alsina@llu.lv

Abstract. Tomatoes are one of the most popular vegetables due of their wide use as food. Tomatoes are not only tasty fruit, but one of its benefits - high carotenoids content is well-known. Non-destructive analyses methods are used more and more in different industries. It is cheaper, faster and environmentally friendly way of analyse than traditional chemical methods. But these methods need references to the traditional ones. The aim of this study was to find the correlation between lycopene and β-carotene content in tomatoes determined with reflectance spectrometer and extraction of pigments. Content of two carotenoids (lycopene and β-carotene) was determined in 27 varieties of tomatoes. Red, pink, orange, yellow and brown fruits were included in experiment. Reflectance spectrums of tomatoes fruits were obtained with remote sensing portable spectroradiometer RS-3500 (Ltd.Spectral Evolution). Tetrahydrofuran was used for extraction of pigments. Absorption spectra of extract were obtained by spectrophotometer UV-Vis -1800 (Ltd. Shimadzu). Linear regression analyses were performed to correlate spectral data with lycopene and β-carotene concentrations measured by pigment extraction. The best reflectance region for lycopene spectral detection was 570 ± 5 nm, but for β-carotene 487 ± 5 nm. Reflectance indexes for both pigments were worked out. High linear correlation ($R^2 > 0.9$) between spectral parameters and lycopene concentration was detected. Correlation between results obtained with methods used for β-carotene determination was lower and depended of colour of tomatoes fruits.

Key words: *Lycopersicon esculentum*, reflectance spectrum, reflectance index.

INTRODUCTION

Tomatoes (*Lycopersicon esculentum* Mill.) are second most consumed vegetable in the world (Clément et al., 2015). Tomatoes differ in size, shape, color, ripening rate, firmness and composition determinating quality and taste (Gastélum-Barrios et al., 2011). They are consumed fresh and in many processed forms Tomatoes and their products are the world richest source of lycopene (Dias, 2012). The average daily intake of lycopene in human diet is about 25 mg and 85% of that is obtained from tomatoes.

Tomatoes contain significant amounts of carotenes and they are the forth leading source of provitamine A in the American diet (Arab & Steck, 2000). Lot of researches demonstrate that lycopene and β-carotene can act as free- radical quencers, prevent aging, tissue damage, heart diseases and certain cancers (Pedro & Ferreira, 2005).

Standart biochemical methods to assay lycopene and β-carotene content are time consuming and use hazardous organic solvents (Davis et al, 2003, Pedro et al., 2005).

Non-destructive analyses are used more and more in different industries. Itis cheaper, faster and environmentally friendly way of analyse than traditional chemical methods. But these methods need references to the traditional ones. They allow to follow on the biochemical changes of the fruits during the ripening process and harvest plants at the optimum time. Non-destructive analyses are used to clarify tomatoes and their products quality as well. Pedro & Ferreira (2005) reported about satisfactory prediction abilities of total solids, lycopene and β-carotene in tomatoe products. Clement et al. (2008) reported about simultaneously measured quality parameters of tomato in a nondestructive manner using vis−NIR reflectance spectroscopy and chemometrics. Results showed well predicted tomatoe color index. Ciaccheri et al. (2018) clarified that lycopene prediction models were dependent on cultivar and season. Clement et al. (2015) informed of determination of lycopene content in vine or pink beaf-type tomatoes and obtained coeficient of determination was 0.65. Davis et al. (2003) reported about light absorbance measurements with scanning xenon flash colorimeter/spectrophotometer, correlation coeficents for lycopene in pureed fresh tomatoes was 0.97, for tomatoes products- 0.88.

The aim of this study was to clarity the correlation between lycopene and β-carotene content in fruits of tomatoes determined with reflectance spectrometer and extraction of pigments.

MATERIALS AND METHODS

Samples

Measurements were done with 27 varieties of tomatoes. Tomatoes were grown in plastic film greenhouse without additional lighting. All fruits were harvest at fully ripening stage. In the experiment red fruit varieties 'Amaneta F1', 'Aurea F1', 'Bellastar F1', 'Berberana F1', 'Conchita F1', 'Elegance F1', 'Gardener's Delight F1', 'Gaurmandia F1', 'Lancelot F1', 'Nectar F1', 'Pozano F1' and Sunstream F1', pink ones 'Cipars F1', 'Dimerosa F1', 'DRK936 F1', 'Fuji Pink F1', 'Pink Wonder F1', 'Rhianna F1', and 'Rosastar F1', orange – 'Apressa F1','Beorange F1', 'Organza F1', and 'Oranjstar F1', yellow – 'Bolzano F1' and 'Gualdinjo F1' and brown – 'Black Cherry F1' and Chocomate F1' were included. Average tomatoe fruit weight varied from 8.6 g ('Bellastar F1') till 212.0 g ('Pink Wonder F1').

Non-destructive determination of lycopene and β-carotene

Reflectance spectrums of tomatoes fruits were obtained with remote sensing portable spectroradiometer RS-3500 (Ltd.Spectral Evolution). 4 – tomatoes fruits depending on fruit size were used for analyses. Totally 16 reflectance spectrums for each variety were obtained. Spectrums were represented as averages for each variety.

Extraction and determination of lycopene and β-carotene

The same tomatoes fruits were used for biochemical analyses. All the chemicals used were with the analytical grade.

Fresh tomatoes were homogenised, 1 ± 0.005 g of sample was placed in test tube, filled up to 10 mL with tetrahydrofurane (THF), mixed and shacked 30 min in the dark. Then the light absorption values (A) at 663, 645, 505 and 453 were noted by UV-VIS spectrophotometer (UV-1800 Shimadzu Corporation, Japan). Equations 1 and 2 were used to calculate lycopene and β-carotene content (Nagata & Yamashita, 1992). Lycopene and β-carotene content was expressed as mg 100 g^{-1} of fresh matter (FM).

$$Lyc = -0.0458A_{663} + 0.204A_{645} + 0.372A_{505} - 0.0806A_{453} \quad (1)$$

$$\beta car = 0.216A_{663} - 1.22A_{645} - 0.304A_{505} + 0.452A_{453} \quad (2)$$

Biochemical analyses were performed in three replicates.

Data analyses

Obtained data were processed by Excel software (Anova and Correlation analyses), data were expressed as means of three replicates for biochemical analyses and 16 replicates for non-destructive analyses.

RESULTS AND DISCUSSION

The reflectance spectrums of tomatoes are shown in Fig. 1. Tomatoes were grouped by their colour and the significant differences between differently coloured fruits are clearly seen in the visible light wavelength (400–700 nm). The major peak of reflectance for red coloured tomatoes fruits was at 652 nm, for pink ones at 643 nm, brown – 636 and for orange and yellow at 612 nm. Decrease of reflectance spectrums in the area between 670–680 nm (minimum at 678 nm for brown coloured tomatoes fruits) indicates chlorophylls presence in tomatoes fruits. Similar evidence of presence of chlorophylls was obtained by Ciaccheri et al. (2018). Rapid increase of reflectance was observed for yellow tomatoes at 457 nm, for orange at 490 nm, but for red, purple and brown ones at 583–587 nm wavelength zone.

Wavelengths area from 1,800–2,500 is less informative due to low reflectance signal (Fig. 1)

Reflectance spectrums at visible light area (400–700 nm) were used to check the correltion of lycopene and β-carotene content determined with biochemical analyses (Fig. 2). The highest coefficient of correlation for lycopene content was detected at the wavelength 570 nm |r| = 0.864, but for β-carotene at the wavelength 487 nm (|r| = 0.682). These wavelengths were used for development of normalized difference indexes for determination of both carotenoids. Normalized difference index is popular in remote sensing and based on ratio of difference and sum of selected wavelengths thus include the effect of average spectra height of sample (Choudhary et al., 2009). In our experiments as reference spectrum 630 nm (cross-point of lycopene and β-carotene correlation curves) was used and equations for index of lycopene (LYC) (Eq. 3) and β-carotene CAR (Eq. 4) was drown up, where RW reflectance at specified wavelength.

$$LYC = \frac{RW_{630} - RW_{570}}{RW_{630} + RW_{570}} \quad (3)$$

$$CAR = \frac{RW_{630} - RW_{487}}{RW_{630} + RW_{487}} \quad (4)$$

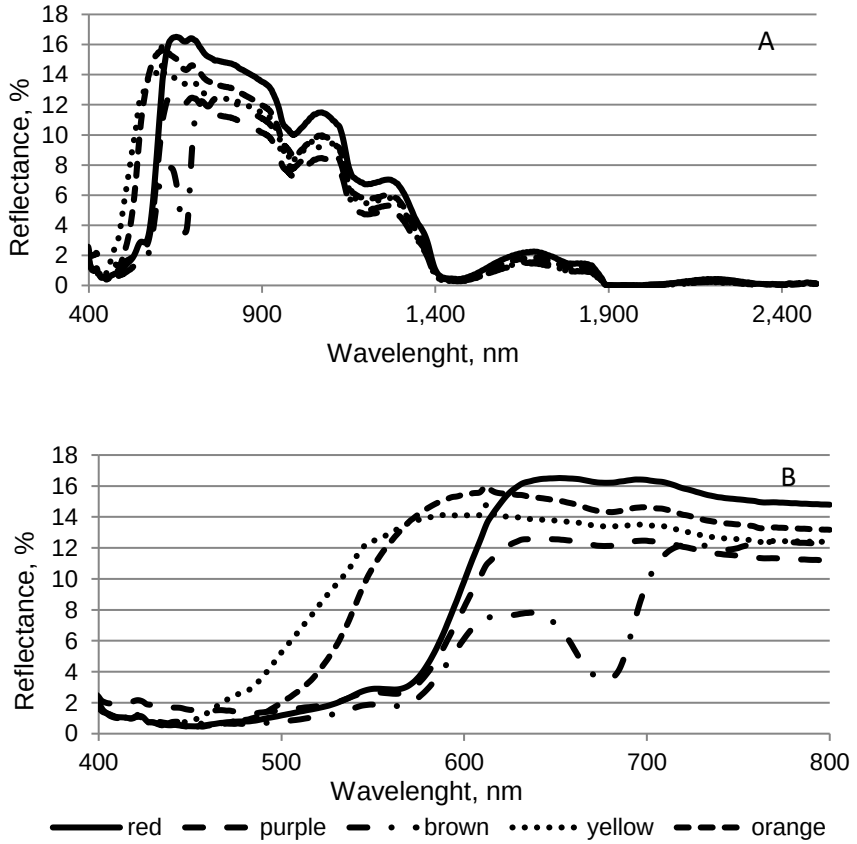

Figure 1. Reflectance spectrums of tomatoes (determined with RS3500); A – in the wavelength region 400–2.500 nm< B – in the wavelength region 400–800 nm.

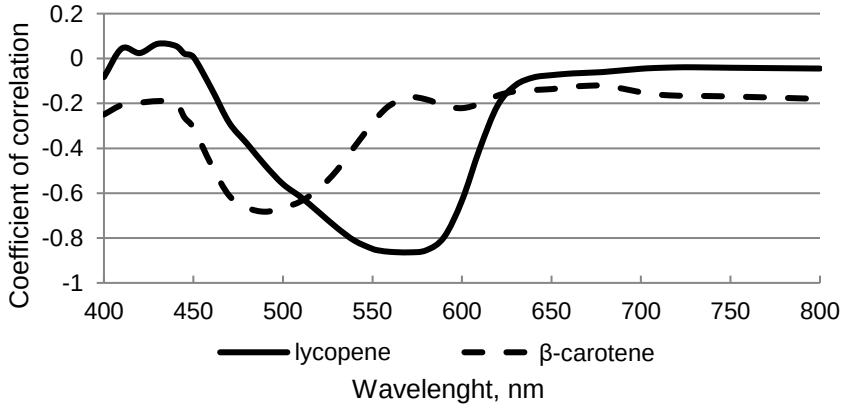

Figure 2. Coefficients of correlation between reflectance at different wavelength and lycopene and β-carotene determined by biochemical methods.

Obtained results showed that calculated lycopene index from reflectance spectrums (LYC) highly correlated with results of biochemical analyses (coefficient of determination $R^2 = 0.889$). There are no differences depending on tomatoes fruit colour. (Fig. 3).

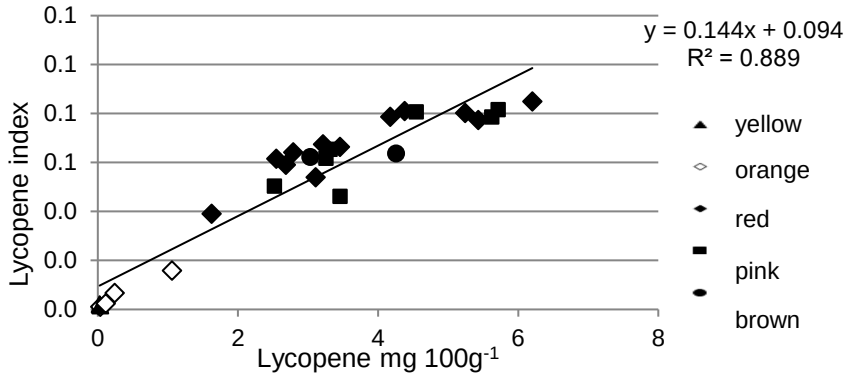

Figure 3. Correlation of lycopene index (LYC) and biochemically tested lycopene content in tomatoes fruits (mg 100 g^{-1} FM).

Correlation between calculated carotene index and biochemical analyses is lower. Coefficient of determination is $R^2 = 0.553$. Differences between tomatoes fruit colour are recognized. Pink tomatoes fruits have less value of indexes in comparison with red ones (Fig. 4).

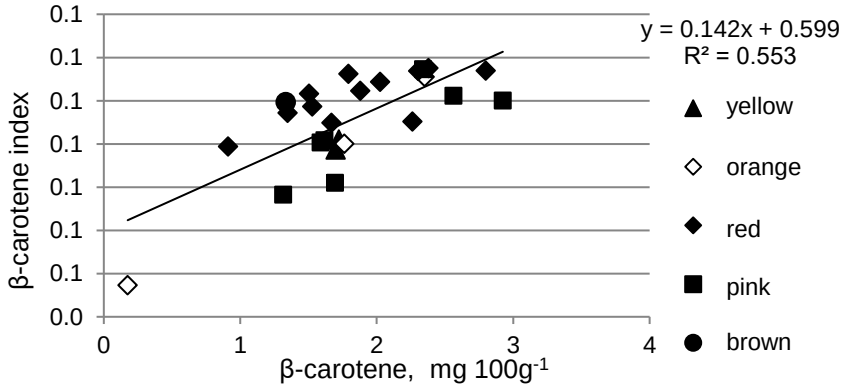

Figure 4. Correlation of β-carotene index (CAR) and biochemically tested l β-carotene content in tomatoes fruits (mg 100 g^{-1} FM).

Several different non-destructive spectroscopic methods have been used to detect lycopene content in tomatoes. Our results corresponds to the same prediction level ($R^2 = 0.889$). Pedro & Ferreira (2005) reported about $R^2 = 0.999$ for lycopene in tomatoes products, Ciaccheri et al. (2018) $0.73 < R^2 < 0.81$, depending on sensor and tomatoes cultivar, Choudhary et al. (2009) $R^2 = 0.88$ for tomatoes puree, Clement et al. (2008) $0.92 < R^2 < 0.98$ for fresh tomatoes, Davis et al. (2003) $R^2 = 0.97$ for fresh tomatoes and 0.88 for tomatoes products, Tilahun et al. (2018) – 0.85 for intact tomatoes fruits. Results depended on used sensors, obtained spectral data, tomatoes cultivars,

growing conditions, but generally the correlation level with biochemical analyses is rather high, that during plant cultivation, fruit storage and processing non- destructive methods are useful for lycopene quantification.

Less information and lower coefficients of determination was reported for β-carotene content. Pedro & Ferreira (2005) reported about $R^2 = 0.996$ for β-carotene in tomatoes products, Tilahun et al. (2018) – 0.77 for intact tomatoes fruits. Our results confirm that future investigations of non-destructive carotene determination is requred.

CONCLUSIONS

Elaborated lycopene index (LYC) can be used with an adequate precision for non-destructive assessment of lycopene in tomatoes fruits.

For assessment of β-carotene content with non-destructive methods future investigations are needed.

ACKNOWLEDGEMENTS. Study was supported by European Regional Development Fund project 'New control methods for energy and ecological efficiency increase of greenhouse plant lighting systems (uMOL)', Grant Agreement Nr. 1.1.1.1/16/A/261.

REFERENCES

Arab, L. & Steck, S. 2000. Lycopene and cardiovascular disease. *Am J Clin Nutr*. **71**(6), 1691S-1695S.

Choudhary, R., Bowser, T., Weckler, P., Maness, N.O. & McGlynn, W. 2009. Rapid estimation of lycopene concentration in watermelon and tomato puree by fiber optic visible reflectance spectroscopy. *Postharvest Biol. Technol.* **52**, 103–109.

Ciaccheri, L., Tuccio, L., Mencaglia, A.A., Mignani, A.G., Hallmann, E., Sikorska-Zimny, K., Kaniszewski, S., Verheul, M. & &Agati, G. 2018. Directional versus total reflectance spectroscopy for the in situ determination of lycopene in tomato fruits. *Journal of Food Composition and Analysis* **71**, 65–71.

Clement, A., Bacon, R., Sirois, S. & Dorais, M. 2015. Mature-ripe tomato spectral classification according to lycopene content and fruit type by visible, NIR reflectance and intrinsic fluorescence. *Quality Assurance and Safety of Crops & Foods* **7**(5), 747–756.

Clement, A., Dorais, M. & Vernon, M. 2008. Nondestructive measurement of fresh tomato lycopene content and other physicochemical characteristics using visible-NIR spectroscopy. *Journal Agricultural Food Chemical* **56**(21), 9813–9818.

Davis, A.R., Fish, W.W. & Perkins-Veazie, P. 2003. A rapid spectrophotometric method for analyzing lycopene content in tomato and tomato products. *Postharvest Biology and Technology* **28**, 425–430.

Dias, J.S. 2012. Nutritional Quality and Health Benefits of Vegetables: A Review. *Food and Nutrition Sciences* **3**, 1354–1374.

Gastélum-Barrios, A., Bórquez-López, R.A., Rico-García, E. & Soto-Zarazúa, G.M. 2011. Tomato quality evaluation with image processing: A review. *African J. Agric. Res.* **6**(14), 3333–3339.

Nagata, M. & Yamashita, I. 1992. Simple method for simultaneous determination of chlorophyll and carotenoids in tomato fruit. *Nippon Shokuhin Kogyo Gakkaish*, **39**, 925–928.

Pedro, A. M. & Ferreira, M. M. 2005. Nondestructive determination of solids and carotenoids in tomato products by near-infrared spectroscopy and multivariate calibration. *Analytical Chemistry* **77**, 2505–2511.

Tilahun, S., Park, D.S., Seo, M.H., Hwang, I.G., Kim, S.H., Choi, H.R. & Jeong, C.S. 2018. Prediction of lycopene and β-carotene in tomatoes by portable chroma-meter and VIS/NIR spectra. *Postharvest Biol. Technol.* **136**, 50–56.

Agronomy Research **17**(2), 349–357, 2019
https://doi.org/10.15159/AR.19.119

RGB vegetation indices applied to grass monitoring: a qualitative analysis

B.D.S. Barbosa[1], G.A.S. Ferraz[1], L.M. Gonçalves[1], D.B. Marin[1], D.T. Maciel[1], P.F.P. Ferraz[1] and G. Rossi[2]

[1]University Federal of Lavras, Department of Engineering, Federal University of Lavras, BR37200-000 Lavras-Minas Gerais, Brasil
[2]University of Florence Studies, Department of Agricultural, Food, Environment and Forestry (DAGRI), Via San Bonaventura, 13, IT50145 Firenze, Italia
*Correspondence: gabriel.ferraz@ufla.br

Abstract. In developing countries such as Brazil, research on low-cost remote sensing and computational techniques become essential for the development of precision agriculture (PA), and improving the quality of the agricultural products. Faced with the scenario of increasing production of emerald grass (Zoysia Japônica) in Brazil, and the value added the quality of this agricultural product. The objective of this work was to evaluate the performance of RGB (IV) vegetation indices in the identification of exposed soil and vegetation. The study was developed in an irrigated area of 58 ha cultivated with emerald grass at Bom Sucesso, Minas Gerais, Brazil. The images were obtained by a RGB digital camera coupled to an remotely piloted aircraft. The flight plan was setup to take overlapping images of 70% and the aircraft speed was 10 m s^{-1}. Six RGB Vegetation index (MGVRI, GLI, RGBVI, MPRI, VEG, ExG) were evaluated in a mosaic resulting from the images of the study area. All of the VIs evaluated were affected by the variability of lighting conditions in the area but MPRI and MGVRI were the ones that presented the best results in a qualitative evaluation regarding the discrimination of vegetation and soil.

Key words: ARP, emerald grass, index vegetation RGB.

INTRODUCTION

The increasing demand for grass and for higher-quality grass by the consumer market is responsible for the increased grass production area in Brazil, especially in locations near large consumer centres (Godoy et al., 2012). Given the increased demand, the monitoring of this crop is extremely important and is viable using precision agriculture (PA) techniques. In developing countries, the use of remote sensing techniques with low financial and computational costs has become essential for the development of small agricultural businesses (Ponti, 2013) and generates higher profitability for the agricultural enterprise.

For the success of PA, the use of remotely piloted aircraft (RPA) has increasing potential for agricultural monitoring by obtaining data with remote sensing techniques. The advantages of RPA include lower acquisition costs than other platforms for

obtaining aerial data, flight speeds that are suitable for collecting aerial data, high spatial resolution, and low risk of accidents involving human operators (Xiang & Tian, 2011; Vega et al., 2015).

In agricultural research, the use of conventional consumer cameras has increased due to the low acquisition cost, but the potential and costs of this branch of agricultural research requires further studies (Zhang et al., 2016).

Consumer cameras on aircraft have been used for several applications in agricultural monitoring, including forage yield prediction (Hunt et al., 2013), plant detection (Barrero & Perdomo, 2018), agricultural pest monitoring (Yang & Hoffman, 2015), and green vegetation distinction (Romeo et al., 2013; Kazmin et al., 2015). Cameras are already being used for crop monitoring and protection by several farmers with high levels of technology deployed on their properties (Zhang et al., 2016).

One way to better identify changes in agricultural fields is to use a vegetation index (VI) (Xiao & Moody, 2005). To determine the effect of UV radiation on the vegetation canopy, MRI is determined by the electromagnetic radiation (EMR) reflected by vegetation canopies that is detected by the passive optical sensor, but the reflected REM varies according to the chemical and structural structure of each species (Liu et al., 2016; Zhang & Kovacs, 2012). In the case of a conventional camera, REM is detected in the portion of the visible in the electromagnetic spectrum (Red-R, Blue-B and Green-G), more commonly to evaluate characteristics such as the nutritional state of the plant (Vergara-Diaz et al., 2016). VIs are also used in the management of agricultural practices, mainly in crops of high economic value and with high production costs (Hamuda et al., 2016), benefiting farmers with cost reduction in different agricultural operations.

Meyer & Neto (2018) emphasize the importance of research into developing a highly effective VI for distinguishing biomass, soil, and residues (e.g., straw, twigs, dried leaves), which can improve automated remote sensing applications, machine learning, plantation monitoring, and the application of precision farming techniques.

Several types of VIs are available in the literature; however, they are not efficient under non-uniform lighting conditions (Romeo et al., 2013).

Thus, the objective of this study was to analyse the behaviours of several VIs applied to images captured by a conventional RGB camera onboard a civil-use recreational RPA.

MATERIALS AND METHODS

Study site

The study was conducted in a grass (*Zoysia japonica*) cultivation area (Fig. 1), which covers a total of 58 ha. The area is irrigated by centre pivot irrigation equipment and is located in the municipality of Bom Sucesso, Minas Gerais (MG), Brazil (UTM 23K 509402.45 m E, 7662306.20 m s).

The planting of grass area is divided into 8 plots with different planting dates, which causes regions with different densities of vegetation as shown in Fig. 1, c.

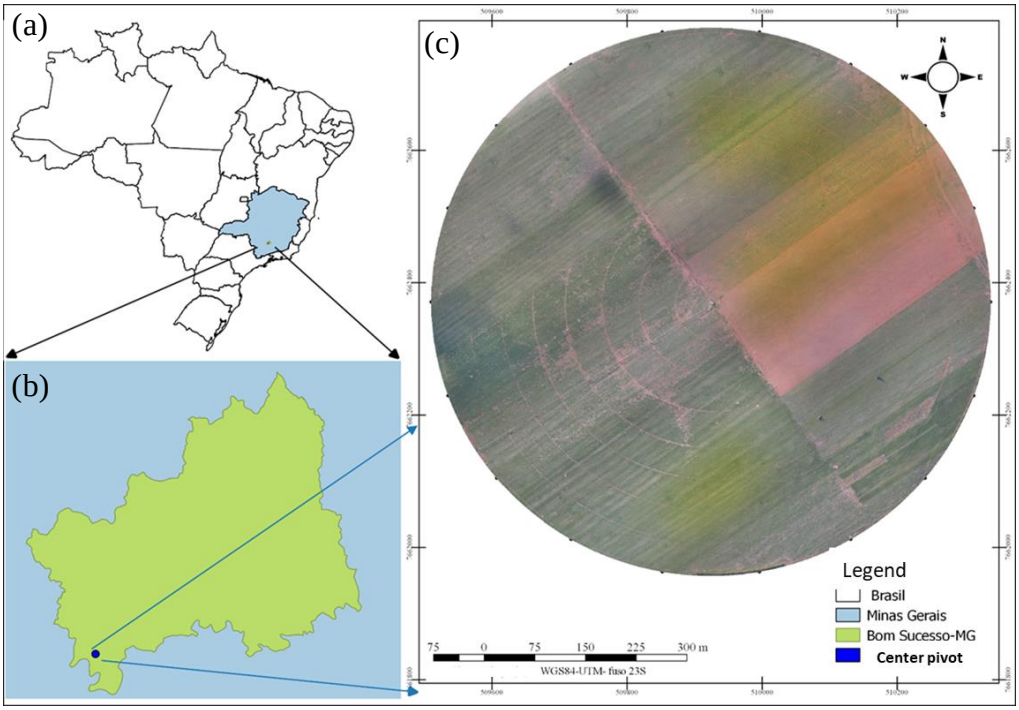

Figure 1. Study site location. (a) Brazil; (b) City; (c) Field of study.

Acquisition of aerial images

The images used in this study were obtained using an RPA (Phantom 3, DJI, Shenzhen, China) equipped with a Sony EXMOR 1/2.3 camera with 12.76 megapixels, a 94° FOV, an f/2.8 optical aperture, and sensors that capture electromagnetic radiation in the RGB spectral bands. The camera was coupled to a gimbal to stabilize it while in flight. The images were stored on an SD card.

Flight planning was done using the free application DroneDeploy, which is available for smartphones. The flight parameters are calculated based on the sensor information and the desired final spatial resolution. A spatial resolution of 6 cm was adopted for this study. To achieve this resolution, a flight height of 110 m and an average flight speed of 10 m s^{-1} were adopted as the flight parameters for the entire mission, and 70% longitudinal and lateral image overlaps were used. Rasmussen et al. (2014) recommend a frontal overlap of at least 75% and a lateral overlap of 60% for orthomosaic construction to obtain RGB images with conventional cameras. However, Kakaes et al. (2015) report that there is no globally accepted standard on the best overlap of frontal and lateral images and that the definition depends on the target to be imaged. The image overlaps and flight speed used in this study were first defined based on the operational capability of the equipment (flight time) at 10 m s^{-1}.

The flight schedule was set to between 12:00 and 2:00 p.m. to obtain good lighting conditions, as recommended by Bater et al. (2011), who reported that the images of RGB cameras are strongly influenced by hourly, daily, and seasonal lighting changes.

Image processing

The collected images were sent via the internet for image seaming (mosaicing) using the free trial version of the online DroneDeploy platform (www.dronedeploy.com). This platform returns a final product to the user in GeoTIFF format (mosaic) representing the fusion of the obtained images of the study site.

This mosaic was imported into the free geographic information system (GIS) software Quantum GIS version 14.2 (QGIS Development Team, Open Source Geospatial Foundation), in which the raster calculator tool was used to calculate the VIs (Table 1). The VIs are the results of algebraic operations between the spectral R, G and B bands that make up the mosaic.

Table 1. Vegetation Indices used in the study

IV	Name	Equation	Reference
MGVRI	Modified Green Red Vegetation Index	$\frac{(G)^2 - (R)^2}{(G)^2 + (R)^2}$	Bendig, et al. (2015)
GLI	Green Leaf Index	$\frac{2G - R - B}{2G + R + B}$	Louhaichi, Borman & Johnson (2001)
MPRI	Modified Photochemical Reflectance Index	$\frac{G - R}{G + R}$	Yang et al. (2008)
RGVBI	Red Green Blue Vegetation Index	$\frac{G - (B * R)}{(G)^2 + (B * R)}$	Bendig, et al.(2015)
ExG	Excess of green	$2G - R - B$	Woebbecke et al. (1995)
VEG	Vegetativen	$\frac{G}{(R)^{a^*} * B^{(1-a)}}$	Hague et al. (2006)

a* = constant with value of 0.667; B = blue, G = green, R = red.

RESULTS AND DISCUSSION

The RGB mosaic showed areas with cloud shading (shaded area) and with higher reflectance (Area with spots), demarcated by polygons in the images (Fig. 2, A). The values found for all VIs represent that the higher the number presented by the evaluated VI, the greater the presence of vegetation in a certain area (green coloration), and for the exposed soil, the observed values are smaller (red coloration).

Rasmussen et al. (2014) suggest that in order to avoid this undesirable effect on images obtained by RPAs, images should be acquired on completely cloudy days or when the angle of light incidence is the same as the orientation of the camera so that the lighting conditions are as as possible. Bannari et al. (2009) emphasizes that the IVs are subject to variations in their values due to several factors, mainly due to the presence of shadows, solar brightness and pixel mix, which does not reflect the real surface condition.

According to Rasmussen et al. (2014), mosaicing software can cause spots to be present due to changes in the light reflection angle; thus, several software packages should be tested to determine which is best for each VI to be applied. Faced with this problem, Ortega-Terol et al. (2017) developed software for flight planning, processing images acquired with RPAs, and detecting areas with changes in sunlight reflectance. Their analysis was successful, thus providing an additional tool for noise detection in orthomosaics.

Another factor that should be discussed and investigated is the thresholds of the flight planning parameters that must be adopted to obtain the images. In this study, based on flight safety concerns, frontal, and lateral overlaps of 70% were adopted initially due to the limitations of the available flight time, which may have affected the quality of the generated mosaic. According to Torres-Sánchez et al. (2018), the definition of better overlap rates between images requires further study because this definition affects both the flight time and the processing time of the images.

According to Feng et al. (2015), processing aerial images obtained by RPAs, including orthorectification and image seaming, is not a trivial task due to the large number of images obtained, which have different characteristics, such as variations in lighting conditions.

All VI evaluated were probably affected by the solar reflection angle (area with spots), which was not evaluated in this study, or by the presence of shadows (Shaded area). Among the VI studied, the modified photochemical reflectance index (MPRI) had a smaller effect of yellow spots on the image (Area with spots)

MPRI can be inferred as the most adequate index to evaluate vegetation variability and soil cover, since it provided the best visual distinction between these variables. However, in the upper left portion of Fig. 2, B, MPRI is affected by cloud shading (indicated by arrows). This interference by means of shadows can lead the producer to believe that the vegetation present in these areas is at a higher stage of development than in neighboring areas, ready for harvest. This type of information can lead to erroneous crop management decisions and can lead to economic losses.

Ortega-Terol et al. (2017) point out that in multispectral images in which the normalized difference vegetation index (NDVI) is applied, errors of approximately 20% in the prediction of the VI values may compromise decision-making on crop management, irrigation planning, and other agricultural practices. These authors emphasize that when areas affected by variations in sunlight reflectance are identified, they should be eliminated from agronomic analysis when VIs are applied for vegetation analysis.

GLI (Fig. 2, C) had an inverse behavior to that observed for MPRI. This VI was effective only in the identification of exposed soil (Red coloration), not being efficient in the vegetation enhancement. In regions with spots (indicated by arrows in Fig. 2, C) GLI presented high values (GLI > 0.11) indicating a higher vegetation cover in this region, which is not confirmed by the analysis presented in Fig. 2, a and by field analysis.

MGRVI (Fig. 2, D) also provided good results, being able to efficiently highlight vegetation and soil, with results close to results obtained visually by MPRI (Fig. 2, B). The factor of not being chosen in this study as the best performing LV is due to the fact that it is more affected by the shadows (indicated by the arrows in Fig. 2D) than MPRI. The MGRVI has potential for studies of agricultural productivity and, according to Bending et al. (2015), this VI is promising for the prediction of barley biomass. These authors encourage further studies on the behavior of this VI, especially in other cultures.

The red-green-blue vegetation index (RGBVI) (Fig. 2, E) had the same behavior of the excess of green (ExG) (Fig. 2, H) and GLI (Fig. 2, C), being qualitatively inferior to the results presented by the MPRI (Fig. 2B). The RGBVI shows a different behavior of the vegetation in areas with the presence of yellow spots indicated with arrows in Fig. 2, E, in comparison with the MPRI and Fig. 2, A, showing a higher density of vegetation.

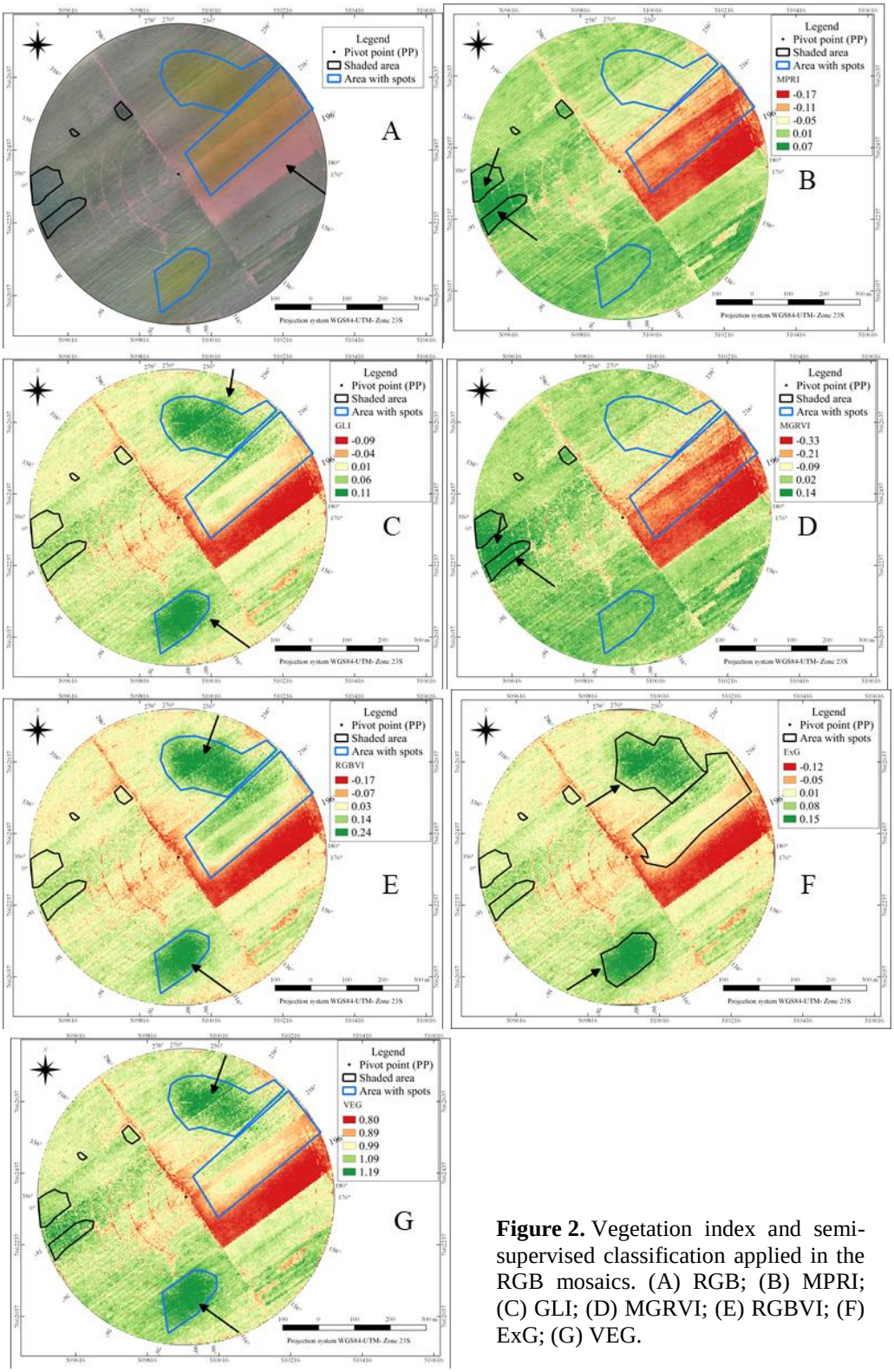

Figure 2. Vegetation index and semi-supervised classification applied in the RGB mosaics. (A) RGB; (B) MPRI; (C) GLI; (D) MGRVI; (E) RGBVI; (F) ExG; (G) VEG.

Bending et al. (2015) indicate that this VI is more efficient in the initial stages of development of the culture. Barret et al. (2015) found that RGBVI was highly correlated with NDVI, which is the VI most used in the research, and these authors emphasize that pasture monitoring can be performed with an aerial platform (eg an RPA) and an RGB camera. However, it is noteworthy that few studies have investigated the effects of light variations on RGB images obtained by APRs and their effects on the decision process.

In this study the IV ExG (Fig. 2, F) in comparison as Fig. 2, A and MPRI (Fig. 2, B) was not able to distinguish vegetation (represented by green coloration) of soil (represented by red color) effectively, indicating a vegetation less dense (which is represented by a color lighter, with values close to 0.01). In the areas indicated by arrows indicating in Fig. 2, F a dark green coloration is observed, this fact is due to the fact that ExG classified this region as being an area with vegetation in a greater stage of development, which is not proven in the field and by Fig. 1, A. Such behavior is due to the presence of noises (yellow spots in Fig. 2, A).

Torrez-Sánchez et al. (2015) evaluated the effectiveness of vegetation segmentation using ExG VI with automatic classification methods, and the results reached an accuracy of approximately 90%, indicating an additional possibility for the use of this IV. The divergence between the result obtained by the authors and that of this study may be associated with the lack of ideal lighting conditions at the time of images collection, however, it is necessary to study more about which parameters cause greater influence in this type of IV.

VEG VI (Fig. 2, G) was able to enhance vegetation and soil exposed vegetation; however, this VI was also affected by areas with spots (indicated by the arrows in Fig. 2, G), as well as the ExG and RGBVI. Therefore, this VI should also be used with caution in agricultural monitoring, where there are significant variations in lighting conditions.

CONCLUSIONS

All of the evaluated VIs were affected by the variability in the lighting conditions at the site. The MPRI and MGRVI provided the best results in a qualitative assessment of the discrimination between vegetation and soil, but their use in images containing regions affected by shading should be evaluated carefully.

ACKNOWLEDGMENTS. We thank Itograss Agrícola, the Brazilian Federal Agency for Support and Evaluation of Graduate Education (CAPES), the National Council for Scientific and Technological Development (CNPQ), the Federal University of Lavras (UFLA), and the UFLA Office of Graduate Studies (PPGEA-UFLA) for their support in the development and presentation of this study.

REFERENCES

Bannari, A., Morin, D., Bonn, F. & Huete, A.R. 2009. A review of vegetation indices. *Remote sensing reviews*, 13(1–2), 95–120.

Bareth, G., Bolten, A., Hollberg, J., Aasen, H., Burkart, A. & Schellberg, J. 2015. Feasibility study of using non-calibrated UAV-based RGB imagery for grassland monitoring: case study at the Rengen Long-term Grassland Experiment (RGE), Germany. *DGPF Tagungsband*, **24**, pp. 1–7.

Barrero, O. & Perdomo, S.A. 2018. RGB and multispectral UAV image fusion for Gramineae weed detection in rice fields. *Precision Agriculture* **19**(5), 809–822.

Bendig, J., Yu, K., Aasen, H., Bolten, A., Bennertz, S., Broscheit, J. & Bareth, G. 2015. Combining UAV-based plant height from crop surface models, visible, and near infrared vegetation indices for biomass monitoring in barley. *International Journal of Applied Earth Observation and Geoinformation* **39**, pp. 79–87.

de Godoy, L.J.G., Bôas, R.L.V. & Backes, C. 2012. Production of Saint Augustine grass carpets submitted to nitrogen doses. *Semina: Ciências Agrárias* **33**(5), 1703–1716.

Feng, Q., Liu, J. & Gong, J. 2015. UAV remote sensing for urban vegetation mapping using random forest and texture analysis. *Remote Sensing* **7**(1), 1074–1094.

Hamuda, E., Glavin, M. & Jones, E. 2016. A survey of image processing techniques for plant extraction and segmentation in the field. *Computers and Electronics in Agriculture* **125**, 184–199.

Hunt, E.R., Cavigelli, M., Daughtry, C.S., Mcmurtrey, J.E. & Walthall, C.L. 2005. Evaluation of digital photography from model aircraft for remote sensing of crop biomass and nitrogen status. *Precision Agriculture* **6**(4), 359–378.

Kakaes, K., Greenword, F., Lippincott, M., Dosemagen, S., Meier, P. & Wich, S.A. 2015. Drones and Aerial Observation: New Technologies for Property Rights. Human Rights, and Global Development: *A Primer (New America, 2015*), 514–519.

Kazmi, W., Garcia-Ruiz, F.J., Nielsen, J., Rasmussen, J. & Andersen, H.J. 2015. Detecting creeping thistle in sugar beet fields using vegetation indices. *Computers and Electronics in Agriculture* **112**, 10–19.

Liu, C., Sun, P.S. & Liu, S.R. 2016. A review of plant spectral reflectance response to water physiological changes. *Chinese Journal of Plant Ecology* **40**, 80–91.

Louhaichi, M., Borman, M.M. & Johnson, D.E. 2001. Spatially Located Platform and Aerial Photography for Documentation of Grazing Impacts on Wheat. *Geocarto International* **16**(1), 65–70.

Meyer, G.E. & Neto, J.C. 2008. Verification of color vegetation indices for automated crop imaging applications. *Computers and electronics in agriculture* **63**(2), 282–293.

Ortega-TeroL, D., Hernandez-Lopez, D., Ballesteros, R. & Gonzalez-Aguilera, D. 2017. Automatic Hotspot and Sun Glint Detection in UAV Multispectral Images. *Sensors* **17**(10). 2352.

Ponti, M.P. Segmentation of low-cost remote sensing images combining vegetation indices and mean shift. *IEEE Geoscience and Remote Sensing Letters* **10**(1), pp. 67–70.

Rasmussen, J., Ntakos, G., Nielsen, J., Svensgaard, J., Poulsen, R.N. & Christensen, S. 2016. Are vegetation indices derived from consumer-grade cameras mounted on UAVs sufficiently reliable for assessing experimental plots?. *European Journal of Agronomy* 74, 75–92.

Romeo, J., Pajares, G., Montalvo, M., Guerrero, J. M., Guijarro, M. & de la Cruz, J.M. 2013. A new Expert System for greenness identification in agricultural images. *Expert Systems with Applications* **40**(6), 2275–2286.

Torres-Sánchez, J., López-Granados, F. & Peña, J.M. 2015. An automatic object-based method for optimal thresholding in UAV images: Application for vegetation detection in herbaceous crops. *Computers and Electronics in Agriculture* **114**. 43–52.

Vega, F.A., Ramírez, F.C., Saiz, M.P. & Rosúa, F.O. 2015. Multi-temporal imaging using an unmanned aerial vehicle for monitoring a sunflower crop. Biosystems Engineering 132, 19–27.

Vergara-Díaz, O., Zaman-Allah, M.A., Masuka, B., Hornero, A., Zarco-Tejada, P., Prasanna, B.M., ... & Araus, J.L. 2016. A novel remote sensing approach for prediction of maize yield under different conditions of nitrogen fertilization. *Frontiers in plant science 7*, 666.

Woebbecke, D.M., Meyer, G.E., Von Bargen, K. & Mortensen, D.A. 1995. Color indices for weed identification under various soil, residue, and lighting conditions. *Transactions of the ASAE* **38**(1), 259–269.

Xiang, H. & Tian, L. 2011. Development of a low-cost agricultural remote sensing system based on an autonomous unmanned aerial vehicle (UAV). *Biosystems engineering* **108**(2), 174–190.
Xiao, J.,& Moody, A. 2005. A comparison of methods for estimating fractional green vegetation cover within a desert-to-upland transition zone in central New Mexico, USA. *Remote sensing of environment* **98**(2-3), 237–250.
Yang, Z., Willis, P. & Mueller, R. 2008. Impact of band-ratio enhanced AWIFS image to crop classification accuracy. *Pecora* **17**, 18–20.
Zhang, J., Yang, C., Song, H., Hoffmann, W.C., Zhang, D. & Zhang, G. 2016. Evaluation of an airborne remote sensing platform consisting of two consumer-grade cameras for crop identification. *Remote Sensing* **8**(3), 257.
Zhang, C. & Kovacs, J.M. 2012. The application of small unmanned aerial systems for precision agriculture: a review. *Precision agriculture* **13**(6), 693–712.

Agronomy Research **17**(2), 358–370, 2019
https://doi.org/10.15159/AR.19.132

An experimental investigation of performance levels in a new root crown cleaner

V. Bulgakov[1], S. Pascuzzi[2], M. Arak[3], F. Santoro[2], A.S. Anifantis[2], Y. Ihnatiev[4] and J. Olt[3,*]

[1]National University of Life and Environmental Sciences of Ukraine, 15 Heroyiv Oborony street, UA03041 Kyiv, Ukraine
[2]Department of Agricultural and Environmental Science University of Bari Aldo Moro, Via Amendola, 165/A, IT70125 Bari, Italy
[3]Estonian University of Life Sciences, Institute of Technology, Kreutzwaldi 56, EE51006 Tartu, Estonia
[4]Tavria State Agrotechnological University, 18 B, Khmelnytsky Ave, UA72310 Melitopol, Ukraine
[*]Correspondence: jyri.olt@emu.ee

Abstract. For the purposes of carrying out field experiments using the vertical-type cleaner with its elastic cleaning blades to remove haulm residues from the crowns of standing roots, the programme for this process and the technique behind it have both been developed by basing the process on the measurement of the volume of haulm residues that are left on the root crowns after they have been cleaned by a cleaning tool that operates at pre-set values in terms of its translational velocity, its height above the soil surface, and its rate of revolution. In addition, the cleaner's energy-and-force performance has also been determined. In this process, the new laboratory and the field experimental unit have been put together. The unit comprises a rear-mounted root crown cleaner of the rotary type with a vertical axis of rotation. During the field experiments, the general-purpose tractor which carries it moves at a pre-set velocity as registered by the track measuring wheel; the general height of the cleaning tool's position is set within the specified range by the use of two pneumatic feeler wheels that are equipped with adjustment mechanisms. The results of the completed investigations have been statistically processed with the use of the regression analysis and correlation analysis methods. On the basis of the developed multiple-factor experiment technique, empirical mathematical models have been generated in the form of regression equations for the process of cleaning the crown's of sugar beet roots. In accordance with the results of the calculations, it has been established that the translational velocity of the implement has the greatest level of impact on the volume of haulm residue that remains on the spherical surfaces of root crowns after cleaning. The rate of rotation for the vertical cleaning rotor and its height above the soil surface which are controlled by the two pneumatic feeler wheels have a lesser effect on the process under consideration.

Keywords: cleaner, elastic blade, harvesting, haulm, sugar beet root, experimental unit.

INTRODUCTION

The topping of standing roots and the removal of haulm residues from their crowns is a key problem in the work process where this involves sugar beet harvesting

(Vasilenko, 1996; Gruber, 2005; Wang & Zhang, 2013; Gu et al., 2014). It has been established by previous research that within the context of state-of-the-art sugar beet topping technologies which require shearing off the upper parts of the root crowns, perhaps around 14–17% of the sugar-bearing mass is lost. In view of the above, the problem of removing haulm and cleaning the root crowns of sugar beets of haulm residues without losing any sugar-bearing mass is an economically justified research and development problem which should be of current concern. In order to be able to resolve said problem, it is necessary to develop a design of crown cleaning unit which not only provides for the cleaning of standing root crowns of haulm residues, but one which also features the design and technology embodiment that ensures that the quality and cost-performance indices of the operation are both increased. It is also necessary to develop a technique that can be used in experimental investigations into the cleaning unit that is under consideration, to carry out the comprehensive field testing of that unit, and then process the results of said field studies with the use of a PC in order to verify its technological and process properties. Providing a solution to the aforementioned tasks gives this paper its relevancy.

The scientific and practical problems that have been set out when it comes to cleaning the crowns of standing roots of haulm residues and other plant impurities that may be present in the inter-row spaces for sugar beet plantations after shearing off the bulk of the haulm from the roots are areas that can be solved through the development and implementation of modular-design tractor-implementation units - the modular concept provides some important advantages in the application of units under production conditions (Bulgakov, 2011).

A definitive contribution to the theory behind and practice of the process of post-cleaning standing root crowns of haulm residues was made at various times by the following scientists and design engineers (Pogorely et al., 1983; Pogorely et al., 2004; Bentini et al., 2005; Wu et al., 2013; Zhang et al., 2013, Bulgakov et al., 2016; Bulgakov et al., 2017, etc).

At the same time, the fundamental theoretical and field experiments which were carried out by the aforementioned authors as well as the specific relations between the parameters of the work process that are under consideration and the practical results of their application that have been obtained as a result are not sufficient for the substantiation of the design and process parameters and the operating modes of the newly-designed cleaning unit.

The aim of the study was to improve the quality of the work process when it comes to cleaning root crowns of haulm residues with the use of the new cleaning unit through the development of the improved technique of obtaining results from the experimental investigations that have been carried out for the estimation of the rational parameters of the process.

MATERIALS AND METHODS

The subject of the experimental investigations is the roots, haulm, and the work process that is required to remove haulm residues with the use of the newly-designed cleaning unit with a vertical drive shaft. The schematic model of the cleaning unit that is under consideration is presented in Fig. 1.

The relation between the design and kinematic parameters and the operating modes of the cleaning unit and its performance quality levels is the subject matter of these experimental investigations.

Therefore, in the quest for the further improvement of tools for root crown post-cleaning and the estimation of the performance quality levels of the tools in real operational conditions (depending upon the plant development status, the uniformity of root positioning in the rows, the kinematic modes of operation, and the parameters for being able to adjust the tools for the work process), standard experimental investigation practices have been used, and case-specific field testing procedures have also been developed.

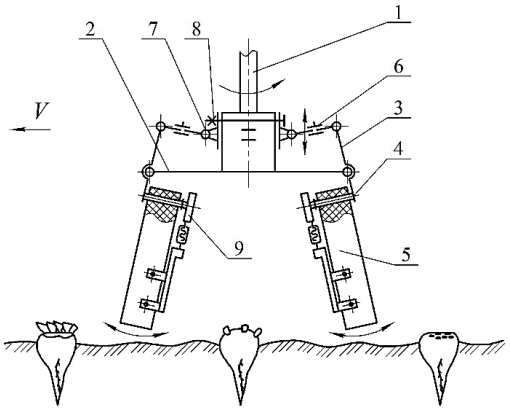

Figure 1. Design and process schematic model for a unit for cleaning root crowns of haulm residues (Bulgakov et al., 2018): 1 – vertical shaft; 2 – disk; 3 – double-arm lever; 4 – axles; 5 – blade; 6 – articulated arm; 7 – slide; 8 – lock; 9 – blade rigidity control unit.

As a result of processing the *a priori* information and carrying out theoretical investigations and expert analysis, it has been established that the principal input parameters (variable factors) in the experimental investigations are the rotation rate for the vertical drive shaft with its cantilevered elastic cleaning blades, the travel rate of the cleaning unit, and the position of the cleaning tool above the soil's surface level. The other parameters that describe the operation of the cleaning unit that is under consideration as well as the characteristics of the conditions under which the investigations are carried out are fixed but controlled factors.

In order to determine the indicators of the agronomical appraisal of the beet root plantation, in the field that features a relatively smooth relief and a stable yield, test plots have been marked off, each plot consisting of several rows with a length of at least 25 m planted with sugar beet, and in those plots field experiments have been carried out using fivefold replication.

The biological yield has been recorded with the use of blanket gathering and the weighing of the roots of sugar beets from the test plot with a total area of 27 m^2, measuring 1.3 m widthwise (incorporating three rows) and 30 m lengthwise (taking into account the fivefold replication of each experiment).

The operational quality of the unit - in terms of cleaning root crowns of haulm residue has - been evaluated with the use of the procedure that is described here. Firstly, the haulm of each test plot is gathered using a commercial haulm-gatherer, which carries out the process of the blanket shearing-off of the haulm without feelers and supports across the entire operating span and without post-cleaning the root crowns of any haulm residues. Next, the indicators are determined and recorded for quality in terms of blanket shearing-off and the removal of the bulk of the haulm herbage. In order to obtain a more in-depth assessment of the quality of the operation of the new cleaning unit, the haulm gatherer's haulm cutting tool is set up for a height of cutting which ensures that the

wasted mass of the roots does not exceed 5.0%. At the same time, the amount and degree of the damage are both measured where it is inflicted on the sugar beet root crowns. This measurement process is carried out in accordance with the following formula:

– slightly damaged roots of sugar beets are classed as being those roots in which the cracks and chips on the crowns have a depth of less than 10 mm;

– severely damaged roots are classed as those roots in which chips and cracks (nicks) on the crowns are deeper than 10 mm.

During the experimental investigation of the newly-designed cleaning unit, the vertical position of the cleaning shaft with its elastic blades is changed so that the cleaning blades are situated at the level of the reference surface - 0 cm (in practice this means touching the beet root crowns), and above the reference surface that is formed by the root crowns, that is at heights of 2 cm and 4 cm above the soil's surface level. It ought to be noted that the lower setting for the cleaning blades relative to the soil surface results in a lower quality of root crown cleaning of haulm residues, knocking out roots from the soil and increasing energy consumption during the work process that is under consideration.

The samples are taken after root crown cleaning has been completed, with fivefold replication at every setting of the cleaning blade elevation process and at operating travel speeds of V_p = 1.0; 1.5, and 2.0 m s^{-1} for the cleaning unit. The above conditions during the experimental investigation are applied along with switching between three values for the angular velocity ω of the cleaning tool's rotation - this being the vertical drive shaft: ω = 46.9, 56.5, and 76.8 rad s^{-1} (448 rpm, 540 rpm, and 734 rpm respectively).

Prior to carrying out a run by the cleaning unit, two similar contiguous rows of planted sugar beet are selected. A one metre-long frame is laid over one of them in such a manner that it encloses the row of sugar beet roots on both sides (Fig. 2).

Figure 2. Assessing the degree of sugar beet root crown cleaning.

After that, all of the haulm residues on the root crowns are cut off manually and are weighed on electronic scales with an accuracy of ± 0.1 g. The next step is to evaluate the quality of the cleaning unit's operations. To that end, upon the completion of the measurements, on the adjacent, similar row of planted beet roots, the root crowns are cleaned by the cleaning unit. Then, the frame is laid over that cleaner-processed plantation row (opposite the previous place in which measurements were taken), and a comparative analysis of the degree of root crown cleaning of haulm residues is carried out by means of collecting and weighing the haulm residues. For that purpose, all haulm residues which remain on those root crowns that have already been cleaned (root crowns already cleaned by the cleaning unit) are manually cut off and are accurately weighed. When comparing the weighing data that was obtained previously and then again after the run by the cleaning unit, final results are arrived at which indicate the efficiency of root crown cleaning of haulm residues.

The degree of root crown cleaning of haulm residues is calculated with the use of the following Eq.:

$$\delta = \frac{M - M_o}{M} \cdot 100\% \qquad (1)$$

where δ – is the degree of root crown cleaning, %; M – mass of haulm residues before the run by the cleaning unit; M_o – mass of haulm residues after the run by the cleaning unit.

From this it can be found that haulm residues per running metre (g m^{-1}) that remain on the beet root crowns after the cleaning shaft with its elastic cleaning blades has passed over them is the indicator that specifies the quality of the operation of the root crown cleaning unit. This parameter has been chosen as the function of optimisation - the dependent variable in this multi-factored experiment.

It is already well-known that the velocity of the translation of the cleaning unit and the rate of rotation of its tool are in a two-way interrelation, which is considered as being the kinematic mode of operation, and this is specified by the ratio of the cleaning blade's circumferential velocity to the velocity of the translation of the cleaning unit itself over the field.

In further statistical computation, the following factors are considered as being independent ones, which can be purposefully and quantitatively changed when carrying out field experiments:

1) the velocity of the translational motion of the experimental unit over the field;

2) the angular velocity of the rotational motion of the cleaning tool of the newly-designed cleaning unit;

3) the elevation of the line that is circumscribed by the lower end of the cleaning blade with reference to the soil's surface level.

The field experiments have been carried out in view of the problems that have been outlined above, and in accordance with the technique described above. For this end, the field experiment unit (Fig. 3) has been manufactured by modelling in full the operation of the newly-designed unit which cleans root crowns of haulm residues.

Figure 3. Experimental unit with attached implement for cleaning root crowns of haulm residues with a vertical cleaning drive shaft during field investigations.

During the experimental investigations, the following indicators have been determined for the operational quality of the new root crown cleaning tool with its vertical drive shaft: the level of cleaning of haulm residues from root crowns and the sweeping of plant residues outside the operating zone within any planted row of sugar beet.

The experiments have been carried out in accordance with a programme which involves comprehensive fact-based experimentation. It ought to be noted that all items in this programme, which involves the investigation of the levels of quality inherent in

the performance of the vertical cleaning tool, have been accomplished using fivefold replication, which totals:

$$N = 5P^k = 5 \cdot 3^3 = 5 \cdot 27 = 135 \text{ experiments} \quad (2)$$

In accordance with the preliminary theoretical studies (Bulgakov et al., 2018), three values are assumed for the cleaning unit's translation velocity; that is, the unit travels using the first, third, and reduced fifth gears of the carrying tractor, which is equivalent to the following values for the cleaning unit's speed of travel: 0.6, 0.9, and 1.9 m s^{-1} respectively. The precise value for the translational motion velocity is monitored with the use of a track-measuring wheel that is mounted on the tractor.

The positioning of the cleaning tool with respect to the soil's surface level is determined by three positions. Due to the design of the multi-purpose experimental unit, the height at which the tool is carried can be adjusted within quite a wide range. The three following values are assumed for the elevation at which the tool's blades are mounted with respect to the soil's surface level: 0 m, 0.02 m, and 0.04 m, which is stipulated by the biological properties of sugar beet roots.

The angular velocity of rotation of the cleaning tool - its vertical drive shaft - is set at three levels: 46.9, 56.5, and 76.8 rad s^{-1}. Adjustments are made by changing the transmission ratio of the drive sprockets that are used in the vertical shaft's drive mechanism and by means of their respective replacement. The precise value for the angular velocity of rotation for the vertical shaft in relation to the number of teeth on the drive sprocket is calibrated in laboratory conditions with the use of a tachometer.

RESULTS AND DISCUSSION

After completing all of the experiments using fivefold replication in accordance with the comprehensive fact-based experimental programme, a total of 135 samples of haulm residues have been obtained. Each haulm residue sample that was obtained after running the cleaning unit with various parameters has been weighed using electronic laboratory scales.

The weighing results that were obtained have been sorted and inputted into the PC database, with statistical processing then being carried out. The results of the PC-assisted processing of the considerable amount of collected data are shown in Table 1.

Furthermore, the mathematical model for the subject of the research as a response function has been generated. In this function, the optimisation parameter is y – the haulm residues on the root crowns. The parameter represents the results of the experiment as a function of the following variable factors that assume different values during the experiments: x_1 – the velocity of the linear translational motion of the cleaning unit over the field; x_2 – the angular velocity of rotation of the cleaning tool; x_3 – the elevation of the cleaning blades with reference to the soil's surface level:

$$y = f(x_1, x_2, x_3). \quad (3)$$

When the correlations are studied, two principal issues can be seen to arise: it is necessary to determine the density - the relation between the factors in their effect on the optimisation parameter - and the shape of such a relation. In order to determine the density and the shape of relation, the use was made of regression and correlation statistical methods.

Correlation and regression analysis of the experimental data was carried out with the use of Analysis ToolPak in Microsoft Excel.

Table 1. Operational quality indicators for the root crown cleaning unit with its vertical drive shaft and elastic cleaning blades

Angular velocity of rotation (rad s^{-1})	Combined unit travel speed in field								
	0.8 m s^{-1}			1.3 m s^{-1}			1.9 m s^{-1}		
	Elevation of cleaning blade (cm)								
	0	2	4	0	2	4	0	2	4
	Haulm residue, g m^{-2}			Haulm residue, g m^{-2}			Haulm residue, g m^{-2}		
734	4	1	5	12	14	0	43	83	79
	2	6	5	11	20	3	28	51	25
	9	23	12	5	14	17	37	44	23
	4	8	7	17	28	6	13	39	27
	0	19	6	9	10	11	9	38	21
540	8	4	24	10	32	60	9	2	116
	12	30	13	30	16	119	16	9	88
	16	9	21	4	28	72	5	19	61
	4	6	15	4	15	168	9	12	35
	5	4	53	21	13	128	19	19	169
448	80	64	234	41	9	52	2	18	14
	65	72	189	28	28	82	4	11	1
	57	94	142	29	29	79	2	11	28
	37	69	98	30	18	73	4	12	24
	83	52	126	38	34	111	7	18	8

The empirical dependencies have been computed with the use of the multivariate regression analysis in the form of a second degree polynomial with the possibility of being able to eliminate minor variables when carrying out the calculations. The computational work was done on a PC by means of dedicated software that was developed with the use of the experimental data computation technique.

The calculations that were carried out have resulted in a mathematical model being obtained of the volume of haulm residues on sugar beet root crowns, y, varying as a function of x_1, x_2, and x_3 which, after estimating the significance of the regression coefficients in accordance with Fisher's ratio test, assumes the following form:

$$y = 335.891 - 192.079x_1 - 5.075x_3 + 3.034x_1x_3 + 2.522x_2x_2. \quad (4)$$

Therefore the principal factors that have an effect on the process of post-cleaning root crowns of haulm residues are the velocity of the translational motion of the cleaner and the angular velocity of the rotation of its cleaning tool.

In order to determine the effect that the main design and kinematic parameters of the cleaner (its variable factors) may have on the optimisation parameter - in order to establish the relation between the volume of haulm residue on the root crowns and the angular velocity of the rotation of the cleaning drive shaft, the velocity of the cleaning unit's translational motion, and the elevation of the cleaning blades above the soil's surface level - the computer programme, STATISTICA-5.0 for Windows 95, has been used which has provided plotting for the graphical representation of the intermediate regression models in the form of quadratic response surfaces for the amount of sugar beet haulm residues as a function y_i of two variable factors x_i, with the third factor being

an invariable constant. The aforementioned response surfaces are presented in Figs 4, 5, 6, 7, 8, 9, 10, 11, and 12.

As a result of processing the experimental data, the intermediate regression equations which describe the effect that is produced by the velocity of the translational motion of the cleaning unit and the elevation of the cleaning blades above the soil's surface level at fixed values of the angular velocity of rotation for the cleaning tool have been generated, with these being, respectively, as follows:

at ω_1 = 76.8 rad s^{-1}

$$y_{1.1} = 30.817 - 58.533x_1 + 10.34x_2 + 30.687x_1x_1 + 1.445x_1x_2 - 2.883x_2x_2, \quad (5)$$

at ω_2 = 56.5 rad s^{-1}

$$y_{1.2} = -98.753 + 191.745x_1 - 32.195x_2 + 73.445x_1x_1 + 14.321x_1x_2 + 7.317x_2x_2. \quad (6)$$

at ω_3 = 46.9 rad s^{-1}

$$y_{1.3} = 157.991 - 156.173x_1 - 14.296x_2 + 42.444x_1x_1 - 18.547x_1x_2 + 5.75x_2x_2. \quad (7)$$

Through an analysis of the response surfaces of the dependencies between the volume of haulm residue on the root crowns and the velocity of the translational motion of the cleaning unit and the elevation of the cleaning blades above the soil's surface level as shown in Figs 4, 5, and 6, it has been established that the rational design and kinematic parameters of the work process which is involved in post-cleaning standing root crowns of haulm residues are found within the following ranges: the velocity of the translational motion of the cleaning unit - between 0.9–2.5 m s^{-1}, the and elevation of the cleaning blades above the soil's surface level - between 1.0–2.7 cm.

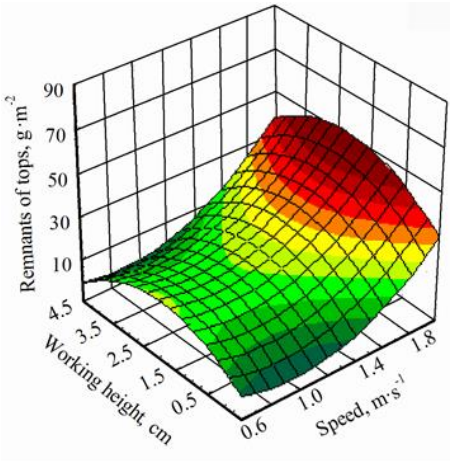

Figure 4. The response surface of haulm residues on root crowns against the speed of the cleaner and the elevation of the blades at the angular velocity of the cleaning tool's rotation of 76.8 rad s^{-1}.

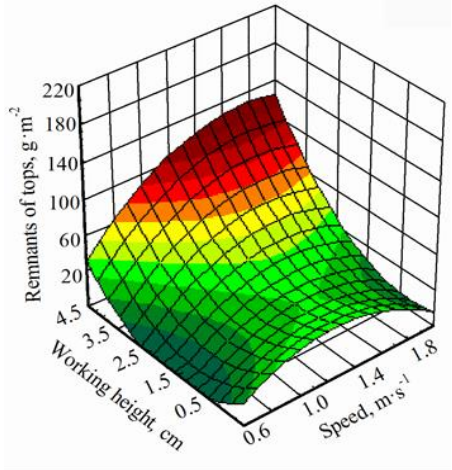

Figure 5. The response surface of haulm residues on root crowns against the speed of the cleaner and the elevation of the blades at the angular velocity of the cleaning tool's rotation of 56.5 rad s^{-1}.

When the angular velocity of the rotation of the vertical shaft rises from 46.9 to 76.8 rad s^{-1} at the velocity of the translational motion of the cleaning unit equal to 1.5 m s^{-1}, the volume of haulm residues on the root crowns decreases from 32.36 to

6.41 g m^{-2} with the elevation of the cleaning blades above the soil's surface level varying within 0–4 cm. Accordingly, at the velocity of the translational motion of the cleaning unit equal to 2.0 m s^{-1} this figure increases from 12.6 to 16.5 g m^{-2}. Therefore changing the elevation of the cleaning blades above the soil's surface level produces only an insignificant effect on the optimisation parameter.

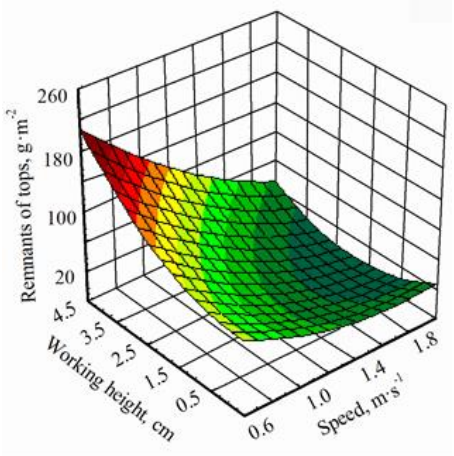

Figure 6. The response surface of the haulm residues on root crowns against the speed of the cleaner and the elevation of the blades at the angular velocity of the cleaning tool's rotation of 46.9 rad s^{-1}.

After processing the experimental data, the intermediate regression equations have been obtained that specify the influence of the velocity of the translational motion of the cleaning unit and the angular velocity of the rotation of its cleaning tool at the following fixed values for the elevation of the cleaning blades above the soil's surface level, with these being, respectively:

at h_1 = 0 cm

$$y_{2.1} = 559.575 - 156.264x_1 - 13.743x_2 + 3.475x_1x_1 + 2.265x_1x_2 + 0.081x_2x_2, \quad (8)$$

at h_2 = 2 cm

$$y_{2.2} = 657.136 - 239.272x_1 - 15.609x_2 + 24.424x_1x_1 + 2.72x_1x_2 + 0.094x_2x_2, \quad (9)$$

at h_3 = 4 cm

$$y_{2.3} = 236.016 - 180.451x_1 + 0.974x_2 - 30.222x_1x_1 + 4.13x_1x_2 - 0.071x_2x_2, \quad (10)$$

After analysing the response surfaces for the dependencies between the volume of haulm residues on the root crowns and the velocity of the translational motion of the cleaning unit and the angular velocity of rotation of its cleaning tool as shown in Figs 7, 8, and 9, it has been established that the rational design and kinematic parameters of the work process involved in the post-cleaning process are found within the following ranges: the velocity of the translational motion of the unit, which falls between 0.9–2.5 m s^{-1}, and the angular velocity of rotation of the cleaning tool, which falls between 63.0–81.0 rad s^{-1}.

When the elevation of the cleaning blades with reference to the soil's surface level rises from 0 cm to 4.0 cm at the velocity of translational motion of the cleaning unit which is equal to 1.5 m s^{-1}, the volume of haulm residues on the root crowns increases from 25.7 to 90.5 g m^{-2} at the angular velocity of the cleaning blade's rotation of 46.9 rad s^{-1}. This provides an angular velocity of rotation that is equal to ω = 56.5 rad s^{-1} - between 18.04 and 62.9 g m^{-2}, and at ω = 76.8 rad s^{-1} - between 2.7 and 7.6 g m^{-2}.

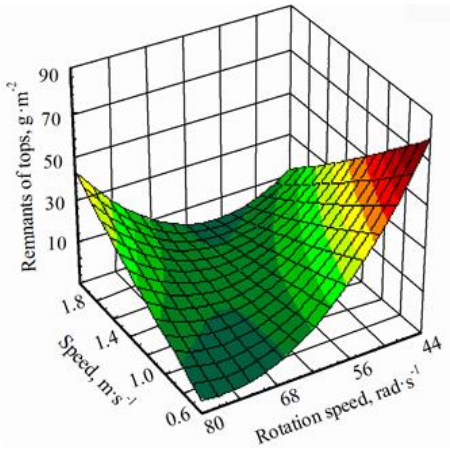

Figure 7. The response surface of haulm residues against the translational motion speed and angular velocity of the rotation of the cleaning tool at the elevation of the blades at 0 cm.

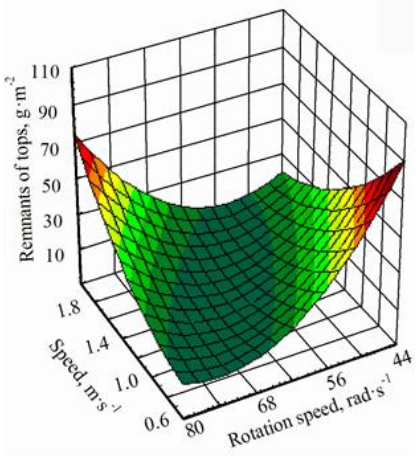

Figure 8. The response surface of haulm residues against the translational motion speed and angular velocity of the rotation of the cleaning tool at the elevation of the blades at 2 cm.

When the velocity of the translational motion of the cleaning unit rises to 2.0 m s^{-1}, the total volume of haulm residues on the root crowns increases from 18.4 to 62.9 g m^{-2}. Therefore an increase in the elevation of the cleaning blades above the soil's surface level from 0cm to 4.0 cm results in around a threefold growth in the volume of haulm residues on the root crowns, while the rise in the velocity of the translational motion of the cleaning unit reaches 2.0 m s^{-1} - a growth of about 3.4 times.

After processing the experimental data, the intermediate regression equations that specify the influence of the elevation of the cleaning blades above the soil's surface level and the angular velocity of the rotation of the cleaning tool at the following fixed values for the velocity of the translational motion of the cleaning unit have been obtained, with these being, respectively, as follows:

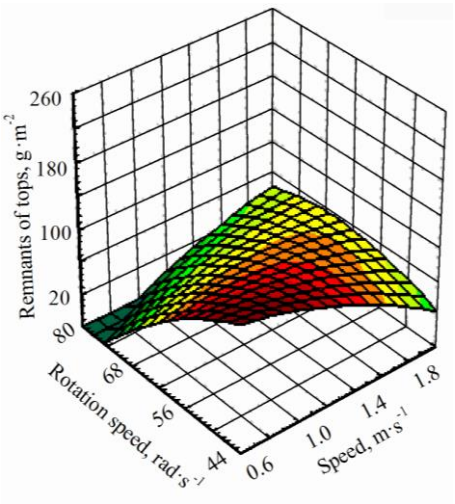

Figure 9. The response surface of haulm residues against the translational motion speed and angular velocity of the rotation of the cleaning tool at the elevation of the blades at 4 cm.

at V_1 = 0.8 m s^{-1}

$$y_{3.1} = 1135.99 + 35.358x_1 - 35.721x_2 + 3.45x_1x_1 - 0.662x_1x_2 + 0.275x_2x_2, \quad (11)$$

at V_2 = 1.3 m s^{-1}

$$y_{3.2} = -229.977 + 22.151x_1 + 8.454x_2 + 5.45x_1x_1 - 0.54x_1x_2 - 0.069x_2x_2, \quad (12)$$

at V_3 = 1.9 m s^{-1}

$$y_{3.3} = -430.304 + 1.745x_1 + 13.756x_2 + 1.283x_1x_1 - 0.156x_1x_2 - 0.102x_2x_2, \quad (13)$$

After analysing the response surfaces of the dependencies between the volume of haulm residues on the root crowns, the elevation of the cleaning blades above the soil's surface level, and the angular velocity of rotation of the cleaning tool as shown in Figs 10, 11, and 12, it has been established that the rational design and kinematic parameters of the work processes that are involved in post-cleaning are to be found within the following ranges: the elevation of the cleaning blades above the soil's surface level, between 0–1.21 cm, and the angular velocity of rotation of the cleaning tool, which is between 57.9–66.0 rad s^{-1}.

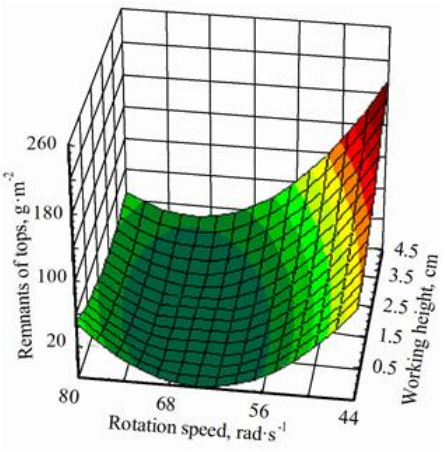

Figure 10. The response surface of haulm residues against the elevation of the blades and the angular velocity of the rotation of the cleaning tool at the velocity of the translation of 0.8 m s^{-1}.

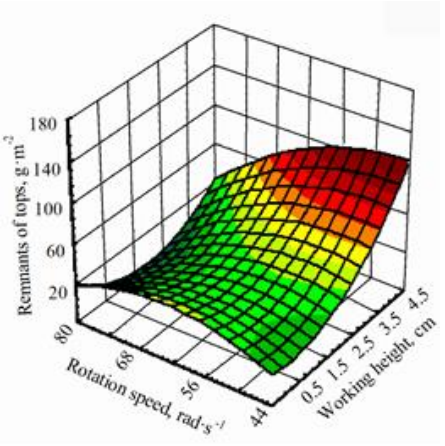

Figure 11. The response surface of haulm residues against the elevation of the blades and the angular velocity of the rotation of the cleaning tool at the velocity of the translation of 1.3 m s^{-1}.

When the velocity of the translational motion of the cleaning unit increases from 0.8 to 1.9 m s^{-1} at the elevation of the cleaning blades above the soil's surface level where this is equal to 2.0 cm, then the total volume of haulm residues falls from 58.1 to 3.1 g m^{-2} at an angular velocity of rotation for the cleaning tool of 46.9 rad s^{-1}. Further, when the angular velocity of rotation of the cleaning tool is increased to 56.5 and to 76.8 rad s^{-1}, the volume of haulm residues on the root crowns grows from 19.1 to 22.6 g m^{-2} and from 19.1 to 30.5 g m^{-2} respectively.

When the elevation of the cleaning blades above the soil's surface level is increased to 4.0 cm, the volume of haulm residues on the root crowns in practical terms does not change, and totals 58.1, 54.9, and 55.8 g m^{-2} at the velocity of the translational motion of the cleaning unit which is equal to 0.8, 1.3, and 1.9 m s^{-1} respectively, and the fixed angular velocity of the rotation of the cleaning tool which is equal to ω = 56.5 rad s^{-1}.

According to the results of the analysis of the quadratic response surfaces that has been presented in Figs 4–12, the optimum mode of operation for the cleaning unit has the parameters that are described below, subject to being able to minimise the volume of haulm residue on the root crowns (g m^{-2}), which is the principal quality indicator of the

root crown post-cleaning. The velocity of the translational motion of the cleaning unit has to be within the range of1.5–2.0 m s^{-1}. It has been established that operating the cleaning unit for the design that is under consideration outside the aforementioned translational motion velocity range, at lower speeds, results in damage being suffered by the sugar beet root crowns, while in the case of higher speeds the quality of the cleaning declines. The angular velocity of the rotation of the cleaning tool - its vertical drive shaft- on the cleaning unit of the design that is under consideration has to be within the range of 57–85 rad s^{-1}. Any departure from said angular velocity range also results in a deterioration of the quality of post-cleaning or damage to the sugar beet root crowns. The elevation of the cleaning blades above the soil's surface level has no significant effect on the quality indicators of the process in regard to post-cleaning root crowns of haulm residues. Nevertheless, a range of between 0–2 cm should be assumed as the most rational parameter range when it comes to positioning the cleaning blades above the soil's surface level.

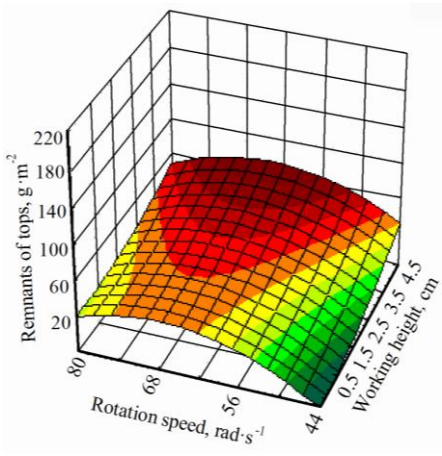

Figure 12. The response surface of haulm residues against the elevation of the blades and the angular velocity of the rotation of the cleaning tool at the velocity of the translation of 1.9 m s^{-1}.

Therefore, according to the results of the experimental research into the operation of the newly-designed cleaning unit which was carried out in real-life field conditions where sugar beet root crowns were cleaned of their haulm residues after a blanket feeler-free topping was carried out, the conclusion can be drawn that the operation quality indicators for the cleaning unit meet the existing agronomical requirements, which implies the expediency of its wide application in production conditions.

CONCLUSIONS

1. In the paper, the technique being used for experimental investigations into the unit that cleans root crowns of haulm residues has been substantiated. The technique involves investigating the effect that the modes of operation of the root crown cleaning unit have on the quality of being able to eliminate haulm residues - meaning an experimental determination in field conditions for the principal quality indicators in the performance of this design of cleaning unit.

2. It has been established that, in regard to the principal indicators for the quality of operation in field conditions, the unit that has been developed for cleaning standing root crowns of haulm residues not only meets agronomical requirements, but exceeds them.

3. The analysis of the regression equation that describes the effect of the main design and kinematic parameters regarding the degree of success of root crown post-cleaning of haulm residues has shown that the angular velocity of rotation of the cleaning

tool and the velocity of the translational motion of the cleaning unit are the principal factors that have an effect on the optimisation parameter.

4. After analysing the quadratic response surfaces, it has been established that the rational mode of operation for the cleaning unit, subject to minimising the post-cleaning quality indicator - in other words the volume of haulm residue on the root crowns (g m^{-2}) - is achieved within the following parameter ranges: the cleaning unit's travelling speed is between 1.5–2.0 m s^{-1} and the angular velocity of the rotation of the cleaning tool is between 57–85 rad s^{-1}. The most rational parameter range for the elevation of the cleaning blades above the soil's surface level is between 0–2 cm.

5. Following the results that have been obtained in terms of the field experiments, it has been established that the extent of root crown cleaning of haulm residue is 95.9%, while the degree of sweeping haulm and plant residues which is outside the planted row of sugar beet is 99.96%, which exceeds the world's standard agronomical requirements for the process of post-cleaning sugar beet root crowns of haulm residue.

REFERENCES

Bentini, M., Caprara, C. & Rondelli, V. 2005. Mechanical properties of sugar beet roots. *Transactions of the American Society of American Engineers* **48**(4), 1429–1439.

Bulgakov, V.M. 2011. *Sugar beet harvesting machines*. Kiev: Agricultural Science, 351 pp.

Bulgakov, V., Adamchuk, V., Arak, M. & Olt, J. 2018. The theory of cleaning the crowns of standing beet roots with the use of elastic blades. *Agronomy Research* **16**(5) 1931–1949. DOI:10.15159/AR.18.213

Bulgakov, V., Adamchuk, V., Arak, M. & Olt, J. 2017. A theoretical study of haulm loss resulting from rotor topper oscillation. *Chemical Engineering Transactions* **58**, 223−228. DOI: 10.3303/CET1758038.

Bulgakov, V.; Adamchuk, V, Arak, M. & Olt, J. 2016. Theory of impact interaction between the feeler and standing sugar beet root crowns during their scalping. *Book of proceedings*: *VII International Scientific Agriculture Symposium "Agrosym 2016", Jahorina, October 6-9, 2016.* Ed. Dušan Kovacević. University of East Sarajevo, 63−70. DOI: 10.7251/AGRENG1607004

Gruber, W. 2005. Trends in sugar beet harvesting. *Landtechnik* **60**(6), 320–321.

Gu, F., Hu, Z., Wu, H., Peng, B., Gao, X. & Wang, S. 2014. Development and experiment of 4LT-A staggered-dig sugar beet combine. *Nongye Gongcheng Xuebao/Transactions of the Chinese Society of Agricultural Engineering* 30(23), 1–9. DOI: 10.3969/j.issn.1002-6819.2014.23.001

Pogorely, L.V. & Tatyanko, N.V. 2004. *Beet-harvesting machines: History, Construction, Theory, Prognosis*. Feniks, Kyiv, 232 pp. (in Ukrainian).

Pogorely, L.V., Tatyanko, N.V. & Bray, V.V. 1983. *Beet-harvesting machines (designing and calculation)*. Tehnika, Kyiv, 168 pp. (in Russian).

Vasilenko, P.M. 1996. *Introduction to agricultural mechanics*. Agricultural Education, Kiev, 252 pp. (in Russian).

Wang, F. & Zhang, D. 2013. Design and experiment of disc-dig sugar beet combine. *Nongye Gongcheng Xuebao/Transactions of the Chinese Society of Agricultural Engineering* **29**(13), 7–14. DOI: 10.3969/j.issn.1002-6819.2013.13.002

Wu, H., Hu, Z., Peng, B., Wang, H. & Wang, B. 2013. Development of auto-follow row system employed in pull-type beet combine harvester. *Nongye Gongcheng Xuebao/Transactions of the Chinese Society of Agricultural Engineering* 29(12), 17–24. DOI: 10.3969/j.issn.1002-6819.2013.12.003

Zhang, G., Xu, W. & Fan, S. 2013. Analysis and parameter optimization of adjustable beet top cutting mechanism. *Nongye Gongcheng Xuebao/Transactions of the Chinese Society of Agricultural Engineering* **29**(18), 26–33. DOI: 10.3969/j.issn.1002-6819.2013.18.004

Agronomy Research **17**(2), 371–377, 2019
https://doi.org/10.15159/AR.19.106

Effect of environmental temperature during the of brooding period on growing period of pullets viscera and tibia

M.G.L. Cândido[1,*], I.F.F. Tinôco[1], M. Barbari[2], L.C.S.R. Freitas[1], T.C. dos Santos[1], R.R. Andrade[1], R.S. Gates[3], L. Conti[2] and G. Rossi[2]

[1]Federal University of Viçosa, Department of Agricultural Engineering, Peter Henry Rolfs Ave, s/n, BR 36570-000 Viçosa-MG, Brazil
[2]University of Firenze, Department of Agricultural, Food, Environmental and Forestry, Via San Bonaventura, 13, IT50145 Firenze, Italy
[3]University of Illinois, Department of Agricultural and Biological Engineering, 1304 West Pennsylvania Avenue, US61820 Urbana-IL, United States of America
[*]Correspondence: marciagl.candido@gmail.com

Abstract. Poultry production in subtropical and tropical regions faces many problems, one of which is the high air temperature causing thermal stress, particularly dangerous in high-producing birds. Thus, the negative effects caused by heat stress (HS) must be managed. The objective of this study was to evaluate the effects of four different levels of HS in viscera and tibia of pullets. A total of 648 chicks (Lohmann LSL Lite) were used in this study in two different phases. The pre-experimental phase (PEP) was from day 1 through 6 weeks of age. The birds were reared with three different environmental temperatures: thermal comfort, hot and cold. The experimental phase (EP) was conducted from the 7th to the 17th week. Pullets from each thermal environment of the PEP were submitted to: 20 °C, 25 °C, 30 °C, 35 °C. At the end of the 17th week of age 120 pullets were euthanatized and the organs, heart, liver, spleen and gizzard were weighed, as also their tibias. Effects of PEP, and its interaction with EP, were not significant ($P < 0.05$) for viscera and tibia weight. However, a significant increase ($P < 0.05$) in heart weight with the decrease of the environmental temperature was observed, being the pullets subject to 20ºC and 25 °C with the heaviest weights. For the liver, pullets subject to the 35 °C had the lowest weight and were different ($P < 0.05$) from the other three treatments. For gizzard, the difference ($P < 0.05$) was between the treatments 20ºC and 35 °C. These results indicate that brooding temperatures tested during the first 6 weeks of life did not affect the viscera and bone weight during the growing phase.

Key words: heat stress, poultry, pullet, thermoregulation, viscera.

INTRODUCTION

Tropical and subtropical, characterized by high average temperatures in most of the year, are responsible for high animal protein production requiring special care regarding thermal stress, to which birds are predominantly submitted in most of the year. In this sense, the production environment is essential to reach high levels of productivity, with maintenance of the thermal comfort of the birds. Thus, the climatic environment cannot

be a determining factor for reducing production, and the heat stress (HS) negative effects must be managed.

The HS is a well-known cause of decreased development, growth and productivity of poultry (Cassuce et al., 2013; Lara & Rostagno, 2013; Cândido et al., 2016; Freitas et al., 2017; Santos et al., 2017; Arcila et al., 2018). When birds are exposed to stressful environments, physiological changes may occur, such as increased plasma corticosterone, changes in thyroid hormone levels triiodothyronine (T_3) and thyroxine (T_4), immunosuppression, elevation of heart rate and respiratory rate (Donkoh, 1989; Moraes et al., 2002; Sahin et al., 2002; Mack et al., 2013). Other changes resulting from stress are the behavioral changes of the birds, which can be reflected in anomalous behaviors (Zimmerman et al., 2000; Moura et al., 2008; Xie et al., 2015).

Also, the proper development of organs and the skeleton is determinant for a long productive life and birds' welfare, especially during the first phases of life. However, viscera and bone development may be also affected by HS (Moraes et al., 2002; Regmi et al., 2015; Casey-Trott et al., 2017). The laying hens skeleton becomes fully developed during the growing period, when the bird is a pullet. An underdevelopment in this phase may cause laying problems during the productive phase (Whitehead, 2004; Casey-Trott et al., 2017).

A hen spends over 76 weeks of her life laying eggs. To avoid economic losses during this period, the thermoregulation system must be prepared for cope to high environment temperatures. However, it is inferred that, possibly adapting to the Brazilian climate, the physiological responses of the birds can be altered, so that the areas currently considered as comfort in temperate climates may be different from those occurring in hot climates or tropical. This difference can occur due to changes in genetic and nutritional standards, environmental and breeding management, especially acclimatization to the conditions of the tropical climate (Cassuce et al., 2013; Arcila et al., 2018).

In this sense, objective of this study was to evaluate the effects of four different levels of HS in pullets viscera and tibia, when they were previously acclimatized to three different temperatures during the brooding phase.

MATERIALS AND METHODS

Experimental Design

All animal care procedures were approved by Ethics Commission on the use of Farm Animals of the Federal University of Viçosa (CEUAP-UFV Protocol No. 37/2016).

The research was conducted in two phases, pre-experimental and experimental. The pre-experimental phase was from day one through the 6th week of age, and the experimental phase started at the 7th week through the 17th week.

A total of 648 commercial replacement chicks (Lohmann LSL Lite) were randomly allocated to one of four controlled-environment chambers, housed from day one to 17 weeks of age. Each chamber measured 3.20 m x 2.44 m x 2.38 m (LxWxH). Chicks were placed inside steel cages measuring 0.50 m x 0.50 m x 0.50 m (LxWxH). The placement density was 140 cm² chick^{-1} for the first four weeks (17 chicks cage^{-1}), and 357 cm² chick^{-1} (seven pullets) from the 5th week to the 17th week per industry guidelines (Lohmann, 2016). The cages were equipped with 0.5 m of linear feeder at the cage front,

and one nipple drinker placed on a side midway between the front and back. Birds were provided with feed and water ad libitum and fed with a starter feed till the 6th week, and a grower feed thereafter (Rostagno et al., 2011).

The light program used was that recommended by the industry guidelines (Lohmann., 2016). The Light:Dark (L:D) hourly schedule was 24L:0D and 16L:8D, for days 1–2, and 3–6 respectively. It was then reduced by 1 hour per day, until the 6th week, finishing with 10L:14D applied for the remainder of the experiment.

Chamber temperatures were individually controlled with a microcontroller (model MT-531R Plus, Full Gauge Controls, Canoas/RS, Brazil), connected to an air heater (Model AB Split 1, Britania Eletrodomesticos S.A. Pirabeiraba, SC, Brazil) and an air conditioner (Model ABS 12FC 2LX, Komeco, Manaus, AM, Brazil). Relative humidity was maintained in the range of 40–60% with an ultrasonic humidifier (Model HUL535W, Kaz USA, Inc., Marlborough, MA) and the air conditioner. Ventilation was provided by two 10 cm axial fans (model FD08025 S1M, Ambition Technology Company, Guangdong, China), providing approximately 1.08 $m^3 min^{-1}$ (3.6 air changes hr^{-1}) Air quality was monitored daily for ammonia (Gas Alert Extreme NH3 Detector, BW Technologies®, Oxfordshire, UK) and carbon dioxide (AZ 77535, AZ Instrument Corp., Taichung City, Taiwan). Chamber temperature and relative humidity were recorded by a datalogger (Model HOBO U14-001, Onset, USA), each five minutes for the entire experiment.

***Pre-Experimental Phase*.** The pre-experimental phase of this work had the purpose of acclimatizing groups of chicks to one of three different air temperatures prior to assignment to different HS levels during the experimental phase. During this pre-experimental phase, the chicks were divided randomly into groups of 216 and placed into one of three environmental chambers, each one with a different air temperature (mild cold stress, thermal comfort, mild heat stress) as shown in Table 1. The chicks were subjected to the Pre-Experimental Phase temperatures 24h per day. Evaluation of performance and physiological responses of these chicks at the end of the pre-experimental phase are reported separately in Andrade et al. (2017). As important note for this study, the body weight of pullets at the start of this experiment were similar, averaging 418 g $bird^{-1}$.

Table 1. Air temperatures during the pre-experimental phase

Thermal Environment	1st week	2nd week	3rd week	4th week	5th and 6th week
Mild cold stress	28	25	23	20	17
Thermal comfort[1]	31-35	28	26	23	19
Mild heat stress	38	31	29	26	22

[1]Per Lohmann (2016); Albino & Carvalho, 2014.

***Experimental Phase*.** The period from the 7th to the 17th week of age involved a total of 420 pullets, 140 of which were obtained from each of the three pre-experimental phase temperatures and divided into four groups of 35 pullets (five cages) and placed separately into one of the four experimental phase temperature treatments, as depicted in Fig. 1. These temperature treatments were denoted as: Thermal Comfort (TC, 20 °C); presumed Mild Heat Stress (MiHs, 25 °C); presumed Moderate Heat Stress (MoHs,

30 °C); presumed Severe Heat Stress (SeHs, 35 °C). During the night the air temperature was set to 20 °C, from 7:00 p.m. to 7:00 a.m. for all chambers.

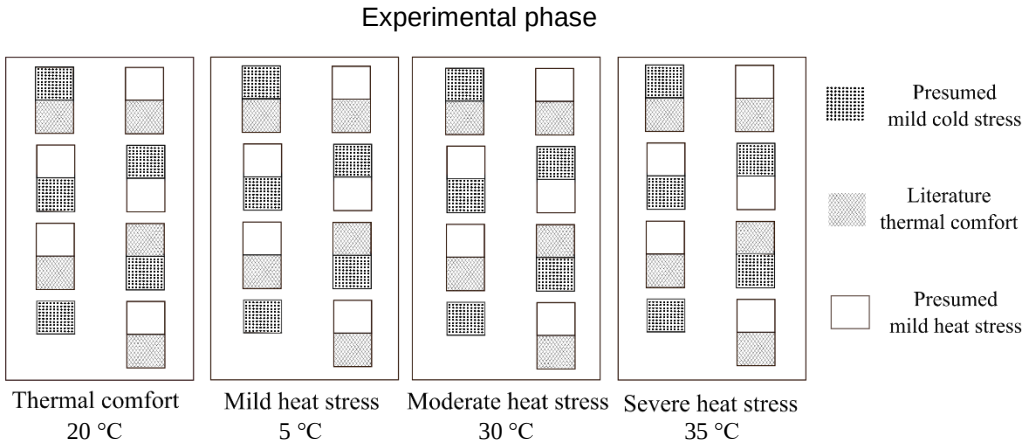

Figure 1. Experimental design of pullets' distribution in the environmentally controlled chambers during the Phase II, from the 7th through the 17th weeks of age.

Bone and Viscera Measurements

The bone and viscera measurements were assessed by weight measurements at the 17th week. For these measurements 2 pullets for cage (120 pullets) were obtained randomly and subjected to cervical dislocation. The viscera heart, liver, spleen and gizzard were removed and immediately weighed. The same procedure was done with the tibias.

Statistical Analyses

The experimental design was completely randomized in subdivided parcels (chambers), with four treatments (experimental phase temperatures - TC; MiHs; MoHs; SeHs), three sub-parcels (pre-experimental phase temperatures), their interactions, and five replicate cages per treatment x sub-parcel combination. The quantitative analysis of relative visceral weight (expressed as percentage of body weight) for heart, liver, spleen and gizzard, and the tibias weights was performed using analysis of variance (SAEG, 2007). Differences between group means were compared by Tukey's test, with a 5% confidence level ($P < 0.05$) for significance of treatment effects, interactions and differences between means.

RESULTS AND DISCUSSION

The target temperature levels were maintained each day of the 17-week experiment within 1.0ºC deviation. Effects of pre-experimental temperature treatment, experimental temperature and its interaction were not significant ($P > 0.05$) for tibia weight at 17th week of life, Table 2. In an experiment with chick broilers in the first week of life Moraes et al. (2002) found a difference in tibia weight between the ones at 20 °C compared with 25 °C and 35 °C. Also, Bruno et al. (2000) found difference between tibia weight for broilers raised in hot and thermoneutral environments. It is well-known that the fast

development of broilers may cause leg disorders and skeletal problems and, that hens have slower body development than broilers (Bruno et al., 2000; Whitehead, 2004). With this in mind, the contrast between the literature and the results of this work may be due the development velocity between the two types of birds.

Relative viscera weight from heart, liver, spleen and gizzard of pullets subjected to the 4 different experimental temperatures during the growing phase (TC, 20 °C; MiHs, 25 °C; MoHs, 30 °C; SeHs, 35 °C) are presented in Table 2. Effects of pre-experimental temperature treatment and its interaction with experimental temperatures were not significant ($P < 0.05$) for all evaluated viscera. Pullets subjected to 20 °C and 25 °C, had higher weight, for heart ($P < 0.01$) compared with pullets subjected to 30 °C, 35 °C. Pullets subjected to 35 °C had less weight, for heart ($P < 0.01$) and spleen ($P < 0.01$) compared with pullets subjected to 20 °C, 25 °C and 30 °C treatments. For the gizzard, only the treatments TC, 20 °C and SeHs, 35 °C were different from each other ($P < 0.01$).

Moraes et al. (2002), found higher absolute values for heart and liver weight in broilers subjected to cold stress, but this difference was not significant ($P > 0.05$). The difference between the viscera weight pattern in cold and hot environments can be due the fact of when birds are exposed to lower temperatures, especially in the first week of life if related to high metabolic rate, and increased oxygen demand to maintain the body temperature (Yang & Siegel, 1997).

Deaton et al. (1969) in an experiment with broilers reported lower liver weight for birds subject to heat stress when compared to the ones in thermoneutral and cold stress. These findings corroborate with this study. In stressed poultry is well-known the reduction in mass of lymphoid tissues, like thymus, spleen and bursa of Fabricius (Etches et al., 2000). In this experiment the spleen weight was reduced in pullets subject to severe heat stress.

Table 2. Relative visceral weight and tibia weight (expressed as percentage of body weight) of pullets subjected to 4 levels of experimental temperature, pre-experimental temperature, and interactions on the performance of pullets at 17 weeks of age

Thermal Environments	Performance Parameters				
	Heart (%)	Liver (%)	Spleen (%)	Gizzard (%)	Tibia (%)
TC, 20 °C	0.53[a]	1.57[ab]	0.17[a]	2.05 [a]	0.62
MiHs, 25 °C	0.50[a]	1.69[a]	0.17[a]	2.12[ab]	0.63
MoHs, 30 °C	0.49[b]	1.46[bc]	0.17[a]	2.05 [ab]	0.65
SeHs, 35 °C	0.43[c]	1.56[c]	0.16[b]	2.11[b]	0.70
SEM	0.49	1.39	0.26	2.29	0.46
P-value (Experimental phase)	< 0.001	< 0.001	< 0.001	< 0.01	ns
P-value (Pre - Experimental phase)[1]	ns	ns	ns	ns	ns
P-value (Interactions)	ns	ns	ns	ns	ns

[a–c] Means within a column with different superscripts differ significantly ($P < 0.05$); [1] Temperatures used in the Phase I are listed in Table 1; Treatments were: Thermal Comfort – 20/20 °C (TC); Mild Heat Stress – 25/20 °C (MiHs); Moderate Heat Stress – 30/20 °C (MoHs); and Severe Heat Stress – 35/20 °C (SeHs); ns = not significant; SEM: Root Mean Square Error.

CONCLUSIONS

The results of the study indicate that brooding temperatures tested during the first 6 weeks of life did not affect the viscera and bone weight during the growing phase.

The thermal environment affected pullets' viscera weight, as proved by the birds subjected to 35 °C, which resulted the most affected. The tibia relative weight was not affected either by the brooding temperatures tested nor by the temperatures during the growing phase.

ACKNOWLEDGEMENTS. AMBIAGRO research group, Department of Agricultural Engineering and Department of Animal Science of Federal University of Viçosa (UFV); Department ABE of University of Illinois at Urbana-Champaign and Department DAGRI of University of Florence. We also thank the Brazilian Government support through CAPES - Finance Code 001, CNPq and FAPEMIG. The authors would like to thank also Marcos Borges of Lohmann do Brasil for donating the birds.

REFERENCES

Albino, L.F.T. & Carvalho, B.R. 2014. *Laying Hens*. 1st ed. Aprenda Fácil, Viçosa. 376 pp. (in Portuguese).

Andrade, R.R., Tinôco, I.F.F., Baêta, F.C., Barbari, M., Conti, L., Cecon, P.R., Cândido, M.G.L. & Martins, I.T.A. Teles. Junior, C.G.S. 2017. Evaluation of the surface temperature of laying hens in different thermal environments during the initial stage of age based on thermographic images. *Agron. Res*. **15**, 629–638.

Arcila, J.C.P., Tinôco, I.F.F., Saraz, J.A.O., Rocha, K.S.O. & Candido, M.G.L. 2018. Zootechnical and physiological performance of broilers in the final stage of growth subjected to different levels of heat stress. *Rev. Fac. Nac. Agron*. **71**, 1–8.

Bruno, L.D.G., Furlan, R.L., Malheiros, E.B. & Macari, M. 2000. Influence of early quantitative food restriction on long bone growth at different environmental temperatures in broiler chickens. *Br. Poult. Sci*. **41**, 389–394.

Cândido, M.G.L., Tinôco, I.F.F., Pinto, F. de A. de C., Santos, N.T. & Roberti, R.P. 2016. Determination of thermal comfort zone for early-stage broilers. *Eng. Agrícola* **36**, 760–767.

Casey-Trott, T.M., Korver, D.R., Guerin, M.T., Sandilands, V., Torrey, S. & Widowski, T.M. 2017. Opportunities for exercise during pullet rearing, Part I: Effect on the musculoskeletal characteristics of pullets. *Poult. Sci*. **96**(8), 2518–2527.

Cassuce, D.C., Tinôco, I.F.F., Baêta, F. da C., Zolnier, S., Cecon, P.R. & Vieira, M.F.A. 2013. Thermal comfort temperature update for broiler chickens up to 21 days of age. *Eng. Agric*. **33**, 28–36.

Deaton, J.W., Reece, F.N., McNally, E.H. & Tarver, W.J. 1969. Liver, heart and adrenal weights of broilers reared under constant temperatures. *Poult. Sci.* **48**, 283–288.

Donkoh, A. 1989. Ambient temperature: a factor affecting performance and physiological response of broiler chickens. *Int J Biometeorol.* **33**, 259–265.

Etches, R.J., John, T.M. & Gibbins, A.M.V. 2000. *Behavioral, physiological, neuroendocrine and molecular responses to heat stress*. in Poultry Production in hot climates. Daghir, N.J., ed. Second Edi. CAB International, Wallingford. 387 pp.

Freitas, L.C.S.R., Tinôco, I.F.F., Baêta, F.C., Barbari, M., Conti, L., Teles Júnior, C.G.S., Cândido, M.G.L., Morais, C.V. & Sousa, F.C. 2017. Correlation between egg quality parameters, housing thermal conditions and age of laying hens. *Agron. Res*. **15**, 687–693.

Lara, L.J. & Rostagno, M.H. 2013. Impact of heat stress on poultry production. *Animals* **3**, 356–369.

Lohmann. 2016. LSL-Lite Commercial Management Guide. Lohmann Tierzucht. Cuxhaven, Germany.

Mack, L.A., Felver-Gant, J.N., Dennis, R.L. & Cheng, H.W. 2013. Genetic variation alter production and behavioral responses following heat stress in 2 strains of laying hens. *Poult. Sci*. **92**, 285–292.

Moraes, V.M.B., Malheiros, R.D., Furlan, R.L., Bruno, L.D.G., Malheiros, E.B. & Macari, M. 2002. Effect of Environmental Temperature During the First Week of Brooding Period on Broiler Chick Body Weight, Viscera and Bone Development. *Rev. Bras. Ciência Avícola* **4**(1), 1–8.

Moura, D.J., Nääs, I.D.A., Alves, E.C.D.S., de Carvalho, T.M.R., do Vale, M.M. & Lima, K.A.O. 2008. Noise analysis to evaluate chick thermal comfort. *Sci. Agric*. **65**, 438–443.

Regmi, P., Deland, T.S., Steibel, J.P., Robison, C.I., Haut, R.C., Orth, M.W. & Karcher, D.M. 2015. Effect of rearing environment on bone growth of pullets. *Poult. Sci.* **94**, 502–511.

Rostagno, H.S., Albino, L.F.T., Donzele, J.L., Gomes, P.C., de Oliveira, R.F., Lopes, D.C., Ferreira, A.S. & Barreto, S.L. de T. 2011. *Brazilian Tables for Poultry and Swine*. Universidade Federal de Viçosa, Viçosa (in Portuguese).

Sahin, K., Sahin, N., Onderci, M., Gursu, F. & Cikim, G. 2002. Optimal dietary concentration of chromium for alleviating the effect of heat stress on growth, carcass qualities, and some serum metabolites of broiler chickens. *Biol. Trace Elem*. Res. **89**, 53–64.

Santos, T.C., Gates, R.S., Tinôco, I.F.F., Zolnier, S. & Baêta, F. da C. 2017. Behavior of Japanese quail in different air velocities and air temperatures. *Pesqui. Agropecu. Bras*. **52**, 344–354.

Whitehead, C.C. 2004. Overview of bone biology in the egg-laying hen. *Poult. Sci*. **83**, 193–199.

Xie, J., Tang, L., Lu, L., Zhang, L., Lin, X., Liu, H.C., Odle, J. & Luo, X. 2015. Effects of acute and chronic heat stress on plasma metabolites, hormones and oxidant status in restrictedly fed broiler breeders. *Poult. Sci*. **94**, 1635–1644.

Yang, A. & Siegel, P.B. 1997. Late embryonic and early posthatch growth of heart and lung in White Leghorn lines of chickens. *Growth Development & Aging: GDA* **61**, 119-126.

Zimmerman, P.H., Koene, P. & Van Hooff, J.A.R.A.M. 2000. The vocal expression of feeding motivation and frustration in the domestic laying hen, Gallus gallus domesticus. *Appl. Anim. Behav. Sci*. **69**, 265–273.

Agronomy Research **17**(2), 378–384, 2019
https://doi.org/10.15159/AR.19.117

Thermal comfort of pigs housed in different installations

D. Cecchin[1], P.F.P. Ferraz[2,*], A.T. Campos[2], F.A. Sousa[3], P.I.S. Amaral[4], J.O. Castro[2], L. Conti[5] and V.M.F da Cruz[6]

[1]Federal Fluminense University (UFF), Department of Agricultural Engineering and Environment, Street Passo da Pátria, n.156, Boa Viagem, Niterói-RJ, Brazil
[2]Federal University of Lavras (UFLA), Campus Universitário, BR 3037, Lavras-MG, Brazil
[3]SEMAG/Aracruz, Av. Morobá, n.20, BR 29192-733 Bairro Morobá-ES, Brazil
[4]José do Rosário Vellano University (UNIFENAS), Department of Veterinary Medicine. Rodovia Mg-179 km 0, s/n - Bairro Trevo, BR 37130-000 Alfenas-MG, Brazil
[5]University of Firenze, Department of Agriculture, Food, Environment and Forestry (DAGRI), Via San Bonaventura, n.13, IT 50145 Firenze, Italy
[6]Évora University (UE), Pólo da Mitra, PT 7002-554, Évora, Portugal
[*]Correspondence: patricia.ponciano@ufla.br

Abstract. In an intensive production system, the environment directly influences the comfort and welfare of pigs. Animals under heat stress may exhibit behavioural changes and changes in physiological parameters, such as increased body temperature, respiratory and cardiac movements. The aim of this study was to evaluate the thermal comfort of growing and finishing pigs housed in facilities with different construction typologies. The evaluated pens were: pen with water depth (WDP) and pen with partially slatted floor (SLF). Data on the ambient thermal environment in the pens and in the outside were collected automatically using Hobo dataloggers, model U12-013. This equipment recorded the air temperature, relative humidity of the air and black globe temperature in intervals of five minutes. Subsequently the variables were used in the calculation of the temperature index of the globe and humidity. The physiological responses of the animals were collected: Surface Temperature (ST) and Respiratory Rate (RF). When analyzing the parameters: ST and RF, it was observed that the WDP pen presented a significant difference in all the observed hours, with an increase observed throughout the day, and the SLF pen presented a difference at 9:00 a.m. presenting a lower value than the other schedules evaluated. The BGHI inside the pens showed average values in the hottest period of the day slightly above what is recommended for adult pigs. Both facilities during the hottest time of the day demonstrated a similar trend in relation to the evaluated variables, so it was concluded that both pens provided the same conditions of thermal comfort for the animals.

Key words: rural buildings, pigs, house design.

INTRODUCTION

Brazilian pig farms have the challenge of providing environmental comfort to the animals, aiming at the productive benefits (Morales, 2010). The environment has great influence on the welfare of the pigs (Machado Filho, 2000), an improper environment

causes discomfort to the animals. The low level of animal welfare can affect production, reproduction, health and quality of the final product.

Ambience is the science that analyzes the characteristics of the environment as a function of the thermal comfort zone of the species, associated with physiological characteristics that regulate the internal temperature of the animal (Bridi, 2006).

The knowledge and identification of climatic variables that directly influence the performance of the animal in the form of thermal stress are the main measures to seek out and execute mitigating measures of discomfort and loss of production (Bloemhof et al., 2008; Nazareno et al., 2012).

Pigs grow and function better under thermoneutral temperature conditions. Pigs exposed to temperatures outside the thermoneutral zone may have behavioral and physiological changes, consequently reducing weight gain (Kiefer et al., 2010). Studies by MacLean (1969) found that in a situation of thermal stress, the immune system of the animals becomes weak, resulting in an inefficiency to resistance to infections.

The objective of this study was to evaluate the thermal comfort of growing and finishing pigs in facilities with different types of floors.

MATERIALS AND METHODS

The study was carried out in a commercial swine farm (Granja Niteroi) (21° 11' 37" S; 45° 02' 49'' W; 918 m) in the municipality of Lavras-MG, Brazil, from July to August 2014.

The climate of the region, according to Köppen's classification, is Cwa, i.e., rainy temperate (mesothermal) with dry winter and rainy summer, subtropical.

The evaluated housing system was intensive confinement, in which the animals do not have access to the outside of the facilities. The thermal environment and air quality of facilities with swine in growing and finishing stages were evaluated.

The animals were housed in pens as follows: with mean weight of 28.69 kg (pen with water depth, WDP); and with 28.5 kg (pen with partially slatted floor, SLF). The animals remained in the pens during the growing and finishing stages, reaching final mean weights of 83.47 kg (WDP pen) and 87.67 kg (SLF pen).

The animals were housed in masonry buildings covered with fiber-cement roofing, supporting structures in reinforced concrete, concrete floor and East-West orientation. Each pen was equipped with two automatic feeders and four nipple drinkers, with total area of 72 m² (8 x 9 m), ceiling height of 3 m, containing 72 animals each. The WDP pen had, on one of its sides, a lowering in the concrete floor (1 m wide and 10 cm deep), filled with water, and was fenced by masonry dividers with ceramic bricks covered with a layer of concrete render and painted in white. The SLF pen had dividers made of steel wire ropes, ceiling height of 3 m and concrete floor, with sides made of slotted precast concrete plates.

The surface temperature of the animals was determined in three times (09:00 a.m, 12:00 a.m and 03:00 p.m) with a surface thermometer, non-contact, infrared, Fluke 62 Mini model brand, with accuracy of ± 1% of reading. Five animals were chosen at random in each pen, where surface temperatures were collected. The temperature was collected at three points (back of neck, palette and ham), by calculating the average of the same, as performed by Amaral et al. (2014). These measures were performed during 40 days, within a two month interval.

For the collection of respiratory frequency was adopted methodology used by Amaral et al. (2014), where is made the measurement and counting of the movements of the animal for 15 seconds, later by multiplying by four to get the amount of movement per minute. Five randomly selected animals were observed in controlled trials (in each pen) during the hours of 09:00 a.m., 12:00 p.m. and 03:00 p.m., during the days of data collection. These measures were performed during 25 days, within a two month interval.

Data relative to the ambient thermal comfort in the pens and outside were automatically collected using data loggers (Hobo, model U12-013), with accuracy of ± 0.5° C. These devices recorded the dry bulb temperature, relative air humidity and black globe temperature in intervals of five minutes. To obtain the black globe temperatures (Tbg), the external sensors of the data loggers, inserted in black balloons, were used. The data loggers were positioned inside the facilities at a height of 1.20 m from the floor, as described in Sampaio et al (2004).

Based on the Tdb (bulb temperature), RH (relative air humidity) and Tbg values, the temperature and humidity index (THI), and the black globe temperature and humidity index were determined (BGHI). The BGHI, THI, and h were used to evaluate the thermal environment. Based on the BGHI, the effects of air velocity and radiation can be quantified indirectly.

The THI index was calculated using the equation proposed by Thom (1958):

$$THI = Tdb + 0.36\ Tdp + 41.2$$

where Tdb = dry bulb temperature (°C) and Tdp = dew point temperature (°C).

The BGHI index was calculated using the equation proposed by Buffington et al. (1981):

$$BGHI = Tbg + 0.36\ Tdp - 330.08,$$

where Tbg = black globe temperature (K) and Tdp = dew point temperature (K).

The thermal environment data (THI, BGHI, Tdb and RH) and the physiological variables (RF and ST) were subjected to analysis of variance using the "F" test and the means subsequently compared by the Scott knott test at 5% of significance. The analysis was conducted adopting a completely randomized design. The results were obtained with the aid of statistical software SISVAR 5.3.

RESULTS AND DISCUSSION

It was observed a significant difference for the variable Tdb between the pens and between the schedules, and the SLF pen presented mean values higher for 9:00 a.m. and 12:00 a.m. than in the WDP pen ($P < 0.05$, Scott-Knott test). The WDP pen presented a significant difference in all the observed hours, with an increase observed throughout the day, and the SLF pen presented a difference at 9:00 a.m, presenting a lower value than the other schedules evaluated (Table 1).

Sampaio et al. (2004) limit the thermoneutral zone between 15 and 21 °C. However, for pigs in the growing phase the values are: 18 °C to 25 °C, and 15 °C as critical cold limit and 26 °C as the critical heat limit. The average temperature values observed in the present study, in the afternoon, are a little above the range cited by Agroceres Pic (2008).

When pigs are exposed to high temperatures, performance is affected (Kiefer et al., 2010), mainly by reducing food intake and energy expenditure associated with thermoregulation processes (Manno et al., 2006).

Table 1. Mean values of environmental variables observed during the evaluated period, along the day, in swine growing and finishing facilities with floor with water depth (WDP), and pen with slatted floor (SLF)

Pens	Tdb (°C)			RH (%)		
	9:00 a.m.	12:00 p.m.	03:00 p.m.	9:00 a.m.	12:00 p.m.	03:00 p.m.
WDP	19.0aA*	25.8aB	26.9aC	73.9aA	49.8aB	45.2aC
SLF	22.8bA	26.6bB	27.1aB	57.9bA	44.96bB	40.6bC

Dry bulb temperature (Tdb); Relative air humidity (RH). *Averages followed by the same letter, lowercase in the column and uppercase in the row, do not differ by the Scott-Knott test at 5% probability.

The average RH showed a significant difference between the pens ($P < 0.05$, Scott-Knott test) and the pen with a water depth had the highest average values during the analyzed times, which was already expected due to the microclimate inside the pen created by the evaporation of the water present in the water depth.

According to Muller (1989), for pigs weighing over 30 kg and in thermal comfort, the optimal RH is between 50 and 70%. It was observed that in the evaluation of 9:00 a.m. the average RH in SLF pen was within the range quoted by Muller, however in the times of 12:00 p.m. and 03:00 p.m. it was below the value recommended by the author. The WDP pen presented a higher RH compared to the SLF pen at all evaluated times.

There were no significant differences between the pens for the THI and BGHI indices, but a significant difference was observed between the hours for each pen, the evaluation at 9 a.m. recorded lower values than for the other times in both pens for THI and BGHI (Table 2).

Table 2. Mean values of environmental indices observed during the evaluated period, in swine growing and finishing facilities with floor with water depth (WDP), and pen with slatted floor (SLF)

Pens	THI			BGHI		
	9:00 a.m.	12:00 p.m.	03:00 p.m.	9:00 a.m.	12:00 p.m.	03:00 p.m.
WDP	65.3aA	72.2aB	73.1aB	68.4aA	73.1aB	73.6aB
SLF	69.0aA	72.7aB	72.8aB	69.4aA	74.5aB	73.8aB

Temperature and humidity index (THI), Black globe-humidity index (BGHI); *Averages followed by the same letter, lowercase in the column and uppercase in the row, do not differ by the Scott-Knott test at 5% probability.

Turco et al. (1998) found that the BGHI upper limit of thermal comfort for adult pigs was 72. In the present study, although there were no statistical differences between the two facilities, at 12:00 and 03:00 p.m. mean values were above that recommended by Turco et al. (1998).

The THI values followed the same trend as the BGHI values, increasing due to the increase in Tbd, but values were below the values mentioned by Chase (2006) and Botto et al. (2014), who consider that THI below 74 is normal for pigs.

There was a significant difference in respiratory frequency, between the pens, as well as between times, between pens the difference occurred at the 9 o'clock time (Table 3), the animals housed in the WDP pen presented lower RF in comparison to the housed animals in the SLF pen, this was possibly due to the influence of the environmental variables (Tdb, RH). Both facilities presented significant differences

between the schedules, the movements per minute increased in the higher temperature schedules (12:00 p.m. and 03:00 p.m.).

Table 3. Mean physiological variables observed in animals in the growth and termination phase confined in a water depth pen (WDP), and pen with slatted floor (SLF)

Pens	RF (mov.min^{-1})			ST (°C)		
	9:00 a.m.	12:00 p.m.	03:00 p.m.	9:00 a.m.	12:00 p.m.	03:00 p.m.
WDP	40.0aA*	48.8aB	54.0aC	31.5aA	33.4aB	33.7aB
SLF	48.0bA	51.6aB	59.2aC	32.9bA	33.7aB	34.0aB

RF: Respiratory Rate; ST: Surface Temperature. *Averages followed by the same letter, lowercase in the column and uppercase in the row, do not differ by the Scott-Knott test at 5% probability.

According to Hannas (1999), the first response of the pigs when exposed to the temperature above the upper limit of the thermal comfort zone is the increase of the respiratory rate, due to the direct stimulation of the hypothalamic center.

According to Ferreira (2011) the RF of adult pigs in comfort is 44 ± 7.9 movements per minute, the values found in the present study are within the range quoted only in the time of 9:00 am for both pens and at 12:00 p.m. for the WDP pen. According to Kiefer et al. (2009) the respiratory rate of pigs in the growth and finishing phase in comfort (21 °C) is 45.90 mov min^{-1}. However, Manno et al. (2006) found 48 ± 8 mov min^{-1} for swine (30 to 60 kg) maintained in thermal comfort. Correlation of RF and BGHI, it is possible to observe that the increase of BGHI influenced RF. High environmental temperatures may increase respiratory rate (Manno et al., 2006), the RF is one of the mechanisms for body heat loss, thus allowing the maintenance of homeostasis (Christon, 1988).

The ST also presented significant difference between the pens at the 9 o'clock time. It was also observed a difference between the schedules for both pens, the average surface temperatures at 12:00 p.m. and 3:00 p.m. were higher than at 9:00 a.m.

The ST values found in the present study are below those observed by Kiefer et al. (2010), which was 36.24 °C for swine in thermal comfort (21 °C). However, the values found are close to those obtained in the afternoon by Santos et al. (2018) when studying different environments. The variation of the surface temperature is high and may vary, among others, depending on the breeding system (Nazareno et al., 2012), race, environmental factors, metabolism adjustments, with the purpose of dissipating heat (Soerensen & Pedersen, 2015).

CONCLUSIONS

The BGHI inside the pens showed average values in the hottest period of the day slightly above what is recommended for adult pigs.

Both facilities during the hottest times of the day demonstrated a similar trend in relation to the evaluated variables, so it was concluded that both pens provided the same conditions of thermal comfort for the animals.

It recommends, that new studies should be carried out in the warmer period (summer season) to analyze the comfort of these animals.

REFERENCES

Agroceres Pic. 2008. *Females management guide (Guia de manejo de fêmeas)*. 2. ed. São Paulo, 31 pp. Avaiable in: <http://www.agrocerespic.com.br/servlet/navSrvt?cmd=detNot&id=284&idcat=17>. Accessed: 14.08.2016.

Amaral, P.I.S., Ferreira, R.A., Pires, A.V., Fonseca, L.S., Gonçalves, S.A. & Souza, G.H.C. 2014. Performance, behaviour and physiological responses of finishing pigs under different lighting programs. *Journal Animal Behaviour and Biometeorology* **2**, 54–59 (in Portuguese).

Botto, Ľ., Lendelová, J., Strmeňová, A. & Reichstädterová, T. 2014. The effect of evaporative cooling on climatic parameters in a stable for sows. *Res. Agr. Eng.* **60**(Special Issue), S85–S91.

Bloemhof, S., Van Der Waaij, E.H., Merks, J.W. & Knol, E.F. 2008 Sow line differences in heat stress tolerance expressed in reproductive performance traits. *Journal of Animal Science* **86**, 3330–3337.

Bridi, A.M. 2006. Facilities and environment in animal production (Instalações e ambiência na produção animal). In: *curso sobre qualidade da carne suína*, 2., 2006, Londrina. Anais... Londrina: Universidade Estadual de Londrina, pp. 1–16.

Buffington, D.E., Collazo-Arocho, A., Canton, G.H., Pitt, D., Thatcher, W.W. & Collier, R.J. 1981. Black globe-humidity index (BGHI) as comfort equation for dairy cows. *Transactions of the ASAE* **24**,711–714.

Chase, L.E. 2006. Climate change impacts on dairy cattle. Climate change and agriculture: Promoting practical and profitable responses. < https://www.uvm.edu/vtvegandberry/ClimateChange/ClimateChangeImpactsDairyCattle.pdf > Accessed 15.03.19.

Christon, R. 1988. The effect of tropical ambient temperature on growth and metabolism in pigs. *Journal Animal Science* **66**, 3112–3123.

Ferreira, R.A. 2011. *Greater production with better environment: for poultry, pigs and cattle.* 2. Ed. Viçosa, MG, 401 pp. (in Portugueses).

Hannas, M.I. 1999. *Physiological aspects and production of swine in hot weather (Aspectos fisiológicos e a produção de suínos em clima quente)*. In: Silva, I. J.O. Ambiência e qualidade na produção industrial de suínos. Piracicaba: FEALQ, pp. 1–33.

Kiefer, C., Meignen, B.C.G., Sanches J.F. & Carrijo, A.S. (2009) response of growing swine maintained in different thermal environments. *Arch. Zootec.* **58**(221). 55–64 (in Portuguese).

Kiefer, C., Moura, M.S., Silva, E.A., Santos, A.P., Silva, C.M., Luz, M.F. & Nantes, C.L. 2010. Response of finishing swine maintained in different thermal environments. *Revista Brasileira de Saúde e Produção Animal.* 11:496–504. (in Portuguese).

Machado Filho, L.C.P. (2000) *Pig welfare and meat quality A Brazilian view.* In: conferencia internacional virtual sobre qualidade de carne suína, 1., 2000, Concórdia. Anais... Concórdia: Embrapa Suínos e Aves. p. 34–40 (in Portuguese).

Maclean, C.W. 1969. Observations on non-infectious infertility in sows. *The Veterinary Record*, 85:675–682.

Manno, M.C., Oliveira, R.F.M., Donzele, J.L., Oliveira, W.P., Vaz, R.G.M.V., Silva, B.A.N., Saraiva, E.P. & Lima, K.R.S. 2006. Effects of environmental temprerature on performance of pigs from 30 to 60 kg live weight. *Revista Brasileira de Zootecnia* **35**, 471–477 (in Portuguese).

Morales, O.E.S. 2010. Influence of different farrowing house cooling systems on the productivity of sows and their litters. 52 pp. Dissertação (Mestrado em Ciências Veterinárias) – Universidade Federal do Rio Grande do Sul, Porto Alegre. (in Portuguese).

Muller, P.B. 1989. Biodimatology applied to domestic animals.3. Ed. Porto Alegre: Editora Sulina, 158 pp. (in Portuguese).

Nazareno, A.C., Silva, I,J.O., Nunes, M.L.A., Castro, A.C., Miranda, K.O.S. & Trabachini, A. 2012. Bioclimatic characterization of outdoor and confined systems for pregnant sows. *Revista Brasileira de Engenharia Agrícola e Ambiental* **16**, 314–319 (in Portuguese).

Sampaio, C.A.P., Cristani, J., Dubiela, J.A., Boff, C.E. & Oliveira, M.A. 2004. Evaluation of the thermal environment in growing and finishing swine housing using thermal comfort indexes under tropical conditions. *Ciência Rural* **34**, 785–790 (in Portuguese).

Santos, T.C., Carvalho, C.C.S., Silva, G.C., Diniz, T.A., Soares, T.E., Moreira, S.J.M. & Cecon, P.R. (2018). Influence of the thermal environment on the behavior and performance of pigs. *Revista de Ciências Agroveterinárias* **17**(2), 241–253 (in Portuguese).

Soerensen, D.D. & Pedersen, L.J. 2015. Infrared skin temperature measurements for monitoring health in pigs: a review. *Acta Veterinaria Scandinavica* **57**, 1–11.

Thom, E.C. 1958 Cooling Degree: Day Air Conditioning. Heating, And Ventilating. *Transaction of the American Society of Heating* **55**, 65–72.

Turco, S.H.N., Ferreira, A.S., Baêta, F.C., Aguiar, M.A., Cecon, P.R., Araújo, G.G.L. 1998. Environmental Thermal Evaluation of Different Conditioning Systems in Pigs Nursery. (Avaliação térmica ambiental de diferentes sistemas de acondicionamento térmico em maternidades suinícolas). *Revista Brasileira de Zootecnia* **27**, 974–981.

Agronomy Research **17**(2), 385–395, 2019
https://doi.org/10.15159/AR.19.115

Spatial distribution of thermal variables, acoustics and lighting in compost dairy barn with climate control system

F.A. Damasceno[1*], C.E.A Oliveira[1], G.A.S Ferraz[1], J.A.C Nascimento[1], M Barbari[2] and P.F.P Ferraz[1]

[1]Federal University of Lavras, Engineering Department, BR37200-000 Lavras, Minas Gerais, Brazil
[2]University of Florence, Department of Agriculture, Food, Environment and Forestry, Via San Bonaventura, 13, IT50145 Firenze, Italy
[*]Correspondence: flavio.damasceno@deg.ufla.br

Abstract. The main objective of this research was to evaluate the spatial distribution of the thermal variables, acoustics and lighting in climate controlled compost dairy barn. The experiment was conducted in October 2017, in a farm located in the west of Minas Gerais state, Brazil. For the study, the interior of the animal facility was divided into 120 meshes equidistant points, in which air temperature (t_{db}), relative humidity (RH), noise, illuminance, and air speed (V_{air}) were manually collected. The technique of geostatistics was used to evaluate the distribution and spatial dependence of variables. Spatial distribution maps showed the occurrence of high variability of attributes and content within the animal facility. Thermal environment variables showed alert situations throughout practically the entire facility. The noise and luminance levels were within the recommended values.

Key words: animal welfare, dairy cattle, geostatistics.

INTRODUCTION

In Brazil, extensive systems of milk production predominated for a long time, and it is still feasible for the producers to raise the animals in the fields (Bond et al., 2012). However, due to the introduction of animals genetically developed for temperate climate conditions to increase the productivity of the herds, problems related to the animal comfort are increased mainly due to the tropical climate of the country with the occurrence of elevated temperatures throughout the most of the year (Faria et al., 2008).

Confinement of animals emerged as a way to improve productivity, through the control of environmental conditions, associated with a good management of genetics, nutrition, reproduction and sanity. Intensive production systems, in which animals remain housed in functional facilities, have been used as a way to provide a comfortable environment, reducing stress and, consequently, increasing the welfare and productive capacity of the animal (Perissinotto et al., 2009).

The compost dairy barn (Compost Bedded Pack, CBP) consists of a large, open resting area. It is usually bedded with sawdust or dry fine wood shavings that are composted in place, along with manure, and mechanically stirred on a regular basis

(Barberg et al., 2007; Shane et al., 2010; Black et al., 2013). Virginia dairy farmers developed the CBP barn concept to improve cow comfort, increase cow longevity, reduce initial barn costs (Barberg et al., 2007), and potentially reduce the mastitis risks associated with the conventional deep bedding.

In the CBP, the ventilation system is responsible for the maintenance of a comfortable environment for the animals, for the removal of gases and heat, and for the drying of bedding material (Janni et al., 2007; Lobeck et al., 2011).

In CBP barns, different natural and mechanical ventilation systems can be used. In the case of mechanical ventilation, the main types of fans used are low volume and high speed (LVHS) and high volume and low speed (HVLS) (Leso et al., 2018). For farms with inadequate climatic conditions, where only fan use is not sufficient to ensure a comfortable environment for the animals, climate control systems are used (Nääs & Arcaro Júnior, 2001). In this case, the design and adaptation to the hot climate condition can allow the maintenance of the ideal temperature and air velocity, but relative humidity, ammonia and carbon dioxide concentration have to be well managed.

In the climate controlled systems, the monitoring and evaluation of the environment of the animal facilities can be useful to aid decision-making regarding adjustments and corrections of the systems (Sales et al., 2011). Among the models used for the evaluation of spatial variability, the geostatistical methods allow the understanding of the randomness of the data and the establishment of a spatial dependence function, making possible the interpretation of the results based on their spatial variability (Yamamoto & Landim, 2015).

The main objective of this research was to evaluate the spatial distribution of the thermal variables, acoustics, and lighting in compost dairy barn with a climate control system.

MATERIALS AND METHODS

Characterization of the animal facility

The study was carried out during the month of October, 2017, at a farm located in the West of Minas Gerais state, Brazil (latitude 20° 47' 30" S, longitude 45° 18' 52" W, and altitude 921 m), According to classification of Köppen, the climate is Cwa - humid temperate, with dry winter and hot, subtropical summer, and hottest month temperature above 22 °C (Sá Júnior et al., 2012).

The data were collected in a climate controlled compost dairy barn (CBP), equipped with a ventilation system in air-conditioned tunnel mode (negative pressure). This system had 22 exhaust fans (Equipaves®, model 53", diameter of 1.42 m, six propellers and power of 1.0 CV) installed in the southwestern face of the installation, and evaporative cooling of porous material type moistened through porous plate of pulp with dimensions 18.0 x 3.0 m, installed in the northeast face of the CBP barn. The system remained switched on whenever the temperature was above 21 °C, and its monitoring and actuation was performed by means of two sensors that were located inside the installation.

The CBP barn had a width of 23.0 m and a length of 180.0 m, eave height of 4.0 m, roof pitch of 15°, and cover in metallic tiles (thickness of 0.50 mm). The orientation of barn was northeast-southwest (Fig. 1). The floor of the feed alley was covered in concrete. The lateral closure was done by means of plastic curtains of blue colour with

3.5 m of height. Throughout the barn, baffle curtains were installed, starting at 2.5 m in height, spaced every 12 m and used to direct the air towards the bedding. The lighting of the CBP barn was realized by means of 90 tubular fluorescent lamps with power of 36 W, installed equally spaced. The surrounding vegetation was composed of *Eucalyptus* trees.

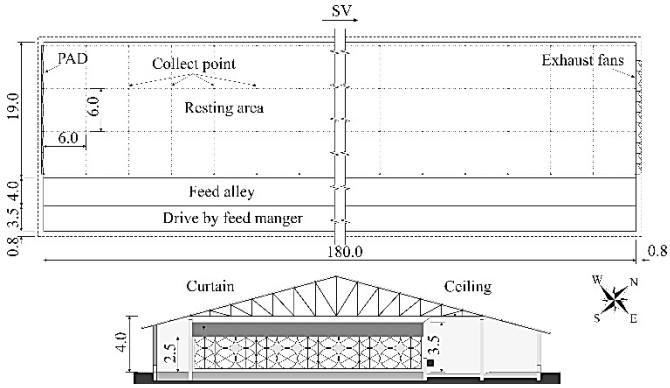

Figure 1. Schematic representation of the CBP barn with collection points and cross section.
* SV – sense of ventilation; PAD – evaporative cooling plate. Dimensions in meters (m).

Inside of CBP barn 325 Holstein cows (305 lactating and 20 pre-calving) were housed. The lactating cows were distributed in 5 groups divided according to the order of production of the animals. Larger animals were housed in lots 1 and 2, located near the evaporative cooling plate (PAD). The milk production per cow was 28 kg day^{-1}.

The CBP barn had a total area of 4,770 m^2, where 3,420 m^2 were resting area (wood sawdust with depth of 0.4 m). The stirring was performed twice a day at milking times (7:00 a.m. and 2:00 p.m.) by means of a rototiller with cultivator, coupled to a small tractor.

Data collection

The resting area of the CBP barn was divided into a rectangular grid containing 120 equidistant points (6 x 6 m), arranged according to the constructive characteristics of the barn (Fig. 1, a). The data collection was performed between 12:00 to 16:00 h.

The environmental variables were collected near the geometric centres of the animals (1.5 m height). A portable digital thermo-higro-decibel-lux meter was used to collect air temperature (t_{bs}), relative humidity (RH) and noise level (Instrutherm®, model THDL-400, with accuracy of ± 3.5%). The air velocity was measured by means of a hot wire anemometer (Instrutherm®, model TAFR-190, with accuracy of ± 0.1 m s^{-1}).

For the evaluation of the thermal comfort inside the CBP, the Temperature and Humidity Index (THI) was used, according to the model proposed by Buffington et al. (1983):

$$THI = 0.8 \cdot t_{bs} + RH \cdot \left(\frac{t_{bs} - 14.3}{100} \right) + 46.3 \quad (1)$$

where t_{bs} is dry-bulb air temperature (°C); *RH* is the relative humidity (%).

For dairy cattle, the limits of THI that characterize a situation of comfort or discomfort are not fully agreed among the scientific community. In general, the limits proposed by Thom (1959) and Hubbard et al. (1999) for dairy cattle are: THI < 74 - thermal comfort condition; $74 \leq$ THI < 79 - an alert condition for producers; $79 \leq$ THI < 84 - a hazard condition, and safety measures must be taken to prevent disastrous losses, especially for confined herds; and, THI > 84 - emergency situation, and urgent steps must be taken to avoid loss of staff. However, THI values above 72 represent a stress condition for Holstein cows, which may lead to reduced productivity (Johnson, 1980).

Geostatistics analysis

In order to verify the spatial behaviour of the variables within the CBP barn, as well as to predict their levels in non-sampled locations and the occurrence of spatial dependence, the geostatistical technique was used. The analyses were performed using the R (Development Core Team, 2016) software, through the geoR library (Ribeiro Junior & Diggle, 2001). The evaluation of the spatial dependence of the variables inside the CBP facilities was made through semivariogram adjustments. For the estimation of the semivariogram we used the estimator of Matheron (1962):

$$\hat{\gamma}(h) = \frac{1}{2N(h)} \sum_{i=1}^{N(h)} \left[Z(X_i) - Z(X_i + h) \right]^2 \qquad (2)$$

where $N(h)$ corresponds to the number of experimental pairs of observations $Z(X_i)$and $Z(X_i + h)$, separated by a distance h.

The coefficients of the theoretical model for semivariogram, called nugget effect - C_0, plateau - $C_0 + C_1$, and reach - a, were obtained from a mathematical model for the calculated values of Bachmaier & Backers (2008).

The degree of spatial dependence (GDE) was determined by the ratio between the nugget effect (C_0) and the threshold ($C_0 + C_1$), multiplying by 100. Dependency analysis was performed using Cambardella et al. (1994). According to this classification, a strong spatial dependence is considered for the semivariograms that have nugget effect of less than 25% of the plateau, a moderate spatial dependence for the semivariograms that have a nugget effect between 25% and 75% of the plateau and a weak spatial dependence for the semivariograms that present nugget effect greater than 75% of the plateau.

Due to the small grouping of data, the Restricted Maximum Likelihood Estimation (REML) method was used, as suggested by Marchant & Lark (2007). The model tested for the adjustment of the experimental semivariogram was the Spherical, a model widely used in geostatistics and that returns good results.

In order to make maps of the spatial distribution of the levels of variables within the CBP barn, the ordinary data kriging technique was used. From the interpolated data, response surface maps were generated, using the ArqGIS® software, version 10.1.

The descriptive statistics were used to determine the fraction of area occupied by the intervals of each of the analysed variables and to better characterize the spatial distribution of the variables inside the climate controlled CBP barn.

RESULTS AND DISCUSSION

The estimated models and parameters of experimental semivariograms adjusted for the variables and THI, acoustic and lighting environment within the evaluated facility are reported in Table 1. The experimental semivariograms were adjusted by the spherical model. According to Isaaks & Srivastana (1989), from a value of the distance between points, there is no more spatial dependence and the variance of the difference between pairs of samples becomes invariant.

Table 1. Estimated models and parameters of experimental semivariograms adjusted for the variables and THI, acoustic and lighting environment within the evaluated facility

Variable	Method	Model	C_0	C_1	C_0+C_1	*a*	GDE	Classification
t_{bs}	REML	Spherical	0.08	1.62	1.69	96.90	4.45	Strong
RH	REML	Spherical	9.91	38.78	48.69	104.71	20.35	Strong
THI	REML	Spherical	0.31	1.88	2.19	100.16	13.96	Strong
V_{air}	REML	Spherical	0.15	0.28	0.43	22.45	34.85	Moderate
Noise	REML	Spherical	6.09	26.02	32.11	112.27	18.96	Strong
Illuminance	REML	Spherical	46.08	29.54	75.62	21.61	60.94	Moderate

*C_0 – nugget effect; C_1 – contribution; $C_0 + C_1$ – threshold; a – reach; GDE – degree of spatial dependence; t_{bs} – dry-bulb air temperature; RH – air relative humidity; THI – temperature-humidity index; and V_{air} – air velocity.

According to Ferraz et al. (2017a), the nugget effect (C_0) is an important parameter of the semivariogram, since it indicates the unexplained variability. The importance of this parameter is related to the discontinuity check of the semivariograms for distances less than the shortest distance between the collection points, being this discontinuity caused by errors during collection and analysis, local variations, among others, and it is not possible to perform the quantification of each of these components.

The individual quantification of the nugget effect was performed according to the classification suggested by Cambardella et al. (1994). For the variables that compose the thermal environment (t_{bs}, RH, THI and V_{air}), the highest value of C_0 was verified for RH, which presented a value equal to 9.91. However, when the contribution of this one at the level was analysed, it was verified that it was less than 25%, being classified as a strong spatial dependence, in the same way as for t_{bs} and THI. The same condition was not verified for the V_{air} attribute, which, despite having a low C_0 value, was higher than 25% of the plateau, indicating the occurrence of moderate spatial dependence.

The noise variable presented initial variability at 6.06, but its contribution at the level was less than 25%, characterizing a strong spatial dependence. The same condition was not observed for the illuminance, which presented quite high C_0 and with contribution higher than 25% of the plateau, classifying its dependence as moderate.

The determination of the spatial dependence limit was performed from the scope assessment (*a*), which indicates how far a variable is influenced by space. These values, related to semivariograms, are of considerable importance in determining the limit of spatial dependence (Ferraz et al., 2017b).

Samples separated by smaller distances are correlated with one another, allowing interpolations to be performed for smaller spacing than sampling. In this case, if *a* is less than the smallest sample spacing, the semivariogram is constant and equal to any value,

the absence of spatial dependence, and the spatial distribution is completely random, and the geostatistical methods must not be applied (Vieira, 2000).

For all attributes evaluated, the value of *a* was higher than the smaller distance between sampling points, allowing the application of geostatistics techniques in a satisfactory way. The lowest range values *a* were verified for the variables illuminance (21.61 m) and air velocity (22.45 m), which still presented values above the shortest distance between samplings (6.0 m).

All variables evaluated in this study presented different spatial dependence ranges, from lower values, such as 21.61 m, to quite high values, such as 104.71 m. From this information, it can be inferred that it is possible to use larger distances between sampling points. This distance is variable according to the attribute of interest. It is also worth noting that for variables with values *a* closely related to each other, such as t_{bs}, RH and THI, it is possible to use the same sampling mesh.

The results obtained infer that the variables and indexes evaluated did not have a random distribution in the space, since they presented strong or moderate spatial dependence and the superior one to the smaller distance between points sampled, indicating that it is appropriate to apply the geostatistical technique. The occurrence of spatial dependence allows to perform data interpolation using the ordinary kriging technique and to make spatial distribution maps. These maps give important information (Fig. 2), such as the location and magnitude of the areas with the highest and lowest levels of the variables and index evaluated, allowing the precise management of the required interventions (Ferraz et al., 2017b).

The t_{bs} varied throughout the CBP barn (Fig. 2, a), presenting values between 23 and 29 °C. The greatest variation was observed in the region between the evaporative cooling plate (PAD) and the central part of the barn, where there was initially a decrease of t_{bs}, followed by its increase. In general, t_{bs} tends to have lower levels in the area close to the PAD, due to the system for climate control. However, the predominance of remarkably high t_{bs} values was observed, due to the bad side seal related to the presence of a gate located in the entrance of the feed alley, which was damaged, remaining partially open. The infiltration of air (sealing faults) through the sides and parts damaged in this gate, as well as its opening, cause leaks of cooled air and the entrance of outside warm air. This can be the reason for the increase of t_{bs} in this region. Except for this particular condition present near the PAD of the CBP barn, an increase of t_{bs} with the distance of the cooling device was observed, with emphasis on the occurrence of higher levels and greater uniformity in the region near the exhaust fans.

According to Nääs (1989), the air temperature range characterized as a thermal comfort situation for lactating cows is between 4.0 and 24.0 °C and may be restricted to the limits of 7.0 to 21.0 °C, depending on RH and solar radiation. According to Huber (1990), the zone of thermoneutrality for lactating Holstein cows is between 4.0 and 26.0 °C.

Considering the temperature range recommended by Huber (1990), it is verified that t_{bs} inside the CBP barn was above the upper critical temperature limit indicated for lactating Holstein cows, with the most critical conditions in areas close to PAD and the entrance of the feed alley.

A high spatial variability of RH inside the climate controlled CBP barn was observed (Fig. 2, b), with an amplitude of variation equal to 35%. Areas with the highest RH were observed near the PAD, where the levels were predominantly greater than 65%.

It is also worth noting the occurrence of regions with higher RH in the feeding alley. A trend towards lower RH values (> 60% RH) along the entire north-west face of the facility was observed, due to faults in the lateral closure provided by the plastic curtains, as well as the presence of the openings of the gates for access to the lots, necessary for the management of the animals.

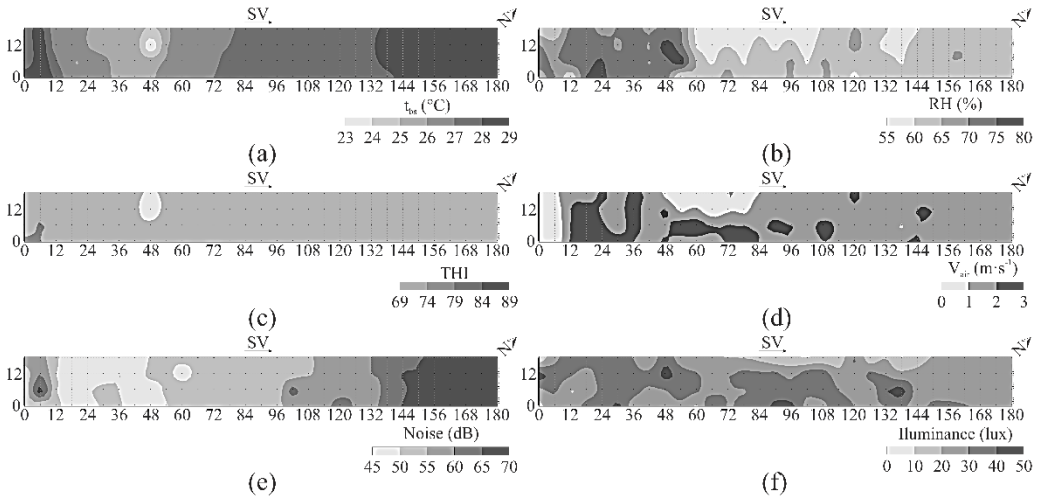

Figure 2. Spatial distribution of the variables: (a) dry bulb air temperature (t_{bs}); (b) relative humidity (RH); (c) Temperature and Humidity Index (THI); (d) air velocity (V_{air}); (e) noise levels and (f) illuminance.

According to Nääs & Arcaro Jr. (2001), the RH value of 70% is considered as the upper limit for cooling an environment for animals through the use of water. Above this value, the heat exchanges between the animals and the environment are impaired, and the animals may suffer from heat stress. Notably in the region close to the PAD, values of RH were close to or even above this limit, indicating that, despite the climate control system, the animals could be exposed to heat stress, not being able to exchange heat with the environment in the form of latent heat.

The THI presented uniform distribution throughout the CBP barn, with the predominance of the condition characterized as alert to the producer (Fig. 2, c). In a small region close to the PAD and the feed alley, the occurrence of a condition characterized as a hazard was observed, due to the combination of the high t_{bs} and RH values verified for this region. The results show that the THI inside the facility is above the required values for lactating Holstein cows, which should be less than 72 (Johnson, 1980).

The air velocity (V_{air}) presented considerable spatial variability inside the CBP barn, with values ranging from 1.0 to 3.0 m s^{-1}, and lower values (< 1.0 m s^{-1}) observed at the locations farthest from the exhaust fans and near the sides of the CBP barn (Fig. 2, d). Since the exhaust fans are the direct source of elevation of the V_{air} within the CBP barn, it is expected that the highest levels of such an attribute can be observed close to the face on which such equipment is installed. The results indicated that the regions with the highest values of V_{air} did not occur in the area near the exhaust fans, but in areas located between the central part of the facility and the PAD, notably near the feed alley

(Fig. 2, d). It can be inferred that its occurrence is due to the formation of preferred paths for the air currents inside the facility, as well as the occurrence of infiltrations of air through the side curtains. The difficult explanation of spatial distribution for this attribute is due to its high spatial and temporal variability, since it can change of magnitude and direction abruptly (Faria et al., 2008).

The noise levels presented considerable spatial variability within the CBP barn (Fig. 2, e), with values ranging from 45 to 70 dB. The results evidenced the increase of the noise levels as it approached the exhaust fans, the highest values being observed in the area immediately next to the face where they were located, allowing to infer that their occurrence is due to the characteristic noise caused by the rotation of the exhaust fans. A small area with higher noise near the PAD (> dB) was also observed, due to the noise caused by the passage of air through the PAD and other external sources.

The results of intensity of illumination showed the occurrence of variation of distribution inside CBP barn, which presented amplitude of variation equal to 50 lux (Fig. 2, f). The illuminance was greater than 20 lux throughout the CBP barn, being less than that value only in the region of the northwest face of the facility. Since the lamps were uniformly arranged inside the facility, a uniform spatial distribution of the illuminance was expected. However, the presence of air deflecting curtains throughout the installation in some cases may act as obstacles to the passage of light and cause lower levels in some places. Also the faults in the lateral closing system, allowing the entrance of solar rays and elevation of the intensity of illumination, can be responsible of the irregular light distribution in the barn.

The spatial distribution maps do not provide detailed numerical information about the area occupied by each class of attributes or indexes. Frequency distribution graphs were generated in order to allow the best characterization of the CBP barn. Fig. 3 shows the frequency distribution graphs of the all variable evaluated in this study.

The t_{bs} was higher than the recommended upper critical limit for lactating cows (26 °C) in 85.6% of the resting area, characterizing a condition of thermal discomfort by heat (Fig. 3, a).

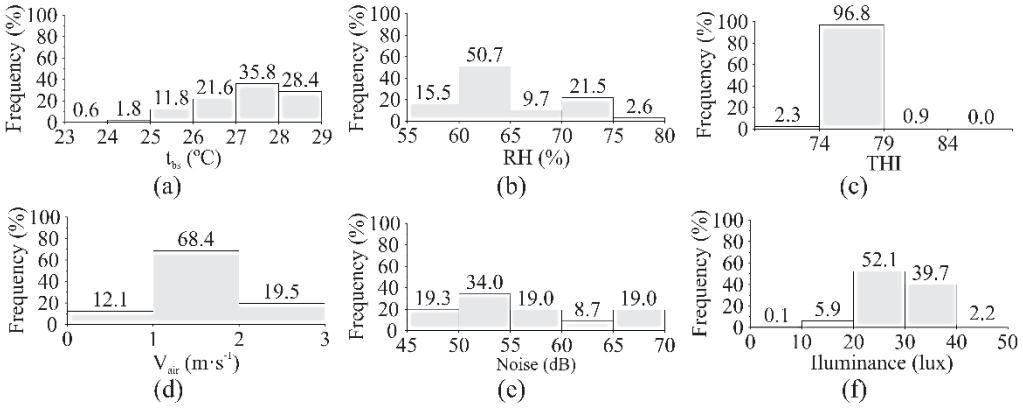

Figure 3. Frequency distribution of the variables: (a) dry bulb air temperature (t_{bs}); (b) relative humidity (RH); (c) Temperature-Humidity Index (THI); (d) air velocity (V_{air}); (e) noise levels; (f) illuminance.

The RH was higher than the recommended upper limit for cooling cows with water (70% RH) in 24.1% of the area, making the dissipation of heat in a latent form difficult. In this area the animals were exposed to heat stress conditions (Fig. 3, b).

According to Fig. 3, c, only 2.2% of the total resting area of the facility presented thermal conditions of adequate comfort (THI < 74); in 96.8%, the environmental attributes indicated the occurrence of alert condition (74 ≤ THI < 79) and in 0.9% a hazard condition (79 ≤ THI <84). The results show that despite the use of the climate control system, in almost the whole area of the barn the environmental conditions were not adequate to the thermal needs of the animals. These results showed that the performance of the animals may be affected by the heat stress and, therefore, measures must be taken to make the environment adequate to the physiological needs of the animals, in order to avoid losses that can go from production drops to death of animals.

The results corroborate with those described by Faria et al. (2008), which, studying the spatial variability of the microclimate in a free-stall with forced ventilation associated with a nebulization system, found values of t_{bs}, RH and THI above the ideal condition comfort.

The V_{air} was between 1.0 and 2.0 m s^{-1} in 68.4% of the resting area, being higher than 2.0 m s^{-1} in 19.5% (Fig. 3d). In general, maintenance of V_{air} at levels of 1.8 m s^{-1} should be ensured in order to allow drying of the bed, removal of gases and favouring the temperature changes between the animal and the environment (Black et al., 2013). Thus, the exhaust fans system used was satisfactory in promoting the increase of the V_{air}, since it guaranteed its maintenance at levels higher than 1.0 m s^{-1} in 87.9% of the resting area.

Fig. 3, e shows that the frequency distribution of noise levels was approximately uniform, given the occurrence of values close to 20% for most classes. It should be noted that in 72.3% of the CBP barn area, noise levels were between 40 and 60 dB, indicating a condition of tranquillity, according to the scale proposed by Bistafa (2006).

The illuminance levels was between 20 and 40 lux, which occupied 91.8% of the CBP barn area, while only 6.0% of the area was below 20 lux (Fig. 3, f).

According to Dahl & Petitclerc (2003), dairy production can be increased by using a daily period of 16 to 18 hours with intensity of 200 lux, regardless of the adopted production system. Considering the value proposed by the authors, the results presented in Fig. 3, f show that the light intensity inside the installation was lower than the recommendations. According to the recommendation of minimum intensity suggested by Harmon & Peterson (2011) and the University of Wisconsin-Madison's Guide to Good Agricultural Practices for Energy Efficiency in Agriculture (Wisconsin Focus on Energy, 2016) for livestock facilities of 20 to 30lux, in general the luminous intensity delivered is in compliance with the recommended minimum values for housed lactating cows.

CONCLUSIONS

The spatial dependence of the variables of the thermal, acoustic and lighting environment was verified by means of the geostatistics technique, with strong spatial dependence predominating.

The spatial distribution maps showed the occurrence of high variability of attributes and indexes within a compost dairy barn (CBP) provided with a climate control system.

The thermal variables, air temperature and relative humidity presented high spatial variability, but their combination returned values of temperature and humidity index (THI) characterized as alert situation throughout practically the entire facility. Also the levels of noise and illuminance had considerable variability, presenting values between 45 and 70 dB, and 10 and 50 lux, respectively.

The geostatistics technique was able to assist the decision making regarding the definition of the pattern of air flow based on exhaust fans for air exchange and air cooling in the CBP barn.

ACKNOWLEDGEMENTS. The authors are thankful to the Federal University of Lavras for this great opportunity; the Brazilian State Government Agency, FAPEMIG; the National Counsel of Technological and Scientific Development (CNPq - Brazil); Federal agency, CAPES, for their financial support.

REFERENCES

Bachmaier, M. & Backers, M. 2008. Variogram or semivariogram? Understanding the variances in a variogram. *Precision Agriculture* **9**, 173–175.

Barberg, A.E., Endres, M.I., Salfer, J.A. & Reneau, J.K. 2007. Performance and welfare of dairy cows in an alternative housing system in Minnesota. *J. Dairy Sci.* **90**(3), 1575–1583.

Bistafa, S.R. 2006. *Acoustics applied to noise control*. São Paulo: Edgard Blücher, 368 pp. (in Portuguese).

Black, R.A., Taraba, J.L., Day, G.B., Damasceno, F.A. & Bewley, J.M. 2013. Compost bedded pack dairy barn management, performance, and producer satisfaction. *J. Dairy Sci.* **96**(12), 8060–8074.

Buffington, D.E., Collier, R.J. & Canton, G.H. 1983.Shade management systems to reduce heat stress for dairy cows in hot, humid climates. *Trans. ASAE* **26**(6), 1798–1802.

Cambardella, C.A., Moorman, T.B., Novak, J.M., Parkin, T.B., Karlen, D.L., Turco, R.F. & Konopka, A.E. 1994. Field scale variability of soil properties in Central Iowa soils. *Soil Sci. Soc. Am. J.* **58**, 1501–1511.

Dahl, G.E. & Petitclerc, D. 2003. Management of photoperiod in the dairy herd for improved production and health. *J. Anim. Sci.* **81**(15), 11–17.

Faria, F.F., Moura, D.J., Souza, Z.M & Matarazzo, S.V. 2008. Spatial variability of the microclimate of a shed used for confinement of dairy cattle. *Ciência Rural* **38**(9), 2498–2505 (in Portuguese).

Ferraz, G.A.S., Silva, F.M., Oliveira, M.S., Custódio, A.A.P. & Ferraz, P.F.P. 2017ª. Spatial variability of plant attributes of a coffee crop. *Revista Ciência Agronômica* **48**(1), 81–91 (in Portuguese).

Ferraz, P.F.P., Yanagi Junior, T.Y., Ferraz, G.A.S. & Damasceno, F.A. 2017b. Spatial distribution of the temperature index of the globe and humidity in chicken shed in the first week of life heated by industrial furnace. *Energ. Agric.* **32**(4), 356–363 (in Portuguese).

Harmon, J.D. & Peterson, D. 2011. Farm Energy: Indoor lighting for livestock, poultry, and farm shop facilities. *Agriculture and Environment Extension Publications*, **32**, 1–4.

Hubbard, K.G., Stooksbury, D.E., Hahn, G.L. & Mader, T.L.A 1999. Climatological perspective on feedlot cattle performance and morality related to the temperature-humidity index. *J. Prod. Agric.* **12**(4), 650–653.

Huber, J.T. 1990. Feeding of high production cows under conditions of thermal stress. *Dairy cattle.* Piracicaba: FEALQ, pp. 33–48 (in Portuguese).

Isaaks, E.H. & Srivastava, R.M. 1989. *An Introduction to Applied Geostatistics.* Oxford University Press, New York, 561 pp.

Janni, K.A., Endres, M.I., Reneau, J.K. & Schoper, W.W. 2007. Compost dairy barn layout and management recommendations. *Appl. Eng. Agric*. **23**(1), 97–102.

Johnson, H.D. 1980. Environmental management of cattle to minimize the stress of climatic change. *Int. J. Biometeorol*. **24**, 65–78.

Leso, L., Conti, L., Rossi, G. & Barbari, M. 2018. Criteria of design for deconstruction applied to dairy cows housing: a case study in Italy. *Agron. Res.* **16**(3), 794–805.

Lobeck, K.M., Endres, M.I., Shane, E.M., Godden, S.M. & Fetrow, J. 2011. Animal welfare in cross-ventilated, compost-bedded pack, and naturally ventilated dairy barns in the upper Midwest. *J. Dairy Sci*. **94**(11), 5469–5479.

Marchant, B.P. & Lark, R.M. 2007. Robust estimation of the variogram by residual maximum likelihood. *Geoderma* **140**, 62–72.

Matheron, G. 1962. *Treaty of applied geostatistics*. Vol. I: Mémoires du Bureau de Recherches Géologiques et Minières, n. 14, Editions Technip, Paris, 333 pp. (in French).

Nääs, I.A. 1989. *Principles of thermal comfort in animal production*. São Paulo, Brazil: Ícone, 183 pp. (in Portuguese).

Nääs, I.A. & Arcaro Jr., I. 2001. Influence of ventilation and spraying on artificial shading systems for lactating cows in hot conditions. *Rev. bras. eng. agríc. ambient*. **5**(1), 139–142 (in Portuguese).

Perissinotto, M., Moura, D.J., Cruz, V.F., Souza, S.R.L., Lima, K.A.O. & Mendes, A.S. 2009. Thermal comfort of dairy cattle confined in subtropical and Mediterranean climates by the analysis of physiological parameters using the fuzzy set theory. *Ciência Rural* **39**, 1492–1498 (in Portuguese).

R Development Core Team. 2016. R: a language and environment for statistical computing. R Foundation for Statistical Computing, Vienna, Austria. *http://www.R-project.org/*. Accessed 22.10.2017.

Ribeiro Junior, P.J. & Diggle, P.J. 2001. GeoR: a package for geostatistical analysis. *R-News* **1**, 14–18.

Sá Júnior, A., Carvalho, L.G., Silva, F.F. & Alves, M.C. 2012. Application of the Köppen classification for climatic zoning in the state of Minas Gerais, *Brazil. Theor. Appl. Climatol*. **108**(1–2), 1–7.

Sales, F.A., Barbosa Filho, J.A.D., Aquino, T.M.F., Brito, I.F. & Carvalho, L.E. 2011. Environmental monitoring of the horizontal profile of a shed for pigs, in the gestation phase, using precision livestock farming. *Revista Científica de Produção Animal* **13**(1), 7–12 (in Portuguese).

Shane, E.M., Endres, M.I. & Janni, K.A. 2010. Alternative bedding materials for compost bedded pack barns in Minnesota: a descriptive study. *Appl. Eng. Agric*. 26(3) 465–473.

Thom, E. 1959. The discomfort index. *Weatherwise* **12**(1), 57–60.

Vieira, S.R. 2000. Geostatistics in studies of soil spatial variability. In: NOVAIS, R.F. et al. (eds): *Tópicos em ciência do solo*. Viçosa: Sociedade Brasileira de Ciência do Solo, v.1, pp. 1–54 (in Portuguese).

Wisconsin Focus on Energy. 2016. *Energy Efficiency Best Practices Guide: Agriculture*. Madison: University of Wisconsin–Madison, 74 pp.

Yamamoto, J.K. & Landim, P.M.B. 2015. *Geostatístics: concepts and applications* (Geoestatística: conceitos e aplicações). Oficina de textos, São Paulo, Brazil, 215 pp. (in Portuguese).

Agronomy Research **17**(2), 396–407, 2019
https://doi.org/10.15159/AR.19.063

The effect of Minituber Weight on their Field Performance under a Northern European environment

I. Dimante[1,2,*], I. Mežaka[2] and Z. Gaile[1]

[1]Latvia University of Life Sciences and Technologies, Faculty of Agriculture, Liela street 2, LV 3001 Jelgava, Latvia
[2]Institute of Agricultural Resources and Economics, Zinatnes street 2, LV 4126 Priekuli, Latvia
[*]Correspondence: ilze.dimante@arei.lv

Abstract. Weight of potato minitubers as well cultivar affects field performance of minitubers. The aim of this study was to compare minitubers of four weight classes (MtC) (3 to 4.99 g, 5 to 9.99 g, 10 to 19.99 g, and > 20 g) with respect to their field performance. Three year experiments were conducted at AREI, Latvia (57°19′ N, 25°20′ E) between 2014 and 2016. Cultivars 'Monta', 'Prelma' and 'Mandaga' were used. A significant relationship between the number of stems and the number of progeny tubers per plant was detected and the number of stems explained 74% of variation in progeny tuber number. Multiplication rate, expressed as the number of progeny tubers > 25 mm per planted minituber, was in range from 4.2 to 13.1 tubers and was significantly affected by the cultivar and MtC. Cultivar and MtC had significant effect on the number of tubers and tuber yield per m^2. The number of progeny tubers and yield increased with increases for MtC. The highest number of progeny tubers (size > 25 mm) per m^2 were obtained from minitubers > 20 g of 'Prelma' (93.4), but the highest yield was from minitubers > 20 g of 'Mandaga' (4.92 kg m^{-2}). The effect of MtC was more pronounced on number of tubers than on tuber yield. Cultivar and MtC determined mean size (diameter (μ)) of progeny tubers. Mean size increased as MtC decreased. MtC had a significant effect on standard deviation (σ) only for 'Prelma'. When σ was recalculated to coefficient of variation (*CV*), no significant effect of MtC remained.

Key words: multiplication rate, seed potato, tuber yield, tuber size distribution.

INTRODUCTION

Nowadays seed potato (*Solanum tuberosum* L.) programmes worldwide include production of small tubers called minitubers that are grown from *in vitro* derived potato plantlets (Struik, 2007). That is the initial stage of seed potato production performed under protected environments. Depending on production technology, minitubers differ in their size or weight. The size of planted minitubers can significantly influence their performance in the field (Struik & Lommen, 1999; Barry et al., 2001). Therefore, it is important to determine the minimal feasible minituber weight to have acceptable field performance when further multiplied in the field under particular conditions.

Potato yield is determined by multiple factors: the number of plants per unit area, the number of tubers produced by one plant and by the average weight of progeny tubers (Struik & Lommen, 1999).

The number of tubers per plant is affected by number of stems per plant (Knowles & Knowles, 2006) which in turn affects stem density per unit area. Bigger seed tubers produce more stems (Wurr et al., 2001) and it leads to more progeny tubers per plant (Knowles & Knowles, 2006; Bussan et al., 2007). The association between heavier tubers and larger number of stems has been observed on minitubers as well (Ozkaynak & Samanci, 2006; Dimante & Gaile, 2018).

Many authors investigating field performance of minitubers have reported significant differences between cultivars with respect to the number of tubers, yield and average weight of progeny tubers (Karafyllidis et al, 1997; Gopal et al., 2002; Radouani & Lauer, 2015; Rykaczewska, 2016; Fulladolsa et al., 2018). Cultivar can influence whether size or weight of minitubers will affect yield of progeny tubers. For example, for cultivar 'Nicola' the size of minitubers did not affect total tuber number and yield, whereas a significant effect of the size of minitubers on these variables were observed for 'Russet Burbank' (Radouani & Lauer, 2015).

For seed potato multiplication purposes it is probably more important to know multiplication rate expressed as the number of progeny tubers above a certain weight per plant than the weight produced per seed tuber (Lommen & Struik 1995). The number of progeny tubers determines replantable area or seed potential of planted minitubers. Seed potential is defined as an area (e.g. ha^{-1}) that can be replanted by seed that has been produced at unit area (e.g. ha^{-1}) planted with minitubers (Rykbost & Charlton, 2004).

Tuber size is one of the main aspects that determine yield quality (Haverkort & Verhagen, 2008). The size of marketable tubers depends on the intended use. As marketable yield is always lower than the total yield, mean tuber size and low variation in this parameter is very important not only in potato production for processing or table consumption, but also for seed potatoes. Low variation of tuber size is especially desirable. Thus due to the sizing requirements limiting minimum and maximum tuber size within a lot, low variation in tuber size can benefit minimizing certification expenses because the yield could be certified as one lot.

Many factors determine tuber size distribution of the yield. Most of them, such as number of stems per plant and the rate of crop growth, are difficult to manipulate. One of the most controllable factors is seed size (Struik et al., 1990).

Many approaches have been used in the previous studies to show tuber size distribution. Probably the most common approach is when the yield (or tuber number) of a particular grade of tubers is expressed as percentage (Georgakis et al., 1997; Fulladolsa et al., 2018) or proportion to the total yield (Bussan et al., 2007; Oliveira et al., 2017). Blauer et al. (2013) applied polygonal plots for graded yield and compared the effect of treatments on tuber size distribution. The approach developed by Travis (1987) is considered to be a very straightforward model for comparison of different field experiments. The method allows to compare results and is especially useful when different units or different size grades of the yield have been used (Wurr et al., 1993). The model of Travis (1987) allows calculation of mean size (μ) and standard deviation (σ) measuring the spread of yield across the size grades.

Little published data exists on productivity of plants from minitubers in the Northern Europe and particularly of Baltic States. Minitubers are planted relatively late

(in the second part of May) in the region and growing season is relatively short. Ware potato growing habits in Baltics limit seed potato production because heavy virus pressure occurs almost every growing season. Good field performance of minitubers can favour decreasing the field generations needed for the seed multiplication and thus help maintain acceptable health status of seed potato. As a result, availability of the locally bred cultivars can be improved.

This study was conducted in a Northern European environment using three Latvian origin varieties differing in maturity class to investigate field performance of minitubers with focus on the impact of the weight class of minitubers.

MATERIALS AND METHODS

Experiments were conducted for three growing seasons (2014–2016) in the Priekuli Research Centre (PRC) at the Institute of Agricultural Resources and Economics, Latvia (57°19′ N, 25°20′ E). Cultivars bred in PRC ('Monta' – early, 'Prelma' – medium early and 'Mandaga' – medium late) were used in the study.

Minitubers were grown from *in vitro* plantlets in greenhouses at PRC and harvested in August on average 78 days ('Monta' and 'Prelma') to 92 days after planting ('Mandaga'). The storage period of obtained minitubers was nine months including seven months in cold storage (3 °C). Minitubers were de-sprouted two weeks before planting in the field and then pre-sprouted under diffused natural light.

Minitubers of four weight classes (MtC) 3.00 to 4.99 g, 5.00 to 9.99 g, 10.00 to 19.99 g, and > 20 g were hand planted on 15 May 2014, 19 May 2015 and 16 May 2016.

The content of organic matter in the soil was low to optimal. Availability of phosphorus and potassium in the soil was medium to high (Table 1). Fertilizers were applied to the experimental field one week before planting at the rate of 60 kg.

Table 1. Characteristics of the soil at the study site, 2014–2016

Indices	2014	2015	2016
Soil	Sod-podzolic loamy sand		
Soil pH KCl	4.5	5.0	5.3
Organic matter content,%	2.1	2.1	1.8
K_2O mg kg^{-1}	189	142	143
P_2O_5 mg kg^{-1}	164	150	120
Pre-crop	winter cereals		

N ha^{-1}, 55 kg P_2O_5 ha^{-1} and 90kg K_2O ha^{-1}. Deep tillage (25–26 cm) was performed after the broadcasting of the fertilizers. Plant protection measures were aligned with the integrated pest management practice.

A split-plot design was used for the study. Weight classes of minitubers were randomized as sub-plots within the cultivars as main plots. Three replications were applied in 2014 and four replications in 2015 and 2016. The distance between rows was 0.7 m. In-row spacing between planted minitubers was 0.2 m. In each sub-plot 48 minitubers (12 tubers × 4 rows) were planted. Plants from two outer rows as well as one plant at the beginning and one at the end of each inner row were excluded from the yield assessment to minimize the effects of plant competition between plots with different treatments and to exclude the border effect.

The overall meteorological conditions at the location of the conducted experiments are shown in Table 2.

Table 2. Meteorological conditions in Priekuli, long term average and 2014–2016

Period	Average air temperature, °C				Sum of precipitation, mm			
	LTA*	2014	2015	2016	LTA*	2014	2015	2016
Last 10 days of May	13.2	15.5	11.6	16.6	21.1	36.5	24.3	0.5
June	14.9	13.5	14.3	16.4	81.2	108.3	39.4	144.5
July	17.5	19.5	15.9	17.9	86.0	76.5	91.5	109.5
First 10 days of August	17.7	21.8	19.1	16.7	24.5	30.2	16	54.5
Last 20 days of August	15.7	14.4	17.1	16.1	57.1	128	8.1	121.3

*LTA is long term (1981–2010) average.

In 2015 and 2016 air temperature of the end of May exceeded the long term average (LTA) thus promoting emergence of the plants. After the warm beginning of the season, cooler weather followed in the last 20 days of June 2014 (3.1 °C below the LTA). In the same period of 2016 the air temperature was close to the norm. The precipitation was unevenly distributed across the growing season in these two years. In the last 20 days of June 2014 and the first 10 days of July the sum of the precipitation reached 169 to 222% of the average from long term data. In the last 20 days of July 2014 less than average rain was recorded (43 to51%). Precipitation in August 2014 again exceeded long term average data and prolonged rain periods burdened the harvesting. In 2016 precipitation exceed the long term data in all periods of the growing season except the last 10 days of July. Heavy rain fell (58 mm) over 24 hours at the end of June 2016. Despite of the optimal air temperature, canopy closure was slowed down because of the water logging in the field. However, further conditions favoured yield formation.

The situation in 2015 was slightly different. Plant emergence from minitubers was considerably delayed as a result of low air temperatures at the end of May and dry conditions (7 mm of precipitation in the first 20 days of June) later in first part of June. In the last 10 days of June 2015 the amount of precipitation increased, thus favouring canopy development of the plants and weather conditions were favourable for yield formation.

In 2014 cultivars ‘Monta’ and ‘Prelma’ were harvested on August 14 and 15 (91 and 92 days after planting), cultivar ‘Mandaga’ was harvested on September 4 (112 days after planting). Harvest time was influenced by the meteorological conditions as described above. In 2015 and 2016 ‘Monta’ and ‘Prelma’ were harvested in the first days of August and the length of vegetation season for these cultivars was 78 to 80 days, whereas vegetation season for ‘Mandaga’ was 94 to 98 days.

Tubers from each individual plot were harvested by hand and then graded in the following size grades (TSG): < 25 mm, 25–35 mm, 35–45 mm, 45–55 mm, > 55 mm by passing tubers through a square mesh hand grader. Yield and the number of tubers per size grade were determined.

Multiplication rate was calculated as the number of tubers > 25 mm (the minimal size of potato seed according to UNECE standard S-1 seed potatoes) derived from each planted minituber.

Analysis of variance (ANOVA) using R studio running against R version 3.2.5 was applied to determine the effects of two main factors – cultivar and MtC. Differences between the treatments were compared using Tukey’s HSD test ($\alpha = 0.05$).

A linear regression was performed to relate progeny tuber number to number of above ground stems as well as to relate mean weight of progeny tuber to total tuber number per m^2.

Data on tuber numbers and total weight per size grade were used for the determination of tuber size distribution according to Travis (1987).

To uncover the variance and mean of the grouped data the formulas (1) and (2) were used:

The mean was calculated as

$$\bar{\mu} = \sum \frac{f\mu}{n} \quad (1)$$

Variance, denoted by σ was defined as

$$\sigma = \sqrt{\frac{\sum f(\mu - \bar{\mu})^2}{n}} \quad (2)$$

Where σ is standard deviation, $\bar{\mu}$ is the mean, μ stands for each data value in turn, and f is the frequency with which data value μ, occurs, n is data-set extent.

The means and variances were calculated for individual plots and then obtained values were subjected to analysis of variance (ANOVA) to verify if variety and MtC have significant impact on mean and variance of progeny tuber size.

RESULTS AND DISCUSSION

Relation between stem number and progeny tuber number

In our previous research, significantly more above ground stems were produced by the heavier minitubers (Dimante & Gaile, 2018). Linear regression analysis revealed a highly significant ($P < 0.001$) relationship between the number of stems and the number of progeny tubers per plant (Fig. 1).

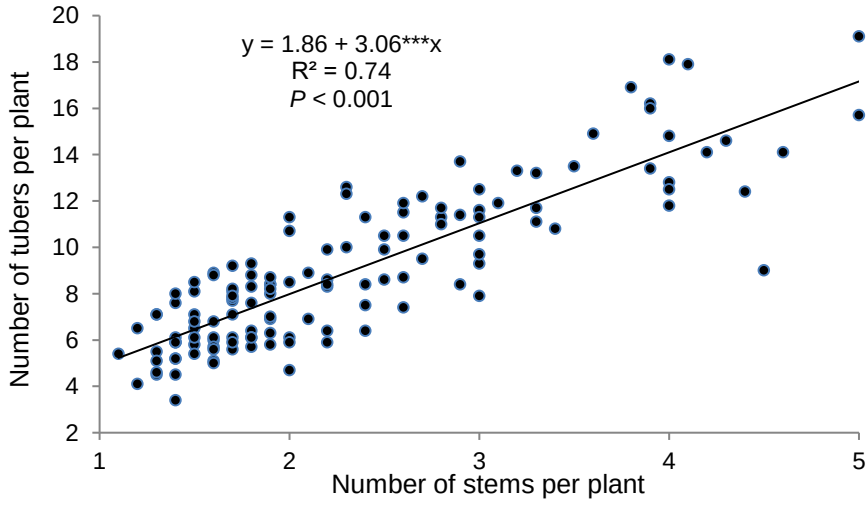

Figure 1. Relationship between number of tubers and number of stems per plant.
*** Significant at 0.001 probability level by *t*-Test.

The number of progeny tubers per plant increased by 3.06 units as a result of an increase in stem number by 1 unit per plant. The obtained regression trend for minitubers is in line with the data reported previously by Knowles & Knowles (2006), Bussan et al. (2007) and Goeser et al. (2012) which found that increases in stem number significantly increased number of tubers per plant for conventional seed potato. Furthemore, in our research, number of stems explained 74% of variation in tuber number in comparison with 55% obtained by Bussan et al. (2007).

Multiplication rate

Multiplication rate-expressed as the number of progeny tubers > 25 mm obtained from one planted minituber was affected by both the cultivars ($P < 0.001$) and MtC ($P < 0.001$). Cultivar by MtC interaction was significant too ($P < 0.001$). For all cultivars, the largest MtC produced significantly higher number of seed tubers (> 25 mm) per plant. No significant differences were found between the two smallest MtC (Fig. 2). However, the pattern of the increase of multiplication rate with increases of MtC was different for the studied cultivars.

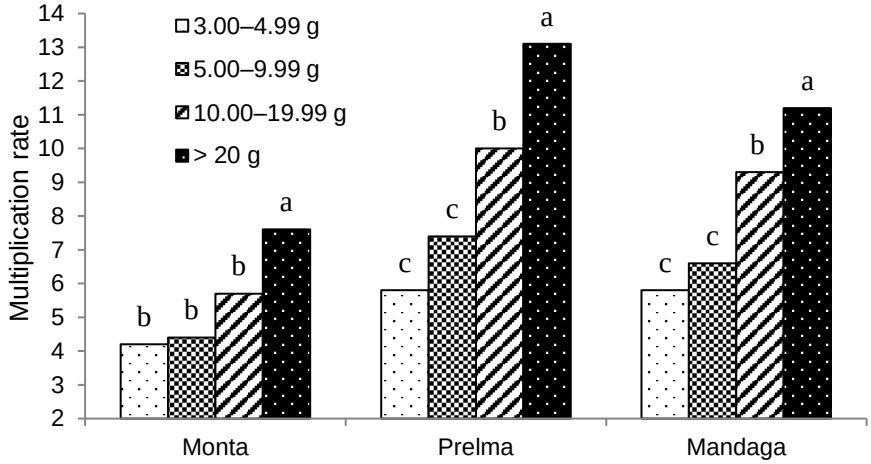

Figure 2. Number of progeny tubers of size > 25 mm obtained from one planted minituber (multiplication rate) depending on weight class of minituber.
Different letters indicate significant differences ($P < 0.05$) between MtC within cultivar by Tukey's test ($P < 0.05$).

The increase of multiplication rate for cultivar 'Monta' was the least pronounced. The lightest MtC produced 4.2 tubers of size > 25 mm, while 7.6 seed size tubers per plant were obtained from MtC > 20 g. Only the latter MtC significantly ($P < 0.001$) differed from other classes.

Minitubers from the lightest class of cultivars 'Prelma' and 'Mandaga' had the same multiplication rate: 5.8 tubers of size > 25 mm. Multiplication rate of 'Prelma' had a tendency to have relatively more pronounced increase compared with 'Mandaga'. The gap between MtC continued to increase until the heaviest MtC. This resulted in the highest multiplication rate among all treatments – 13.1 progeny tubers were produced per one minituber > 20 g from cultivar 'Prelma'. 'Mandaga' had significant increase of

multiplication rate with increase of MtC as well, however, the magnitude of increase slightly declined between the two heaviest MtC.

Dimante & Gaile (2018) observed significantly lower emergence rate of 'Monta' in comparison with 'Prelma' and 'Mandaga'. Averaged across the years and MtC, emergence rate of 'Monta' was 87%. However, the low emergence rate of this cultivar only partially explains the low multiplication rate. When we recalculated multiplication rate to the number of progeny tubers > 25 mm per emerged tuber, it still remained relatively low, ranging from 5.4 to 8.3 progeny tubers per emerged plant. However, the approach when multiplication rates have been calculated as progeny tubers per emerged tuber demonstrates the potential of the cultivar.

The results obtained in our research agree with those published by the other authors (Barry et al., 2001; Gopal et al., 2002; Ozkaynak & Samanci, 2006; Wrobel, 2015). Moreover, as we used only progeny tubers of size > 25 mm for calculation of the multiplication rate, we can assume that this parameter is even higher, especially minitubers > 20 g of the cultivar 'Prelma' had an exceptionally high multiplication rate.

The number of progeny tubers and their yield

The number of progeny tubers and tuber yield per m^2 was significantly affected by the cultivar ($P < 0.001$) and MtC ($P < 0.001$). The interaction between the main factors was significant for number of progeny tubers ($P < 0.001$). Yield data of progeny tubers (all tubers and those of size above 25 mm) did not interact significantly between the main factors ($P = 0.542$ and $P = 0.545$ respectively). The data in Table 3 shows an increase of all variables with the increases of MtC and this trend is generally consistent with findings of other authors (Struik & Lommen, 1999; Barry et al., 2001; Ozkaynak & Samanci, 2006; Radouani & Lauer, 2015).

Table 3. Number of progeny tubers and tuber yield produced by minitubers of four weight classes (MtC), 2014–2016

Variable	Weight class of minitubers, g	Cultivar			*Mean of MtC*
		Monta	Prelma	Mandaga	
Number of progeny tubers per m^2	3.00–4.99	$34.10^{b\,B}$	$46.80^{c\,A}$	$45.10^{c\,A}$	42.00^{c}
	5.00–9.99	$35.70^{b\,B}$	$59.50^{c\,A}$	$51.40^{c\,A}$	48.90^{c}
	10.00–19.99	$47.30^{ab\,B}$	$82.10^{b\,A}$	$73.80^{b\,A}$	67.70^{b}
	> 20.00	$62.30^{a\,B}$	$109.50^{a\,A}$	$92.40^{a\,A}$	88.10^{a}
Tuber yield, kg m^{-2}	3.00–4.99	$2.08^{b\,C}$	$2.90^{c\,B}$	$3.82^{bc\,A}$	2.930^{b}
	5.00–9.99	$2.16^{b\,B}$	$3.54^{bc\,A}$	$3.75^{c\,A}$	3.15^{b}
	10.00–19.99	$2.80^{ab\,B}$	$4.02^{ab\,A}$	$4.73^{ab\,A}$	3.85^{a}
	> 20.00	$3.16^{a\,B}$	$4.78^{a\,A}$	$4.98^{a\,A}$	4.30^{a}
Number of progeny tubers of size > 25 mm per m^2	3.00– 4.99	$30.20^{b\,B}$	$41.10^{c\,A}$	$41.20^{c\,A}$	37.50^{c}
	5.00– 9.99	$31.20^{b\,B}$	$53.00^{c\,A}$	$46.70^{c\,A}$	43.70^{c}
	10.00–19.99	$40.50^{b\,B}$	$71.30^{b\,A}$	$66.50^{b\,A}$	59.40^{b}
	> 20.00	$54.30^{a\,B}$	$93.40^{a\,A}$	$80.00^{a\,A}$	75.90^{a}
Tuber of size > 25 mm yield, kg m^{-2}	3.00–4.99	$2.05^{b\,C}$	$2.85^{c\,B}$	$3.79^{bc\,A}$	2.90^{b}
	5.00–9.99	$2.12^{b\,B}$	$3.49^{bc\,A}$	$3.71^{c\,A}$	3.11^{b}
	10.00–19.99	$2.76^{ab\,B}$	$3.95^{ab\,A}$	$4.70^{ab\,A}$	3.80^{a}
	> 20.00	$3.11^{a\,B}$	$4.69^{a\,A}$	$4.92^{a\,A}$	4.24^{a}

Means within variable in the same column followed by different lowercase letter and means in the same row followed by different capital letter are significantly different by Tukey's test ($P < 0.05$).

However, in some studies the results are not that straightforward. For example Karafyllidis et al. (1997) in a study conducted in Greece with four sizes of minitubers concluded that only minitubers of size below 10 mm were unsuitable for field planting as they produced significantly less tubers and yield than those which size was between 10 and 25 mm. Additionally Radouani & Lauer (2015) found even decrease in number of progeny tubers and insignificant increase of the yield as a result of increase in planted minituber weight for the cultivar 'Nicola'.

Significant differences between the two smallest MtC (3.00–4.99 g and 5.00–9.99 g) according the number of progeny tubers and tuber yield were not observed in the present study for all cultivars. The highest number of progeny tubers per m^2 were produced by the cultivar 'Prelma'. Although minitubers of cultivar 'Mandaga' produced less tubers, the obtained yield was higher than that of 'Prelma', though insignificantly.

The most pronounced relative increase of number of progeny tubers and tuber yield per m^2 with increase of MtC was observed for cultivar 'Prelma'. Thus from MtC > 20.00 g we obtained 2.3 times more progeny tubers and 1.6 times higher yield (kg m^{-2}) than from MtC 3.00–4.99 g. In comparison, the number of progeny tubers for cultivar 'Monta increased only 1.8 times, which was the smallest increase between cultivars, whereas 'Mandaga' had the smallest increase of tuber yield (1.3 times).

In general the obtained results show more pronounced effect of MtC on number of progeny tubers than on tuber yield. This can be explained by the decrease of mean weight of progeny tubers in plots with higher number of progeny tubers (Knowles & Knowles, 2006; Bussan et al., 2007; Blauer et al., 2013). In our study the relationship between the number of tubers per m^2 and mean weight of tubers (g) was significant ($R^2 = 0.31$; $P < 0.001$). In a study by Rykaczewska (2016), a decrease in the mean weight of tubers resulted in insignificant differences of progeny tuber yield between sizes of minitubers, while in our study we still observed a significant effect of MtC on progeny tuber yield (Table 3).

Tuber yield obtained from the smallest MtC of 'Mandaga' exceeded the yield obtained from the biggest MtC of 'Monta'. Low tuber numbers and yield of cultivar 'Monta' can be a result of low emergence rate which was on average 87% over all MtC (Dimante & Gaile, 2018).

Despite the short growing season, number of progeny tubers per m^2 and tuber yield per m^2 in the present research was similar to those in other studies with longer growing seasons and even exceeded some of the previously published data. Thus Radouani & Lauer (2015) obtained 44–63 tubers and the yield was 1.63–5.8 kg m^{-2} under 120 days of vegetation season in Morocco. Besides, relatively big minitubers in the range of 15–60 g were used in the study. Rykaczewska (2016) investigated field performance of conventionally grown minitubers of size 15–22 g under 144–147 days of vegetation season in Poland. In the study, 68–71 progeny tubers were obtained per m^2 and yield was 2.90 to 5.3 kg m^{-2}. In Turkey, Ozkaynak & Samanci (2006) used minitubers of three weight classes (6–8 g, 8–16 g and 16–18 g) and reported only 1.3–1.5 kg of progeny tubers per m^2 harvested 88 to 102 days after planting. The investigation conducted by Barry et al. (2001) in Ireland with an unspecified length of growing season showed 33.2–53.5 progeny tubers m^{-2}.

Results of our study suggest considerable potential to obtain high yields and numbers of progeny tubers in our region despite of the late planting and short growing season.

Progeny tuber size distribution

Progeny tuber size distribution was expressed in kilos per m^2 per each mm progeny tube size (Fig. 3).

The common pattern for all cultivars was that yield of progeny tubers from minitubers > 20 g was approximately normally distributed. As MtC decreased, a shift of the size distribution towards higher yield proportion of larger tubers was observed. Knowles & Knowles (2006) observed similar shift in tuber size distribution for plots where conventional seed potatoes produced less stems. Acquired relationship can be attributed to our results as less stems were produced by smaller minitubers.

Mean tuber size (μ) was significantly affected by the cultivar and MtC ($P < 0.001$). There was no significant interaction between the treatments ($P = 0.470$). The effect of MtC on standard deviation of tuber size (σ) was significant ($P < 0.01$) too, whereas no significant effect of the cultivar ($P = 0.188$) and no significant cultivar by MtC interaction was observed ($P = 0.340$).

The only cultivar showing a significant effect of MtC on σ ($P < 0.05$) was 'Prelma'. Smaller MtC had larger values of tuber size (μ) expressed in mm. The increase of μ values led to an increase in variability of tuber size (σ). According to Wurr et al. (1993), a positive relation between σ and μ exists. This relation was also found in the case of 'Prelma'. Wurr et al. (1993) suggested use of coefficient of variation (CV) as more stable measure of variability. Following the suggestion of Wurr et al. (1993), we recalculated variability to CV, and the effect of MtC was not more significant ($P = 0.354$). Overall, the calculated value of CV ranged between 17 and 19% across all treatments and variation of progeny tuber size did not depend on MtC. As a result, the yield obtained from every single MtC was quite uniform in terms of the tuber size. This suggests good potential for obtaining a high proportion of marketable yield.

Georgakis et al. (1997) expressed tuber size distribution as a percentage and found that the size of minitubers did not affect the size distribution of progeny tubers. For all cultivars and minituber sizes, > 50% of progeny tubers were in range of 25–50 mm. However, the proportion of undersized tubers (< 25 mm) was quite high, and depending on cultivar and planted minituber size, it ranged from 15 to 41%. These results can hardly be compared to ours as the proportion of progeny tubers smaller than 25 mm was below 15% for all treatments used in our study. In addition, the proportion of undersized progeny tubers tended to be lower in plots planted with the lightest classes of minitubers (data not shown). Fulladolsa et al. (2018) compared minitubers and conventional tubers with respect to the tuber size distribution. The obtained results on effects of seed source on progeny tuber size distribution were not convincing over years, however, the proportion of undersized and standard sized progeny tubers obtained from minitubers (i.e. smaller seed) was higher than that from conventional tubers (i.e. larger seed). These findings are not consistent with results of our research, as the proportion of larger tubers increased with decrease of MtC (i.e. seed size). Fulladolsa et al. (2018) explained that these minitubers produced significantly more culls that were discarded from the total yield.

The data on the number and yield of progeny tubers and their size distribution can help estimate the appropriate amount and size of minitubers that are necessary to obtain certain yield level of desired size of progeny tubers.

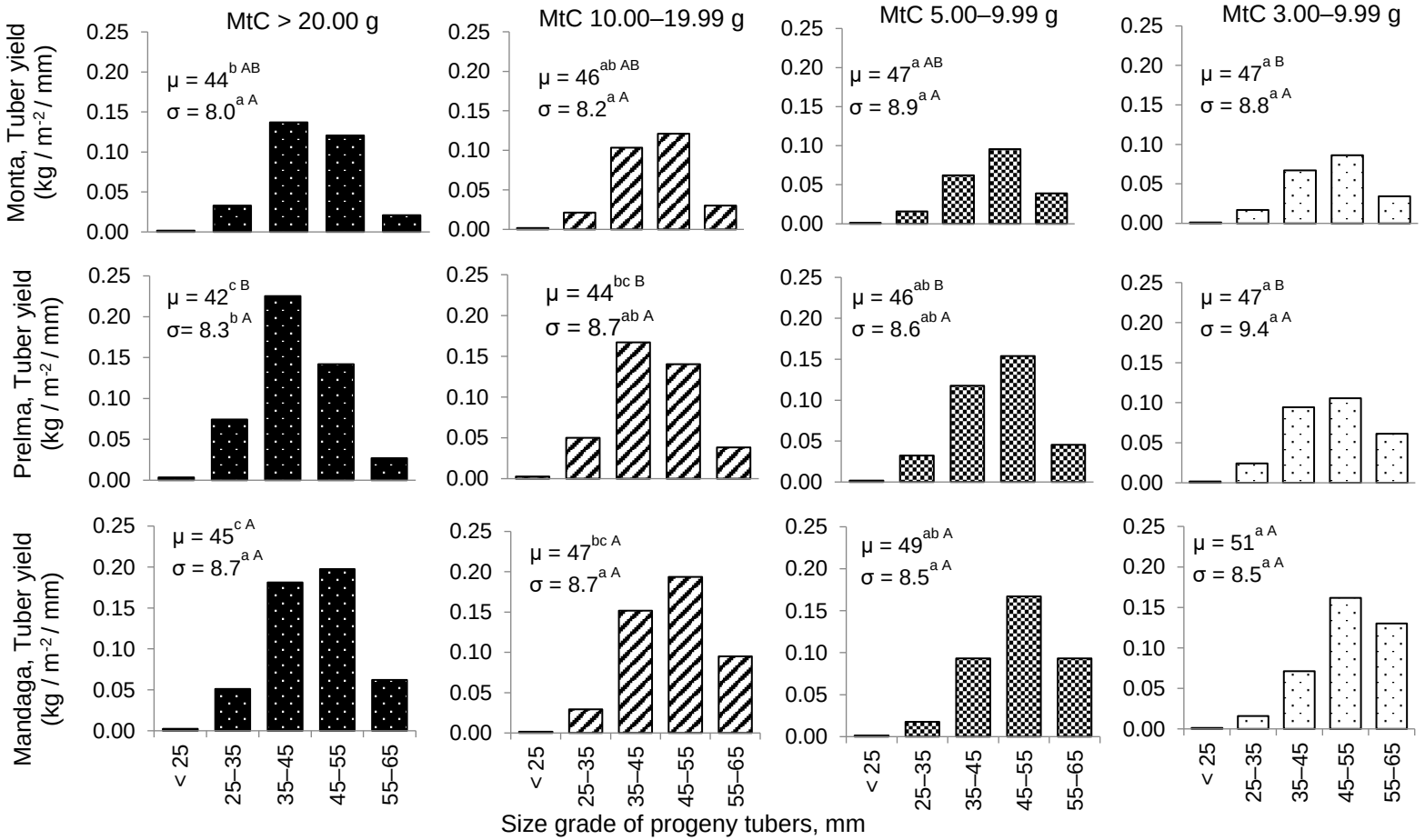

Figure 3. Progeny tuber size distribution depending on weight class of planted minituber (MtC) and cultivar.

μ – mean tuber size; σ – standard deviation of tuber size; Means within cultivar and between MtC followed by different lowercase letter and means within MtC between cultivars followed by different capital letter are significantly different by Tukey's test ($P < 0.05$).

CONCLUSIONS

The choice of cultivar and weight class of planted minituber (MtC) significantly affected field performance variables such as yield, the number of progeny tubers, multiplication rate, and tuber size distribution.

The larger was the planted minituber, the higher yield and more progeny tubers were obtained. However, the magnitude of increase in the yield and number of progeny tubers between MtC significantly depended on the cultivar. The decrease of the mean weight of progeny tubers in plots with higher number of progeny tubers resulted in more pronounced effect of MtC on number of progeny tubers than on tuber yield. The magnitude of increase of multiplication rate was also cultivar-dependent. Mean size (μ) of progeny tubers significantly increased as MtC decreased, but the standard deviation (σ) measuring the spread of yield across the grades was significantly affected by MtC only for the cultivar 'Prelma'. Furthermore, coefficient of variation as relative measure of variability was not MtC-dependent.

Results of our study suggested considerable potential for obtaining high yields and numbers of progeny tubers in our region despite of the late planting and short growing season. Relatively low variation of mean tuber size of progeny tubers within each treatment was detected and no effect of MtC was observed. These findings show potential to obtain a high proportion of marketable yield from minitubers with weight over 3 g and to grade the greatest part of the yield into one seed lot.

ACKNOWLEDGEMENTS. The authors thank Dr. agr. Ilze Skrabule for her great support in organizing the field trials and valuable advices during data assessment. We greatly acknowledge the role of Potato tissue culture laboratory technical staff in growing of minitubers and in assistance during the field trials and data collection.

REFERENCES

Barry, P., Clancy, P.C. & Molloy, M. 2001. The effect of seed size and planting depth on the yield of seed potatoes grown from minitubers. *Irish Journal of Agricultural and Food Research* **40(**1), 71–81.

Blauer, J.M., Knowles, L.O. & Knowles, N.R. 2013. Manipulating stem number, tuber set and size distribution in specialty potato cultivars. *American Journal of Potato Research* **90**(5), 470–496.

Bussan, A.J., Mitchell, P.D., Copas, M.E. & Drilias, M.J. 2007. Evaluation of the effect of density on potato yield and tuber size distribution. *Crop Science* **47**(6), 2462–2472.

Dimante, I. & Gaile, Z. 2018. Assessment of potato plant development from Minitubers. *Agronomy Research* **16**(4), 1630–1641.

Fulladolsa, A.C., LaPlant, K.E., Groves, R.L. & Charkowski, A.O. 2018. Potato plants grown from minitubers are delayed in maturity and lower in yield, but are not at a higher risk of potato virus Y infection than plants grown from conventional seed. *American Journal of Potato Research* **95**(1), 45–53.

Georgakis, D.N., Karafyllidis, D.I., Stavropoulos, N.I., Nianiou, E.X. & Vezyroglou, I.A. 1997. Effect of planting density and size of potato seed-minitubers on the size of the produced potato seed tubers. *Acta Horticulturae* **462**, 935–942.

Goeser, N.J., Mitchell, P.D., Esker, P.D., Curwen, D., Weis, G. & Bussan, A.J. 2012. Modeling Long-Term Trends in Russet Burbank Potato Growth and Development in Wisconsin. *Agronomy* **2**(4), 14–27.

Gopal, J., Kumar, R. & Kang, G.S. 2002. The effectiveness of using a minituber crop for selection of agronomic characters in potato breeding programmes. *Potato Research* **45**, 145–151.

Haverkort, A.J. & Verhagen, A. 2008. Climate change and its repercussions for the potato supply chain. *Potato Research* **51**(3–4), 223–237.

Karafyllidis, D.I., Georgakis, D.N., Stavropoulos, N.I., Nianiou, E.X. & Vezyroglou, I.A.1997. Effect of planting density and size of potato seed-minitubers on their yielding capacity. *Acta Horticulturae* **462**, 943–950.

Knowles, N.R. & Knowles, L.O. 2006. Manipulating stem number, tuber set, and yield relationships for northern- and southern-grown potato seed lots. *Crop Science* **46**(1), 284–296.

Lommen, W.J.M. & Struik, P.C. 1995. Field performance of potato minitubers with different fresh weights and conventional seed tubers: Multiplication factors and progeny yield variation. *Potato Research* **38**(2), 159–169.

Oliveira, J.S., Brown, H.E., Gash, A. & Moot, D.J. 2017. Yield and weight distribution of two potato cultivars grown from seed potatoes of different physiological ages. *New Zealand Journal of Crop and Horticultural Science* **45**(2), 91–118.

Ozkaynak, E. & Samanci, B. 2006. Field performance of potato minituber weights at different planting dates. *Archives of Agronomy and Soil Science* **52**(3), 333–338.

Radouani, A. & Lauer, F.I. 2015. Field Performance of Cultivars Nicola and Russet Burbank Micro and Minitubers. *American Journal of Potato Research* **92**(2), 298–302.

Rykaczewska, K. 2016. Field performance of potato minitubers produced in aeroponic culture. *Plant, Soil and Environment* **62**(11), 522–526.

Rykbost, K.A. & Charlton, B.A. 2004. Effects of prenuclear minituber seed size on production of Wallowa Russet seed. *Research in the Klamath Basin 2004 Annual Report*, 38–43.

Struik, P.C., Haverkort, A.J., Vreugdenhil, D., Bus, C.B. & Dankert, R. 1990. Manipulation of tuber-size distribution of a potato crop. *Potato Research* **33**(4), 417–432.

Struik, P.C. & Lommen, W.J.M. 1999. Improving the field performance of micro-and minitubers. *Potato Research* **42**(3–4), 559–568.

Struik, P.C. 2007. The Canon of Potato Science: Minitubers. *Potato Research* **50**(3–4), 305–308.

Travis, K.Z. 1987. Use of a simple model to study factors affecting the size distribution of tubers in potato crops. *The Journal of Agricultural Science* **109**(3), 563–571.

UNECE STANDARD S-1 concerning the marketing and commercial quality control of Seed Potatoes. 2018. http://www.unece.org/fileadmin/DAM/trade/agr/standard/potatoes/S-1_SeedPotatoes_2018_E.pdf. Accessed 11.2.2019.

Wrobel, S. 2015. Assessment of potato microtuber and in vitro plantlet seed multiplication in field conditions – Growth, development and yield. *Field Crops Research* **178**, 26–33.

Wurr, D.C.E., Fellows, J.R., Akehurst, J.M., Hambidge, A.J. & Lynn, J.R. 2001. The effect of cultural and environmental factors on potato seed tuber morphology and subsequent sprout and stem development. *Journal of Agricultural Science* **136**, 55–63.

Wurr, D.C.E., Fellows, J.R., Lynn, J.R. & Allen, E.J. 1993. The impact of some agronomic factors on the variability of potato tuber size distribution. *Potato Research* **36**(3), 237–245.

Agronomy Research **17**(2), 408–417, 2019
https://doi.org/10.15159/AR.19.112

Spatial variability of litter temperature, relative air humidity and skin temperature of chicks in a commercial broiler house

P.F.P. Ferraz[1*], G.A.S. Ferraz[1], L. Schiassi[1], V.H.B. Nogueira[1], M. Barbari[2] and F.A. Damasceno[1]

[1]Federal University of Lavras, Agricultural Engineering Departament, Campus Universitário, PO Box 3037, Lavras, Minas Gerais, Brazil
[2]University of Firenze, Department of Agriculture, Food, Environment and Forestry, Via San Bonaventura, 13, IT50145 Firenze, Italy
[*]Correspondence: patricia.ponciano@ufla.br

Abstract. The thermal environment inside a broiler house has a great influence on animal welfare and productivity during the production phase. Among the importance of the chicken litter is the function of absorbing moisture, provide thermal insulation and provide a soft surface for broilers. The skin temperature is an important physiological parameter to quantify the thermal comfort of animals, its variations may occur as a function of thermal variables. So, the aim of this work was to analyse the magnitude and spatial variability of chicken litter temperature and relative humidity of the air and to correlate them with the spatial distribution of chicks' skin surface temperature throughout the broiler house during the 7th, 14th and 21st days of the chicks' life, using geostatistical techniques. The experiment was performed in a commercial broiler house located in the western mesoregion of Minas Gerais, Brazil, where 28,000 male Cobb chicks were housed. The heating system consisted of an industrial indirect-fired biomass furnace. The heated air was inflated by an AC motor, 2,206 W of power, 1,725 RPM. Geostatistical techniques were used through semivariogram analysis and isochore maps were generated through data interpolation by kriging. The semivariogram was fitted by the restricted maximum likelihood method. The used mathematical model was the spherical one. After fitting the semivariograms, the data were interpolated by ordinary kriging. The semivariograms along with the isochore maps allowed identifying the non-uniformity of spatial distribution of the broiler litter temperature throughout the broiler house for 3 days of chicks' life. It was observed that skin surface presented a positive correlation with the litter temperature and a negative correlation with the air humidity. The semivariograms along with the isochore maps allowed identifying the non-uniformity of spatial distribution of the litter temperature, air humidity and skin temperature of chicks throughout the broiler aviary for the three days. In addition, the use of geostatistics and distribution maps made possible to identify different environmental conditions in regions inside the broiler house that may harm the development of chicks.

Key words: environment, geostatistics, thermal comfort, physiological responses.

INTRODUCTION

Broiler facilities should provide thermal comfort conditions that ensure animal welfare and enable animals to maximise their genetic potential for production with the least possible energy expenditure (Nascimento et al., 2014).

Environmental factors, such as air temperature and relative humidity, are crucial for animal husbandry because they affect the broiler's most important vital function – homeothermy (Amaral et al., 2011). According to Ferraz et al. (2018), animals housed at adequate air temperatures avoid wasting the metabolic energy contained in the feed because they expend almost no energy maintaining their body temperatures. Therefore, the housing system climate must be controlled so that broiler maintain their normal physiological functions and achieve satisfactory production.

Usually in a facility for broiler commercial production, the animals are commonly raised in open-plan facilities with a litter covered floor (Dunlop et al., 2015). Shepherd & Fairchild, (2010) and Collett (2012) describe litter as a mixture of bedding materials and manure that is used to provide a cushioning and insulating barrier between the broiler and the ground. Some researches in the literature have shown a very complex nature of the heat exchange between air, broiler body and the litter (Bieda & Kobia, 1999, Nawalany et al., 2010, Said et al., 2016). The welfare, health and productivity of broiler chickens can only be achieved by ensuring optimum thermal conditions in the living area of the chicks. Nawalany et al. (2010) affirm that thermal conditions in the living area of chickens are significantly affected not only by air temperature but also by bedding temperature.

The optimal range of relative humidity for chicken during and after brooding is 60–80 and 50–70%, respectively (Xiong et al., 2017). Higher relative air humidity combined with high temperatures cause the poultry to have greater difficulty releasing internal heat through their airways, thus increasing the animals' physiological responses, including respiratory rate, cloacal temperature (Cassuce et al., 2013) and skin surface temperature (Nascimento et al., 2014).

Abreu et al. (2017) suggest that variations in dry-bulb temperature, relative humidity and lighting are the main causes of changes in the animals' physiological responses. Among the physiological responses used to assess chicks' thermal comfort, skin surface temperature stands out because it can be measured to determine the animal's physical status (Nääs et al., 2014).

Under high ambient temperature conditions, animal body temperatures increase, and metabolic heat must be dissipated to lower the body temperature. Per Whittow (1986), part of the heat is transported through the blood stream via the blood flow to the skin surface or mucosa. Thus, under high temperature conditions, the blood vessels will be at their maximum vasodilatation, and much of the heat inside the body will be transported through the blood stream and tissues. Whittow (1986) further explains that when animals are housed under low temperature conditions, their blood vessels will be at their maximum vasoconstriction, and the heat will be transferred through the tissues.

Nowadays, geostatistical techniques are considered an efficient tool to evaluate the thermal variables inside the animal facilities and it have been used by many researches (Cemek et al., 2016, Ferraz et al., 2016; Curi et al., 2017,). Queiroz et al., 2017 suggest that geostatistical mapping using kriging maps can be a highly important tool for

analysing environmental conditions in broiler houses because these maps are easily interpreted.

Thus, this study analysed the magnitude and spatial variability of the litter temperature (t_{litter}) and relative air humidity (RH) and correlated these parameters with the spatial distribution of the broilers' skin surface temperatures (t_{skin}) while in the broiler house at days 7, 14 and 21 of the chicks' lives using geostatistical mapping methods.

MATERIALS AND METHOD

This experiment was conducted in a broiler house on a commercial farm in Minas Gerais, Brazil (20°11'58" latitude South and 45°02'08" longitude West), in the spring. The area's Köppen climate classification is type Cwa, or humid mild climate with dry winters and hot summers (de Sá Junior et al., 2012).

The broiler house in which the experiment was conducted was 13 m wide, 160 m long and 3 m high (Fig. 1) and was oriented northeast-southwest. The broiler house was made of reinforced concrete and bricks, fibre cement roof tiles, concrete flooring, and rice husk litter approximately 10 cm high. The broiler house housed 28,000 Cobb male chicks aged 1 to 21 days.

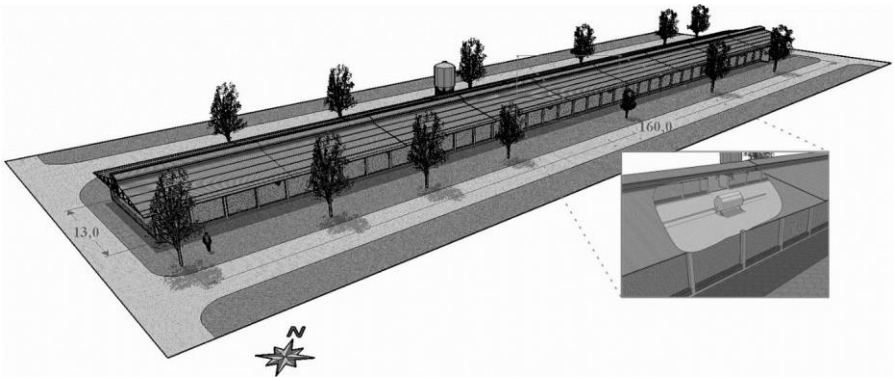

Figure 1. Three-dimensional diagram of the broiler house and heating system evaluated in this study, indicating the main dimensions in metres.

The broiler house's heating system consisted of a 2.23-m-long, 1.23-m-wide and 1.85-m-high metallic industrial indirect biomass fired hot-air furnace. The heated air was blown by a three-phase alternating current (AC) motor, 2,206 W power, and 1,725 RPM, distributed along metal pipes of approximately 28.60 m long on the northeast side and 22.45 m long on the southwest side installed in the central inner portion of the broiler house. The pipes were 23.00 cm wide and had 5.00-cm-wide holes every 1.00 m alternately on each side to release heated air.

Throughout the study period, the litter temperature (t_{litter}), relative air humidity (RH) and the animals' skin surface temperatures (t_{skin}) were measured on days 7, 14 and 21 of the chicks' lives. A digital infrared sensor Raynger ST (Raytek, Berlin, Germany), accurate to 0.5 °C was used to measure the t_{litter} and t_{skin}. The t_{skin} was measured under the wing, using the method proposed by Amaral et al. (2011). The RH was measured using a humidity probe, with a ± 3.00% reading accuracy. The sensors used to measure

the t_{litter}, t_{skin} and RH were placed forming a 1.00 × 1.00 m grid, totalling 75 collection points per variable on each day of analysis.

The variables' spatial variations during the experimental period were analysed by semivariogram fitting and ordinary kriging interpolation. The classic semivariogram was estimated using Eq. 1:

$$\hat{\gamma}(h) = \frac{1}{2N(h)} \sum_{i=1}^{N(h)} [Z(x_i) - Z(x_i + h)]^2 \quad (1)$$

where N (h) is the number of experimental observation pairs, Z(xi) and Z (xi + h), separated by a distance, h.

The semivariogram was fitted using the restricted maximum likelihood (REML) method, which results in less biased estimates. The mathematical model used to fit the semivariogram was the spherical model, which is widely used in geostatistical studies. The data were interpolated by ordinary kriging. The free software environment for statistical computing and graphics, R (R Development Core Team, 2018), was used for geostatistical analysis and map plotting.

Multivariate principal component analysis was used to plot the surface temperature variations with environmental variables in the broiler house. The free software environment for statistical computing and graphics, R (R Development Core Team, 2018), was used for this purpose.

RESULTS AND DISCUSSION

Fig. 2 shows the air temperature results for the collection period. Maximum values near 35 °C were observed in the first week because a firewood furnace was used to heat the facility.

Macari et al. (2004), Ferreira (2005) and Medeiros et al. (2005) found that thermal comfort conditions for broilers range from 32 to 34 °C in the first week, 28 to 32 °C in the second week and 26 to 28 °C in the third week of age. This explains the decrease in the maximum values for each week of observation as shown in the figure below.

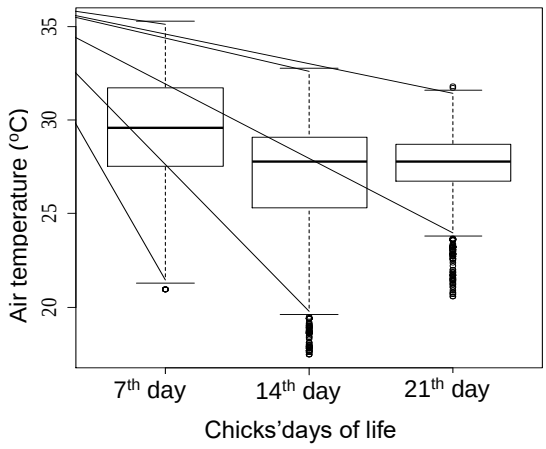

Figure 2. Air temperature distribution on days 7, 14 and 21 of the chicks' lives.

Principal component analysis was used to associate the t_{skin}, t_{litter}, and RH data. Fig. 3 shows that the chicks' skin surface temperatures were strongly positively correlated with the t_{litter} and negatively correlated with the RH. Thus, the data suggest that an increase in t_{litter} as a function of an increase in air temperature will increase the chicks' t_{skin}. Conversely, an increase in RH will decrease the chicks' t_{skin}.

The findings of this study indicate a positive association between t_{skin} and t_{litter} and corroborate the study published by Nascimento et al. (2014), who confirmed the importance of using building materials with low thermal conductivity to help maintain thermal insulation from external temperatures and decrease heat transfer from the facilities to the animals.

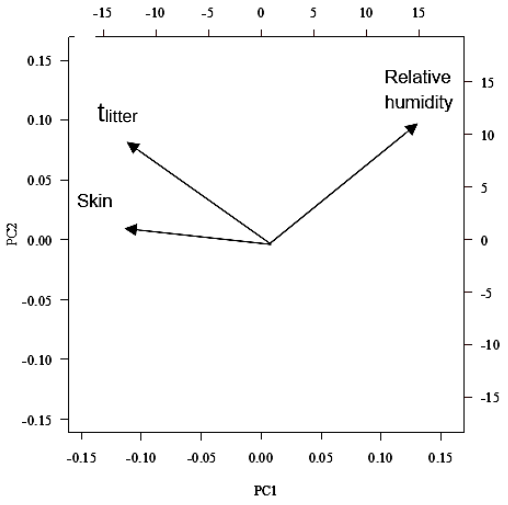

Figure 3. Principal component analysis of the chicks' skin surface temperature (t_{skin}), litter surface temperature (t_{litter}) and relative humidity (RH).

Table 1 lists the estimated experimental semivariograms for the t_{litter}, t_{skin} and RH inside the broiler house on days 1, 7 and 14 of the chicks' lives.

The data varied because the environmental conditions inside the broiler house lacked homogeneity during the experimental period. The nugget effect (C0) is a parameter that indicates unexplainable variability, which can be expressed as the sill ratio, which allows for comparing the degree of spatial dependence (DSD) of the studied variables (Trangmar et al., 1985).

Table 1. Estimated parameters of the experimental semivariograms for litter temperature, skin surface temperature and relative air humidity on days 7, 14 and 21 of the chicks' lives

Variables	C0	C1	C0 + C1	a	SDD		ME
$t_{litter}7$	2.07	0.94	3.01	34.92	68.79	Moderate	-0.0008
$t_{litter}14$	2.01	2.32	4.33	38.53	46.45	Moderate	0.0003
$t_{litter}21$	2.07	0.24	2.31	40.60	89.48	Weak	0.0003
$t_{skin}7$	0.37	0.13	0.50	33.37	74.00	Moderate	0.0003
$t_{skin}14$	0.29	0.09	0.37	22.28	76.92	Weak	0.0004
$t_{skin}21$	0.23	0.03	0.26	4.99	87.66	Weak	3.89E-05
RH7	0.79	16.87	17.66	39.36	4.47	Strong	-0.0002
RH14	0.48	13.43	13.90	43.18	3.46	Strong	-0.0094
RH21	0.15	3.60	3.76	43.41	4.04	Strong	-0.0033

C0: nugget effect; C1: contribution; C0 + C1: sill; a: range; DSD: degree of spatial dependence; ME: mean error.

The range (a) is a relevant parameter of a semivariogram because it is related to the spatial dependence threshold, indicating the threshold at which the variable is spatially

correlated among the evaluated points. In the present study, the range of the variable t_{litter} varied from 34.92 m to 40.60 m throughout all days and periods under study.

T_{skin} ranged from 4.99 to 33.37 °C, and the RH ranged from 39.36 to 43.41%.

Per Cambardella et al. (1994), semivariograms can be classified as follows: nugget effect < 25.00% of the sill = strong spatial dependence; nugget effect between 25.00 and 75.00% = moderate spatial dependence; and nugget effect > 75.00% = weak spatial dependence.

All DSD values were strong for the RH, whereas the t_{litter} values were moderate on days 7 and 14. The other DSD values were classified as weak; however, all study variables showed spatial dependence.

Per Faraco et al. (2008), the mean error should be as close as possible to zero, which indicates the semivariogram's goodness of fit. The variables outlined in Table 1 met this criterion.

Subsequently, the t_{litter}, RH and t_{skin} values were estimated based on the semivariogram models' spatial dependence (Faraco et al., 2008; Souza et al., 2010). Therefore, kriging performed well in estimating the non sampled values of this variable considering the best-fitting semivariogram. Thus, spatial distribution maps were constructed for all study variables (Figs 4–6), enabling visualising the data's spatiotemporal variability.

Each spatial distribution map shows the image for each day analysed (7, 14 and 21). Analysis of the maps shows that t_{litter} decreased after day 7 (Fig. 4, a), compared with days 14 (Fig. 4, b) and 21 (Fig. 4, c). According to the researches made by Said et al. (2016) comparing the litter temperature in the 10th and 20th day of chicken's age, it was observed biggest values of litter temperature in the 10th day of life. Probably in both cases this effect is directly related to air temperature control during the first days of the chicks' lives, when the broiler house heating systems were turned on.

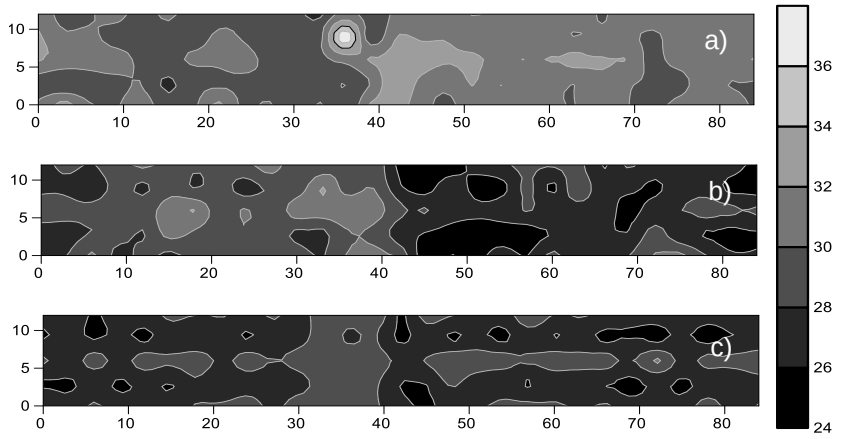

Figure 4. Spatial distribution of the litter temperature for days 7 (a), 14 (b) and 21 (c) of the chicks' lives.

The spatial distribution maps in Fig. 5 show that the heating system with the firewood furnace used in the study facility decreased the RH on days 7 (Fig. 5, a) and 14 (Fig. 5, b) compared with that on day 21 (Fig. 5, c). The increased relative air humidity

also led to higher faecal concentrations during the study period because chicks experience increased thermal stress and gain weight as they age; therefore, they drink more water and thus eliminate more water in their excreta, which increases the litter water content (Oliveira et al., 2000). Besides, it can be observed that during all the experimental period the litter humidity exceeded the allowable limit recommended by Butcher & Miles (2014) that is between 25 and 35% relative humidity. According to Said et al. (2016) in case of high humidity it requires regulation of the ventilation system and to monitor constantly the air quality in the broiler house so as not to exceed the levels of harmful substances in the air and minimize of chick's activity.

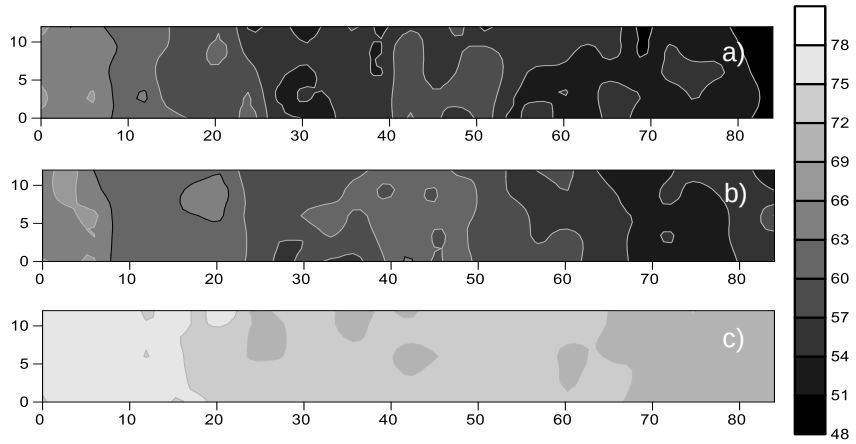

Figure 5. Spatial distribution of the relative humidity on days 7 (a), 14 (b) and 21 (c) of the chicks' lives.

Per Tankson et al. (2001), when broilers are in their thermal comfort zone, their t_{skin} is approximately 33 °C. The results shown in Fig. 6 indicate the effect of the heating system with the firewood furnace used in the study facility on the chicks as they reached maximum t_{skin} values near 40 °C, whereas on subsequent days, the maximum value was 39 °C, and the minimum value was 36 °C.

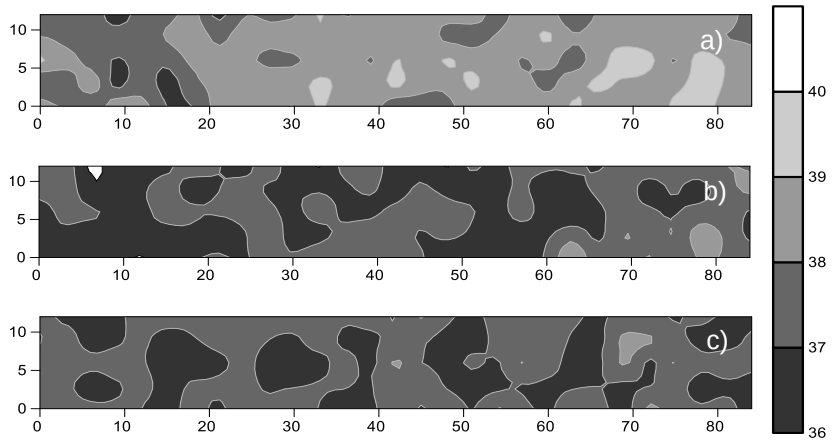

Figure 6. Spatial distribution of the skin temperature on days 7 (a), 14 (b) and 21 (c) of the chicks' lives.

These values highlight the need to control the thermal environment to reduce the chicks' heat stress after their second week of life at the study facility.

A visual analysis of all maps shows how the study data vary in space and the different spatial distribution patterns in each case, which are similar to the findings of Silva et al. (2013) and Curi et al. (2014).

Per Barbosa Filho et al. (2007), broiler tend to exchange body heat via contact with the litter or soil, which is usually at temperatures lower than those of the body, thus favouring heat exchange by thermal conduction. Therefore, the sites where the litter temperature is higher may hinder the chicks' heat exchange by thermal conduction with the litter and favour heat stress conditions, which may negatively affect production.

CONCLUSIONS

The semivariograms and maps enabled efficiently characterising the magnitude and spatial variability of the litter temperature, chick skin temperature and relative air humidity inside the broiler house.

The results showed a positive correlation between litter temperature and the chicks' skin temperature and a negative correlation between relative air humidity and the chicks' skin temperature.

Furthermore, the results showed an uneven spatial distribution of the study variables, which may indicate heating system failures in sections of the broiler house, which may affect the chicks' thermal comfort and welfare.

ACKNOWLEDGEMENTS. The authors thank the Brazilian Federal Agency for Support and Evaluation of Graduate Education (CAPES), the National Council for Scientific and Technological Development (CNPq), and the Minas Gerais Research Foundation (FAPEMIG) for funding the project.

REFERENCES

Abreu, L.H., Yanagi Junior, T., Campos, A.T., Bahuti, M. & Fassani, É.J. 2017. Cloacal and surface temperatures of broilers subject to thermal stress. *Engenharia Agrícola* **37**, 877–886.

Amaral, A.G., Yanagi Junior, T., Lima, R.R., Teixeira, V.H. & Schiassi, L. 2011. Effect of the production environment on broiler chickens reared in commercial shed. *Arq. Bras. Med. Vet. Zootec.* **63**, 649–658 (in Portuguese).

Barbosa Filho, J.A.D., Silva, I.J.O., Silva, M.A.N. & Silva, C.J.M. 2007. Behavior evaluation of laying hens using image sequences. *Eng. Agríc.* **27**, 93–99 (in Portuguese).

Bieda, W. & Kobia, M. 1999. Effect of litter, floor and ground on thermal conditions of broiler house in the winter period. *Roczniki Nauk Zootechnicznych* **26**, 265–274 (in Polish).

Butcher, G.D. & Miles, R.D. 2014. Causes and Pre vention of Wet Litter in Broiler Houses. [Online]. Available at: https://www.edis.ifas.ufl.edu/pdffiles/VM/VM02000.pdf Accessed 02.04.2019.

Cambardella, C.A., Moorman, T.B., Novak, J.M., Parkin, T.B., Karlen, D.L., Turco, R.F. & Konopka, A.E. 1994. Field scale variability of soil properties in Central Iowa soils. *Soil Science Society of America Journal* **58**, 1501–1511.

Cassuce, D.C., Tinôco, I.de F.F., Baêta, F.C., Zolnier, S., Cecon, P.R. & Vieira, M.de F.A. 2013. Thermal comfort temperature update for broiler chickens up to 21 days of age. *Eng. Agríc.* **33**, 28–36.

Cemek, B., Kucuktopcu, E. & Demir, Y. 2016. Determination of spatial distribution of ammonia levels in broiler houses. *Agronomy Research* **14**, 359–366.

Collett, S.R. 2012. Nutrition and wet litter problems in poultry. *Anim. Feed Sci. Technol*. **173**, 65–75.

Curi, T.M.R. de C., Conti, D., Vercellino, R.A., Massari, J.M., Moura, D.J., Souza, Z.M. & Montanari, R. 2017. Positioning of sensors for control of ventilation systems in broiler houses: a case study. *Scientia Agricola* **74**, 101–109.

Curi, T.M.R. de C., Vercellino, R. do A., Massari, J.M., Souza, Z.M. & Moura, D.J. de. 2014. Geostatistic to evaluate the environmental control in different ventilation systems in broiler houses. *Eng. Agríc.* **34**, 1062–1074 (in Portuguese).

de Sá Júnior, A. 2012. Application of the Köppen classification for climatic zoning in the state of Minas Gerais, Brazil. *Theoretical and Applied Climatology* **108**, 1–7.

Dunlop, M.W., Blackall, P.J. & Stuetz, R.M. 2015. Water addition, evaporation and water holding capacity of poultry litter. *Science of the Total Environment* **538**, 979–985.

Faraco, M.A., Uribe-Opazo, M.A., Silva, E.A.A., Johann, J.A. & Borssoi, J.A. 2008. Selection criteria of spatial variability models used in thematical maps of soil physical attributes and soybean yield. *Rev. Bras. de Ciênc. Solo* **32**, 463–476 (in Portuguese).

Ferraz, P.F., Yanagi Junior, T., Ferraz, G.A., Schiassi, L., & Campos, A.T. 2016. Spatial variability of enthalpy in broiler house during the heating phase. *Rev. bras. eng. agríc. Ambiental* **20**, 570–575.

Ferraz, P.F.P., Yanagi Junior, T., Hernandez-Julio, Y.F., Ferraz, G.A.E.S., Silva, Maria A.J.G., & Damasceno, F.A. 2018. Genetic fuzzy system for prediction of respiratory rate of chicks subject to thermal challenges. *Rev. bras. eng. agríc. Ambiental* **22**, 412–417.

Ferreira, R.A. 2005. *Greater production with better environment for poultry, pigs and cattle*. Viçosa, MG: Aprenda Fácil, 371 pp. (in Portuguese).

Macari, M., Furlan, R.L. & Maiorka, A. 2004. *Physiological and management aspects for the maintenance of thermal homeostasis and control of metabolic syndromes*. In: Mendes, A.A., Nããs, I.A., Macari, M. (Ed.). Production of broilers. Campinas: FACTA, pp. 137–155 (in Portuguese).

Medeiros, C.M., Baêta, F.D.C., de Oliveira, R.F., de F.F. Tinôco, I., Albino, L.F. & Cecon, P.R. 2005. Environmental thermal index of productivity for broiler chickens. *Revista Brasileira de Engenharia Agrícola e Ambiental* **9**, 660–665 (in Portuguese).

Nääs, I.A., Garcia, R.G. & Caldara, F.R.2014. Infrared thermal image for assessing animal health and welfare. *Jour. anim. behav. biomet.* **2**, 66–72.

Nascimento, G. R. do, Nääs, I.A., Baracho, M.S., Pereira, D.F. & Neves, D.P. 2014. Infrared thermography in the estimation of thermal comfort of broilers. *Rev. bras. eng. agríc. ambient*. **18**, 658–663 (in Portuguese).

Nawalany, G., Bieda, W. & Radon, J. 2010. Effect of floor heating and cooling of bedding on thermal conditions in the living area of broiler chickens. *Archiv fur Geflugelkunde* **74**, 98–101.

Oliveira, J.E. de, Sakomura, N.K., Figueiredo, A.N., Lucas Júnior, J. de & Santos, T.M.B. dos. 2000. Effect of thermal insulation under the roof on performance of broiler chickens stocked in different densities. *R. Bras. Zootec* **29**, 1427–1434 (in Portuguese).

Queiroz, M.L.V, Barbosa Filho, J.A.D., Sales, F.A.L., de Lima, L.R. & Duarte, L.M. 2017. Spatial variability in a broiler shed environment with fogging system. *Revista Ciência Agronômica* **48**, 586–595 (in Portuguese).

R Development Core Team. R: a language and environment for statistical computing. Vienna: *R Foundation for Statistical Computing*, 2018. Disponível em: <http://www.R-project.org/>. Accessed 22.4.2018.

Said, J., Bod'o, S., Saady, T., Galik, R., Sardary, S. & Abbas, K. 2016. Effect of broiler chickens living conditions on results of fattening. *Agronomy Research* **14**, 228–235.

Shepherd, E.M. & Fairchild, B.D., 2010. Footpad dermatitis in poultry. *Poult. Sci.* **89**, 2043–2051.

Silva, E.G.D., Santos, A.C.D., Ferreira, C.L.S., Sousa, J.P.L.D., Rocha, J.M.L.D. & Júnior, O.S. 2013. Spatial variability of the environmental characteristics and weight of broilers in shed negative ventilation. *Rev. bras. saúde prod. anim.* **14**, 132–141 (in Portuguese).

Souza, G.S., Lima, J.S.S., Xavier, A.C. & Rocha, W.S.D. 2010. Ordinary kriging and inverse-square-distance in espacialization in the chemical attributes of the ultisol. *Scientia Agraria* **11**, 73–81 (in Portuguese).

Tankson, J.D., Vizzier-Thaxton, Y., Thaxton, J.P., May, J.D. & Cameron, J.A. 2001. Stress and nutritional quality of broilers. *Poultry Science* **80**, 1.384–1.389.

Trangmar, B.B., Yost, R.S. & Uehara, G. 1985. Applications of geostatistics to spatial studies of soil properties. *Advances in Agronomy* **38**, 45–94.

Xiong, Y., Meng, Q.S., Jie, G.A.O., Tang, X.F. & Zhang, H.F. 2017. Effects of relative humidity on animal health and welfare. *Journal of integrative agriculture* **16**, 1653–1658.

Whittow, G.C. 1986. Energy metabolism. In: Avian Physiology (P.D. Sturkie, ed.), 4th edition, Springer-Verlag, New York, pp. 253–268.

Agronomy Research **17**(2), 418–429, 2019
https://doi.org/10.15159/AR.19.114

Principal components in the study of soil and plant properties in precision coffee farming

G.A.S. Ferraz[1], P.F.P. Ferraz[1], F.B. Martins[2], F.M. Silva[1], F.A. Damasceno[1] and M. Barbari[3]

[1]Federal University of Lavras – UFLA, Departament of Agricultural Engineering, University Campus, BR37200-000 Lavras-MG, Brazil
[2]Rural Federal University of Rio de Janeiro – UFRRJ, BR-465, Km 7, BR 23.897-000 Seropédica- RJ, Brazil
[3]Department of Agriculture, Food, Environment and Forestry (DAGRI), Università degli Studi di Firenze, Via San Bonaventura, 13, IT50145 Firenze, Itália
*Correspondence: gabriel.ferraz@ufla.br

Abstract. In this work, a principal component analysis was performed to evaluate the possibility of discarding obsolete soil and plant variables in a coffee field to eliminate redundant and difficult-to-measure information in precision coffee farming. This work was conducted at Brejão Farm in Três Pontas, Minas Gerais, Brazil, in a coffee field planted with 22 ha of Topázio cultivar. The evaluated variables were the yield, plant height, crown diameter, fruit maturation index, degree of fruit maturation, leafing, soil pH, available phosphorus (P), remaining phosphorus (Prem), available potassium (K), exchangeable calcium (Ca2+), exchangeable magnesium (Mg2+), exchangeable acidity (Al3+), potential acidity (H + Al), aluminium saturation ($N_{(Al)}$), potential CEC (CECp), actual CEC (CECa), sum of bases (SB), base saturation (BS) and organic matter (OM). The data were evaluated by a principal component analysis, which generated 20 components. Of these, 7 representing 88.98% of the data variation were chosen. The variables were discarded based on the preservation of the variables with the greatest coefficients in absolute values corresponding to the first component, followed by the variable with the second highest absolute value corresponding to the second principal component. Based on the results, the variables V, OM, fruit maturity index, plant height, yield, leafing and P were selected. The other variables were discarded.

Key words: Multivariate analysis, coffee plant, precision agriculture, fertility, management.

INTRODUCTION

Precision agriculture in coffee production has been called Precision Coffee Farming (Ferraz et al., 2012a), and it can be defined as the set of techniques and technologies based on the spatial variability of soil and plant properties capable of assisting the coffee farmer in crop management to maximize profitability and increase fertilizer, spraying and harvesting efficiency, thereby leading to increased yield and final quality of the product (Ferraz et al., 2012b).

However, the use of precision coffee farming often requires the use of several variables for more accurate decision-making, which makes the work more complex and,

in some cases, more costly (Almeida et al., 2011). With a high number of variables, many of them can contribute to the characteristics under evaluation. Thus, redundant and difficult-to-measure variables can be eliminated, thus reducing the time and costs of experiments (Leite et al., 2009).

According to Olive (2017) principal component analysis is used to explain the dispersion structure with a few linear combinations of the original variables. Jolliffe & Cadima (2016) affirms that large datasets are increasingly widespread in different areas and in order to interpret such datasets, methods are required to drastically reduce their dimensionality in an interpretable way. Principal component analysis (PCA) is used to obtain a small number of linear combinations (principal components) of a set of variables that retain as much information on the original variables as possible (Jolliffe, 1972; Jolliffe & Cadima, 2016; Olive, 2017). According to Morais (2011), PCA helps to reduce the size of a data set by selecting the principal components (PCs), discarding the original variables and excluding possible outliers and Jolliffe & Cadima (2016) affirms that PCA is one of the oldest and most widely used methods to perform it.

The principal components were used for different aspects of coffee farming, such as evaluating characters related to the vegetative growth of Arabica coffee cultivars (Freitas et al., 2007), discriminating between maturation stages and types of post-harvest processing (Arruda et al., 2011), performing multiple linear regression modelling of coffee crop yield (Carvalho et al., 2004), evaluating morphological characters of Arabica coffee (Teixeira et al., 2013) and studying the spatial variability of chemical attributes of a soil cultivated with coffee plants (Silva et al., 2010b; Silva & Lima 2012). But all of these studies had just focused on soil or on plant features separately. It is known that plant and soil can affect the coffee production, so they need to be studied together in order to obtain more and better information about the coffee production.

Thus, the aim of this work was to perform a principal component analysis of data obtained by precision coffee farming and evaluate the possibility of discarding soil and plant variables in a coffee field to eliminate redundant and difficult-to-measure information in precision coffee farming, so making the precision coffee farming more feasible to farmers.

MATERIALS AND METHODS

The experiment was carried out at the Brejão farm, which is located in the Três Pontas Municipality in southern Minas Gerais, Brazil. The study area was cultivated with 22 hectares of coffee (*Coffea arabica* L.) of the Topazio cultivar, which was transplanted in December 2005 at a spacing of 3.8 m between rows and 0.8 m between plants, for a total of 3289 plants ha^{-1}. The geographical coordinates of the central point of the area are 21° 25' 58" south latitude and 45° 24' 51" west longitude.

The local climate is characterized as mild, tropical of altitude, with moderate ambient temperatures and hot and rainy summer, classified by Köppen as Cwa (Sá Junior et al., 2012). The soil was classified as Haplustox (EMBRAPA, 2016).

In this study, 20 variables were used, and 14 of these variables were soil related, and 6 were coffee plant related. Thus, sampling was carried out in the study area, in which a regular 57 x 57 m sampling grid was delimited, and a total of 64 georeferenced points (average of 2.9 points per hectare) were sampled using the Topcon FC-100 GPS data collector (Topcon Positioning Systems Inc, Livermore, Calif., USA), whose mean

error was 10 cm. Within this grid, another four regular sampling grids (called zoom) were created, and the points were spaced at 3.8 x 3.8 m. These grids were positioned at four different points of the main grid. Each magnification will correspond to 10 georeferenced sampling points (one point of the main grid and nine points of the new grid). Therefore, the grid was composed of 100 georeferenced sampling points (Fig. 1).

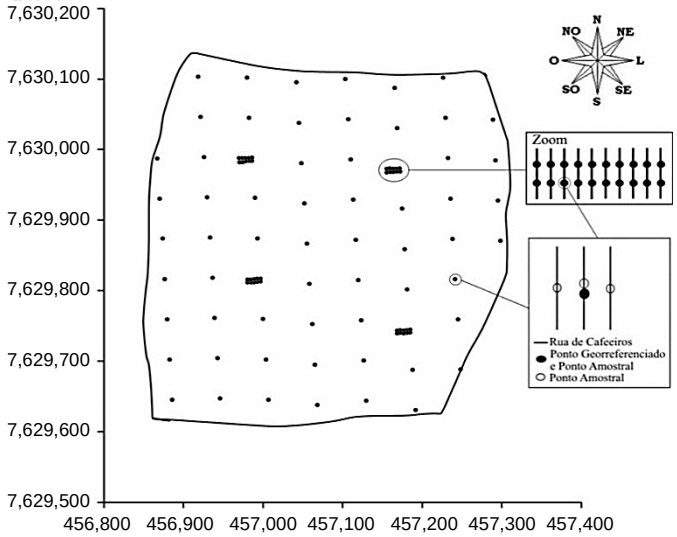

Figure 1. Sampling grid and procedure.

Each sampling point corresponded to four plants: two plants located in the coffee row where the point was georeferenced and the other two plants located in each row to the side of the reference point.

The soil samples were collected by subsampling in the canopy projection of the coffee plants at a depth of 0 to 20 cm using a Dutch auger. The traditional soil sampling diffused for coffee cultivation, recommends that soil sampling should be performed from 0–20 cm (Guimarães et al., 2002; Matiello et al., 2010) depth and it was performed by many studies (Ferraz et al., 2012b; Silva et al., 2010a; Silva et al., 2013; Silva & Lima 2012). At each sampling point, a sub-sample of each of the four plants that make up this point was collected. The subsamples of each sampling point were homogenized to form a composite sample for the point.

The evaluated soil chemical properties were as follows: soil pH, available phosphorus (P) (Mehlich 1), remaining phosphorus (Prem), available potassium (K) (Mehlich 1), exchangeable calcium (Ca^{2+}) (extractor: KCL – 1 mol L^{-1}), exchangeable magnesium (Mg^{2+}) (extractor: KCL – 1 mol L^{-1}),exchangeable acidity (Al^{3+}) (extractor: KCL – 1 mol L^{-1}), potential acidity (H + Al) (extractor: SMP), aluminium saturation ($N_{(Al)}$), potential cation exchange capacity (CECp) actual cation exchange capacity (CECa), sum of bases (SB), base saturation (BS) and organic matter (OM). The soil samples were sent to the soil analysis laboratory of the Department of Soil Science of the Federal University of Lavras for proper analysis of these properties.

The six coffee plant-related variables studied were yield (YIELD), plant height (HEIGHT), crown diameter (CROD), fruit maturation index (FMI), degree of fruit maturation (DFM) and leafing (LEAF).

The coffee YIELD (L plant^{-1}) was obtained by manual harvesting on cloths around the four plants at the sampling point, and the volume harvested from each plant after shaking was measured in a container graduated in litres. After this measurement, the mean YIELD of these four plants was obtained and used as the YIELD for the sampling point.

At each sampling point, after the YIELD measurements, the fruits collected from the four plants composing the point were placed in the same container, where they were homogenized to obtain a 0.5-L sample of fruits (Carvalho et al., 2003; Silva, 2008). Using this sample, the number of fruits at each maturation stage (dry, raisin, cherry and green) was counted and transformed to a percentage for use in equation 1 described by Alves et al. (2009) to calculate the FMI.

$$FMI = \sum \%cherry, \%raisin, \%dry \quad (1)$$

The same fruits used to obtain the FMI were also used to determine the DFM. According to Silva et al. (2010a), the literature does not provide information about the maturation stage parameters or aims and only reports the indices related to fruit colour and days after flowering. Thus, these authors stipulated a scale of scores ranging from 1 to 4, where a value of 1.0 is given for the green maturation stage, 2.0 is given for the cherry maturation stage, 3.8 is given for the raisin maturation stage and 4.0 is given for the dry maturation stage. Thus, the authors created an index called the DFM, and it is presented in Eq. 2.

$$DFM = \frac{4(\%\, dry) + 3.8(\%\, raisin) + 2(\%\, cherry) + 1(\%\, green)}{(\%\, dry + \%raisin + \%cherry + \%\, green)} \quad (2)$$

In the four plants that represented the sampling point, the HEIGHT and CROD were measured using a ruler graduated in millimetres. HEIGHT was measured from the soil surface to the top of the plant, and the CROD represented the measurement of the longest branch. After this measurement, the mean height and CROD of each sampling point was obtained in metres.

The visual scale proposed by Boldini (2001) was used to evaluate the LEAF, and the classes range from 0 to 20%, from 21 to 40%, from 41 to 60%, from 61 to 80% and from 81 to 100%.

Souza et al. (2008) reinforced that the multivariate analysis technique has an advantage relative to the univariate analysis methods in that it evaluates the level to which each characteristic studied explains the total variance among the evaluated treatments. Thus, less discriminating characteristics could be discarded since they are already correlated with other redundant variables or present invariance.

The methodology proposed by Jolliffe (1972) was used to select the number of principal components (PCs), where the p number of significant PCs can be defined by the number of PCs required to explain a percentage of the total data variance (cumulative) greater than 90% or by a value of the associated eigenvalue (λ) greater than 0.7. The eigenvalue can be obtained by Eq. 3.

$$det([T]_A - \lambda I_n) = 0 \quad (3)$$

where I_n is the identity matrix of order n and is called the characteristic equation. From this equation, the polynomial $[T]_A - \lambda I_n$ is obtained, which is the polynomial characteristic of *T*, and its roots in R are the eigenvalues of the linear operator *T*.

In addition, the classical B4 method for discarding variables proposed by Jolliffe (1972), which is based on the preservation of most of the variation in the data, was adopted for discarding the variables. The B4 method involves the use of the first p PCs selected, and the variable with the greatest absolute value of eigenvectors corresponding to the first PC is selected. The next variable to be selected will be the highest absolute value of the eigenvectors corresponding to the second PC, which continues until the selected p PC. Unselected variables will be discarded. In this way, the number of variables selected is equal to the number p of PCs.

All analyses were performed using the R (R Development Core Team, 2018) statistical platform.

RESULTS AND DISCUSSION

The PCA generated 20 PCs, and the first 7 PCs explained 88.98% of the total variance of the data under study and presented a variance greater than 0.7 (eigenvalue greater than 0.7); thus, they were considered significant PCs (Table 1). Moreover, 45.10%of the data variation can be explained by the first PC. Silva et al. (2010b) studied 22 soil variables and observed that the first PC explained 42.00% of the data variation.

Following the B4 method for discarding variables proposed by Jolliffe (1972) the values with the highest absolute value of each of the significant PCs (PC1, PC2, PC3, PC4, PC5, PC6 and PC7) can be selected: BS, OM, FMI, HEIGHT, YIELD, LEAF and P, respectively. These variables correspond to the values highlighted in bold in Table 2. The other variables can be discarded.

The variables to be discarded showed significant simple linear correlations with the other variables (Table 3) and thus were redundant because such correlations present a statistical relationship that involves dependence between variables.

Table 1. Principal components (PCs), eigenvalues, percentage of variance explained by the PCs (% VPC) and cumulative percentage of variance explained by the PCs of the soil and plant attributes of the studied coffee plants

	Eigenvalue	%VPC	Cumulative %VPC
PC1	**9.02**	45.10	45.10
PC2	**2.28**	11.40	56.50
PC3	**1.96**	9.81	66.31
PC4	**1.67**	8.35	74.66
PC5	**1.13**	5.63	80.28
PC6	**0.92**	4.60	84.90
PC7	**0.82**	4.09	88.98
PC8	0.58	2.90	91.88
PC9	0.53	2.64	94.52
PC10	0.36	1.79	96.32
PC11	0.32	1.62	97.93
PC12	0.17	0.84	98.77
PC13	0.10	0.51	99.29
PC14	0.08	0.38	99.67
PC15	0.05	0.22	99.90
PC16	0.01	0.05	99.95
PC17	0.01	0.05	100.00
PC18	0.00	0.00	100.00
PC19	0.00	0.00	100.00
PC20	0.00	0.00	100.00

Table 2. Coefficients of the 20 principal components (eigenvectors)

	PC1	PC2	PC3	PC4	PC5	PC6	PC7	PC8	PC9	PC10	PC11	PC12	PC13	PC14	PC15	PC16	PC17	PC18	PC19	PC20
YIELD	0.111	-0.178	-0.074	0.004	**-0.479**	-0.556	0.404	-0.219	-0.430	0.064	0.072	0.000	0.010	0.075	0.034	-0.006	0.010	0.000	0.000	0.000
HEIGHT	-0.012	-0.135	0.098	**0.624**	-0.261	0.081	0.053	-0.201	0.406	-0.315	0.382	0.221	-0.006	0.064	-0.021	0.010	-0.009	0.000	0.000	0.000
CROD	0.033	-0.330	-0.056	0.413	-0.305	0.255	-0.019	**0.625**	-0.176	0.233	-0.258	-0.111	0.049	-0.017	0.017	-0.004	0.011	-0.001	0.000	0.000
FMI	-0.011	0.290	**-0.599**	0.105	-0.108	-0.116	0.051	0.095	0.101	-0.132	-0.053	0.018	-0.299	-0.616	-0.097	0.009	0.014	-0.001	0.000	0.000
DFM	-0.005	0.319	-0.594	0.087	-0.049	-0.052	-0.118	0.057	0.057	-0.046	-0.080	0.038	0.229	**0.669**	0.051	0.008	-0.008	0.001	0.000	0.000
LEAF	0.024	0.182	0.297	0.265	0.285	**-0.645**	-0.148	0.414	0.001	-0.301	-0.047	-0.146	-0.011	0.038	-0.018	0.029	-0.005	0.000	0.000	0.000
Ph	0.322	-0.046	0.019	-0.026	-0.016	0.084	-0.043	-0.033	-0.061	-0.058	-0.019	-0.113	-0.352	0.229	**-0.793**	0.236	0.035	-0.002	0.001	0.000
P	-0.042	0.308	0.090	0.200	0.272	0.290	**0.776**	0.023	-0.153	-0.180	-0.142	-0.116	0.038	0.063	-0.008	0.008	0.000	0.000	0.000	0.000
K	0.256	-0.078	0.022	0.208	-0.049	-0.019	-0.145	-0.467	0.151	-0.121	**-0.626**	-0.408	0.104	-0.078	0.122	-0.013	-0.084	0.084	0.036	0.000
Ca	0.320	-0.067	-0.021	-0.044	0.116	-0.034	0.103	0.102	0.083	0.063	-0.049	0.333	-0.152	0.043	0.167	0.128	-0.244	**0.712**	0.308	0.000
Mg	0.290	-0.073	-0.169	0.004	0.155	-0.021	0.069	0.048	0.087	0.139	0.437	-0.410	**0.599**	-0.212	-0.167	0.078	0.003	0.153	0.066	0.000
Al	-0.310	-0.109	-0.064	0.093	0.109	-0.092	0.061	-0.080	0.145	0.229	0.045	-0.275	-0.247	0.111	0.052	0.040	0.585	0.323	0.015	-0.417
H + Al	-0.302	-0.211	-0.088	0.047	0.151	-0.107	0.051	-0.059	0.029	0.018	-0.157	0.149	0.160	-0.030	-0.265	-0.125	-0.002	-0.216	**0.780**	0.000
SB	0.325	-0.072	-0.044	-0.015	0.114	-0.032	0.078	0.045	0.093	0.061	-0.022	0.156	-0.008	-0.009	0.116	0.109	-0.201	-0.393	-0.016	**-0.779**
CECp	0.264	-0.217	-0.129	0.058	0.286	-0.136	0.185	0.004	0.285	0.305	0.004	0.015	-0.233	0.085	0.239	0.216	0.186	-0.367	-0.014	0.468
CECa	-0.229	-0.351	-0.155	0.059	0.292	-0.176	0.125	-0.057	0.102	0.066	-0.242	0.317	0.226	-0.050	-0.309	-0.093	-0.130	0.150	-0.539	0.000
BS	**0.328**	-0.002	-0.009	-0.017	0.051	-0.007	0.055	0.058	0.097	0.049	0.056	-0.020	-0.142	0.073	-0.066	**-0.910**	0.101	0.006	-0.008	0.000
$N_{(Al)}$	-0.314	-0.045	-0.057	0.069	0.043	-0.054	0.050	-0.032	0.099	0.241	0.186	**-0.414**	-0.314	0.123	0.011	-0.086	**-0.698**	0.001	-0.001	0.000
OM	0.029	**-0.443**	-0.292	0.036	0.337	0.140	-0.146	-0.059	-0.446	**-0.495**	0.181	-0.106	-0.163	0.035	0.203	-0.028	0.009	0.002	0.000	0.000
Prem	0.075	0.281	0.033	0.490	0.259	0.023	-0.258	-0.287	**-0.448**	0.446	0.093	0.197	-0.019	-0.090	-0.032	-0.027	-0.003	0.000	0.000	0.000

Table 3. Simple correlation coefficient between the studied variables

	YIELD	HEIGHT	CROD	FMI	DFM	LEAF	Ph	P	K	Ca	Mg	Al	H + Al	SB	CECp	CECa	BS	N(Al)	MO	Prem
YIELD	1.00																			
HEIGHT	0.09	1.00																		
CROD	0.17	0.45	1.00																	
FMI	0.05	-0.05	-0.06	1.00																
DFM	-0.05	-0.11	-0.09	0.90	1.00															
LEAF	-0.02	0.11	-0.10	-0.12	-0.13	1.00														
Ph	0.31	-0.04	0.13	-0.10	-0.07	0.00	1.00													
P	-0.19	0.07	-0.13	0.10	0.05	0.11	-0.16	1.00												
K	0.28	0.23	0.16	-0.07	-0.04	0.06	0.76	-0.16	1.00											
Ca	0.31	-0.09	0.10	-0.05	-0.05	0.07	0.92	-0.11	0.68	1.00										
Mg	0.28	-0.05	0.10	0.09	0.11	-0.01	0.81	-0.13	0.59	0.85	1.00									
Al	-0.26	0.13	-0.02	0.04	0.01	-0.06	-0.90	0.08	-0.65	-0.87	-0.72	1.00								
H + Al	-0.22	0.08	0.02	0.00	-0.03	-0.09	-0.87	0.02	-0.62	-0.81	-0.71	0.94	1.00							
SB	0.32	-0.06	0.11	-0.03	-0.03	0.06	0.93	-0.12	0.73	0.99	0.89	-0.87	-0.81	1.00						
CECp	0.29	0.02	0.16	-0.02	-0.03	0.04	0.75	-0.13	0.63	0.88	0.84	-0.55	-0.52	0.89	1.00					
CECa	-0.11	0.07	0.10	-0.03	-0.07	-0.10	-0.67	-0.05	-0.43	-0.53	-0.46	0.80	0.93	-0.54	-0.18	1.00				
BS	0.30	-0.05	0.08	-0.02	-0.01	0.08	0.95	-0.10	0.72	0.97	0.88	-0.90	-0.89	0.98	0.83	-0.66	1.00			
N(Al)	-0.28	0.10	-0.04	0.07	0.04	-0.08	-0.91	0.10	-0.71	-0.90	-0.73	0.98	0.89	-0.90	-0.63	0.71	-0.91	1.00		
OM	0.05	0.01	0.28	-0.01	0.00	-0.25	0.15	-0.25	0.11	0.15	0.27	0.03	0.20	0.17	0.32	0.40	0.08	-0.04	1.00	
Prem	-0.13	0.24	0.03	0.12	0.21	0.35	0.18	0.25	0.30	0.13	0.17	-0.18	-0.27	0.16	0.10	-0.29	0.19	-0.18	-0.08	1.00

The parameter BS is an important index of soil acidity for establishing adequate limestone doses for crops and management strategies for agricultural production (Fageria, 2011). The concept of BS is related to the supply of bases (Ca, Mg, K) at optimal levels for the development of plants (McLean, 1977). Thus, the choice of BS can be explained since this variable indicates the percentage of cation exchange sites that are occupied by bases, that is, the percentage of negative charges at pH 7,0 occupied by Ca^{2+}, K^{+}, (Na^{+}) compared to the sites occupied by H^{+} and Al^{3+}.

PC1 included BS and presented correlation values with the items included in this index (Table 2). A positive correlation was observed with Ca, K and CEC at pH 7,0 (CECp), and a negative correlation was observed with Al and with H + Al, which justifies the choice of V since these parameters are already included in the composition of the index.

PC2 included OM as the variable to be chosen. According to Mielniczuk et al. (2003), OM is one of the main parameters in the evaluation of soil quality and had a strong effect on the physical, chemical and biological characteristics of the soil.

Xavier et al. (2006) stated that soil OM is one of the main sources of energy and nutrients to the system, and it is capable of maintaining the soil YIELD in general. Silva & Resck (1997) reported that the benefits generated by OM include improvements in the physical conditions of the soil and the energy supply for microbial growth, which Paes et al. (1996) indicated leads to increased nutrient cycling and soil CEC. Table 3 shows that the t and T are directly correlated with the OM. These two variables are also correlated with PC2.

It should be noted that the behaviour of PC1 and PC2 in this study was similar to that observed by Silva et al. (2010b).

According to Novais & Smyth (1999), P is one of the most limiting elements for crops grown under tropical soil conditions due to their soil-sink characteristics. In the coffee crop, Guimarães et al. (2002) indicated that the P requirement is small in the adult stage of the crop relative to the nitrogen and K requirements. In the young stage, the P requirement is greater, which is also observed for the other nutrients. P affects the development of the root system and formation of the xylem of the plant, and it is also very important in grain formation. Therefore, the study of this variable is very important.

The plant characteristics selected by the PCs were HEIGHT, FMI, YIELD and LEAF. DFM was excluded because its information was already included in the FMI, which made it redundant.

The study of YIELD in precision coffee farming is of great importance because these data can be used to infer soil parameters that may be detrimental to the good productive performance of the plant, and they are also important for the adequate planning and management of the harvesting stage and for determining whether to implement manual, semi-mechanized or mechanized strategies.

According to Silva et al. (2006), the maturation index can be used to define the harvest period of a given plot. A plot that exhibits plants with 20 to 25% of green fruits (FMI of 75 to 80%) is considered to be at the beginning of the harvest; a plot that exhibits between 10 and 15% of green fruit is considered to be at the middle of the harvest (FMI of 85 to 90%); and a plot that exhibits less than 5% of green fruit is considered to be at the end of harvest (FMI of 95%).

Boldini (2001) developed a grading scale for classifying the LEAF a coffee plant: 0 to 20% LEAF is assigned a score of one, 21 to 40% is assigned a score of two, 41 and

60% is assigned a score of three, 61 to 80% is assigned a score of four; and from 81 to 100% is assigned a score of five. This variable is analysed to assess the effect of pest organisms in the crop LEAF (Silva et al., 2013).

PC4 indicated that HEIGHT is a variable to be evaluated. This parameter is an important growth trait of the plant and indicates its development. This characteristic is closely related to the crop management conditions. When analysing PC4 (Table 2), CROD also stood out as one of the characteristics strongly related to this PC, and it is also an indicator of plant development. Therefore, because HEIGHT is a sufficient indicator of plant development, CROD was redundant and discarded.

The study of fruit detachment force, both for green and cherry fruits, can be an important indicator for selecting selective mechanized harvesting. Silva et al. (2010b) reported that a greater difference in the detachment force between green and cherry fruits corresponds to improved selective mechanized harvesting of the coffee fruits. In addition, this variable can be used to indicate when to start this type of harvest (Silva, 2008).

When studied together, these four coffee plant-related variables provide the foundation for the study of crop development based on the type of management implemented and allow for the identification of abnormal development. These variables can also be used to define the most adequate crop management activities.

Therefore, the selection of these soil and plant variables can be valuable for the coffee grower. The use of precision agriculture can generate a lot of information that may not always be useful to producers who may be still being spent on time and money. So, focusing your time on variables that can really give accurate information to farm management becomes essential. This paper proves that was possible reduce the number of variables that can be useful for the coffee producers.

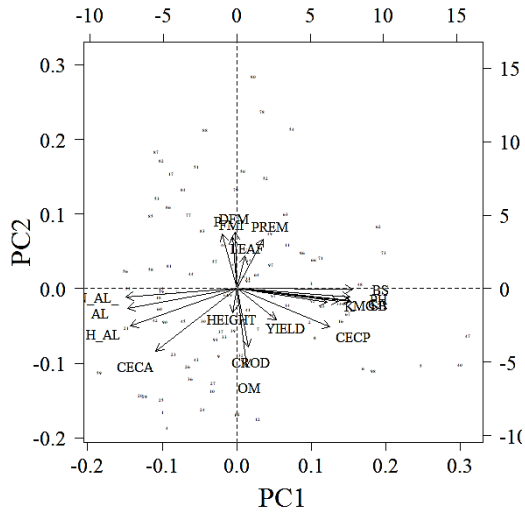

Figure 2. Biplot of the first two principal components.

The PCA analyses can also give us a good information about the relationship between variables. So, in order to study the relationship of the chosen variables with the yield it was performed a biplot chart of PC1 and PC2 (Fig. 2). It is possible to observe in the Fig. 2 that exists a direct relationship between BS and YIELD, OM and YIELD and HEIGHT and YIELD. Otherwise, there are an inverse relationship between FMI and YIELD, LEAF and YIELD and P and YIELD. So, the right management of this variables will be important to increase the coffee yield.

CONCLUSIONS

The use of the PCA is important in the field of precision coffee farming because it can identify soil and plant variables that can be discarded to remove repetitive and difficult-to-measure information. Thus, the variables selected for this study were SB, OM, FMI, HEIGHT, YIELD, LEAF and P. It was possible as well to use the PCA to study the relationship among the coffee yield among the other six selected variables. So, with the results present in this study the coffee farmer could be more focused in some variables, so reduce time consuming to analyse all of the many data that precision agriculture can generate.

ACKNOWLEDGEMENTS. The authors thank the National Council for Scientific and Technological Development (CNPq), the Coordination for the Improvement of Higher Education Personnel (CAPES), the Foundation for Research of the State of Minas Gerais (FAPEMIG), the Federal University of Lavras (UFLA), the Federal Rural University of Rio de Janeiro (UFRRJ) the Postgraduate Program in Agricultural and Environmental Engineering (PGEAAmb).

REFERENCES

Almeida, A.P.S. 2011. Impact of the ICMS Credit on the Cost of Production in Coffee Production: a Study of the Main Producing Regions of Arabica Coffee in Brazil. 2011. Available: < https://repositorio.ufu.br/handle/123456789/11948> Accessed 7.12.2018 (in Portuguese).

Alves, M.C., Silva, F.M., Ferreira, T.A. & Silva, F.C. 2009. Neuro-fuzzy operational performance of a coffee harvester machine. *Journal of convergence information technology* **4**, n.2, 52–59.

Arruda, N.P., Hovell, A.M., Rezende, C.M., Freitas, S.P., Couri, S. & Bizzo, H.R. 2011. Discrimination between maturation stages and types of post-harvest processing of arabica coffees by solid phase microextraction and principal component analysis. *Química Nova*, São Paulo **34**(5), 819–824 (in Portuguese).

Boldini, J.M. 2001. *Epidemiology of rust and cercosporiosis in irrigated and fertigated coffee.* 67 pp. Dissertation (Masters in Phytopathology), Federal University of Larvas, Lavras, 2001 (in Portuguese).

Brazilian Agricultural Research Corporation. National Soil Research Center. *Brazilian classification soil system (*Empresa Brasileira de Pesquisa Agropecuária. Centro Nacional de Pesquisas de Solos. Sistema Brasileiro de classificação do Solo - in Portuguese). 2 ed. Rio de Janeiro, 2006, 306 pp.

Carvalho, G.R., Mendes, A.N.G., Carvalho, L.F. & Bartholo, G.F. 2003. Ethephon efficiency in the uniformization and anticipation of fruit maturation (Coffea arabica L.) and beverage quality. *Science and Agrotechnology* **27**(1), 98–106 (in Portuguese).

Carvalho, L.G.D., Sediyama, G.C., Cecon, P.R. & Alves, H.M. 2004. Regression model for the coffee produdivity forecast in the State of Minas Gerais. *Brazilian Journal of Agricultural and Environmental Engineering* **8**, 204–211 (in Portuguese).

Fageria, N.K. 2001. Response of upland rice, dry bean, corn and soybean to base saturation in cerrado soil. *Brazilian Journal of Agricultural and Environmental Engineering* **5**(3), 416–424. (in Portuguese).

Ferraz, G.A.S, Silva, F.M., Alves, M.C., Bueno, R.L. & da Costa, P.A.N. 2012a. Geostatistical analysis of fruit yield and detachment force in coffee. *Precision Agriculture* **13**(1), 76–89.

Ferraz, G.A.S., Silva, F.M.D., Carvalho, L.C., Alves, M.D.C. & Franco, B.C. 2012b. Spatial and temporal variability of phosphorus, potassium and of the yield of a coffee field. *Engenharia Agrícola* **32**(1), 140–150 (in Portuguese).

Freitas, Z.M.T.S.D., Oliveira, F.J.D., Carvalho, S.P.D., Santos, V.F.D. & Santos, J.P.D.O. 2007. Evaluation of quantitative traits related to the vegetative growth among cultivars of low size Arabica coffee. *Bragantia*, Campinas, **66**(2), 267–275 (in Portuguese).

Guimarães, R.J., Mendes, A.N.G., Souza, C.A.S. 2002. Coffee Nutrition: Extraction of Nutrients, Liming and Gessam in the Planting, Training and Production phases. In: *Coffee*. Lavras: UFLA / FAEPE, pp. 194–234 (in Portuguese).

Jolliffe, I.T. & Cadima, J.2016. Principal component analysis: a review and recent developments. *Philosophical Transactions of the Royal Society A: Mathematical, Physical and Engineering Sciences*, **374**(2065), 1–16.

Jolliffe, I.T. 1972. Discarding variables in a principal component analysis. I. Artificial data. *Applied Statistics* **21**, 160–173.

Leite, C.D.S., Corrêa, G.D.S.S., Barbosa, L.T., Melo, A.L.P.D., Yamaki, M., Silva, M.D.A. & Torres, R.D.A. 2009. Evaluation of performance and carcass characteristics of cutting quails by principal components analysis. *Brazilian Journal of Veterinary Medicine and Animal Science* **61**(2), 498–503 (in Portuguese).

Matiello, J.B., Santinato, R., Garcia, A.W.R., Almeida, S.R. & Fernandes, D.R. 2010. *Coffe crop in Brazil*: *recommendation manual*. Rio de janeiro e Varginha: Fundação Procafé (in Portuguese).

McLean, E.O. 1977. Contrasting concepts in soil test interpretation: Sufficiency levels of available nutrients versus basic cation saturation ratios. In: Stelly, M. (Ed.) *Soil testing: Correlating and interpreting the analytical results*. Madison: American. Society of Agronomy, pp. 39–54.

Mielniczuk, J., Bayer, C., Vezzani, F.M., Lovato, T., Fernandes, F.F. & Debarba, L. 2003. Soil and crop management and their relationship with carbon and soil nitrogen stocks. In: Curi, N.; Marques, J.J., Guilherme, L.R.G., Lima, J.M., Lopes, A.S., Alvarez, V.H., eds. *Topics in soil science*. Viçosa, MG, Brazilian Society of Soil Science, **3**, pp. 209–248 (in Portuguese).

Morais, J.T.G. 2011. *Principal components analysis integrated to artificial neural networks for prediction of organic matter*. 67 pp. Dissertation (Master in Industrial Engineering) - Federal University of Bahia (in Portuguese).

Novais, R.F. & Smyth, T.J. Source-drain relationship of phosphorus in soil. In*: Phosphorus in soil and plant in tropical conditions*. UFV, 1999. 2–6 (in Portuguese).

Olive, D.J. 2017. Principal Component Analysis. In: Robust Multivariate Analysis. Springer, Cham, pp. 189–217.

Paes, J.M.V., Andreola, F., Brito, C.H. & Loudes, E.G. 1996. Decomposition of coffee straw in three types of soil and its influence on CTC and pH. *Ceres* **43**, 337–392.

R DEVELOPMENT CORE TEAM. R: a language and environment for statistical computing. Vienna: R Foundation for Statistical Computing, 2018. Available <http://www.R-project.org/>. Accessed:13.8. 2018.

Sá Junior, A., Carvalho, L.G., Silva, F.F. & Alves, M.C. 2012. Application of the Köppen classification for climatic zoning in the state of Minas Gerais, Brazil. *Theoretical and Applied Climatology* **108**, 1–7.

Silva, A.F., Lima, J.S.D.S., Souza, G.S. & Oliveira, R.B. 2010b. Spatial variability of chemical attributes of a humic red-yellow latosol cultivated with coffee. *Revista Brasileira de Ciências do Solo* **34**, 15–32 (in Portuguese).

Silva, F.C.D., Silva, F.M.D., Alves, M.D.C., Barros, M.M.D. & Sales, R.D.S. 2010a. Behavior of the detachment force of fruits of coffee trees during the harvest period. *Science and Agrotechnology* **34**(2), 468–474 (in Portuguese).

Silva, F.C. *Effect of the Detachment force and maturation of coffee fruits on mechanized harvesting*. 2008. 106 pp. Dissertation (Master in Agricultural Engineering) - Federal University of Lavras (in Portuguese).

Silva, F.M.D., Oliveira, E., Guimarães, R.J., Figueiredo, C.A.P.D. & Silva, F.C. 2006. Operational and economical performance of the coffee harvest with the use of the lateral harvester. *Coffee Science* **1**(2), 119–125 (in Portuguese).

Silva, F.M., Ferraz, G.A.S., Alves, M.C. 2013. Study case on precision coffee cultivation. In: Silva, F. M., Alves, M. C. (Ed). *Precision coffee makers*. Lavras: Editora UFLA, pp. 179–208. (in Portuguese).

Silva, J.E. & Resck, D.V.S. 1997. Soil organic matter. In: Vargas, M.A.T. & Hungary, M., ed. C*errado soils Biology*. Planaltina: Embrapa-CPAC, 467–524 (in Portuguese).

Silva, S.A. & Lima, J.S.S. 2012. Evaluation of the variability of nutritional status and coffee productivity through principal component analysis and geostatistics. *Ceres* **59**(2), 271–277 (in Portuguese).

Souza, J.M.L., Negreiros, J.R.S., Álvares, V.S., Leite, F.M.N, Souza, M.L., Reis, F.R & Felisberto, F.Á. V. 2008. Physicochemical variability of cassava flour. *Food Science and Technology* **28**(4), 907–912 (in Portuguese).

Teixeira, A.L., Gonçalves, F.M.A., Rezende, J.C., Rocha, R.B., Pereira, A.A. 2013. Principal components analysis on morphological characters of arabica coffee in juvenile stage. *Coffee Science* **8**(2), 205–210 (in Portuguese).

Xavier, F.A.D.S., Maia, S.M.F., Oliveira, T.S.D. & Mendonça, E.D.S. 2006. Microbial biomass and light organic matter in soils under organic and conventional agricultural systems in Ibiapaba - CE. *Brazilian Journal of Soil Science* **30**, 247–258 (in Portuguese).

Agronomy Research **17**(2), 430–437, 2019
https://doi.org/10.15159/AR.19.046

Evaluating the effects of application modes and soil types on the herbicide efficacy and crop yield of pendimethalin and clomazone on transplanted pepper (*Capsicum annuum* L.)

G. Glatkova[1,*] and Z. Pacanoski[2]

[1]University Ss. Cyril and Methodius, Agriculture Institute, 16-ta Makedonska brigada 3A, MK1000 Skopje, Republic Macedonia
[2]University Ss. Cyril and Methodius, Faculty for Agricultural Sciences and Food, 16-ta Makedonska brigada 3, MK1000 Skopje, Republic of Macedonia
[*]Correspondence: gordana_glatkova@yahoo.com

Abstract. Field experiment was carried out in 2014 and 2015 in two locations Kochani and Drachevo in Republic of Macedonia to evaluate the efficacy and crop safety of pendimethalin and clomazone on transplanted pepper according to mode of application, (pretransplant -PRE-T and pretransplant incorporated -PTI) and soil types (alluvial soil and vertisol). The weed population in both years and locations mainly consisted annual spring and summer grasses and broadleaf weeds. Weed competition significantly reduced pepper yield. There was no recorded difference between the efficacy of pendimethalin PRE-T and pendimethalin PTI. However, the efficacy of clomazone PTI was higher than that of clomazone PRE-T in both experimental years and locations, indicating incorporation into soil if critical for clamazone. Both pendimethalin and clomazone had low efficacy on *Solanum nigrum L*. Pepper plants were not visibly injured by any herbicides treatments. In summary, locations and soil types did not affect herbicide efficacy and pepper selectivity. Pepper yield was markedly affected by herbicide efficacy in both years and locations.

Key words: pepper, weeds, herbicides, pretransplant, pretransplant incorporated, soil type, effectiveness, injury.

INTRODUCTION

Pepper *(Capsicum annuum L.)* is an economically important vegetable crop in Republic of Macedonia, which is currently grown in about 8,522 ha, with total pepper production of 175,867 t and average pepper production in about 20.6 t ha^{-1} (Anonymous, 2015). Pepper is grown, in areas with a warm climate and a long growing season, which are also favorable to the growth of weeds, which results in increased weed pressure (Granberry & Colditz, 1990). Pepper is not a very competitive crop and weeds can significantly reduce pepper yield (Eshel et al., 1973; Frank et al., 1988). The weed infestation may reduce pepper yield by 60–80% (Sharma et al., 1988; Narayana, 1990, Khan et al., 2012). Weed management in pepper is required to minimize decrease of yield and quality of the fruit. Subhra & Pabirta (2014) noticed that the decrease in the pepper fruits/plant was proportional to the duration of weeds competition.

In Republic of Macedonia weed control in pepper are a combination of inter-row cultivation, hand weeding and herbicide application. For Macedonian farmers the use of soil applied herbicides before transplanting is most acceptable. This time of application leaves the soil surface without weeds at the beginning of the growing season. According to Isik et al. (2009) immediately after transplanting, chilli pepper seedlings grow slowly whereas weeds emerge fast, grow rapidly and compete with the crop for nutrients, moisture, sunlight and growing space during all growing season.

Some soil applied herbicides can be used pre-transplanting (PRE-T) or pre-transplanting incorporated (PTI) depending on the soil and weather conditions. Soil incorporation can increase the efficacy of the herbicide, but on the other hand, it can cause phytotoxicity on crops. Also, soil incorporation increases farmers' costs. The choice of any weed control measures therefore, depends largely on its effectiveness and costs (Subhra & Pabitra, 2014).

Pendimethalin is a herbicide of the dinitroaniline class used in premergence and early postemergence applications to control annual grasses and certain broadleaf weeds. Pendimethalin inhibits root and shoot growth. It controls the weed population and prevents weeds from emerging, particularly during the crucial development phase of the crop. Its primary mode of action is to preventing plant cell division and elongation in susceptible species. Pendimethalin is used in major crops such as corn, potatoes, sunflower, wheat, rice, vegetables like pepper, carrot, parsley, etc. Incorporation of pendimethalin into the soil by cultivation or irrigation is recommended (Janic, 1985 and 2005).

Clomazone, whose active ingredient is isoxazolane, is a selective herbicide with both contact and residual activity. Clomazone systemically enters through the roots and shoots and translocates via the xylem. This herbicide is used for the control of annual broadleaf weeds and grasses. It inhibits the biosynthesis of photosynthetic pigments of both chlorophyll and carotenoids. Susceptible plants sprayed with the herbicide typicallyshow signs of whitening or bleaching, followed by necrosis. Clomazone is used on major crops such as oilseed rape, cotton, tobacco, soybeans, rice and sugar cane and vegetables like peas, beans, carrots, pepper and potatoes. Incorporation of clomazone into the soil is not mandatory but is recommended (Dan, et al., 1989; Cabral, 2017).

To identify the best application method and the effects of soil types for pendimethalin and clomazone on Pepper, the study aimed at evaluating the efficacy and phytotoxicity of the two herbicides. Results from this study will provide guidance for farmers in Republic of Macedonia to adopt the right weed control programs to achieve better weed control in pepper.

MATERIALAS AND METODS

Field experiment was carried out in 2014 and 2015 at two locations Kochani and Drachevo, in eastern and northern Macedonia on alluvial soil and vertisol, respectively (Filipovski, 2006).

The experiment was laid out in a randomized block design having four replications and harvest plot size of 20 m^2. The field studies was carried with local pepper variety 'Kurtovska kapija' which was transplanted in a well-prepared seedbeds on June 13th, 2014 and June 16th, 2015 in Kochani location and June 16th, 2014 and June 18th, 2015 in

Drachevo location. The inter-row spacing was 60 cm and intra-row spacing was 30 cm. Standard agronomic practices were used in both locations and both experimental years. Tested treatments are described in Table 1.

Table 1. Trade names, active ingridients, rates and time of aplications of herbicides

Treatments	Concentration of active ingredient (a.i) in herbicide	Trade name of herbicide	Rate L ha^{-1}
Untreated Control	/	/	/
Weed-free control	/	/	/
Pendimethalin PTI	330 g L^{-1}	Stomp 330 E	5.00
Pendimethalin PRE-T	330 g L^{-1}	Stomp 330 E	5.00
Clomazone PTI	480 g L^{-1}	Gamit 4 EC	0.75
Clomazone PRE-T	480 g L^{-1}	Gamit 4 EC	0.75

PTI (pretransplant incorporated); PRE-T (pretransplant).

Application of the herbicides were with a CO_2 – pressurized backpack sprayer with 350 L ha^{-1} water. Both herbicides were applied in two method (PTI and PRE-T). Time of application were one day before pepper transplanting. Incorporation was performed with two parallel passes of a field cultivator with 25 cm sweeps operation to a depth of 8 cm. Untreated and weed free control were included in the studies. Weed free control was maintained with two runs of hoeing. Weed control efficacy was estimated 30 days after treatment (DAT) by weed plants counting and herbicides efficacy was calculated using the following equation (Mani et al., 1968).

$$\mathrm{Wce} = \frac{\mathrm{Wup} - \mathrm{Wtp}}{\mathrm{Wup}} \cdot 100 \qquad (1)$$

where Wce – weed control efficiency; Wup – number of weeds in the untreated plots; Wtp – number of weeds in the treated plots.

Pepper plant injury including bleaching, chlorosis, necrosis, stunting and minor leaf malformation were recorded 30 days after treatments (DAT). Injury was based on a scale of 0 to 100% where 0% = no pepper injury and 100% = all pepper plants death (Frans et al., 1986). Peppers in all plots (variants) were harvested two times based on the visual maturity of the pepper in weed free plots. The average yield for each variant is calculated. Pepper fruits were classified into marketable and non-marketable categories, based on factors such as size and colour Non-marketable materials were removed. The data were subjected to statistical analysis applying LSD- test (Steel & Torrie, 1980).

RESULTS AND DISCUSSION

Weed population: The weed population in both years and locations mainly consisted annual spring and summer grasses and broadleaf weeds. In both years Kochani weed population consisted 9 species, and total number of weeds was 223.7 plant m^{-2} in 2014 and 173.5 plant m^{-2} in 2015, respectively. In Drachevo region weed population in both years was consisted of 8 species, and total number of weeds was 126.2 plant m^{-2} in 2014 and 122.4 plant m^{-2} in 2015, respectively. (Table 2).

Table 2. Weed infestation in the study (for both years and locations) in the untreated plots

Weed species		Weeds No m^{-2}			
		Kochani		Drachevo	
		2014	2015	2014	2015
1.	*Portulaca oleraceae L.*	94.0	70.0	12.0	19.0
2.	*Amaranthus retroflxus L.*	38.8	42.0	68.0	51.0
3.	*Echinochloa crus gali (L.) P. Beauv*	24.7	12.1	10.9	15.6
4.	*Galinsoga parviflora Cav.*	24.3	10.6	1.5	2.8
5.	*Chenopodium album L.*	17.0	10.5	15.0	9.8
6.	*Solanum nigrum L.*	9.7	17.8	9.0	12.3
7.	*Setaria spp. (L.) P. Beauv*	7.1	5.3	8.6	10.0
8.	*Polygonum lapathifolium L.*	6.5	3.1	1.2	1.9
9.	*Abuthilon theofrasti Medik.*	1.6	2.1	/	/
Total weed species		9	9	8	8
Total weeds No m^{-2}		223.7	173.5	126.2	122.4

Herbicides efficacy: All herbicide treatment showed a highly significant ($P < 0.01$) effect on weed density per m^2 compared to the untreated control. Efficacy of herbicides in 2014 (Table 3.) ranged from 90.5% (clomazone PRE-T) to 98.3% (pendimethalin PTI) in Kochani and from 89.0% (clomazone PRE-T) to 98.0% (pendimethalin PTI) in Drachevo. In 2015 herbicide efficacy ranged from 85.3% (clomazone PRE-T) to 93.5% (clomazone PTI) in Kochani and from 82.8% (clomazone PRE-T) to 92.3% (pendimethalin PTI) in Drachevo. Method of application did not affect the efficacy of pendimethalin. Efficacy of clomazone PTI was significantly higher compared to clomazone PRE-T. (Table 3). John et al. (1998) emphasizes that clomazone must be incorporated to reduce vaporization.

Lower total herbicide efficacy in 2015 in both locations was caused by the lower efficacy of both herbicides on *Solanum nigrum* (Table 5). No effect of location/soil type on efficacy of both tested herbicide was observed. (Table 3).

Table 3. Total herbicides efficacy at 30 days after treatment (DAT) in both experimental locations and years

Treatments	Total herbicide efficacy/Weed control (%)			
	2014		2015	
	Kochani	Drachevo	Kochani	Drachevo
Untreated Control	0.0	0.0	0.0	0.0
Pendimethalin PTI	98.3 **	98.0 **	92.5 **	92.3 **
Pendimethalin PRE-T	97.5 **	97.0 **	91.5 **	91.8 **
Clomazone PTI	97.8 **	97.5 **	93.5 **	91.3 **
Clomazone PRE-T	90.5 **	89.0 **	85.3 **	82.8 **
LSD 0.05	1.2	1.0	1.3	1.0
LSD 0.01	1.7	1.4	1.8	1.4

(*) Significant level $P < 0.05$; (**) Significant level $P < 0.01$.

In 2014, efficacy of herbicides on dominant weeds 30 DAT ranged from 88.0% (ECHCG treated with clomazone PRE-T) to 99.8% (CHEAL treated with clomazone PTI) in Kochani and from 85.0% (SETSP treated with clomazone PRE-T) to 99.5% (POROL treated with clomazone PTI) in Drachevo (Table 4). In 2015, herbicide efficacy

on dominant weeds ranged from 70.3% (SOLNI treated with clomazone PRE-T) to 99.5% (GALPA treated with clomazone PTI) in Kochani and from 63.0% (SOLNI treated with clomazone PRE-T) to 99.3% (POROL treated with clomazone PTI) in Drachevo (Table 5).

Table 4. Herbicide efficacy on predominant weeds in both locations 30 DAT in 2014

Treatments	Kochani					Drachevo				
	POROL	AMARE	ECHCG	GALPA	CHEAL	POROL	AMARE	ECHCG	SETSP	CHEAL
Untreated Control	0	0	0	0	0	0	0	0	0	0
Pendimethalin PTI	98.3	95.3	94.8	97.3	99.5	97.8	95.0	96.5	97.8	98.3
Pendimethalin PRE-T	97.5	93.5	93.8	96.3	99.0	96.3	93.5	95.0	97.3	97.5
Clomazone PTI	97.8	95.0	95.0	95.3	99.8	99.5	91.0	96.8	98.0	98.0
Clomazone PRE-T	89.8**	89.5**	88.0**	90.5**	92.0**	88.5**	87.8**	90.0**	85.0**	88.8**
LSD 0.05	0.9	1.3	0.9	1.2	1.0	1.5	1.5	1.2	1.2	1.2
LSD 0.01	1.3	1.8	1.2	1.7	1.4	2.1	2.2	1.7	1.6	1.7

(*) Significant level $P < 0.05$; (**) Significant level $P < 0.01$;

POROL – *Portulaca oleracea*; AMARE – *Amaranthus* retroflexus; ECHCG – *Echinochloa* crus galli; GALPA – *Galinsoga parviflora*; CHEAL – *Chenopodium album*; SETSP – *Setaria spp*.

Table 5. Herbicide efficacy on predominant weeds in both locations 30 DAT in 2015

Treatments	Kochani					Drachevo				
	POROL	AMARE	ECHCG	GALPA	SOLNI	POROL	AMARE	ECHCG	GALPA	SOL NI
Untreated Control	0	0	0	0	0	0	0	0	0	0
Pendimethalin PTI	97.0	93.5	94.3	98.3	75.0	98.8	95.5	95.3	91.8	75.3
Pendimethalin PRE-T	95.8	92.0	92.8	98.3	74.3	98.3	94.8	94.3	91.3	74.3
Clomazone PTI	97.8	93.5	96.8	99.5	75.5	99.3	92.0	95.3	90.8	74.3
Clomazone PRE-T	86.8**	89.8**	90.3**	83.8**	70.3**	87.0**	86.3**	86.3**	86.0**	63.0**
LSD 0.05	1.2	1.3	1.2	1.4	1.0	0.9	1.2	1.0	1.2	1.7
LSD 0.01	1.7	1.8	1.7	2.0	1.4	1.3	1.7	1.4	1.7	2.4

(*) Significant level $P < 0.05$; (**) Significant level $P < 0.01$;

POROL – *Portulaca oleracea*; AMARE – *Amaranthus* retroflexus; ECHCG – *Echinochloa* crus galli; GALPA – *Galinsoga parviflora*; SOLNI – *Solanum nigrum.*

Most of tested herbicide treatments provided good controll (efficacy above 90%) on *Portulaca oleracea, Amaranthus retroflexus, Echinochloa crus galli, Galinsoga parviflora, Setaria spp*. and *Chenopodium album*, except that the efficacy of clomazone PRE-T was significantly lower. Both herbicides showed very low efficacy on *Solanum nigrum* (63.0–75.5%). According to John, et al. (1998), efficacy of clomazone PTI on *Chenopodium album* and *Datura stramonium* ranged between 77.0% and 95.0% without injury to bell pepper. Efficacy of pendimethalin in Subhra & Pabitra (2014) trials 30 DAT was 74.7%. In Gare et al. (2015) higher weed control efficiency was noted in treatments with pendimethalin, butachlor and fenoxaprop-P-ethyl combinated with two runs of hoeings and one hand weeding than in herbicides used alone without hoeing and hand weeding.

Visual injury of pepper: Pepper plants was not visibly injured by any herbicide treatments except clomazone PTI which caused transient bleaching on 2–3 leaves (0.3–0.7%) (Table 6). The injured plants recovered without affecting the pepper yield.

Table 6. Efects of herbicide treatments on pepper yield and crop injury

Treatments	Pepper yield kg ha^{-1}				Crop injury %			
	2014		2015		2014		2015	
	Kochani	Drahcevo	Kochani	Drachevo	Kochani	Drachevo	Kochani	Drachevo
Untreated Control	17,347	21,008	21,051	22,391	/	/	/	/
Weed-free control	45,719	44,922	44,193	43,829	/	/	/	/
Pendimethalin PTI	44,788	44,290	43,420	43,033	/	/	/	/
Pendimethalin PRE-T	44,430	44,166	43,368	43,120	/	/	/	/
Clomazone PTI	44,875	44,375	43,480	43,111	0.7	0.3	0.6	0.4
Clomazone PRE-T	39,176 **	38,667 **	38,568 **	36,658 **	/	/	/	/
LSD 0.05	1,134	1,100	637	629				
LSD 0.01	1,569	1,522	880	870				

(*) Significant level $P < 0.05$; (**) Significant level $P < 0.01$.

Weather and soil condition had no impact on the herbicide phytotoxicity. However according to Timothy et al. (2001) clomazone at application rate 1.12 kg ha^{-1} PTI and PRE-T significantly injured (leaf bleaching or chlorosis) 'Sweet Banana' (40% and 20%, respectively) and 'Red Chili' (30% and 18%, respectively) varieties in early season evaluations. However this injury was transient and did not significantly affect total fruit number or yield.

Pepper yield: Weed competition caused large reductions of pepper yield. Comparison of untreated and weed free control indicated that weeds reduced pepper yield from 53% to 63% without herbicide applications. Tested herbicide treatments in both experimental years at both locations had a significant ($P < 0.01$) effect on pepper yield. In both years, the lowest yield was recorded in untreated control (Table 6.). Absence of the weeds led to the increase of the pepper yield. Among herbicide treatments the pepper yield in 2014 ranged from 39,176 kg ha^{-1} (clomazone PRE-T) to

44,875 kg ha^{-1} (clomazone PTI) in Kochani and from 38,667 kg ha^{-1} (clomazone PRE-T) to 44,375 kg ha^{-1} (clomazone PTI) in Drachevo. In 2015 pepper yield ranged from 38,568 kg ha^{-1} (clomazone PRE-T) to 43,480 kg ha^{-1} (clomazone PTI) in Kochani and 36,658 kg ha^{-1} (clomazone PRE-T) to 43,120 kg ha^{-1} (pendimethalin PRE-T) in Drachevo. According to Yadav, R.S. (2001) all weed control treatments including pendimethalin produced significantly higher dry chilli yield compared with weedy check.

In both experimental years and locations, the lowest pepper yields among tested herbicide treatments was recorded on plots treated by clomazone PRE-T (from 36,658 kg ha^{-1} to 39,176 kg ha^{-1}) (Table 6), which correlated with the efficacy of the same herbicide variant. However, in the Mohsen & Douglas (2015) studies clomazone PRE-T did not reduce banana pepper yield.

According to Rodrigo et al. (2016) herbicides clomazone and pendimethalin applied PTI caused slight foliar chlorosis and necrosis but did not affect fruit yield, whereas the same herbicides applied posttransplant reduced fruit yield significantly. Cavero et al. (1996) noted insignificant reductions of seeded peppers yield after postemergence application of clomazone (1.0 and 2.0 kg ha^{-1}) at growth stage 6–8 leaves. Stall et al. (1996) also noted that pepper was tolerant to clomazone and pendimethalin applied PPI. Phillip & Tim (2006) study has shown that pendimethalin and clomazone gave best control when applied PRE-T. Both tested herbicide applied at double rates on soils with very low organic carbon and clay content did not cause any crop injury. Yield and quality of tested pepper cultivars were also not affected by these herbicides.

CONCLUSIONS

In the pepper production, pepper yields was markedly affected by weed competition. Weed management is important for increasing both the yield and quality of the pepper. Weeds reduced pepper yield about 53–63%. Pendimethalin and clomazone showed very good efficacy when they were incorporated into soil. Efficacy of clomazone was lower, if it was not incorporated into soil before transplanting. Pepper plants was not significantly visible injured by any herbicides treatments. Soil and weather conditions had no impact on the herbicides efficacy and crop yield.

REFERENCES

Anonymous. 2015. Agricultural statistic of Republic of Macedonia, Ministry for agriculture, forestry and water utilization, Government of RM, Skopje, R Macedonia

Cabral, C.M., Santos, J.B., Ferreira, E.A., Costa, S.S.D., Dalvi, V.C. & Francino, D.M.T. 2017. Structural evaluation of damage caused by herbicide clomazone in leaves of arborescent species native to Brazil. *Planta Daninha* **35**.

Cavero, J., Zaragoza, C. & Gil-Ortega, R. 1996. Tolerance of direct-seeded pepper (*Capsicum annuum*) under plastic mulch to herbicides. *Weed Technology* **10**, 900–906.

Dan, E.W., Lawrence ,R.O, & Robert E.F. 1989. Weed Control with Clomazone Alone and with Other Herbicides. *Weed Technology* **3**, 678–685.

Eshel, Y., Katan, J. & Palevitch, D. 1973. Selective action of diphenamid and napropamide in pepper and weeds. *Weed Research* **13**, 379–384.

Filipovski, G. 2006. Soil Classification of the Republic of Macedonia. MASA. (in Macedonian)

Frank, J.R., Schwartz, P.H. & Bourke, J.B. 1988. Insect and weed interactions on bell peppers. *Weed Technol*ogy **2**, 423–428.

Frans, R.E., Talbert, R., Marx, D. & Crowley, H. 1986. *Experimental sesign and tehniques for measuring and analyzing to weed control practices.* In N.D. Camper ed. Research Metods in Weed Science. rd ed. Champaing, IL: Southern Weed Science Society, pp. 37–38.

Gare, B.N., Raundal, P.U. & Burli, A.V. 2015. Integrated weed management in rainfed chilli (*Capsicum annum L.),* Karnataka *Journal of Agricultural Science* **28**, 164–167.

Granberry, D.M. & Colditz, P. 1990. Pepper culture and varieties, In Commercial pepper production. Coop. Ext. Service. U.S. Dept. Of Agr. The Univ. of Georgia College of Agr. *And Environ. Sci*., Athens, pp. 3–5.

Isik, D., Kaya, E., Ngouajio, M. & Mennan, H. 2009. Weed suppression in organic pepper (*Capsicum annuum* L.) with winter cover crops. *Crop Protection* **28**, 356–363.

Janic, V. 1985. *Herbicidi,* Naucna knjiga, Beograd pp. 335–336 (in Serbian).

Janic, V. 2005. *Fitofarmacija,* Drustvo za zastitu bilja Srbija, pp. 529–530 (in Serbian).

John, A.A., Henry, P.W. & Thomas, E.H. 1998. Weed Management in Transplanted Bell Pepper (Capsicum frutescens) with Clomazone and Rimsulfuron, *Weed Technology* **12**, 458–462.

Khan, A., Muhammad, S., Hussain, Z. & Khattak, A.M. 2012. Effect of different weed control methods on weeds and yield of chillies (*Capsicum annuum* L.). *Pakistan Journal of Weed Science Research* **18**, 71–78.

Mani, V.C., Gautam, K.C. & Chakraberty, T.K. 1968. Losses in crop yield in India due to weed growth. *PANS* **42**, 142–158.

Mohsen, M. & Douglas, D. 2015. Banana Pepper Response and AnnualWeed Control with S-metolachlor and Clomazone, *Weed Technology* **29**, 544–549.

Narayana, R.K. 1990. Effect of herbicides under different soil regimes on weed control, yield and quality of chillies *(Capsicum annum L.). Abstract of Papers Presented in Biennia Conference of Indian Society of Weed Sciences*, pp. 140–141.

Phillip, R.F. & Tim, L.H. 2006. *Evaluation of new herbicides for capsicums and chillies*, Research report, Serve -Ag Research Ag Research Pty Ltd, Australia, 3 pp.

Rodrigo, F., Fernanda, P., Connie, E., Gabriela, C. & Nathalie, K. 2016 Effects of Preemergence Herbicides on Bell Pepper, Crop Injury, and Weed Management in Irrigated Chilean Fields, *Weed Tehnology* **30**(2), 587–594.

Sharma, P.P., Lankroo, G.M. & Arya, P.S. 1988. Chemical weed control in bell pepper *(Capsicum annum* L.). *Vegetable Science* **15**, 113–119.

Stall, W.M. & Gilreath, J.P. 1996. Evaluation of pepper tolerance to selected preplant herbicides. *Proceedings of the Florida State Horticultural Society* **109**, 187–190.

Steel, R.G.D. & Torrie, J.H. 1980. *Principles and procedures of statistics*: A Biological Yield Approach. 2nd Ed. Mcgraw Hill Book Co., New York, 633 pp.

Subhra, S. & Pabitra, A. 2014. Weed management in transplanted chilli. *Indian Journal of Weed Science* **46**, 261–263.

Timothy, L.G., David, C.B. & Scott, D. 2001. Response of Several Transplanted Pepper Cultivars to Variable Rates and Methods of Application of Clomazone. *Hortscience* **36**,104–106.

Yadav, R.S. 2001. Integrated Weed Management in Transplanted Chilli Under Irrigated Conditions of Arid Zone. *Annals of Arid Zone* **40**, 53–56.

Agronomy Research **17**(2), 438–446, 2019
https://doi.org/10.15159/AR.19.093

Measurements of wireless detectors used to monitor animal movements in livestock farms

J. Hart[1,*] and V. Hartová[2]

[1]Czech University of Life Sciences Prague, Faculty of Engineering, Department of Technological Equipment of Buildings, Kamýcká 129, CZ165 00 Prague, Czech Republic
[2]Czech University of Life Sciences Prague, Faculty of Engineering, Department of Vehicles and Ground Transport, Kamýcká 129, CZ165 00 Prague, Czech Republic
[*]Correspondence: janhart77@gmail.com

Abstract. At present, there is a great interest in monitoring and automating farm animals and livestock farming. There are many systems and methods to check the movement of animals in certain areas. One option is to use motion detectors. However, some installations are so specific that they require the use of wireless motion detectors. They not only have to fulfill their functional part but also have a sufficiently strong signal that should not interfere outside the defined ISM bands. Due to the frequent deployment of different types of these detectors, research has been carried out to monitor shortcomings in frequently used types of wireless detectors. This research defines which tested detectors are fully usable according to the standards and which need to be modified by the manufacturer. Also, based on measurements, the basic risks and recommendations for the use of individual types of tested detectors are defined.

Key words: livestock, measurement, wireless, ISM band, detector.

INTRODUCTION

At present, there is a great interest in monitoring and automating farm animals and livestock farming. There are many systems and methods to check the movement of animals in certain areas. These methods can be divided into contact and non-contact. Contact methods can use different systems, such as pedometers or RFID technology (Porto et al., 2012). These detections can affect the comfort of animals and must be placed on each monitored place. If only a passage is required to be monitored, so-called non-contact measuring systems, such as laser gates, infrared gates, and others, are also used. All of these monitoring systems are part of so-called systems to maximize animal welfare (Firk et al., 2002; Barbari et al., 2008; Martiskainen et al., 2009; Ilie-Zudor et al., 2011; Alsaaod et al., 2012; Chanvallon et al., 2014).

One of the possibilities for non-contact detection is the use of passive motion detectors. However, there is a problem with the fact that only wireless detectors can be installed in certain locations. These detectors may not only meet the requirements for a given measurement but also require wireless transmission (Mathie et al., 2004; Robert et al., 2009; Ilie-Zudor et al., 2011; Alsaaod et al., 2012; Chanvallon et al., 2014).

ISM bands (Industrial, Scientific and Medical) are typically used for wireless transmission. Many researches have shown that not every transmitter meets the ISM band. These bands are free of charge and are specified by the telecommunication authorities. It was therefore a question of whether motion detectors meet the necessary requirements of telecommunication authorities. Failure to meet the requirements would lead to complications in their installation. (Kuchta et al., 2009; Nikonowicz et al., 2019; Zgaren et al., 2018; Yang et al., 2018).

Aim of the paper was of whether the selected wireless detectors meet the requirements for wireless communication in the ISM bands. An evaluation was also made based on the wireless transmitting intensity of individual motion detectors (Kuchta et al., 2009; Schmidt et al., 2017; Hart & Hartová, 2018; Nikonowicz et al., 2019).

MATERIALS AND METHODS

Test were performed accurately to determine the breadth of broadcast for each motion detector. Motion detectors for which the tests were conducted are standard motion detectors used to frequent occurrence. These are the following types:

ISM868: JA-83P, PMD75, PMD2P, IR8M, RWT95P

ISM433: PMD75, AZ-10P.

SPECTRAN HF-6060 spectrum analyser (Fig. 1) was used, which investigated the size of the frequencies at tested motion detectors. Within the measurement the following values were set on the SPECTRAN HF-6060 spectrum analyzer:

- Sampletime – 50 ms
- Samples – 500
- Bandwidth – 1 MHz

Figure 1. Spectrum analyser SPECTRAN HF-6060 with an antenna.

At the beginning of the measurement, the hypothesis 'The wireless signal base is in the ISM433 (433–434,79 MHz) or ISM868 (868–870 MHz) band' is determined. The measurements were made by the detector being installed in a laboratory 4 m from the spectral analyzer. When the detector was in the state of guarding, there was a disturbance of the guarded space (moving in front of the detector). Detected signals were also recorded through a spectral analyzer into the MSC SpectrumAnalyzer software. Subsequently, a graph of transmission characteristics was created with the help of the software. Measurement was performed on all motion detectors cyclically and measured at least 500 cycles.

The Figs 2–10 show the intensity of the wireless transmission motion detectors in bandwith ISM868. Among these figures, Figs 3, 5, 7 and 9 show the origin of the transmitted signal range for individual motion detectors.

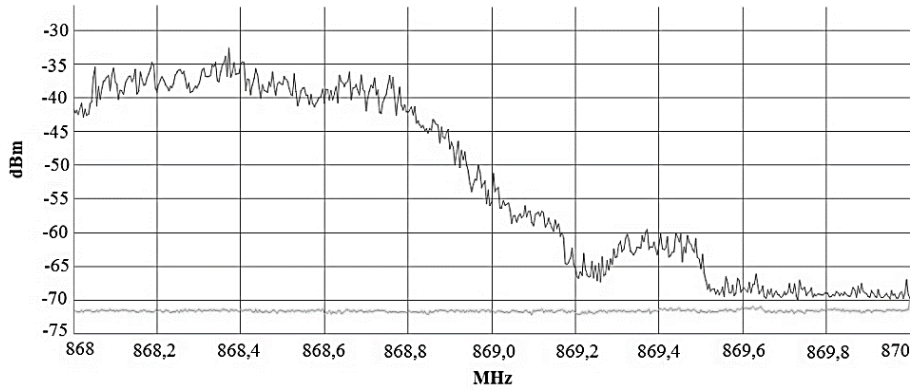

Figure 2. Motion detector JA-83P (ISM bandwidth).

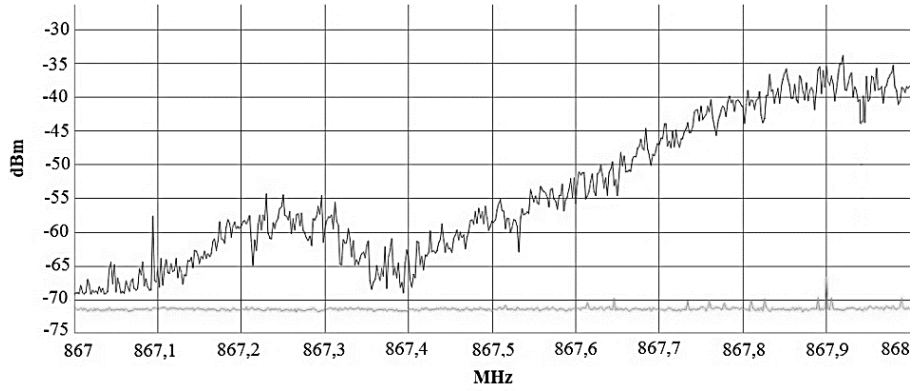

Figure 3. Motion detector JA-83P (origin of the transmitted signal range).

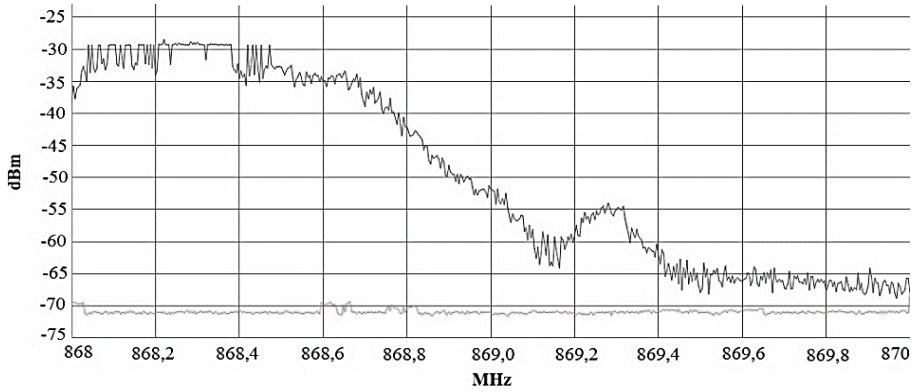

Figure 4. Motion detector PMD75 (ISM bandwidth).

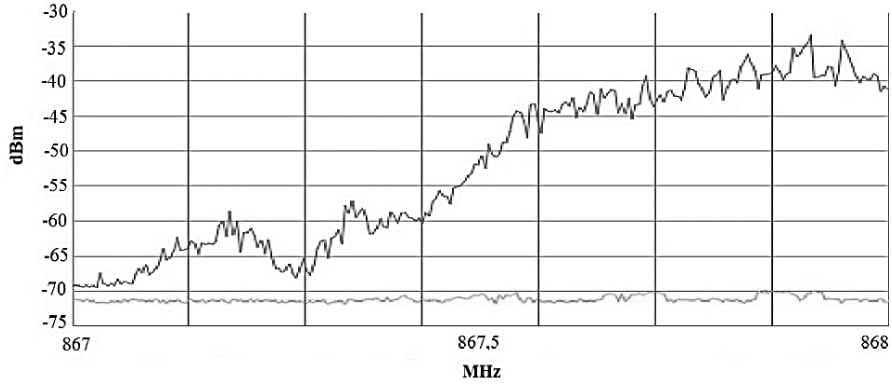

Figure 5. Motion detector PMD75 (origin of the transmitted signal range).

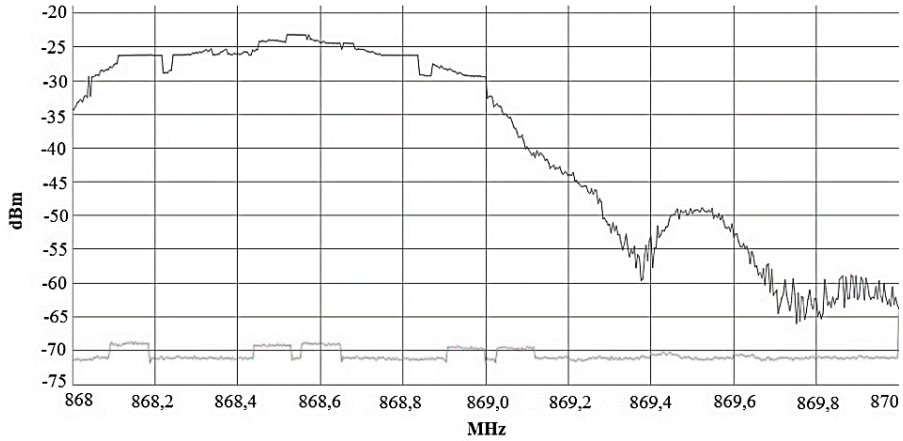

Figure 6. Motion detector PMD2P (ISM bandwidth).

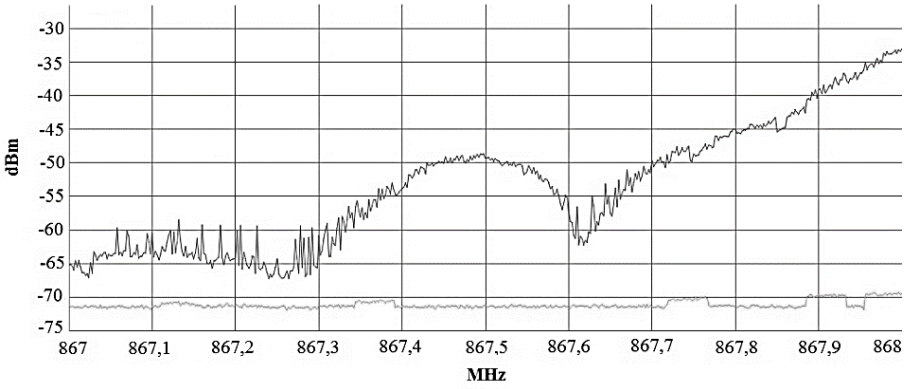

Figure 7. Motion detector PMD2P (origin of the transmitted signal range).

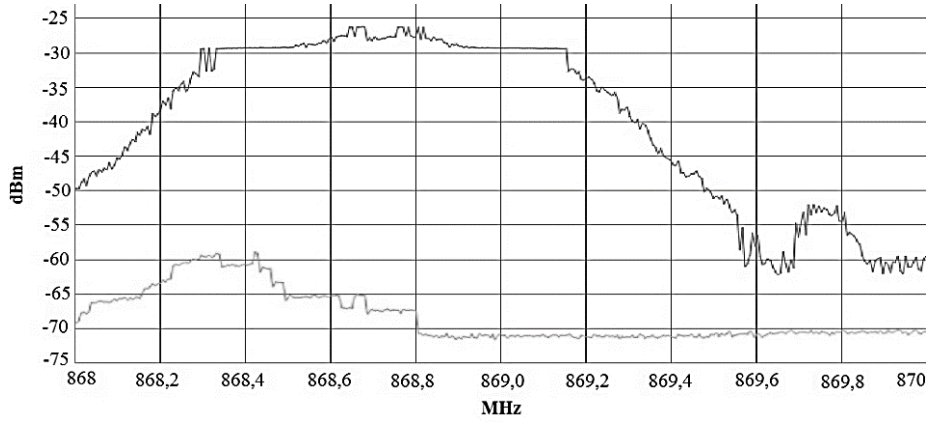

Figure 8. Motion detector IR8M (ISM bandwidth).

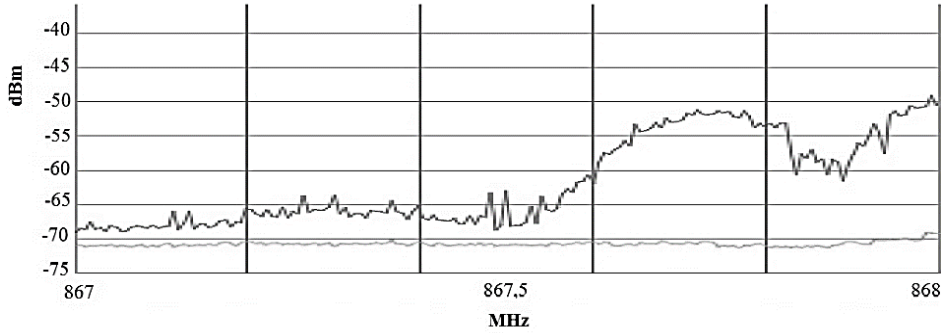

Figure 9. Motion detector IR8M (origin of the transmitted signal range).

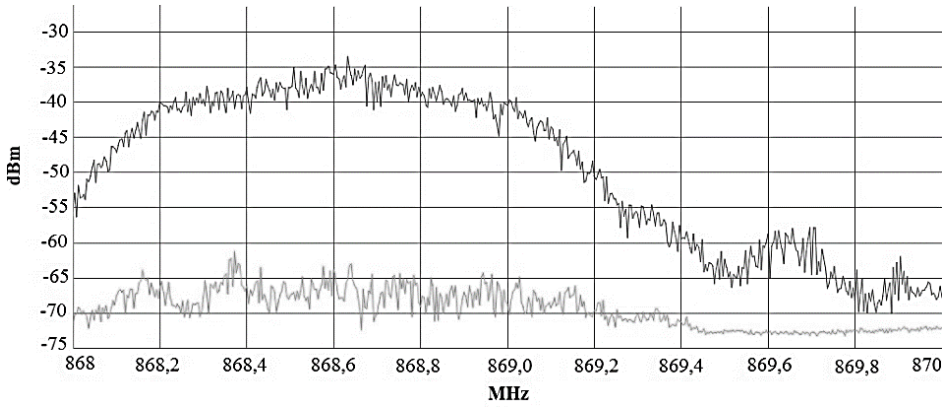

Figure 10. Motion detector RWT95P (ISM bandwidth).

The Figs 11 and 12 show the intensity are an evident intensity of the wireless transmission motion detectors in bandwith ISM433.

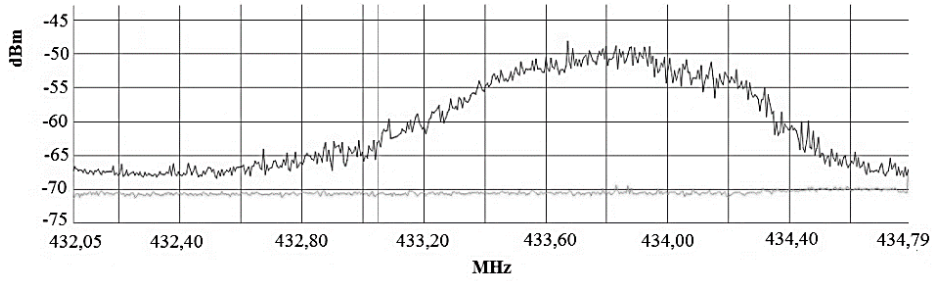

Figure 11. Motion detector PMD75 (ISM bandwidth).

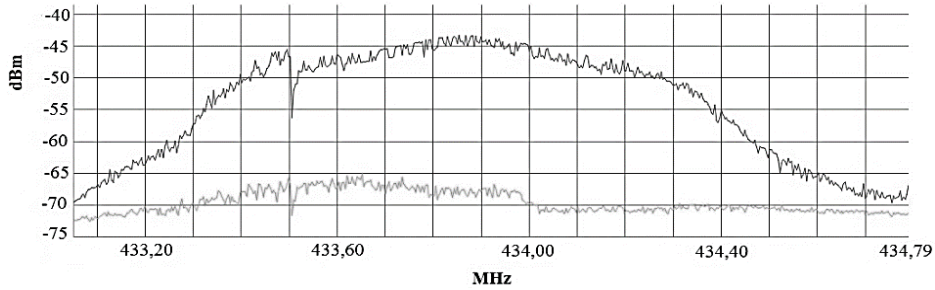

Figure 12. Motion detector AZ-10P (ISM bandwidth).

In the following figures (Figs 11 and 12) are an evident intensity of the wireless transmission motion detectors in bandwith ISM433.

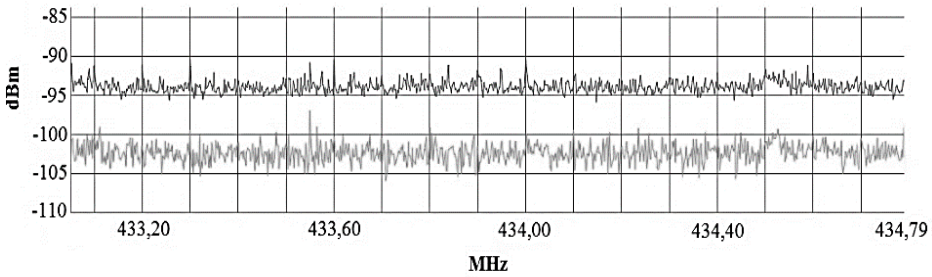

Figure 13. Motion detector AZ-10P (ISM bandwidth).

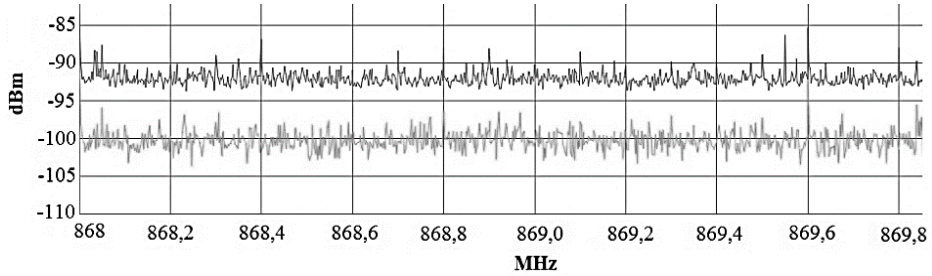

Figure 14. Motion detector AZ-10P (ISM bandwidth).

RESULTS AND DISCUSSION

All charts show two values, referred to the maximum measured value and the current trend. For detector measurements, the maximum value of the detector transmission is given. For ISM band measurements, the maximum value is the limit over which it is normally possible to transmit.

It is obvious that all tested detectors meet signal intensity. According to the measurement of natural interference in a given area (Figs 13 and 14) it is obvious that all tested detectors have higher signal strength. It was found that the JA-83P, PMD75, PMD2P and IR8M detectors did not meet the requirements of the ISM bands and hit their part beyond the defined values (Figs 3, 5, 7 and 9).

The evaluation of the individual criteria, which are the signal strength, the base of the transmission signal and the exact range defined by the ISM bands, can be seen in Fig. 15. The graph was created by a multi-criteria point analysis of variants. The ratio between the criteria evaluated was: exact range defined by the ISM bands (0.5), the signal strength (0.3) and the base of the transmission signal (0.2).

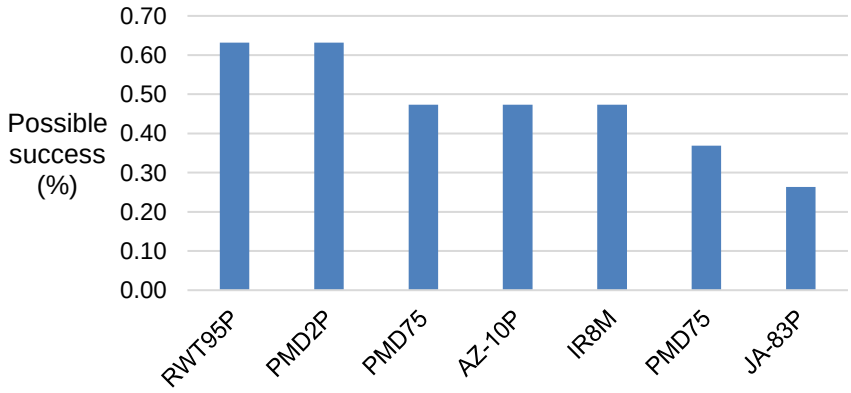

Figure 15. The evaluation of the individual criteria at motion detectors.

Possible success has been identified. This is the percentage of intensity, width and meeting the scope of ISM wireless transmission. Although two detectors (RWT95P and PMD2P) were placed in the first place, it can be determined that the detector RWT95P is better. This is because it meets the ISM868 transmission band.

In the past, many tests have been carried out on different systems that have proven that not every manufacturer adheres to the exact range of ISM bands. For the proper functioning of cattle pass testing, it is advisable to use motion detectors that meet the requirements for their use. The use functional detectors that do not have a well defined ISM band can result in the need to uninstall the system. This initiative may arise from a telecommunication office that can evaluate the system being used as a disruptive element in a given area (Kuchta et al., 2009; Schmidt et al., 2017; Hart & Hartová, 2018; Zgaren et al., 2018; Yang et al., 2018; Nikonowicz et al., 2019).

CONCLUSIONS

On the basis of this study, some conclusions can be taken. It is important to have an overview of the reliability and functionality of each wireless transmissions. When using wireless transmissions, it is also important for motion detectors to have bidirectional communication, which increases the system's chances to detect band interference, and also allows the transmission to be switched to a free zone.

The RWT95P is the best-rated detector due to its features. Detectors JA-83P, PMD75, PMD2P and IR8M detected overlapping outside ISM bands. It is therefore recommended to change the wireless technology of these detectors.

All of the measured data are important for end users and manufacturers as feedback on their products. In the future, there will be efforts to expand similar tests to other manufacturers, as the reliability of these systems is very important, and it will be necessary to check them.

ACKNOWLEDGEMENTS. It is a project supported by the CULS IGA TF 'The University Internal Grant Agency' (31170/1312/3121).

REFERENCES

Alsaaod, M., Romer, C., Kleinmanns, J., Hendriksen, K., Rose-Meierhofer, S., Plumer, L. & Buscher, W. 2012. Electronic detection of lameness in dairy cows through measuring pedometric activity and lying behavior, In: *APPLIED ANIMAL BEHAVIOUR SCIENCE*, pp. 134–141.

Barbari, M., Conti, L. & Simonini, S. 2008. Spatial identification of animals in different breeding systems to monitor behaviour. *Proceedings of the VIII Congress on Livestock Environment*. Iguassu Falls, Brazil, 31 August-4 September, 937–942.

Chanvallon, A., Coyral-Castel, S., Gatien, J., Lamy, J.M., Ribaud, D., Allain, C., Clement, P. & Salvetti, P. 2014. Comparison of three devices for the automated detection of estrus in dairy cows, In: *THERIOGENOLOGY*, pp. 734–741.

Firk, R., Stamer, E., Junge, W. & Krieter, J. 2002. Automation of oestrus detection in dairy cows: a review, In: *LIVESTOCK PRODUCTION SCIENCE*, pp. 219–232.

Hart, J. & Hartová, V. 2018. Testing of ISM band at remotes for unlocking vehicles. *Agronomy Research* **16** (S1), 1017–1024.

Ilie-Zudor, E., Kemeny, Z., van Blommestein, F., Monostori, L. & van der Meulen, A. 2011. A survey of applications and requirements of unique identification systems and RFID techniques, In: *COMPUTERS IN INDUSTRY*, pp. 227–252.

Kuchta, R., Vrba, R. & Sulc, V. 2009. IQRF Smart Wireless Platform for Home Automation: A Case Study, In: 5*th International Conference on Wireless and Mobile Communications*, Cannes, France, pp. 168–173.

Martiskainen, P., Jarvinen, M., Skon, J.P., Tiirikainen, J., Kolehmainen, M. & Mononen, J. 2009. Cow behaviour pattern recognition using a three-dimensional accelerometer and support vector machines, In: *APPLIED ANIMAL BEHAVIOUR SCIENCE*, pp. 32–38.

Mathie, M.J., Coster, A.C.F., Lovell, N.H. & Celler, B.G. 2004. Accelerometry: providing an integrated, practical method for long-term, ambulatory monitoring of human movement, In: *PHYSIOLOGICAL MEASUREMENT*, pp. R1–R20.

Nikonowicz, J., Mahmood, A., Sisinni, E. & Gidlund, M. 2019. Noise Power Estimators in ISM Radio Environments: Performance Comparison and Enhancement Using a Novel Samples Separation Technique, In: *IEEE TRANSACTIONS ON INSTRUMENTATION AND MEASUREMENT*, pp. 105–115.

Porto, S.M.C., Arcidiacono, C., Cascone, G., Anguzza, U., Barbari, M. & Simonini, S. 2012. Validation of an active RFID-based system to detect pigs housed in pens. *J. Food, Agriculture & Environment* **10**(2), 468–472.

Robert, B., White, B.J., Renter, D.G. & Larson, R.L. 2009. Evaluation of three-dimensional accelerometers to monitor and classify behavior patterns in cattle, In: *COMPUTERS AND ELECTRONICS IN AGRICULTURE*, pp. 80–84.

Schmidt, M., Block, D. & Meier, U. 2017. Wireless Interference Identification with Convolutional Neural Networks, In: *2017 IEEE 15TH INTERNATIONAL CONFERENCE ON INDUSTRIAL INFORMATICS (INDIN*), pp. 180–185.

Yang, H., Kim, B., Lee, J., Ahn, Y. & Lee, C. 2018. Advanced Wireless Sensor Networks for Sustainable Buildings Using Building Ducts, In: *SUSTAINABILITY*, Ar. Num. 2628.

Zgaren, M., Moradi, A., Tanguay, L.F. & Sawan, M. 2018. ISM-band 902-to 928-MHz FSK transceiver with scalable performance for medical devices, In: *INTERNATIONAL JOURNAL OF CIRCUIT THEORY AND APPLICATIONS*, pp. 2266–2282.

Agronomy Research **17**(2), 447–455, 2019
https://doi.org/10.15159/AR.19.102

Assessment of production zones modelling accuracy based on satellite imaging and yield measurement of selected agriculture plot

Z. Jelínek*, K. Starý and J. Kumhálová

Czech University of Life Sciences Prague, Faculty of Engineering, Department of Machinery Utilization, Kamýcká 129, CZ165 00 Prague, Czech Republic
*Correspondence: jelinekzdenek@tf.czu.cz

Abstract. Currently, remote sensing or yield monitor equipment offer possibilities how to estimate productivity of the agriculture field. That is why the main aim of this study is to assess how the latest satellite images from vegetation season and final yield data from combine harvester can be used to predict yield and to assess site-specific zones productivity. The study is focused on the accuracy of these systems for the field productivity estimation. The 24.7 ha experimental field is located near to Vendoli village (the Czech Republic) and it is cultivated by conventional agricultural practices with emphasis on typical agricultural crops growing in the Czech Republic (winter wheat, spring barley and winter rape). The results showed that both methods of estimation can be used for yield prediction. Nevertheless, each of them need specific processing and has typical limitations.

Key words: Spectral indices, yield data, growth stages, geoinformatics.

INTRODUCTION

Agricultural systems are modified ecosystems. Change in one component of a system makes changes in other systems, because of mutual interactions. For example change in humid or in weather to warm can lead to the development of a crop diseases and losing of crop yield potential. Adaptation to managing technological processes is very difficult. Systems are influenced by the weather condition and other inputs. Murthy (2012) described nine types of agricultural meteorology models, which are classified into different types or groups, i.e statistical, mechanistic, deterministic, stochastic, dynamic, static, simulation, descriptive and explanatory model. These models explain influence of weather on agricultural systems.

Remote sensing in agricultural application has been used more than three decades (Knipling, 1970; Tucker et al., 1981; Moran et al., 1994; Wardlow & Egbert, 2008) and one of the aim of remote sensing is to optimize crop yield in large plot and predict yield (Mulla, 2013). Generally mapping of yields and weather models are important for projecting impact of climate change on linked environmental outcomes (Rosenzweig et. Al., 2013). Currently many information about individual zones are accumulated and are used for the analysis of crop growth a yield patterns and also can be used for management zones (Mulla, 2013). In studies focused on monitoring of health crop with the help of

remote sensing are used especially spectral indices, mainly Normalized Difference Vegetation Index (NDVI, Rouse et al., 1974), the normalized ratio between RED and NIR bands. Most of spectral indices are based on leaf area index (LAI) or absorption photosynthetically radiation (Asrar et al., 1984; Baret & Guyot, 1991). More than 100 spectral indices have been reviewed by Xue & Su (2017). They described spectral indices along with their representativeness, applicability and implementation in precision agriculture.

Weather data is usually used as an input to crop models. Thornton et al. (1997) described these models and their link to simulation of crop growth, development and impacts of climate change. Crop models and simulation are very often used in USA and also in Europe by farmers, public and private agencies and policy makers to a greater extent for decision making (Murthy, 2012). In addition, basic knowledges about inputs provide valuable informations applicable in yield prediction. There are also many studies showing the benefits of crop prediction and geostatistical analysis for agricultural management (Seelan et al., 2003).

It is clear that many inputs data play a key role in yield prediction and crop simulations. Nevertheless appropriate data collection can be limited for farmers in practical use. The main aim of this study is to use only the most common data from agronomical praxis as yield, mostly free satellite images and weather data (temperature and precipitation) and phenology expressed by BBCH scale for yield or NDVI frequency maps modelling for the yield prediction and crop structure estimation.

MATERIALS AND METHODS

Study area

The study area is an 24.7 ha experimental field located near to Vendolí village (N 49°43'48", E 16°24'14"), The Czech Republic. The experimental field is undulated with elevation ranges from 543 m to 571 m a.s.l. and 6% slope. The soil can be classified as modal cambisols on limestone sandstones. Some parts of this plot are strongly eroded, especially those sloping. The average precipitation is 700 mm per year and the average temperatures ranges between 6 and 7 °C. Table 1 contents the temperature and precipitation data from monitored years (2014 to 2018). The experimental field is owned by Agricultural Company Vendolí used conventional arable soil technology (ploughing) on all their plots. Since 2014 the crop rotation has been as follows: winter wheat (2014), spring barley (2015), winter rape (2016), winter wheat (2017) and spring barley (2018).

Table 1. Weather conditions (precipitations and temperatures) at different phenological phases by BBCH scale for experimental field in 2014–2018

	Precipitation (mm)					Temperature (°C)				
	2014	2015	2016	2017	2018	2014	2015	2016	2017	2018
BBCH 0–19	37.0	30.4	69.0	32.8	21.1	8.8	5.5	12.1	3.6	15.2
BBCH 20–29	97.8	7.6	191.0	224.2	37.7	2.8	9.7	3.0	2.7	17.0
BBCH 30–59	127.2	35.8	44.2	75.9	24.8	9.6	13.0	6.7	16.1	19.8
After BBCH 60	201.8	132.6	177.5	173.8	53.8	17.1	18.6	15.9	19.6	19.4
Sum	463.8	206.4	481.7	506.7	137.4	-	-	-	-	
Mean	115.9	51.6	120.4	126.7	34.4	9.6	11.7	9.4	10.5	17.9

Yield and remote sensing data

The yield was measured by a combine harvester New Holland CR9080 equipped with yield monitor and DGPS receiver with EGNOS correction. The accuracy of this system is ± 0.1-0.3 m in horizontal and ± 0.2–0.6 m in vertical direction. The yield data are saved every 1 second with coordinates to the external memory. Failure on external memory caused the data loses in 2017. The yield data were process by basic statistical method in order to eliminate the errors of yield measurement system. The yield data sets were then interpolated to kriging maps (see Fig. 1) using experimental variograms. Details about yield data processing are more described in Kumhálová et al., 2011. Relative yield values were calculated for each yield data set with the aim to standardize the yield data (the actual yield value to average yield value of the plot converted to percentages). The relative yield maps were then converted to rasters, resampled to equal spatial resolution (10 m according to Sentinel 2 spatial resolution) and recalculated to yield frequency maps (Maphanyane et al., 2018) with help of Cell Statistics tool in ArcGIS 10.4.1 SW (ESRI, Redlands, CA, USA). The maximum values of the input's yield data were used for yield frequency maps calculation. The yield frequency maps were derived from the all measured years and from cereals only (except winter rape yield) – see Fig. 2, (a, b).

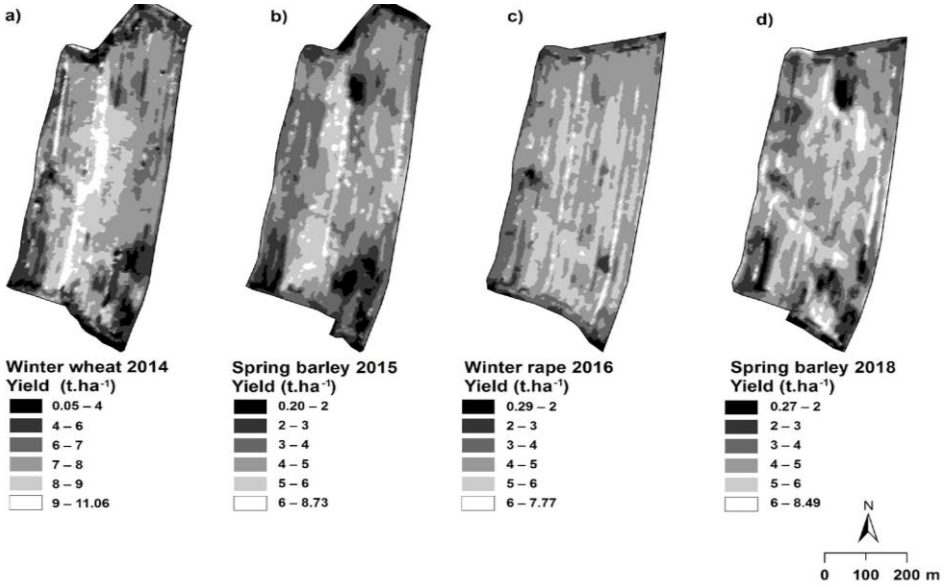

Figure 1. Yield maps (in t ha^{-1}) for the years 2014 with winter wheat (a); 2015 with spring barley (b); 2016 with winter rape (c); 2018 with spring barley (d).

The Landsat 8 satellite image for 2014 was downloaded from USGS (https://earthexplorer.usgs.gov/), Sentinel 2A images for 2016, 2017 and 2018 were downloaded from Copernicus Open Access Hub (https://scihub.copernicus.eu/) and SPOT 7 image for 2015 was purchased from ArcDATA Company (https://www.arcdata.cz/). The last satellite images from each vegetation season were selected, pre-processed to the level of BOA reflectance (Bottom of Atmosphere) and resampled to 10 m spatial resolution except Landsat image in 2014 (see Table 2 and

Fig. 3) with the help of SW ENVI 5.5 (Excelis, Inv. Mc Lean, USA) or SNAP 6.0.4 (ESA, http://step.esa.int/main/). Normalized Difference Vegetation Index was calculated from each image. NDVI frequency maps with the help of Cell Statistics tool were created in four variations, where maximum values of the input data were used. The NDVI frequency maps were derived on the base of – all NDVI images [1], NDVI images for cereals only (without 2016 – winter rape) [2], all NDVI images except 2014 (with 30 m spatial resolution/Landsat image) [3] and NDVI for cereals (except 2014 and 2016) [4] – see Fig. 2(c–f).

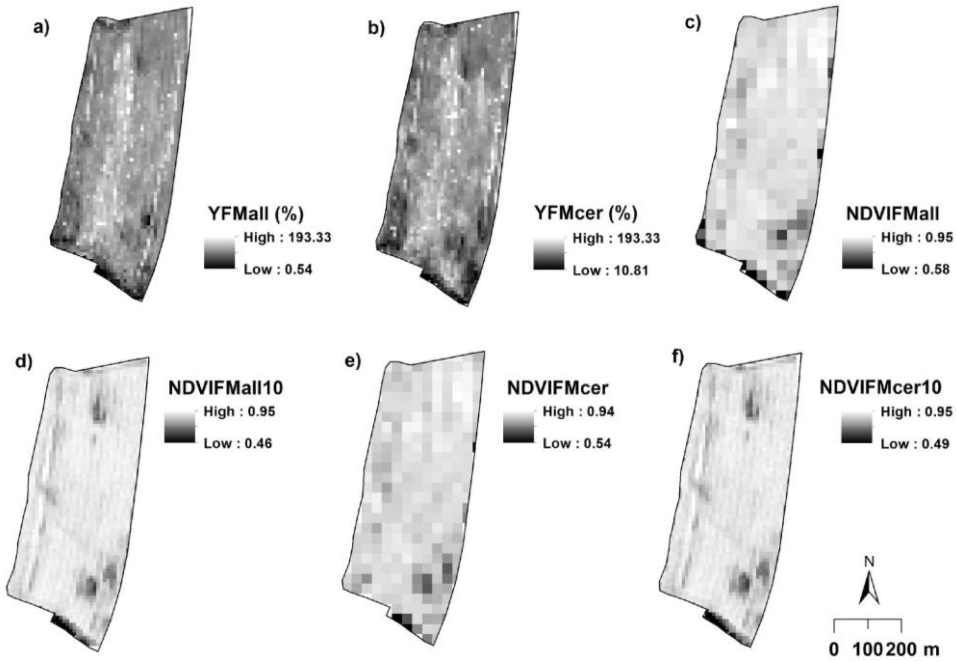

Figure 2. Yield and Normalised Difference Vegetation Index (NDVI) frequency maps: YFMall = yield frequency map derived from all yield maps (a); YFMcer = yield frequency map derived from cereals yield maps only (b); NDVIFMall = NDVI frequency map for all years (c); NDVIFMall10 = NDVI frequency map for all years without Landsat image/2014 (d); NDVIFMcer = NDVI frequency map derived for cereals only (e); NDVIFMcer10 = NDVI frequency map derived for cereals without Landsat image/2014 (f).

Table 2. Satellite images used in this study

Satellite	Sensor	Spatial resolution	RED range (nm)	NIR range (nm)	Date
Landsat 8	OLI	30 m	636–673	851–879	7-July 2014
SPOT 7	NAOMI	6 m	625–695	760–890	4-July 2015
Sentinel 2A	MSI	10 m*	650–680	785–900	5-June 2016 20-June 2017 17-June 2018

RED = reflectance in RED band; NIR = reflectance in near infrared band; OLI = Operational Land Imager; NAOMI = New AstroSat Optical Modular Instrument; MSI = Multispectral Instrument; * 10 m for RED and NIR bands.

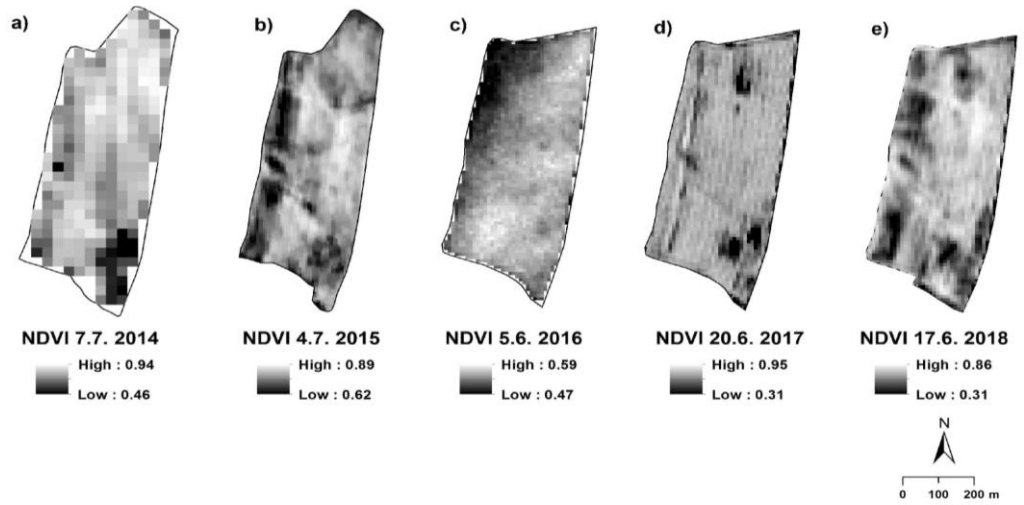

Figure 3. Normalised difference Vegetation Index (NDVI) for the years 2014 with winter wheat (a); 2015 with spring barley (b); 2016 with winter rape (c); 2017 with winter wheat (e); 2018 with spring barley (f).

Coefficients of determination were calculated in Statistica 8.0 SW (StatSoft Inc., Tulsa, OK, USA) between each crop yield data, NDVI images, yield frequency maps and NDVI frequency maps (see Table 3 and 4).

RESULTS AND DISCUSSION

The coefficients of determination for selected parameters are shown in Table 3 and 4. The coefficients of determination were calculated for a 5% significance level.

Table 3. Coefficients of determination between yield from selected years and Yield/NDVI frequency maps and NDVI (at 5% significance level)

Models	Yield 18	Yield 16	Yield 15	Yield 14
YFMcer	0.56	0.15	0.59	0.45
YFMall	0.24	0.16	0.46	0.44
NDVIFMcer	0.12	0.01	0.22	0.14
NDVIFMcer10	0.24	0.03	0.24	0.13
NDVIFMall	0.10	0.31	0.07	0.07
NDVIFMall10	0.30	0.08	0.36	0.16
NDVI180617	0.52	0.10	0.36	0.16
NDVI170620	0.27	0.08	0.34	0.16
NDVI160605	0.05	0.13	0.05	0.03
NDVI150704	0.18	0.09	0.27	0.08
NDVI140707	0.06	0.05	0.26	0.19

NDVI = Normalised Difference Vegetation Index for selected terms; YFMcer = yield frequency map derived from cereals yield maps only; YFMall = yield frequency map derived from all yield maps; NDVIFMcer = NDVI frequency map derived for cereals only; NDVIFMcer10 = NDVI frequency map derived for cereals without Landsat image/2014; NDVIFMall = NDVI frequency map for all years; NDVIFMall10 = NDVI frequency map for all years without Landsat image/2014.

Table 4. Coefficients of determination between NDVI from selected terms and Yield/NDVI frequency maps (at 5% significance level)

	NDVI180617	NDVI170620	NDVI160605	NDVI150704	NDVI140707
YFMcer	0.38	0.24	0.04	0.17	0.14
YFMall	0.18	0.16	0.08	0.12	0.14
NDVIFMcer	0.20	0.31	0.006	0.12	0.35
NDVIFMcer10	0.18	0.38	0.008	0.07	0.14
NDVIFMall	0.06	0.03	0.14	0.06	0.05
NDVIFMall10	0.26	0.96	0.02	0.12	0.18

NDVI = Normalised Difference Vegetation Index for selected terms; YFMcer = yield frequency map derived from cereals yield maps only; YFMall = yield frequency map derived from all yield maps; NDVIFMcer = NDVI frequency map derived for cereals only; NDVIFMcer10 = NDVI frequency map derived for cereals without Landsat image/2014; NDVIFMall = NDVI frequency map for all years; NDVIFMall10 = NDVI frequency map for all years without Landsat image/2014.

Table 3 showed that winter rape yield prediction based on yield frequency maps had lower usability (r^2 = 0.15 /0.16 for both cases) than the yield prediction maps for cereals yield estimations (r^2 from 0.24 to 0.59). On the other hand the cereals yield prediction was more accurate for model which included the yield form cereals only (except winter rape, see Fig. 2, b). The yield frequency map for cereals explained from 56% to 59% of actual yield variability for spring barley and 45% for winter wheat yield. No significant difference was found in yield prediction for winter wheat in 2014 between both yield models (see Fig. 2, a and b). On the contrary yield frequency map for cereals (see Fig. 2b) explained actual spring barley yield more significantly than the other model.

NDVI frequency map from all year except 2014 with Landsat image, resampled to 10 m (see Fig. 2, d), seemed to be the best model for actual cereal yields explaining. Nevertheless the actual yields were explained from 30 to 36% for spring barley and 16% for winter wheat. Winter rape actual yield was best explained, but not too much significantly (31%), by the model derived from all NDVI from 2014 to 2018 (see Fig. 2, c).

Coefficients of determination between actual yields and actual NDVI map generally fits best for individual years. The exception was NDVI in 2018, where NDVI image fits best for both spring barley yield maps (in 2015 and 2018 – see Figs 1 and 3).

Table 4 showed coefficient of determination between NDVI from selected terms and Yield / NDVI models. The models generally better explain the cereal crop variability, crop health and structure in individual terms in years 2017 and 2018. It can be caused by weather conditions, when ore water supply was during crop tillering (BBCH 20–29) with higher temperature in comparison with previous years. The best model for crop condition estimation seems to be the NDVI frequency map in spatial resolution of 10 m according to Sentinel 2 image from all years except 2014 (see Fig. 2, d). This model explains winter wheat crop structure from 96%. The best model for crop yield estimation is then yield frequency map for cereals (see Fig. 2, b) that explain the yield variability from 44% in average for all selected years.

The yield is made up of many variables among which belong especially weather condition, soil type, pH, soil nutrients and topography (Kumhálová et al. 2011). In time of climate warming it is obvious that the crop growth and then resulting yield is mostly influenced by water supply as in our study in 2017 and 2018. Crops benefit better in places with better water and nutrients supply, especially in drier years. This statement is

in accordance with Schmidt & Persson (2003) or Kumhálová & Matějková (2017). The places with better productivity are good bounded by derived yield or NDVI frequency maps. Each of these models used in this study has its positive or negative sides that can influence their usability. The yield frequency maps depend on annual measurement of yield data. It can be a problem for farmers who do not have the appropriate equipment (active yield monitor on combine harvester). The problem may also occur during recording and storing yield data on combine harvester. This was case of our study in 2017. In order to obtain as accurate data as possible, it is necessary to calibrate the yield monitor system and to properly process the yield data using advanced tools (Chung et al., 2002, Maldaner et al., 2016). Currently, many commercial or freely available softwares allow relatively simple data processing to resulting yield frequency map (Pink & Dobermann, 2005). The NDVI frequency maps depend on satellite images access. Currently satellite images from Copernicus Earth observation programme offers optical satellite images with high spatial (from 10 to 60 m) and radiometric (13 bands) resolution and very good revisit frequency (5-days on equator). Fiuzal et al. (2017) stated that the main limitation of using optical data is heavy cloud cover. This is in accordance with our study. The satellite images were selected according to criteria (1) last satellite image in vegetation season and (2) cloud-free image. For this reason, there is a relatively large data range in the images used for the purposes of this study (5 June 2016 and 7 July 2014). To ensure these criteria, it was also necessary to use various satellite images (Landsat, Sentinel 2 and SPOT) regardless of their properties. The spectral and spatial differences can be one of the limitations in comparison and use data sets. This corresponds well with Scudiero et al. (2016) study, where the suitability of sensor measurements to geographical region and use purposes was assessed.

Many studies have been written to evaluate cereals using optical remote sensing. The first was publicated in the 1970s with the most widely used NDVI spectral index. As can be seen from the results of this study, the models used are more suitable to evaluate and predict the yield of cereals than winter rape. Our results are in good agreement with the findings of Domínguez et al. (2017). They found out that different winter rape canopy architecture and leaf structure cause different spectral properties then in the case of cereals. Winter rape crops have also other growth requirements than cereals.

CONCLUSIONS

The results showed that information about crop yield and crop condition derived from satellite images can be useful for frequency map modelling. Yield frequency map and NDVI frequency map can be helpful tool for agriculture plots management. These models have their limitations that can be crucial for agricultural praxis. Nevertheless, our study showed that the best model for crop yield estimation is yield frequency map for cereals explaining the yield variability from 44% in average for all selected years. The best model for crop condition estimation seems to be the NDVI frequency map in spatial resolution of 10 m according to Sentinel 2 image from all years. This model explain winter wheat crop structure from 96% and from 38% for all selected NDVI images. The models were more significant for cereals and in drier and warmer years.

ACKNOWLEDGEMENTS. This study was supported by Czech University of Life Sciences Prague, when conducted under grant IGA no. 31180/1312/3118. The authors wish to deep thank the farmers in Agricultural Company Vendolí for their time, inputs data and provided experimental field.

REFERENCES

Asrar, G., Fuchs, M., Kanemasu, E.T. & Hatfield, J.L. 1984. Estimating absorbed photosynthetic radiation and leaf-area index from spectral reflectance in wheat. *Agron. J.* **76**, 300–306.

Baret, F. & Guyot, G. 1991. Potentials and limits of vegetation indexes for LAI and APAR assessment. *Remote Sens. Environ*. **35**, 161–173.

Copernicus Open Access Hub. *https://scihub.copernicus.eu/* Accessed 18.12.2018.

Chung, S.O., Sudduth, K.A. & Drummond, S.T. 2002. Determining yield monitoring system delay time with geostatistical and data segmentation approaches. *Transactions of the ASAE* **45**(4), 915–926.

Domínguez, J.A., Kumhálová, & J. Novák, P. 2017. Assessment of the relationship between spectral indices from satellite remote sensing and winter oilseed rape yield. *Agronomy Research* **15**, 055–068.

Fieuzal, R., Marais Sicre, C. & Baup, F. 2017. Estimation of corn yield using multi-temporal optical and radar satellite data and artificial neural networks. *International Journal of Applied Earth Observation and Geoinformatio*n **57**, 14–23.

Gianquinto, G., Orsini, F., Fecondini, M., Mezzetti, M., Sambo, P. & Bona, S. 2011. A methodological approach for defining spectral indices for assessing tomato nitrogen status and yield. *Eur. J. Agron.* **35**(3), 135–143.

Knipling, E.B. 1970. Physical and physiological basis for the reflectance of visible and near-infrared radiation from vegetation. *Remote Sens. Environ*. **3**, 155–159

Kumhálová, J., Kumhála, F., Kroulík, M. & Matějková, Š. 2011. The impact of topography on soil properties and yield and the effects of weather conditions. *Precision Agriculture* **12**, 813–830.

Kumhálová, J. & Matějková, Š. 2017. Yield variability prediction by the remote sensing sensors with different spatial resolution. *International Agrophysics* **31**, 195–202.

Maldaner, L.F., Molin, J.P. & Canata, T.F. 2016. Processing yield data from two or more combines. In: *Proceedings of the 13th International Conference on Precision Agriculture (unpaginated, online).* Monticello, IL: International Society of Precision Agriculture. Accessed: *https://www.researchgate.net/publication/308168387* 19.10.2018.

Maphanyane, J.G., Mapeo, R.B.M. & Akinola, M.O. 2018. *Handbook of research on Geospatial Science and Technologies.* IGI Global, Hershey PA USA, 457 pp.

Moran, M.S., Clarke, T.R., Inoue, Y. & Vidal, A. 1994. Estimating crop water deficit using the relation between surface-air temperature and spectral vegetation index. *Remote Sens. Environ.* **49**, 246–263.

Mulla, D.J. 2013. Twenty five years of remote sensing in precision agriculture: Key advances and remaining knowledge gaps. *Biosystems Engineering* **114**(4), 358–371.

Murthy, V.R.K. 2002. Basic principles of Agricultural Meteorology. Book syndicate publishers, Koti, Hyderabad, India, 261 pp.

Pink, J.L. & Dobermann, A. 2005. Processing of Yield Map Data. *Precision Agriculture* **6**, 193–212.

Rosenzweig, C., Jones J.W, Hatfield J.L., Ruane, A.C., Boote, K.J., Thorburn, P., Antle, J.M., Nelson, G.C, Porter, C., Janssen, S., Asseng, S., Basso, B., Ewert, F., Wallach, D., Baigorria, G. & Winter, J.M. 2013. The Agricultural Model Intercomparison and Improvement Project (AgMIP): Protocols and pilot studies. *Agric. Forest Meteorol*. **170**, 166–182.

Rouse, J.W., Haas, R.H., Schell, J.A. & Deering, D.W. 1974. Monitoring vegetation systems in the Great Plains with ERTS. In: *Freden, S. C., Mercanti, E. P., Becker, M. (Eds.), Third Earth Resources Technology Satellite-1 Symposium*, Vol. 1: Technical Presentations, NASA SP-351. National Aeronautics and Space Administration, Washington, DC, pp. 309–317.

Schmidt, F. & Persson, A. 2003. Comparison of DEM data capture and topographic wetness indices. *Precision Agriculture* **4**, 179–192.

Scudiero, E., Corwin, D.L., Wienhold, B.J., Bosley, B., Shanahan, J.F. & Johnson, C.K. 2016. Downscaling Landsat 7 canopy reflectance employing a multi-soil sensor platform. *Precision Agriculture* **17**, 53–73.

Seelan, S.K., Languette, S., Casady, G.M., Seielstad, G.A. 2003. Remote sensing applications for precision agriculture: A learning community approach. *Remote Sensing of Environment* **88**, 157–169.

SNAP 6.0.4. ESA. *http://step.esa.int/main/* Accessed 19.12.2018.

Thornton, P.K., Bowen, W.T., Ravelo, A.C., Wilkens, P.W., Farmer, G., Brock, J. & Brink, J.E. 1997. Estimating millet production for famine early warning: an application of crop simulation modelling using satellite and ground-based data in Burkina Faso. *Agricultural and Forest Meteorology* **83**, 95–112.

Tucker, C.J., Holben, B.N., Elgin, J.H. & McMurtrey III, J.E. 1981. Remote sensing of total dry matter accumulation in winter wheat. *Remote Sens. Environ*. **11**, 171–189.

USGS. *https://earthexplorer.usgs.gov/* Accessed 19.12.2018.

Wardlow, B.D. & Egbert, S.L., 2008. Large-area crop mapping using time-series MODIS 250 m NDVI data: an assessment for the U.S. Central Great plains. *Remote Sens. Environ*. **112**, 1096–1116.

Xue, J. & Su, B. 2017. Significant remote sensing vegetation indices: a review of developments and applications. *Journal of Sensor*, 2017, 17.

Agronomy Research **17**(2), 456–465, 2019
https://doi.org/10.15159/AR.19.053

Ranking irrigation schemes based on principle component analysis in the arid regions of Turkey

S. Kartal[1], H. Değirmenci[2,*] and F. Arslan[2]

[1]University of Akdeniz, Kumluca Vocational School, Plant and Animal Production Department, TR07350, Antalya, Turkey
[2]University of Kahramanmaraş Sütçü İmam, Faculty of Agriculture, Biosystem Engineering Department, TR46040, Kahramanmaraş, Turkey
[*]Correspondence: hdegirmenci46@gmail.com

Abstract. Water is a scarce resource and thus irrigation schemes in arid regions have become more important. The irrigation sector which uses most of the water resources has to cope with global warming, disasters and water scarcity around the world, particularly in the Mediterranean countries, including Turkey. Irrigation schemes, which were built by DSI (State Hydraulic Works) and whose operation and maintenance management was transferred to water user associations, play a crucial role in irrigated agriculture in Turkey. In order to improve the performance, weakness and strengths of irrigation schemes are determined by performance indicators (system operation, financial and production efficiency) which show the overall information about them. In the present study, seven irrigation schemes located in an arid region of central Anatolia were chosen to assess the irrigation performance using principal component, correlation and cluster analysis while quality index showed the rank of the irrigation schemes. We found that the average total annual volume of irrigation supply was 7,648.58 m^3 ha^{-1} and the average relative water supply was 1.91 during the 11 years between 2006 and 2016. In this region, higher inverse correlations were due to using surface irrigation methods (51.3%). As of 2017, the irrigation schemes have weak water distribution systems, on an average, consisting of 55.5% open canals, 22.5% canalette and only 10% pipes. According to the quality index, financial and system operation indicators are more effective than that of production efficiency indicators. In conclusion, average irrigation ratio (55.68%) can be increased by improving the water distribution system, and the technology used on both management and farm levels.

Key words: Principal components analysis, irrigation performance indicators, irrigation schemes, quality index.

INTRODUCTION

Water is the most important and an indispensable resource for supporting life. Due to both climatic changes and anthropogenic causes, the amount of available water on earth is decreasing over time. Hence, it is necessary to maximise the output from all the water that is still available. A research conducted by the National Aeronautics and Space Administration of the United States Federal Government (NASA) showed that the consumption of available water in the world is increasing at a higher rate than that of its rate of replenishment (Anonymous, 2017a).

The scarcity of water resources necessitates the efficient use of water in agriculture. In this respect, it is mandatory to choose efficient irrigation methods and systems in agricultural systems, and to increase the skills and training of the labour force in the agricultural field (Değirmenci, 2004).

Turkey is not a water-rich country where the average annual precipitation is about 643 mm and groundwater potential is approximately 112 billion m^3 $year^{-1}$ out of which 44 billion m^3 of water is consumed. The amount of water available per capita is approximately 1,519 m^3 annually indicating that Turkey is already facing a water deficit (DSI, 2017). Turkey spans over 78 million ha and, 28 million ha, constituting about one-third of the land area, is under cultivation. Studies show that it is possible to economically irrigate approximately 8.5 million ha of land with the existing water potential. Within this area, 5.9 million ha of land is equipped for irrigation. The responsibility of the operation and maintenance of irrigation networks in Turkey has been transferred to water user associations since 1993. Approximately 86% of the area open to total irrigation in Turkey has been transferred to irrigation unions, 5.9% to cooperatives, 5.5% to municipalities and 1.6% to village legal entities (Anonymous, 2017b). The transfer of responsibilities of the operations, maintenance and management of the irrigation facilities, is aimed to protect the facilities, carry out timely maintenance, reduce maintenance costs and to achieve fair water distribution. However, research has indicated that the above aims have not been achieved (Kartal, 2018).

Evaluation of the performance of irrigation schemes and an assessment of the current situation is of great importance in determining whether the targets have been achieved. For this purpose, performance evaluation studies should be performed for all the irrigation schemes including an assessment of the irrigation management. The performance of the irrigation schemes operated by the DSI in Turkey is monitored and evaluated annually. Performance indicators that are used include water supplied to users, irrigation efficiency, cost and benefit. However, the information available from the monitoring and evaluation efforts is not sufficient. Hence, the performance of the irrigation systems has not adequately been determined. As a result, efforts are used to establish a performance indicator set compatible with that used for irrigation systems in other countries (Nalbantoğlu & Çakmak, 2007).

Several studies such as Bareng et al. (2015) and Bumbudsanpharoke & Prajamwong (2015) have been carried out to evaluate the performance of irrigation networks. Alcon et al. (2017) evaluated five irrigation schemes in the Segura river basin of south-eastern Spain using data from 2002–2010 with a total of 10 water use efficiency indicators, energy use and agricultural production efficiency indicators. They used the panel data regression model in the evaluation. Using their approach, Arslan & Değirmenci (2018) evaluated the performance of Kahramanmaraş left bank irrigation scheme in Turkey using RAP-MASSSCOTE (Mapping System and Services for Canal Operation Techniques) with both management and operational indicators. Zema et al. (2018a) evaluated 10 water user associations using performance indicators in Calabria region in southern Italy. Data enveloping analysis and principal components analysis were used in the statistical evaluation. Rodriguez-Diaz et al. (2008) evaluated nine water user associations with a new methodology called quality index to determine overall performance of 27 system operations, production efficiency and financial indicators in the Spanish Andalusian region. Corcoles et al. (2011) evaluated seven water user associations in the Castilla - La Mancha region of Spain, using the basic components and

cluster analysis using data from 2006–2008. A total of 79 financial activity, system operating activity, production activity and environmental activity indicators were used in the evaluation. Energy indicators were also used depending on features such as conceptual, operational, efficiency and quality of supply.

The effective use of water resources is particularly important in arid regions such as central Anatolia. In order to achieve this goal, irrigation schemes, responsible for water management in the agricultural areas where 70% of water is consumed, should be evaluated. Performance indicators aid in the evaluation and provide the irrigation managers the direction of the current situation of the irrigation schemes.

The main aim of this current study is to evaluate seven irrigation schemes in the Anatolia region of central Turkey using 14 performance indicators (water distribution, finance and productivity) with the data from 2008 to 2015. Quality index, a statistical method, was chosen to rank irrigation schemes based on the overall performance score.

MATERIALS AND METHODS

Çumra, Ayrancı, Altınapa, Ivriz, Karaman, Ilgin and Kıreli irrigation schemes located in the central Anatolian region were selected. Data from 2008 to 2015 including the command area, irrigated area, water diverted or pumped from reservoir, irrigation water requirement, operation-maintenance cost, total annual expenditure and production value were obtained from DSI (State Hydraulic Works) monitoring and evaluation reports. General features of the irrigation schemes are presented in Table 1.

Table 1. General features of the irrigation schemes

Irrigation schemes	First operation year	Command area (ha)	Water diversion	Main crops
Çumra	1912	59,650	Gravity-pumped	Grain-Sugar beet-Sunflower
Ayrancı	1962	4,600	Gravity	Cereals-Fruit-Forage crops
Altınapa	1968	1,015	Gravity	Fruit-Vegetable-Cereals
İvriz	1983	36,108	Gravity-pumped	Cereals-Corn-Sunflower
Karaman	1988	15,040	Gravity-pumped	Cereals-Corn-Fruit
Ilgın	1993	5,214	Pumped	Sugar beet-Cereals-Corn
Kıreli	2002	1,0511	Gravity-pumped	Sugar beet-Corn-Forage crops

Calculation of performance indicators

Comparison indicators of Malano & Burton (2001) and Molden et al. (1998) were used in the calculation (formulae and correction factors) of performance indicators in the current study (Table 2). In the calculation of output, the Central Bank's average dollar rate was used for the local currency for the relevant year in Turkey.

Statistical evaluation

According to Rodriguez-Diaz et al. (2008) and Zema et al. (2015), the quality index, which is present in all indicators, can be calculated to give overall performance as a score. To calculate the score of the irrigation schemes considering performance indicators, the following procedure which consists of the factor analysis was used:

1- Calculating min, max and mean values of the land fragmentation indices for irrigation schemes.

2- Normalising the performance indicators from 0 to 1. The aim of this step is to normalise the smallest value to 0, the maximum value to 1 and to spread all other data to the range of 0–1.

3- Applying the principal component analysis to the performance indicators which were calculated according to Table 2 for each irrigation scheme.

Table 2. Calculation of the performance indicators

	Indicators	Formula	Code	Correction factor
Water distribution	Irrigation ratio (%)	$\frac{\text{Irrigated area} \cdot 100}{\text{Command area}}$	A	+1
	Annual irrigation water supplied per unit irrigated area (m^3 ha^{-1})	$\frac{\text{Annual irrigation water supplied}}{\text{Irrigated area}}$	B	-1
	Annual irrigation water supplied per unit command area (m^3 ha^{-1})	$\frac{\text{Annual irrigation water supplied}}{\text{Command area}}$	C	-1
	Annual relative water supply	$\frac{\text{Annual irrigation water supplied}}{\text{Annual irrigation water requirement}}$	D	-1
Financial	Total MOM cost per unit irrigated area ($ ha^{-1})	$\frac{\text{Total MOM cost}}{\text{Irrigated area}}$	E	-1
	Total MOM cost per unit command area ($ ha^{-1})	$\frac{\text{Total MOM cost}}{\text{Command area}}$	F	-1
	Total MOM cost per unit irrigation water supplied to users ($ m^{-3})	$\frac{\text{Total MOM cost}}{\text{Annual irrigation water supplied}}$	G	-1
	Total cost per unit irrigated area ($ ha^{-1})	$\frac{\text{Total cost}}{\text{Irrigated area}}$	H	-1
	Total cost per unit command area ($ ha^{-1})	$\frac{\text{Total cost}}{\text{Command area}}$	I	-1
	Total cost per unit irrigation water supplied ($ m^{-3})	$\frac{\text{Total cost}}{\text{Annual irrigation water supplied}}$	J	-1
Productivity	Output per unit irrigated area ($ ha^{-1})	$\frac{\text{Total annual value of agricultural production}}{\text{Irrigated area}}$	K	+1
	Output per unit command area ($ ha^{-1})	$\frac{\text{Total annual value of agricultural production}}{\text{Command area}}$	L	+1
	Output per unit irrigation water supplied to users ($ m^{-3})	$\frac{\text{Total annual value of agricultural production}}{\text{Annual irrigation water supplied}}$	M	+1
	Output per unit irrigation water requirement ($ m^{-3})	$\frac{\text{Total annual value of agricultural production}}{\text{Annual irrigation water requirement}}$	N	+1

*MOM: Maintenance, operation and management; A: Irrigation ratio (%); B: Annual irrigation water supplied per unit irrigated area (m^3 ha^{-1}); C: Annual irrigation water supplied per unit command area (m^3 ha^{-1}); D: Annual relative water supply; E: Total MOM cost per unit irrigated area ($ ha^{-1}); F: Total MOM cost per unit command area ($ ha^{-1}); G: Total MOM cost per unit irrigation water supplied to users ($ m^{-3}); H: Total cost per unit irrigated area ($ ha^{-1}); I: Total cost per unit command area ($ ha^{-1}); J: Total cost per unit irrigation water supplied ($ m^{-3}); K: Output per unit irrigated area ($ ha^{-1}); L: Output per unit command area ($ ha^{-1}); M: Output per unit irrigation water supplied to users ($ m^{-3}); N: Output per unit irrigation water requirement ($ m^{-3}).

4- Calculating % weight of the coefficients obtained from principal component analysis.

5- Correcting coefficient values according to the correction factor (Table 2) of the indices.

6- Calculation of the weighted indicator values.
7- Calculation of the overall holding scores.

RESULTS AND DISCUSSION

The calculated performance indicators' minimum, maximum, average and standard deviation values of the irrigation schemes are shown in Table 3. Average value of irrigation ratio (A) was the highest (100%) in the Ayrancı and lowest (9.16%) in the Altınapa irrigation scheme. The average performance of the irrigation schemes in Turkey was 62% in 2017 (DSI, 2017). In this context, irrigation schemes with an irrigation ratio lower than 62% are insufficient in terms of the irrigated area in Turkey. Annually, irrigation water supplied per unit irrigated area (B) was highest (63,440.86 m^3 ha^{-1}) while Altınapa irrigation scheme had the lowest (190.65 m^3 ha^{-1}). Annual relative water supply (D) of 0.43 was the lowest in Kıreli and the highest (13.63) in Altınapa. Annual relative water supply values in Turkey were found to be between 1.55 and 1.98 in Akıncı irrigation scheme (Nalbantoğlu & Çakmak 2007), and according to results of Değirmenci (2001) it was changed from 0.91 to 7.15 in the irrigation schemes that were transferred. Average total MOM cost per unit irrigated area was the highest (\$ 499.25 ha^{-1}) in Kıreli and the lowest (\$ 4.41 ha^{-1}) in the Altınapa irrigation scheme. On the other hand, average total MOM cost per unit command area was the highest (\$ 143.01 ha^{-1}) in Karaman and the lowest (\$ 1.44 ha^{-1}) in the Altınapa irrigation scheme. Total MOM cost per unit area did not show high performance. In this current study, we took into consideration this indicator to be as low as possible, and the lower values of the indicator showed higher performance. However, some modernisation expenditure could have increased the indicator, and the higher values of the indicator could have increased the performance. Average total cost per unit irrigated area (H) was found to be the highest (\$ 5,737.77 ha^{-1}) in Kıreli and the lowest (\$ 237.28 ha^{-1}) in Karaman. Total cost per unit irrigation water supplied (J) shows that the Altınapa irrigation scheme had the lowest performance while Kıreli had the highest. Output per unit irrigated area and per unit irrigation water requirement was the highest in the Altınapa and the lowest in the Ayrancı irrigation scheme. These observations suggest that the Altınapa irrigation scheme has the best performance in terms of productive indicators.

Principal component analysis

The Kaiser-Mayer-Olkin (KMO) and the Bartlett test were applied to understand whether the data set (performance indicators) is appropriate for the basic component analysis. It is basically a test for sampling adequacy. Based on the results of the KMO and the Bartlett test shown in Table 4, the dataset was found to be suitable for the principal component analysis.

Table 4 shows that treatments D and B are in the second group while M, N and K are in the third group. According to the results it may be suggested that the first component, which explains most of the variation, represents indicators related to water in just one variable which is the first group.

Table 3. Descriptive statistics of performance indicators

Indicator	Code*	A	B	C	D	E	F	G	H	I	J	K	L	M	N
Çumra	Min.	84.58	3,686.60	3,262.76	1.20	45.83	40.79	0.01	620.39	552.27	0.07	2,367.27	2,107.37	0.25	0.41
	Max.	97.61	1,1873.12	10,231.70	3.25	108.52	93.52	0.01	939.88	805.61	0.22	3,071.11	2,764.53	0.73	1.00
	Mean	88.38	8273.43	7,283.13	2.34	75.07	66.23	0.01	792.81	700.21	0.11	2,690.72	2,376.93	0.37	0.78
	Ss.	3.93	2,594.73	2,206.48	0.74	21.01	18.16	0.00	86.57	78.68	0.05	218.57	207.22	0.16	0.16
Ayrancı	Min.	17.76	3,817.50	1,086.96	1.25	4.51	1.70	0.00	421.26	421.26	0.05	1,247.64	267.35	0.15	0.22
	Max.	100.00	8,913.04	8,913.04	2.95	342.16	65.18	0.06	2,810.59	560.67	0.46	5,188.23	3,945.97	1.08	1.83
	Mean	79.73	6,598.25	5,404.89	1.88	65.80	29.95	0.01	937.46	482.40	0.15	2,946.03	2,287.06	0.51	0.90
	Ss.	32.33	1,620.69	2,813.58	0.51	107.04	26.59	0.02	837.15	40.82	0.14	1,337.57	1,217.79	0.32	0.50
Altınapa	Min.	9.16	9,419.08	1,379.31	2.12	4.41	1.44	0.00	491.28	230.75	0.03	2,864.85	394.90	0.07	0.64
	Max.	83.74	63,440.86	15,665.02	13.63	99.03	70.13	0.01	2,875.29	411.42	0.22	8,921.87	4,549.63	0.72	2.06
	Mean	28.49	26,095.26	5,813.92	5.67	57.61	15.47	0.00	1,654.47	295.63	0.08	5,508.32	1,559.48	0.30	1.20
	Ss.	23.03	18,383.81	4,281.29	4.14	33.81	20.83	0.00	985.71	48.67	0.06	1,686.72	1,295.67	0.19	0.45
İvriz	Min.	41.73	4,948.06	3,048.83	1.61	108.88	62.71	0.01	614.12	353.71	0.06	2,029.81	847.05	0.24	0.41
	Max.	67.36	10,424.15	6,003.96	2.59	243.93	127.34	0.04	1,055.30	560.57	0.18	3,808.19	2,446.93	0.77	1.24
	Mean	60.24	7,513.43	4,492.35	2.17	156.16	92.07	0.02	751.54	444.85	0.11	2,835.04	1,733.05	0.40	0.85
	Ss.	7.66	1,627.92	996.69	0.35	41.37	18.02	0.01	137.32	53.12	0.04	572.93	480.61	0.16	0.26
Karaman	Min.	49.87	4,335.88	2,413.56	0.89	149.82	88.56	0.03	237.28	118.34	0.03	2,875.47	1,625.41	0.48	0.64
	Max.	59.11	6,998.69	3,550.53	1.80	259.71	143.01	0.05	2,217.39	1,154.10	0.40	5,494.82	2,846.17	1.18	1.42
	Mean	53.30	5,722.30	3,030.31	1.41	209.82	111.11	0.04	1,605.01	858.87	0.29	4,085.21	2,169.16	0.73	1.00
	Ss.	2.88	890.64	362.34	0.31	41.48	19.54	0.01	562.62	297.15	0.11	868.91	441.82	0.19	0.23
Ilgın	Min.	20.50	1,930.65	843.88	0.72	144.07	46.33	0.03	866.35	424.23	0.19	2,714.95	752.97	0.54	0.55
	Max.	60.57	6,466.30	2838.51	1.97	312.18	98.01	0.08	2,490.64	635.17	0.57	6,259.13	2,660.98	1.87	1.55
	Mean	42.79	4,163.60	1629.22	1.20	196.01	77.07	0.05	1,410.79	523.24	0.37	3,693.61	1,496.54	1.05	1.09
	Ss.	15.49	1,649.	657.72	0.45	52.86	17.01	0.01	566.86	59.13	0.13	1,083.95	530.61	0.51	0.28
Kıreli	Min.	9.95	3,095.44	611.64	0.43	199.62	24.24	0.03	2,640.16	497.61	0.61	5,154.36	512.93	0.70	0.75
	Max.	22.13	7,959.02	04,960.90	1.70	499.25	49.68	0.08	5,737.77	647.18	0.93	6,856.49	1,200.86	1.75	1.46
	Mean	15.11	5,311.94	731.92	1.04	279.41	39.41	0.06	4,108.97	572.33	0.80	5791.40	873.91	1.23	1.11
	Ss.	4.26	1,856.39	112.81	0.43	96.39	7.67	0.02	1,198.31	41.44	0.11	588.24	246.91	0.42	0.18

*A: Irrigation ratio (%); B: Annual irrigation water supplied per unit irrigated area (m^3 ha^{-1}); C: Annual irrigation water supplied per unit command area (m^3 ha^{-1}); D: Annual relative water supply; E: Total MOM cost per unit irrigated area (\$ ha^{-1}); F: Total MOM cost per unit command area (\$ ha^{-1}); G: Total MOM cost per unit irrigation water supplied to users (\$ m^{-3}); H: Total cost per unit irrigated area (\$ ha^{-1}); I: Total cost per unit command area (\$ ha^{-1}); J: Total cost per unit irrigation water supplied (\$ m^{-3}); K: Output per unit irrigated area (\$ ha^{-1}); L: Output per unit command area (\$ ha^{-1}); M: Output per unit irrigation water supplied to users (\$ m^{-3}); N: Output per unit irrigation water requirement (\$ m^{-3}).

Table 4. Principal component analysis conformity test

Kaiser-Meyer-Olkin Measure of Sampling Adequacy		.581
Bartlett's Test of Sphericity	Approx. Chi-Square	1,080.642
	Df	91
	Sig.	.000*

*Significance level at $p < 0.01$

Differences between these indicators are higher in the first group, but lower in the third group. In short, values of the indicators in the third group are more similar to each other than that compared to the indicators in the first group. However, the primary aim of the principal component analysis was to use the coefficient as a parameter to calculate the quality index. In this case, it can be interpreted that the indicators in the first group are more effective in the ranking of irrigation schemes because they explain the variance better than the others (Table 5). On the other hand, the effects of indicators in the second and third groups had a lower effect on the ranking.

Table 5. Principal component matrix

Indicators*	Component		
	1	2	3
L	**-.867**	-.136	.250
A	**-.863**	-.133	-.313
H	**.833**	.035	.335
E	**.808**	-.157	-.046
J	**.737**	-.456	.359
C	**-.714**	.493	-.174
G	**.691**	-.477	.087
D	-.032	**.934**	.162
B	.040	**.923**	.170
M	.303	-.674	**.545**
N	.013	.052	**.908**
K	.302	.120	**.871**
F	-.012	-.117	-.309
I	-.038	-.221	.124

*A: Irrigation ratio (%); B: Annual irrigation water supplied per unit irrigated area (m^3 ha^{-1}); C: Annual irrigation water supplied per unit command area (m^3 ha^{-1}); D: Annual relative water supply; E: Total MOM cost per unit irrigated area ($ ha^{-1}); F: Total MOM cost per unit command area ($ ha^{-1}); G: Total MOM cost per unit irrigation water supplied to users ($ m^{-3}); H: Total cost per unit irrigated area ($ ha^{-1}); I: Total cost per unit command area ($ ha^{-1}); J: Total cost per unit irrigation water supplied ($ m^{-3}); K: Output per unit irrigated area ($ ha^{-1}); L: Output per unit command area ($ ha^{-1}); M: Output per unit irrigation water supplied to users ($ m^{-3}); N: Output per unit irrigation water requirement ($ m^{-3}).

Quality index

The success of ranking of the irrigation schemes resulting from the calculation of the quality index is given in Table 6. This ranking shows the most successful irrigation schemes by reducing all the performance indicators to a single number.

According to the quality index ranking, Ayrancı had the highest score and was the most successful irrigation scheme. However, this comparison only shows the rank among the irrigation schemes in the current study. Water was used more efficiently in Ayrancı while Kıreli irrigation scheme had ineffective water usage during the study period. The second most successful irrigation scheme was Çumra having 59,650 ha of command area. Ayrancı, Altınapa and Ilgın are small-scale irrigation schemes compared with the others and have less than 10,000 ha of command area. Thus, large scale irrigation schemes have more importance in the region. We observed that the last and the second last irrigation schemes, Kıreli with 10,511 ha and Karaman with 15,040 ha of command area, need more focus in terms of water management.

After identifying the strengths and weakness using direct methods such as external and internal (Değirmenci, 2001; Değirmenci et al., 2013; Arslan & Değirmenci, 2018), Çakmak et al. (2006) suggest that best management practices should be applied to irrigation schemes to achieve good water management in agriculture. Inefficient use of water is still one of the most important problems (Değirmenci et al., 2017) in the transferred irrigation schemes. These problems may be explained with some features of the irrigation schemes (Alcon et al., 2018; Zema et al., 2018a; Zema et al., 2018b).

Table 6. Quality index rank

Irrigation schemes	Quality index	Rank
Ayrancı	-62.7275	1
Çumra	-322.605	2
Altınapa	-370.725	3
İvriz	-458.451	4
Ilgın	-835.736	5
Karaman	-914.8	6
Kıreli	-1320.47	7

Particularly in central Anatolia, irrigation schemes have different types of features such as water diversion type, and the irrigation method used by farmers. Further studies should focus at determining more effective features in the region.

On the other hand, modernisation requirement may help increase performance of the irrigation schemes (Playán & Mateos, 2006; Renault, 1998). These modernisation processes should be continued to reach the goals with go gear technology considering energy requirement (Diaz et al., 2011; Lamaddalena & Khila, 2012).

CONCLUSIONS

Assessment of irrigation schemes with a large number of performance indicators make it cumbersome for evaluation and monitoring. In this respect, the principal component analysis and subsequent quality index can be used to evaluate these data without any issues. As a result of the analysis, the extent to which the indicator affects the irrigation schemes can easily be found. The quality index ranking showed that the Ayrancı scheme had the highest score and was the most successful irrigation scheme in the region but due to the small size of its command area, it had a relatively lower impact than the ones with higher impact. Thus Çumra, which had the biggest command area and is ranked at two, is important with respect to using irrigation water in the arid region. With the lowest score, Kıreli had the worst performance, and having more than 10,000 ha of command area, contributed to its lower score. Despite the higher agricultural production, the larger financial indicator values placed Kıreli irrigation scheme in the lowest rank. This shows that water usage is the most important factor in the central Anatolia region, indicating that further research should focus on improvising the water use efficiency. Based on principal component analysis, and general statistics, the average amount of irrigation water supplied to users per unit irrigated area is approximately 9000 m^3 ha^{-1} annually, a figure which is very high for an arid region. Thus, the problems that prevent effective use of irrigation water should be eliminated.

REFERENCES

Alcon, F., Bastida, P.A.G., Garcia, M.S., Alvarez, V.M., Gorriz, B.M. & Baille, A. 2017. Explaining the Performance of Irrigation Communities in a Water scarce Region. *Irrigation science* **35**(3), 193–203.

Anonymous 2017a. Dünyada tatlı su kaynakları tükeniyor mu? (https://www.bbc.com/turkce/vert-fut-39646356). Last access date: 19.01.2019.

Anonymous 2017b. 2017 Yılı Faaliyet Raporu. Devlet Su İşleri Genel Müdürlüğü (2017 State Hyraulic Works Activity Report). Ankara, Turkey.

Arslan, F. & Değirmenci, H. 2018. RAP-MASSCOTE Aproach of Modernizing Operatıon-Maintanence and Management of Irrigation Schemes: A Case Study of Kahramanmaraş Left Bank Irrigation Scheme. *Atatürk University Journal of the Agricultural Faculty* **49**(1), 45–51, 2018

Bareng, J.L.R., Balderama, O.F. & Alejo, L.A. 2015. Analysis of Irrigation Systems Employing Comparative Performance Indicators: A Benchmark Study for National Irrigation and Communal Irrigation Systems in Cagayan River Basin. *Journal of Agricultural Science and Technology* A **5**, 325–335.

Bumbudsanpharoke, W. & Prajamwong, S. 2015. Performance Assessment for Irrigation Water Management: Case Study of the Great Chao Phraya Irrıgatıon Scheme. *Irrig. and Drain.* **64**, 205–214.

Çakmak, B., Yapılar, T. & Aküzüm, T. 2006. Water management in agriculture in Turkey, problems and solutions (Türkiye'de tarimda su yönetimi, sorunlar ve çözüm önerileri). TMMOB Chamber of Civil Engineers Water Policies Congress (*TMMOB İnşaat Mühendisleri Odası Su Politikaları Kongresi)* **2**, 349–359.

Córcoles, J.I., de Juan, J.A., Ortega, J.F., Tarjuelo, J.M. & Moreno, M.A. 2011. Evaluation of Irrigation Systems by Using Benchmarking Techniques. J*ournal of Irrigation and Drainage Engineering* **138**(3), 225–234.

Değirmenci, H. & Arslan, F. 2018. Operation and Maintenance Cost Analysis of Turnover Irrigation Schemes to Irrigation Associations. *Su Kaynakları (Water resources)* **3**(1), 16–23.

Değirmenci, H. 2001. Evaluation of Water Use Efficiency in transferred Irrigation Schemes (Devredilen sulama şebekelerinin karşılaştırma göstergeleri ile değerlendirilmesi). *Uludag Universtiy Journal of Agriculture Faculty* **15**, pp. 31–41.

Değirmenci, H. 2004. Assessment of Irrigation Schemes with Comparative Indicators in Kahramanmaraş Region. *KSU Journal of Science and Engineering* **7**(1), 104–110.

Değirmenci, H., Tanrıverdi, Ç., Arslan, F. & Gönen, E. 2017. Benchmarking Performance of Large Scale Irrigation Schemes with Comparative Indicators in Turkey. *Scientific Papers Series E. Land Reclamation, Earth Observation and Surveying, Environmental Engineering* **VI**, 87–92.

Díaz, J.R., Urrestarazu, LP., Poyato, E.C. & Barrios, M.P.M. 2011. The paradox of irrigation scheme modernization: more efficient water use linked to higher energy demand. *Spanish Journal of Agricultural Research* **4**, 1000–1008.

Kartal, S. 2018. Performance Assessment Of Irrigation Schemes with Multivariate Some Statistical Methods: A Case Study of Turkey. Institute for Graduate Studies in Science and Technology Department of Biosystem Engineering, *PhD THESIS*, pp. 175–182.

Lamaddalena, N. & Khila, S. 2012. Energy saving with variable speed pumps in on-demand irrigation systems. *Irrigation science* **30(**2), 157–166.

Malano, H. & Burton, M. 2001. Guidelines for Benchmarking Performance in the Irrigation and Drainage Sector. IPTRID and FAO, Rome, Italy.

Molden, D.J., Sakthivadivel, R., Perry, C.J., Fraiture, C.D. & Kloezen, W.H. 1998. Indicators for Comparing Performance of Irrigated Agricultural Systems. IWMI, Research Report 20, Colombo, 26 p.

Nalbantoğlu, G. & Çakmak, B. 2007. Benchmarking of Irrigation Performance in Akıncı Irrigation District. *Journal of Agricultural Sciences* **13**(3), 213–223.

Playán, E. & Mateos, L. 2006. Modernization and optimization of irrigation systems to increase water productivity. *Agricultural water management* **80**(1–3), 100–116.

Renault, D. 1998. Modernizations of irrigation systems: a continuing process. In Modernization of Irrigation System Operations. Maharashtra (India). 28-30 Oct 1998.

Rodríguez-Díaz, J.A., Camacho-Poyato, E., Lopez-Luque, R. & Pérez-Urrestarazu, L. 2008. Benchmarking and Multivariate Data Analysis Techniques for Improving the Efficiency of Irrigation Districts: An Application in Spain. *Agricultural systems* **96**(1–3), 250–259.

State Hydraulic Works (DSI). 2017. 2017 Annual Report Ministry of Water Affairs General Directorate of State Hydraulic Works, Ankara.

Zema, D.A., Nicotra, A. & Zimbone, S.M. 2018b. Diagnosis and improvement of the collective irrigation and drainage services in Water Users' Associations of Calabria (Southern Italy). *Irrigation and Drainage* **67(**5), 629–644.

Zema, D.A., Nicotra, A., Tamburino, V. & Zimbone, S.M. 2015. Performance Assessment of Collective Irrigation in Water Users' Associations of Calabria (Southern Italy). *Irrigation and drainage* **64(**3), 314–325.

Zema, D.A., Nicotraa, A., Mateosb, L. & Zimbonea, S.M. 2018a. Improvement of the Irrigation Performance in Water Users Associations Integrating Data Envelopment Analysis and Multi-Regression Models. *Agricultural Water Management* 205, 38–49.

Agronomy Research **17**(2), 466–480, 2019
https://doi.org/10.15159/AR.19.071

Assessment of applied microwave power of intermittent microwave-dried carrot powders from Colour and NIRS

M. Keskin[1,*], Y. Soysal[1], Y.E. Sekerli[1], A. Arslan[1] and N. Celiktas[2]

[1]Department of Biosystems Engineering, Faculty of Agriculture, Hatay Mustafa Kemal University, TR31040 Antakya, Hatay, Turkey
[2]Department of Field Crops, Faculty of Agriculture, Hatay Mustafa Kemal University, TR31040 Antakya, Hatay, Turkey
[*]Correspondence: keskin@mku.edu.tr, mkeskinhatay@gmail.com

Abstract. Applied microwave (MW) power level is an essential factor on the quality of the dried agricultural products. Even if higher MW powers result in shorter drying times, they lead to quality degradations. It is almost impossible to know the applied MW power of a dried and powdered product by human vision. Thus, the aim of this study was to predict the applied MW power of carrot powders by using two different instruments, a chromameter and FT-NIRS. The experiments were carried out at nine different power levels (100–500 W) with three replications (N = 27). The colour and NIR reflectance was measured using a chromameter and NIRS system. The data was analysed using PLS regression. The drying time of intermittent MW drying at the highest applied power of 500 W was 1.12–5.47 times shorter than those of other lower applied powers. Applied MW power was a crucial factor on all colour parameters of the powdered carrots. Brightness (L*) decreased significantly with the increase of applied MW power resulting in darker product colours. Data analysis results showed that the NIRS system (R^2 = 0.99; SEP = 16.1 W) can predict the microwave power of powdered carrots with significantly better performance than a chromameter (R^2 = 0.95; SEP = 29.9 W). But, the chromamater is far more inexpensive when compared with the NIRS system and hence, it can also be used to predict the applied MW power from the colour data relatively well. Also, a mathematical model was developed to predict applied MW power from the colour parameters.

Key words: Microwave drying, applied power, carrot, reflectance, chromameter, FT-NIRS.

INTRODUCTION

Water content of fresh agricultural products has to be decreased by using different drying methods to prolong their shelf life (Onwude et al., 2016). Drying methods can be divided into four groups including convective drying in cabinet, kiln, belt, and conveyors as first generation, spray and drum drying as second generation, freeze and osmotic drying as third generation and microwave and RF related drying as innovative fourth generation methods (Kumar & Karim, 2017). Microwave (MW) drying has some advantages including volumetric heating, higher drying rate, shorter process time, cost reduction and better product quality and is generally combined with other methods to improve its performance (Ekezie at al., 2017; Kumar & Karim, 2017). Applying MW continuously results in uneven heating, overheating and lower product quality; thus,

intermittent or pulsed MW is applied to eliminate the drawbacks (Ekezie at al., 2017; Pham et al., 2017). Various studies were carried out on intermittent MW drying of agricultural products such as strawberry (Changrue, 2006), banana (Baini & Langrish, 2007), potato (Soysal, 2009), red pepper (Soysal et al., 2009a), oregano (Soysal et al., 2009b), carrot (Arikan et al., 2012), fig fruit (Sharifian et al. 2012), wheat seeds (Li et al., 2014), kiwi (Pham et al., 2016), pumpkin (Junqueira et al., 2017), pistachio nuts (Kermani et al., 2017), apple (Aghilinategh et al., 2016; Dehghannya et al., 2018) and mushroom (Das & Arora, 2018).

Drying temperature or applied microwave (MW) power is a crucial factor on the quality of the dried agricultural products. Even if higher drying temperatures and MW powers result in shorter drying times, they cause quality degradations (Moraes et al., 2013; Karam et al., 2016; Kumar & Karim, 2017). Cracks, casehardening, colour deterioration, phytochemical depletion, antioxidant activity reduction, degradation of nutrients, poor rehydration and shrinkages are the main damages occurring at high drying temperatures and MW powers (Cao et al., 2016; Karam et al., 2016). It is almost impossible to differentiate the food products dried by different methods and applied MW powers with human vision by consumers. On the other hand, chromatographic and spectroscopic methods along with chemometrics could be useful to differentiate the food products dried by different drying methods (Hwang et al., 2017). The food industry is often encountered with adulteration and it is hard to determine if products have been adulterated by a human observer; thus, practical systems could be used to detect adulteration. Some techniques such as FTIR have potential to monitor food adulteration (Rodriguez-Saona & Allendorf, 2011; Khan et al., 2015).

Some electro-optic instruments including digital camera, spectroradiometer, spectrophotometer, chromameter and near infrared reflectance spectroscopy (NIRS) can be utilized to evaluate the quality of food products (Rodriguez-Saona & Allendorf, 2011; Keskin et al., 2017). NIRS systems (800–2500 nm) and Fourier Transform (FT) NIRS systems are rapid, non-invasive, quick and non-destructive for food quality and adulteration studies (Tripathi & Mishra, 2009; Lim et al., 2015; Toledo-Martín et al., 2015; Wu et al., 2017; Li et al., 2018). Colour is an important feature in food product quality evaluation (Ordonez-Santos et al., 2014; Yang et al., 2018) and can be quantified by using a colorimeter (chromameter) or spectrophotometers (Pathare et al., 2013). Chromameters are regularly used in the colour assessment of food because of their easy usage and colour elucidation (Pathare et al., 2013). These systems have been used to assess fruit and vegetable ripeness, quality of the dried products and the colour of raw and processed foods including meat, bread, flour, dough, juice, molasses, chocolate, oils, milk, dairy products, pasta, jam, etc. (Keskin et al., 2017).

Carrot (*Daucus carota* L.) is an important root vegetable with carotenoids, flavonoids, vitamins and minerals that provide various nutritional and health benefits (da Silva Dias, 2014). It is a medicinal and industrial crop as it is a plentiful and inexpensive source of minerals, vitamins and fibre. It is consumed fresh or used for the production of dried powders for soups and other food products. The total global carrot production (including turnips) was about 42.7 million tonnes in 2016 (FAO, 2018). China was the first producer country with around 20.6 million tonnes followed by Uzbekistan and Russian Federation with about 2.3 and 1.9 million tonnes, respectively while Turkey ranked thirteenth with about 0.56 million tonnes (FAO, 2018).

Applied microwave power level in drying process is a vital factor for the final quality of the dried product. But, to our best knowledge, no study was found on the determination of applied microwave power of dried carrot powders using reflectance data. Thus, the aim of this study was to predict the applied microwave power of carrot powders dried by intermittent microwave drying with different applied power levels by using two different instruments, a chromameter and FT-NIRS.

MATERIALS AND METHODS

Carrot Samples

Carrots (*Daucus carota* 'Nantes') produced in open fields in Konya province of Turkey were obtained from a wholesale market located in Antakya, Hatay, Turkey (Fig. 1). They were stored at +4 °C in refrigerator until drying. The middle size carrots (15–20 cm) were selected and used in the study in November 2018.

Intermittent Microwave Drying of Carrot Samples

A lab-scale microwave oven (Beko, MD 1605, Turkey) with a maximum rated power of 900 W at 2450 MHz was used in the drying experiment. The size of the microwave cavity was about 22 x 35 x 33 cm. The actual power of the microwave oven was calculated as 736 W by using the IMPI-2L test (Buffler, 1993). The experiment were carried out at nine different power levels (100, 150, 200, 250, 300, 350, 400, 450 and 500 W) by changing the on and off times (T_{on} and T_{off}) of the microwave oven as controlled by a PLC (Table 1). The mass of the microwave turntable with the grated carrot sample and the microwave cavity inside air temperature were recorded at every minute during the drying process. A fan was used to aspirate air from the microwave cavity with about 2 ms^{-1} airflow speed. The ambient air entered the cavity at near room temperature (22 ± 2 °C). The drying procedure was repeated three times at each microwave power level giving a total 27 (9×3) drying experiments.

Table 1. Applied microwave power and related parameters used in the drying study

	AP (W)	IM (g)	SP (W g^{-1})	PP* (-)	T_{on} (s)	T_{off} (s)	PR** (-)	MCT (°C)
1	100	300	0.33	0.14	15	95	7.36	38.2
2	150	300	0.50	0.20	15	59	4.91	42.6
3	200	300	0.67	0.27	15	40	3.68	46.0
4	250	300	0.83	0.34	15	29	2.94	50.6
5	300	300	1.00	0.41	15	22	2.45	53.7
6	350	300	1.17	0.48	15	17	2.10	57.1
7	400	300	1.33	0.54	15	13	1.84	59.9
8	450	300	1.50	0.61	15	10	1.64	62.2
9	500	300	1.67	0.68	15	7	1.47	64.7

AP: Applied Power; IM: Initial Mass; SP: Specific Power; PP*: Power Proportion; T_{on}: On Time; T_{off}: Off Time; PR: Pulse Ratio; MCT: Mean Cavity Temperature; *PP was calculated by dividing the AP by microwave oven's actual power (736 W); **PR = (T_{on} + T_{off}) / T_{on} (Arikan et al., 2012).

Carrots were washed with tap water, peeled off and grated as long and thin strips (mean thickness: 1.1 ± 0.24 mm) by using a hand-operated stainless steel grater and placed homogenously on the microwave oven's turntable with sample thickness of about

10–15 mm. The initial water content of the fresh material was in the range of about 8.5–9.5 kg H_2O kg^{-1} DM (89.5–90.5% wet basis) as determined by oven method by drying a sample of about 50 g in oven at 103 °C for 24 hours. Fresh grated carrot of about 300 g was dried applying intermittent microwave energy until the water content declined to about 0.11 kg H_2O kg^{-1} DM for each drying procedure by recording the time, mass and temperature every minute during the drying process. The dried samples were ground by using an electric grinder to make them ready for colour and NIRS measurement (Fig. 1).

Figure 1. Whole carrots (left), grated fresh carrot and powdered carrot samples (right).

Colour Measurement

Colour of fresh and powdered carrots was measured by using a hand-held chromameter (Minolta CR-400, Osaka, Japan). Two colour models of CIE L*a*b* and L*C*h were employed. In both colour models, the colour is expressed in three dimensions and the meaning of each parameter is given below (Keskin et al., 2017):

L*: Brightness of the colour (0: black, 100: white),

a*: Redness-greenness (–60: green, +60: red),

b*: Yellowness-blueness (–60: blue, +60: yellow),

C* Chroma having a value from 0 to 60,

h: Hue angle (0°: red, 90°: yellow, 180°: green, 270°: blue).

The chromameter was utilized with illuminant C standard and calibrated using its white reflector plate. In measuring the colour of the samples, ground material measurement apparatus was employed. Colour change of the material was evaluated by using the total chromatic aberration (ΔE*) and colour difference values (ΔL*, Δa*, Δb*, ΔC* and Δh) (Soysal et al., 2009b):

$$\Delta L^* = L^*_d - L^*_f$$

$$\Delta a^* = a^*_d - a^*_f$$

$$\Delta b^* = b^*_d - b^*_f$$

$$\Delta E^* = [(\Delta L^*)^2+(\Delta a^*)^2+(\Delta b^*)^2]^{0.5}$$

$$\Delta C^* = C^*_d - C^*_f$$

$$\Delta h = h_d - h_f$$

where *d* and *f* refers to the dried and fresh products, respectively.

NIRS measurement

The powdered carrot samples (N = 27) were placed on glass petri plates (9 cm of diameter). The near infrared (NIR) reflectance of the samples was quantified by using a FT-NIRS system (NIRFlex N-500, Büchi Labortechnik AG, Flawil, Switzerland) covering the wave numbers of 4,000–10,000 cm^{-1} (1,000–2,500 nm) with a resolution of 4 cm^{-1} (total number of reflectance variables: 1,500). All spectra were recorded as the average of 32 scans with three repetitions for each powder sample.

Data Analysis

Powdered carrot sample data included 27 samples (three samples for each of the nine microwave power levels). The colour data were analysed using PLS (Partial Least Squares) regression method in a multivariate statistics program (UnScrambler, v.9.7, Camo, Oslo, Norway). PLS regression was selected since it is more suitable in comparison to other methods (MLR and PCR) with many inter-correlated variables (Keskin et al., 2004; Keskin et al., 2008; Keskin et al., 2013). Correlation coefficients between applied microwave power and colour data were calculated in MS Excel program. The influence of applied microwave power on the colour of the powdered samples was statistically evaluated with a statistic software (SPPS, v.17, IBM, NY, USA) using one-way analysis of variance (ANOVA) and the means were compared with Duncan's test ($p = 0.05$). The NIRS data were explored using the chemometric software of the FT-NIRS system (NIRCal, v5.5, Büchi Labortechnik AG, Flawil, Switzerland) with PLS regression method. 2/3 of the data (n = 18) were used in calibration and the remaining 1/3 of the data (n = 9) were included in the validation set in both colour and NIRS data analysis. Outlying samples were determined and excluded from the colour data set (N = 4) and NIRS data set (N = 1) in the data analysis.

RESULTS AND DISCUSSION

Drying Kinetics of Carrots

Intermittent microwave drying (IMWD) at 500 W applied power with a pulse ratio (PR) of 1.47 had the lowest drying time (Fig. 2, a) among the drying treatments. The drying time of IMWD at 500 W was 1.12–5.47 times shorter than those of other lower applied powers (Fig. 2a). Similarly, the drying rate of IMWD at 500 W was 1.18–5.63 times higher than that of other applied powers (Fig. 2b). As PR increased from 1.47 to 7.33, the drying time increased from 34 to 186 min and the drying rate decreased 5.63 times. The drying rate curve became flatter with the increase in PR indicating gentle drying of the product (Fig. 2b and Fig. 3). After a short heating period, the drying rates of carrot samples dried at PRs from 1.47 (300 W) to 2.45 (300 W) reached to the maximum at specific moisture ratios and then, fast falling rate periods were observed. However, further increase in the PR from 2.45 (300 W) to 7.36 (100 W) resulted in significant changes in the drying rate curves and the constant rate drying periods revealed below the 2.47 PR value (Fig. 2b). As PR increased, the length of the constant rate period progressively increased since microwave power off time (T_{off}) provided a rest time for moisture and temperature redistribution inside the product during the following microwave on time after the warming-up period (Fig. 2b and Fig. 3) (Gunasekaran, 1999; Beaudry et al., 2003, Esturk, 2010).

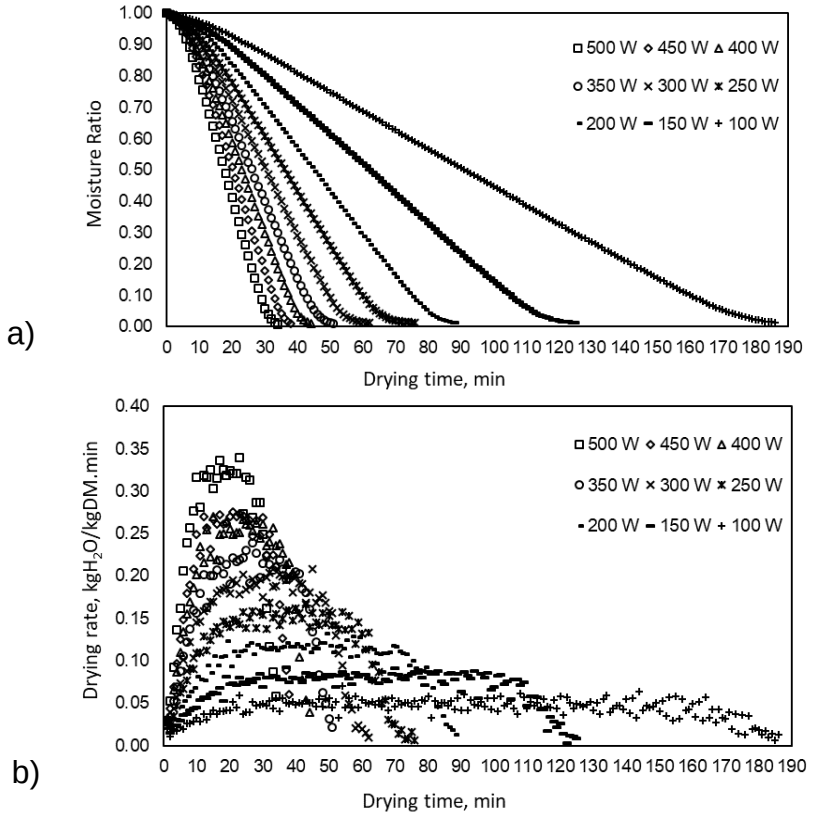

Figure 2. Intermittent microwave drying curves (a) and drying rates (b) of grated carrot at different microwave power levels (DM: dry matter, v_a = 2.0 m s^{-1}).

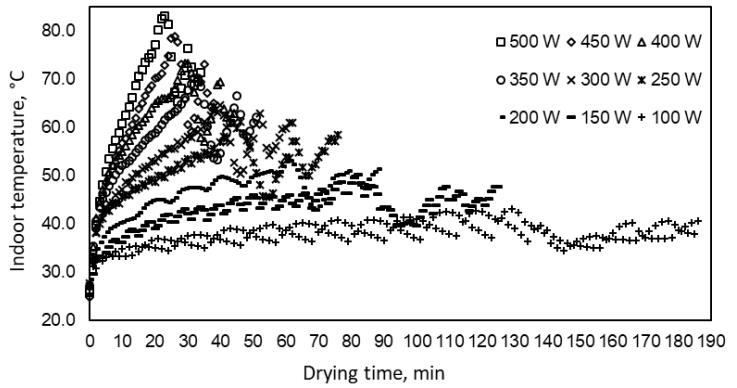

Figure 3. Within-cavity air temperature during intermittent microwave drying of grated carrot

The findings of the current study are supported by several previous studies. Arikan et al. (2012) reported that there was a short heating up period which was followed by a constant rate period until the product moisture content decreased to 1.5–2.0 kg H_2O kg^{-1} DM during IMWD of grated carrots. They further stated that the constant rate period

was 3/5 of the total drying time. Changrue (2006) reported that there was a constant rate period observed in continuous and IMWD of carrot and strawberry without pre-drying. Cui et al. (2004) stated that drying took place at a constant rate period of microwave-vacuum drying of carrot slices with 3–5 mm thickness until the moisture content decreased to 2.0 kg H_2O kg^{-1} DM. It was reported that there was a long constant rate period in convective air drying of carrot until the moisture content decreased to 1.5 kg H_2O kg^{-1} DM (May & Perre, 2002). Cui et al. (2004) conducted continuous and IMWD under vacuum for carrot slices with the thickness of 4, 8 and 10 mm. They stated that the temperature recorded on the surface and in the center of the product was same and there was a uniform temperature distribution in the product less than 8 mm in thickness. They also observed the heating up and constant rate periods followed by a falling rate period in drying of carrots with less than 8 mm thickness.

Effect of Applied Microwave Power on the Colour of Powdered Carrots

The relations between applied microwave (MW) power level determined by the IMPI-2L test (Buffler, 1993) and colour values were also studied (Table 2). The data presented are the means of nine independent measurements from three subsamples and the values after the ± sign represent the standard deviation. The mean L*, a* and b* colour values of fresh carrot samples were 49.79, 21.20 and 37.54, respectively which relates to matte yellowish–orange colour. L* values of the dried samples were higher compared to fresh samples which means that the dried samples were darker than the fresh ones. Also, L* decreased significantly at higher applied MW powers (400, 450 and 500 W) resulting in darker product colours (lower L* values). Similar findings of reduction in L* when the drying temperature increased were reported in dried carrot (Arikan et al., 2012) and dried red peppers (Ning et al., 2012; Swain et al., 2014; Keskin et al., 2018). The a*, b* and C* values were close to the values of the fresh samples for lower applied MW powers (100, 150 and 200 W) while they significantly decreased at higher MW powers (400, 450 and 500 W) which means that the colour of the dried samples got matte at higher applied MW powers. On the other hand, h value was similar to the values of the fresh samples for lower applied MW powers but they significantly increased as the applied MW power was increased meaning that higher powers made the samples matte and more yellowish orange colour.

Table 2. Influence of applied microwave power on the colour of the powdered carrots

AMP* (W)	L*	a*	b*	C*	h
Fresh	49.79 ± 0.65^{a}	21.20 ± 0.56^{e}	37.54 ± 0.81^{b}	43.11 ± 0.96^{cd}	60.55 ± 0.28^{a}
100	71.46 ± 0.81^{def}	22.18 ± 1.15^{e}	39.12 ± 0.22^{b}	44.98 ± 0.72^{d}	60.46 ± 1.18^{a}
150	74.33 ± 1.06^{f}	16.79 ± 4.61^{d}	37.87 ± 1.73^{b}	41.43 ± 3.58^{bcd}	66.15 ± 4.59^{b}
200	72.95 ± 0.69^{ef}	16.12 ± 4.60^{cd}	39.54 ± 1.53^{b}	42.72 ± 3.42^{cd}	67.83 ± 4.61^{b}
250	70.50 ± 2.65^{cde}	12.87 ± 2.08^{ab}	39.66 ± 1.84^{b}	41.72 ± 2.51^{bcd}	72.08 ± 1.64^{c}
300	68.48 ± 2.97^{cd}	12.74 ± 1.09^{ab}	39.07 ± 1.19^{b}	41.12 ± 1.52^{bcd}	71.98 ± 0.71^{c}
350	67.38 ± 0.52^{c}	11.87 ± 2.55^{ab}	39.04 ± 0.55^{b}	40.81 ± 1.15^{bc}	73.11 ± 2.70^{c}
400	67.56 ± 1.73^{c}	13.44 ± 1.50^{bc}	39.17 ± 0.92^{b}	41.43 ± 0.97^{bcd}	71.13 ± 1.98^{c}
450	63.35 ± 4.26^{b}	10.33 ± 2.64^{ab}	36.68 ± 0.81^{ab}	38.12 ± 1.60^{ab}	74.35 ± 3.08^{c}
500	61.16 ± 1.46^{b}	10.13 ± 2.76^{a}	34.47 ± 0.97^{a}	35.95 ± 1.79^{a}	73.69 ± 3.15^{c}

Same letters within the same column are not significantly different ($p < 0.05$); *AMP: Applied Microwave Power (W).

The colour difference data that is essential in the assessment of dried material quality is shown in Table 3. It was found that the change of brightness (ΔL*) and total colour change (ΔE*) was lower at higher applied microwave (MW) powers. A similar finding was reported by Keskin et al. (2018) for powdered peppers dried by infrared energy. Also, Rhim & Hong (2011) reported that the ΔE value depended on both drying temperature and water activity (Aw) and ΔE was lower in high temperature (50 °C) only in low Aw conditions. Even if the total colour difference (ΔE*) values were lower at higher applied powers (400, 450 and 500 W), the higher power levels made the samples darker which is not preferable. However, since bright coloured products are more preferred by consumers, the ΔE* value should not be considered as a single indicator of colour evaluation and thus, ΔL* should also be taken into account. Also, the hue angle difference (Δh) can be considered as a good indicator to explain the colour changes of the carrot powders at different MW powers. The Δh value was relatively smaller at lower applied MW powers (100, 150 and 200 W) as compared to higher MW powers (Table 3).

Table 3. Effect of applied microwave power on the colour difference of powdered carrots

AMP* (W)	ΔL*	Δa*	Δb*	ΔC*	Δh	ΔE*
100	21.67 ± 0.81^{cd}	0.98 ± 1.15^{d}	1.58 ± 0.22^{b}	1.86 ± 0.72^{d}	-0.09 ± 1.18^{a}	21.78 ± 0.73^{cd}
150	24.54 ± 1.06^{d}	-4.41 ± 2.08^{c}	0.33 ± 1.84^{b}	-1.68 ± 2.51^{bcd}	5.60 ± 1.64^{b}	25.03 ± 1.29^{e}
200	23.16 ± 0.69^{d}	-5.08 ± 1.50^{bc}	2.00 ± 0.92^{b}	-0.40 ± 0.97^{cd}	7.28 ± 1.98^{b}	23.84 ± 0.46^{de}
250	20.71 ± 2.65^{bcd}	-8.32 ± 2.22^{a}	2.12 ± 1.00^{b}	-1.39 ± 1.65^{bcd}	11.53 ± 2.43^{c}	22.53 ± 2.31^{cde}
300	18.69 ± 2.97^{bc}	-8.46 ± 1.85^{a}	1.53 ± 0.57^{b}	-2.00 ± 1.03^{bcd}	11.43 ± 2.30^{c}	20.71 ± 2.01^{bc}
350	17.59 ± 0.52^{b}	-9.32 ± 1.15^{a}	1.50 ± 1.13^{b}	-2.31 ± 1.42^{bc}	12.56 ± 1.07^{c}	20.00 ± 0.83^{bc}
400	17.77 ± 1.73^{bc}	-7.76 ± 2.13^{ab}	1.63 ± 2.09^{b}	-1.68 ± 2.57^{bcd}	10.59 ± 2.12^{c}	19.60 ± 1.77^{bc}
450	13.56 ± 4.26^{a}	-10.86 ± 1.95^{a}	-0.86 ± 3.17^{ab}	-4.99 ± 3.58^{ab}	13.81 ± 1.53^{c}	17.90 ± 2.27^{ab}
500	11.37 ± 1.46^{a}	-11.07 ± 1.44^{a}	-3.07 ± 2.21^{a}	-7.16 ± 2.50^{a}	13.14 ± 1.22^{c}	16.33 ± 1.04^{a}

Same letters within the same column are not significantly different ($p < 0.05$); *AMP: Applied Microwave Power (W).

Consequently, statistical analysis showed that applied MW power level was a crucial factor on all colour parameters of the powdered carrots (Table 2 and Table 3). The colours of carrot samples dried at lower applied MW powers (100, 150 and 200 W) were comparatively brighter and more vivid yellowish-orange and increase of applied MW power (400, 450 and 500 W) led to development of matte darker yellowish-orange product colour, which was considered as unacceptable for consumer preference.

Estimating Applied Microwave Power from Colour Data

Correlation coefficients between applied microwave (MW) power and colour parameters were also investigated (Fig. 4). It was observed that high correlation and dependence was present between applied MW power and the colour parameters. The highest correlation coefficient was found as –0.87 for the colour parameter of L* while the parameter b* had the lowest correlation (–0.55). Parameters of L*, a*, b* and C* were in a decreasing trend as response to increasing applied MW power while h was in a rising trend as the applied MW power increased.

Colour data were used to develop a mathematical model to estimate applied microwave (MW) power of the samples using PLS regression. Three different models were investigated with X variables of L*a*b, L*C*h and L*a*b*C*h (all colour

parameters) and Y variable of applied MW power (100, 150, 200, 250, 300, 350, 400, 450, 500 W). The model with all colour values (L*a*b*C*h) provided better outcomes in terms of R^2 and SEP as compared to other two models with L*a*b and L*C*h. The validation R^2 and SEP values were around 0.95 and 29.9 W for the model with L*a*b*C*h while they were around 0.94 and 35.3 W for the model with L*a*b and around 0.95 and 31.9 W with the L*C*h, respectively.

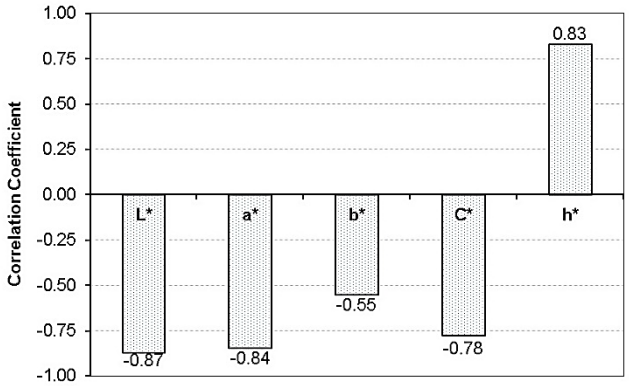

Figure 4. Correlation coefficients between applied MW power and colour parameters.

The score plot for PC1 and PC2 for the model with L*a*b*C*h (Fig. 5) revealed that the powdered carrot samples dried by different power rates were dispersed very well in a way that the samples which were dried with higher power rates (400, 450, 500 W) were on the right-hand side as the ones with lower power levels (100, 150, 200 W) were on the left-hand side. The model had three significant PCs and they explained 100% of the variability of X (colour) and 96% of variability of Y (power). It can be stated that PC1 significantly explained the differences of powdered carrot samples dried by different applied MW power rates.

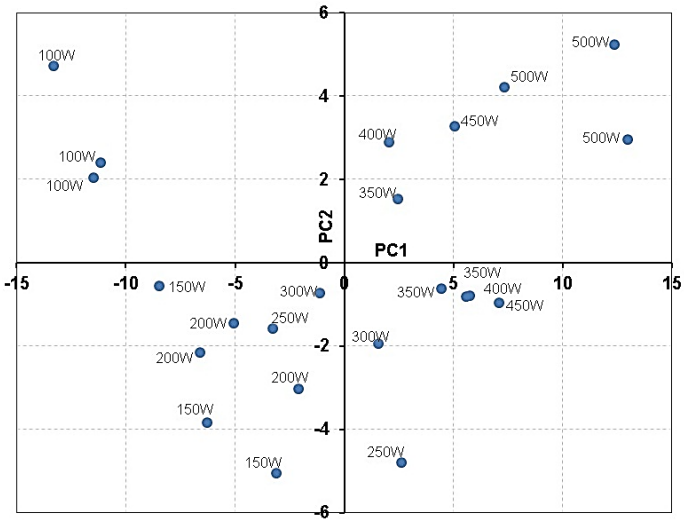

Figure 5. Score plot of PLS regression model of powdered carrots using colour data.

The original vs. predicted applied microwave (MW) power for the model of L*a*b*C*h is presented on Fig. 6. The validation R^2 and SEP values were around 0.95 and 29.9 W for the model with L*a*b*C*h. This means that the applied MW power of the dried and powdered carrot samples can be estimated relatively well using L*a*b*C*h colour data obtained from the hand-held chromameter. Similarly, Keskin et al. (2018) reported that the drying temperature of infrared-dried powdered peppers could be predicted from the colour data ($R^2 = 0.98$). The mathematical model to predict the applied MW power of dried and powdered carrot samples was computed as:

$$AMWP = 1227.78 - 21.03 \times L^* - 6.18 \times a^* + 1.92 \times b^* - 0.99 \times C^* + 8.28 \times h$$

where AMWP: Applied microwave power (W);

L*: Brightness of colour (0: black, 100: white);

a*: Redness and greenness (–60: green, +60: red);

b*: Yellowness and blueness (–60: blue, +60: yellow);

C*: Chroma value (0–60);

h: Hue angle value (0°: red, 90°: yellow, 180°: green, 270°: blue).

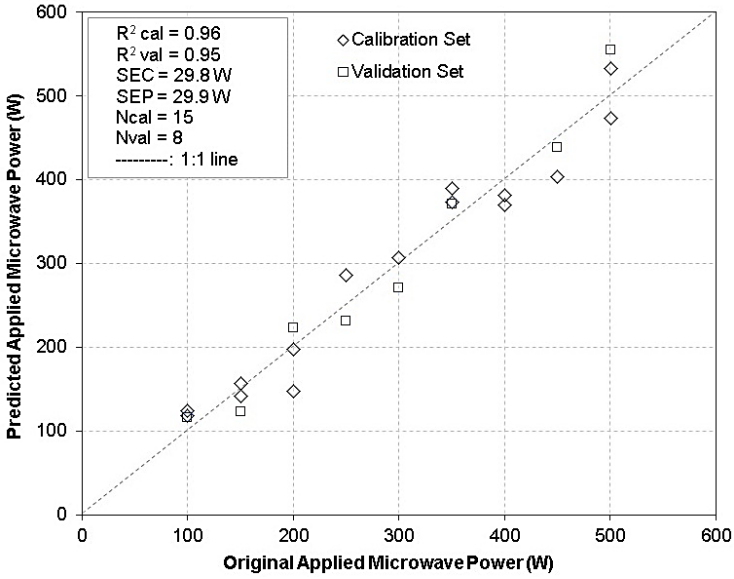

Figure 6. Original vs. Predicted applied microwave power of powdered carrots with colour data.

Estimating Applied Microwave Power from FT-NIRS Data

The raw mean near infrared (NIR) reflectance data is shown on Fig. 7. Each line in the figure represents the average reflectance of the three replicated powdered carrot samples. It was observed that the fresh carrot samples had lower reflectance (higher absorbance) values as compared to the dried powdered samples. The important absorbance bands were found to be around the wavenumbers of 4,300–4,400 cm^{-1} (CH2, aminoacid, CH3, starch), 4,700–4,800 cm^{-1} (CONH2, CONHR, starch), 5,100−5,200 cm^{-1} (H2O, CO2R, CONH2, amide), 6,700–6,900 cm^{-1} (CONHR, CONH2, cellulose) and 8,200–8,400 cm^{-1} (CH2, CH3).

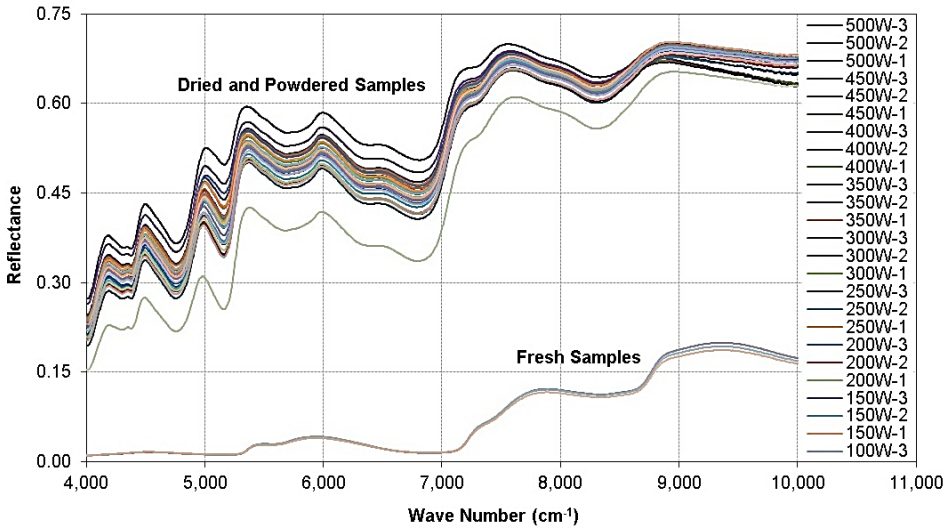

Figure 7. Near infrared reflectance spectra of the powdered carrot samples from FT-NIRS.

In the NIRS data analysis with PLS regression, different data pre-treatment methods were utilized and combination of four treatments being SNV (Standard Normal Variate), First Derivative BCAP, Variance Scaling and MSC Offset (Multiplicative Scatter Correction) provided better results in terms of higher R^2 and lower SEP. Based on the PC1 and PC2 score plot (Fig. 8), it was seen that the samples were separated very well in a way that the samples dried with lower applied microwave power (100, 150, 200 W) were on the left-bottom side and the ones from higher applied microwave power (400, 450, 500 W) were on the right-top hand side. From this observation, it can be inferred that a successful model can be developed to estimate applied microwave power from the NIR reflectance data.

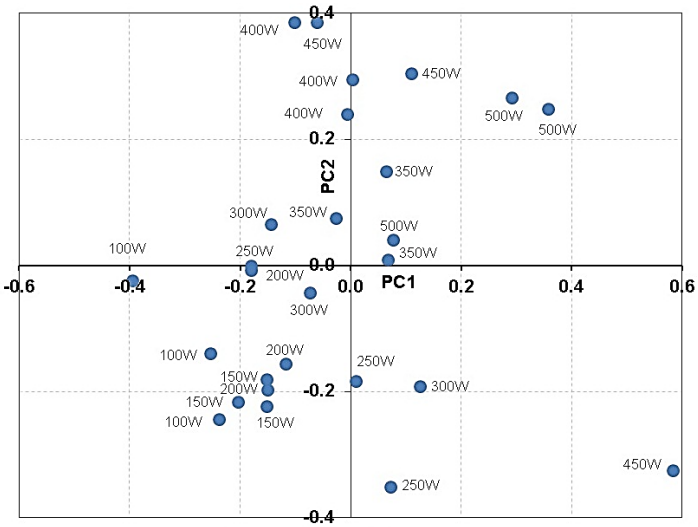

Figure 8. Score plot of FT-NIRS model of powdered carrots dried by intermittent microwave.

Based upon the original vs. predicted applied microwave power for the model using NIRS reflectance data (Fig. 9), the validation R^2 and SEP values were around 0.99 and 16.1 W. This means that the applied microwave power of the dried and powdered carrot samples can be estimated very well using NIR reflectance data. Similarly, Keskin et al. (2018) reported that the drying temperature of infrared-dried powdered peppers could be predicted from the NIRS data (R^2 = 0.98). Thus, it can be inferred that NIRS is a useful tool for the estimation of drying temperature or applied microwave power for dried and powdered carrot samples.

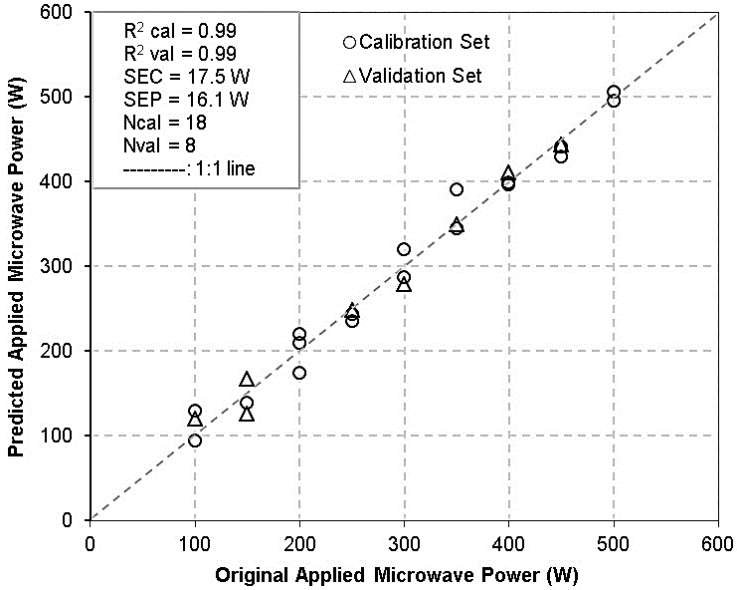

Figure 9. Original vs. Predicted applied microwave power of powdered carrots using FT-NIRS.

As a comparison between the chromameter and the NIRS system, it was observed that the NIRS system (R^2 = 0.99; SEP = 16.1 W) can predict the applied microwave (MW) power of powdered carrots with significantly better performance than a chromameter (R^2 = 0.95; SEP = 29.9 W). Yet, cost of the equipment is also a crucial factor. The chromamater is far more inexpensive as compared with the NIRS system and it can predict the applied MW power from the colour data relatively well.

It is not feasible to assess the quality of fresh or dried agricultural products by human vision since it is not subjective and standard (Keskin at al., 2008; Keskin et al., 2017); thus, various electro-optical instruments including chromameters and NIRS systems are used for this purpose owing to their benefits being non-destructive, fast, inexpensive, repeatable, environment-friendly and performing analysis in situ and online (Garcia-Sanchez et al., 2017). In intermittent microwave (MW) drying, applied MW power, pulse ratio and temperature are crucial factors to obtain high quality dried products (Ekezie et al., 2017). The current study aimed at prediction of applied MW power of powdered carrots dried by intermittent MW energy. Further studies have been planned to include other drying methods including hot air convective and infrared drying

methods and the combined drying methods at different drying temperatures for other agricultural products.

CONCLUSIONS

This study was conducted to predict the applied microwave (MW) power of carrot powders dried by intermittent MW drying with varying applied MW powers (100-500 W) by using two different instruments, a chromameter and FT-NIRS.

The drying time with the highest applied power of 500 W was 1.12–5.47 times shorter than those of lower applied powers. However, intermittent MW drying with longer power-off time (lower applied power) resulted in a more stable and gentle drying process and could be preferred as a drying method to produce higher quality products in terms of product colour. Statistical analysis showed that applied MW power was a crucial factor on all colour parameters of the powdered carrots. Brightness (L*) decreased significantly with the increase of applied MW power resulting in darker product colours.

Results showed that the NIRS system ($R^2 = 0.99$; SEP = 16.1 W) can predict the microwave power of powdered carrots with comparatively better performance than a chromameter ($R^2 = 0.95$; SEP = 29.9 W). The chromamater is far more inexpensive when compared with the NIRS system and it can predict the applied microwave power from the colour data relatively well.

ACKNOWLEDGEMENTS. The authors recognize the financial support from TUBITAK (the Scientific and Technological Research Council of Turkey).

REFERENCES

Aghilinategh, N., Rafiee, S., Hosseinpour, S., Omid, M. & Mohtasebi, S.S. 2016. Real-time color change monitoring of apple slices using image processing during intermittent microwave convective drying. *Food Science and Tech. International* **22(**7), 634–646.

Arikan, M.F., Ayhan, Z., Soysal, Y. & Esturk, O. 2012. Drying characteristics and quality parameters of microwave-dried grated carrots. *Food Bioprocess Tech*. **5**, 3217–3229.

Baini, R. & Langrish, T.A.G. 2007. Choosing an appropriate drying model for intermittent and continuous drying of bananas. *Journal of Food Engineering* **79(**1), 330–343.

Beaudry, C., Raghavan, G.S.V. & Rennie, T.J. 2003. Microwave finish drying of osmotically dehydrated cranberries. *Drying Technology* **21**(9), 1797–1810.

Buffler, C.R. 1993. Microwave cooking and processing: engineering fundamentals for the food scientist. New York, USA: Avi Book, p. 39, 54.

Cao, Z., Zhou, L., Bi, J., Yi, J., Chen, Q., Wu, X., Zheng, J. & Li, S. 2016. Effect of different drying technologies on drying characteristics and quality of red pepper (*Capsicum frutescens* L.): a comparative study. *Journal of the Sci. of Food and Agr.* **96**, 3596–3603.

Changrue, V. 2006. Hybrid (Osmotic, microwave-vacuum) drying of strawberries and carrots. PhD thesis, McGill University, Quebec, Canada.

Cui, Z.W., Xu, S.Y. & Sun, D.W. 2004. Microwave-vacuum drying kinetics of carrot slices. *Journal of Food Engineering* **65(**2), 157–164.

da Silva Dias, J.C. 2014. Nutritional and health benefits of carrots and their seed extracts. *Food and Nutrition Sciences* **5**, 2147–2156.

Das, I. & Arora, A. 2018. Alternate microwave and convective hot air application for rapid mushroom drying. *Journal of Food Engineering* **223**, 208–219.

Dehghannya, J., Farshad, P. & Heshmati, M.K. 2018. Three-stage hybrid osmotic–intermittent microwave–convective drying of apple at low temperature and short time. *Drying Technology* **36**(16), 1982–2005.

Ekezie, F.C., Sun, D.W., Han, Z. & Cheng, J.H. 2017. Microwave-assisted food processing technologies for enhancing product quality and process efficiency: A review of recent developments. *Trends in Food Science & Technology* **67**, 58–69.

Esturk, O. 2010. Intermittent and continuous microwave-convective air-drying characteristics of sage (*Salvia officinalis*) leaves. *Food and Bioprocess Technology* **5**(5), 1664–1673.

FAO, 2018. Crop Production Statistics. Food and Agriculture Organization (FAO). www.fao.org (Accessed: 13.11.2018)

Garcia-Sanchez, F., Galvez-Sola, L., Martinez-Nicolas, J.J., Muelas-Domingo, E. & Nieves, M. 2017. Using near-infrared spectroscopy in agricultural systems. DOI: http://dx.doi.org/10.5772/67236.

Gunasekaran, S. 1999. Pulsed microwave-vacuum drying of food materials. *Drying Technology* **17**(3), 395–412.

Hwang, I.M., Choi, J.Y., Nho, E.Y., Lee, G.H., Jamila, N., Khan, N., Jo, C.H. & Kim, K.S. 2017. Characterization of red peppers (*Capsicum annuum*) by high-performance liquid chromatography and near-infrared spectroscopy. *Analytical Letters* **50**(13), 2090–2104.

Junqueira, J.R.J., Correa, J.L.G. & Emesto, D.B. 2017. Microwave, convective, and intermittent microwave–convective drying of pulsed vacuum osmodehydrated pumpkin slices. *Journal of Food Process Preserv*. DOI: 10.1111/jfpp.13250.

Karam, M.C., Petit, J., Zimmer, D. & Djantou, E.B. 2016. Effects of drying and grinding in production of fruit and vegetable powders: A review. *Journal of Food Eng.* **188**, 32–49.

Kermani, A.M., Khashehchi, M., Kouravand, S. & Sadeghi, A. 2017. Effects of intermittent microwave drying on quality characteristics of pistachio nuts. *Drying Technology* **35**, 1108–1116.

Keskin, M., Dodd, R.B., Han, Y.J. & Khalilian, A. 2004. Assessing nitrogen content of golf course turfgrass clippings using spectral reflectance. *Applied Eng. Agric.* **20**(6), 851–860.

Keskin, M., Han, Y.J., Dodd, R.B. & Khalilian, A. 2008. Reflectance-based sensor to predict visual quality ratings of turfgrass plots. *Applied Eng. in Agriculture* **24**(6), 855–860.

Keskin, M., Karanlık, S., Görücü Keskin, S. & Soysal, Y. 2013. Utilization of color parameters to estimate moisture content and nutrient levels of peanut leaves. *Turkish Journal of Agriculture and Forestry* **37**, 604–612.

Keskin, M., Setlek, P. & Demir, S. 2017. Use of color measurement systems in food science and agriculture. *International Advanced Researches & Engineering Congress*. 16–18 November 2017. Osmaniye, Turkey. pp. 2350–2359 (Abstract in English).

Keskin, M., Soysal, Y., Sekerli, Y.E., Arslan, A. & Celiktas, N. 2018. Predicting Drying Temperature of Infrared-Dried Pepper Powders Using FT-NIRS and Chromameter. I*nternational Conference on Energy Research* (ENRES 2018), Alanya, Turkey.

Khan, U., Afzaal, M., Arshad, M.S. & Imran, M. 2015. Non-destructive analysis of food adulteration and legitimacy by FTIR technology. *Journal of Food Industry and Microbiology* DOI:10.4172/2572-4134.1000103.

Kumar, C. & Karim, M.A. 2017. Microwave-convective drying of food materials: A critical review. *Critical Reviews in Food Science and Nutrition*. DOI: 10.1080/10408398.2017.1373269.

Li, Y., Zhang, T., Wu, C. & Zhang, C. 2014. Intermittent Microwave Drying of Wheat (*Triticum aestivum* L.) Seeds. *Journal of Exp. Biology and Agric. Sci.* **2**(1), 32–36.

Li, X., Lu, R., Wang, Z., Wang, P., Zhang, L. & Jia, P. 2018. Detection of corn and whole wheat adulteration in white pepper powder by near infrared spectroscopy. *American Journal of Food Science and Tech*. **6**, 114–117.

Lim, J., Kim, G., Mo, C. & Kim, M.S. 2015. Design and fabrication of a real-time measurement system for the capsaicinoid content of Korean red pepper (*Capsicum annuum* L.) powder by visible and near-infrared spectroscopy. *Sensors* **15**, 27420–27435.

May, B.K. & Perre, P. 2002. The importance of considering exchange surface area reduction to exhibit a constant drying flux period in foodstuffs. *Journal of Food Eng.* **54**(4), 271–282.

Moraes, I.C.F., Sobral, P.J.A., Branco, I.G. & Gomide, C.A. 2013. Dehydration of "dedo de moça" pepper: kinetics and phytochemical concentration. *Ciênc. Tecnol. Aliment., Campinas* **33**, 134–141.

Ning, X.F., Han, C.S. & Li, H. 2012. A mathematical model for color changes in red pepper during far infrared drying. *Journal of Biosystems Engineering* **37**(5), 327–334.

Onwude, D.I., Hashim, N. & Chen, G. 2016. Recent advances of novel thermal combined hot air drying of agricultural crops. *Trends in Food Science & Technology* **57**, 132–145.

Ordonez-Santos, L.E., Tanganan, L.M. & Mendez-Molano, G.X. 2014. A study of degradation kinetics regarding green peppers' (Capsicum spp.) surface colour. *Orinoquia, Universidad de los Llanos* **18**(1), 16–20.

Pathare, P.B., Opara, U.L. & Al-Said, F.A.J. 2013. Color measurement and analysis in fresh and processed foods: A Review. *Food Bioprocess Technology* **6**, 36–60.

Pham, N.D., Kumar, C., Joardder, M.U.H., Khan, M.I.H., Martens, W. & Karim, M.A. 2016. Effect of different power ratio mode of intermittent microwave convective drying on quality attributes of kiwi fruit slices. *20th Int. Drying Symposium*, Gifu, Japan.

Pham, N.D., Khan, M.I.H., Joardder, M.U.H, Rahman, M.M., Mahiuddin, M., Abesinghe, A.M.N. & Karim, M.A. 2017. Quality of plant-based food materials and its prediction during intermittent drying. Critical Reviews in Food Science and Nutrition. doi: 10.1080/10408398.2017.1399103

Rhim, J.W & Hong, S.I. 2011. Effect of water activity and temperature on the color change of red pepper (Capsicum annuum L.) powder. *Food Sceince and Biotech.* **20**(1), 215–222.

Rodriguez-Saona, E. & Allendorf, M.E. 2011. Use of FTIR for rapid authentication and detection of adulteration of food. *Annual Review of Food Science and Tech.* **2**, 467–483.

Sharifian, F., Motlagh, A.M. & Nikbakht, A.M. 2012. Pulsed microwave drying kinetics of fig fruit (Ficus carica L.). *Australian Journal of Crop Science* **6**(10), 1441–1447.

Soysal, Y. 2009. Intermittent and continuous microwave-convective air drying of potato (Lasy rosetta): Drying kinetics, energy consumption and product quality. *Journal of Agricultural Machinery Science* **5**(2), 139–148.

Soysal, Y., Ayhan, Z., Esturk, O. & Arikan, M.F. 2009a. Intermittent microwave–convective drying of red pepper: Drying kinetics, physical (colour and texture) and sensory quality, *Biosystems Eng*. **103**, 455–463.

Soysal, Y., Arslan, M. & Keskin, M. 2009b. Intermittent microwave-convective air drying of oregano. *Food Science Tech Int.* **15**(4), 397–406.

Swain, S., Samuel, D.V.K., Bal, L.M. & Kar, A. 2014. Thermal kinetics of colour degradation of yellow sweet pepper (CapsicumAnnum L.) undergoing microwave assisted convective drying. *International Journal of Food Properties* **17**(9), 1946–1964.

Toledo-Martin, E.M., Garcia, M.C., Font, R., Rojas, J.M., Gomez, P., Navarro, M. & Celestino, M.D. 2015. Application of visible/near-infrared reflectance spectroscopy for predicting internal and external quality in pepper. *Sci Food Agric*. **96**, 3114–3125.

Tripathi, S. & Mishra, H.N. 2009. A rapid FT-NIR method for estimation of aflatoxin B1 in red chili powder. *Food Control* **20**, 840–846.

Wu, X.Y., Zhu, S.P., Huang, H. & Xu, D. 2017. Quantitative identification of adulterated Sichuan pepper powder by near-infrared spectroscopy coupled with chemometrics. *Journal of Food Quality*. Article ID: 5019816, 7 pp.

Yang, X.H, Deng, L.Z., Mujumdar, A.S., Xiao, H.W., Zhang, Q. & Kan, Z. 2018. Evolution and modeling of colour changes of red pepper (*Capsicum annuum* L.) during hot air drying. *Journal of Food Eng*. **231**, 101–108.

Agronomy Research **17**(2), 481–490, 2019
https://doi.org/10.15159/AR.19.103

Methodology of the stress detemination in the tool module during the work of the agriculture machine

A. Kešner[1,*], R. Chotěborský[1], M. Linda[2] and M. Hromasová[2]

[1]Czech University of Life Sciences Prague, Facult of Engineering, Department of Material Science and Manufacturing Technology, Kamýcká 129, CZ165 21 Prague, Czech Republic
[2]Czech University of Life Sciences Prague, Faculty of Engineering, Department of Eletrical Engineering and Automation, Kamýcká 129, CZ165 21 Prague, Czech Republic
*Correspondence: kesner@tf.czu.cz

Abstract. Machine construction is designed using by mathematical models. The frame is a fundamental part of an agricultural soil cultivation machine so that forces were transfered during transport and machine work to frame. The stress in the machine frame is important to know for the best frame design of the machine. The mathematical model included measued strain can able to design or detect deficiencies on the machine frame. Due to the transfer of forces from the tools, stress is created in the machine frame. High requirements are placed on the determination of boundary conditions for mathematical models in agricultural machinery. Various types, sizes and equipment of agricultural tools significantly affect the transfer of draught force to the machine. The direction and magnitude of the forces, that are caused by agricultural tools, it is important to find out. Ansys mechanical solver have been used to determination strain like response of frame from chisel module. The results can be used as a boundary condition for mathematical models.

Key words: agricultural machine, mathematical model, stress, simulation

INTRODUCTION

The design of an agricultural machine is currently being built using modern technologies such as computer simulation (Kheybari & Salehpour, 2015). When creating a mathematical model it is necessary to know its load on the frame of the agricultural machine (Abo Al-kheer et al., 2011). The transporting and working position of the agricultural machine are important positions when designing the machine. Frames of agricultural machines are stressed from the tool module during working of machine on the field (Ani et al., 2018). Exertion from tool modules causes disturbances such as cracks or deformations on the frame of agricultural machines (Paraforos et al., 2014). Farm machinery manufacturers use the same tool modules for multiple types of machines (the width of the machine, etc.). Stress is an important boundary condition for creating mathematical models of agricultural machinery (Govindarajan & Gnanamoorthy, 2007).

Stress measurement is used for components and machines in many different fields – as residual stresses in production and machining (Sutanto & Madl, 2018), design of

combined agricultural machinery (Bulgakov et al., 2016). Measurement conditions are important for real stress measurement from strain gauges (Lindblom & Cashion, 2005).

During the operation of the agricultural machine, the force tool acts to stress the machine frame (Nurmiev et al., 2018). The forces generated by the tool model are very fast, when the stress is rapidly declining and rising. The soil resistance play an important role (Chotěborský & Linda, 2016). It this reason, why the manufacturers of agricultural machinery report the maximum resistance of the land that the location can have for the work of the machine (Cardei et al., 2018). An obstacle in the soil can cause an immediate increase in strength (Bulgakov et al., 2016). For this reason, the tool modules are protected. Protecting the tool module will allow it to deflect so that the tool module position is deflected when the obstacle impacts. The machine stress is not exceeded by changing the tool module position. The protection is set so that when the maximum machine resistance is reached, the machine's working depth is reduced. Increased stress can not occur on the machine than it is designed on (Bulgakov et al., 2016).

The magnitude of stress from the tool module determines its size and shape (Chotěborský & Linda, 2015). In order to determine the appropriate place on the flexi-tine and the position on the machine frame, it is possible to repeat the measurement for different chisels and coulters and to determine the influence of the tool on the stress (Ahmed et al., 2014).

The main reason for this measurement is to find out the boundary conditions for calculating mathematical models. Mathematical models are part of the design solution for machine design.

The aim of this work was to design a suitable procedure for detecting stress acting on the machine frame from the tool module.

MATERIALS AND METHODS

The workflow consisted of several parts. The first, it was to determine the measuring points in assemble frame and it calibrate the stress measurement devices. It was also the detection of maximum values of strain in the machine frame. Field experiments were carried out subsequently.

Measuring equipment

The stress was measured on the machine frame and the tool module. The device was built for 8 measuring points. Data transfer was performed via WiFi. Critical places were chosen on a mathematical model. The chosen places were grinded before gluing of strain gauges. The strain gauges were silicon resistance type AP130-6-35/BP/Au. The measurement procedure is described in the literature (Furrer & Semiatin S.L., 2009).

$$\varepsilon_M = \frac{-C_1 + \sqrt{C_1^2 + 4 \times C_2 \times \left(1 - \frac{R_{REL}}{R_2}\right)}}{2 \times C_2} \quad (1)$$

where ε_M – deformation on surface [-], C_1 – linear coefficient of deformation equation [-]; C_2 – quadratic coefficient of deformation equation [-], R_2 – semiconductor compensation strain gauge [Ω], R_{REL} – relative strain gauge [Ω].

Fig. 1 shows the location of strain gauges on the machine. The location of the strain gauges was selected according to the mathematical model where the force on the tip of

chisel of the tool modules was loaded. The forces were assume in the x, y, z axes in ratio 1:0.1:0.01 and the strain was determine in a mathematical model. The stain gauge were glued in place with ideal direction of strain in place 1 – 3 and 6 – 8 on frame and 4 and 5 were place on flexi tine.

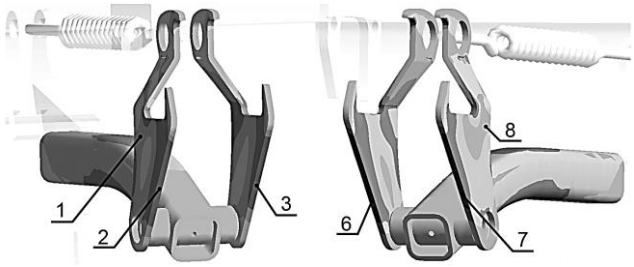

Figure 1. Left – Location of strain gauges 1, 2, 3, to the right the location of strain gauges 6,7,8 on frame of test machine.

Fig. 2 shows a tool module that is fitted with strain gauges. The module thus prepared is ready for installation on the machine.

Figure 2. The tool module is ready for installation on the test machine.

1 module allowed to connect 8 measuring points. The device is powered by an integrated battery. Connectors CAN 9 are used to connect measuring positions. The measuring application was designed to control the module. The application can be used to set the measurement mode, the sequential buffer and the number of channels. Fig. 3 shows the entire connection of the measuring device.

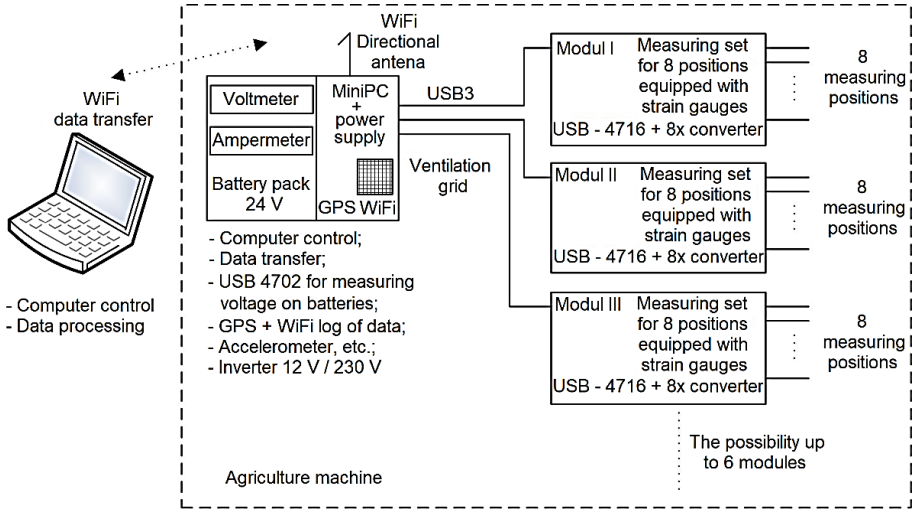

Figure 3. Scheme of a measuring device for recording strain from strain gauges during experimental tests on the field.

Detecting maximum stress values

The type of sandyclay soil is important to follow when designing the machine. It is necessary to determine the limit conditions that may occur during machine operation. These limit conditions have been ensured by the design of an experimental ride with blocked fuse of tool module. These conditions ensure that the maximum load is determined during the experimental ride.

Experimental rides

Two agricultural tools (chisels) were selected for tests. One chisel was fitted with wings, the second was without wings – see Fig. 4.

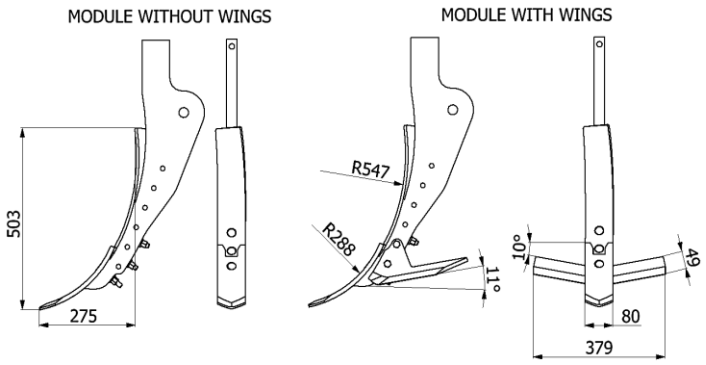

Figure 4. Modules of tools used for tests (in millimetres).

Soil resistance is defined by the module surface – chisels, ridging body and wings. According to Fig. 4 the area module for soil resistance is 40,240 mm^2 (80 mm x 503 mm) and for chisel with wings is area of soil resistance 54,891 mm^2 [80 mm x 503 mm + ((379 mm – 80 mm) x 49 mm)].

The tool modules were installed on a test machine – see Fig. 5.

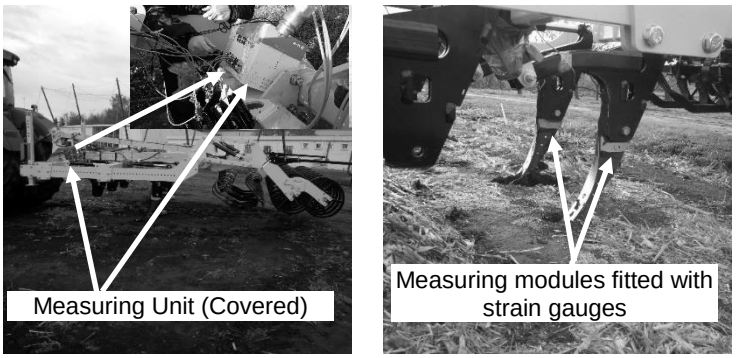

Figure 5. Test machine with installed tool modules for experimental rides – left all machine during work, right detail of module with tools.

The securing was provided by means of hydraulic cylinders for the tool modules. The pressure in the hydraulic cylinders is controlled by a pressure regulator. The pressure

in the hydraulic cylinders for active secure was set at 12 MPa. A pressure of 18 MPa was set to lock the fuse. Two experimental rides were carried out. The first experimental ride was carried out with the active fuse of the flexi-tine. The second experimental ride was performed with blocked fuses. The experimental rides parameters are summarized in Table 1.

Table 1. Setting up and parameters for modules of tools

	1st experimental ride	2nd experimental ride
Type of fuse (-)	hydraulic cylinder	hydraulic cylinder
Pressure in hydraulic cylinder (MPa)	12	18
Fuse of protection module (-)	on	off
Force in hydraulic cylinder (kN)	28.50	42.76
Working depth (m)	0.3	0.3
Area of modulus resistance in soil without wings (m^2)	0.040 24	0.040 24
Area of modulus resistance in soil with wings (m^2)	0.054 981	0.054 981
Working speed ($km \times h^{-1}$)	10.6	10.6
Tractor power (kW)	239	239
Place of measuring (-)	50.127652 14.374566	50.127510 14.374756

The course of the experimental ride was measured from the beginning of the tool's work in the soil of the tool until the tool was finished work in the soil.

The diagram of the connection of the measuring tool module to the machine frame is shown in Fig. 6.

The FEM model was used to determination of boundary condition. Measured strain was response of model and forces and moments were used as variables in parametric modelling in steady state for blocked fuse. Step by step algorithm cycles found a solution which will be under closely to real average strain. The limit was used 10% error. Model of tool module was calculated on Intel® Xeon® Processor CPU E5 - 1650 v3@, processor base frequency 3.50 GHz.

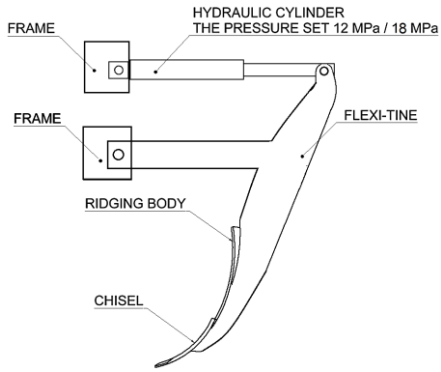

Figure 6. Module mounting diagram – active fuse 12 MPa, blocked fuse 18 MPa.

RESULTS AND DISCUSSION

The time frequency *t* is shown for the beginning work of the tool in soil, the classic machine work in soil, and the finish work of the tool in Figs 7 to 10. The individual distortions ε correspond to the position of the measuring points. The measuring points were selected according to the mathematical model with the prevailing stress in one axis.

The deformation distribution distortion for the experimental ride with the set activared fuse is shown in Figs 7 and 8.

The same course was observed for measuring points 2 and 6 as well as for measuring points 3 and 7.

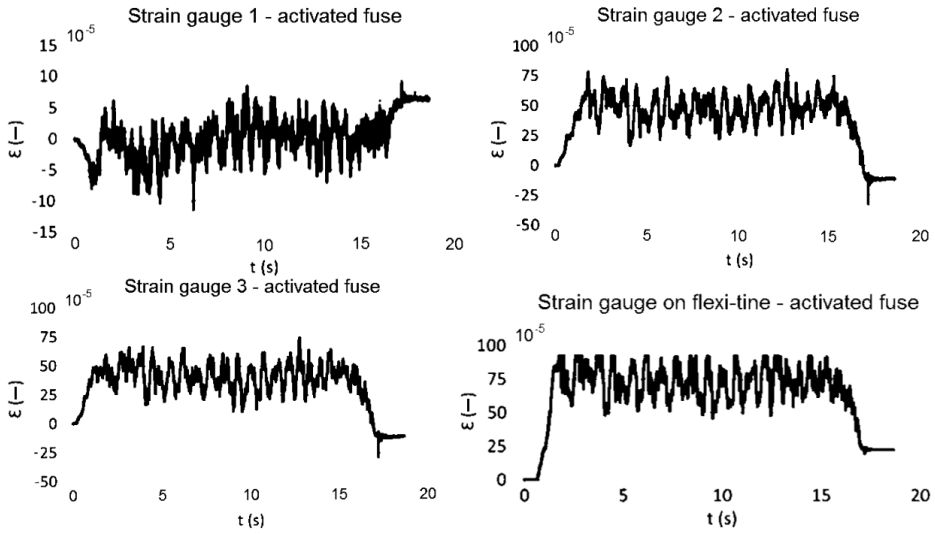

Figure 7. Dependence between deformation ε and time during the experimental ride, tools with wings, active fuse.

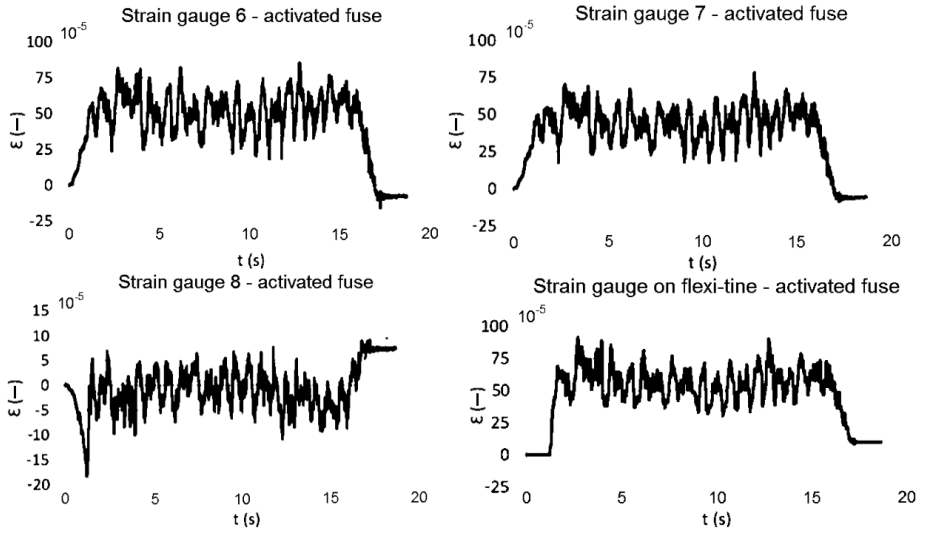

Figure 8. Dependence between deformation ε and time during the experimental ride, tools without wings, active fuse.

The course is clipped for the measuring point in flexo-tine. The reason for this clip is the small measurement range for the strain gauge in flexi-tine. The location of this strain gauge shows large deflections during measurement. The beginning of the tool's work in the soil is value for ε 0 m. Values ε of 0.0005 m to 0.001 m and higher are for

working tool in the soil. For the end of work tool, the value ε again drops to 0 m. This fact was also found for the same measuring point for the second experimental ride.

The deformation distribution distortion for the experimental ride with the set blocked fuse is shown in Figs 9 and 10.

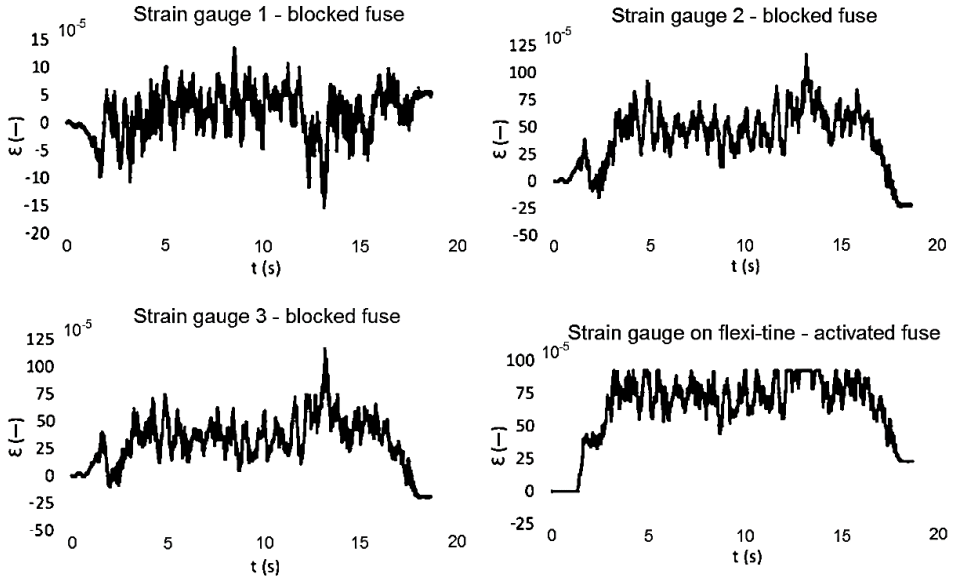

Figure 9. Dependence between deformation ε and time during the experimental ride, tools with wings, blocked fuse.

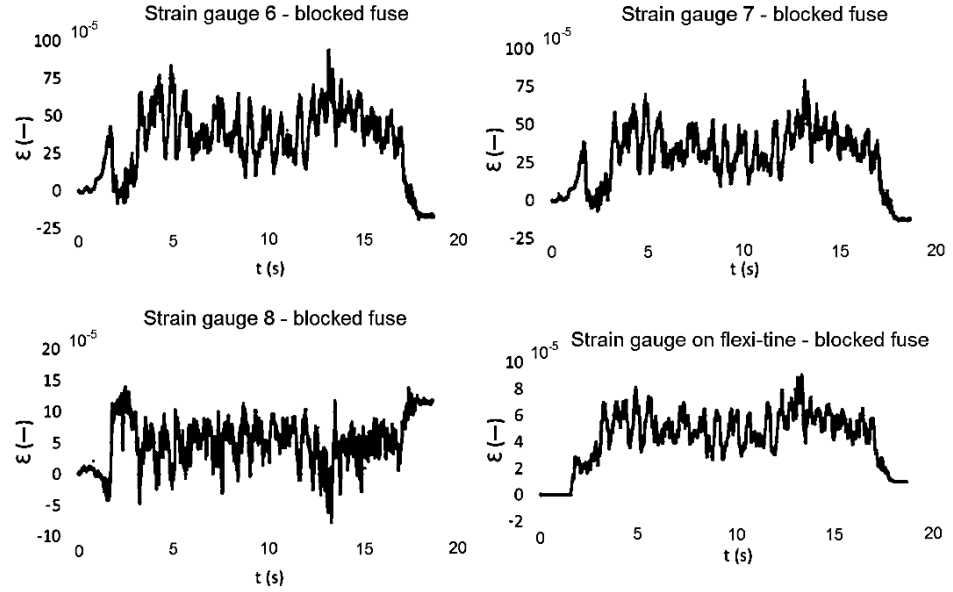

Figure 10. Dependence between deformation ε and time during the experimental ride, tools without wings, blocked fuse.

The measurement courses are similar for measuring points 1 and 8 for 3 and 7. Measurement courses show the same magnitude of deformation ε for measuring points 2 and 6 and 3 and 7.

Large amplitude was detected for blocked fuse for both fixed-tine in 13 second. Machine crossing over an obstacle in the ground (stone) or compressed part of the soil may be the reason for the occurrence of large amplitudes. The opposite direction of the amplitude was found for measurement points 1 and 8. The reason is the opposite orientation of the forces in the measuring point.

Large differences of course were found for the characteristics of experimental rides between activated fuse and blocked fuse. The activated fuse eliminates the force transfer to the frame more than the blocked fuse. All strain is transmitted to the machine frame for blocked fuse.

The chisel with wing has a 26.7% higher area than the wingless chisel. Comparison of strain gauges located at the same locations (1 and 8, 2 and 6, 3 and 7) shown a resuts where it seem higher draght force but lower moment around vertical axis.The courses were analyzed from experimental rides. The entire course was recorded for each experimental ride. The course was divided into parts. The first course was always the beginning of the tool's work in the soil – the time before the tool reached the required working depth – marked by t_1 in Fig. 11. The work of the tool in the soil is recorded by t_2 for the required working depth. The end of working for tool is recorded at t_3. The period t_4 shows the increase in resistance for the tool while working at the standard depth.

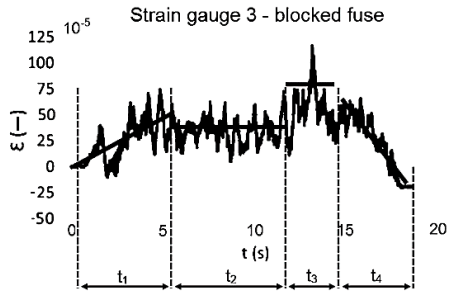

Figure 11. Dependence between deformation ε and time during experimental ride, without wings, blocked fuse.

The direction, magnitude of the acting force in the x, y, z axes of the tool module is a necessary boundary condition for the construction of mathematical models. Measured data were used for a parametric computation of frame part in FEM. Final parametric cycle of steady state FEM algorithm for mean strain during t_2 shown an acceptable boundary condition which are presented in Table 2. Results shown higher draught force for wings chisel and also higher stability in x-axis determined lateral forces and lower moment in tool module.

Table 2. Boundary conditions for steady state during field tests

	Fx (N]	Fy (N)	Fz (N)	Mx (Nm)	My (Nm)	Mz (Nm)
module with wings	2 553	-36,334	-291	139	70	4,871
modelu without wings	1,642	-42,567	-5,690	78	74	4,482

Many authors are concerned with detecting traction resistance in agricultural machinery. No literature has been found that deals directly with strain measurements.

(Kumar et al., 2016) work is concerned with detecting the traction resistance of an agricultural machine using its own developed digital system. Their results make it

possible to optimize tractor consumption. The tractor's consumption depends on the size of the traction resistance of the agricultural machine. In this work, the traction resistance can also be calculated based on the measured courses. The fuel consumption of the tractor and other quantities can be calculated from the traction resistance in this work.

The influence of plow angles in dependence on traction resistance was studied in (McKyes & Desir, 1984). The impact of tool resistance with wings and tool without wings has been investigated in this work. The ratio of areas correspond with ratio of strain. Significant impact of the wings was detected on the resistance of the tool module.

(Onwualu, 1998) examined the influence of velocity on traction resistance. A constant speed was used in this work. The design of the test runs identified the maximum traction resistance that can be developed on the machine frame. Different speeds can be neglected due to the size of the traction resistance.

CONCLUSIONS

A method was developed to measure the stress on the frame of the agricultural machine. Stress is generated from the tool module in the machine frame. The magnitude of stress is one of the marginal conditions for creating a mathematical model design.

Depending on the models and measured stress, the geometry of the tool can be modified.

The maximum traction resistance was determined by the fuse protection system. For this reason, the type of soil was not detected. Soil served only as a load for experimental drives.

The effect of the tool module resistance has been detected. The effect is shown in the course for wing and without modules.

The effects of the tool modules can be detected for different sizes and shapes by the procedure described in this paper. The procedure can be used, for example, for disk machines. However, the discs are affected by the momentum created by angled disk operation.

From the measurements used in this work, more data can be calculated such as traction resistance, tractor fuel consumption, resistance in various work dumps, effect of tool size and shape, etc.

REFERENCES

Abo Al-kheer, A., Eid, M., Aoues, Y., El-Hami, A., Kharmanda, M.G. & Mouazen, A.M. 2011, Theoretical analysis of the spatial variability in tillage forces for fatigue analysis of tillage machines. *Journal of Terramechanics* **48**(4), 285–295.

Ahmed, S.F., Zein Eldin, A.M. & Abdulaal, S.M. 2014. Reducing draft required for a simple chisel tool. *AMA, Agricultural Mechanization in Asia, Africa and Latin America* **45**(4), 26–31.

Ani, O.A., Uzoejinwa, B.B., Ezeama, A.O., Onwualu, A.P., Ugwu, S.N. & Ohagwu, C.J. 2018. Overview of soil-machine interaction studies in soil bins. *Soil and Tillage Research* **175**, 13–27.

Bulgakov, V., Adamchuk, V., Arak, M., Nadykto, V., Kyurchev, V. & Olt, J. 2016, Theory of vertical oscillations and dynamic stability of combined tractor-implement unit. *Agronomy Research* **14**(3), 689–710.

Cardei, P., Vladutoiu, L., Chisiu, G., Tudor, A., Sorica, C., Gheres, M. & Muraru, S. 2018. Research on friction influence on the working process of agricultural machines for soil tillage. *IOP Conference Series: Materials Science and Engineering* **444**.

Chotěborský, R. & Linda, M. 2015. FEM based numerical simulation for heat treatment of the agricultural tools. *Agronomy Research* **13**(3), 629–638.

Chotěborský, R. & Linda, M. 2016. Determination of chemical content of soil particle for abrasive wear test. *Agronomy Research* **14**, 975–983.

Furrer, D. & Semiatin, S.L. 2009. ASM Handbook Volume 22A: Fundamentals of Modeling for Metals Processing. *ASM International*, 284–325.

Govindarajan, N. & Gnanamoorthy, R. 2007. Rolling/sliding contact fatigue life prediction of sintered and hardened steels. *Wear* **262**(1–2), 70–78.

Kheybari, S. & Salehpour, R. 2015. The optimization of the paddy field irrigation scheduling using mathematical programming. *Water Science and Technology: Water Supply* **15**(5), 1048–1060.

Kumar, A.A., Tewari, V.K. & Nare, B. 2016. Embedded digital draft force and wheel slip indicator for tillage research. *Computers and Electronics in Agriculture* **127**, 38–49.

Lindblom, G.P. & Cashion, B.S. 2005, Operational considerations for optimum deposition efficiency in aerial application of dispersants. In *2005 International Oil Spill Conference, IOSC 2005*, pp. 5923.

McKyes, E. & Desir, F.L. 1984. Prediction and field measurements of tillage tool draft forces and efficiency in cohesive soils. *Soil and Tillage Research* **4**(5), 459–470.

Nurmiev, A., Khafizov, C., Khafizov, R. & Ziganshin, B. 2018. Optimization of main parameters of tractor working with soil-processing implement. *Engineering for Rural Development* **17**, 161–167.

Onwualu, A. 1998. Draught and vertical forces obtained from dynamic soil cutting by plane tillage tools. *Soil and Tillage Research* **48**(4), 239–253.

Paraforos, D.S., Griepentrog, H.W., Vougioukas, S.G. & Kortenbruck, D. 2014, Fatigue life assessment of a four-rotor swather based on rainflow cycle counting. *Biosystems Engineering* **127**, 1–10.

Sutanto, H. & Madl, J. 2018, Residual stress development in hard machining - a review. *IOP Conference Series: Materials Science and Engineering* **420**, 012031.

Agronomy Research **17**(2), 491–498, 2019
https://doi.org/10.15159/AR.19.033

The course of drying and colour changes of alfalfa under different drying conditions

P. Kic

Czech University of Life Sciences Prague, Faculty of Engineering, Department of Technological Equipment of Buildings, Kamýcká 129, CZ165 21 Prague, Czech Republic
*Correspondence: kic@tf.czu.cz

Abstract. One of the conditions for successful livestock breeding and efficient livestock production is to ensure quality feed. High quality feed for livestock is alfalfa, which has a very high nutritional value and its cultivation is also important for crop production in terms of improving the soil structure and nitrogen enrichment. The aim of this paper is to inform about the experimental investigations of alfalfa drying and colour changes under different drying conditions. The results of natural convection at 27.5 °C and 40% relative air humidity are compared with forced convection at 1.2 m s^{-1} air flow velocity at the same air temperature and with results of drying by natural convection at 50 °C. The dry matter content was measured gravimetrically after drying in a hot air dryer at 105 °C. Higher drying rates shorten the time required for drying and earlier preservation and storage in the hayloft or in the hay bales. This reduces the risk of wetting of feed such by rain and degradation by fungi, etc. A shorter drying time is also important in terms of energy savings. The precise knowledge of the drying process and drying curves allows also to determine the appropriate time for storage and conservation for production of another type of fodder e.g. haylage or silage. The measurement results show a positive effect of higher drying speeds as well as increased air temperature. Higher drying air temperature during convection led to the partial lightening and greater yellowing of the feed.

Key words: forced drying, natural drying, moisture, spectrophotometer, temperature.

INTRODUCTION

Alfalfa (*Medicago sativa*) is used because of its high protein content and highly digestible fibre for cattle, horses and other domestic animals. Alfalfa is most often harvested and conserved as hay, but can also be made into haylage or silage. The differences are according to the moisture. Dry matter content (DM) is one of fundamental characteristics in conservation of alfalfa (Bebb 1990; Maloun, 2001). The DM content in fresh plants depends on the weather and on phenophases in a wide range from 11 to 25%. During the conservation it is necessary to increase the amount of DM at least to 35% (preferably 40%) for the production of silage in horizontal or tower silos.

For the production of haylage (silage with higher DM) it is necessary to increase DM content to 45% (in horizontal or tower silos), for production of round bale wrapped in foil to DM content from 45 to 65%. DM content of 75–85% allows storage of forage in round bales without using the packaging film (under shelter) or in hayloft for longer

periods. In the production of uncoated hay bales it is needed to prevent mould growth by increased DM content at least to 75%.

For the production of quality hay the DM of 75–85% should be achieved, which requires drying time 2–4 days of favourable weather. High-quality alfalfa hay should be green, soft to the touch, with a high proportion of leaves, smelling well and without admixtures. Moisture level should not be higher than 15%.

Drying time and temperature together with the moisture influence the quality of the final dry fodder. There are many different applications of drying for the agricultural (Jokiniemi et al., 2012; Aboltins & Palabinskis, 2013; Jokiniemi et al., 2014) purposes. Problems of natural drying applied to drying of special plants are solved also in some scientific publications, e.g. (Aboltins & Kic, 2016).

The increased air velocity for convection or suitable material preparation can influence the drying process positively. But too high air velocity, needed to accelerate the drying process, can cause problems with losses of light particles particularly at the final stage of drying when forage has low water content and thus low density of small particles. In practice, sometimes DM is not sufficient in the production or storage of hay, haylage or silage, or on the contrary, DM is too high which can cause higher losses of fodder. DM is an important determinant of intake by animals (Pond & Pond, 2000). The attention of alfalfa drying under artificial conditions is paid in different scientific publications, e.g. (Adapa et al., 2004; Osorno & Hensel, 2012).

The aim of this work is to bring some new experimental and theoretical investigations of alfalfa drying by natural and forced convection with different air velocities compared with drying with increased temperature to 50 °C.

In recent years, great attention has been paid to the colour, as an important parameter for determination of some data in agriculture and food industry. This includes e. g. parameters relevant to determine the appropriate harvest period or properties of vegetation and plants (Hernandez & Larsen, 2013; Kross et al., 2015; Prabhakara et al., 2015; Rigon et al., 2016) and similar agro – technical or even ecological data (Tillack et al., 2014). This is mainly used by remote sensing methods.

In order to determine the quality of some agricultural products, the CIELAB colour scheme is used, where colours are expressed by L* value (lightness), redness (a* values) and yellowness (b* values), e.g. Orazem et al., 2013; Kic, 2018; Peralta et al., 2018. Since these methods are still rather difficult to access, they are used for expensive products, where colour determination can be important for consumers. The use for measurements of traditional crops, such as fodder, is not yet common.

In practice, however, some practical advice and recommendations for farmers are used on the basis of farmers' experience for centuries, e.g. hay should not be brown, dark, etc. This study therefore shows the possibility of using exact colour measurement as a parameter describing the properties of a harvested or stored feed crops such as alfalfa. It can be assumed that further research from this point of view will continue and further develop this issue.

MATERIALS AND METHODS

The laboratory measurements were carried out at the Faculty of Engineering CULS Prague during summer weather conditions in July. Three different drying conditions of alfalfa were selected for this research work.

To study the drying kinetics, alfalfa samples which were cut up into a particle length from 2 to 5 cm, were placed in a thin layer about 50 mm on sieve tray with mesh 3 x 4 mm of total area approximately 20,400 mm^2. Initial weight of each sample on the tray was approximately 60 g.

The drying conditions of first sample A were natural, with average temperature of drying air 27.5 ± 0.8 °C and relative humidity 39.9 ± 2.7% and natural convection. The forced drying of the second sample B was in drying chamber with air velocity 1.2 m s^{-1} and the same air temperature and humidity.

To study the influence of higher temperature on the drying process, the third sample C was put in the drying chamber with increased air temperature 50 °C and 0 m s^{-1} air velocity.

The moisture content in the alfalfa samples was identified by the gravimetric measurement in regular time intervals. Samples were weighed during the drying on the digital laboratory balance KERN-440-35N with maximum load weight 400 g, with resolution 0.01 g and accuracy ± 10 mg and values were recorded. Each measuring tray was weighed every 30 min. The total drying time 46 h was adapted to the need for a determination of lowest moisture content, which can be achieved by convective drying with air temperature 27.5 °C, and 21 h for drying with increased air temperature 50 °C.

Air speed was measured by anemometer CFM 8901 Master with resolution 0.01 m s^{-1} and accuracy ± 2% of final value. Air temperature and humidity was measured by the sensor FHA646-E1C connected to the data logger ALMEMO 2690-8.

The DM in alfalfa samples was identified by gravimetric measurement using an MEMERT UNB-200 air oven under temperature 105 °C. Samples were weighed on a KERN 440-35N laboratory balance in regular time intervals. The total drying time was adapted to the need for a determination of the equilibrium moisture.

The following main parameters are calculated from the measured values of all alfalfa samples. Water content, dry basis u is defined as the ratio of the mass of water m_W contained in a solid to the mass of dry basis m_S, expressed in Eq. (1):

$$u = \frac{m_W}{m_S} \tag{1}$$

where u – water content, dry basis, g g^{-1}; m_W – mass of water, g; m_S – mass of dry basis, g.

Water content, wet basis w is the ratio of the mass of water m_W contained in a solid to the mass of the moist solid $m = m_S + m_W$, expressed in Eq. (2):

$$w = \frac{m_W}{m} 100 \tag{2}$$

where w – water content, wet basis, %.

Changes of the water content du during the time difference dt describe the drying rate N expressed in Eq. (3):

$$N = \frac{\Delta u}{\Delta t} \tag{3}$$

where N – drying rate, g g^{-1}min^{-1}; t – time, min.

The colour was evaluated according to the CIELAB system where colour attributes lightness (L* value), redness (a* value) and yellowness (b* value) were measured five times of each fresh sample, after convection (natural or forced) drying and after hot air drying in 105 °C. The instrument used for this research, Spectrophotometer CM-600d

Konica Minolta, was first calibrated. Calibration is based on the black ($L^* = 0$) and white ($L^* = 100$) standards.

The obtained results of colour range coordinates of tested alfalfa samples were processed by Excel software and verified by statistical software Statistica 12 *(ANOVA* and *TUKEY HSD Test*) to recognise if the differences are significant. Different superscript letters (*a, b*) in common are significantly different from each other in the columns of the tables *(ANOVA; Tukey HSD Test; $P \leq 0.05$)*, e.g. if there are the same superscript letters in the columns (before drying, after natural drying and after drying in oven) it means the differences between the values of the same homogenous group are not statistically significant at the significance level of *0.05*.

RESULTS AND DISCUSSION

The kinetics of alfalfa drying process of A, B and C samples described by the curves calculated according to equations (1), (2) and (3) is in Figs 1–5. The whole convection drying time 46 h was sufficient to the maximal drop of water content which can be achieved by convection with air temperature 27.5 °C and relative humidity 39.9%.

The curves of water content, dry basis u (g g^{-1}) in Fig. 1 show that the increased air velocity to 1.2 m s^{-1} (sample B) in comparison with natural convection (sample A) reduced the time of drying considerably. The biggest drop of water content and shortest time for drying (only 21 h) is in the case of sample C, which has been caused by the increased air temperature to 50 °C.

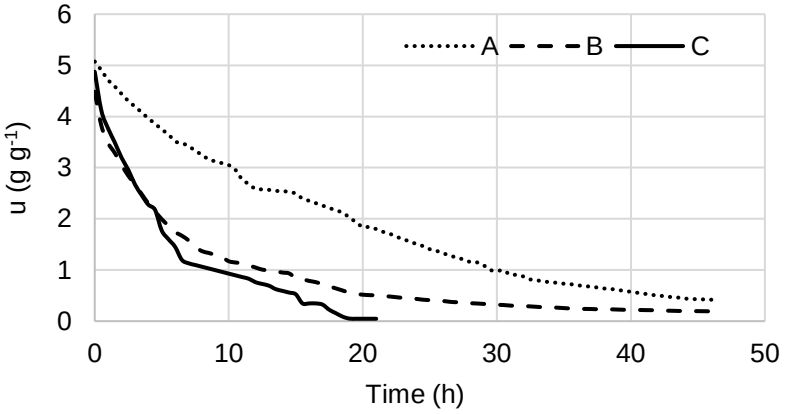

Figure 1. Water content, dry basis u (g g^{-1}) of all 3 alfalfa samples during the drying process.

The course of water content, wet basis w (%) during the drying is presented in Fig. 2. The decrease of water content, wet basis is significantly slower in the case of natural convection (sample A) than with forced convection (sample B). The water content, wet basis achieved by convection drying was 29.57% in the case of natural convection (sample A), 16.11% in the case of forced convection (sample B). The fastest drop of water content, wet basis and the lowest reached water content, wet basis (w = 4.5%) was in the case of drying by air at 50 °C (sample C).

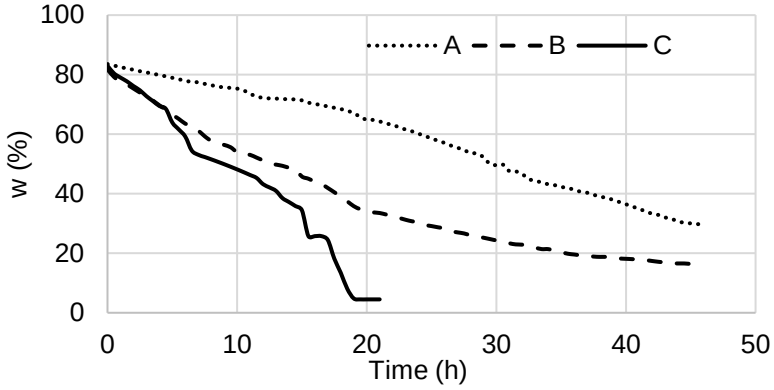

Figure 2. Water content, wet basis w (%) of all 3 alfalfa samples during the drying process.

The course of drying rate N (g $g^{-1}min^{-1}$) during 46 h of drying is presented in Fig. 3. To see better differences influenced by different drying conditions, drying rates from the first 10 hours are presented in Fig. 4.

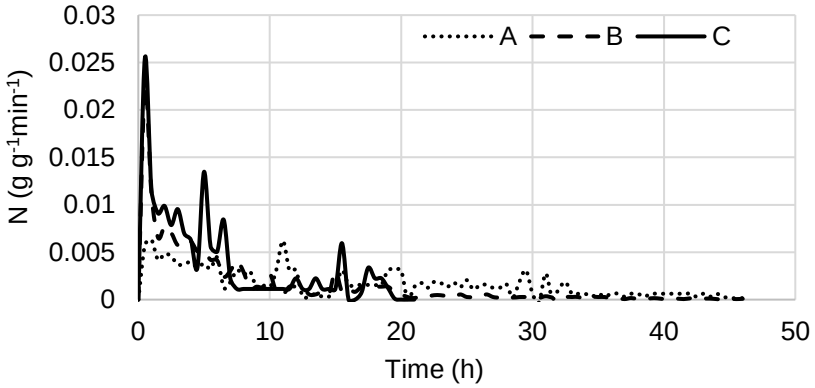

Figure 3. Drying rate N (g $g^{-1}min^{-1}$) of 3 alfalfa samples during 46 h of drying.

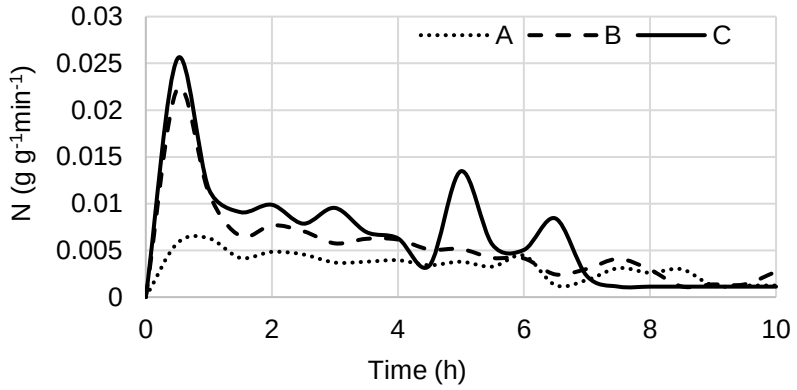

Figure 4. Drying rate N (g $g^{-1}min^{-1}$) of 3 alfalfa samples during the first 10 h of drying.

The biggest drying rates N (g $g^{-1}min^{-1}$) were achieved during the first 30 min. According to Fig. 4 the difference between the sample B and C is not significant during that time. This can be explained by the evaporation of the first portion of moisture from the surface parts of the plants. The drying rate of sample A by natural convection is significantly smaller than the sample B and C during the first 7 hours.

Rather interesting is the dependence of drying rate N (g $g^{-1}min^{-1}$) on the water content, dry basis (g g^{-1}) presented in Fig. 5, describing both very important parameters of drying process. The best relation between the drying rate and water content is achieved if the water content is high and with increased temperature (sample C) or higher air velocity of forced drying (sample B). There is a big difference between the drying with air velocities 1.2 m s^{-1} (sample B) and natural convection (sample A). The increased air velocity has positive impact on the whole process of drying.

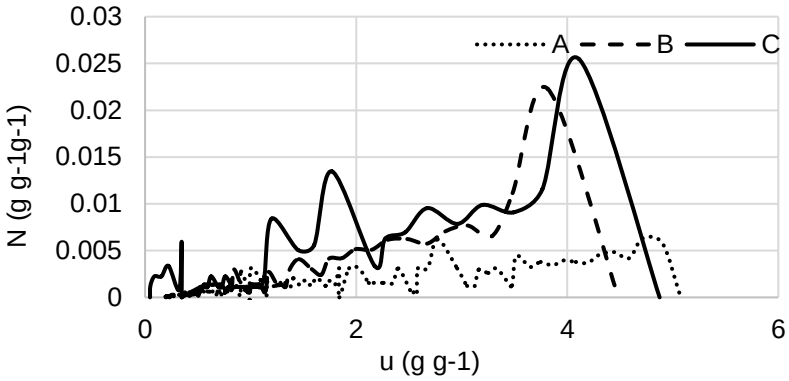

Figure 5. Drying rate N (g $g^{-1}min^{-1}$) of 3 alfalfa samples as a function of water content u (g g^{-1}) during the drying process.

The mean values and standard deviations (SD) calculated from the results of measurements of the lightness L^* are presented in the Table 1. There are also included in the Table 1 the colour specification a^* and b^* mean values with SD.

The results of lightness L* in the Table 1 indicate that the measured samples were slightly lighten by all types of drying process, which is statistically significant. The smallest change of lightness ($\Delta L^* = 2.58$) was in the case of the sample C from $L^* = 37.49 \pm 0.30$ after drying with a higher air temperature of 50 °C to $L^* = 40.07 \pm 1.29$. The smallest change of lightness ($\Delta L^* = 0.59$) was also in this case after the subsequent hot air drying at 105 °C oven.

The biggest increase of lightness ($\Delta L^* = 5.91$) was in the case of sample B. Lightness increased from $L^* = 35.80 \pm 0.94$ due to the natural drying by increased air flow velocity to lightness ($L^* = 41.71 \pm 2.80$). However, the following hot air drying by 105 °C did not cause such a high change of lightness.

There are recognised also changes in colour shades, a* and b*. The greenness (-a*) of all samples was only slightly reduced by the drying process, which was not in any case statistically significant. The yellowness (b*) was increased. Statistically significant increase of yellowness was in the case of natural drying A and in the case of hot air drying samples C by 50 °C; the yellowness was increased from $b^* = 13.41 \pm 0.46$ to the value of $b^* = 20.47 \pm 0.55$, which causes the difference $\Delta b^* = 7.06$.

Table 1. Colour range coordinates (L*, a* and b* mean values with SD) of tested alfalfa samples. Different letters (*a, b, c*) in the superscript are the sign of high significant difference (*ANOVA; Tukey HSD Test; $P \leq 0.05$*)

State of the measured alfalfa samples A, B, C	Parameter Drying conditions	L* ± SD	a *± SD	b* ± SD
Sample A before natural drying	t = 27.5 °C, natural conv.	38.70 ± 4.58^{a}	-9.04 ± 0.46^{a}	15.72 ± 2.77^{a}
Sample A after natural drying	t = 27.5 °C, natural conv.	$42.28 \pm 1.86^{a, b}$	-8.60 ± 0.44^{a}	$19.55 \pm 1.39^{a, b}$
Sample A after drying in oven	t = 105 °C, natural conv.	48.81 ± 0.87^{b}	-8.61 ± 0.45^{a}	24.20 ± 2.53^{b}
Sample B before forced drying	t = 27.5 °C, natural conv.	35.80 ± 0.94^{a}	-9.01 ± 0.5^{a}	14.66 ± 1.99^{a}
Sample B after forced drying	t = 27.5 °C, v = 1.2 m s^{-1}	41.71 ± 2.80^{b}	-8.84 ± 0.92^{a}	18.98 ± 3.23^{a}
Sample B after drying in oven	t = 105 °C, natural conv.	$39.77 \pm 3.31^{a, b}$	-8.51 ± 0.07^{a}	18.87 ± 1.23^{a}
Sample C before natural hot air drying	t = 27.5 °C, natural conv.	37.49 ± 0.30^{a}	-8.93 ± 0.22^{a}	13.41 ± 0.46^{a}
Sample C after natural hot air drying	t = 50 °C, natural conv.	40.07 ± 1.29^{b}	-8.52 ± 0.50^{a}	20.47 ± 0.55^{b}
Sample C after drying in oven	t = 105 °C, natural conv.	40.66 ± 0.84^{b}	-8.98 ± 1.75^{a}	19.70 ± 3.02^{b}

SD – Standard deviation.

The influence of hot air drying in oven (105 °C) after the natural or forced drying did not cause significant changes of lightness or greenness or yellowness. The greatest change of lightness due to hot-air drying at 105 °C ($\Delta L^* = 6.53$) was in the case of sample A, but this small changes are not statistically significant.

CONCLUSIONS

This research is useful for verification of the influence of different air parameters on the drying process of alfalfa. In order to achieve the suitable water content of alfalfa for different conservation applications with economic benefits, the optimization of drying time should be provided and respected.

It has been found that the increased temperature and forced convection has a strong and positive influence on drying time in comparison with free drying by natural convection. There are big differences between the results of drying with air velocities 0 m s^{-1} and 1.2 m s^{-1}, nevertheless more progressive results in this research were achieved by the increased temperature to 50 °C. Future research in this area, partly described and expressed by drying coefficient, should be focused on the study of other factors influencing the drying process especially by different air temperatures.

Measured changes of colours during the drying process create the background for further research on this field. The results of lightness L* indicate that the measured samples were slightly lighten after the drying process. Drying alfalfa by air with temperature 50 °C increased yellowness.

Changes of colours are important parameters describing the changes of crops quality which should be studied also for other levels of drying conditions and also for other types of materials. New information about these properties should be respected during the harvest and storage of agricultural products.

REFERENCES

Aboltins, A. & Palabinskis, J. 2013. New types of air heating solar collectors and their use in drying agricultural products. *Agronomy Research* **11**, 267–274.

Aboltins, A. & Kic, P. 2016. Research of some medical plants drying process. In: *15th International Scientific Conference Engineering for Rural Development*. Latvia University of Agriculture, Jelgava, pp. 1145–1150.

Adapa, P.K., Schoenau, G.J. & Arinze, E.A. 2004. Fractionation of alfalfa into leaves and stemps using a three pass rotary drum dryer. *Biosystems Engineering* **91**, 455–463.

Bebb, D.L. 1990. *Mechanised livestock feeding*.BSP professional books, Oxford, 209 pp.

Hernandez, L.F. & Larsen, A.O. 2013. Visual definition of physiological maturity in sunflower (Helianthus annuus L.) is associated with receptacle quantitative color parameters. *Spanish Journal of Agricultural Research* **11**(2), 447–454.

Jokiniemi, T., Mikkola, H., Rossner, H., Talgre, L., Lauringson, E., Hovi, M. & Ahokas, J. 2012. Energy savings in plant production. *Agronomy Research* **10**, 85–96.

Jokiniemi, T., Jaakkola, S., Turunen, M. & Ahokas, J. 2014. Energy consumption in different grain preservation methods.*Agronomy Research* **12**, 81–94.

Kic, P. 2018. Mushroom drying characteristics and changes of colour. In: *17th International Scientific Conference Engineering for Rural Development*. Latvia University of Agriculture, Jelgava, pp. 432–438.

Kross, A., McNairn, H., Lapen, D., Sunohara, M. & Champagne, C. 2015. Assessment of RapidEye vegetation indices for estimation of leaf area index and biomass in corn and soybean crops. *International Journal of Applied Earth Observation and Geoinformation* **34**, 235–248.

Maloun, J. 2001. *Technological equipment and main processes in the production of fodder*. CULS, Faculty of Engineering, Prague, 201 pp. (In Czech).

Orazem, P., Mikulic-Petkovsek, M., Stampar, F. & Hudina, M. 2013. Changes during the last ripening stage in pomological and biochemical parameters of the 'Redhaven' peach cultivar grafted on different rootstocks. *Scientia Horticulturae* **160**, 326–334.

Osorno, F.L. & Hensel, O. 2012. Drying homogeneity of grass mixture components in a rotary drum. *Drying Technology* **30**, 1931–1935.

Peralta, D.V., Rodgers, J.E., Knowlton, J.L. & Fortier, C.A. 2018. Upland Cotton Surface Amino Acid and Carbohydrate Contents vs. Color Measurements. *Journal of Cotton Science* **22**, 142–152.

Pond, W.G. & Pond, K.R. 2000. *Introduction to animal science*. John Wiley & sons, inc. New York, 687 pp.

Prabhakara, K., Hively, W.D. & McCarty, G.W. 2015. Evaluating the relationship between biomass, percent groundcover and remote sensing indices across six winter cover crop fields in Maryland, United States. *International Journal of Applied Earth Observation and Geoinformation* **39**, 88–102.

Rigon, J.P.G., Capuani, S., Fernandes, D.M. & Guimarães, T.M. 2016. A novel method for the estimation of soybean chlorophyll content using a smartphone and image analysis. *Photosynthetica* **54**(4), 559–566.

Tillack, A., Clasen, A., Kleinschmit, B. & Fŏrster, M. 2014. Estimation of the seasonal leaf area index in an alluvial forest using high-resolution satellite-based vegetation indices. *Remote Sensing of Environment* **141**, 52–63.

Agronomy Research **17**(2), 499–508, 2019
https://doi.org/10.15159/AR.19.045

Properties of soil and peat humic substances from Latvia

M. Klavins*, O. Purmalis, S. Grandovska and L. Klavina

University of Latvia, Department of Environmental Science, Raiņa bulv. 19, LV 1586 Riga, Latvia
*Correspondence: maris.klavins@lu.lv

Abstract. The acidity, elemental, functional and spectral (UV, fluorescence, IR spectra) characteristics of humic substances isolated from soils of different origin and peat in Latvia are described and compared with values common for humic substances of different origin, to evaluate the character of processes during humification. Substantial dependence of properties of humic substances on the humification conditions are found.

Key words: humic substances, soil, peat.

INTRODUCTION

Humic substances (HS) are the most widely found naturally occurring organic substances. Humic substances are a general category of naturally occurring, biogenic, heterogeneous organic substances that can generally be characterized as being yellow to black in colour, of high molecular weight and refractory. Humic substances can be divided in three fractions: a) humin is the fraction of humic substances that is not soluble in water at any pH; b) humic acid (HA) is the fraction of humic substances that is not soluble in water under acidic conditions (below pH 2), but becomes soluble at greater pH; c) fulvic acid is the fraction of humic substances that is soluble under all pH conditions (Gerke, 2018). Humic substances form most of the organic component of soil, peat and natural waters, they influence the process of formation of fossil fuels, they play a major role in the global carbon geochemical cycle. About 60–85% of the organic matter in soil consists of humic substances (Thurman, 1985) and their concentrations change depending on the soil origin. Interaction of humic substances with xenobiotics may modify the uptake and toxicity of these compounds, and affect fate of pollutants in environment (Lipczynska-Kochany, 2018). In the same time the soil and peat humic substances may be regarded as a valuable resource for applications in agriculture (Gerke, 2018). Thus humic substances are of great importance not only considering processes in environment, but also as an important resource.

Despite the long history of humus research, comparatively recently reliable and unified methods have been introduced for isolation of humic substances (Mallick, 2017) to adequately determine the HS structure and properties, depending on its sources. The major questions are concerning the changes in properties of humic matter depending on their origin. It has been shown, that the structure and properties of soil humic matter differ between soil humic matter of different origin (Орлов, 1990), in the same time, considering the great variability in soil properties and thus the humification conditions, the actual

relationship is far from being explained. Another open question can be related to the genesis of soils and development of peat soils. Just as soil humic substances also humic matter form peat has been studied in comparatively few studies (Wiszniewska et al., 2016).

The aim of the present paper is to describe the properties of soil humic substances isolated from different soils in Latvia and peat humic substances, to evaluate the impact of the soil and peat composition on the humus structure (humification process, generally) and soil formation.

MATERIALS AND METHODS

Humic substances were isolated from peat of Latvia, representing different peat types and mechanisms of their formation. Soil samples were from different sites in Latvia from upper horizon during summer season 2018. The selected soils (for some soils several samples were taken to get representative samples) from all territory of Latvia represent the principal soil types in Latvia. The soils were classified according to the International Soil classification system (IUSS Working Group WRB, 2015). The analytical characterisation of soil samples were done within 1 month. The taxonomic and chemical properties of the soils and peat are presented in Table 1. Organic carbon content was determined by wet combustion (Walkley-Black method) and soil, and peat pH in a 0.1 M KCl solution.

Table 1. Characteristics of soil and peat samples

Soil group/peat type	Symbol	Organic carbon, %	pH (in 0.1M KCl)
Leptosols	VKz	5.8	7.32
Phaozems	VKt	2.7	7.13
Stagnosol	VKg	6.3	7.24
Luvisol	BRt	22.9	6.51
Retisols	PVv	3.7	6.87
Podzols	Pot	4.6	6.76
Anthrosols	ANt	20.6	6.73
Technisols	ANu	3.7	7.23
Gleysols	GLh	6.3	6.48
Histosols	TZh	31.3	5.64
Peat			
Pine peat	P-1	34.5	6.2
Sedge-*hypnum* peat	P-2	22.4	6.4
Wood-*Sphagnum* peat	P-3	28.4	5.3
Fuscum- *Sphagnum* peat	P-4	16.3	4.7
Cotton-grass- *Sphagnum* peat	P-5	26.4	4.8

Humic acids were extracted and purified using procedures recommended by the International Substance Society (Klavins, 1998). Briefly, 1 kg of 2 mm (sieved) air dry soil or peat was reacted with 10 L of 0.1 M HCl for 1 h. The slurry was allowed to settle, and the aqueous phase was decanted and discarded. Approximately 1 L of H_2O was added to the soil or peat mass and the resulting slurry was allowed to incubate for 30 min, after which the pH of the slurry was adjusted to 7 with the addition of 1 M NaOH. This was followed by the addition of a sufficient quantity of 0.1 M NaOH (done under N_2 gas), to bring the total volume of the solution phase to 10 L and the resulting slurry was

stirred under N_2 gas. After 24 h the alkaline slurry was filtered through glasswool and the particle free filtrate was acidified to a pH value of 1, with the addition of 6 M HCl. This solution was then allowed to settle then it was centrifuged, and the supernatant was discarded. The sediment (which contained humic acid) was washed with distilled water and repeatedly centrifuged discarding the supernatant. Solid residue after centrifugation was then suspended in a mixture of 0.1 M HCl and 0.3 M HF, to remove mineral particles. This treatment was repeated until the ash content was reduced less than 2%. Afterwards humic acid dispersion in distilled water were dialyzed against water to remove chlorides and resulting humic acids were lyophilized. Clear brown coloured solution containing the fulvic acids (FA) were obtained after acidification with HCl. The obtained FA solutions were transferred to the H^+ form by passing through a strong cationite KY-23 column and finally freeze dried. To ensure representative samples for analysis two extractions were made for some soil samples.

The obtained humic substances were characterized as follows:

1. Elemental analysis: C, H, N and ash concentrations were determined by a Perkin Elmer 240/A CHN-Analyzer. Oxygen concentrations were calculated by difference;
2. Concentrations of functional groups were determined by standard methods (Klavins, 1998);
3. Molecular weight distribution was determined with gel filtration on Sephadex G-100 (bead diameter 40–120 μm) column (1 × 40 cm). The eluent: 0.01 M Tris-HCl buffer (pH 9.0) was pumped through the column at 1 mL min^{-1}, gathering 1 mL fractions. 25 mg of humic substances were applied on the top of the column as 1% solution in 0.1 M NaOH. A standard set of proteins was used for column calibration. The void volume of the column was determined using Blue Dextran 2000000. Detection was performed at 280 nm;
4. UV-Vis spectra were obtained over a range of 200 to 700 nm using a Specord UV 40 UV-Vis spectrophotometer on 0.05 N $NaHCO_3$ solutions at a concentration of 50 mg L^{-1} for FA and 33 mg L^{-1} for HA and a pH between 8 and 9. For analysis of E4/E6 ratio the humic matter samples (2 mg) were dissolved in 10 mL 0.05 M $NaHCO_3$ and absorbances at 465 and at 665 nm were measured against a reference of 0.05 M $NaHCO_3$.
5. Fluorescence spectra were recorded using a Hitachi 850 fluorescence spectrometer, on aqueous solutions of each sample at a concentration of 100 mg L^{-1}, adjusted to pH 8 with 0.0 M NaOH. Emission spectra were recorded (scan speed 60 nm min^{-1}, response 2 s) over the wavelength range 360 to 640 nm at a fixed excitation wavelength of 335 nm.
6. Infrared (IR) spectra were recorded, in the 4,000 to 500 cm^{-1} wavenumber range using a Perkin Elmer 400 IR spectrophotometer, of KBr pellets obtained by pressing mixtures of 1 mg samples and 400 mg KBr with precautions taken to avoid moisture uptake;
7. The Van Krevelen graphical-statistical method was applied as used for the study of the structure on the basis of elemental analysis data (Орлов, 1990).

RESULTS AND DISCUSSION

The selected soils and peat samples (Table 1) are representative for Latvia. To study the processes influencing their properties soil humic substances have been compared

with aquatic humic substances studied in previous paper (Klavins et al., 1997). The composition of major elements, atomic ratios and ash contents of HA and FA samples examined are presented in Table 2. The elemental composition of humic substances from soils and peat of Latvia is generally similar to that of humic substances presented in literature (Орлов, 1990).

Table 2. Elemental and functional composition of humic substances from soils, peat and related environments of Latvia

Humic substances	C, %	H, %	N, %	O, %	COOH, mmol g^{-1}	ArOH, mmol g^{-1}
Humic acids						
HA-VkzA	52.34	4.83	3.08	38.92	2.85	1.94
HA-VKzB	52.05	4.69	3.16	39.23	3.10	2.15
HA-VktA	53.46	4.81	3.61	36.78	2.85	2.10
HA-VKtB	53.96	4.76	3.85	35.95	2.20	2.05
HA-VKtC	52.76	4.95	3.55	37.39	2.50	1.50
HA-VKg	51.32	4.53	4.38	38.60	2.15	2.48
HA-BrtA	55.10	5.23	4.35	33.17	1.90	1.85
HA-BRtB	57.03	5.04	4.35	33.17	1.90	1.05
HA-BRtC	56.13	4.89	3.86	34.00	2.10	0.95
HA-PVv	54.05	5.21	3.71	35.89	2.10	1.56
HA-Pot	53.68	5.12	3.56	36.68	2.15	1.15
HA-Ant	57.91	4.03	3.85	32.89	2.85	2.10
HA-Anu	57.25	3.94	2.95	34.71	2.95	2.05
HA-GLh	54.68	4.08	3.84	36.55	1.90	0.75
HA-TZh	53.01	5.03	1.07	38.63	1.95	0.80
HA-Rāznas Lake	48.74	4.06	1.65	44.17	5.56	0.72
HA-Rusonu Lake	50.38	4.03	1.04	37.40	4.28	0.65
HA-Nordic Reference	55.20	4.12	1.04	39.02	4.12	1.21
HA-P-1	48.11	5.60	1.95	43.00	n.d.	n.d.
HA-P-2	52.47	4.18	2.15	39.06	n.d.	n.d.
HA-P-3	50.71	4.43	2.73	40.95	n.d.	n.d.
HA-P-4	53.01	5.03	1.65	38.63	n.d.	n.d.
HA-P-5	51.39	4.08	2.25	41.03	n.d.	n.d.
Fulvic acids						
FA-VkzA	49.31	4.64	2.95	41.93	3.28	2.16
FA-VKzB	48.65	4.54	2.87	42.98	3.80	2.20
FA-VktA	43.68	4.81	3.65	46.18	3.68	1.75
FA-VKtB	44.36	4.31	3.48	46.51	3.75	1.60
FA-VKtC	42.95	4.55	3.71	47.64	3.75	1.70
FA-VKg	48.75	3.85	2.63	43.59	3.30	2.20
FA-BrtA	48.23	4.43	3.93	41.54	2.82	0.90
FA-BRtB	49.35	4.56	2.76	42.19	2.85	1.15
FA-BRtC	48.17	4.15	2.83	43.90	2.70	0.85
FA-PVv	46.13	4.09	2.48	45.99	3.10	1.65
FA-Ant	45.53	4.31	2.95	46.06	3.50	1.60
FA-Nordic Reference	52.62	4.09	0.74	41.93	7.53	1.53

Humic acids commonly have much higher carbon concentrations than fulvic acids, but at the same time oxygen, carboxylgroup concentrations are higher in fulvic acids. To

characterise elemental composition, atomic ratios (Van Krevelen graphs) are often used. H/C versus O/C ratios (Fig. 1) reflect the relative percentage of aromaticity in structures of humic substances. Chemical processes influencing the formation of HA's can be evaluated by the van Krevelen diagram. As far as most important processes influencing the structure of HS can be described as demethylation (removal of $-CH_3$ group), dehydration and decarboxylation (removal of – COOH group), the same diagram (Fig. 1) can be also used to study humification process. Demethylation, dehydration and decarboxylation processes result in increased aromaticity and increased humification degree. Fig. 1 shows that demethylation and dehydration processes dominate in the generation of humic acids. Highest is the aromaticity of peat HA and HA from hydromorphic soils. Lowest among humic acids is the humification degree for HA's from *Anthrosol* and *Phaozem* soils.

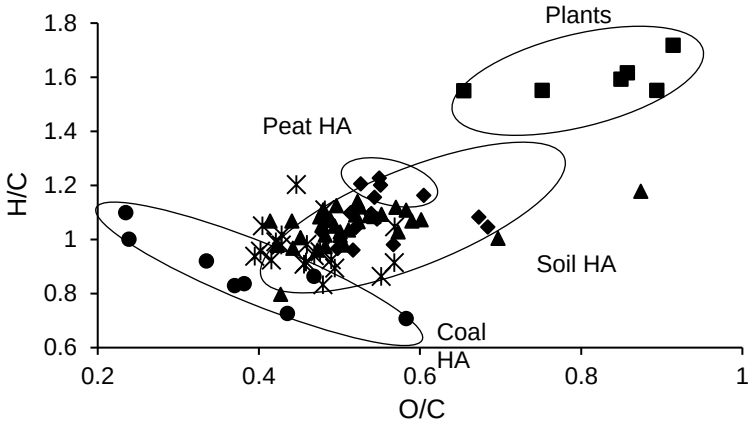

Figure 1. Van Krevelen (H/C *vs.* O/C atomic ratio) graph of humic matter precursors (Klavina et al., 2015)) (plants) (■); peat humic acids (◆), coal humic acids (Krumins et al., 2017) (•) and soil humic acids (▲★).

In humic substances from *Gleysol*, *Histosol* and *Podzol* soils, concentrations of carboxylgroups and phenolic hydroxylgroups are lower (Table 1), than in humic substances from *Phaozem* soils. The most dominant functional groups in the structure of AHS are carboxyl and phenolic hydroxylgroups. The concentrations of carboxylgroups are higher in fulvic acids (3.5–6 mmol g^{-1}), while humic acids have more phenolic hydroxylgroups (1.0–1.5 mmol g^{-1}). In general, the concentrations of carboxylgroups correlate to the O/C ratio, thus indicating that the dominant portion of the oxygen in humic molecules is in form of carboxylgroups. Nitrogen concentrations in humic acids are ~ 1.5 times higher than in fulvic acids.

The UV-Vis spectra of soil and peat HA examined (Fig. 2) are featureless, and they monotonically decrease with increasing wavelength. Only in case of humic substances from *Anthrosol* soils shoulders at 360 nm can be observed. The ultraviolet spectra of both humic and fulvic acids are similar, differing only slightly in optical density.

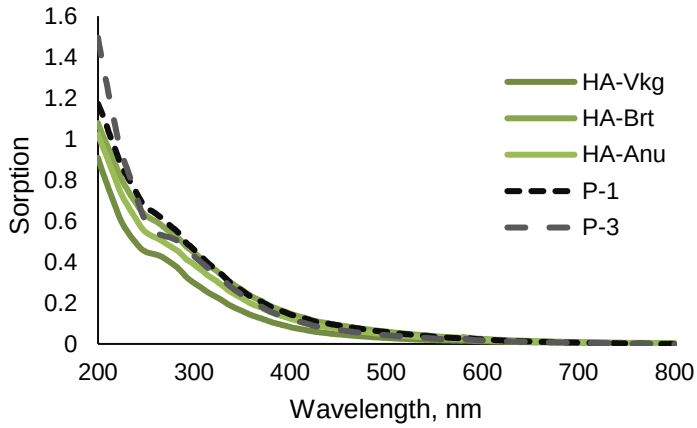

Figure 2. UV-Vis spectra of soil and peat humic substances (*Phaozem* soil VKg *Cambisol* soil BRt *Anthrosol* soil ANu Pine peat P-1 Wood-*Sphagnum* peat P-3).

Table 3. Light absorbance properties and aromaticity of soil humic substances

Sample*	Molar absorption, L (mole C)$^{-1}$ cm^{-1}	E_4/E_6	Aromaticity, %	M_w
FA Missouri River**	247	13.9	20.4	-
FA Ohio River**	274	17.2	24.3	-
FA Minnesota groundwater**	122	3.53	12.6	-
FA Suwannee River**	389	20.7	24.8	880
FA Lake Fryxell**	150	-	13	-
FA Coal Creek**	401	20.7	27.4	-
FA Lake Burtnieku***	214	8.6	17.4	2,200
FA Lake Liepajas***	189	9.4	16.1	1,650
HA-VKg	501	5.4	41.4	8,200
HA-BrtA	444	6.5	36.7	4,250
HA-PVv	392	7.8	32.4	3,800
HA-Pot	379	6.7	31.4	5,100
HA-GLh	269	6.3	22.3	4,400
HA-TZh	681	5.6	56.3	9,300

* – for soil symbols see Table 1; ** – Chin et al., 1994; *** – Klavins, 1998.

The slope of the adsorption curves as measured by the ratios of UV absorbancy at 465 and 665 nm, have been suggested to be inversely related to the condensation of aromatic groups (aromaticity), and also to particle size and molecular weight. The higher E4/E6 ratios measured for the aquatic FA, with respect to those of soil origin, are in general agreement with data in the literature and suggest a lower degree of condensed aromatic systems and smaller particle sizes or molecular weights than for aquatic HS. The E4/E6 ratio for fulvic acids is higher than for humic acids, thus this ratio correlates with the changes in molecular mass of humic substances (Table 3). Within the UV spectra, the molar absorptivities of the humic substances were measured at 280 nm. This wavelength was chosen, since $\pi - \pi^*$ electron transition occurs in this region for phenolic substances, aniline derivatives, benzoic acids, polyenes, and polycylic aromatic

hydrocarbons (Fuentes et al., 2018). Since many of these substances are precursors of components of certain types of humic substances, molar absorptivity (ɜ) may serve as a basis for calculation of aromaticity of humic mater and evaluation of its origin using the following equation (Chin et al., 1994):

aromaticity = 0.05 ɜ + 6.74

(ɜ – molar absorption, L (mole C)$^{-1}$ cm^{-1})

Comparison of molar absorptivities and calculated values of aromaticity found in this study, with those from literature (Table 3) allows to evaluate the impact of different sources on the structure and properties of humic substances. Humic substances from *Histosol* soils have a high degree of aromaticity and molar absorptivity.

Fluorescence emission spectra (excitation at 330 nm) of humic and fulvic acids (Fig. 3) are characterised by broad bands centered around λ = 435 nm and between λ = 445 nm and λ = 485 nm, respectively. Some samples of humic substances influenced by human activities show also shoulders at lower wavelengths. Although the exact nature of the fluorescing groups is still far from clarified, fluorescence at the higher wavelengths, typical for humic substances from *Cambisol* and *Histosol* soils, may be attributed to either highly substituted aromatic nuclei, possibly bearing at least one electron-donating group, and/or conjugated unsaturated systems capable of high degrees of resonance. Soil humic and fulvic acids have fluorescence spectra with maximum at lower wavelengths than aquatic HS (Klavins, 1998), indicating low degrees of aromatic polycondensation and lower levels of conjugated chromophores. Also, lignin-derived, coumarin-like structural units and conjugated phenolic aldehydes, which have λ_{em} max = 465–470 can be suggested as possible contributors to fluorescence of soil humic substances (Shirshova et al., 2017). The presence of lignin-like structures seem to play a secondary role. Substantially different are spectra for humic substances influenced by human activities (*Anthrosol* soils) which have spectral maximums possibly related to conjugation products with contaminants.

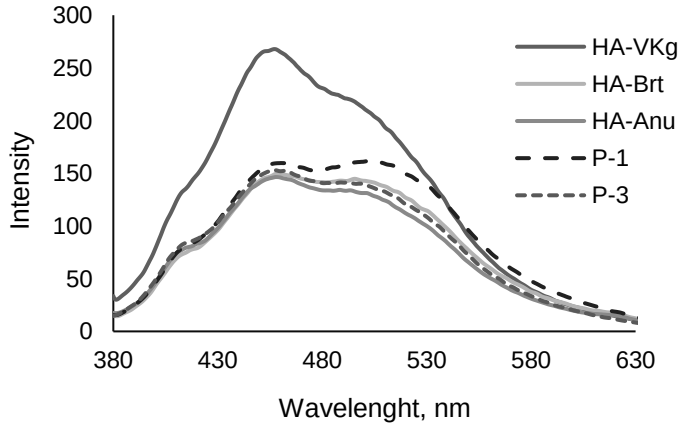

Figure 3. Fluorescence emission spectra of soil and peat humic substances (*Phaozem* soil VKg *Cambisol* soil BRt *Anthrosol* soil ANu Pine peat P-1 Wood-*Sphagnum* peat P-3).

The IR spectra (Fig. 4) of the peat and soil HA examined are in general similar to one another in the main position of adsorption, but differences of various entity are apparent in the relative intensity of some bands, depending of origin and nature of the sample. IR spectra of analysed humic substances can be divided by regions depending on informativity and the presence of important functional groups. Absorption bands in spectral region 3,600–2,800 cm^{-1} are very broad and are typical not only for humic substances, but also for mineral constituents. Absorbance in this spectral region is determined by the presence of $^{-}$OH groups. Sorption at wavelengths 2,920 and 2,860–2,850 cm^{-1} identifies the presence of CH_3^- and CH_2^- groups. IR spectra data of soil humic substances show that methylene groups $-(CH_2)_n-$ exist in the form of comparatively short alkane chains ($n < 4$). Typical intensive sorption lines are common for the region around 1,700 cm^{-1} (1,725–1,700 cm^{-1}), which is characteristic for carbonylgroups in aldehydes, ketones and carbonic acids. The actual sorption maximum greatly depends on the conjugation degree, presence of substituents and hydrogen bonding. In spectral region 1,690–1,500 cm^{-1} it is possible to identify the sorption maximum of amide bonds (1,650–1,640 cm^{-1} and 1,550–1,540 cm^{-1}). In region 1,625–1,610 cm^{-1}, the sorption indicates the presence of aromatic C = C and carbonylgroups, quinones. At wavelengths 1,470–1,370 cm^{-1}, there are bands typical for C-H and O-H bonding and sorption maximums typical for C-O. For wavelengths below 1,000 cm^{-1} fingerprint patterns are evident. Sorption in this spectral region provide information about possible role of carbohydrate percentage in the structure in humic molecules. Sorption at 1,080 cm^{-1} shows OH deformation or C-O stretch of phenol and alcohol OH groups, and 1,040 cm^{-1} indicates C-O stretch of polysaccharide components.

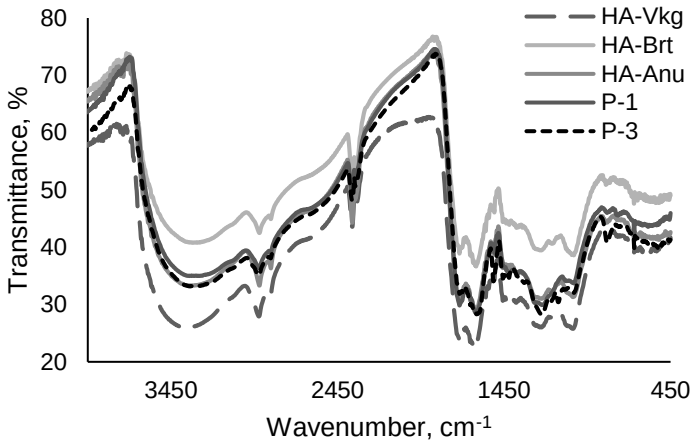

Figure 4. Fourier transform infra-red spectra of studies humic substances Fluorescence emission spectra of soil and peat humic substances (*Phaozem* soil VKg *Cambisol* soil BRt *Anthrosol* soil ANu Pine peat P-1 Wood-*Sphagnum* peat P-3).

The distinctive distribution of functional groups and the major building blocks of humic substances may reflect the way of their production and structure alteration due to microbial degradation and geochemical alteration. Fulvic acid formation may occur through condensation reactions involving compounds derived from precursor organic materials or through production of residual recalcitrant compounds in the microbial

degradation of precursor organic material. For peat humic acids, lignin is not included in the set of precursor materials and carbohydrates and aliphatic structures are relatively abundant. Carbohydrate structures, however, are the most labile and are rapidly degraded by microorganisms. Similarity between humic substances from peat and soil indicate either the dominance of allochtohonous peat humus or the deep transformation of autochthonous humic material.

CONCLUSIONS

The elemental, functional, mass-molecular and spectral characterization of soil and peat humic substances stresses the role of their origin on the properties of humic substances. Humic substances from different soil and peat types differ in properties. The similarity in the structure and properties of humic substances originating from *Podzol, Phaozems, Gleysol* soils on one hand and *Cambisol* and *Histosol* soils on other hand, suggests the importance of intensity of biological transformation of organic matter on their structure. Humic substances from *Cambisol* and *Histosol* soils are similar to peat humic substances and they are highly aromatic. The pattern of differences between Latvian peat and soil humic substances, demonstrates that even within small territory as Latvia it is impossible to isolate one reference sample that would be representative of soil humic substances.

ACKNOWLEDGEMENTS. Authors would like to express gratitude to Latvian Council of Science Council of Latvia for providing a grant 'Properties and structure of peat humic substances and possibilities of their modification' lzp-2018/1-0009.

REFERENCES

Chin, Y-P., Aiken, G. & O'Loughlin, E. 1994. Molecular weight, polydispersity, and spectroscopic properties of aquatic humic substances. *Environ. Sci. Technol*. **28**(11), 1853–1858.

Fuentes, M., Baigorri, R., González-Gaitano, G. & García-Mina, J.M. 2018. New methodology to assess the quantity and quality of humic substances in organic materials and commercial products for agriculture. *J. Soils Sedim.* **18**(4), 1389–1399.

Gerke, J. 2018. Concepts and misconceptions of humic substances as the stable part of soil organic matter: A review. *Agronomy* **8**(5), 1–16.

IUSS Working Group WRB. 2015. World Reference Base for soil resources 2014. International soil classification system for naming soils and creating legends for soil maps. Update 2015. World Soil Resources Report 106. FAO, Rome: 188 pp.

Klavina, L., Springe, G., Nikolajeva, V., Martsinkevich, I., Nakurte, I., Dzabijeva, D. & Steinberga, I. 2015. Chemical composition analysis, antimicrobial activity and cytotoxicity screening of moss extracts (moss phytochemistry). *Molecules* **20**(9), 17221–17243.

Klavins, M. 1998. *Aquatic humic substances: Characterisation, Structure and Genesis*. Rîga: LU, 286 pp.

Krumins, J., Yang, Z., Zhang Q., Yan M. & Klavins, M. 2017. A study of weathered soil spectroscopic properties. *Energy Proc.* **128**, pp. 51–58.

Lipczynska-Kochany, E. 2018. Humic substances, their microbial interactions and effects on biological transformations of organic pollutants in water and soil: A review. *Chemosphere* **202**, 420–427.

Mallick, S.P. 2017. *Method Development for Aquatic Humic Substance Isolation and Its Application to Landfill Leachate*. Lamar University. Beaumont, 87 pp.

Shirshova, L.T., Gilichinsky, D.A., Ostroumova, N.V. & Yermolayev, A.M. 2017. Investigation of humic substances from permafrost sediments using diagrams of optical parameters. *METHODS* **21**(2), 62–71.

Thurman, E.M. 1985. *Organic Geochemistry of Natural Waters*. Martinus Nijhoff/Dr.W.Junk Publishers, Wageningen, 234 pp.

Орлов Д.С. 1990. *Soil humic acids and general humification theory* [Гумусовые кислоты почв и овщая теория гумификации]. Москва, Изд. МГУ 324 с. (in Russian).

Wiszniewska, A., Hanus-Fajerska, E., Muszynska, E. & Ciarkowska, K. 2016. Natural organic amendments for improved phytoremediation of polluted soils: a review of recent progress. *Pedosphere* **26**(1), 1–12.

Agronomy Research **17**(2), 509–517, 2019
https://doi.org/10.15159/AR.19.038

Modular sensory hardware and data processing solution for implementation of the precision beekeeping

V. Komasilovs[1], A. Zacepins[1], A. Kviesis[1], S. Fiedler[2] and S. Kirchner[2]

[1]Latvia University of Life Sciences and Technologies, Faculty of Information Technologies, Department of Computer Systems, Liela iela 2, LV-3001 Jelgava, Latvia
[2]University of Kassel, Department of Agricultural and Biosystems Engineering, Mönchebergstraße 19, DE34109 Kassel, Germany
[*]Correspondence: aleksejs.zacepins@llu.lv

Abstract. For successful implementation of the Precision Apiculture (Precision Beekeeping) approach, immense amount of bee colony data collection and processing using various hardware and software solutions is needed. This paper presents standalone wireless hardware system for bee colony main parameters monitoring (temperature, weight and sound). Monitoring system is based on Raspberry Pi 3 computer with connected sensors. Power supply is granted by the solar panel for reliable operation in places without constant source for power. For convenient data management cloud based data warehouse (DW) is proposed and developed for ease data storage and analysis. Proposed data warehouse is scalable and extendable and can be used for variety of other ready hardware solutions, using variety of data-in/data-out interfaces. The core of the data warehouse is designed to provide data processing flexibility and versatility, whereas data flow within the core is organized between data vaults in a controllable and reliable way. Our paper presents an approach for linking together hardware for bee colony real-time monitoring with cloud software for data processing and visualisation. Integrating specific algorithms and models to the system will help the beekeepers to remotely identify different states of their colonies, like swarming, brood rearing, death of the colony etc. and inform the beekeepers to make appropriate decisions/actions. This research work is carried out within the SAMS project, which is funded by the European Union within the H2020-ICT-39-2016-2017 call. To find out more visit the project website https://sams-project.eu/.

Key words: Precision beekeeping, data warehouse, bee colony monitoring.

INTRODUCTION

Bee health and sustainable beekeeping are a key for sustainable agriculture worldwide (Gallai et al., 2009; Kaplan, 2008). Risks of depleting honey production threatens livelihoods of beekeepers, but degradation of pollination power of suffering bee colonies threats overall agricultural production and affects entire population. Approximately 75% of the crops, used for human feeding depends on pollination (Ollerton et al., 2011; Potts et al., 2016). The European honeybee *Apis mellifera* is the most economically valuable pollinator of agricultural crops worldwide. These insects can provide pollination generally to any fruit and vegetable, playing a crucial ecosystem service for agricultural food production and for wild plant diversity and conservation

(Bommarco et al., 2013; Klein et al., 2006). Many national and international projects like ITAPIC[1], Swarmonitor[2], Smartbees[3], PoshBee[4] and others were implemented or are ongoing to study factors and parameters that may contribute to the bee health. In addition, several monitoring sensors have been developed for automatic beehive monitoring thus facilitating the development of the Precision Beekeeping (Meikle & Holst 2015). Precision Beekeeping is defined as an apiary management strategy based on the monitoring of individual bee colonies to minimise resource consumption and maximise the productivity of bees (Zacepins et al., 2015). Nevertheless, there still is a lack of a system which can be widely used and is very affordable for the end users (beekeepers).

Despite the fact there are number of implemented solutions for data collection about bee colonies, only few of them offer basic functionality for data analysis and decision making. This paper describes authors' developed bee colony hardware system for temperature, humidity, weight and sound monitoring linked together with a cloud data warehouse, specially designed for on-line data storage and close to real-time analysis and decision support actions. The proposed approach integrates two stages of the three-phase cycle of the Precision Beekeeping, including data collection and data analysis. Third phase – application of control actions, remains responsibility of the beekeeper. This phase, called also data utilization, usually involves the adjustment of important parameters and making the needed actions (Pentjuss et al., 2011). Author's approach can be integrated into a beekeeping practice to help the bees and pollination service they provide.

Research idea brings clear economic impact for the beekeepers. Proposed solution helps to remotely monitor bee colonies, recognize various states (for example normal, swarming, colony death) and minimise the necessity for on-site colony visits, therefore reducing beekeeper's spending on unneeded travelling to remote apiary. As well, bee colony health can be increased by minimising the number of beehive openings (see Fig. 1) (Stalidzans et al., 2017).

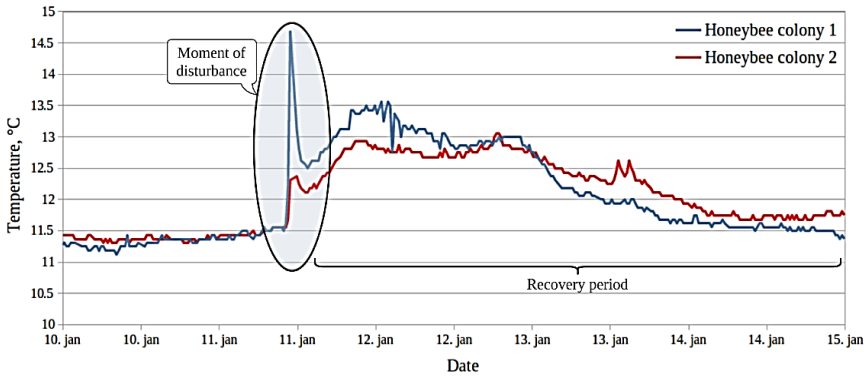

Figure 1. Temperature changes in the bee colony during manual hive weighing.

1 Application of Information Technologies in Precision Apiculture – http://www.itapic.eu
2 http://www.swarmonitor.com
3 Sustainable management of resilient bee populations – http://www.smartbees-fp7.eu
4 Pan-European assessment, monitoring, and mitigation of stressors on the health of bees – http://www.poshbee.eu

Every time when hive is opened and bee colony is inspected or any other manipulations with hive are done an additional stress is posed for the colony. Such stress can also be caused by manual weighting procedure.

In overall, developed approach facilitates optimization of operational beekeeping costs and minimises colony losses, increasing the profitability and stability of beekeeping.

This research is done within the SAMS[5] project. SAMS is a project funded by the European Union within the H2020-ICT-39-2016-2017 call. SAMS enhances international cooperation of ICT (Information and Communication Technologies) and sustainable agriculture between EU and developing countries in pursuit of the EU commitment to the UN Sustainable Development Goal "End hunger, achieve food security and improved nutrition and promote sustainable agriculture". SAMS proposes implementation of Precision Beekeeping by allowing active monitoring and remote sensing of bee colonies and beekeeping by developing appropriate ICT solutions supporting management of bee health and bee productivity and a role model for effective international cooperation. The outcome of the project will be a technologically enhanced beehive system and service including several components, like decision support system, advisory support tool, bee management business concept.

SENSORY HARDWARE FOR BEE COLONY MONITORING

Many parameters of the bee colony can be monitored by the automated system, but not all of them can provide the beekeeper with valuable information. According to literature review and results of recent researches it is concluded, that system should measure temperature, humidity, weight and acoustic parameters of the colony. Temperature and humidity are the most commonly used metrics in precision beekeeping (Meikle & Holst 2015; Zacepins et al., 2015; Meikle et al., 2017). Hive weight is also a useful metric for monitoring the productivity of a colony with a correlation between honey production and different parameters of meteorological conditions (Fitzgerald et al., 2015; Ruan et al., 2017). In addition, monitoring of acoustics of bee colonies can be used for the prediction of e.g. swarming behaviour (Ferrari et al., 2008; Bencsik et al., 2011).

Developed system's architecture is based on proposed approach by (Kviesis & Zacepins 2015), where measurement node sends data to remote server via mobile network. According to the demands, a Raspberry Pi 3 (RPi) was used as Single-Board-Computer (SBC). The RPi was extended with a RPi-Shield-Audio Card and a microphone. A script addresses the sound card and converts the analog audio signals of the microphone. These signals are further broken down into their frequency components by means of a Fast Fourier Transformation (FFT). Using Wi-Fi and a mobile GSM router, the measured values are uploaded to a cloud server and deleted from the SBC memory. In case, radio transmission is not possible, the data remains on the device memory until a connection is established. Conversely, the SBC can also receive updates from the cloud server. Settings, such as the intervals of the data logger, can be changed by user from any computer with internet availability. In addition to the interval sizes for

5 International partnership on innovation in smart apiculture management services –http://www.sams-project.eu

updates and uploads, variables that can be changed including the recording length of the audio signals and the sampling rate. The source codes will be available as open source on SAMS project website (https://sams-project.eu/).

The sensory hardware (see Fig. 2) is capable to obtain temperature data of the inside and outside temperature as well as weight data of the bee colony. A RPi capable sensor for temperature and a load cell in combination with an A/D converter is used for weight measurements. Additional sensors can be connected optionally.

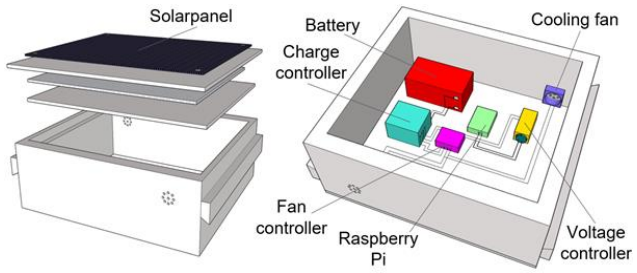

Figure 2. Sensory hardware with casing, solar energy supply, single board computer and cooling.

Sensor placement in a modified broodframe is shown in Fig. 3, and the bee hive with installed monitoring system is demonstrated in Fig. 4.

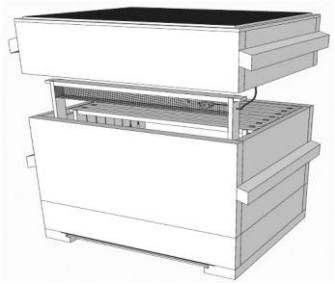

Figure 3. Sensory placement in a modified broodframe connected with cable.

Figure 4. Bee hive with monitoring system prototype at the test site Witzenhausen of the University of Kassel.

In order to supply the system with electricity, a polycrystalline photovoltaic module with a system voltage of 12 V DC was used as a solar generator. To protect the battery from overcharging, a pulse-width modulated shunt controller with depth discharge protection was selected. To store energy a 12 V lead batteries with a capacity of 18 Ah was built in. For adequate ventilation, a temperature controller was installed in combination with two housing fans.

The energy consumption of the RPi depends on the specific sensor constellation. For the hardware configuration used here, the power consumption was less than 0.5 A. To reduce the consumption, the RPi can simply be started for the relevant measuring intervals using a time-controlled ‘power switch’. The component costs for the sensory system run to about 300 euros (see Fig. 5). If several sensor systems are used at one location, the power supply is designed to be shared. This reduces the specific costs

accordingly. Still it can be seen, that costs for granting power supply with alternative methods (photovoltage system) is already expensive. System costs can be significantly decreased if the system is connected to the electrical grid available at the apiary. A honey chamber of a standard magazine hive for honey bees was selected as the casing for the hardware components. This is familiar to every beekeeper and can easily be placed on a beehive. In addition the construction principle can be transferred to magazine hives of other dimensions easily.

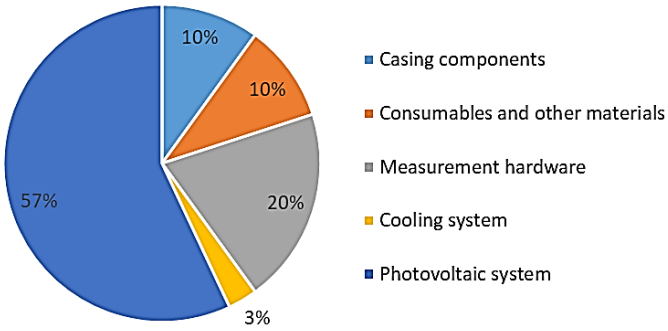

Figure 5. Cost distribution of the monitoring device. Complete system costs are about 300 euros.

DATA WAREHOUSE CONCEPT

Data warehouse (DW) can be considered as a universal system, which is able to operate with different data inputs and have flexible data processing algorithms.

By the definition data warehouse is like an intermediate layer between data provider systems and data consumer systems or end-users (Inmon, 2010). DW provides customizable facilities for data storage management, processing, analysis and output. The DW should be used to help beekeepers run the apiary more effectively by utilising higher amount of available data and accumulated data interpretation knowledge.

Authors suggest implementing DW as a cloud based data storage and processing unit with capabilities to combine different data sources like existing systems and available on-apiary generated data.

Architecture of the developed DW is demonstrated in Fig. 6. DW is capable to analyse data in the real-time or store it for future analysis.

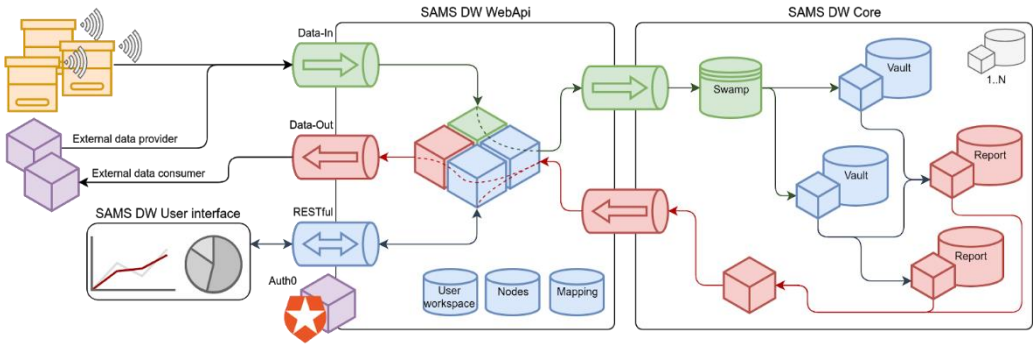

Figure 6. Architecture of the developed data warehouse.

DW consists of three modules: a) Core – main data storage and processing unit; it receives data about various beekeeping objects in predefined format and distributes it through number of vaults and reports, which apply needed transformation to the data (e.g. aggregation, modelling, decision making); b) WebApi – intermediary unit between 'outer world' and DW Core; it provides number of HTTP interfaces for machine-to-machine interaction with external systems via Internet; main functions of the unit include request authentication and authorization, user private workspace management, data-in and data-out interface configuration and data conversion to/from DW Core supported formats; c) Graphical user interface – single-page web application provides user convenient way for managing the sources of incoming data (e.g. hives with monitoring devices) and getting insights into produced outputs (e.g. reports).

DW Data-in interface provides data input functionality for various data sources – it can be in a form of data files uploaded manually via user interface or via automated (scheduled) scripts, a bee colony measurement system configured, accordingly, to send data in accepted format, or third-party services, like weather station data.

Benefit of the DW is that data are processed almost immediately by involving different models for data aggregation and reporting. Modular architecture of the solution ensures isolation boundaries both for reliability reasons, maintenance and development considerations.

LINKING REMOTE HARDWARE WITH CLOUD SOFTWARE

Remote hive monitoring systems (like Raspberry Pi based solution described previously in section 'Sensory hardware for bee colony monitoring') need special authentication mechanisms before sending data to the data warehouse. Since access to the Web API's interfaces are protected by Auth0 authentication and authorization service, non-interactive Machine-to-Machine authentication flow is required (https://auth0.com/docs/applications/machine-to-machine). During such flow Auth0 service provides access token (a credential) that is issued to an authorized device and must be included into each HTTP request to DW endpoints. The access token has an expiration time (for example, 24 hours) and should be eventually renewed by the device. Remote measurement system is sending HTTP POST request to DW data-in interface, including authentication token within request header and JSON formatted data as a body of the request. A temperature and humidity HTTP POST example is shown below (where <token> is issued by Auth0 service and source IDs are arbitrary identifiers used for mapping incoming data to beekeeping objects like hives):

```
POST /api/data HTTP/1.1
Host: example.host.com:port
Authorization: Bearer <token>
Content-Type: application/json

[{"sourceId": "temp-id-123",
   "values": [{"ts": "2018-10-10T23:06:00Z", "value": 33.2},
         {"ts": "2018-10-10T23:07:00Z", "value": 33.5}]},
 {"sourceId": "hum-id-234",
   "values": [{"ts": "2018-10-10T23:06:00Z", "value": 42.8}]}]
```

Upon receiving such request, it is validated against registered/allowed devices, and only then it is converted to appropriate format and sent to DW Core. Data processing involves various stages of pre-aggregation and actions performed by DW Core (see Fig. 6): temporary incoming data storing (swamp), data flow management, data vault activation, etc. Example of temperature measurements pre-aggregated into hourly record is shown below:


```
{"_id" : "hive-549:2018101510",
   "count" : 5,
   "max" : 45.5,
   "min" : 39.099998474121094,
   "sum" : 213.39999771118164,
   "values" : {
            "15" : 44.400001525878906,
            "17" : 45.5,
            "20" : 41.599998474121094,
            "23" : 39.099998474121094,
            "27" : 42.79999923706055}}
```


Described DW was implemented as a set of microservices and modules, built using Spring Boot 2.0 (back-end) and Angular 6 with Bootstrap 4 framework (front-end). MongoDB, a NoSQL database was used as a persistent storage for metadata and measurements.

Developed solution was approbated by building end-to-end data flow from hive prototype located in Witzenhausen, Germany to DW cloud service (physically hosted on servers in Jelgava, Latvia). In addition, for testing purposes room micro-climate monitoring hardware prototype was adapted to send temperature and humidity measurements to DW using the same data-in interfaces. Both devices are sending their measurements according to their schedules and become available in DW user interface in a form of quick overview of latest values as well as detailed parametrized reports. During implementation and testing period, several new versions of device and DW software were deployed. Modular architecture and flexible interfaces contributed to fast new feature development and deployment cycle.

CONCLUSIONS

Development of the Precision Beekeeping direction is in active state nowadays, as many scientists and also industrial sector are heading toward development of solutions for improvement the management and monitoring of the apiary, minimising the beekeepers direct influence on the process.

Described systems and approach integrates two stages of the Precision Beekeeping, including data collection and data analysis. Third phase - application, remains still for the beekeeper.

Developed system should be used to minimise the number of manual bee colony inspections, which should lead to the minimisation of the impact to the bee colony health.

The advantage of developed system is the possibility to detect abnormal behaviour of the colony at an early stage giving the beekeeper the chance to save their colonies.

At this moment system's prototype is used in experimental apiary in Germany, but in the future systems will be installed in apiaries in Ethiopia and Indonesia.

ACKNOWLEDGMENT. Scientific research, publication and presentation are supported by the Horizon 2020 Project SAMS 'Smart Apiculture Management Services'. This project receives funding from the Horizon 2020 European Union Research and Innovation Framework under Grant Agreement Nr.780755 – SAMS. This project receives funding from the German Federal Ministry for Economic Cooperation and Development.

REFERENCES

Bencsik, M., Bencsik, J., Baxter, M., Lucian, A., Romieu, J. & Millet, M. 2011. Identification of the honey bee swarming process by analysing the time course of hive vibrations. *Computers and electronics in agriculture* **76**(1), 44–50. Available at: http://dx.doi.org/10.1016/j.compag.2011.01.004

Bommarco, R., Kleijn, D. & Potts, S.G. 2013. Ecological intensification: Harnessing ecosystem services for food security. *Trends in Ecology and Evolution* **28**(4), 230–238.

Ferrari, S., Silva, M., Guarino, M. & Berckmans, D. 2008. Monitoring of swarming sounds in bee hives for early detection of the swarming period. *Computers and electronics in agriculture* **64**(1), 72–77.

Fitzgerald, D.W., Murphy, F.E., Wright, W.M., Whelan, P.M. & Popovici, E.M. 2015. Design and development of a smart weighing scale for beehive monitoring. *In 26th Irish Signals and Systems Conference* (ISSC), pp. 1–6.

Gallai, N., Salles, J.M., Settele, J. & Vaissière, B.E. 2009. Economic valuation of the vulnerability of world agriculture confronted with pollinator decline. *Ecological economics* **68**(3), 810–821. Available at: http://dx.doi.org/10.1016/j.ecolecon.2008.06.014

Inmon, B.H. 2010. Data Warehousing, 2.0 Modeling and Metadata Strategies for Next Generation Architectures. *Architecture*, pp.1–13.

Kaplan, J. 2008. Colony Collapse Disorder. A Complex Buzz. *Agricultural Research Magazine* **56**(5), 8–11.

Klein, A.M., Vaissiere, B.E., Cane, J.H., Steffan-Dewenter, I., Cunningham, S.A., Kremen, C. & Tscharntke, T. 2006. Importance of pollinators in changing landscapes for world crops. *Proceedings of the royal society B: biological sciences* **274**(1608), pp. 303–313.

Kviesis, A. & Zacepins, A. 2015. System architectures for real-time bee colony temperature monitoring. *In Procedia Computer Science*, **43**, pp. 86–94.

Meikle, W.G., Weiss, M., Maes, P.W., Fitz, W., Snyder, L.A., Sheehan, T., Mott, B.M. & Anderson, K.E. 2017. Internal hive temperature as a means of monitoring honey bee colony health in a migratory beekeeping operation before and during winter. *Apidologie* **48**(5), 666–680.

Meikle, W.G. & Holst, N. 2015. Application of continuous monitoring of honeybee colonies. *Apidologie* **46**(1), 10–22. Available at: http://link.springer.com/article/10.1007/s13592-014-0298-x

Ollerton, J., Winfree, R. & Tarrant, S. 2011. How many flowering plants are pollinated by animals? *Oikos* **120**(3), 321–326.

Pentjuss, A., Zacepins, A. & Gailums, A. 2011. Improving precision agriculture methods with multiagent systems in Latvian agricultural field. *In Proceedings of the 10th International Scientific Conference "Engineering for Rural Development."* Jelgava, Latvia, pp. 109–114.

Potts, S.G., Ngo, H.T., Biesmeijer, J.C., Breeze, T.D., Dicks, L.V., Garibaldi, L.A., Hill, R., Settele, J. & Vanbergen, A. 2016. *IPBES:* Summary for policymakers of the assessment report of the Intergovernmental Science-Policy Platform on Biodiversity and Ecosystem Services on pollinators, pollination and food production.

Ruan, Z.Y., Wang, C.H., Lin, H.J., Huang, C.P., Chen, Y.H., Yang, E.C., Tseng, C.L. & Jiang, J.A. 2017. An Internet of Things-Based Weight Monitoring System for Honey. International *Journal of Agricultural and Biosystems Engineering* **11(**6), 478–482.

Stalidzans, E., Zacepins, A., Kviesis, A., Brusbardis, V., Meitalovs, J., Paura, L., Bulipopa, N. & Liepniece, M. 2017. Dynamics of Weight Change and Temperature of Apis mellifera (Hymenoptera: Apidae) Colonies in a Wintering Building With Controlled Temperature. *Journal of Economic Entomology* **110**(1), 13–23. Available at: http://jee.oxfordjournals.org/lookup/doi/10.1093/jee/tow282

Zacepins, A., Brusbardis, V., Meitalovs, J. & Stalidzans, E. 2015. Challenges in the development of Precision Beekeeping. *Biosystems Engineering* **130**, pp.60–71.

Agronomy Research **17**(2), 518–539, 2019
https://doi.org/10.15159/AR.19.065

A research on models of the photosynthetic light response curves on the example of evergreen types of plants

S. Korsakova[1], Yu. Plugatar[1], O. Ilnitsky[1] and M. Karpukhin[2]

[1]FSBSI ' The Labor Red Banner Order Nikita Botanical Gardens – National Scientific Center of Russian Academy of Sciences'298648, Russia, The Republic of Crimea, Yalta, urban vil. Nikita, Nikita Botanical Gardens
[2]Federal State Budget Educational Institution of Higher Education 'Ural State Agrarian University', 42, Karla Libknehta street, RU620075 Yekaterinburg, Sverdlovsk region, Russia
[*]Correspondence: Xoshyn@gmail.com

Abstract. The peculiarities of CO_2 exchange in the leaves of ornamental evergreen plant species that are common in the Southern coast of Crimea were studied: *Nerium oleander* L., *Laurus nobilis* L., *Aucuba japonica* Thunb., and *Melissa officinalis* L. The results of approximation of the most commonly used four models of P_N/I curves with the measured data were compared. The values of the parameters P_{gmax}, $\varphi_{(I_{comp})}$, R_D, I_{max}, which were calculated from the modified Michaelis-Menten model in comparison with the measured values were higher by 5–15%, and those that were calculated by the hyperbolic tangent model – lower by 3–13%. The use of a modified rectangular hyperbola model, which is capable of describing the photoinhibition by the nonrectangular hyperbola and the modified nonrectangular hyperbola model, showed a high degree of adequacy of the proposed models for describing the true dependence between the rate of photosynthesis and the light intensity for *Nerium oleander* L., *Laurus nobilis* L., *Aucuba japonica* Thunb. and *Melissa officinalis* L. Measurements of CO_2 exchange in leaves under similar environmental conditions showed significant differences in the parameters of the P_N/I curves: the light compensation point, the rate of photosynthesis and dark respiration, light saturation, and quantum yield. The highest values of photosynthesis efficiency were observed in *Nerium oleander*, the lowest values in *Aucuba japonica* – the light saturation was noted at a very low photosynthetically active radiation. The lower values of the light compensation point and the saturation constants in *Laurus nobilis* and *Aucuba japonica* indicate their effective use of the photosynthetically active radiation, which allows them to survive in conditions of durable shade.

Key words: evergreen species, CO_2 exchange, photosynthetic light response curves, fitting, nonlinear regression

INTRODUCTION

Many problems of plant physiology can be solved with proper completeness if quantitative methods are used in the studies (Drozdov et al., 2008). Studies in which we are using methods that do not violate the integrity of the plant have a particular relevance. One of such approaches is the construction of light dependences of CO_2 exchange, which

allows us to evaluate the efficiency of the use of light energy by the plant organism, incorporated in its genetic system, the mechanism of its utilization of light energy and the transformation of inorganic compounds of biogenic elements into organic substances (Zalensky, 1977; Zvalinsky, 2006). The analysis of the photosynthetic light-response curves (P_N/I curve) gives an important potential ecological and physiological characterization of this species, which allows us to compare different plant species growing in similar conditions of CO_2 exchange indicators; to receive important information about the adaptive mechanisms of the genotype, the plant diversity by competitiveness in such a narrow ecological niche, stress resistance and productivity (Kaibeyainen, 2009; Bolondinsky & Vilikainen, 2014). The use of methods of mathematical modeling contributes to the more detailed quantitative understanding of the mechanisms of plant functioning and their responses to external conditions (Thornley, 1982). Since there does not exist theoretically based solid model would be an ability to handle all experimental data of the real P_N/I curves,, currently, the number of models have been used to assess the relationship between the photosynthetic rate (P_N) and photosynthetically active radiation (PAR) are more than two dozen (Zvalinsky, 2006). Various experimental light curves are described by various functions: rectangular, nonrectangular hyperbola, Blackman's equation, exponential, hyperbolic tangent (Zvalinsky, 2006). All the curves have a similar shape, but they differ in the region of inflection and in achieving the maximum of photosynthesis. In the work of Lobo et al. (2013a), calculations of the statistical indices are presented and the method for selecting the approximating function of the P_N/I dependence by the method of least squares is shown (the error sum of squares, SSE) by means of add-in 'Solver' in 'Microsoft Excel 2010'.

The problems that a researcher encounters while quantitatively describing the real photosynthetic light curves, and the merits of the 'Statistica' system, which had analyzed the photosynthetic rate of light intensity in evergreen plant species growing in the Southern coast of the Crimea, are described in this paper.

The purpose of this work is to study the peculiarities of net CO_2 assimilation in leaves of ornamental evergreen plant species for the subsequent determination of their physiological differences in relation to the light factor. On the basis of experimental data, to examine the parameters of the photosynthetic light curve response models, to compare them with the measured data, determine the problems of each model using photosynthetic parameters calculated on the basis of the statistical function.

MATERIAL AND METHODS

Four evergreen plant species that are common in the landscaping of the Southern coast of the Crimea were used in the experiment: Oleander (*Nerium oleander* L.), Bay laurel (*Laurus nobilis* L.), Spotted laurel (*Aucuba japonica* Thunb.) and Lemon balm (*Melissa officinalis* L.).

Part of the experiments were carried out in a greenhouse of the Nikitsky Botanical Garden (NBG) under conditions of moderate shading (about 50–60% of total illumination), with the 4 year old seedlings, growing in 10-L vegetation vessels; another part of the experiments were in the field conditions with full sunlight, in the place of growth of the plants – in the upper park of the Arboretum Nikitsky Botanical Garden and the experimental area, located in the central branch of the NBG 'Lavrovoye'.

The maximal intensity of photosynthesis occurs in perennial evergreen plants after completion of leaf formation by its area and biomass (Tobias et al., 1995; Miyazawa & Terashima, 2001), so the intensity of carbon dioxide exchange of leaves was determined three times on well-developed intact leaves of the upper part of the plant shoot every 10–15 min using an automatic 4-channel open system for CO_2 exchange and leaf transpiration monitoring 'Monitor photosynthesis RTM-48A' (Bioinstruments S.R.L., Moldova) (Balaur et al., 2009). To measure the CO_2 exchange, a single-channel infrared gas analyzer (IRGA) with an open gas metering system by 'PP Systems' (USA) was used (Balaur et al., 2013). The CO_2 exchange is determined by decrement of CO_2 concentration at the outlet (C_{out}) of the leaf chamber, which is compared with the concentration of incoming ambient air (C_{in}). The CO_2 exchange rate (E) is calculated as follows: $E = k\times(C_{in} - C_{out})\times F$, where F is air flow rate and k is a dimension factor, which depends on air temperature and pressure and is calculated automatically by the system. The standard air flow rate is 0.9 ± 0.1 liter per minute. The cycle starts from the pump switching on and leaf chamber connected to the analyzer channel. Within 1 min the channel of the leaf chamber is purging with ambient air; at the same time there is an automatic calibration for the gas analyzer, which lasts about 20 seconds. The reference concentration (C_{in}) is measured twice – at the end of this stage (C_{in1}) and after the closed chamber phase (C_{in2}). The arithmetic mean (C_{in}) of these two values is substituted in formula. In measurement cycle, the leaf is enclosed for 30 seconds only. An air pump provides an air stream from the circumference to the center of leaf chamber; then this air is fed through a connecting tube into the gas analyzer unit (Balaur et al., 2009). The leaf chamber was configured so that its elements did not obscure the leaf; the area of the window of the leaf chamber was 20 cm^2. The photosynthetically active radiation (PAR) and other environmental parameter, such as air temperature (in °C) and humidity (in %), were measured by the sensors of the RTH-48 Meteo module connected to the digital input of the RTM-48A system; leaf temperature (in °C) was measured with LT-1P leaf temperature sensor; soil moisture (in %) was measured with mineral soil sensor SMS-5M connected to the RTM-48A analog inputs. To obtain the P_N/I dependence, CO_2 exchange measurements were carried out in the PAR range from 0 to 2,000 μmol photons m^{-2} s^{-1}, at the natural CO_2 concentration in the air of 0.04%. During experiments in the well-ventilated greenhouse the input gas for the CO_2 measurement was used the air of the greenhouse (at the CO_2 concentration in the air also of 0.04%).

Statistical processing of data was carried out in programs 'Statistica 10' ('Statsoft Inc.', USA) and 'Microsoft Excel 2010'. All calculations were performed at a given significance level $P \leq 0.05$.

Experimental measurements in the field and in the greenhouse were carried out on sunny, mostly clear days in September 2015 and 2016. The investigated plants experienced neither a lack of soil moisture nor stress due to high temperature: the air temperature in the daytime varied within 26–31 °C, while that in the nighttime was within 19–24 °C, with the relative air humidity of 50–68% and soil moisture of 60–80% field capacity. The maximum measured value of PAR under treatment of full sunlight varied within 1,270–1,830 μmol photons m^{-2} s^{-1}, under treatment moderate shading in greenhouse was within 470–630 μmol photons m^{-2} s^{-1}.

Taking into account the frequency of application of the models (Jassby & Platt, 1976; Platt et al., 1977; Kaibeyainen, 2009; Dalke et al., 2013; Bolondinsky & Vilikainen, 2014), critical remarks, and the advantages of the proposed modern empirical

approaches and original projects (Thornley, 1982; Zvalinsky, 2006, Ye, 2007; Zvalinsky, 2008; Lobo et al., 2013b), in this study we compared the measured and the calculated photosynthetic parameters using four different well-described mathematical expressions of the P_N/I curve: the modified Michaelis-Menten model (Eq. 1) (Kaibeyainen, 2009), the hyperbolic tangent model (Eq. 2) (Jassby & Platt, 1976; Platt et al., 1977), the modified model of a rectangular hyper which can describe the photoinhibition by the nonrectangular hyperbola (Eq. 3) (Ye, 2007) and the modified model of the nonrectangular hyperbola (Eq. 4) (Zvalinsky, 2006, 2008).

$$P_N = \frac{IP_{gmax}}{I + I_{(50)}} - R_D\,, \tag{1}$$

$$P_N = P_{gmax}\, tanh\left(\frac{\varphi_{(I_0)} I}{P_{gmax}}\right) - R_D\,, \tag{2}$$

$$P_N = \varphi_{(I_0 - I_{comp})} \frac{1 - \beta I}{1 + \gamma I}\left(I - I_{comp}\right), \tag{3}$$

$$V = \frac{1 + [I]}{2\gamma_I}\left\{1 - \sqrt{1 - \frac{4\gamma_I [I]}{(1 + [I])^2}}\right\} \; were\; V = P_N/P_{gmax}\; and\; [I] = I/I_K \tag{4}$$

where P_{gmax} is the maximum of gross photosynthetic rate at the 'optimal' light intensity (below the level when the photoinhibition begins) (Zvalinsky, 2006), μmol CO_2 m^{-2} s^{-1}; P_N is the net photosynthetic rate, μmol CO_2 m^{-2} s^{-1}; R_D is the dark respiration rate, μmol CO_2 m^{-2} s^{-1}; I is the photosynthetically active radiation (PAR), μmol photons m^{-2} s^{-1}; I_{comp} is the light compensation point (LCP) – the light intensity at which the total CO_2 exchange ($P_N/I_{(x,t)}$) equals zero, μmol photons m^{-2} s^{-1}; $I_{(50)}$ is the point of light saturation for $P_N + R_D$, equal (50%) from P_{gmax}, μmol photons m^{-2} s^{-1}; I_{sat} is the light saturation point, μmol photons m^{-2} s^{-1}; I_k is the light constant, μmol photons m^{-2} s^{-1}; $[I]$ is relative light intensity (dimensionless); $\varphi_{(I)}, \varphi_{(I_0)}, \varphi_{(I_{comp})}, \varphi_{(I_0 - I_{comp})}$ are the quantum yield of photosynthesis (the tangent of the slope of the light curve, calculated as the derivative of P_N at point I) for different light intensities, for $I = 0$; $I = I_{comp}$; $I = I_0 - I_{comp}$, μmol CO_2 μmol photons^{-1}; β *and* γ are coefficients that are independent of irradiance (Ye, 2007), m^2 s μmol photons^{-1} and β is a correction factor for the decreasing trend of P_N when PAR exceed light saturation point due to photoinhibition and is similar to the convexity (Thornley, 1982), γ is a conversion factor for the initial slope of the P_N/I curve and the maximum photosynthetic rate; γ_I is the convexity factor ('curvature') of the non-rectangularity of the hyperbola, dimensionless.

Parameters P_{gmax}, R_D and I_{sat} for Eq. (3) were calculated from formulas (5–7) (Ye, 2007):

$$P_{gmax} = \varphi_{(I_0 - I_{comp})} \frac{1 - \beta I_{sat}}{1 + \beta I_{sat}}\left(I_{sat} - I_{comp}\right) + R_D, \tag{5}$$

$$R_D = \varphi_{(I_0 - I_{comp})} \cdot I_{comp}\,, \tag{6}$$

$$I_{sat} = \left(\sqrt{\frac{(\beta+\gamma)\left(1+\gamma I_{comp}\right)}{\beta}} - 1 \right) / \gamma \,. \quad (7)$$

The general forms of the P_N/I curve of Eqs (1)–(3) and calculation of the main photosynthetic characteristics ($\varphi_{(I)}$, I_{comp}, $I_{sat(n)}$) in 'Excel' (Eq. (5)–(15) developed by F.A. Lobo et al. (Lobo et al., 2013a, 2013b):

$$\varphi_{(I)} = \frac{I_{(50)} P_{gmax}}{\left(I + I_{(50)}\right)^2}, \quad (8)$$

$$\varphi_{(I)} = \varphi_{(I_0)} sech^2 \left(\frac{\varphi_{(I_0)} I}{P_{gmax}} \right) = \varphi_{(I_0)} \left[\frac{1}{cosh^2 \left(\frac{\varphi_{(I_0)} I}{P_{gmax}} \right)} \right], \quad (9)$$

$$\varphi_{(I)} = \varphi_{(I_0 - I_{comp})} \frac{1 - \beta\gamma I^2 - 2\beta I + (\gamma+\beta) I_{comp}}{(1+\gamma I)^2}, \quad (10)$$

$$I_{comp} = \frac{I_{(50)} R_D}{P_{gmax} - R_D}, \quad (11)$$

$$I_{comp} = arctanh \left(\frac{R_D}{P_{gmax}} \right) \frac{P_{gmax}}{\varphi_{(I_0)}}, \quad (12)$$

$$I_{sat(n)} = \frac{I_{(50)} \left(R_D \frac{n}{100} - P_{gmax} \frac{n}{100} - R_D \right)}{P_{gmax} \left(\frac{n}{100} - 1 \right) + R_D \left(1 - \frac{n}{100} \right)}, \quad (13)$$

$$I_{sat(n)} = arctanh \left[\frac{\frac{n}{100} \left(P_{gmax} - R_D \right) + R_D}{P_{gmax}} \right] \frac{P_{gmax}}{\varphi_{(I_0)}}, \quad (14)$$

$$I_{sat(n)} = \frac{A I_{comp} - B\gamma + C}{2A} - \frac{\sqrt{\left(B\gamma - A I_{comp} - C \right)^2 - 4A\left(C I_{comp} + B \right)}}{2A}, \quad (15)$$

$I_{sat(n)}$ in Eq. (13)–(15) is the light saturation point (LSP), determined at the photosynthesis rate $P_N + R_D$ equal (n%) from P_{Nmax} (Lobo et al., 2013a). To calculate any value of $I_{sat(n)}$, we can substitute the desired percentile value instead of (n) in the formula.

RESULTS AND DISCUSSION

Eq. (4) has three main parameters: the maximum rate of photosynthesis P_{gmax}, the light I_k constant and the non-rectitude parameter of the hyperbola γ_I (Zvalinsky, 2006, 2008). The parameter I_k(*I-constant)* is the main one for the light curve, the tangent of the slope angle $\varphi_{(I_0)}$on its initial section is a dependent parameter. $I_k = P_{gmax}/\varphi_{(I_0)}$. $\varphi_{(I_0)} = a \times \varphi_{max}$ the a is the absorption, φ_{max} is the maximum quantum yield.

Theoretically, the maximum quantum yield is 0.1250 μmol CO_2 μmol photons^{-1}, which means that 8 photons are required per one molecule of CO_2 fixed (Singsaas et al., 2001).

If we substitute V and $[I]$ with P_N/P_{gmax} *and* I/I_K, respectively, into Eq. (4), taking into account that $P_{gmax} = P_N + R_D$ (Ye, 2007), the photosynthetic rate will be equal to:

$$P_N = P_{gmax}\frac{I + I_k - \sqrt{(I + I_k)^2 - 4\gamma_I I I_k}}{2\gamma_I I_k} - R_D\ . \tag{16}$$

For any value of I in the set of the experimental data, an arbitrary quantum yield of photosynthesis φ_I is calculated as the derivative of the P_N/I curve in relation to I (Lobo et al., 2013a). The calculated derivative for the mathematical model (16) is presented in Eq. (17):

$$\varphi_{(I)} = \frac{P_{gmax}}{2\gamma_I I_k}\left(1 - \frac{I + I_k - 2\gamma_I I_k}{\sqrt{(I + I_k)^2 - 4\gamma_I I I_k}}\right). \tag{17}$$

When $I = 0$, Eq. (17) takes the next form:

$$\varphi_{(I_0)} = P_{gmax}/I_k\ . \tag{18}$$

Eq. (19) for calculation of the light compensation point I_{comp} from the model (16) was obtained after the transfer of the term I to the left side of the equation with the total CO_2 exchange equal to zero ($P_N = 0$):

$$I_{comp} = I_k R_D \frac{1 - \gamma_I \frac{R_D}{P_{gmax}}}{P_{gmax} - R_D}\ . \tag{19}$$

The general formula for calculating $I_{sat(n)}$ is obtained from the mathematical model (16), and is presented in Eq. (20):

$$I_{sat(n)} = \frac{I_k\left(\frac{n}{100}\left[R_D - R_{gmax}\right] - R_D\right)\left(1 - \gamma\left[\frac{\frac{n}{100}\left(P_{gmax} - R_D\right) + R_D}{P_{gmax}}\right]\right)}{\left(\frac{n}{100} - 1\right)\left(P_{gmax} - R_D\right)}. \tag{20}$$

In addition to the main cardinal points of the light curve using the add-in 'Solver' in 'Microsoft Excel 2010', applying the Lobo approach (Lobo et al., 2013) for each model and species, we found the maximum light intensity I_{max} saturating P_N, as a point beyond which there is no significant increase in the rate of net photosynthesis. At this point, the maximum net photosynthetic rate saturated with light ($P_{N(Imax)}$) was calculated in the absence of photoinhibition. These variables are more realistic for representing the photosynthetic potential of plants, since their magnitude is always within the range of measurements (Lobo et al., 2013a). Taking into account the technical characteristics of the photosynthesis monitor RTM-48A (Balaur et al., 2009), the calculation of I_{max} was carried out if the maximum change in the measured values ΔP_N did not exceed 0.1 μmol CO_2 m^{-2} s^{-1} in the interval of light intensity increment ΔI = 50 μmol photons m^{-2} s^{-1}.

Module: Advanced Analysis / Nonlinear Estimation (Advanced Linear / Nonlinear Models) in the 'Statistica' system. Nonlinear estimation in the 'Statistica' system involves finding the best fit for the relationship between the values of the

dependent variable and the values of the set of one or more independent variables. Since the selection process is iterative, estimates of the primary parameters of the curve must be given. The initial estimates and ranges were based on our own experience with the study of species and the literature data. Only one initial guess of the free parameters was used. The maximum and minimum limits imposed for the parameters $P_{gmax}, \varphi_{(I_0)}, R_D$, LPC: the maximal rate of the net CO_2 uptake for C_3 species is up to 59 μmol CO_2 m^{-2} s^{-1}; the initial estimates of R_D obtained as approximately about 10% of P_{Nmax}, since both these estimates are interrelated (Lobo et al., 2013a); the maximum quantum yield is 0.1250 μmol CO_2 μmol photons^{-1} (Singsaas et al., 2001); the LCP – from 2 to 150 μmol photons m^{-2} s^{-1} (Lobo et al., 2013a; Korsakova, et al., 2016); the range for the correction coefficients in Eq. (3) and the non-rectitude parameter of the hyperbola in Eq. (16) are from 0 to 1 ($0 < (\beta;\ \gamma;\ \gamma_l) < 1$) (Zvalinsky, 2006, 2008; Lobo et al., 2013a). The above indices help to choose the correct value for the parameters; however, the measured data are taken into account (Lobo et al., 2013a).

In order to determine the restrictions on the parameter change area, you should add to the loss function (in the 'Loss function' field) a penalty function equal to zero for the allowed values of the parameter and very large for invalid values. You can see an example below, which shows the input of a modified model of a rectangular hyperbola (Eq. (3) and the loss function including the imposition of a penalty if the parameter γ is less than or equal to zero:

The estimated function: $\mathrm{v2} = \varphi_{(I_0 - I_{comp})} * ((1 - \beta * \mathrm{v1})/(1 + \gamma * \mathrm{v1})) * (\mathrm{v1} - I_{comp})$

The loss function: $\mathrm{L} = (\mathrm{OBS} - \mathrm{PRED}) ** 2 + (\gamma <= 0) * 100{,}000{,}000$

where v1 is the photosynthetically active radiation (I); μmol photons m^{-2} s^{-1}; v2 is the net photosynthesis rate (P_N), μmol CO_2 m^{-2} s^{-1}.

In this paper to obtain the equations parameters, mathematical fitting of P_N/I curve models were performed with the Quasi-Newton method.

The user is given the complete control over all aspects of the evaluation procedure (initial values, step size, stopping criterion, etc.). The approximation of the model to the experimental dependence is considered to be best if the error sum of squares (SSE) of the desired analytic function from the experimental dependence is minimal. Even if the distribution of the dependent variable is not normal, the R^2 helps to evaluate how well the selected model is consistent with the original data (Stukach, 2011).

Comparison and experimental estimation of the model parameters. There is no single definitive universal mathematical model for application in all cases when describing real light curves; therefore, when carrying out specific studies, the best P_N/I curve from all existing ones will be the one that best corresponds to the initial data (Lobo et al., 2013a). Taking into account that the classical reaction of plant adaptation in response to changes in light conditions is characterized, as a rule, by changing the angle of inclination of the initial section of the light curve, the level of the light saturation plateau and the rate of the dark respiration, was carried out the comparative analysis of the consistency of approximating functions for P_N/I dependencies under different conditions of irradiance: under full sunlight and under moderate shading treatment (Fig. 1).

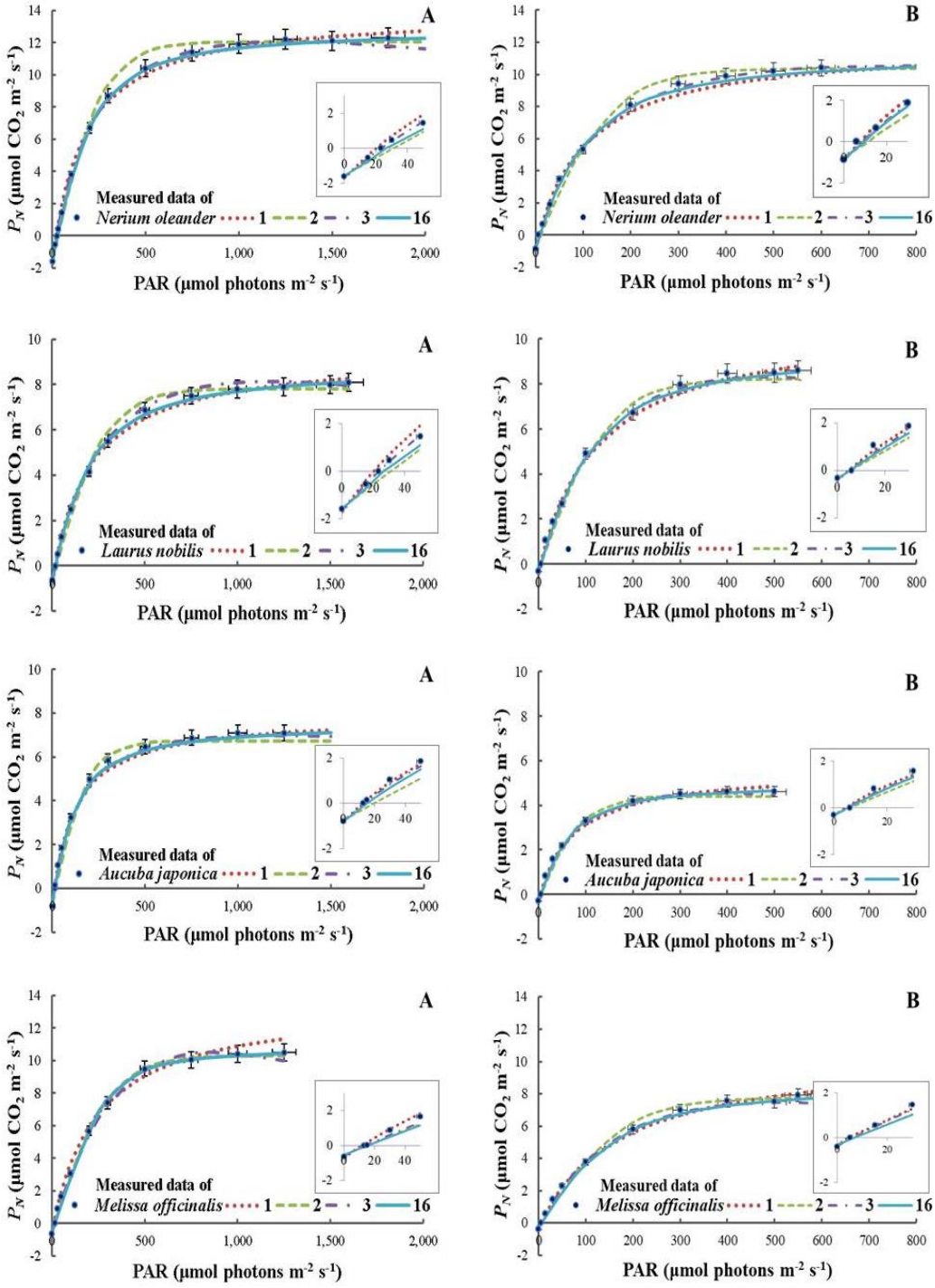

Figure 1. Fitting of the P_N/I curves using different mathematical models: A – full sunlight; B – moderate shading; 1, 2, 3, 16 – corresponding models of light response curves; P_N – net photosynthetic rate; PAR – photosynthetically active radiation.

Tables 1–4 show the average values and their standard deviations (±) of the experimental data, the parameters of the light curve models (Eqs (1), (2), (3) and (16), as well as the variables calculated from these models (Eqs (5)–(15), (17)–(20).

Statistical analysis showed that the P_N/I dependencies for *Nerium oleander*, *Laurus nobilis*, *Aucuba japonica* and *Melissa officinalis* are well described by the presented models (1), (2), (3) and (16) (Tables 1–4). The consistency of the calculated and measured data makes it possible to draw a conclusion about the adequacy of the studied models, which are in satisfactory coordination with each other. The check on the Student t-test of the regression coefficients showed that all the factors included in the model are significant at the 5% significance level. The parameters P_{gmax}, $\varphi_{(I_0-I_{comp})}$, R_D, I_{comp}, $I_{(50)}$ and I_K of the models of the light curves used in this study are highly significant ($p < 0.0001$). The significance level of the t-statistics of the correction coefficients γ and β (Eq. (3), as well as the 'curvature' γ_I index (Eq. (16) were predominantly within $p < 0.001$–0.05, however, in about 40% of cases, the significance of the corrective coefficient of inhibition of photosynthetic reactions by light β (Eq. (3) were only at the 10–20% level (Korsakova et al., 2018). The resulting models of light curves of photosynthesis are characterized by a high degree of determination (the values of the determination coefficients were 94–99). In this study the mathematical model which fitted the best the measured data of P_N/I curve of *Nerium oleander* and *Laurus nobilis* was the modified rectangular hyperbola model (Eq. (3), Tables 1–2) because it had the lowest SSE. The best fitted for the measured data of P_N/I curve of *Aucuba japonica* and *Melissa officinalis* under full sunlight treatment was the modified rectangular hyperbola model (Eq. (3), Tables 3–4), under moderate shade treatment was the modified nonrectangular hyperbola model (Eq. (16), Tables 3–4).One of the reasons for the better coordination of these models with the experimental data are that equations (1) and (2) have constant values of internal convexity ('curvature'), so they are not as universal as equations (3) and (16) , with a variable parameter of the value of internal convexity ('curvature').

The parameter γ_I in Eq. (16) can take any value from 0 to 1 (Zvalinsky, 2006) so that it can be used to describe light curves of any curvature that have the same initial slope angle and maximum saturation level. At $\gamma_I = 0.0$, Eq. (16) becomes the equation of the rectangular hyperbola of Michaelis-Menten (Eq. (1)), and as the parameter increases to $\gamma_I \approx 0.999$ – the equation goes to the Blackman's broken line. The intermediate position is occupied by the function of the exponent ($\gamma_I \approx 0.8$) and the hyperbolic tangent ($\gamma_I \approx 0.95$) – Eq. (2) (Zvalinsky, 2006). The parameter γ_I has a clear biological meaning – the relative limitation of reactions beyond the limits of the substrate cycle. The high value of the parameter γ_I ($\gamma_I \approx 0.95$) means that the relative resistance of the substrate cycle (photochemical reactions of photosynthesis) is about 20 times lower (and the rate of these reactions is correspondingly 20 times higher) compared with the total resistance of reactions outside the substrate cycle (i.e. the dark reactions of photosynthesis and the 'processing' reactions) (Zvalinsky, 2008).

The modified Michaelis-Menten model (Eq. (1) with low internal convexity shows a relatively rapid decrease in the slope of the curve with increasing of I, which indicates a more gradual transition from light limitation to saturation, and leads to higher values of P_{gmax} and $\varphi_{(I)}$ in comparison with other models and initial data (Tables 1–4). The

models with low internal convexity have a very short quasilinear section and tend to give high values of $\varphi_{(I)}$ in the case when the initial data does show high convexity (Henley, 1993). The average value of the parameter P_{gmax} (Tables 1–4), found by Eq. (1), is the highest in comparison with other models, and by 7–10% higher than in accordance with Eq. (2).

One of the oldest and most used in the description of light dependencies is the parameter of saturating light intensity I_K (substrate light constant) which is equal to the value of light intensity at the intersection of the maximum photosynthetic rate and the line found by extrapolating the initial slope of the light curve. The parameter $I_K = P_{gmax}/\varphi_{(I_0)}$was empirically introduced by J.F. Talling (Talling, 1957). The magnitude of the parameter I_K characterizes the light conditions, when photosynthesis is limited by the dark reactions under which the protective mechanisms begin to act, and can be used to evaluate the adaptive properties of the species (Gaevsky et al., 2012). The adaptation of the photophysical and photochemical stages to changes in the light regime determines the nature of the dark reactions of photosynthesis. A low I_K often indicates an ineffective use of the PAR, rather than an effective low utilization, and vice versa (Henley, 1993).

It should be noted that when using various functions in the description of light curves, the ratio between the value of the photosynthetic rate P_{gIk} at the point I_K and the maximum P_{gmax}will be different. When using an equation with a constant value of internal convexity ('curvature'), the ratio P_{gIk}/P_{gmax} (the mass fraction of light saturation of photosynthesis) is *const*. For example, when describing the P_N/I dependence by the Michaelis–Menten rectangular hyperbola function, the P_{gIk} rate will always reach 50% of the P_{gmax} ($P_{gIk}/P_{gmax} = 0.50$) at the I_K point, and if the hyperbolic tangent is $P_{gIk}/P_{gmax} = 0.76$ or 76% from P_{gmax} (see Tables 1–4). When using models with a variable parameter, the values of internal convexity ('curvature'), for example, in our studies this Eq. ((3) and (16), the ratio P_{gIk}/P_{gmax} is not constant, but can vary in the range from 0.50 to 1.00 (Tables 1–4).

In connection with the fact that a significant increase in photosynthesis is observed above I_K (Tables 1–4), quantitative equating I_K to light saturation is not justified. At the same time, this indicator actually approximately corresponds to light saturation, since it qualitatively determines the transition region from electron transfer control to carbon assimilation control (Henley, 1993).

In the proposed mathematical models, the main one is that P_{gmax} is the maximum specific rate of photosynthesis at the 'optimal' light intensity (below the level of irradiance when photoinhibition starts) (Zvalinsky, 2006). However, it should be taken into account that when describing the P_N/I dependence by the mathematical model of the hyperbola without taking into account the photoinhibition condition (Eqs (1) and (16), the P_{gmax} is the asymptote of the hyperbola as $I \to \infty$. In this case, the parameter P_{gmax} cannot be used as an independent variable to determine the maximum potential of photosynthetic species, since it does not exist in real life (Lobo et al., 2013a). In order to overcome the difficulty, a number of investigators suggested that the light saturation constant I_{sat} must be determined at a photosynthetic rate equal to 50% ($I_{sat(50)}$), 90% ($I_{sat(90)}$), 95% $I_{sat(95)}$ and 99% ($I_{sat(99)}$) from P_{gmax} or P_{Nmax} (Kaibeyainen, 2009; Greer & Weedon, 2012; Lobo et al., 2013a). The maximum possible amount of the

photosynthetic active radiation reaching the Earth's surface is about 2,435 μmol photons m^{-2} s^{-1} (Jones et al., 2003) or slightly higher due to scattered radiation, which can increase this value. At higher altitudes, in connection with the tenuous air, higher values of the PAR can be observed. It is obvious that the values of I_{sat} above these maximum limits do not have a realistic eco-physiological meaning. From the statistical indices given in Tables 1–4, it can be seen that the values $I_{sat(95)}$, obtained from equations (1) and (16) were higher than the maximum theoretically possible value that can reach Earth's surface or were are out of the range employed to obtain the measurements.

Comparatively good comparability both with the results of measurements and with the results of calculations using the models (1), (2), (3) and (16), showed the maximum values of the parameter of saturating P_N at the light intensity of I_{max} – a point beyond which there is no significant changes in the net photosynthetic rate under the given conditions (Tables 1–4). A light-saturated rate of net photosynthesis ($P_{N(Imax)}$) was found for this point. The results are consistent with the conclusion of F.A. Lobo (Lobo et al., 2013a) that I_{max} and $P_{N(Imax)}$ more realistically represent the photosynthetic potential of a plant, their interpretation is immediate and obvious, since their values are always within the range of measurements.

The results of the studies given in Tables 1–4 show that the values of P_{gmax}, calculated using the modified Michaelis-Menten model (1), are on average 12–22% higher than using models (2), (3), and (16) and 15% higher than in the experimental data. Using the hyperbolic tangent model (model (2), this indicator, in comparison with other models, was on average 3–18% lower and 6% lower than the measured values.

The values of the visible quantum yield of photosynthesis $\varphi_{(I_{comp})}$ and dark respiration R_D, calculated from the model (1), compared to other models, were higher by an average of 18–60% and 5–15%, respectively, and calculated according to the model (2) – lower by 15–38% and 3–13%, respectively.

In comparison with the initial data, the average values of the parameters R_D and I_{max}, found from the function (1), exceeded the values measured in the experiments by 8% and 28%, respectively, and those calculated by the function (2), on the contrary, understated them by 65 and 19%, respectively. The position of the light compensation point I_{comp} on the light curve when using the model with low internal convexity (Michaelis-Menten model, Eq. (1), as a rule, was shifted to a lower irradiance field in comparison with the measured values by an average of 7%, and when using models with high internal convexity (hyperbolic tangent model, Eq. (2) – in the area of higher irradiance, on average by 20–30%. The difference between the values of this parameter, using Eq. (1) and Eq. 2), reached 30–40%.

One of the reasons for such discrepancies, both with the results of measurements and with the results of calculations for other models, is the variability of the real values of internal convexity ('curvature'), which is assumed constant in models (1) and (2).

Approximate values of the parameters $P_{gmax}, \varphi_{(I_{comp})}, I_{comp}, R_D, I_{max}$ were obtained in the calculations using model equations (3) and (16). Their values on average did not differ by more than 5–13%. The average values of the photosynthetic indices, calculated using these model equations, in comparison with the values measured in the experiments, did not differ by more than 1–14% on average (Tables 1–4).

Table 1. Results fitted by four models P_N/I curve and measured data in *Nerium oleander* L. seedlings under different light conditions

Parameters	P_N/I models				Measured
	(1)	(2)	(3)	(16)	value
P_{gmax}	15.6 ± 2.7	13.6 ± 2.4	14.1 ± 2.6	14.4 ± 2.0	14.7 ± 2.7
(μmol CO_2 m^{-2} s^{-1})	12.8 ± 1.3	11.1 ± 0.9	11.5 ± 0.9	12.2 ± 1.2	12.3 ± 1.3
$\varphi_{(I_0)}$	0.10 ± 0.02	0.05 ± 0.01	0.08 ± 0.01	0.06 ± 0.01	
(μmol CO_2 μmol $photons^{-1}$)	0.13 ± 0.02	0.07 ± 0.01	0.11 ± 0.01	0.10 ± 0.02	
$\varphi_{(I_{comp})}$	0.08 ± 0.02	0.05 ± 0.01	0.06 ± 0.01	0.05 ± 0.01	
(μmol CO_2 μmol $photons^{-1}$)	0.11 ± 0.03	0.07 ± 0.01	0.10 ± 0.02	0.09 ± 0.02	
$\varphi_{(I_0-I_{comp})}$			0.07 ± 0.01		
(μmol CO_2 μmol $photons^{-1}$)			0.10 ± 0.02		
R_D	1.7 ± 0.2	1.6 ± 0.2	1.6 ± 0.1	1.6 ± 0.1	1.6 ± 0.1
(μmol CO_2 m^{-2} s^{-1})	0.9 ± 0.3	0.7 ± 0.3	0.8 ± 0.3	0.8 ± 0.3	0.8 ± 0.2
I_{comp}	20.3 ± 2.1	31.2 ± 2.5	23.6 ± 1.4	26.5 ± 3.4	23.3 ± 5.6
(μmol photons m^{-2} s^{-1})	7.9 ± 3.9	11.6 ± 5.8	8.6 ± 4.1	9.6 ± 4.8	5.8 ± 1.8
$I_{(50)}$	165 ± 7				
(μmol photons m^{-2} s^{-1})	100 ± 6				
I_K	165 ± 7	269 ± 14	163 ± 13	253 ± 43	
(μmol photons m^{-2} s^{-1})	100 ± 6	164 ± 15	101 ± 1	128 ± 11	
I_{sat}			1,387 ± 214		880 ± 27
(μmol photons m^{-2} s^{-1})			918 ± 309		440 ± 10
β			0.0002 ± 0.0001		
(m^2 s μmol $photons^{-1}$)			0.0002 ± 0.0001		
γ			0.004 ± 0.001		
(m^2 s μmol $photons^{-1}$)			0.007 ± 0.001		
γ_I				0.71 ± 0.17	
				0.55 ± 0.01	
P_{gIk}	7.82 ± 1.33	10.36 ± 1.85	8.07 ± 1.75	9.95 ± 2.69	
(μmol CO_2 m^{-2} s^{-1})	6.40 ± 0.66	8.45 ± 0.66	6.48 ± 0.69	7.28 ± 0.65	
P_{gIk}/P_{gmax}	0.50 ± 0.00	0.76 ± 0.00	0.57 ± 0.02	0.68 ± 0.08	
	0.50 ± 0.00	0.76 ± 0.00	0.56 ± 0.02	0.60 ± 0.01	
$I_{sat(95)}$	2,815 ± 94[1]	509 ± 25	782 ± 72	1,600 ± 611	
(μmol photons m^{-2} s^{-1})	1,773 ± 52	306 ± 31	488 ± 126	1,249 ± 121	
I_{max}	958 ± 34	617 ± 15	845 ± 21	756 ± 59	
(μmol photons m^{-2} s^{-1})	661 ± 87	403 ± 1	540 ± 24	541 ± 84	
$P_{N(Imax)}$	15.2 ± 2.8	11.9 ± 2.4	12.2 ± 2.8	11.6 ± 2.3	13.1 ± 2.6
(μmol CO_2 m^{-2} s^{-1})	12.0 ± 1.1	10.0 ± 1.4	10.5 ± 1.2	10.0 ± 1.6	11.5 ± 1.5
SSE	22.4 ± 26.4	16.9 ± 16.9	15.4 ± 17.8	15.8 ± 18.3	
	28.8 ± 10.4	31.6 ± 9.2	25.1 ± 7.6	27.3 ± 9.8	

Designation: in the numerator – in the field under light treatments: full sunlight; in denominator – in greenhouse under light treatments: moderate shading; P_{gmax}– maximum gross photosynthetic rate; $\varphi_{(I_0)}, \varphi_{(I_{comp})}, \varphi_{(I_0-I_{comp})}$ – quantum yield of photosynthesis for different light intensities; R_D – dark respiration rate; I_{comp} – light compensation point; $I_{(50)}$ – point of light saturation for $P_N + R_D$, equal (50%) from P_{gmax}; I_k – light constant; I_{sat} – light saturation point; β *and* γ – coefficients; γ_I – convexity factor, P_{gIk}– gross photosynthetic rate at the point I_K; P_{gIk}/P_{gmax} – relative saturation of photosynthesis at the point I_K; $I_{sat(95)}$ – light saturation point for photosynthetic rate of $P_N + R_D$, equals to 95% of P_{Nmax}; I_{max} – light saturation point beyond which there is no significant increase in P_N; $P_{N(Imax)}$ – maximum net photosynthetic rate, calculated and measured at $I = I_{max}$; SSE – error sum of squares; 1 – Isat(n) estimates derived from Eqs. are higher than the maximum theoretical value that can reach Earth's surface; ± – standard deviation.

Table 2. Results fitted by four models P_N/I curve and measured data in *Laurus nobilis* L. seedlings under different light conditions

Parameters	P_N/I models				Measured value
	(1)	(2)	(3)	(16)	
P_{gmax}	10.1 ± 0.8	8.5 ± 0.7	8.7 ± 0.8	9.6 ± 0.9	9.2 ± 0.5
(μmol CO_2 m^{-2} s^{-1})	11.2 ± 0.6	8.5 ± 0.6	8.7 ± 0.5	9.8 ± 0.9	9.3 ± 0.6
$\varphi_{(I_0)}$	0.05 ± 0.01	0.03 ± 0.01	0.04 ± 0.01	0.04 ± 0.01	
(μmol CO_2 μmol photons^{-1})	0.09 ± 0.01	0.06 ± 0.01	0.08 ± 0.01	0.07 ± 0.01	
$\varphi_{(I_{comp})}$	0.05 ± 0.01	0.03 ± 0.01	0.04 ± 0.01	0.04 ± 0.01	
(μmol CO_2 μmol photons^{-1})	0.09 ± 0.01	0.06 ± 0.01	0.08 ± 0.01	0.07 ± 0.01	
$\varphi_{(I_{0-}I_{comp})}$			0.04 ± 0.01		
(μmol CO_2 μmol photons^{-1})			0.08 ± 0.01		
R_D	0.8 ± 0.4	0.7 ± 0.3	0.7 ± 0.3	0.7 ± 0.4	0.6 ± 0.2
(μmol CO_2 m^{-2} s^{-1})	0.4 ± 0.1	0.3 ± 0.1	0.4 ± 0.1	0.4 ± 0.1	0.4 ± 0.1
I_{comp}	16.5 ± 9.2	25.1 ± 13.5	19.0 ± 10.7	19.5 ± 10.2	16.3 ± 5.1
(μmol photons m^{-2} s^{-1})	4.6 ± 0.6	5.5 ± 0.7	4.9 ± 0.6	5.2 ± 0.7	5.9 ± 0.6
$I_{(50)}$	197 ± 29				
(μmol photons m^{-2} s^{-1})	122 ± 13				
I_K	197 ± 29	295 ± 46	201 ± 33	234 ± 30	
(μmol photons m^{-2} s^{-1})	122 ± 13	150 ± 21	111 ± 10	140 ± 14	
I_{sat}			1,190 ± 206		737 ± 16
(μmol photons m^{-2} s^{-1})			493 ± 73		343 ± 78
β			0.0002 ±		
(m^2 s μmol photons^{-1})			0.0001		
			0.0005 ±		
			0.0001		
γ			0.003 ± 0.001		
(m^2 s μmol photons^{-1})			0.005 ± 0.001		
γ_I				0.50 ± 0.10	
				0.64 ± 0.09	
P_{gIk}	5.06 ± 0.42	6.48 ± 0.56	5.10 ± 0.47	5.62 ± 0.50	5.06 ± 0.42
(μmol CO_2 m^{-2} s^{-1})	5.62 ± 0.28	6.51 ± 0.43	5.35 ± 0.30	6.17 ± 0.24	5.62 ± 0.28
P_{gIk}/P_{gmax}	0.50 ± 0.00	0.76 ± 0.00	0.59 ± 0.01	0.59 ± 0.02	0.50 ± 0.00
	0.50 ± 0.00	0.76 ± 0.00	0.61 ± 0.01	0.63 ± 0.03	0.50 ± 0.00
$I_{sat(95)}$	3,457 ± 406[1]	554 ± 92	719 ± 104	2,466 ± 639[1]	
(μmol photons m^{-2} s^{-1})	2,224 ± 240[2]	278 ± 38	319 ± 45	1,105 ± 324	
I_{max}	826 ± 85	618 ± 82	750 ± 95	741 ± 90	
(μmol photons m^{-2} s^{-1})	730 ± 51	381 ± 43	438 ± 54	549 ± 87	
$P_{N(Imax)}$	8.9 ± 1.0	7.5 ± 0.4	7.6 ± 0.4	7.4 ± 0.4	7.0 ± 0.4
(μmol CO_2 m^{-2} s^{-1})	10.0 ± 0.4	8.1 ± 0.6	8.3 ± 0.6	8.5 ± 0.7	8.9 ± 0.4
SSE	7.2 ± 2.5	8.7 ± 3.3	6.1 ± 2.1	6.9 ± 2.4	
	9.6 ± 1.1	9.6 ± 0.6	8.7 ± 0.9	8.8 ± 0.8	

Designation: in the numerator – in the field under light treatments: full sunlight; in denominator – in greenhouse under light treatments: moderate shading; P_{gmax}– maximum gross photosynthetic rate; $\varphi_{(I_0)}, \varphi_{(I_{comp})}, \varphi_{(I_{0-}I_{comp})}$ – quantum yield of photosynthesis for different light intensities; R_D – dark respiration rate; I_{comp}– light compensation point; $I_{(50)}$ – point of light saturation for $P_N + R_D$, equal (50%) from P_{gmax}; I_k – light constant; I_{sat} – light saturation point; β *and* γ – coefficients; γ_I – convexity factor, P_{gIk}– gross photosynthetic rate at the point I_K; P_{gIk}/P_{gmax} – relative saturation of photosynthesis at the point I_K; $I_{sat(95)}$ – light saturation point for photosynthetic rate of $P_N + R_D$, equals to 95% of P_{Nmax}; I_{max} – light saturation point beyond which there is no significant increase in P_N; $P_{N(Imax)}$ – maximum net photosynthetic rate, calculated and measured at $I = I_{max}$; SSE – error sum of squares; [1] – Isat(n) estimates derived from Eqs. are higher than maximum theoretical value that can reach Earth's surface; [2] – estimates of Isat(n) derived from Eqs. are out of range employed to obtain the measurements; ± – standard deviation.

Table 3. Results fitted by four models P_N/I curve and measured data in *Aucuba japonica* Thunb. seedlings under different light conditions

Parameters	P_N/I models				Measured
	(1)	(2)	(3)	(16)	value
P_{gmax}	8.7 ± 0.4	7.5 ± 0.5	7.8 ± 0.5	8.3 ± 0.4	8.2 ± 0.3
(μmol CO_2 m^{-2} s^{-1})	5.9 ± 0.1	4.7 ± 0.1	4.9 ± 0.1	5.3 ± 0.1	6.3 ± 1.2
$\varphi_{(I_0)}$	0.07 ± 0.01	0.04 ± 0.01	0.07 ± 0.01	0.06 ± 0.01	
(μmol CO_2 μmol photons^{-1})	0.09 ± 0.01	0.05 ± 0.01	0.07 ± 0.01	0.06 ± 0.01	
$\varphi_{(I_{comp})}$	0.06 ± 0.01	0.04 ± 0.01	0.06 ± 0.01	0.05 ± 0.01	
(μmol CO_2 μmol photons^{-1})	0.08 ± 0.01	0.05 ± 0.01	0.07 ± 0.01	0.06 ± 0.01	
$\varphi_{(I_0-I_{comp})}$			0.06 ± 0.01		
(μmol CO_2 μmol photons^{-1})			0.07 ± 0.01		
R_D	0.8 ± 0.1	0.7 ± 0.1	0.8 ± 0.1	0.8 ± 0.1	0.8 ± 0.1
(μmol CO_2 m^{-2} s^{-1})	0.3 ± 0.1	0.3 ± 0.1	0.3 ± 0.1	0.3 ± 0.1	0.3 ± 0.1
I_{comp}	12.1 ± 1.5	19.6 ± 2.3	13.3 ± 1.7	15.1 ± 2.00	12.6 ± 3.4
(μmol photons m^{-2} s^{-1})	4.3 ± 0.3	6.0 ± 0.5	4.8 ± 0.4	5.2 ± 0.3	6.0 ± 0.7
$I_{(50)}$	119 ± 4				
(μmol photons m^{-2} s^{-1})	71 ± 5				
I_K	119 ± 4	199 ± 11	119 ± 6	152 ± 6	
(μmol photons m^{-2} s^{-1})	71 ± 5	95 ± 8	67 ± 6	83 ± 6	
I_{sat}			1,283 ± 187		685 ± 93
(μmol photons m^{-2} s^{-1})			402 ± 47		270 ± 20
β			0.0001 ± 0.0001		
(m^2 s μmol photons^{-1})			0.0005 ± 0.0001		
γ			0.007 ± 0.001		
(m^2 s μmol photons^{-1})			0.010 ± 0.002		
γ_I				0.50 ± 0.03	
				0.64 ± 0.07	
P_{gIk}	4.34 ± 0.21	5.69 ± 0.36	4.28 ± 0.24	4.87 ± 0.28	
(μmol CO_2 m^{-2} s^{-1})	2.97 ± 0.02	3.58 ± 0.01	2.87 ± 0.04	3.32 ± 0.07	
P_{gIk}/P_{gmax}	0.50 ± 0.00	0.76 ± 0.00	0.55 ± 0.01	0.59 ± 0.01	
	0.50 ± 0.00	0.76 ± 0.00	0.59 ± 0.02	0.63 ± 0.02	
$I_{sat(95)}$	2,065 ± 98[2]	375 ± 21	643 ± 50	1,681 ± 62	
(μmol photons m^{-2} s^{-1})	1,266 ± 99	177 ± 15	240 ± 13	673 ± 154	
I_{max}	624 ± 10	453 ± 21	600 ± 15	572 ± 9	
(μmol photons m^{-2} s^{-1})	413 ± 14	244 ± 14	312 ± 8	323 ± 25	
$P_{N(Imax)}$	8.1 ± 0.5	6.6 ± 0.4	6.6 ± 0.3	6.4 ± 0.3	6.5 ± 0.1
(μmol CO_2 m^{-2} s^{-1})	5.4 ± 0.1	4.3 ± 0.0	4.5 ± 0.0	4.5 ± 0.0	5.6 ± 0.5
SSE	8.5 ± 3.1	10.5 ± 3.4	8.1 ± 3.2	8.2 ± 3.1	
	8.4 ± 3.3	8.4 ± 3.1	7.8 ± 3.2	7.76 ± 3.0	

Designation: in the numerator – in the field under light treatments: full sunlight; in denominator – in greenhouse under light treatments: moderate shading; P_{gmax}– maximum gross photosynthetic rate; $\varphi_{(I_0)}, \varphi_{(I_{comp})}$, $\varphi_{(I_0-I_{comp})}$ – quantum yield of photosynthesis for different light intensities; R_D – dark respiration rate; I_{comp} – light compensation point; $I_{(50)}$ – point of light saturation for $P_N + R_D$, equal (50%) from P_{gmax}; I_k – light constant; I_{sat} – light saturation point; β *and* γ – coefficients; γ_I – convexity factor, P_{gIk}– gross photosynthetic rate at the point I_K; P_{gIk}/P_{gmax} – relative saturation of photosynthesis at the point I_K; $I_{sat(95)}$ – light saturation point for photosynthetic rate of $P_N + R_D$, equals to 95% of P_{Nmax}; I_{max} – light saturation point beyond which there is no significant increase in P_N; $P_{N(Imax)}$ – maximum net photosynthetic rate, calculated and measured at $I = I_{max}$; SSE – error sum of squares; [2] – estimates of Isat(n) derived from Eqs. are out of range employed to obtain the measurements; ± – standard deviation.

Table 4. Results fitted by four models P_N/I curve and measured data in *Melissa officinalis* L. seedlings under different light conditions

Parameters	P_N/I models				Measured
	(1)	(2)	(3)	(16)	value
P_{gmax}	14.2 ± 0.3	10.9 ± 0.5	11.3 ± 0.6	11.3 ± 0.2	11.5 ± 0.2
(μmol CO_2 m^{-2} s^{-1})	10.9 ± 1.4	8.1 ± 0.7	8.2 ± 0.6	8.9 ± 0.6	9.0 ± 0.8
$\varphi_{(I_0)}$	0.06 ± 0.01	0.04 ± 0.01	0.04 ± 0.01	0.03 ± 0.01	
(μmol CO_2 μmol $photons^{-1}$)	0.07 ± 0.01	0.05 ± 0.01	0.06 ± 0.01	0.05 ± 0.01	
$\varphi_{(I_{comp})}$	0.06 ± 0.01	0.04 ± 0.01	0.04 ± 0.01	0.03 ± 0.01	
(μmol CO_2 μmol $photons^{-1}$)	0.06 ± 0.01	0.05 ± 0.01	0.06 ± 0.01	0.05 ± 0.01	
$\varphi_{(I_0-I_{comp})}$			0.04 ± 0.01		
(μmol CO_2 μmol $photons^{-1}$)			0.06 ± 0.01		
R_D	0.7 ± 0.2	0.5 ± 0.2	0.6 ± 0.1	0.5 ± 0.1	0.6 ± 0.2
(μmol CO_2 m^{-2} s^{-1})	0.4 ± 0.1	0.3 ± 0.1	0.4 ± 0.1	0.3 ± 0.1	0.4 ± 0.1
I_{comp}	11.1 ±2.0	14.8 ± 3.7	13.6 ± 3.5	15.2 ± 4.4	13.0 ± 3.3
(μmol photons m^{-2} s^{-1})	5.8 ± 0.9	6.9 ± 1.6	6.3 ± 1.3	6.9 ± 1.7	5.0 ± 1.0
$I_{(50)}$	231 ± 32				
(μmol photons m^{-2} s^{-1})	163 ± 60				
I_K	231 ± 32	304 ± 12	263 ± 22	332 ± 16	
(μmol photons m^{-2} s^{-1})	163 ± 60	188 ± 50	145 ± 48	188 ± 66	
I_{sat}			810 ± 13		723 ± 18
(μmol photons m^{-2} s^{-1})			557 ± 64		440 ± 53
β			0.0004 ± 0.0001		
(m^2 s μmol $photons^{-1}$)			0.0005 ± 0.0001		
γ			0.001 ± 0.001		
(m^2 s μmol $photons^{-1}$)			0.004 ± 0.002		
γ_I				0.90 ± 0.04	
				0.74 ± 0.12	
P_{gIk}	7.10 ± 0.14	8.26 ± 0.35	7.49 ± 0.59	8.70 ± 0.58	
(μmol CO_2 m^{-2} s^{-1})	5.46 ± 0.71	6.15 ± 0.53	5.19 ± 0.62	6.07 ± 0.83	
P_{gIk}/P_{gmax}	0.50 ± 0.00	0.76 ± 0.00	0.66 ± 0.01	0.77 ± 0.04	
	0.50 ± 0.00	0.76 ± 0.00	0.63 ± 0.04	0.68 ± 0.07	
$I_{sat(95)}$	4,195±645[1]	565±22	575±14	955±277	
(μmol photons m^{-2} s^{-1})	2,990±1,116[1]	347±93	370±47	940±210	
I_{max}	1,072 ± 61	670 ± 22	725 ± 16	680 ± 62	
(μmol photons m^{-2} s^{-1})	799 ± 171	440 ± 92	484 ± 53	530 ± 47	
$P_{N(Imax)}$	12.4 ± 0.4	10.1 ± 0.3	10.7 ± 0.5	10.0 ± 0.2	10.8±0.3
(μmol CO_2 m^{-2} s^{-1})	9.5 ± 0.9	7.6 ± 0.7	7.8 ± 0.6	7.8 ± 0.6	8.6±0.1
SSE	39.5 ± 26.4	34.9 ± 26.9	34.4 ± 25.9	35.1 ± 27.1	
	19.4 ± 5.2	19.0 ± 6.5	17.9 ± 5.4	17.8 ± 5.5	

Designation: in the numerator – in the field under light treatments: full sunlight; in denominator – in greenhouse under light treatments: moderate shading; P_{gmax}– maximum gross photosynthetic rate; $\varphi_{(I_0)}, \varphi_{(I_{comp})}$, $\varphi_{(I_0-I_{comp})}$ – quantum yield of photosynthesis for different light intensities; R_D – dark respiration rate; I_{comp} – light compensation point; $I_{(50)}$ – point of light saturation for $P_N + R_D$, equal (50%) from P_{gmax}; I_k – light constant; I_{sat} – light saturation point; β *and* γ – coefficients; γ_I – convexity factor, P_{gIk}– gross photosynthetic rate at the point I_K; P_{gIk}/P_{gmax} – relative saturation of photosynthesis at the point I_K; $I_{sat(95)}$ – light saturation point for photosynthetic rate of $P_N + R_D$, equals to 95% of P_{Nmax}; I_{max} – light saturation point beyond which there is no significant increase in P_N; $P_{N(Imax)}$ – maximum net photosynthetic rate, calculated and measured at $I = I_{max}$; SSE – error sum of squares; [1] – Isat(n) estimates derived from Eqs. are higher than the maximum theoretical value that can reach Earth's surface; ± – standard deviation.

The parameters of the P_N/I curve, obtained with the use of model Eqs (3) and (16) with a sufficient accuracy for practical purposes, correspond with each other and with direct measurements, and they can be used as a basis for calculating the dependence of photosynthetic rate on the light intensity for these species of evergreen plants. The proposed models have a high degree of adequacy to real P_N/I dependencies, however, it should noticed that any model calculations grade a number of possible specific deviations, associated with the conditions of plant development or a sudden change in environmental conditions.

Fig. 2 shows the change in the quantum yield of photosynthesis of $\varphi_{(I)}$ in *Nerium oleander*, *Laurus nobilis*, *Aucuba japonica* and *Melissa officinalis*, depending on the photosynthetic photon flux density I under full sunlight (A) and moderate shading (B). $\varphi_{(I)}$ is calculated as a derivative of light curves models: model Eq. (1) – 1A, 1B; model Eq. (2) – 2A, 2B; the model Eq. (3) – 3A, 3B, and the model Eq. (16) – 16A, 16B. With increasing light intensity, the quantum yield decreased and reached zero at the point of light saturation. Comparison of the results of the calculations, presented in the Fig. 2, showed that at low intensities of I in the evaluated models, the values of $\varphi_{(I)}$ differ more than twofold (for example, 1AB and 2AB). Therefore, the search for the most accurate model becomes fundamentally important for the interpretation of all information. When evaluating the quantum yield, it should be taken into account that the values of $\varphi_{(I_0)}$ and $\varphi_{(I_{0-I_{comp}})}$, representing the 'maximum quantum yield', do not correspond to the original concept of this parameter, since photosynthesis is impossible in the dark. First of all, it is important to understand that $\varphi_{(I_0)}$ is the derivative of the model, when I equals zero. Secondly, nonlinear models do not have a 'linear section' in the literal sense of the word, so these sections can not be correctly inscribed in curvilinear dependencies, which in most cases are P_N/I dependencies. In this case, it is quite obvious that $\varphi_{(I_0)}$ is always the maximum value of the quantum yield, higher than any other point on the P_N/I curve. However, the $\varphi_{(I_0)}$ does not have a realistic value in terms of plant ecophysiology, since positive net assimilation in total darkness is impossible.

At the same time, the maximum visible quantum yield is the most accurate way to express the effectiveness of plant use of light in photosynthesis. It shows the amount of CO_2 bound during the photosynthesis process per one photon of light energy in the plant (Falkowski & Raven, 2007). The apparent quantum yield reflects the efficiency of the photosynthetic mechanism and affects the rate of photosynthesis, mainly at low and medium light intensities (Golovko, 1999). Since plant growth occurs most often under light that does not reach photosynthetic saturations, the magnitude of the apparent quantum yield can determine the rate of their primary production.

The magnitude of the visible quantum yield of photosynthesis is not constant, but varies depending on the conditions under which photosynthesis takes place. However, it is important to note that the relationship between the absorbed light and the O_2 release may differ from the ratio between the absorption of light and the absorption of CO_2. For ecophysiological purposes, it is preferable to use the term 'apparent quantum yield', since it does not use the light absorbed by the leaves, but the incident light, and no correction to eliminate the effect of photorespiration. (Singsaas et al., 2001). The maximum quantum yield appears to be better represented as the ratio of the net CO_2 evolution to the absorbed (or incident) light in the area of the P_N/I curve, where posi net

CO_2 assimilation begins (Ye, 2007). Depending on the emphasis, from the point of view of ecophysiological studies, it seems much more reasonable to use one theoretical maximum quantum yield ($\varphi_{(max)} = 0.125$) as a recommendation to determine how stress factors or specific conditions, affecting the plant, can affect the quantum yield or any other P_N/I parameter or calculated values (Golovko, 1999). This approach allows analyzing all points on the curve for ecophysiological purposes: if P_N is above the light compensation point, this means that there is net CO_2 absorption, the quantum yield values $\varphi_{(I)}$ can be analyzed not only when P_N depends on I, but also when P_N becomes increasingly independent of I. This possibility is very useful for assessing the differences in the efficiency of photosynthesis between sunny and shadow leaves, for which, not always, but often, there is no difference in $\varphi_{(I)}$ by the primary part of the P_N/I-curve. The slope of the linear portion of the light curve is primarily determined by the pigment content (Tarchevsky, 1977). In light species, the pigment content and the slope are usually at a less amount than in the shade-tolerant plants (Clayton, 1984).

Investigation of the parameters of light curves (Tables 1–4, Fig. 2) *Nerium oleander*, *Laurus nobilis*, *Aucuba japonica* and *Melissa officinalis* showed an increase in the efficiency of the use of light in moderate shade treatment, which indicates the adaptation of the photosynthetic mechanism to the growth conditions. Comparison of the dynamics of the quantum yield of photosynthesis in the irradiance range 0–100 μmol photons m^{-2} s^{-1}, in Fig. 2, letters A and B, indicates an increase in the efficiency of using low light intensities by *Nerium oleander*, *Laurus nobilis*, *Aucuba japonica*, when there is deterioration of light conditions, which indicates a high degree of adaptation of the photosynthetic mechanism of these species to moderate shading. The absence of significant changes in the effectiveness of the CO_2 exchange of *Melissa officinalis* indicates that is sun plant with low-level activity of using low light intensities. With moderate shading, the intensity of respiration in the studied plant species decreased by 1.5–2.5 times on average, which can be regarded as a direct reaction to a decrease in the formation of assimilates due to the PAR decrease.

Analysis of photosynthesis light curve of *Nerium oleander*, *Laurus nobilis*, *Aucuba japonica* and *Melissa officinalis* showed that *Nerium oleander* possessed the photosynthetic apparatus characterized by a high rate of photochemical reactions (Table 1). The average value of the light compensation center *Nerium oleander* was in the range of 20–30 μmol photons m^{-2} s^{-1} under full sunlight; the light saturation was noted at PAR of 750–900 μmol photons m^{-2} s^{-1}; the level of the dark respiration was at 1.6 μmol CO_2 m^{-2} s^{-1}, which indicates a light species. Shade-tolerant species generally have lower dark respiration rates and hence lower light compensation points (Loach, 1967), and lower light saturation points for photosynthesis than do shade-intolerant species (Pallardy, 2008). At the same time, the values of the angle of inclination of the initial section of the light curve and the parameter I_K indicate the ability of *Nerium oleander* to efficiently use light in photosynthesis in the low level of light intensities (160–250 μmol photons m^{-2} s^{-1} (Table 1).

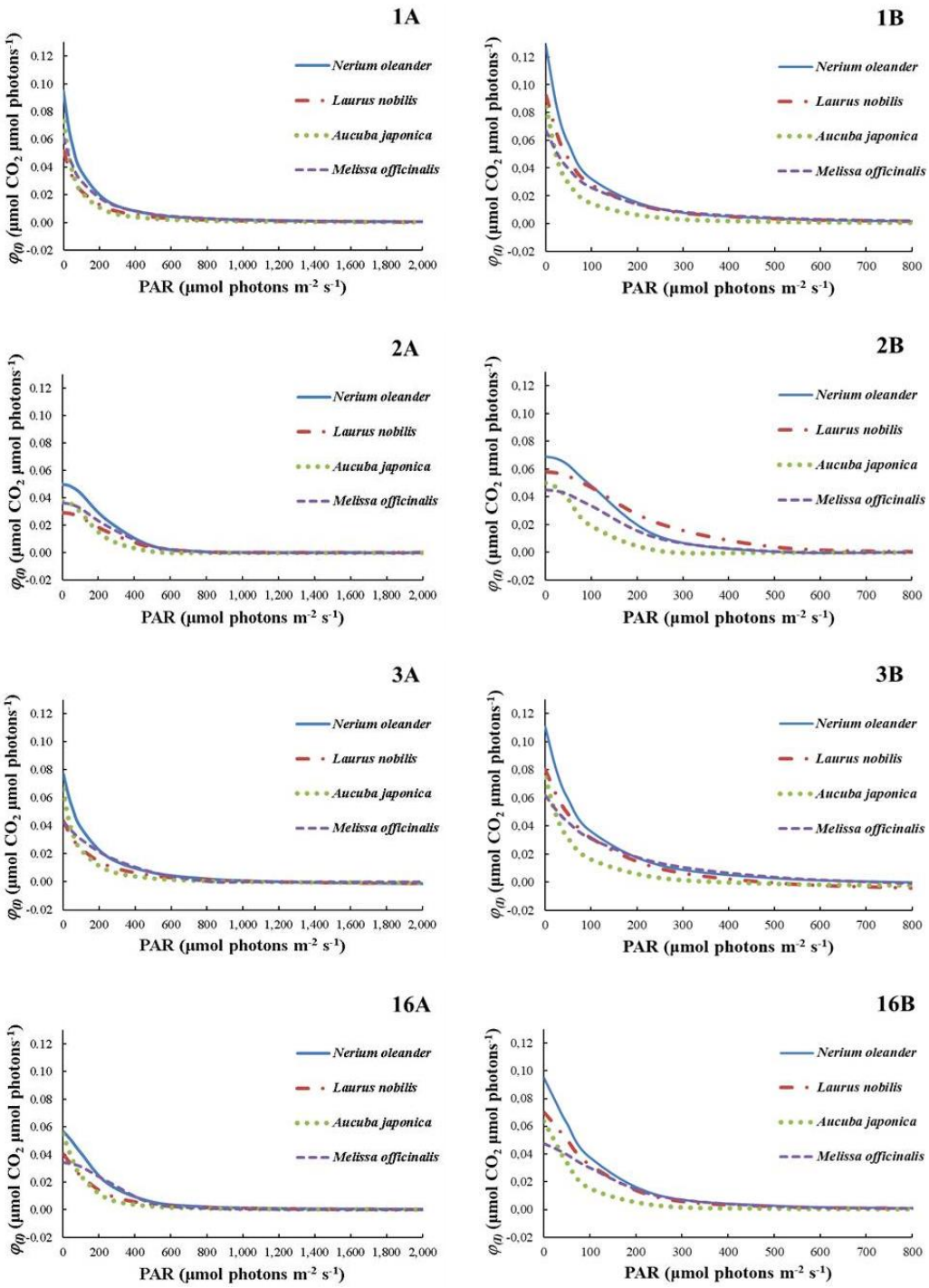

Figure 2. Dynamic curves of the quantum yield of photosynthesis) $A(\varphi_1)$ of *Nerium oleander*, *Laurus nobilis*, *Aucuba japonica* and *Melissa officinalis*: A – full sunlight; B – moderate shading; 1, 2, 3, 16 – derivatives of the corresponding models of light response curves; PAR – photosynthetically active radiation.

Moderate shading had a significant effect on the nature of the light curves of *Laurus nobilis*. With shading, the efficiency of the photosynthetic mechanism in the low values of PAR increased, which can be related to the formation of a more powerful pigment complex. The formation of the photosynthetic mechanism, adapted to shading, provided the ability of the leaves to maintain the rate of P_N not lower, but even higher than in plants under full sunlight (Table 2). Under conditions of moderate shading, the gross photosynthetic rate of leaves of P_{gIk} in the field of the light constant I_K was also higher than that of leaves under full sunlight. The intensity of the dark respiration decreased, which can be regarded as a direct reaction to a decrease in the formation of assimilates due to PAR reduction (Table 2). With moderate shading, the plants retained the intensity of growth of organic material due to an increase in the rate of photosynthesis. This was also facilitated by a slight decrease in the respiration rate of plants.

Based on the study of CO_2 exchange, it can be concluded that *Laurus nobilis* belongs to the group of light plants with well-marked signs of shadow tolerance. The presence of a flexible photosynthetic mechanism, the ability to function effectively in wide range of PAR, facilitate the adaptation of the species when growing on the Southern coast of the Crimea under conditions of intense insolation in open areas and under the canopy of plants of the first layer in conditions of predominance of diffuse radiation.

The most shade-tolerant of all the studied species was *Aucuba japonica*, which is characterized by the lowest activity of photosynthesis, a low rate of dark respiration, which most effectively uses low light intensities (Table 3, Fig. 2, A, B) both under full sunlight and under moderate shading. The light saturation of *Aucuba japonica*, in comparison with other species, occurred in weaker irradiance: under full sunlight treatment at 570–680 μmol photons m^{-2} s^{-1} PAR; under moderate shading conditions at 270–320 μmol photons m^{-2} s^{-1}. The light constant I_K in this case decreased from 119–150 to 67–83 μmol photons m^{-2} s^{-1}.

The light range that can provide the maximum of the photosynthetic intensity of *Melissa officinalis* is about 680–720 μmol photons m^{-2} s^{-1}; the light constant I_K is at 260–330 μmol photons m^{-2} s^{-1}; the slope of the initial segment of the light response curve is at 0.033–0.041 μmol CO_2 μmol photons^{-1}, which indicates its light species. Lower slope in the beginning it is a typical light response curve for a heliophytes plants (Blackman, 1905; Penning et al., 1989).

CONCLUSION

Under conditions of full sunlight and moderate shading significant differences in parameters $P_{gmax}, \varphi_{(I_{comp})}, I_{comp}, R_D, I_{max}$ were found. The average values of the indices calculated from the four model equations differed from 2 to 60%, depending on the type of the parameter, and when compared with the measured data – from 1 to 30%. Values calculated by modified Michaelis-Menten model, overestimated the measured values of photosynthetic rates by 5–15%, and according by hyperbolic tangent model – understated the values by 3–13%. The highest level of consistency between the calculated and measured data for *Nerium oleander, Laurus nobilis, Aucuba japonica* and *Melissa officinalis* was observed using modified rectangular hyperbola model able to fit the photoinhibition stage by nonrectangular hyperbola and modified form of nonrectangular hyperbolic model.

The performed calculations allowed us to conclude that when using various functions to describe the photosynthetic response on the increase in the light flux even when using the same input values, the calculated characteristics for each individual function can differ significantly not only in absolute values, but also have opposite in signs in comparison with the experimental data, while maintaining a general tendency. Considering this fact in order to avoid distortion of the results of the parameters estimation when comparing plant species with relation to the light factor or when studying that relationship in the dynamics during the growing season, it is preferable to use one most suitable function for all investigation plant species.

These results of our studies are consistent with the findings of F.A. Lobo (Lobo et al., 2013a), where the variables I_{max}, $P_{N(Imax)}$ and $\varphi_I$better reflect the saturating light intensity, the maximum absorption rate of CO_2 at light saturation and the quantum yield of photosynthesis. They represent the photosynthetic potential of plants more realistically, because their values are always in the range of measurements.

Applying of methods, using the 'Statistica' system, can be an interesting alternative for users selecting the best light response curve of photosynthesis for the experimental data and its evaluation and interpretation of the results.

This new knowledge that we gained on physiological differences in relation to the light factor, provides valuable information on the adaptation of decorative plants that are have high potential for growing in the South coast of the Crimea, due to the light environment. This knowledge is important as potential ecological and physiological characteristic of these species when creating their ecological and physiological passports.

ACKNOWLEDGEMENTS. This study was supported by a research grant № 14-50-00079 of the Russian Science Foundation and founded by ST. 0829-2019-0021 of FSFIS 'NBG-NSC'.

REFERENCES

Balaur, N.S., Vorontsov, V.A., Kleiman, E.I. & Ton, Yu.D. 2009. New technology for monitoring CO2 exchange in plants. *Physiology of plants* **56**, 466–470 (in Russian).

Balaur, N.S., Vorontsov, V.A. & Merenyuk, L.F. 2013. Features of photorespiration of photosynthetically active organs in C3 plants. *Physiology of Plants* **60**(2), 174–183 (in Russian).

Blackman, F.F. 1905. Optima and limiting factors. *Annals of Botany*. **9**, 281–295.

Bolondinsky, V.K. & Vilikainen, L.M. 2014. Investigation of the light dependence of photosynthesis in the Karelian birch and silver birch under different conditions with different elements of mineral nutrition. *Proceedings of the Karelian Research Center of the Russian Academy of Sciences* **5**, 207–213 (in Russian).

Clayton, R. 1984. *Photosynthesis. Physical Mechanisms and Chemical Models*. Mir, Moscow, 350 pp. (in Russian).

Dalke, I.V., Butkin, A.V., Tabalenkova, G.N., Malyshev, R.V., Grigorai, E.E. & Golovko, T.K. 2013. Efficiency of the use of light energy in a greenhouse salad culture. *Izvestiya Timiriazevskaya Agricultural Academy* **5**, 60–68 (in Russian).

Drozdov, S.N., Kholoptseva, E.S. & Popov, E.G. 2008. Nett photosynthesis of plants as an ecological indicator of biodiversity. In: *Fundamental and practical problems of botany in the early 21st century*. *Part 6: Ecological physiology and biochemistry of plants. Introduction of plants.* Karelian Research Center of the RAS, Petrozavodsk, pp. 47–49 (in Russian).

Falkowski, P.G. & Raven, J.A. 2007. *Aquatic Photosynthesis*. Princeton University Press, Princenton, 488 pp.

Gaevsky, N.A., Ivanova, E.A. & Dubrovskaya, M.A. 2012. Comparative evaluation of photosynthetic activity in a number of plants in Southern Siberia (Pearl Island, Republic of Khakassia). In: *Geoecological problems of steppe regions. The 6th Internacional Symposium*. IPK 'Gazprompechat' LLC 'Orenburggazpromservis', Orenburg, pp. 165–168 (in Russian).

Golovko, T.K. 1999. *Respiration of plants (physiological aspects)*. Nauka, Leningrad, 204 pp. (in Russian).

Greer, D.H. & Weedon, M.M. 2012. Modelling photosynthetic responses to temperature of grapevine (Vitis vinifera cv. Semillon) leaves on vines grown in a hot climate. *Plant, Cell and Environment*. **35**, 1050–1064.

Henley, W.J. 1993. Measurement and interpretation of photosynthetic light-response curves in algae in the context of photoinhibition and diel changes. *J. Phycol*. **29**, 729–739.

Jassby, A.D. & Platt, T. 1976. Mathematical formulation of the relationship between photosynthesis and light for phytoplankton. *Limnol. Oceanogr*. **21**, 540–547.

Jones, H.B., Archer, N., Rotenberg, E. & Casa, R. 2003. Radiation measurement for plant ecophysiology. *J. Exp. Bot*. **54**, 879–889.

Kaibeyainen, E.L. 2009. Parameters of the light response curve of photosynthesis in *Salix dasyclados* and their variation during vegetation. *Physiology of plants* **56**(4), 490–499 (in Russian).

Korsakova, S.P., Ilnitsky, O.A. & Plugatar, Yu.V. 2016. Comparative evaluation of photosynthetic activity in some evergreen ornamental plants on the Southern coast of the Crimea. In: *Biotechnology as an Instrument for Plant Biodiversity Conservation (physiological, biochemical, embryological, genetic and legal aspects). The VII International Scientific and Practical Conference*. ARIAL, Simferopol, pp. 173.

Korsakova, S.P., Ilnitsky, O.A. & Plugatar, Yu.V. 2018. Comparison of photosynthetic light-response curves models by the example of evergreen plant species. *Sc. in the south of Rus*. **14**(3), 88–100 (in Russian).

Loach, K. 1967. Shade tolerance in tree seedlings. 1. Leaf photosynthesis and respiration in plants raised under artificial shade. *New Phytol.* **66**, 607–621.

Lobo, F.A., Barros, M.P., Dalmagro, H.J., Dalmonin, Â.C., Pereira, W.E., Souza, É.C., Vourlitis, G.L. & Rodriguezortiz, C.E. 2013a. Fitting net photosynthetic light-response curves with Microsoft Excel – a critical look at the models. *Photosynthetica* **51**(3), 445–456.

Lobo, F.A., Barros, M.P., Dalmagro, H.J., Dalmonin, Â.C., Pereira, W.E., Souza, É.C., Vourlitis, G.L. & Rodriguezortiz, C.E. 2013b. Erratum to: Fitting net photosynthetic light-response curves with Microsoft Excel – a critical look at the models. *Photosynthetica* **52**(3), 479–480.

Miyazawa, S.-I. & Terashima, I. 2001. Slow Development of Leaf Photosynthesis in an Evergreen Broad-Leaved Tree, Castanopsis sieboldii: Relationships between Leaf Anatomical Characteristics and Photosynthetic Rate. *Plant Cell Environ*. **24**, 279–291.

Pallardy, S. 2008. *Physiology of Woody Plants, 3rd ed*. Academic Press (Elsevier): Burlington, MA, USA, 453 pp.

Platt, T., Denman, K.L. & Jassby, A.D. 1977. Modelling the productivity of phytoplankton. *The sea: ideas and observations of progress in the study of the seas*. *N.Y.: John Wilye & Sons*. **6**, 807–856.

Penning de Vries, F.W.T., Jansen, D.M., Ten Berge, H.F.M. & Bakema, A. 1989. *Simulation of ecophysiological processes of growth in several annual crops.* Simulation Monographs, Pudoc, Wageningen, Netherlands, 271 pp.

Singsaas, E.L., Ort, D.R. & DeLucia, E.H. 2001. Variation in Measured Values of Photosynthetic Quantum Yield in Ecophysiological Studies. *Oecologia* **128**, 15–23.

Stukach, O.V. 2011. *The program complex 'Statistica' in solving problems of quality management: a textbook*. Publishing house of Tomsk Polytechnic University, Tomsk, 163 pp. (in Russian).

Talling, J.F. 1957. Photosynthetic characteristics of some freshwater plankton diatoms in relation to underwater radiation. *New Phytol*. **56**, 29–50.

Tarchevsky, I.A. 1977. *Fundamentals of photosynthesis*. Vysshaya shkola, Moscow, 254 pp. (in Russian).

Thornley, J.H.M. 1982. *Mathematical models in plant physiology*. Naukova dumka, Kiev, 312 pp. (in Russian).

Tobias, D.J., Ikemoto, A. & Nishimura, T. 1995. Leaf Senescence Patterns and Photosynthesis in Four Leaf Flushes of Two Deciduous Oak (*Quercus*) Species. *Photosynthetica* **31**, 231–239.

Ye, Z.-P. 2007. A new model for relationship between irradiance and the rate of photosynthesis in *Oryza sativa*. *Photosynthetica* **45**(4), 637–640.

Zalensky, O.V. 1977. *Ecological and physiological aspects of the study of photosynthesis. The 37th Timiryazev reading*. Nauka, Leningrad, 57 pp. (in Russian).

Zvalinsky, V.I. 2006. Formation of primary production in the sea. *Izv. TINRO*. **147**, 277–304 (in Russian).

Zvalinsky, V.I. 2008. Quantitative description of marine ecosystems. I. General approaches. *Izv. TINRO*. **152**, 132–153 (in Russian).

Agronomy Research **17**(2), 540–550, 2019
https://doi.org/10.15159/AR.19.051

Properties of biofuel fly ash and capabilities of its use for agricultural needs

M. Kulokas[1,*], V. Zaleskas[1], N. Pedišius[1], M. Praspaliauskas[1] and K. Buinevičius[2]

[1]Lithuanian Energy Institute, Laboratory of Heat–Equipment Research and Testing, Breslaujos st. 3, LT-44403 Kaunas, Lithuania
[2]UAB 'Enerstena' Centre of Research and Development, Ateities pl. 30A, LT-52163 Kaunas, Lithuania
[*]Correspondence: kulokas@lei.lt

Abstract. The use of various types of biomass for energy production provides great prospects for reducing the consumption of fossil fuels and the negative impact on the environment. However, the use of biomass, in particular agromass for this purpose, results in relatively large amounts of bottom ashes and fly ashes, the composition and properties of which also raise a number of additional environmental problems. The composition and properties of fly ash are investigated in the paper, taking into account the possibilities of utilizing them for soil fertilization and other applications. Fly ash samples were collected from bunkers of flue gas cleaning equipment (electrostatic precipitator and cyclones) installed after water heating boilers, which are firing wood chips and chuffed straw. The composition of fly ash was determined using Inductively Coupled Plasma Optical Emission Spectrometry (ICP-OES) and Scanning Electron Microscopy with Energy Dispersive Spectroscopy (SEM/EDS) while particle size distribution was obtained using scattered-light aerosol spectrometer. Electrical Low Pressure Impactor (ELPI) was used to separate fly ash into 14 groups by particle diameter, and the analysis of their composition showed differences in the composition of the fly ash collected in cyclones and Electrostatic Precipitators (ESP). An analysis of the composition of samples in regard to the existing heavy metals norms and considering concentrations of elements beneficial to the growth of plants, enables to prepare recommendations for fertilization. The determined alkalinity of fly ash pH 13 confirms the possibility of their use for reducing soil acidity. The analysis of fly ash composition has shown that they contain elements, important for plant growth (Ca, Mg, K, P, N, S), and their concentrations determine the further use for soil quality improvement because the amount of these elements in the acid soils is reduced.

Key words: agromass, biofuel, fly ash, chemical and physical properties.

INTRODUCTION

Biomass is considered as an important renewable energy source the use of which for energy production is constantly increasing. Solid biofuels from wood or waste of agricultures (agromass) make it possible to reduce fossil fuel consumption and greenhouse gas emissions. The quality of solid biofuel, as a raw material, its composition, and the bottom and fly ash that is produced during its combustion

determines the choice of solid biofuel preparation method and the type of incinerator (Olsson et al., 2003). The main cause of concern is the relatively high amount of ash generated by the combustion of solid biofuels produced from agromass, because the chemical compounds contained in the ash causes corrosion of the boiler surfaces, and a large amount of bottom ash increases the equipment surface fouling and the boiler efficiency losses (Zbogar et al., 2009; Frandsen, 2010).

Meanwhile, fly ash particles, which are released into the atmosphere with flue gas, cause environmental pollution and are harmful to human health (Kwauk, 2003; Pui et al., 2014; Xu et al., 2014). Therefore, the constantly tightening emission standards forces to use various methods and equipment, such as cyclones, material filters, electrostatic precipitators and scrubbers, etc., for fly ash deposition. The bottom and fly ash utilization also is a growing concern. The general requirements for the management of non-hazardous waste in Lithuania establish the conditions for the management of the ash of solid biofuel boilers, under which ash can be used in forests and agriculture, for the rehabilitation of damaged areas (Republic of Lithuania... 2011). In general, further use of ash can be carried out in accordance with European Union Directives (European Council Decision 2002; Directive 2006/12/EC) and existing national requirements, which are based on them. However, the use of bottom ash and fly ash collected in flue gas cleaning equipment for forest and agricultural land improvement is only possible if it does not pose a risk to the soil and crop quality and human health (Obernberger & Supancic, 2009). Otherwise, when the maximum permissible concentrations of heavy metals in ashes are exceeded, they must be treated by various methods (e.g. Steenari et al., 1999; Pedersen et al., 2003a; Pedersen et al., 2003b; Mellbo et al., 2008) to reduce their concentrations. When ash is not suitable for fertilization because it does not contain useful elements for plant growth, it can be used in other areas, such as concrete production, road construction, bicycle paths, sidewalks, parking lots, sports grounds, etc. Finally, when the concentration of heavy metals exceeds the limit and it cannot be reduced, collected bottom and fly ash is stored in landfills as hazardous waste.

When ashes are used for fertilization it is important to consider soil acidity, as a key quality indicator, and the elements contained in it. Depending on the elemental composition of ashes which are used for soil fertilization and the acidity of the soil it is possible to increase the yield using the recommended ash rates.

The main purpose of this work is to investigate the elemental composition of the fly ash produced during the burning of wood chips and straw as two major solid biofuel types used for energy production, and to discuss their further use in fertilizing forest and agricultural soils.

MATERIALS AND METHODS

Materials of experiment

Four wood chip and two straw fired plants have been visited to collect the required material for the experiment. Fly ash samples were then taken from flue gas cleaning equipment (ESP and cyclones) bunkers (Table 1). In (A-D) wood chips burning plants, cyclones were installed before the ESP. In (E-F) plants firing straw, only cyclones were installed to clean the flue gas. Dolomite powder was used as a supplement for the straw combustion to increase the melting temperature of the ash in plant F.

Table 1. The sources of investigated wood and straw fly ashes

Biofuel/ fly ash tag	Thermal capacity, MW	Type of separator	Typical temperature of combustion chamber	Approximate composition of burnt solid biofuel	
				Wood chips from forest residue	
A	10	ESP	950 °C	> 90% wood	< 10% bark
B	10	ESP	900 °C	80% softwood and < 20% hardwood	< 10% bark
C	10	ESP	830 °C	80% softwood and < 20% hardwood wood	< 5% bark
D	10	ESP	900 °C	90% softwood and < 10% hardwood wood	< 10% bark
E	1.4	Cyclone	680 °C	Chuffed straw	
F	1.4	Cyclone	1,200 °C		

Determination of ash physico-chemical parameters

The size of the fly ash particles was measured using a scattered light particle spectrometer (Promo 3000). In addition, the size of woody biomass fly ash particles was determined using electrical low pressure impactor (ELPI), which grouped them into 14 fractions in the range of 0.006–10.0 μm during the measurement on-line.

The moisture content of the fly ash particles was determined by weight differences before and after drying (samples were dried for 1 hour at 105 °C) and the density of the test particles was determined according to EN ISO 8130-3 2011, and the bulk density according to EN ISO 60:1977. The morphology of all particles was analyzed using a S-3400N scanning electron microscope (SEM), operated at 5–15 kV accelerating voltage and the angle of repose was determined according to ISO 4324:1977. Since the microscope was equipped with the Bruker Quad 5040 X-ray spectrometer (EDS), additionally information about composition of the analyzed particles was obtained. During the measurements a fully automatic pump and valve control system was used, which provided high vacuum mode, i.e. $\leq 1.5 \times 10^{-3}$ Pa pressure in the sample chamber. The melting temperature of fly ash was determined according to the standard LST CEN/TS 15370-1 :2006 and the pH by hydrogen ion concentration in solution using an ionometer, according to standard LST EN 12176: 2000. The element analyzer (Flash 2000) was used to determine C, H, N, S composition of the solid biofuel and the elemental composition of the fly ash formed during combustion was determined by an inductively coupled plasma optical emission spectrometer (ICP-OES).

RESULTS AND DISCUSSION

The concentrations of basic elements in wood chips and straw (as solid biofuel) and their physical properties (ash content, humidity and lower calorific value) are presented in Table 2. After comparison of this data with analogous literature data (Vesterinen, 2003; Alakangas et al., 2016), a correlation has been established that allows estimating the composition of the selected solid biofuel.

After comparing the (A) and (B) elemental composition of stem without bark, bark, and wood chips from (Vesterinen, 2003; Alakangas et al., 2016) differences in the concentrations of the basic elements were determined which are within the margin of

error and confirm the presence of a stem with bark and branch. The basic elements (C, H, N, S, O and Cl) concentrations of (C) coincided with the composition of the barked stem within the error limits, whereas (D) contained some branches judging from slight differences in O, S, and Cl. Lastly, (E) concentrations of C, H, N, S, O and Cl are close to barley straw, and (F), respectively, close to wheat straw.

The average moisture content of wood chips and straw samples was determined from as received biofuel and correlates with (Alakangas et al., 2016) data. The visible difference between the average moisture content of wood chips and straw in Table 2 is due to the difference in the initial moisture content of the biomass, the difference of which remains when drying biofuel for burning. The average ash content of wood chips and straw samples is related to its composition, inorganic and other mineral substances, which predominantly forms bottom and fly ash. This result correlates with (Alakangas et al., 2016) data and confirms the need for increased researches of ash usages.

Table 2. Results of solid biofuels analysis and their physical properties

	A	B	C	D	E	F
	Composition of basic elements (% of dry basis)					
C	51.8	51.3	51	49.8	49.03	45.6
H	6.1	6.1	6	6.3	5.68	5.8
N	0.3	0.4	0.08	0.13	1.28	0.48
S	0.01	0.02	0	0.02	0.089	0.082
O	41.19	40.85	42.82	43.2	40.25	42.4
Cl	0.0042	0.0076	< 0.0050	0.005	0.069	0.19
Moisture, %	26	24	22	23	1.73	1.75
Ash content, %	1.3	1.9	1.3	2.2	3.67	3.70
NCV_0, MJ kg^{-1}	18.9	19.1	19.2	19	17.9	17.9
	Ash melting temperature					
SST, °C	1,175	1,230	1,180	1,135	896	898
DT, °C	1,225	1,240	1,210	1,165	1,042	1,040
HT, °C	1,245	1,245	1,230	1,185	1,058	1,060
FT, °C	1,260	1,290	1,245	1,205	1,081	1,080

Note: NCV_0 – lower calorific value, MJ kg^{-1}; SST – shrinkage starting temperature; DT – deformation temperature; HT – hemisphere temperature; FT – flow temperature.

Determining the concentrations of heavy metal in collected ash samples (A-F) is necessary for the use of ash in soil fertilization or other areas. Concentrations of heavy metals in wood (A-D) and straw (E-F) ash are shown in Fig. 1. The Ba and Sr, as alkaline earth metal, concentrations is an indicator of poor fuel preparation quality, because burned solid biofuel was slightly polluted with soil. Zn concentration in the (A-F) samples was: (A) – 0.34%, (B) – 1.22%, (C) – 0.77%, (D) – 2.45%, (E) – 0.02% and (F) – 0.02%. Similarly, determination of elements useful for plant vegetation was carried out in order to assess their usefulness as fertilizers in forest and agriculture (Fig. 2).

Permissible limits of heavy metal concentrations according to (Republic of Lithuania ... 2011) are exceeded for fly ash samples (A-D) and they cannot be used in forests and agriculture. On the other hand, fly ash (E-F) can be used in forest and agriculture/ rehabilitation of damaged areas, as the amount of heavy metals does not exceed specified limits. The elemental composition of fly ash (A-D) comparison with composition of fly ash of similar solid biofuel in (Vesterinen, 2003; Alakangas et al.,

2016) shows differences of heavy metals in wood parts and its fuels. Therefore heavy metal concentrations in fly ash can be reduced by proper selection of wood as solid biofuel.

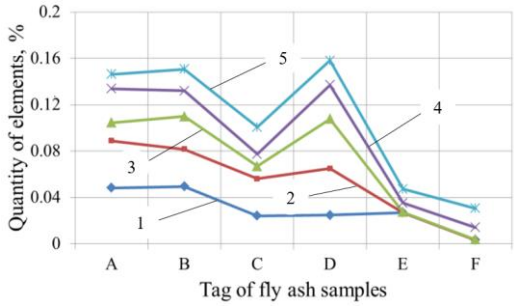

Figure 1. Quantity of heavy metals in fly ash of wood chips – (A-D) and straw – (E-F): 1 – Ba; 2 – Σ(Ba + Sr); 3 – Σ(Ba + Sr + Pb); 4 – Σ(Ba + Sr + Pb + B); 5 – Σ(Ba + Sr + Pb + B + Cu + Cr + Cd + Co + Ni + Mo + As + V + Hg).

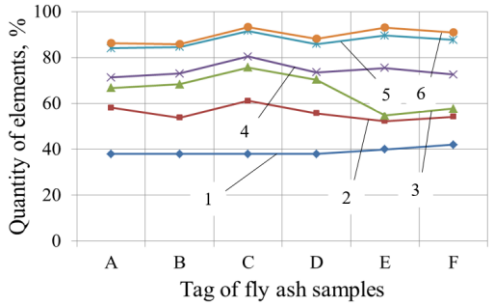

Figure 2. Quantity of elements useful for plant growth in fly ash of wood chips – (A-D) and straw – (E-F): 1 – O; 2 – Σ(O + Ca); 3 – Σ(O + Ca + Si); 4 – Σ(O + Ca + Si + K); 5 – Σ(O + Ca + Si + K + C + S + Cl + P + Mg); 6 – Σ(O + Ca + Si + K + C + S + Cl + P + Mg + B + Fe + Mn + Na + N).

The basic elements required for plant vegetation (Ca, K, Mg and P) and trace elements required for plant nutrient metabolism (B, Cu, Mn, Mo, Zn) also were determined. Concentrations of the elements B, Cu, Ni and Zn from Fig. 1 are assigned to the group of harmful elements because the concentration of these elements required for plants is very low. Other essential trace elements (N, Na, S etc.) also have been identified. Lastly, Si is considered to be a ballast element in this case, while concentration of C is useful to note, as it generally is an indicator of the quality of combustion and fly ash emissions.

On account of fly ash samples being taken from cyclone and ESP bunkers, it was important to analyse the elemental composition of particles precipitated in cyclone and ESP, since cyclones precipitate largely only coarse particles, whereas only small part of the fine particles pass ESP. This analysis could be performed only for fly ash of burnt wood chips since the cyclone was used as the only flue gas cleaning device for the precipitation of straw fly ash, and comparison by elemental composition of wood fly ash is only approximate due to difference on particle size and elemental composition.

The research of the elemental composition and physical properties of fly ash from a wood burning boiler was carried out by using ELPI and EDS for samples of fly ash collected in the cyclone and ESP bunkers (Fig. 3). Elemental composition studies of 14 ash fractions from ELPI have shown that the main constituents of the particles are O, Ca, K, S, Zn, Mg and P, therefore main compounds are Ca and K oxides and sulphates comprising 83–91% of the samples. In addition, 2.4–4.0% of Zn in fly ash from ESP, and 2.4–2.7% of Mg in fly ash from cyclone and 3.4–6.8% of C, i.e. soot, in all fly ash samples were identified. When using EDS on fly ash particles of > 1 μm diameter, concentration of main elements (Ca and K) and additional elements (Mg, Mn, P, S, and Na) was found (Fig. 3). This result can be explained by the natural small and large particles agglomeration in the turbulent flow. Therefore in this case, the sample of the

fine particles of ESP had to have a higher concentration than that measured by ELPI and much more than in the cyclone sample.

A normalized distribution of the mass concentration of particulate matter from the ESP and the cyclone by particle size is provided in Fig. 4, with an obvious difference between ESP and cyclone precipitated particles. When comparing the distribution of the main elements in the fractions of different size particles, the largest elemental composition changes (Fig. 5) can be seen between 0.25–0.38 μm and 0.6–0.94 μm, because it is transition from fine particle mode of its characteristic composition to coarse particle mode, where particle composition depending on the particle size changes more uniformly.

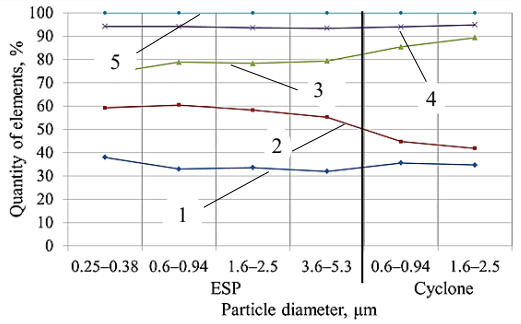

Figure 3. Elemental composition of fly ash samples collected from ESP and cyclone bunker: 1 – O; 2 – Σ(O + K); 3 – Σ(O + K + Ca); 4 – Σ(O + K + Ca + S + C + Zn); 5 – Σ(O + K + Ca + S + C + Zn + Mg + P + Fe + Cl + Mn + Al + Na + Si).

This composition dependence on the particle size is shown in Fig. 5, where element concentrations normalized to the average of the four particle size fractions. There is a consistent increase in Ca, O and S with increasing particle diameter and significant decreases in C and Zn concentrations throughout the range (Fig. 5). Concentration of K in the 0.25–0.38 μm range was lower than in the 0.6–0.94 μm range but from there on continued to decrease steadily. In contrast, Fe concentration slope was reversed: it was lower between 0.6 and 0.94 μm and then continued to increase steadily. Concentration of Mg in the entire range of 0.6–5.3 μm varied slightly and was higher than the concentration in 0.25–0.38 μm particles. The results from Fig. 4 and Fig. 5 correlates to (Lanzerstorfer, 2015) because concentration of Ca and Mg are increasing while K concentration decreasing in the particle size range from 1 μm to 40 μm correlates with the same element concentration variations which have been determined from 1 μm to 4.5 μm.

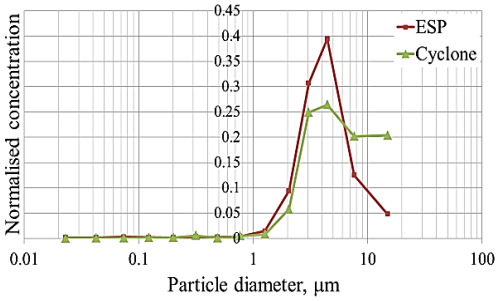

Figure 4. Normalized particle mass size distribution.

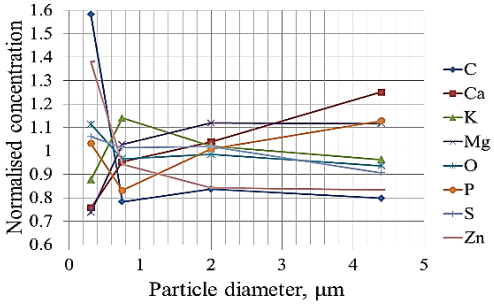

Figure 5. Normalized particle elemental concentration distribution by individual element average.

SEM clearly shows the differences in the particle sizes of the analyzed samples between the different ELPI fraction samples (Fig. 6 (a) and (b)). For many particles that can be clearly distinguished, the measured diameter value corresponds to the particle size range of the individual ELPI fractions (Fig. 6(a) and (c)). From SEM pictures (Fig. 6 (a) and (b)) and Fig. 5 it is obvious that the use of such ashes in the soil will include elements useful for plants (B, Cu, Mn, Mo, Zn) and all heavy metals (As, Cd, Cr, Hg, Ni, Pb) contained in fine particles. Therefore appropriate preparation and spread of either unstabilized or stabilized ash depending on the pH of the soil, the amount of elements in the soil useful for plant vegetation and the ongoing processes is important. This is because unstabilized ash elements get into the soil faster, and stabilized ash elements are washed more slowly, but there is no research on particle size influence on soil and plant element absorption.

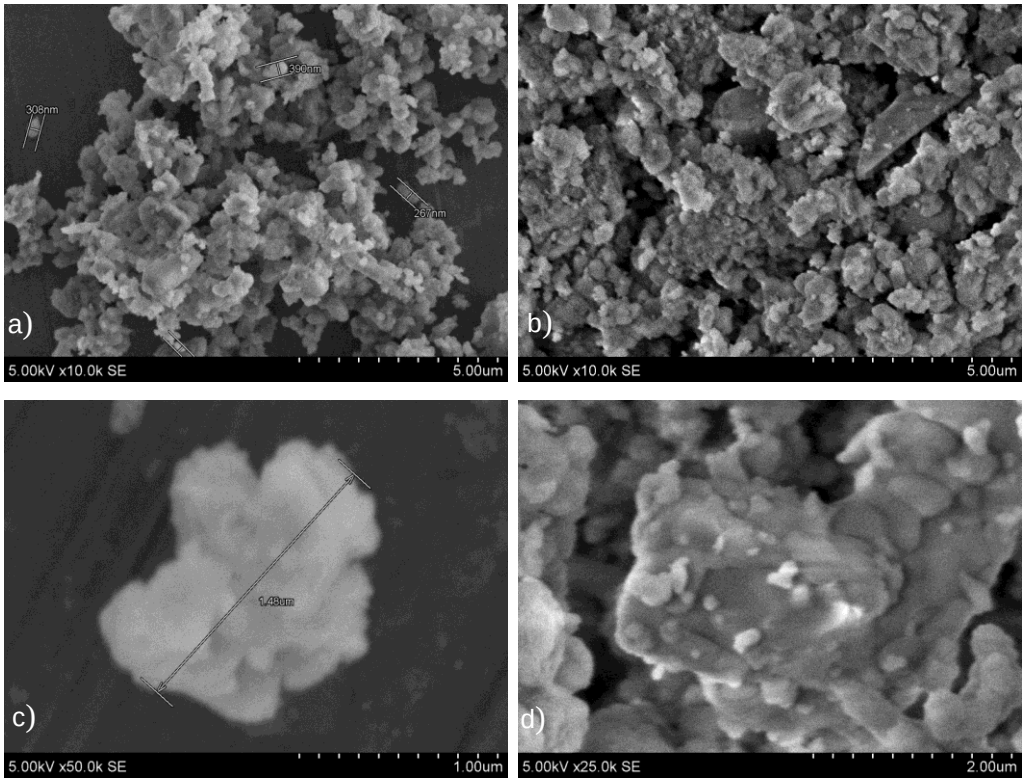

Figure 6.SEM images of particle size distributions from source A: a) 0.25–0.38 μm, 10,000x; b) 3.6–5.3 μm, 10,000x; c),1.6–2.5, μm, 50,000x; d),1.6–2.5, μm, 25,000x.

The physical properties of dry fly ash samples (A-F) (Table 3), as well as the elemental composition previously established, are important for determining additional requirements for combustion equipment, storage tanks, soil fertilization and other areas. Therefore, in this case, it is important to know the sample pH, particle size distribution, density of particles and bulk density of the samples.

Table 3. Physical properties of fly ash

Parameter	Fly ash					
	A	B	C	D	E	F
pH	12.9	12.5	13.1	12.8	13.3	13.3
Mass median diameter d_{50} (μm)	3.1	3.2	5.2	4.8	4.0	1.6
Spread of the size distribution	3.5	4.0	3.5	3.8	4.0	3.6
Density (kg m^{-3})	1,934	1,988	1,937	1,938	1,959	1,960
Bulk density (kg m^{-3})	160	100	140	130	320	290
Voidage	0.74	0,96	0.95	0.95	0.86	0.88
Angle of repose (degree)	50	49	49	50	50	43

The average pH of the fly ash was the same for the (A-D) and (E-F) samples. Meanwhile, the average mass distribution of (A-D) fly ash particles was 4.1 ± 0.8 μm and in the case of (E-F) it was 2.8 ± 0.8 μm. The mean particle size distribution of (A-D) fly ash was 3.7 ± 25 and 3.8 ± 25 for (E-F). (D-E) fly ash particles has a similar mass distribution, but the distribution of particle size (F) is twice as large as (D). The wide particle size distribution correlates with the cyclone and ESP installation of the flue gas cleaning system and its operation, so there are obvious differences between (A-D) and (E-F) samples particles that correlate with the corresponding density data (van Loo & Koppejan, 2008).

The average density of (A-F) fly ash particles was 1,950 kg m^{-3}. The average density of (A-D) fly ash was 133 kg m^{-3}, and 305 kg m^{-3} from (E-F), which may be due to different sampling points for fly ash particles. The average voidage (A-D) and (E-F) is the same, the distribution is very similar and only in the case of (A) the porosity is lower. Finally, in the case of (A-D), the angle of the repos is very narrow (49–50°), and in the case of (E-F) it is broader (43–50°) and determined by the coincidence of (A-D) and (E) angle of repose. When the elemental composition and physical properties of ash is determined, it becomes possible to evaluate the use of ash in forest and agriculture/rehabilitation of damaged areas, the reduction of soil acidity and as a fertilizer additive, e.g. (Muse & Mitchell, 1995). In some cases, ash can be used to improve the composition of sewage sludge suitable for fertilization, composting of organic waste or even paper.

In general, ash can be either untreated or treated reducing heavy metal concentrations to meet the national standards using various leaching methods. In the case at hand, collected volatile ash samples (A-D) should be treated with a variety of leaching methods, as concentrations of heavy metals (B, Cd, Cr, Cu, Pb and Zn) are exceeded, and if it‘s not possible then they would have to be landfilled. Furthermore, even if concentrations of some heavy metals can be reduced by the use of various leaching methods, the elements that are useful for fertilization can be washed off as well making the ash unsuitable as fertilizers.

Soil improvement with unstabilized (dusty) ash activates soil processes, intensifies the mineralization of organic nitrogen and makes an increase in migration of other ions into deeper soil layers and groundwater possible. However, if the ash is used in forestry and spread up to 5 tonnes of ash per hectare, then some heavy metals do not exceed the maximum permissible levels according to regulatory documents. Meanwhile, the impact of stabilized (granulated) ash, according to forest ecosystem studies, has an opposite effect on the soil which can last from 30 to 60 years (Silverberg & Hotanen, 1989;

Korpilahti et al., 1998). Therefore, depending on the leaching of materials from ash granules even if ash doses of 11–44 t ha^{-1} are used for fertilization, the groundwater is not contaminated with either heavy metals or with Ca^{2+}, K^{+}, SO_4^{2-} and other ions (Williams et al., 1996). In the event that even treated ash is not suitable for fertilization, it can be utilized in alternative ways which, unfortunately, are not currently regulated in Lithuania. As a result, landfill disposal is the only treatment even though it is economically disadvantageous.

Alternative use of ash is applied in a number of European Union (EU) countries (e.g. Sweden, Germany, Denmark, France) but it is the most widely developed in Sweden, as ash is used for road construction, landfill reclamation, filling of old shafts or in the manufacture of concrete products including the installation of parking bases. Each alternative use of ash depends on proper dosing, physical properties and elemental composition, as the performance of the product depends on these characteristics. Considering the possible areas of use of bottom and volatile ash, investigated methods of altering their elemental composition it can be expected that developed ash processing and utilization will reduce their amount in landfills and local environmental pollution.

CONCLUSIONS

Samples (A-D) of the wood chips supplied to the boiler plants in operation show that chips are prepared from a fairly diverse range of wood as solid biofuel including tree waste, without paying due attention to their quality. Therefore, the incineration of such chips results in increased amounts of heavy metals in fly ash, which are higher than the permissible limits for soil fertilization set by the Lithuanian minister of environment order No. D1-572, June 25 2014. Such fly ash cannot be used for soil fertilization. In contrast, when the straw is burned, heavy metal concentrations in fly ash are under permissible limits and ash can be used for soil fertilization.

The average pH and porosity of volatile ash are similar between samples and equal to 13 and 0.9 respectively, while (E-F) particles are on average 2.3 times larger than (A-D) volatile ash particles. Average particle density of (A-F) was 1,950 kg m^{-3}, whereas the mean bulk density (E-F) for particles was 2.3 times the average bulk density of (A-D) particles.

Major elements in the fly ash are Ca, K, Zn, S, C and Mg the quantities of which depend on the particle size. The large particles that are retained by the cyclone have higher Ca, Mg and C concentrations. On the other hand, fine particles, retained by the ESP, contain higher concentration of K, Zn, S and other elements. However, in the flow after the boiler particles are affected by turbulence and agglomerate, therefore it is difficult to precisely link the composition of the particles to their size.

The ESP also does not precipitate some of the finest particles, which remain a source of environmental pollution and a threat to human health. Therefore, the research on fine particle agglomeration methods is promising.

ACKNOWLEDGEMENTS. Thanks to KTU Department of Environmental Technology for aerosolization and sizing of cyclone and ESN fly ash samples into 14 fractions using electrical low pressure impactor ELPI and LEI Hydrogen Energy Technology Center for assistance in performing elemental composition analysis of ashes using SEM/EDS.

REFERENCES

Alakangas, E., Hurskainen, M., Laatikainen-Luntama, J. & Korhonen, J. 2016. Properties of indigenous fuels in Finland. Espoo: VTT Technical Research Centre of Finland. *VTT Technical Research Centre of Finland* **272**. 1–222. Access to Document: < http://www.vtt.fi/inf/pdf/technology/2016/T272.pdf >.

Directive 2006/12/EC of the European Parliament and of the Council of 5 April 2006 on waste. Official Journal of the European Communities, L 114/9-21 (27 April, 2006), available from: <http://europa.eu.int/eur-lex>.

European Council Decision of 19 December 2002 on establish criteria and procedures for the acceptance of waste at landfills pursuant to Article 16 of and Annex II to Directive 1999/31/EC. Official Journal of the European Communities, L 11/27-49 (16 January, 2003), available from: <http://europa.eu.int/eur-lex>.

Frandsen, F. 2010. Ash formation, deposition and corrosion when utilizing straw for heat and power production. Technical University of Denmark, Department of Chemical and Biochemical Engineering, ISBN: 978-87-92481-40-5.

Korpilahti, A., Moilanen, M. & Finér, L. 1998. Wood ash recycling and environmental impacts-state-of-the-art in Finland. In *IEA Bioenergy, Task 18: Developing Systems for Integrating Bioenergy into Environmentally Sustainable Forestry*. International Workshop and Study Tour in Finland, September 1998.

Kwauk, M. 2003. Emerging particle science and technology in China. *Powder Technology* **137**, 2–28.

Lanzerstorfer, C. 2015. Cyclone fly ash from a grate-fired biomass combustion plant: dependence of the concentration of various components on the particle size. *Fuel Processing Technology* **131**, 382–388.

Mellbo, P., Sarenbo, S., Stålnacke, O. & Claesson, T. 2008. Leaching of wood ash products aimed for spreading in forest floors – Influence of method and L/S ratio. *Waste Management* **28**, 2235–2244.

Muse, J. K. & Mitchell, C.C. 1995. Paper Mill Boiler Ash and Lime By-Products as Soil Liming Materials. *Agronomy journal* **87**, 432–438.

Obernberger, I. & Supancic, K. 2009. Possibilities of ash utilisation from biomass combustion plants. In: *Proceedings of the 17th European Biomass Conference and Exhibition. Hamburg, ETA-Renewable Energies (Ed.)*, pp. 1–12.

Olsson, M., Kjällstrand, J. & Petersson, G. 2003. Specific chimney emissions and biofuel characteristics of softwood pellets for residential heating in Sweden. *Biomass and Bioenergy* **24**, 51–57.

Pedersen, AJ. 2003a. Characterization and electrodialytic treatment of wood combustion fly ash for the removal of cadmium. *Biomass Bioenergy* **25**, 447–458.

Pedersen, A.J., Ottosen, L.M. & Villumsen, A. 2003b. Electrodialytic removal of heavy metals from different fly ashes – Influence of heavy metal speciation in the ashes. *Journal of Hazardous Materials* **100**, 65–78.

Pui, D.Y.H., Chen, S.C. & Zuo, Z.L. 2014. PM2.5 in China: measurements, sources, visibility and health effects, and mitigation. *Particuology* **13**, 1–26.

Republic of Lithuania minister of environment order No. D1-572, in June 25 2014. Amendments of "On approval of rules for the handling and use of wood fuels ash" order No. D1-14 January 5 2011.

Silverberg, K. & Hotanen, J.P. 1989. Long-term effects of wood ash on a drained mesotrophic Sphagnum papillosum fen in Oulu district, Finland. *Folia Forestalia* **742**, 1–23. Access to Document: < http://urn.fi/URN:ISBN:951-40-1082-5 >

Steenari, B-M., Schelander, S. & Lindqvist, O. 1999. Chemical and leaching characteristics of ash from combustion of coal, peat and wood in a 12 MW CFB – a comparative study. *Fuel* **78**, 249–258.

van Loo, S. & Koppejan, J. 2008. *The Handbook of Biomass Combustion and Co-firing*. Earthscan, London. ISBN 1844072495, 442 pp.

Vesterinen, P. 2003. Wood ash recycling state of the art in Finland and Sweden. *VTT Processes, Jyväskylä*, pp. 1–50.

Williams, T., Hollis, C. & Smith, B. 1996. Forest soil and water chemistry following bark boiler bottom ash application. *Journal of Environmental Quality* **25**(5), 955–960.

Xu, P., Wang, W., Ji, J.W. & Yao, S.Y. 2014. Analysis of the contribution of the road traffic industry to the PM2.5 emission for different land-use types. *Computational Intelligence and Neuroscience* **2014**, 1–6.

Zbogar, A., Frandsen, F., Jensen, P.A. & Glarborg., P. 2009. Shedding of ash deposits. *Progress in Energy and Combustion Science* **35**(1), 31–56.

Agronomy Research **17**(2), 551–558, 2019
https://doi.org/10.15159/AR.19.034

Discrete element simulation of rapeseed shear test

J. Kuře[1,*], L. Hájková[2], M. Hromasová[2], R. Chotěborský[1] and M. Linda[2]

[1]Department of Material Science and Manufacturing Technology Faculty of Engineering, Czech University of Life Sciences Prague, Kamýcká 129, CZ165 21 Prague – Suchdol, Czech Republic
[2]Department of Electrical Engineering and Automation, Faculty of Engineering, Czech University of Life Sciences Prague, Kamýcká 129, CZ165 21 Prague – Suchdol, Czech Republic
[*]Correspondence: kure@tf.czu.cz

Abstract. Suitable equipment are required for storage and transportation of rapeseed which are developed according to rules for bulk matters. It is one of reasons where bulk matter properties are important to the design. Bulk matter properties are important to known as angle of repose, internal friction, external friction, adhesivity force and other bulk properties. Experimental values of bulk properties are added to mathematical models. The model should be calibrated with adequate experiment. The shear test is one of popular calibration test for bulk matters so that be able done experiment and numerical model in one. The aim of this paper is simulation of rapeseed bulk properties during shear strain and flow and its evaluation and calibration with experimental tests. RockyDEM software was used for numerical simulation of rapeseed. Shear test, angle of repose, static and dynamic friction test were used to calibration of the numerical rapeseed model. Sensitivity of numerical model is discussed on the bulk properties.

Key words: oilseed, discrete element methods, angle of friction, shear test.

INTRODUCTION

Use of special equipment is necessary for rapeseed storage and manipulation. These equipment must be designed in a way to accommodate for seamless transportation and storage of the rapeseed. It is possible for a computer simulation to be made in order to lower the design and testing costs. Such simulation requires an accurate mathematical model. To achieve a correct calibration of the mathematical model, it is necessary to acquire rapeseed's mechanical properties. Fundamental bulk properties are angle of repose, internal and external friction. Angle of repose can be determined through experimental measurement (Zhou et al., 2002; Marigo & Stitt 2015). Shear test on a shear device is the most common method for obtain values of internal and external friction (Amšiejus et al., 2014).

Discrete element method (DEM) is a suiTable way of creating the model. Raji & Favier (2004), Wojtkowski et al. (2010) have already dealt with rapeseed modelling, particularly in the area of rapeseed's deformation and processing. High performance of

modern computer technology allows for simulation of bulk matter of rapeseed in 1:1 real rapeseed to simulation ratio. This way, it is possible to achieve accurate results.

The aim of this paper is to create a mathematical model of rapeseed. Model calibration was made on a shear test using shear device. Modelling program RockyDEM was used for the simulation.

MATERIALS AND METHODS

Firstly, it was necessary to acquire rapeseed's basic properties such as size of individual grains, moisture and bulk density. The acquisition of parameters was subject of measurement and experimentation. Secondly, in order to determine the parameters of rapeseed it was necessary to specify its static and dynamic properties. These properties served as input values of the mathematical model. The obtained parameters were then evaluated, inserted to the mathematical model and a calculation was made.

A selected rapeseed sample was subjected to experimental measurement. The first step established the rapeseed grain properties according to (Kanakabandi & Goswami 2019). The diameter of 100 rapeseed grains was measured in order to determine the average grain size. Measured values were then analysed, further processed and finally used to create a histogram. Six measurements were made to specify the bulk density. A 400 mL volume container was filled with rapeseed sample. The weight of the rapeseed was then subtracted.

As (Çalişir et al., 2005; Wiacek & Molenda 2011) have already determined, rapeseed's moisture changes its properties fundamentally. Rapeseed's moisture must be preserved for the entire duration of the measuring process of its properties. The change in the bulk material's moisture affects its cohesive properties and leads to a different behaviour of the material. The moisture content was measured using moisture analyser OHAUS MB 25 (Hromasová et al., 2018). Five different rapeseed measurements were made. Individual samples were heated in the analyser to a temperature of 105 °C. During the test the sample was observed for weight loss. The calculation of moisture was made after the weight of the sample stabilized at a new value. Young's modulus for bulk matter of rapeseed was the next parameter. The test was performed on a tensile testing machine. Rapeseed sample was placed inside a cylindrical chamber with a diameter of 40 mm. Height of the bulk sample was 30 mm. The sample was deformed from 0 N to 10 N. The relative ratio of the volume change and the corresponding load was subsequently evaluated. The result was the Young's modulus.

Shear test was performed on shear device. With the help of shear test it is possible to determine the coefficient of internal and external friction. The internal friction coefficient of bulk materials determines the frictional properties between the individual particles of the material. The coefficient of internal friction determines the frictional properties between the bulk material and the surface of foreign object. (Krc et al., 2016)

Shear device consists of two chambers and a top board. The internal dimensions of the chambers are 90 x 90 mm with the height of 30 mm. Rapeseed sample has been placed inside of the chambers and the upper chamber closed by the top board. See Table 1 for the load for the measurement. See Fig. 1 for the measurement scheme. After load of F_n (N), the upper chamber has been set to motion along horizontal axis at the speed of 1 mm s^{-1}. Tangential force F_s (N) acting on the upper chamber has been progressively subtracted during motion Δl (mm).

Table 1. Values of loads

Number of measures	1	2	3	4	5	6	7	8	9	10
Mass (g)	500	1,000	1,500	2,000	2,500	3,000	3,500	4,000	4,500	5,000

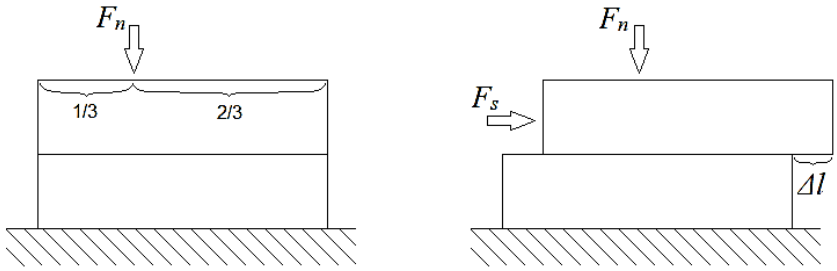

Figure 1. Share device principle.

From each measured force-displacement dependence, a transformation was made based on the stress-deformation dependence (1) (2). Tangential forces at the tearing point and maximal shear forces were subtracted in the overall course. After the construction of Mohr's circles (Fig. 2), a coefficient of static and dynamic friction was obtained.

$$\tau = \frac{F_s}{A} \tag{1}$$

where τ – tangential stress (Pa); F_s – tangential force (N); A – cross section area (m^2)

$$\sigma = \frac{F_n}{A} \tag{2}$$

whre σ – normal stress (Pa); F_n – normal force (N); A – cross section area (m^2)

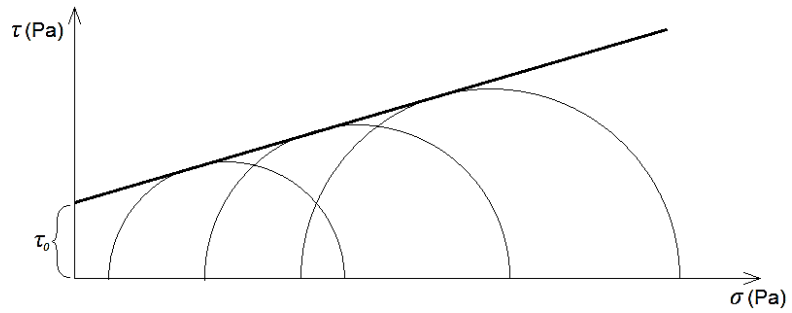

Figure 2. Mohr's circles.

Tangential stress τ (Pa) is given by the formula:

$$\tau = \tau_0 + \sigma \cdot \mathrm{tg}\varphi \tag{3}$$

where τ – tangential stress (Pa); τ_0 – initial tangential stress (Pa); σ – normal stress (Pa); φ – angle of internal friction (°).

The mathematical model is designed in the same way as the shear device and therefore it is possible to observe only the tangential force F_s (N) in the x axis acting on the chamber. RockyDEM software was used to create the mathematical model. Model of the shear device was created using SpaceClaim modelling software, which is a part of Ansys. The model was saved as .stl file and then imported to RockyDEM. (Fig. 3). For the input parameters required for simulation setup see Table 2. These parameters were gathered in previous experiments. After setting up the parameters, the mathematical model was calculated.

Table 2. Input parameters in RockyDEM

Parameter	Value
Particle parameters	
Bulk density	707 kg m^{-3}
Bulk Young's modulus	2.66 MPa
Bulk Poisson's ratio	0.3 (-)
Boundary parameters	
Density	2,700 kg m^{-3}
Young's modulus	70 GPa
Poisson's ratio	0.3 (-)
Material interaction between particle and particle	
Static friction	K (-)
Dynamic friction	0.75 (-)
Tangential stiffness ratio	0.8 (-)
Restitution Coefficient	0.3 (-)
Material interaction between particle and boundary	
Static friction	0.34 (-)
Dynamic friction	0.43 (-)
Tangential stiffness ratio	0.8 (-)
Restitution Coefficient	0.3 (-)

Model verification was made through comparison of experimental results from the shear test and the results of the mathematical module. Output parameters were set once more and another calculation was made. Parameter setting was focused on Static friction, dynamic friction and stiffness. The individual changes were compared based on the adjustment of individual input quantities. It has been found that static friction has the highest effect on the test. To find the optimal parameters, Design of Experiment was followed. Variable K in Table 2 indicates the search parameter.

For normal loads of 500 g, 1,000 g and 2,000 g, simulations with static friction of 0.12, 0.21 and 0.33 were calculated. The results were compared according to individual parameters. The comparison was based on the *T-test* probability in MS Excel 2016.

Parameters that have been selected for the compare of displacement force curves are presented in Fig. 3. Fmax is the maximum value of displacement force curve. Alpha (α) is angle of slope (gradient) displacement force curve. Displacement energy is marked E. Displacement energy is area under displacement force curve.

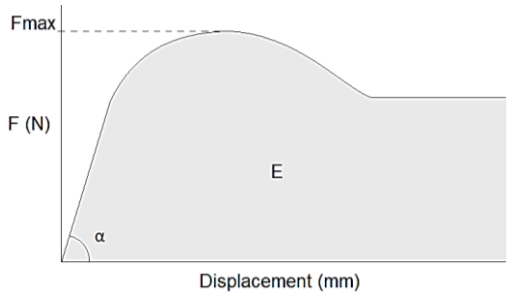

Figure 3. Necessary parameters to compare displacement force curves.

Two computational devices were used for the calculations. The first device was used for preprocessing and post processing: Intel® Xeon® Processor E5-1680 v4, 20MB Cache, 3.40 GHz. The second device was used for solver: HPE NVIDIA Tesla P100 PCIe 16GB Computational Accelerator graphic card.

RESULTS AND DISCUSSION

For the measured rapeseed grain diameter, bulk density and moisture see Table 3. Grain size corresponds to a normal distribution. Measured grain size at the given moisture is comparable to (Çalişir et al., 2005) The value of bulk density; however, was measured higher, but contrary to (Wiacek & Molenda, 2011) the bulk density was lower.

Table 3. Table of measured rapeseed properties

	Value
Size	1.93 mm ± 0.214
Bulk density	707 kg m^{-3} ± 5.469
Moisture	3.5% ± 0.145

Coefficients of static and dynamic friction was calculated of measured tangential stress and normal stress. Results are shown at Fig. 4, a) and b). Coefficient of static friction is 0.29 with $R^2 = 0.97$, coefficient of dynamic friction is 0.76 with $R^2 = 0.99$. Value of bulk Young's modulus is 2.66 MPa.

The coefficient of static and dynamic friction are dependent on moisture content. The coefficient of static friction is approaching to results in (Çalişir et al., 2005; Wiacek & Molenda 2011).

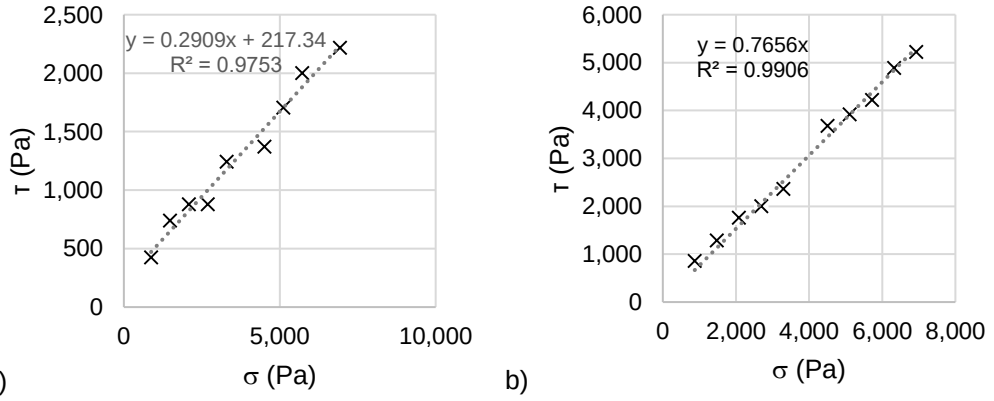

Figure 4. a) The static friction between particle and particle; b) The dynamic friction between particle and particle.

Mathematical model was performed according to Table 2 above. Values were determined by experimental measurements. Poisson ratio and restitution coefficient were left at the default values recommended by the technical manual of Rocky DEM. Tangential stiffness ratio was determined by the DoE when it reached optimal values depending on the model's result. Static friction was set to: 0.12, 0.21 and 0.33.

The final simulation is graphically presented by Rocky DEM (Fig. 5). The simulation shows the particle displacement caused by the top chamber displacement in the horizontal axis.

Fmax, energy and angle α were obtained from measured values and results of simulations. Values are presented in Table 4, 5 and 6.

P values obtained from the *T-tests* were compared and presented in Table 7. The highest value probabilities are bold. These probabilities are significant of model values with real experiment.

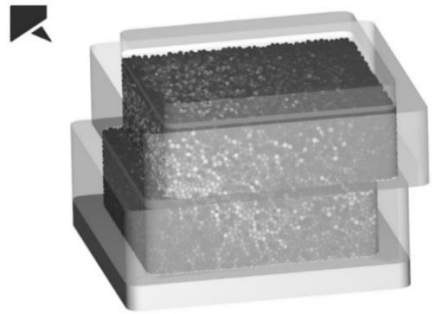

Figure 5. The simulation of share test in Rocky DEM.

Significant value of static friction for relation between computed model and real experiment was determined for value 0.33. However, maximum displacement force of the model with static friction 0.21 is more appropriate in this case.

Table 4. Maximum force values of displacement forces, where S is simulation and SF is static friction

Normal load (g)	Fmax of experiment (N)	Fmax of S with SF 0.12 (N)	Fmax of S with SF 0.21 (N)	Fmax of S with SF 0.33 (N)
500	7.136584	4.635929	5.86799	6.987178
1000	10.0887	7.589752	9.539528	11.03859
2000	16.48494	14.10927	16.97077	20.01202

Table 5. Displacement energies of real experiment and simulations, where S is simulation and SF is static friction

Normal load (g)	Energy of experiment (N)	Energy of S with SF 0.12 (N)	Energy of S with SF 0.21 (N)	Energy of S with SF 0.33 (N)
500	58.25351784	39.49571125	47.77675263	54.73861092
1000	88.69717097	63.95716466	76.82710536	86.53662208
2000	141.9680287	115.7666934	138.7238772	156.3169611

Table 6. Angles α of slope of real experiment and simulations, where S is simulation and SF is static friction

Normal load (g)	Angle α of experiment (N)	Angle α of S with SF 0.12 (N)	Angle α of S with SF 0.21 (N)	Angle α of S with SF 0.33 (N)
500	87.8188913	86.42270722	86.86175238	87.28090587
1000	88.13814944	87.82255397	88.07203203	88.19160679
2000	88.44819378	88.86840589	88.97115811	89.01425526

Table 7. Probability of *T-test* between simulation and real experiment

Static friction in simulation	P value for maximum displacement force	P value for displacement energy	P value for angle of slope displacement force
0.12	0.565523618	0.523194	0.609584
0.21	**0.922420412**	0.825847	0.814835
0.33	0.777313268	**0.944186**	**0.963068**

In Fig. 6, the displacement force of real experiment as continuous line and displacement force of simulations as dashed and dotted lines are presented. Displacement force of simulation with static friction 0.21 shows similar run of curve for real experiment in the initial phase than displacement force of simulation, but the simulation with static friction 0.33 shows better run overall.

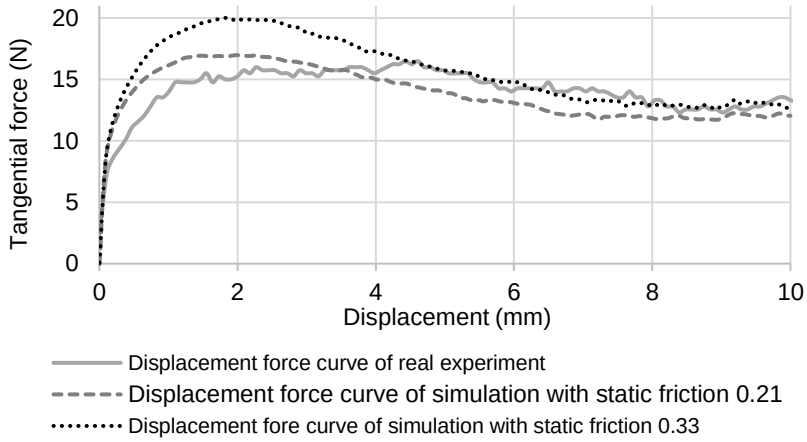

Figure 6. Results of shear tests with normal load of 2,000 g.

The model contains 87,054 particles. The calculation of 10.2 second of simulation need 2.4 hours computation time at the Tesla P100. Time-consumption of simulation of the same time interval is 20.8 hours at the Xeon E5-1680 processor. For the final sensitivity setting of the model was needed 424 hours of calculating.

CONCLUSIONS

The use of this modelling technique is according expanding and it is being exploited in many application. Discrete element method can be used to describe granular problems of rape seed. Parameters are given for moisture content 3.5% and real size of rapeseed grains. For models with a different grain ratio, it may be necessary to change the boundary conditions. When designing a mathematical model of rapeseed, it is important to discuss the purpose of model and use appropriate settings.

ACKNOWLEDGEMENTS. Supported by Internal grant agency of Faculty of Engineering, Czech University of Life Sciences in Prague with name: Influence of input parameters of agricultural bulk matter on the accuracy of solution using discrete element methods.

REFERENCES

Amšiejus, J., Dirgeliene, N., Norkus, A. & Skuodis, Š. 2014. Comparison of Sandy Soil Shear Strength Parameters Obtained by Various Construction Direct Shear Apparatuses. *Archives of Civil and Mechanical Engineering* **14**(2), 327–34.

Çalişir, Sedat, Tamer Marakoğlu, Hüseyin Öğüt & Özden Öztürk. 2005. Physical Properties of Rapeseed (Brassica Napus Oleifera L.). *Journal of Food Engineering* **69**(1), 61–66.

Hromasová, M., Vagova, A., Linda M, & Vaculik, P. 2018. Determination of the Tension Limit Forces of a Barley Malt and a Malt Crush in Correlation with a Load Size. *Agronomy Research* **16**(5), 2037–2048.

Kanakabandi, C.K. & T.K. Goswami, T.K. 2019. Determination of Properties of Black Pepper to Use in Discrete Element Modeling. *Journal of Food Engineering* **246**, 111–18.

Krc, K, Wermager, S., Sneed, L.H. & Meinheit, D. 2016. Examination of the Effective Coefficient of Friction for Shear Friction Design. *PCI Journal* **61**(6).

Marigo, Michele & Edmund Hugh Stitt. 2015. Discrete Element Method (DEM) for Industrial Applications: Comments on Calibration and Validation for the Modelling of Cylindrical Pellets †. *©2015 Hosokawa Powder Technology Foundation KONA Powder and Particle Journal No* **32**, 236–52.

Raji, A.O. & Favier, J.F. 2004. Model for the Deformation in Agricultural and Food Particulate Materials under Bulk Compressive Loading Using Discrete Element Method. I: Theory, Model Development and Validation. *Journal of Food Engineering* **64**(3), 359–71.

Wiacek, J. & Molenda, M. 2011. Moisture-Dependent Physical Properties of Rapeseed – Experimental and DEM Modeling. *International agrophysics* **25**(1995), 59–65.

Wojtkowski, M., Pecen, J., Horabik, J. & Molenda, M. 2010. Rapeseed Impact against a Flat Surface: Physical Testing and DEM Simulation with Two Contact Models. *Powder Technology* **198**(1), 61–68.

Zhou, Y.C., Xu, B.H. Yu, A.B. & Zulli, P. 2002. An Experimental and Numerical Study of the Angle of Repose of Coarse Spheres. *Powder Technology* **125**(1), 45–54.

Agronomy Research **17**(2), 559–573, 2019
https://doi.org/10.15159/AR.19.050

Modeling the functional role of the microorganisms in the daily exchanges of carbon and nitrogen in intercropping system under Mediterranean conditions

M. Latati[1,*], N.Y. Rebouh[2], A. Aouiche[3] and M. Laouar[1]

[1]Ecole Nationale Supérieure Agronomique, Département de Productions Végétales. Laboratoire d'Amélioration Intégrative des Productions Végétales (C2711100). Rue Hassen Badi, El Harrach DZ16200 Alger, Algérie
[2] University of Russia (RUDN University) Department of AgroBiotechnology, Institute of Agriculture,Peoples' Friendship, 6 Miklukho-Maklaya street, RU117198 Moscow, Russia
[3]Ecole Supérieure des Sciences de l'Aliment et des Industries Agroalimentaires (ESSAIA), Avennue Ahmed Hamidouch Route de Beaulieu, El Harrach, DZ16200 Alger, Algérie
[*]Correspondence: m.latati@yahoo.com

Abstract. Carbon (C) and nitrogen (N) sequestration in plants and soil micro-organisms is considered as a major phenomenon against global warming. The modeling of this phenomenon aims at highlighting the role that the legumes-cereals mixed crop can play in the reduction of greenhouse gases. It is based on field experiments in maize (*Zea mays L.*)-common bean (*Phaseolus vulgaris L.*) intercropped system of the cereal agroecosystem in Setif region of Algeria. For this purpose, the MOMOS model was selected and validated in a calcareous soil and low phosphorus (P) conditions. It revealed some mechanisms that control the C and N sequestration in the compartments of the complex soil-plant-atmosphere-microorganism system. CN modeling results show that the daily growth of intercropped maize with common beans is positively correlated with the microbial CN transformation during the cropping cycle, under limited P and N conditions. Thus, this approach revealed the functional role of rhizobial symbiosis in maintaining the balance between the different C and N exchanges from soil to atmosphere and from atmosphere to soil.

Key words: modeling, carbon, nitrogen, sequestration, intercropping.

INTRODUCTION

The superficial layers of the terrestrial globe contain the largest reserves of organic carbon (C) and nitrogen (N) potentially available for plant growth (Ladd et al., 1992). These two elements are also essential constituents of organic matter (OM), which plays a crucial role in maintaining and improving soil fertility by its beneficial effects on physical, chemical and biological properties and more particularly on sequestration of soil C (Ladd et al., 1992). Also, microbial biomass (MB) constitutes a transformation matrix for organic matter in the soil and acts as a labile reservoir of nutrients available to plants, especially for C and N (Srivastava et al., 1989).

The importance of soil organic matter (SOM) pools depends on the input of crop residues and losses of C. These losses are caused either by heterotrophic respiration during the decomposition of SOM by MB or by autotrophic respiration of symbiotic bacteria (Ibrahim et al., 2013).

Several studies focus on crop production and the N cycle including the symbiotic fixation of atmospheric nitrogen (N_2) during crop cycles (Corre-Hellou et al., 2009, Liu et al., 2011). Other studies attempt to link soil respiration to crop production based on pedoclimatic variability (Yuste et al., 2004, Dornbush et al., 2006). However, the data from the literature lack accuracy on the simulation of the daily dynamics of C and N transferred between the plant, soil and atmosphere.

Commonly used cultural practices such as fertilization, pesticide treatments and monoculture, contribute significantly to the degradation of environmental fertility by reducing biological diversity and by increasing the emissions of CO_2 sequestered in the atmosphere (Horrigan et al., 2002). Therefore, the ecosystem approach remains the surest way to avoid the harmful consequences of these practices in conventional agrosystems. This includes, in particular, the ecological services of atmospheric nitrogen fixation and the processes of complementarity and facilitation of legumes by promoting their interactions with soil micro-organisms (Latati et al., 2016, 2017). Indeed, a positive effect on cereals when intercropped with legumes has been demonstrated with biomass accumulation and yield increase (Betencourt et al., 2012, Latati et al., 2013, 2014). This positive effect was confirmed for cowpea-maize (Latati et al., 2014), chickpea-durum wheat (Betencourt et al., 2012) and bean-maize intercropping (Dahmardeh et al., 2010, Latati et al., 2013, 2016 and 2017). However, the increase in cereal yield in intercropping is not due only to the increase in N resources via symbiotic N_2 fixation but also to other mechanisms patterns, i.e. enzyme activity, may show at least similar increases of soil fertility, e.i. C, N and P mobilization abilities (Bargaz et al., 2017, 2018).

To better understand the dynamics of N and C in Mediterranean soils, mechanistic models can answer several pertinent questions. They make it possible, for example, to distinguish the compartments of plant origin, generally located in coarse fractions of the soil, from those of microbial origin located in the finer fractions (Pansu et al., 2009).

In Algerian soils, a first quantification of N, following that of C in an agro-ecosystem cereal production of Setif, revealed a fragility of the reserves and the need to change agricultural practices with a soil preservation management (Latati et al., 2016, 2017). Under different environmental conditions, several modeling studies of stock variations of C and N in several production systems (Pansu et al., 2004, 2009 and 2010) are available and allow a better understanding and adapting the models.

In contrast with other published propositions which need long term comparisons to quantify the C exchanges, our work studies, in the short term, the cycles of C and N by the validation of the MOMOS model (Micro-Organismes et Matière Organique du Sol, i.e. soil microorganism and organic matter model) on the basis of the CN data collected in the cereal agro-ecosystem of Setif region in the northeast of Algeria. It presents the genesis of the MOMOS model which is centred on microbial functioning and appears very sensitive to meteorological, edaphic and biological conditions. It is therefore important to answer two questions: (i) could MOMOS predict the daily evolution at short term of living and dead forms of organic carbon in complex systems, (ii) Could the equations be used to simulate the C and N flows into microbial symbiotic nodules of

intercropped legume roots by checking the simulation against field measurements data of root nodule biomasses?

MATERIALS AND METHODS

Experimental site

The experiment was carried out in the commune of El Kharba (35°58'11"N and 5°14'90"E), Algeria (North Africa), north of Setif region. This site has already been studied in previous researches (Latati et al., 2016; 2017). The choice of this site is justified by the results of Latati et al., (2016 and 2017) which report a high efficiency use of rhizobial symbiosis and the presence of P-deficient and calcareous soils. The climate of Setif is Mediterranean characterized by a harsh winter and a hot and dry summer. The average temperature during the four months of the growing cycle varies between 20.7 °C and 28.1 °C. The maximum temperature (37.1 °C) is recorded during the month of August, while the minimum temperature (13.7 °C) is recorded during the month of September. The maximum rainfall is recorded in September with 28.2 mm. Climatic data are collected from the Meteorological Station of Setif. All the physicochemical characteristics of the soil as well as the experimental device were done as previously reported (Latati et al., 2016).

Sampling and data collection

The data were collected at the first stage of growth at 20 days after sowing (DAS), early flowering (50 DAS), full flowering (75–80 DAS) and at harvest stage (112 DAS). A physicochemical characterization of the initial soil is carried out before sowing. Samples are taken at random. The whole plant is torn off and for each crop modality the rhizospheric soil of the harvested plants is taken. For the fallow, 4 to 5 soil samples on 30 cm deep layer are taken randomly using the same sampling technique used for the other crop modalities.

The complementary data were used for the calibration (field experiment during 2018 growing season at the farmer's plots in the commune of El Kharba) of some parameters such as; the initial values of soil compartments, plant debris and ecophysiological parameters of both intercropped maize and common bean.

Determination of the stable fraction and the labile fraction of humus by NIRS analysis

In order to determine the different labile and stable fractions of the OM, in both root and shoot part of the maize and the common bean, a near-infrared spectroscopy (NIRS) was carried out in the laboratory of INRA Sup-Agro of Montpellier (France) using a NIRS System 6500 reflection spectrometer. NIRS analysis is a non-destructive method of physical analysis based on the selective absorption of electromagnetic radiations with a wavelength near-infrared range (1,100–2,500 nm) by OM components. The absorbance of infrared radiation by a material is characterized by the superposition of the atomic bonds which determines the chemical constitution of the studied material (Barthès et al., 2008). In practice, crushed samples (plant powder) are placed in the spectrophotometer (NIR System 6500) where they are illuminated by monochromatic radiation whose wavelength varies from 400 to 2,500 nm. The amount of light radiation

reflected by the surface of the sample is measured and all these measurements allow obtaining an absorbance spectrum.

Determination of soil microbial biomass

Fumigation-extraction is a reliable technique for measuring the overall size of soil microbial biomass. This method was developed by Vance et al. (1987) and adapted by Wu et al., (1990). It consists in treating the soil with chloroform vapor, which lyses the microorganisms' cells. The cells' compounds obtained were extracted with a solution of K_2SO_4 at 0.05M for C and 0.5M for N. The soil samples (10 mg) were placed in glass Petri dishes and then placed in a desiccator. A Becher containing 50 mL of chloroform ($CHCl_3$) and pumice is introduced into the desiccator until the boiling of $CHCl_3$ for 2 minutes. The desiccator was then placed in the shade at 20–25 °C for 24 h. The microbial biomasses according to N (MBN) and C (MBC) were extracted from the fumigated samples while the extraction of the non-fumigated samples was carried out immediately after weighing the soil samples.

The microbial stock was calculated from the difference between fumigated and non-fumigated soil samples:

$$\mathrm{MBN} = [\mathrm{TN(fumigated)} - \mathrm{TN(not\ fumigated)}]/\mathrm{kn} \quad (1)$$

Total nitrogen (TN) determined by the KJELDAHL method, with a correction factor Kn = 0.54

$$\mathrm{MBC} = [\mathrm{OrgC(fum)} - \mathrm{OrgC(not\ fum)}]/\mathrm{kn} \quad (2)$$

The organic carbon (Org-C) in the solution is determined by the SHUMADZU method, with a correction factor Kc = 0.45 (Joergensen, 1996).

MOMOS Model

The MOMOS model (soil microorganism and organic matter model) is a mechanistic model of OM decomposition defining the functional ecology of MB. It was developed in such a way as to limit the parameters of the system studied to the transfer rates between the compartments which could be adjusted by incubation experiments with isotopic tracing (Pansu et al., 2010, Ibrahim et al., 2013). No application on open complex systems with regular flows has yet been published except for Ibrahim *et al*. (2013). The proposed MOMOS model was coupled with the SAHEL model (soils' water) and the FARPROM model (fallow and plant production) (Pansu et al., 2009).

Mathematical Formulation of MOMOS

All parameters of the MOMOS model are related to soil moisture and temperature (T). This is probably one of the most climate-sensitive models with the general equation:

$$\dot{\mathrm{C}} = \mathbf{f}(\mathbf{T})\mathbf{f}(\theta)\mathrm{Ax} + \mathrm{B} \quad (3)$$

$\dot{\mathbf{C}}$ is the vector of the variable that represents the concentration of C and N in the five compartments of the model (Aerial and root biomass, Microbial biomass, Necromass, Stable humus and labile humus), Ax is the matrix of model parameters, B is the vector representing the C and N inputs, f (T) is the function of the temperature given by equation (Pansu et al., 2004, 2010, Ibrahim et al., 2013).

Data processing and calculation tools

All concentrations of C and N and those of MB in soil (total-C mg g^{-1} and MBC μg mL^{-1}) are converted to C and N stock in the 0 to 30 cm depth layer by applying the following equation:

$$\text{Total C or N g C m} - 2 = 300 \times \text{ds} \times (\text{CN})(1 - \text{Wp})(1 - \text{Cf} \quad (4)$$

$$\text{BC g CBM m} - 2 = 9 \times \text{ds} \times \text{MBCN} \times (1 - \text{Wp})(1 - \text{Cf})/\text{ms} \quad (5)$$

where ds – density of the soil; wp – soil moisture; cf – proportion of coarse fraction of soil; CN – total C and N concentration (mg g^{-1}); ms – weight of the soil sample used in the extraction solution (10 g).

The simulation of the daily soil moisture is carried out by the SAHEL model. This model of soil water management is based on two computational versions of potential evapotranspiration according to available climate data collected at the Setif meteorological station. In this context, two versions of the SAHEL model are used:

There is a simplified version using daily maximum and minimum temperature data and another more elaborate version taking into account wind speed and water vapor pressure (Pansu et al., 2007). In addition, the simulation of daily soil moisture is carried out by the SAHEL model (Penning et al., 1989). Moreover, the daily prediction of the C and N cycles evolution during the vegetative cycle on the MOMOS model coupled with that of TAO is established on the VENSIM 5.9 modeling platform (http://www.vensim.com) under the license 8082006 CIRAD.

RESULTS AND DISCUSSION

Fig. 1 shows a good adjustment of simulated soil volumetric moisture values to those measured in the upper and lower soil layers during all the phenological stages of the cropping cycle. Small differences between the measured and predicted data may exist due to the different soil layers taken into account during sampling. The daily soil moisture data measured on a 0–5 cm layer of depth in our experiment are relatively close to the data predicted by the SAHEL model on a 0–15 cm depth layer. The same simulation results are observed on the deeper layer (15–30 cm) and are well adjusted with the moisture data measured on the 25 to 30 cm layer. All simulations of C and N in the different compartments of the soil were carried out at a depth of 0 to 30 cm using the average values of the simulated volumetric humidity on the two layers of depth 0–15 cm and 15–30 cm.

In the case of C and N transfer into the different organs of the plant and microorganism, Figs 2, 3 and 4 shows a significant adjustment (at 5% significance) based on the F-test between the simulated values of C and N transferred to the different parts of the plant (roots, aerial part and nodules) and those measured in maize-bean intercropping. However, the high significant level between the predicted and the measured data is observed for CN transferred to shoot and nodular biomass, particularly for intercropped common bean (Fig. 2a, 3a and 4), while some simulated values are relatively distant compared with the data measured for the roots (Fig. 2b, Fig. 3b).

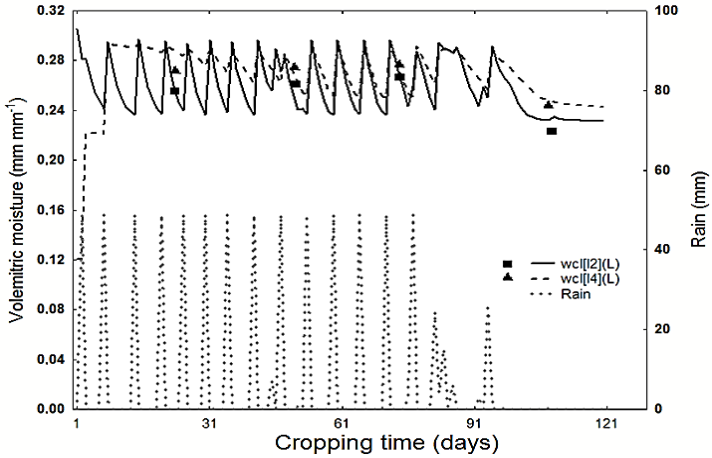

Figure 1. Modelled and measured daily moisture in the surface layer of the soil (wcl2: 0–15 cm) and deeper (wcl4: 15–30) during the growing cycle of the maize-bean intercropping.

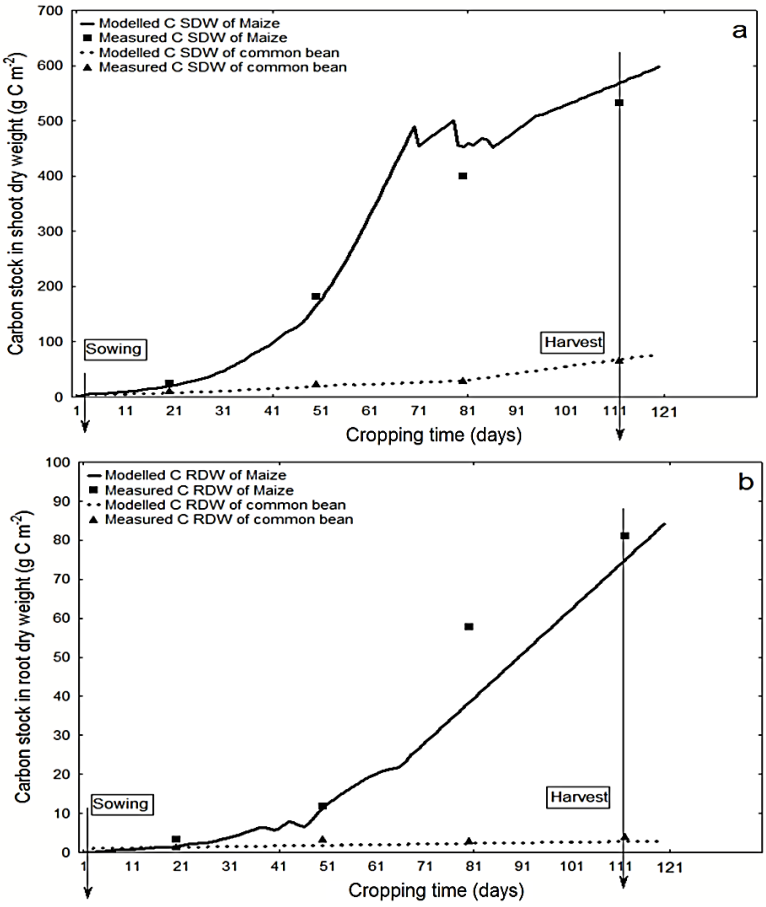

Figure 2. Measured with 95% confidence intervals and modelled values of carbon shoot (a) and root (b) stock in intercropping.

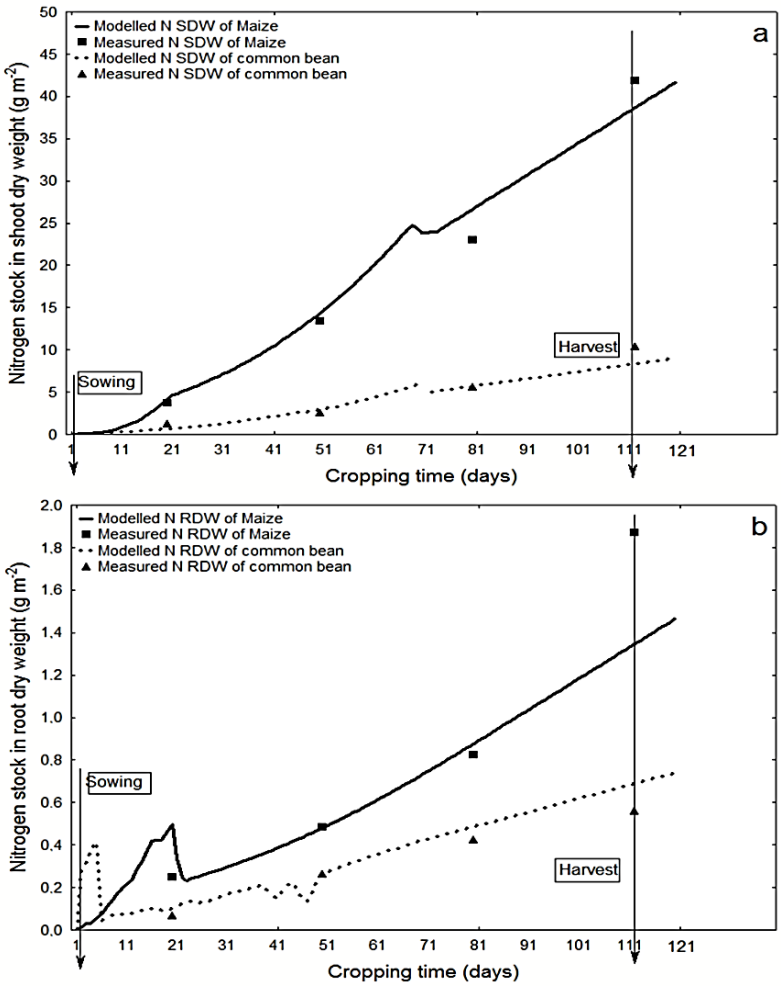

Figure 3. Measured with 95% confidence intervals and modelled values of nitrogen shoot (a) and root (b) stock in intercropping.

However, the transfer of C and N in the shoot and root portion increases from sowing until the end of the crop cycle (harvest). The highest rate is observed during the period from the beginning of flowering (51 DAS) to the full flowering stage (71 DAS). Moreover, the CN transferred to the nodules biomass (NB) reached its optimum (N-NB = 0.88 g m^{-2} and C-NB = 0.06 g m^{-2}) during the flowering stage and then decreased regularly until the end of cropping time (120 days) (Fig. 4).

Indeed, Fig. 5 shows that CN values in soil as well as microbial biomass values are perfectly (at 5% significance) adjusted with field-measured CN data and is fully included in the 95% confidence interval. Moreover, the dynamics of the C and N stock in the soil pass through two phases of evolution (Fig. 5, a). The first phase is characterized by a slight increase in C and N stocks in the soil during the period from sowing to the end of flowering; while the second phase shows a slight decrease in stocks from full flowering to harvest stage.

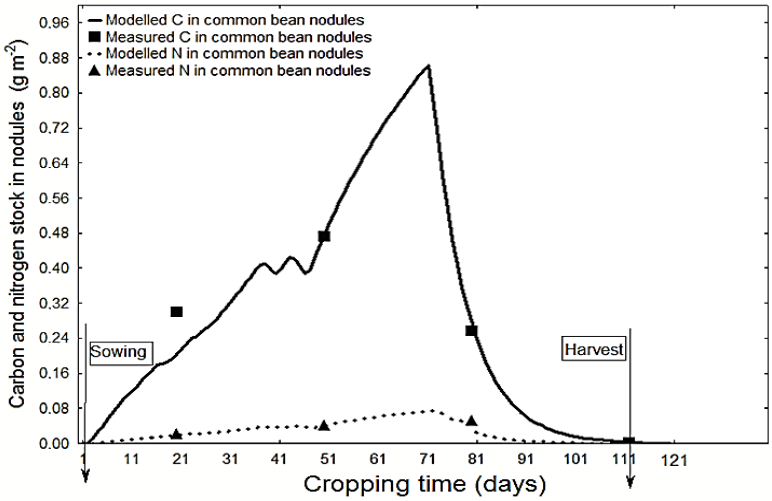

Figure 4. Measured with 95% confidence intervals and modelled values of carbon stock in nodules of intercropped common bean.

The decrease in C and N soil stocks in maize-common beans intercropping is justified by the transfer of these latter elements to shoot and root biomass of intercropped species, particularly during the seeds formation and development. Compared to the relatively stable evolution of CN stocks in soil, CN stocks of MB shows a rapid evolution, particularly at the flowering stage, which recorded the maximum value of MBC (40 g m^{-2}) and MBN (3.5 g m^{-2}) (Fig. 5, b and c). However, MBC and MBN underwent a remarkable decrease, particularly from full flowering to early seed formation (83 DAS) and accompanied by a decrease in CN stocks in nodules during the same period, probably due to the decomposition of the nodules biomass after their senescence (Fig. 5, b).

This study demonstrated the possibility of predicting the daily interactions of CN between the different organs of the plant, soil and atmosphere, by modeling the functional role of microorganisms, in particular N_2-fixing rhizobial bacteria. The MOMOS model defines microbial growth by assimilation of the labile and stable compartments of plant residues and humus as well as root exudates with a simulation of C and N fluxes in the different pools of the soil-plant-microorganism system (Pansu et al., 2009).

The MOMOS model becomes increasingly a generic model since its first application in tropical ecosystems (Pansu et al., 2004, 2010), and its validation under Mediterranean soil conditions in the durum-faba intercropping system at French agrosystems (Ibrahim et al., 2013). F tests showed that the measured data were matched the model predictions at 1 to 5% significance for all studied parameters, the MOMOS model appears to be an effective tool for collecting and analyzing eco-physiological parameters, which are difficult to obtain by experimental methods in different agro-ecological systems.

Despite an increase in C and N stocks in the shoot and root biomass of intercropped maize and common bean, the total C and N stock in the soil remains relatively stable after 21 days of sowing and up to the flowering stage (Fig. 5, a). This dynamics of the

CN fluxes in soil and biomass compartments is identical to the dynamics reported in other experiments describing the assimilated C and N distribution in the plant and soil (Butler et al., 2004, Ibrahim et al., 2013).

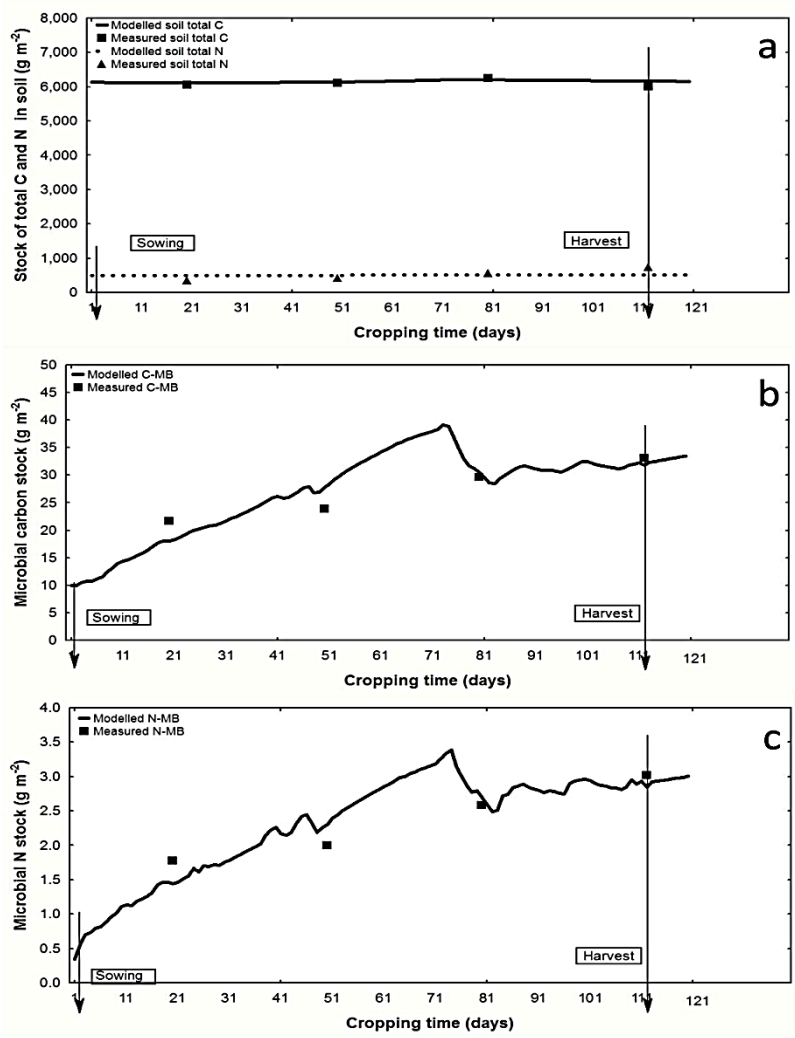

Figure 5. Measured with 95% confidence intervals and modelled values of total carbon and nitrogen in the soil(a), microbial carbon (b) and microbial nitrogen (c) in intercropping.

The increase in the daily CN flow in the plant biomass (Figs 2 and 3) is accompanied by a strong accumulation of these elements in the biomass of the nodules and that of the soil microorganisms particularly during the flowering stage (Fig. 5, b and c). The daily modeling of the CN exchanges between the plant and the soil clearly revealed the role of soil microorganisms in stimulating CN transfers in the maize and common beans grown under intercropping. Moreover, the total C and N inputs did not directly change CN stocks during the cropping cycle. Microbial biomass provides

information on the biological functioning of the soil and is rapidly affected by changes in agricultural practices (Marchand, 2003).

C and N constitute an energy source for micro-organisms, which stimulates their growth and activity. Moreover, microorganisms stimulate rhizodeposition and in this case, C is the most rapidly available to be transferred to the rhizosphere where it would be assimilated by microorganisms (Bazot et al., 2005). The results of simulation of the daily flows of N during the flowering period seem to confirm the high concentration of N observed in both shoot and root biomasses and in the rhizospheric soil of the two intercropped species (Latati et al., 2013 and 2017). These authors reported a strong stimulation of common bean growth when intercropped with maize through the symbiotic N_2 fixation of rhizobial bacteria. Microbial biomass is characterized by rapid turnover compared to other constituents of organic matter especially total C and N (Pansu et al., 2010). It is a sensitive indicator of the evolution of cropping systems according to sustainable cropping practices, particularly in the maize-common bean intercropping system (Sparling et al., 1998).

Furthermore, Fig. 6 shows the CO_2 flux data measured in the maize-common bean intercropping. All respirations (respiration of nodules, roots and microbial respiration) are simulated from the total respiration of the soil. The measured values of the total respiration are strongly adjusted with the daily data simulated during the cropping cycle. A slight difference in simulation, observed in total respiration, is due to an overestimation of the data measured during the first sampling period (21 days after sowing) (Fig. 4). This difference may be explained by the presence of weeds on the experimental field during the growth stage. In addition, autotrophic respiration (root and nodular respiration) and heterotrophic (microbial respiration) increase markedly between sowing and late flowering, reaching the maximum values of this activity. Moreover, a decrease in soil respiration was observed during the same period (83 DAS), indicating a decrease in microbial CN stocks (Fig. 6).

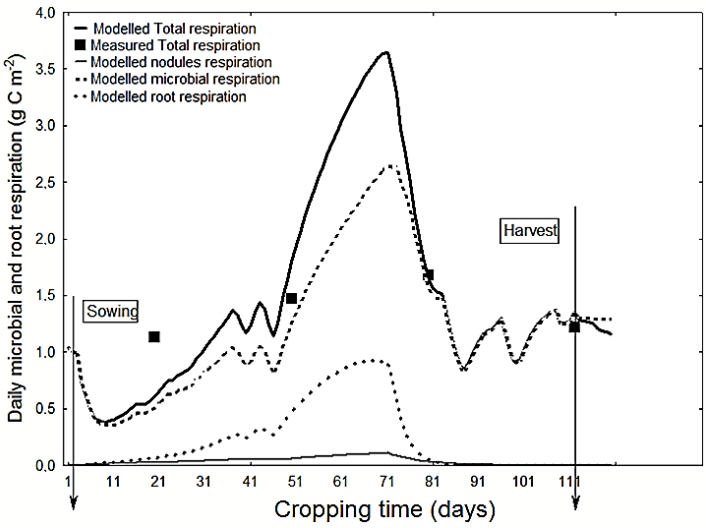

Figure 6. Measured total respiration at soil surface with 95% confidence intervals, and modelled values of root, microbial, nodules and total respirations.

The decrease in both total soil respiration and soil C stocks are accompanied by a strong sequestration of C in the shoot and root of both intercropped maize and common bean especially during seed formation and development (Fig. 6). Plants respire for growth. The results obtained in Fig. 4 show a fast increase in total soil respiration under maize-common bean intercropping during the period from 21 to 70 DAS. Respiration increases due to an increase in biomass production (Schapendonk et al., 1997, Bargaz et al., 2012). Moreover, the decrease in the different components of soil respiration during the harvest stage can be explained by the mortality of the root system which represents the majority respiration of total respiration (Bazot et al., 2005).

Our results are in agreement with those published by Thornton et al. (2004), on the cultivation of ray grass in hydroaeropia. Ibrahim et al. (2013) reported an increase in soil respiration throughout the crop cycle under legumes (faba bean) -cereal (durum wheat) intercropping system. This contradicts our results especially during the last stage of crop development (Fig. 6).

Our results show that the evolution of microbial respiration as well as that of nodules is proportional to that of microbial biomass throughout the flowering period. The same rate of evolution observed between biomass and microbial respiration can be justified by the increasing evolution of the different communities of microorganisms including rhizobia. These results confirm those reported by Pansu et al., (2007, 2009) during the validation of the MOMOS model.

In order to determine the nature and degree of divergence between the different pools of C that may affect N_2 fixation in the common bean-maize intercropping, the relationship between C in the nodular pool and that in the shoot was studied. Moreover, the relationship between the nodular sequestered C and the CN exchanges with the atmosphere via symbiotic N_2 fixation and nodular respiration is studied since nodules formation (21 DAS) to the end of flowering stage (81 DAS).

Fig. 7, a and b show a significant and positive correlation between the C sequestered in the nodules and that stored in the shoot biomass of intercropped common bean ($R^2 = 0.53$*) and maize ($R^2 = 0.51$*). These positive correlations confirm the efficiency of rhizobial symbiosis by intercropped common bean and the contribution of nodules in facilitating C sequestration processes in the shoot biomass of both intercropped common bean and maize (Fig. 7, a and b). The C sequestered in the nodular biomass presents a highly significant and positive correlation ($R^2 = 0.99$ ***) with the flow of C released by nodular respiration (Fig. 7c). Similarly, the fixed nitrogen is positively correlated ($R^2 = 0.69$ **) with the sequestered C in the nodules (Fig. 7, d). This correlation confirms the high efficiency of common beans-rhizobia symbiosis when it was grown intercropped with maize and consequently the increase in N transfers in the different compartments (microbial biomass, stem and nodules) particularly during the flowering stage (Figs 2, 3 and 4).

The simulation results show a positive relationship between the predicted values of the C nodular biomass and the C stock in either common bean or maize shoot in intercropping (Fig. 5). However, the estimation of the use efficiency of rhizobian symbiosis (UERS), defined by the ratio between the simulated C of the nodule and shoot biomass, showed a relatively low value (low coefficient of determination, $R^2 = 0.53$) compared with that measured (Bargaz et al., 2012, Latati et al., 2014, 2016) and in hydroaeropia by Alkama et al., (2009). These authors reported correlations between the shoot and nodule biomass with $R^2 > 0.7$. Recent research has demonstrated the positive

effect of N_2 fixation by legumes intercropped with cereals. It results in biomass accumulation and yield increase through N-resource facilitation especially for intercropped cereals (Zhang et al., 2004, Betencourt et al., 2012, Latati et al., 2016). Several studies have focused on the interaction between nodular permeability to oxygen (nodular respiration) and nodular biomass. These studies have shown in a hydroaeropic-controlled environment that the oxygen nodular permeability is increased under P deficiency (Saber et al., 2008, Alkama et al., 2009).

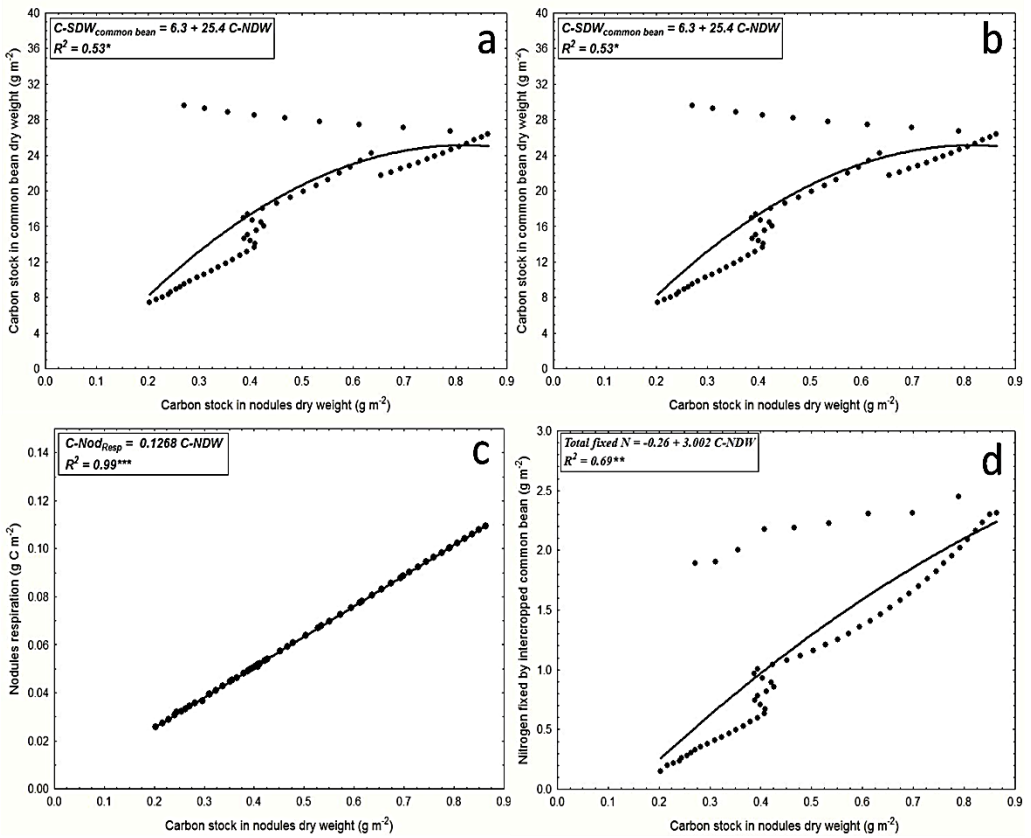

Figure 7. Correlation of modelled values of nodular carbon stock with common bean (a) and maize (b) shoot carbon stock, nodules respiration (c) and the modeled values of fixed nitrogen by intercropped common bean (d).

The application of the MOMOS model allows the simulation of the nodular respiration as well as the quantity of N fixed during the critical phase of symbiotic fixation of N_2. The simulation results show a strong correlation ($R^2 = 0.69$) of N fixed with the C stored in the nodular biomass and, on the other hand, a very strong correlation ($R^2 = 0.99$) of the nodular respiration with the C nodular biomass. It has been shown that the increase in nodular respiration depends on the symbiotic fixation of nitrogen. Alkama et al. (2009) reported that nodular respiration in common beans is positively correlated with the symbiotic fixation of atmospheric nitrogen. The same authors found that the

common bean root nodules excrete in their rhizosphere an amount of H^+ which is correlated with the nodular permeability (nodular respiration).

In this present research the validation of the MOMOS model on the CN data of the maize-bean intercropping system in P-deficient soil revealed two mechanisms, namely the C (nodular respiration) and N (symbiotic N_2 fixation) exchange processes. These mechanisms may explain the physiological behavior of maize and common bean in intercropping with the stimulation of EURS (Latati et al., 2013, 2016) and rhizosphere acidification (Latati et al., 2014), which are relatively related to the nodular respiration of intercropped common bean.

CONCLUSION

The validation of the MOMOS model with the collected CN data in intercropping system makes it possible to demonstrate the functional role of the microorganisms including that of the rhizobial symbiosis via the stimulation of the nodular respiration during the biological N_2 fixation. Indeed, the results obtained make it possible to define relationships between the microbial biomass and its feeding (by the shoot and roots necromasses compartments), the nodulation controlling the N_2 (from the atmosphere to the soil) and CO_2 (from the soil to the atmosphere) exchanges. Also, these results highlighted the crucial role of intercropped common bean symbiosis in maintaining the balance between the different CN exchanges, particularly with the soil and the atmosphere under low P soil conditions. It is now proved that the accuracy of the MOMOS model is perfectly adapted to the study of the CN dynamics in Mediterranean soils, especially Algerian soils which are relatively poor in OM. MOMOS predicted the restoration of soil fertility in C and N using the maize-bean intercropping system. So, this is considered a powerful forecasting tool for the sustainability of cropping systems.

In the face of climate change, the choice of cropping system is of considerable importance in developing sustainable agriculture. For this, the legumes-cereals intercropping is a promising alternative to meet this expectation by sustainably supplying nitrogen and phosphorus, which are essential elements for plant production.

ACKNOWLEDGEMENTS. The paper was prepared with the support of RUDN university program 5–100. The authors thank 'La Direction Génerale de la Recherche Scientifique et du Développement Technologique: DGRSDT-MESRES' for the financial support in the case of ARIMNET2-SEMIARID project. The authors also thank Mr. Marc Pansu for his advice and his orientations in this work.

REFERENCES

Alkama, N., Bolou Bi Bolou, E., Vailhe, H., Roger, L., Ounane, S.M. & Drevon, J.J. 2009. Genotypic variability in P use efficiency for symbiotic nitrogen fixation is associated with variation of proton efflux in cowpea rhizosphere. *Soil Biol Biochem.* **41**, 1814–1823.

Bargaz, A., Ghoulam, C., Amenc, L., Lazali, M., Faghire, M., Abadie, J. & Drevon, J.J. 2012. A phosphoenol pyruvate phosphatase transcript is induced in the root nodule cortex of Phaseolus under phosphorus deficiency. *J. Exp. Bot*. **63**, 4723–4730.

Bargaz, A., Noyce, G.L., Genevieve, F.R., Carlsson, C., Furze, J.R., Jensen, E.J., Dhiba, D. & Isaac, M.E. 2017.Species interactions enhance root allocation, microbial diversity and P acquisition in intercropped wheat and soybean under P deficiency. *Appl. Soil Eco.* **120**, 179–188.

Bargaz, A., Lyamlouli, K., Chtouki, M., Zeroual, Y. & Dhiba, D. 2018. Soil Microbial Resources for Improving Fertilizers Efficiency in an Integrated Plant Nutrient Management System. *Frontiers in microbiology* **9**, 1606. doi:10.3389/fmicb.2018.01606.

Barthès, B.G., Brunet, D., Hien, E., Enjalric, F., Conche, S., Freschet, G., d'Annunzio, R. & Toucet-Louri, J. 2008. Determining the distributions of soil carbon and nitrogen in particle size fractions using near infrared reflectance spectrum of bulk soil samples. *Soil Biol Biochem.* **40**, 1533–1537.

Bazot, S., Mikola, J., Nguyen, C. & Robin, C. 2005. Do defoliation-induced changes in C allocation of field-grown Lolium perenne affect C availability, microbes and microbial feeders in soil? *Functional Ecology* **19**(5), 886–896.

Betencourt, E., Duputel, M., Colomb, B., Desclaux, D. & Hinsinger, P. 2012. Intercropping promotes the ability of durum wheat and chickpea to increase rhizosphere phosphorus availability in a low P soil. *Soil Biol Biochem*. **46**, 21–33.

Butler, J.L., Bottomley, P.J., Griffith, S.M. & Myrold, D.D. 2004. Distribution and turnover of recently fixed photosynthate in ryegrass rhizospheres. *Soil Biol Biochem*. **36**, 371–381.

Corre-Hellou, G., Faure, M., Launay, M., Brisson, N. & Crozat, Y. 2009. Adaptation of the STICS intercrop model to simulate crop growth and N accumulation in pea–barley intercrops. *Field Crops Res.* **113**, 72–81. doi:10.1016/j.fcr.2009.04.007

Dahmardeh, M., Ghanbari, A., Syahsar, B. & A. Ramrodi, M. 2010. The role of intercropping maize (Zea mays L.) and Cowpea (Vigna unguiculata L.) on yield and soil chemical properties. *African J Agric Res.* **5**(8), 631–636.

Dornbush, M.E. & Raich, J.W. 2006. Soil Temperature, Not Aboveground Plant Productivity, Best Predicts Intra-Annual Variations of Soil Respiration in Central Iowa Grasslands. *Ecosyst.* **9**, 909–920. doi: 10.1007/s10021-005-0093-7

Horrigan, L., Lawrence, R.S. & Walker, P. 2002. How Sustainable Agriculture Can Address the Environmental and Human Health Harms of Industrial Agriculture. *Environmental Health Perspectives* **110**, 445–456.

Ibrahim, H., Hatira, A. & Pansu, M. 2013. Modeling the functional role of microorganisms in the daily exchanges of carbon between atmosphere, plants and soil. *Proc Env Sci.* **19**, 96–105.

Joergensen, R.G. 1996. The fumigation-extraction method to estimate soil microbial biomass: Calibration of the k(EC) value. *Soil Biology & Biochemistry* **28**, 25–31.

Ladd, J.N., Jocteur-Monrozier, L. & Amato, M. 1992. Carbon turnover and nitrogen transformations in an alfisol and vertisol amended with [U-14C] glucose and [15N] ammonium sulfate. *Soil Biol Biochem.* **24**, 359–371.

Latati, M., Pansu, M., Drevon, J.J. & Ounane, S.M. 2013. Advantage of intercropping maize (Zea mays L.) and common bean (Phaseolus vulgaris L.) on yield and nitrogen uptake in Northeast Algeria. *International J. Res. Appl.* Sci. **01**, 1–7.

Latati, M., Blavet, D., Alkama, N., Laoufi, H., Pansu, M., Drevon, J.J., Gerard, F. & Ounane, S.M. 2014. The intercropping cowpea-maize improves soil phosphorus availability and maize yields in an alkaline soil. *Plant Soil.* **385**, 181–191.

Latati, M., Bargaz, A., Belarbi, B., Lazali, M., Benlahrech, S., Tellah, S., Kaci, G., Drevon, J.J. & Ounane, S. M. 2016. The intercropping common bean with maize improves the rhizobial efficiency, resource use and grain yield under low phosphorus availability. *Eur. J. Agron.* **72**, 80–90.

Latati, M., Aouiche, A., Tellah, S., Laribi, A., Benlahrech, S., Kaci, G. & Ounan, S.M. 2017. Intercropping maize and common bean enhances microbial carbon and nitrogen availability in low phosphorus soil under Mediterranean conditions. *European Jounal of Soil Biology*. **80**, 8–19.

Liu, Y., Wu, L., Baddeley, J.A. & Watson, C.A. 2011. Models of biological nitrogen fixation of legumes. A review. *Agron Sustain Dev*. **31**, 155–172. doi: 10.1051/agro/2010008

Marchand, A.L. 2003. Rhizosphere study of maize: The influence of Photoassimilates distribution on roots and root morphology. *PhD thesis*. INPL/ENSAIA.

Pansu, M., Bottner, P., Sarmiento, L. & Metselaar, K. 2004. Comparison of five soil organic matter decomposition models using data from a 14C and 15N labeling field experiment. *Global Biogeochemical Cycles* **18**, GB4022.

Pansu, M., Martineau, Y. & Saugier, B. 2009. A modeling method to quantify in situ the input of carbon from roots and the resulting C turnover in soil. *Plant Soil*. **317**, 103–120.

Pansu, M., Sarmiento, L., Metselaar, K., Hervé, D. & Bottner, P. 2007. Modeling the transformations and sequestration of soil organic matter in two contrasting ecosystems of the Andes. *European Journal of Soil Science* doi :10.1111/j.1365–2389.2006.00867.

Pansu, M., Sarmiento, L., Rujano, M.A., Ablan, M., Acevedo, D. & Bottner, P. 2010. Modeling Organic transformations by Micro-Organisms of Soils in six contrasting ecosystems: validation of the MOMOS model. Global Biogeochemical Cycles. **24**, GB1008.

Penning de Vries, F.W.T., Jansen, D.M., Ten Berge, H.F. M. & Bakema, A. 1989. *Simulation of ecophysiological processes of growth in several annual crops*. Pudoc. Wageningen. The Netherlands, 271 pp. ISBN 90-220-0937-8

Saber, S., Alkama, N., Abdelly, C. & Drevon, J.J. 2008. Proton efflux by nodulated roots varies among common-bean genotypes (Phaseolus vulgaris) under phosphorus deficiency. *J. Plant Nutr. Soil Sci.* **171**, 242–248.

Schapendonk, A.H.C.M., Dijkstra, P., Groenwold, J., Pot, C.S. & Van de Geijn, S.C. 1997. Carbon balance and water use efficiency of frequently cut Lolium perenne L. swards at elevated carbon dioxide. *Global Change Biology* **3**, 207–216.

Sparling, G., Vojvodić-Vuković, M. & Schipper, L.A. 1998. Hot-water-soluble C as a simple measure of labile soil organic matter: the relationship with microbial biomass C. *Soil Biol Biochem.* **30**, 1469–1472.

Srivastava, S.C. & Singh, J.S. 1989. Effect of cultivation on microbial biomass C and N of dry tropical forest soil. *Soil Biol. Fert. Soils*. **8**, 343–348.

Thornton, B., Paterson, E., Midwood, A.J., Sim, A. & Pratt, S.M. 2004. Contribution of current carbon assimilation in supplying root exudates of Lolium perenne measured using steady-state 13C labelling. *Physiol Planta* **120**(3), 434–441.

Vance, E.D., Brookes, P.C. & Jenkinson, D.S. 1987. An extraction method for measuring microbial biomass C. *Soi1 Biol. Biochem.* **19**, 703–707.

Wu, J., Joergenson, R.G., Pommerening, B., Chaussod, R. & Brookes, P.C. 1990. Measurement of soi1 microbial biomass C by fumigation-extraction : An automated procedure. *Soi1 Biol Biochem.* **22**, 1167–l169.

Yuste, J.C., Janssens I.A., Carrara, A. & Ceulemans, R. 2004. Annual Q10 of soil respiration reflects plant phenological patterns as well as temperature sensitivity. *Glob Change Biol*. **10**, 161–169.

Zhang, F., Zhang, S., Zhang, J., Zhang, R. & Li, F. 2004. Nitrogen fertilization on uptake of soil inorganic phosphorus fractions in the wheat root zone. *Soil Sci Soc America. J*. **68**, 1890–1895.

Agronomy Research **17**(2), 574–581, 2019
https://doi.org/10.15159/AR.19.107

Effect of two housing systems on performance and longevity of dairy cows in Northern Italy

L. Leso, P. Pellegrini and M. Barbari*

University of Florence, Department of Agriculture, Food, Environment and Forestry, Via San Bonaventura, 13. IT50145 Firenze, Italy
*Correspondence: matteo.barbari@unifi.it

Abstract. The objective of the current study was to evaluate and compare performance of dairy cows housed in compost-bedded pack barns (CBP) and free stall barns, with a focus on longevity-related parameters. Study included 30 commercial dairy farms located in the Po Valley, Italy. Twenty farms had free stall barns, among which 10 used rubber mattresses (FSM) and 10 used deep straw bedding (FSS). The remaining 10 farms had CBP. Monthly dairy herd records were obtained from the Italian DHI association for each farm included in the study over a period of one year. All farms were visited to measure characteristics and dimensions of housing facilities. Linear mixed models were used to evaluate the association between housing system and the outcome variables. In CBP total available area was larger than both in FSM and FSS. However, space per cow over the bedded pack area in CBP (6.8 ± 2.4 m^2 cow^{-1}) was relatively low for this housing system. Milk production was similar among housing systems but somatic cell count and mastitis infection prevalence resulted to be higher in CBP than in FSM and FSS. Calving interval was lower in FSS compared with both FSM and CBP while no differences were found in number of services per pregnancy. Cows housed in CBP were older and had higher parities than those in FSM and FSS while no significant differences in herd turnover rate were detected among housing systems. Results confirm that CBP housing system may improve longevity of dairy cows, which is reported to be one of the most important motivations for building this kind of housing. Nevertheless, CBP housing can pose some challenges in achieving adequate udder health and high milk quality, especially with low space per cow.

Key words: compost-bedded pack barns, freestall, cows, animal welfare, longevity.

INTRODUCTION

The welfare of dairy cattle results from an interaction of several factors. Recent research shows that housing conditions and facility design play a major role in determining cow's health (von Keyserlingk et al., 2009). Gaworsky et al. (2018) in Estonian dairy farms found a decreased tendency in the prevalence of disease cases for udder diseases with an increase in cow herd size. Free stall barns represent the most widespread housing system in intensive dairy farms worldwide. Despite that, recent studies have shown this system can compromise animal welfare and hinder natural cows' behaviour (EFSA, 2009). In recent years, these welfare-related issues concerning free stalls have fostered the interest of farmers and researchers towards alternative loose housing systems, such as compost-bedded pack barns (CBP). Introduced in the US since

2001, the CBP system spread rapidly and nowadays is known worldwide to potentially improve welfare of dairy cows (Bewley et al., 2017).

As opposed to free stalls, in CBP cows are provided with a large open bedded area on which they can lie, stand and walk freely. The bedded pack is aerated once or twice per day to promote evaporation and maintain a soft and hygienic surface for the cows (Leso et al., 2013; Bewley et al., 2017). In CBP, the most commonly used bedding materials are sawdust and wood shavings (Janni et al., 2007). Other materials including straw, peanut shells, woodchips and compost have also been used (Galama, 2014; Favèro et al., 2015; Leso et al., 2018). Generally, CBP requires more space per cow compared with free stalls, as maintaining an adequate animal density over the bedded pack is crucial. Suggested space allowance in CBP ranges from 7.4 to more than 15 m^2 cow^{-1} depending on barn characteristics, bedding availability and pack management (Janni et al., 2007).

Main benefits of CBP include improved feet and leg health and more natural behaviour compared with free stalls, which are likely due to reduced exposure to concrete flooring and injury-causing obstacles within housing (Fulwider et al., 2007). Results with CBP however, strictly depend on pack management (Leso et al., 2013; Mota et al., 2018). Evidence shows that some pack characteristics, especially pack moisture, may affect cows' hygiene and risk of mastitis (Eckelkamp et al., 2016). The main reasons, that producers reported for building CBP, is the improvement of cow comfort and longevity (Barberg et al., 2007; Black et al., 2013). However, little is still known about the effect of this housing system on longevity-related traits. The objective of the current study was to evaluate and compare performance of dairy cows housed in CBP and free stall barns, with a particular interest in longevity.

MATERIALS AND METHODS

This study was performed on 30 dairy farms in the provinces of Mantua (n = 27) and Cremona (n = 3), northern Italy. Twenty farms had FS, among which 10 used rubber mattresses (FSM) and 10 used deep straw bedding (FSS). The remaining 10 farms had CBP. Main bedding materials used in the CBP were sawdust and wood shavings. Producers with CBP cultivated the pack twice or once a day, with an average of 1.4 cultivations per day. Further information about the CBP involved in the current study can be found in Leso et al. (2013). All farms included met the following criteria: used the same housing system for all lactating cows for at least two years before the beginning of the study, the primary breed was Holstein, cows were milked twice daily in a milking parlour, cows were fed with TMR. As all farms involved were located in the production area of Grana Padano cheese all rations were based on corn silage (Mantovi et al., 2015).

Monthly dairy herd records were obtained from the Italian Dairy Association (Associazione Italiana Allevatori, Rome, Italy) for each farm included in the study. The following data were collected over a period of one year (from September 2011 till September 2012): number of cows, daily milk yield, 305-day milk yield, milk fat and protein content, SCC, number of parity, DIM, calving interval, number of services per pregnancy, age at first calving and herd age. Herd age (HA) referred to the mean age (months) of all adult cows in the herd. Mastitis infection prevalence (MIP) was calculated as the number of cows infected divided by the total number of cows. Cows

were considered to be infected when their test-day SCC was greater than 200,000 cells mL^{-1}.

For each farm the monthly herd turnover rate (MHTR) was calculated as the number of cows culled over a period of one month (x100) divided by the mean cow inventory for the same time period (Fetrow et al., 2006). The annual herd turnover rate (AHTR) was obtained by the sum of all the MHTR recorded over a period of one year. Monthly records were grouped by season (fall: September, October and November; winter: December, January and February; spring: March, April, May; summer: June, July and August). Each farm was visited once between July and September 2012 to collect on-site data that included: total available area, laying area (surface covered with bedding or mattresses), number of free stalls (only in free stall barns) and feed fence length. Barn dimensions were measured using a Leica DISTO A5 laser distance meter (Leica Geosystems, Heerbrugg, Switzerland). For each barn a bedded ratio (BR) was calculated by dividing the bedded area inside the barn by the total available area.

Statistical analysis

Descriptive statistics (mean and SD) were used to describe herds' performance and barns' characteristics in each group of farms with the same housing system. One-way ANOVA (R package 'stats'; R Development Core Team, 2018) was used to determine whether housing system produces significant differences in space per cow, BR, number of cows, milk yield, 305ME, SCC, MIP, calving interval, number of services per pregnancy and AHTR. In order to evaluate the association between housing systems, herd records and the main outcome variables (HA and MHTR) a linear mixed model was built. A univariate linear model (R package 'stats'; R Development Core Team, 2011) was used to identify variables to be included in the multivariate model. Variables with P-value < 0.2 were included. An automatic model selection procedure based on the R package 'glmulti' (Calcagno, 2013) was used to build the models. The Bayesian Information Criterion was used for model selection. Variables included were all significant at P-value < 0.05. Housing system was forced in all models as explanatory variable. Residuals were visually checked. Tukey's method was used for multiple comparisons of least squares means (R package 'lsmeans'; Lenth, 2016) in categorically distributed variables within mixed models.

RESULTS AND DISCUSSION

The characteristics of the barns are summarized in Table 1. Total available area per cow in CBP (11.0 ± 4.1 m^2 cow^{-1}) was larger than that in FSM (9.0 ± 2.3 m^2 cow^{-1}) and FSS (9.3 ± 5.4 m^2 cow^{-1}). Cultivated pack barns had higher BR (0.65 ± 0.18) compared with FSM (0.38 ± 0.06) and FSS (0.37 ± 0.10). The pack density in CBP was 6.8 ± 2.4 m^2 cow^{-1}. The space per cow on the bedded area found in this study was lower than that measured in CBP in other countries. Barberg et al. (2007) found an average pack density of 8.6 ± 2.6 m^2 cow^{-1} in Minnesota CBP while Lobeck et al. (2011), studying CBP in the upper Midwest of US, measured an average pack density of 7.6 ± 1.1 m^2 cow^{-1}. Other researchers from the University of Kentucky recommended that the pack area should provide at least 9.3 m^2 of resting space per cow (Bewley et al., 2012). Other experiences with CBP in the Netherlands found that at least 15 m^2 bedded pack space per cow is needed to keep the pack sufficiently dry for the whole year

(Galama, 2014). Also in Israel 15 m^2 cow^{-1} is considered to be an adequate pack density in CBP (Klaas et al., 2010). Although the optimal space per cow in CBP depends on several factors such as climate, type and depth of bedding, barn's characteristics, pack management, breed and size of cows (Bewley et al., 2017), the pack density found in Italian CBP (6.8 ± 2.4 m^2 cow^{-1}) appears to be too high for this housing system.

Table 1. Characteristics of free stall barns with deep straw bedding (FSS), free stall barns with mattresses (FSM) and cultivated pack barns (CBP) in Italy

	FSS		FSM		CBP	
	Mean	SD	Mean	SD	Mean	SD
Total area per cow (m^2 cow^{-1})	9.3	5.4	9.0	2.3	11.0	4.1
Stocking density (cows $stall^{-1}$)	1.09	0.42	0.92	0.10	-	-
Pack density (m^2 cow^{-1})	-	-	-	-	6.8	2.4
Bedded ratio	0.37	0.10	0.38	0.06	0.65	0.18
Space at feed fence (m cow^{-1})	0.63	0.18	0.66	0.07	0.58	0.20

Characteristics and performance of the herds involved in this study are summarized in Table 2. The average number of lactating cows in each housing system was 143 ± 83.9, 147 ± 102.3 and 112 ± 56.6 in FSS, FSM and CBP, respectively. Herds in CBP were smaller than those housed in FSS and FSM ($P = 0.004$), with no difference between FSS and FSM. Other studies from the US also found lower number of cows in CBP compared with free stall barns (Fulwider et al., 2007; Lobeck et al., 2011). Some authors reported an increased interest towards CBP for housing special need cows (Bewley et al., 2017). These findings led to think that although farmers have a positive perception of CBP, especially for welfare related issues, concerns about cost of bedding and ease of management could limit the use of this housing system in bigger operations (Lobeck et al., 2011).

Table 2. Characteristics and performance of cows housed in free stall barns with straw bedding (FSS), free stall barns with mattresses (FSM) and cultivated pack barns (CBP) in Italy

	FSS		FSM		CBP	
	Mean	SD	Mean	SD	Mean	SD
Cows, no.	143[a]	83.9	147[a]	102.3	112[b]	56.6
Day in milk (days)	190	26.3	204	35.7	209	33.1
Parity	2.23	0.27	2.18	0.11	2.39	0.25
Milk yield (kg cow^{-1} day^{-1})	31.4	3.91	29.8	4.6	30.8	3.6
305-day milk yield (kg)	10,901	963	10,450	1,043	10,541	663
% fat	3.93	0.36	3.75	0.32	3.67	0.28
% protein	3.43	0.13	3.38	0.15	3.48	0.16
SCC (cells*1000 mL^{-1})	310[a]	128	259[b]	115	354[a]	171
Mastitis infection prevalence (%)	29.6[a]	9.5	23.2[b]	8.4	32.8[a]	12.7
Calving interval (days)	420[a]	19.1	442[b]	37.3	449[b]	72.9
Services per pregnancy, no.	2.54	0.61	2.59	0.64	2.67	0.50

[a,b] Significant differences among columns ($P < 0.05$).

Milk yield and 305-d mature equivalent milk production (305ME) did not differ among housing systems averaging 31.4 ± 3.91 kg cow^{-1} day^{-1} and 10,901 ± 963 kg, 29.8 ± 4.6 kg cow^{-1} day-^{1} and 10,450 ± 1043 kg, and 30.8 ± 3.6 kg cow^{-1} day^{-1} and

10,541 ± 663 kg in FSS, FSM and CBP, respectively. Somatic cell count in FSM (259,000 ± 115,000 cells mL^{-1}) was lower than that in FSS (310,000 ± 128,000 cells mL^{-1}) and CBP (354,000 ± 171,000 cells mL^{-1}; $P < 0.001$). Mastitis infection prevalence was lower in FSM (23.2 ± 8.4%) compared with FSS (29.6 ± 9.5%) and CBP (32.8 ± 12.7%; $P < 0.001$). No differences in SCC and MIP were detected between CBP and FSS. The SCC measured in CBP involved in this study was similar to 325,000 cell mL^{-1} (Barberg et al., 2007) and 318,000 cell mL^{-1} (Black et al., 2013) previously reported in CBP located in Minnesota and Kentucky, respectively. Another research involving CBP in the upper Midwest of US found higher SCC (434,000 cells mL^{-1}) but similar MIP (33.4%). In the same study the udder health of cows housed in CBP was compared with that of cows in free stall barns finding that both SCC and MIP were lower in free stalls, even though differences were not statistically significant (Lobeck et al., 2011).

These findings suggest that CBP may pose some challenges in achieving adequate udder health and high milk quality. As the bedded pack in CBP is known to contain high bacteria concentrations, the CBP environment appears to be hazardous from an udder health standpoint (Lobeck et al., 2012; Eckelkamp et al., 2016). Many authors highlighted the importance of applying correct pack management procedures (Bewley et al., 2017). In CBP, keeping the pack dry is paramount to achieve sufficient cow hygiene and reduce the risk of mastitis (Favero et al., 2015). Also, excellent teat preparation procedures at milking have also been recommended for dairies with CBP (Janni et al., 2007, Lobeck et al., 2012, Black et al., 2014).

Calving interval was lower in FSS (420 ± 19.1 days) compared with both FSM (442 ± 37.3 days) and CBP (449 ± 72.9 days; $P < 0.001$). The number of services per pregnancy did not differ between FSS (2.54 ± 0.61), FSM (2.59 ± 0.64) and CBP (2.67 ± 0.50). Since in CBP there was more space per cow and higher BR compared with free stall barns a more natural behaviour could have been expected (Fulwider et al., 2007), thus may led to an easier heat detection. Barberg et al. (2007) reported an increase in pregnancy rate in 5 out of 7 farms after shifting from tie stall to CBP. However, results obtained in the current study indicated poorer reproductive performance in CBP than in free stall barns. More exhaustive studies are needed to evaluate effects of this kind of housing system on reproductive performance whereas it is influenced by many environmental and management factors (Schefers et al., 2010).

The open pack area and the soft surface on which cows can stand, walk and rest in CBP is more similar to the pasture environment compared to free stall housing systems (Eckelkamp et al., 2014). This reduces behavioural limitations that may result from individual free stalls and concrete paving, allowing the expression of cattle natural behaviour (Endres & Barberg, 2007). As heat detection is mostly based on behaviour monitoring (Rutten et al., 2013), CBP has the potential to improve fertility, especially in regards of heat detection rate. However, the benefits of CBP housing strictly depend on pack management. If the pack gets too wet cows may sink into the pack and thus deeply limits cow comfort in CBP, leading to undesired behavioural responses and potentially to reduced fertility performance.

Herd age and herd turnover rate

The final model for herd age (HA) included housing system, calving interval and age at first calving (Table 3). Herd age was higher in CBP (48.46 months) than in FSM

and FSS (44.98 and 44.58 months, respectively; $P < 0.001$). No differences were found between FSM and FSS. Each 1-day increase in calving interval was associated with a 0.044-month increase in HA. Herd age also increased with age at first calving by 0.381 months. In literature, information about the effect of CBP on HA or cows' lifespan is still sparse.

Table 3. Least squares means and standard error of herd age (HA) in 3 housing systems: free stall barns with straw bedding (FSS), free stall barns with mattresses (FSM) and cultivated pack barns (CBP) in Italy

Housing system	LSM	SE	
FSS	44.58[b]	0.34	
FSM	44.98[b]	0.33	
CBP	48.46[a]	0.33	
Other parameters	Estimate	SE	P-value
Calving interval (days)	0.044	0.007	< 0.001
Age at first calving (months)	0.381	0.068	< 0.001

[a, b] Significant differences among rows ($P < 0.05$).

The final model for MHTR included housing system, season and housing system × season interaction. Monthly herd turnover rate was 2.98, 2.67 and 2.47% in FSS, FSM and CBP, respectively. No significant difference in MHTR were found between housing systems. Monthly herd turnover rate was higher in fall (3.69%) than in spring, summer and winter (2.38, 2.10 and 2.48%, respectively; $P < 0.001$), with no difference among the latter three.

A housing system × season interaction was observed (Table 4). During fall, MHTR was lower in CBP than in FSS ($P = 0.036$) while, during winter, CBP had lower MHTR than FSM ($P = 0.013$). The FSS barns had higher MHTR in fall than in winter ($P = 0.002$), spring ($P > 0.001$) and summer ($P = 0.008$). Monthly herd turnover rate in FSM was higher in fall than in spring ($P = 0.018$) and summer ($P = 0.005$) and it was higher in winter than in summer ($P = 0.027$). No differences in MHTR were detected among seasons in CBP. This is in contrast to what would have been expected because in CBP the winter season is largely seen as a critical period due to difficulties in keeping the pack dry (Lobeck et al., 2011).

Table 4. Least squares means and standard error of monthly herd turnover rate in 3 housing systems: free stall barns with straw bedding (FSS), free stall barns with mattresses (FSM) and cultivated pack barns (CBP) in Italy

	Housing system					
	FSS		FSM		CBP	
Season	LSM	SE	LSM	SE	LSM	SE
Fall	4.41[a,x]	0.38	3.58[x]	0.38	3.08[b]	0.38
Winter	2.47[y]	0.38	3.26[a,x]	0.38	1.72[b]	0.38
Spring	2.38[y]	0.38	2.00[y]	0.38	2.76	0.38
Summer	2.47[y]	0.47	1.57[y]	0.47	2.47	0.47

[a, b] Significant differences among columns (housing systems) within season ($P < 0.05$); [x, y] Significant differences among rows (seasons) within housing system ($P < 0.05$).

Annual herd turnover rate was 35.70 ± 9.31, 32.37 ± 6.59 and 29.68 ± 11.00% in FSS, FSM and CBP, respectively. No significant differences were detected in AHTR among housing systems ($P = 0.352$). This would be partially explained by the large variation in AHTR among farms. Lobeck et al. (2011) reported similar AHTR (30.1%) in CBP form US. In the same study, AHTR in CBP and free stall barns were compared and no significant differences between types of housing were found. Barberg et al. (2007) reported sensibly lower herd turnover rate (20.9%) in CBP compared with that found in the current study.

Within the dairy literature, the consensus is that lower AHTR are more profitable, with optimal rates of ≤ 3 0% (Fetrow et al., 2006). Annual herd turnover rates measured in CBP remained within this limit or barely above indicating that this alternative housing system can increase profitability of intensive dairy farms which often have higher culling rates. In a large survey carried out in the US including herds from 10 states over a 7-year period, the average culling rate was 35.1% (Hadley et al., 2006).

CONCLUSIONS

Cows housed in CBP were older than cows housed in free stall barns. Although, on average, the turnover rate was lower in CBP than in free stall barns, no significant difference was found in turnover rate among housing system. This would be partially explained by the large variation in turnover rate among farms. Results obtained partially confirm that CBP may improve longevity of dairy cows, which is reported to be one of the most important motivations for building this kind of housing. Further researches are needed to obtain more consistent results, especially about culling rates.

ACKNOWLEDGMENTS. Authors wish to thank all the dairy producers involved in the study for their kind collaboration. We also thank the Associazione Italiana Allevatori for their contribution in providing data.

REFERENCES

Barberg, A.E., Endres, M.I., Salfer, J.A. & Reneau, J.K. 2007. Performance and welfare of dairy cows in an alternative housing system in Minnesota. *J. Dairy Sci.* **90**, 1575–1583.

Bewley, J.M., Taraba, J.L., Day, G.B. & Black, R. 2012. *Compost bedded pack barn design features and management considerations.* Cooperative Extension Publ. ID-206, Cooperative Extension Service, University of Kentucky College of Agriculture, Lexington. 32 pp.

Bewley, J.M., Robertson, L.M. & Eckelkamp, E.A. 2017. A 100-Year Review: Lactating dairy cattle housing management. *J. Dairy Sci.* **100**, 10418–10431.

Black, R.A., Taraba, J.L., Day, G.B., Damasceno, F.A. & Bewley, J.M. 2013. Compost bedded pack dairy barn management, performance, and producer satisfaction. *J. Dairy Sci.* **96**, 8060–8074.

Black, R.A., Taraba, J.L., Day, G.B., Damasceno, F.A., Newman, M.C., Akers, K.A., Wood, C.L., McQuerry, K.J. & Bewley, J.M. 2014. The relationship between compost bedded pack performance, management, and bacterial counts. *J. Dairy Sci*. **97**, 1–11.

Calcagno, V. 2013. glmulti: Model selection and multimodel inference made easy. R package version 1.0.7. *https://CRAN.R-project.org/package=glmulti*. Accessed 16/10/18.

Eckelkamp, E.A., Gravatte, C.N., Coombs, C.O. & Bewley, J.M. 2014. Case study: Characterization of lying behavior in dairy cows transitioning from a freestall barn with pasture access to a compost bedded pack barn without pasture access. *Prof. Anim. Sci.* **30**, 109–113.

Eckelkamp, E.A., Taraba, J.L, Akers, K.A., Harmon, R.J. & Bewley, J.M. 2016. Understanding compost bedded pack barns: Interactions among environmental factors, bedding characteristics, and udder health. *Livest. Sci.* **190**, 35–42.

EFSA. 2009. Scientific report of EFSA prepared by the Animal Health and Animal Welfare Unit on the effects of farming systems on dairy cow welfare and disease. *Annex to the EFSA Journal* **1143**, 1–284.

Endres, M.I. & Barberg, A.E. 2007. Behavior of Dairy Cows in an Alternative Bedded-Pack Housing System. *J. Dairy Sci.* **90**, 4192–4200.

Fávero, S., Portilho, F.V.R., Oliveira, A.C.R., Langoni, H. & Pantoja, J.C.F. 2015. Factors associated with mastitis epidemiologic indexes, animal hygiene, and bulk milk bacterial concentrations in dairy herds housed on compost bedding. *Livest. Sci.* **181**, 220–230.

Fetrow, J., Nordlund, K.V. & Norman, H.D. 2006. Invited review: Culling: Nomenclature, definitions, and recommendations. *J. Dairy Sci*. **89**, 1896–1905.

Fulwider, W.K., Grandin, T., Garrick, D.J., Engle, T.E., Lamm, W.D., Dalsted, N.L. & Rollin, B.E. 2007. Influence of free-stall base on tarsal joint lesions and hygiene in dairy cows. *J. Dairy Sci*. **90**, 3559–3566.

Janni, K.A., Endres, M.I., Reneau, J.K. & Schoper, W.W. 2007. Compost dairy barn layout and management recommendations. *Appl. Eng. Agric*. **23**, 97–102.

Galama, P.J. 2014. *On farm development of bedded pack dairy barns in The Netherlands*. Report 707. Wageningen UR Livestock Research, Lelystad, NL. 35 pp.

Gaworski, M., Leola, A., Kiiman, H., Sada, O., Kic, P. & Priekulis, J. 2018. Assessment of dairy cow herd indices associated with different milking systems. *Agronomy Research* **16**(1), 83–93.

Hadley, G.L., Wolf, C.A. & Harsh, S.B. 2006. Dairy cattle culling patterns, explanations, and implications. *J. Dairy Sci*. **89**, 2286–2296.

Klaas, I.C., Bjerg, B.S., Friedmann, S. & Bar, D. 2010. Cultivated barns for dairy cows: An option to promote cattle welfare and environmental protection in Denmark? *Dansk Veterinærtidsskrift* **93**, 20–29.

Lenth, R.V. 2016. Least-Squares Means: The R Package lsmeans. *J. Stat. Softw.* **69**(1), 1–33.

Leso, L., Conti, L., Rossi, G. & Barbari, M. 2018. Criteria of design for deconstruction applied to dairy cows housing: a case study in Italy. *Agronomy Research* **16**(3), 794–805.

Leso, L., Uberti, M., Morshed, W. & Barbari, M. 2013. A survey of Italian compost dairy barns. *J. Agr. Eng*. **44**(3), 120–124.

Lobeck, K.M., Endres, M.I., Shane, E.M., Godden, S.M. & Fetrow, J. 2011. Animal welfare in cross-ventilated, compost-bedded pack, and naturally ventilated dairy barns in the upper Midwest. *J. Dairy Sci.* **94**, 5469–5479.

Lobeck, K.M., Endres, M.I., Janni, K.A., Godden, S.M. & Fetrow, J. 2012. Environmental characteristics and bacterial counts in bedding and milk bulk tank of low profile cross-ventilated, naturally ventilated, and compost bedded pack dairy barns. *Appl. Eng. Agric.* **28**, 117–128.

Mantovi, P., Dal Prà, A., Pacchioli, M.T. & Ligabue, M. 2015. Forage production and use in the dairy farming systems of Northern Italy. In van den Pol-van Dasselaar, A., Aarts, H.F.M., De Vliegher, A., Elgersma, A., Reheul, D., Reijneveld, J.A., Verloop, J. & Hopkins, A. (eds): *18th EGF Symposium on "Grassland and forages in high output dairy farming systems" Grassland Science in Europe, volume 20*. Wageningen Academic Publishers. Wageningen, The Netherlands, pp. 67–77.

Mota, V.C., Damasceno, F.A. & Leite, D.F. 2018. Fuzzy clustering and fuzzy validity measures for knowledge discovery and decision making in agricultural engineering. *Comput. Electron. Agric.* **150**, 118–124.

R Core Team. 2018. R: A language and environment for statistical computing. R Foundation for Statistical Computing, Vienna, Austria. *https://www.R-project.org/*. Accessed 23/10/18.

Rutten, C.J., Velthuis, A.G.J., Steeneveld, W. & Hogeveen, H. 2013. Invited review: Sensors to support health management on dairy farms. *J. Dairy Sci.* **96**, 1928–1952.

Schefers, J.M., Weigel, K.A., Rawson, C.L, Zwald, N.R. & Cook, N.B. 2010. Management practices associated with conception rate and service rate of lactating Holstein cows in large, commercial dairy herds. *J. Dairy Sci.* **93**, 1459–1467.

von Keyserlingk, M.A.G., Rushen, J., de Passillé, A.M. & Weary, D.M. 2009. Invited review: The welfare of dairy cattle - Key concepts and the role of science. *J. Dairy Sci*. **92**, 4101–4111.

Agronomy Research **17**(2), 582–592, 2019
https://doi.org/10.15159/AR.19.040

Effect of nitrogen rate and forecrop on nitrogen use efficiency in winter wheat (*Triticum aestivum*)

L. Litke*, Z. Gaile and A. Ruža

Latvia University of Life Sciences and Technologies, Institute of Soil and Plant Sciences
2 Liela street, LV-3001 Jelgava, Latvia
*Correspondence: linda.litke@llu.lv

Abstract. Application of plant nutrient is one of the most important measures increasing grain yield and yield quality. Excessive application of nitrogen fertilizers leads to nitrogen leaching and it affects the quality of groundwater and surface water. The objective of this research was to evaluate the effect of nitrogen fertilizer rate on nitrogen use efficiency in winter wheat after two forecrops. The experiment was conducted at the Research and Study farm 'Pēterlauki' of Latvia University of Life Sciences and Technologies (56° 30.658' N and 23° 41.580' E) in four growing seasons: 2014/2015, 2015/2016, 2016/2017 and 2017/2018. Researched factors were crop rotation (wheat/wheat and oilseed rape (*Brassica napus* ssp. *oleifera*/wheat) and five nitrogen fertilizer rates (kg ha^{-1}): N0 or control, N60, N120(90+30), N180(90+60+30) and N240(120+60+60). Nitrogen fertilizer affected winter wheat grain yield significantly ($P < 0.001$) and average grain yield increased significantly ($P < 0.049$) until nitrogen rate N180. But analyzing it after each forecrop separately, yield increased significantly ($P < 0.05$) until N120 after both forecrops. Nitrogen fertilizer affected nitrogen use efficiency (NUE), nitrogen uptake efficiency (NUpE), nitrogen utilization efficiency (NUtE) and protein content significantly ($P < 0.001$). When increasing nitrogen fertilizer rate NUE, NUpE and NUtE decreased, and higher results were observed at the lowest nitrogen rates. Increased nitrogen fertilizer rate also increased crude protein content in grain, and for bread baking suitable grain was obtained only with the highest N rate: N 240. Forecrop did not affect winter wheat grain yield, however, it affected NUtE ($P < 0.01$), NUE ($P < 0.001$) and nitrogen harvesting index ($P < 0.001$) significantly; higher results were observed when wheat was grown after wheat.

Key words: forecrop, nitrogen fertilizer, winter wheat, nitrogen use.

INTRODUCTION

The growth and development of any plant requires optimal supply of plant nutrients. The amount of nutrients in the soil and organic fertilizers cannot provide enough nutrients to produced high grain yields with appropriate quality for processing. Therefore, the use of mineral fertilizers as additional source of plant nutrients plays an important role in agriculture. Nitrogen shows the most apparent effect on yield and quality formation. At the same time, excessive application of nitrogen containing fertilizers not only increases production costs, but also leads to leaching of nitrogen from the soil. In its turn, leaching affected the quality of surface water and groundwater quality.

Nitrogen use efficiency is important indicator showing the amount of grain obtained on the nitrogen unit consumed. Nitrogen use efficiency depends on several factors. The most important factors are: meteorological conditions in growing season and applied cultivation technology. Nitrogen efficiency affected applied fertilizer – type of fertilizer, fertilizer rate and timing of fertilizer application (Haile et al., 2012). Previous studies in Latvia indicate that winter wheat grain yield increased significantly until nitrogen fertilizer rate N120 and with each next nitrogen fertilizer rate nitrogen fertilizer return decreased (Ruža et al., 2003). Other studies also contain information that increasing nitrogen rate decreased nitrogen use efficiency (Rahimizadeh et al., 2010; Haile et al., 2012). However, when changing crop varieties and using intensive cultivation technologies, farmers also use higher fertilizer rates. Therefore, it is important to find out nitrogen fertilizer rates which are agronomically justified. The aim of this paper is to evaluate the effect of nitrogen fertilizer rate on nitrogen use efficiency (NUE) of winter wheat after two forecrops.

MATERIALS AND METHODS

The experiment was conducted at the Research and Study farm 'Pēterlauki' of Latvia University of Life Sciences and Technologies (56° 30.658` N and 23° 41.580` E). Trial was repeated four years: 2014/2015, 2015/2016, 2016/2017 and 2017/2018, and it was arranged using split plot design in four replications, plot size was 25 m^2. As previously described, the researched factors were crop rotation (wheat/wheat and oilseed rape (*Brassica napus* ssp. *oleifera)*/wheat) and nitrogen fertilizer rate (altogether five rates: N0 or control, N60, N120 (90+30), N180 (90+60+30) and N240 (120+60+60). Totally, eight nitrogen rates were used in the trial (in addition to the mentioned: N 90, N150(90+60) and N210(90+70+50) (Litke et al., 2018)), but NUE and other parameters related to nitrogen use by crop (described below) were calculated and analysed only taking into account five rates. Traditional soil tillage with mould-board ploughing at depth of 20–22 cm was used. Straw of both forecrops was incorporated in the soil.

Table 1. Soil agrochemical characteristics depending on forecrop and growing season in winter wheat trial

Growing year and forecrop	pH KCl	Organic matter content, g kg^{-1}	P_2O_5 content, mg kg^{-1}	K_2O content, mg kg^{-1}
2014/2015				
wheat after oilseed rape	6.3	31	69	158
wheat after wheat	6.7	24	237	224
2015/2016				
wheat after oilseed rape	6.9	24	247	328
wheat after wheat	6.7	23	131	195
2016/2017				
wheat after oilseed rape	7.2	32	171	207
wheat after wheat	6.8	21	187	225
2017/2018				
wheat after oilseed rape	6.5	37	112	189
wheat after wheat	6.9	38	175	300

Note: pH KCL was detected potentiometrically in 1 *M* KCl suspension; organic matter content – oxidizing the soil with potassium dichromate ($K_2Cr_2O_7$); P_2O_5 and K_2O content was detected using Egner–Riehm (DL) method.

Soil at the site was loam, *Endocalcaric Abruptic Luvisol* (Cutanic, Hypereutric, Ruptic, Silitic, Protostangnic Epiprotovertic). Soil agrochemical characteristics are described in Table 1.

In the trial, cultivar 'Skagen' was used. This is one of the most commonly used cultivars in Latvia and it is characterized by good winterhardiness, which is combined with disease resistance and baking quality of grain, notably high and stable falling number. Sowing rate depended on sowing time and trial meteorological conditions: 450 germinable seed per m^2 in 2014/2015 (after oilseed rape), 2015/2016 (after both forecrops), but 500 germinable seed m^2 in 2014/2015 (after wheat), 2016/2017 and 2017/2018 (after both forecrops).

In spring, when the vegetation had renewed, nitrogen fertilizer (NH_4NO_3; N 34%) was applied for all variants, except the control variant N0. Second top-dressing was done at GS 29–31 of winter wheat with ammonium sulphate ($(NH_4)_2SO_4$; N 21%, S 24%) at the rate 100 kg ha^{-1} and remaining amount of needed nitrogen was added using ammonium nitrate. The third top-dressing was done at GS 47–51 using ammonium nitrate. The whole rate of fertilizer was applied once for variant N60 and N90; rate was divided into two application for variants N120 and N150, but into three application – for variants N180, N210 and N240. Grain yield was harvested at GS 90–91 using combine Sampo 130. After harvesting, grain was weighted, grain purity and moisture content detected and yield data was recalculated to standard moisture (14%) and 100% purity. Before yield harvesting, plant samples were taken from each plot (from 0.18 m^2) to calculate straw and main root mass (plants were dug out from the top-soil layer) in t ha^{-1}. Samples of grain, straw and roots were used to determine the content of NPK in them. The analysis of N, P, K content was carried out at the Scientific Laboratory of Biotechnology Department of Agronomic Analysis of the Latvia University of Life Sciences and Technologies determining the content of N according the Kjeldahl method (LVS EN ISO 5983–2:2009), P – according the Spectrometric method (ISO 6491:1998), and K – using atomic absorption spectrometry (LVS EN ISO 6869:2002). To convert elements' P and K concentration to oxide, P_2O_5 and K_2O coefficients were used: $P_2O_5 = P \times 2.291$ and $K_2O = K \times 1.204$. Nutrients' removal was calculated using grain, straw and root mass and concentration of nutrient in them. Protein content was calculated by multiplying nitrogen content in grains by coefficient 5.75. Nitrogen use efficiency was calculated according to the following formulas:

Nitrogen use efficiency (NUE, kg kg^{-1}) = G_y / N_{supply}, (1)

where G_y – grain yield, kg ha^{-1}; N_{supply} – sum of nitrogen used from soil in control variant (N-0) and from nitrogen fertilizer, kg.

Nitrogen uptake efficiency (NUpE, kg kg^{-1}) = N_t / N_{supply} (2)

where N_t – total plant N uptake, kg; N_{supply} – explained below formula (1)

Nitrogen utilization efficiency (NUtE, kg kg^{-1}) = G_y / N_t (3)

where G_y – grain yield, kg ha^{-1}; N_t – total plant N uptake, kg

Nitrogen harvesting index (NHI, %) = $(N_g / N_t) \times 100$ (4)

where N_g – total grain N uptake; N_t – total plant N uptake, kg.

Meteorological conditions of three years (2014/2015; 2015/2016 and 2016/2017) were described in detail in our previous paper (Litke et al., 2018). Conditions differed significantly during the last trial year (2017/2018). Meteorological conditions of growing season 2017/2018 differed significantly also from the long-term average data. Autumn of 2017 was warm and excessively rainy. Prolonged drought period started during May 2018. The drought period lasted until yield harvesting. This affected the plant growth and development and use efficiency of applied fertilizer.

Analysis of variance was used for data statistical processing. Bonferroni test was used for comparison of means; the difference was considered statistically significant when $P<0.05$. Significantly different means were labelled with different letters (^{a,b,c,d,e,f,g,h}) in superscript. Data processing was done using R-studio.

RESULTS AND DISCUSSION

Nitrogen fertilizer is important for wheat growing and yield production. According to the research results, nitrogen has great influence on wheat, and different amount of nitrogen fertilizer has different effects on wheat grain yield (Liu & Shi, 2013). Results of our trials also indicated that the nitrogen fertilizer application significantly ($P < 0.001$) increased winter wheat grain yield. Even lower nitrogen fertilizer rates gave a significant yield increase, if compared with control (N0). Average four year winter wheat grain yield (after both forecrops) was 4.72 (N0)–8.96 (N240) t ha^{-1} and significant ($P = 0.049$) increase was observed until nitrogen rate N180 (Fig. 1). If we analyze the grain yield after each forecrop separately, important yield increase was also observed until the rate N180 (8.87 t ha^{-1} after rape, increase +0.67, if compared with N120; 8.69 t ha^{-1} after wheat, increase +0.62 t ha^{-1}, if compared with N120), but this increase, if compared with variant N120, was not mathematically significant ($P = 0.569$ and $P = 0.404$, respectively) (Fig. 1).

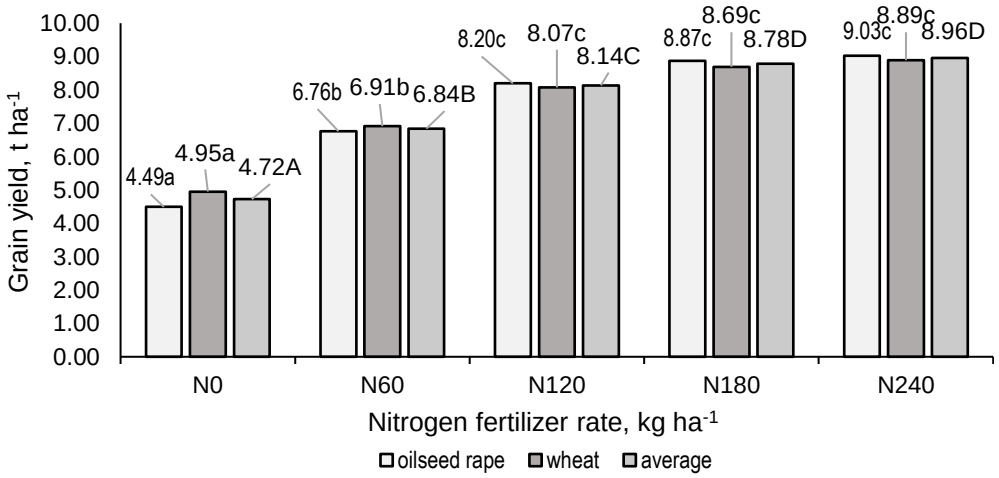

Figure 1. Average four year winter wheat grain yield depending on nitrogen fertilizer rate and forecrop (^{a,b,c} – yields labelled with different small letters are significantly different after specific forecrop depending on N rate.; ^{A,B,C} – average yields labelled with different capital letters are significantly different depending on N rate).

Yield changes in the first three trial years, including calculation of all eight N rates and also effect of soil tillage, were described more in detail in our previous publication (Litke et al., 2018), in which we also showed significant yield increase until the rate N180. But similar studies in Latvia showed that the grain yield increased significantly until nitrogen fertilizer rate N120 (Ruža et al., 2003; Kārkliņš, Līpenīte & Ruža 2017). This can be explained with different agro-meteorological conditions of previous trials, and in addition, average results per 10 winter wheat varieties were described in paper written by Ruža et al. (2003).

Nutrient removal

Nutrient removal is the quantity of nutrients, which are removed with plant material from the field. Nutrient removal with plant material is depending on the size of the harvested yield and its nutrient content. Nutrient removal by harvested yield is one of the ways how nutrients from the soil and given fertilizers leave the field. In our trial, nitrogen fertilizer affected N, P and K content in grain significantly ($P < 0.001$). Results showed that the nitrogen fertilizer rate affected N, P_2O_5 and K_2O removal with grain yield significantly ($P < 0.001$) (Table 2). Results also showed that the increase of nitrogen rate increases also nutrient removal. Nutrients' removal was higher when higher fertilizer rates were used. Depending on nitrogen fertilizer rate, N removal was 66.29–206.05 kg ha^{-1}. Significant increase, depending on forecrop, was observed until nitrogen rate N180 (if forecrop was wheat) – N240 (if forecrop was oil-seed rape). Average P_2O_5 removal with grain yield was 35.26–62.58 kg ha^{-1}, and P_2O_5 removal significantly increased until nitrogen rate N60–N120. Average K_2O removal, depending on nitrogen rate, was 24.68–46.12 kg ha^{-1}, and significant increase of K_2O removal after both forecrops was observed until nitrogen rate N120 (Table 2).

Table 2. Nutrient removal, kg ha^{-1}, with grain yield depending on forecrop and applied N rate on average per trial period

N rate	N removal, kg ha^{-1}		P_2O_5 removal, kg ha^{-1}		K_2O removal, kg ha^{-1}	
	oilseed rape	wheat	oilseed rape	wheat	oilseed rape	wheat
N0	66.29^{a}	68.36^{a}	35.26^{a}	37.90^{a}	26.12^{a}	24.68^{a}
N60	102.24^{b}	105.00^{b}	49.79^{b}	50.43^{ab}	38.40^{b}	36.61^{b}
N120	128.68^{b}	144.91^{c}	56.88^{bc}	56.67^{b}	46.12^{c}	41.23^{bc}
N180	177.28^{c}	181.85^{d}	60.70^{c}	59.22^{b}	44.42^{bc}	43.28^{c}
N240	206.05^{d}	202.12^{d}	62.58^{c}	60.25^{b}	44.21^{bc}	43.48^{c}

$^{a,b,c,d.e}$ – indicators labelled with different letters are significantly different in columns depending on N rate.

Results showed that the forecrop had no significant impact on N ($P = 0.296$, P ($P = 0.545$) and K ($P = 0.612$) content in wheat grain. It coincides with other findings where forecrop had no effect on P and K in wheat grain (Wanic et al., 2018). Results showed that the forecrop affected significantly ($P < 0.05$) only K_2O removal with grain yield. Higher K_2O removal with grains was observed, when wheat was grown after oilseed rape, if compared with wheat growing after wheat. Forecrop did not show any significant effect on N ($P = 0.082$) and P_2O_5 ($P = 0.889$) removal.

Nitrogen fertilizer significantly ($P < 0.001$) affected N and K content in wheat straw, but had no impact ($P = 0.910$) on P content in straw. Ruža et al. (2013) found that by increasing nitrogen rate also K_2O content increased rapidly in straw of barley, and in

its turn also its removal increased. Wheat straw contains the least amount of P_2O_5 and N, but the most amount of K_2O. As a result, straw mass removes the most amount of K_2O from the soil, but the least amount of P_2O_5. Nutrients' (N, P_2O_5, K_2O) removal with straw mass was significantly ($P < 0.001$) affected by nitrogen fertilizer rate. The increase of nitrogen fertilizer rate increases the nutrient removal with straw. Depending on nitrogen fertilizer rate, N removal with straw was 13.41–53.94 kg ha^{-1} (Table 3), P_2O_5 removal was 5.41–10.15 kg ha^{-1}, but K_2O 30.43–138.54 kg ha^{-1}

Table 3. Nutrient removal, kg ha^{-1}, with wheat straw mass depending on forecrop and N rate on average per trial period

N rate	N removal, kg ha^{-1}		P_2O_5 removal, kg ha^{-1}		K_2O removal, kg ha^{-1}	
	oilseed rape	wheat	oilseed rape	wheat	oilseed rape	wheat
N0	13.49^{a}	13.41^{a}	5.78^{a}	5.41^{a}	31.72^{a}	30.43^{a}
N60	22.59^{ab}	21.52^{ab}	6.48^{a}	6.44^{a}	54.67^{b}	49.37^{ab}
N120	35.55^{bc}	28.45^{ac}	7.55^{ab}	7.97^{a}	86.33^{c}	72.51^{bc}
N180	42.62^{cd}	37.27^{bc}	8.62^{ac}	8.54^{a}	108.36^{c}	95.19^{c}
N240	53.94^{d}	44.07^{c}	10.15^{bc}	9.30^{a}	138.54^{d}	91.64^{c}

$^{a,b,c,d.e}$ – indicators labelled with different letters are significantly different in columns depending on N rate.

Forecrop had no significant impact on N ($P = 0.182$), P ($P = 0.492$) and K ($P = 0.074$) content in wheat straw. Our results showed that forecrop had no significant ($P = 0.536$) impact on P_2O_5 removal with straw mass, but it had a significant ($P < 0.001$) impact on N and K_2O removal with straw. When growing wheat after oilseed rape, N and K_2O removal with straw was higher, if compared with the variant where wheat was grown after wheat.

Nitrogen fertilizer affected significantly N ($P < 0.001$) and P ($P < 0.01$) content in the main root mass, but significant impact was not observed on K ($P < 0.227$) content in main root mass. Winter wheat roots mostly remove N and K_2O from the soil, but P_2O_5 removal was the least. Depending on nitrogen rate and forecrop, N removal with main root mass was 2.06–5.05 kg ha^{-1} (Table 4), K_2O removal was 2.00–5.25 kg ha^{-1} and that of P_2O_5 was 0.67–0.96 kg ha^{-1}. Results showed that the nitrogen fertilizer rate had a significant ($P < 0.001$) impact on N and K_2O removal with winter wheat main root mass, but it had no significant ($P = 0.283$) impact on P_2O_5 removal. Increase of nitrogen fertilizer rate also increased N and K_2O removal with main root mass.

Table 4. Nutrient removal, kg ha^{-1}, with wheat main root mass depending on forecrop and N rate on average per trial period

N rate	N removal, kg ha^{-1}		P_2O_5 removal, kg ha^{-1}		K_2O removal, kg ha^{-1}	
	oilseed rape	wheat	oilseed rape	wheat	oilseed rape	wheat
N0	2.17^{a}	2.06^{a}	0.86^{a}	0.77^{a}	2.71^{a}	2.00^{a}
N60	3.26^{ab}	2.43^{ab}	0.96^{a}	0.83^{a}	3.58^{ab}	2.38^{a}
N120	3.65^{bc}	3.01^{bc}	0.85^{a}	0.73^{a}	3.82^{ac}	2.52^{a}
N180	4.54^{bd}	3.46^{c}	0.91^{a}	0.78^{a}	4.66^{bc}	3.19^{a}
N240	5.05^{cd}	3.66^{c}	0.89^{a}	0.67^{a}	5.25^{bc}	2.45^{a}

$^{a,b,c,d.e}$ – indicators labelled with different letters are significantly different in columns depending on N rate.

Forecrop affected significantly ($P < 0.001$) only K content in wheat roots. But forecrop affected significantly ($P < 0.001$) removal of all three nutritional elements with

main root mass. Higher N, P_2O_5 and K_2O removal was observed when wheat was grown after oilseed rape, if compared to wheat growing after wheat.

The total removal of nutrients is the necessary amount of nutrients for crop yield production. Nitrogen fertilizer affected significantly ($P < 0.001$) total nutrients' removal. Increasing nitrogen rate increases also the grain yield, and in its turn – the total nutrient removal increases. Depending on nitrogen fertilizer rate, total N removal was 78.76–257.34 kg ha^{-1}, P_2O_5 removal was 40.86–71.29 kg ha^{-1} and K_2O removal was 56.47–181.47 kg ha^{-1} (Table 5).

Table 5. Total nutrient removal, kg ha^{-1}, with winter wheat biomass depending on forecrop and N rate on average per trial period

N rate	N removal, kg ha^{-1}		P_2O_5 removal, kg ha^{-1}		K_2O removal, kg ha^{-1}	
	oilseed rape	wheat	oilseed rape	wheat	oilseed rape	wheat
N0	78.76^{a}	79.30^{a}	40.86^{a}	42.36^{a}	60.01^{a}	56.47^{a}
N60	124.62^{b}	126.15^{b}	56.45^{b}	55.71^{ab}	98.14^{b}	87.52^{ab}
N120	161.84^{b}	174.32^{c}	63.78^{bc}	63.82^{ac}	134.64^{c}	115.47^{bc}
N180	220.06^{c}	218.29^{cd}	68.61^{bd}	66.60^{bc}	156.39^{cd}	141.10^{c}
N240	257.34^{c}	244.91^{d}	71.29^{cd}	68.52^{bc}	181.47^{d}	136.79^{c}

^{a,b,c,d,e} – indicators labelled with different letters are significantly different in columns depending on N rate.

Results indicated that the forecrop had a significant ($P < 0.001$) impact only on the total K_2O removal, but it had no significant impact on the total N ($P = 0.982$) and P_2O_5 ($P = 0.549$) removal. Higher total K_2O removal was observed when wheat was grown after oilseed rape.

The nitrogen use efficiency

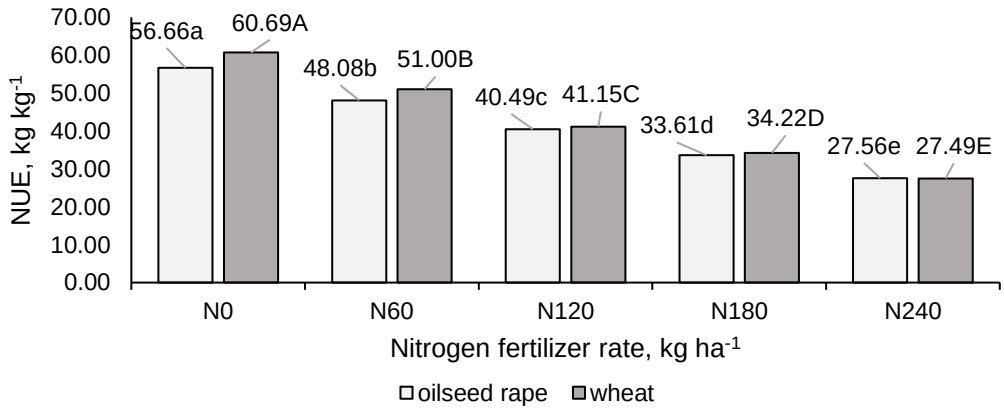

Figure 2. Average winter wheat nitrogen use efficiency (NUE) depending on nitrogen fertilizer rate and forecrop during 2014/2015–2017/2018 (^{a,b,c,d,e} – yield labelled with different letters are significantly different depending on N rate after oilseed rape, ^{A,B,C,D,E} – yields labelled with different letters are significantly different depending on N rate after wheat).

Nitrogen use efficiency (NUE) shows the capacity of given genotype to take advantage of the applied nitrogen and capacity to transform it in grains (Todeschini et al., 2016). Higher NUE of plants can not only enhance crop yields, but also reduce

fertilizer input costs, decrease nutrient loss rate (Baligar et al., 2007). Our results indicated that the nitrogen fertilizer rate affected significantly ($P < 0.001$) NUE, and higher NUE was in the variants with the lowest nitrogen rates. NUE ranged between 27.49–60.69 kg kg^{-1}, depending on nitrogen rate (Fig. 2). In control (N0) variant, the highest NUE (56.66–60.69 kg kg^{-1}) was observed; crop used N only from the soil reserves in this variant. Increase of the nitrogen fertilizer rate decreases NUE. This result was similar with another study, in which it was also found that the increase of nitrogen fertilizer rate gradually decreased the return on 1 kg of nitrogen fertilizer (Haile et al., 2012; Maļecka & Ruža, 2013).

Forecrop has also a significant ($P < 0.001$) impact on NUE (Table 6). Higher NUE was obtained when wheat was grown after wheat. Similarly, Rahimizadeh et al. (2010) found that the forecrop affected NUE, but in his study, the lowest NUE of wheat was observed when wheat was grown after wheat. Our results are different also from the results of Lopez-Bellido Garrido & Lopez-Bellido (2001), who found that nitrogen use efficiency was considerably lower in repeated spring wheat sowings in Mediterranean climate, if compared with wheat growing in different crop rotations.

Table 6. The mean N uptake efficiency (NUpE), N utilization efficiency (NUtE), nitrogen use efficiency (NUE), N harvesting index (NHI) and grain protein content depending on forecrop and nitrogen fertilizer rate

Factor	NUpE, kg kg^{-1}	NUtE, kg kg^{-1}	NUE, kg kg^{-1}	NHI, %	Protein, %
Forecrop					
Oilseed rape	0.84 a	47.36a	41.28a	78.05a	10.1a
Wheat	0.88 a	48.74b	42.91b	81.61b	10.6a
N rate					
N0	0.99 a	58.49 a	58.49 a	80.31 a	8.3 a
N60	0.89 ab	55.13 ab	49.41 b	79.90 a	8.8 a
N120	0.82 b	49.85 b	40.79 c	78.74 a	9.6 a
N180	0.82 bc	41.09 c	33.89 d	80.27 a	11.8 b
N240	0.76 c	35.39 c	27.53 e	79.14 a	13.2 b

$^{a,b,c,d.e}$ – indicators labelled with different letters are significantly different in columns depending on N rate or forecrop.

N uptake efficiency

N uptake efficiency (NUpE) can be defined as the amount of N taken up by the crop as a fraction of the amount available to the crop from all sources. NUpE associated with root structure and functioning. Early root development can promote N scavenge before fertilizer application, root development near to the soil surface enables capture of applied N, and later longer roots and deeper roots can access deeper N reserves and leached N (Hawkesford, 2014). It is mentioned in the literature that the availability of N in soil plays an important role in regulating N uptake by plant roots and the amount of N supply, and dryness in soil constrains the rate of N uptake in crop plants (Keulen & Seligman, 1987). Results showed that the nitrogen fertilizer affected significantly ($P < 0.001$) NUpE and, depending on nitrogen fertilizer rate, average NUpE ranged between 0.76–0.99 kg kg^{-1} (Table 6), decreasing when N rate was increased. Similar results were observed in other studies, where it was found that the nitrogen uptake

efficiency was significantly influenced by nitrogen fertilizer rate, and N uptake efficiency was higher at lower rates of N; it decreased drastically with further increases in the rate of fertilizers (Haile et al., 2012). Forecrop had no significant ($P = 0.354$) impact on NUpE. When growing wheat after wheat, the average NUpE was 0.88 kg kg^{-1}, but growing wheat after oilseed rape – 0.84 kg kg^{-1}. This result differs from other study, where it was found that wheat NUpE was affected by forecrop and the lowest NUpE was observed when growing wheat after wheat (Rahimizadeh et al., 2010).

The nitrogen utilization efficiency

The nitrogen utilization efficiency (NUtE) is the relationship between crop yield and total N absorbed by the plant. Results indicated that the nitrogen fertilizer affected NUtE significantly ($P < 0.001$). It coincides with the results of another study (Haile et al., 2012). In our trial, NUtE was 35.39–58.49 kg kg^{-1}, depending on nitrogen fertilizer rate. Higher average NUtE was observed at lower nitrogen fertilizer rate, and with the increase of nitrogen fertilizer rate NUtE decreased. Forecrop had a significant ($P < 0.01$) influence on NUtE. When growing wheat after wheat, average NUtE was 48.74 kg kg^{-1}, but when growing wheat after oilseed rape the average NUtE was 47.36 kg kg^{-1}.

Nitrogen harvesting index

Nitrogen harvesting index (NHI) is defined as the relation between nitrogen amount in grain to total nitrogen uptake (Rahimizadeh et al., 2010). In our trial, nitrogen fertilizer did not have a significant ($P = 0.3033$) impact on NHI. This result coincides with the results of other authors' research, where it was also found that nitrogen fertilizer did not affect NHI (Rahimizadeh et al., 2010; Haile et al., 2012).

Forecrop affected NHI significantly ($P < 0.001$). Similar results were observed in other study, where it was found that the NHI of wheat varied significantly depending on forecrop (Rahimizadeh et al., 2010).

Protein content

From the economic point of view, grain yield is not the only factor affecting income. Quality of the harvested grains is also important. One of the quality indicators, which is closely related to the applied nitrogen fertilizer rate, is the crude protein (CP) content of grains. In our trial, nitrogen fertilizer affected the CP content significantly ($P < 0.001$). Similar results were obtained by many other researchers (e.g. Rahimizadeh et al., 2010; Abedi et al., 2011; Haile et al., 2012), who found that the grain protein content was significantly affected by N rates. Our results showed that with the increase of nitrogen fertilizer rate, also the CP content of the grains increases significantly ($P < 0.001$). Average grain CP content under different N application rates ranged from 8.3 (N0) to 13.2% (N240). According to the demands of grain milling companies, only the CP content above 12% is suitable for bread baking and for such grain higher price can be obtained. Such appropriate average CP content was provided only by N rate 240 kg ha^{-1}.

Results showed that the forecrop had no significant ($P = 0.215$) impact on the CP content in winter wheat grains (Table 6). This result agrees with the finding of other researchers, where it was found that the choice of forecrops had no significant influence on the protein content of wheat grain (Jankowski et al., 2015).

CONCLUSIONS

Nitrogen fertilizer affected winter wheat grain yield significantly ($P < 0.001$) and average grain yield increased significantly ($P < 0.049$) until nitrogen rate N180. Grain yield increased importantly until N180 also analyzing it separately after every forecrop, but mathematically significant this increase was until N120.

Results indicated that with increasing nitrogen fertilizer rate also removal of N, P_2O_5 and K_2O with wheat biomass increased significantly ($P < 0.001$). Significant increase of nitrogen removal with winter wheat grain yield depending on forecrop was observed until nitrogen fertilizer rate N180–N240, P_2O_5 removal significantly increased until N60 – N120, and K_2O removal significantly increased until nitrogen rate N120.

Nitrogen fertilizer affected nitrogen use efficiency (NUE), nitrogen uptake efficiency (NUpE), nitrogen utilization efficiency (NUtE) and crude protein content significantly ($P < 0.001$), but it did not have any significant ($P = 0.303$) impact on nitrogen harvesting index (NHI). When increasing nitrogen fertilizer rate NUE, NUpE and NUtE decreased, and higher results were observed at the lowest nitrogen rates. Increase in nitrogen fertilizer rate also increased protein content in grain, and suitable for bread baking grain was obtained only with the highest N rate: N 240.

Forecrop did not affect winter wheat grain yield, however, it affected significantly NUtE ($P < 0.01$), NUE ($P < 0.001$) and NHI ($P < 0.001$); higher results were observed when wheat was grown after wheat.

ACKNOWLEDGEMENTS. The research was funded by the 'State and European Union investment for encouragement in agriculture' theme 'Determination of maximal fertilizer norms for crops' and the program of Latvia University of Life Sciences and Technologies 'Strengthening Scientific Capacity in the Latvian University of Life Sciences' Z 24 project.

REFERENCES

Abedi, T., Alemzadeh, A. & Kazemeins, S.A. 2011. Wheat yield and grain protein response to nitrogen amount and timing. *Australian Journal of Crop Science* **5**(3), 330–336.

Baligar, V.C., Fageria, N.K. & He, Z.L. 2007. Nutrient use efficiency in plants. *Communications in Soil Science and Plant Analysis* **32**(7–8), 921–950.

Haile, D., Nigussie, D. & Ayana, A. 2012. Nitrogen use efficiency of bread wheat: Effects of nitrogen rate and time of application. *Journal of Soil Science and Plant Nutrition* **12**(3), 389–409.

Hawkesford, M.J. 2014. Reducing the reliance on nitrogen fertilizer for wheat production. *Journal of Cereal Science* **59**(3), 276–283.

Jankowski, K.J., Kijewski, L. & Dubis, B. 2015. Milling quality and flour strength of the grain of winter wheat grown in monoculture. *Romanian Agricultural Research* **32**, 191–200.

Kārkliņš, A., Līpenīte, I. & Ruža, A. 2017. N fertilizer use and grain yield in Saldus experimental field. In *Proceedings of the Scientific and Practical Conference. Harmonious Agriculture.* Latvia University of Agriculture, Jelgava, Latvia, pp. 42–49 (in Latvian).

Keulen Van, H. & Seligman, N.G. 1987. *Simulation of wheat use nitrogen nutrition and growth of a spring wheat crop. Simulation Monographs*. PUDOC, Wageningen, 310 pp.

Litke, L., Gaile, Z. & Ruža, A. 2018. Effect of nitrogen fertilization on winter wheat yield and yield quality. *Agronomy Research* **16**(2), 500–509.

Liu, D. & Shi, Y. 2013. Effects of different nitrogen fertilizer on quality and yield in winter wheat. *Advance Journal of Food Science and Technology* **5**(5), 646–649.

Lopez-Bellido Garrido, R.J., Lopez-Bellido, L. 2001. Effects of crop rotation and nitrogen fertilizer on soil nitrate and wheat yield under rainfed Mediterranean conditions. *Agronomie* **21**(6–7), 509–516.

Maļecka, S. & Ruža, A. 2013. The impact of nitrogen fertilizer norm on the indicators of nutrient use for spring wheat. In *Proceeding of the Scientific and Practical Conference. Agricultural Science for Successful Farming.* Latvia University of Agriculture, Jelgava, Latvia, pp. 232–237 (in Latvian).

Rahimizadeh, M., Kashani, A., Zare-Heizabadi, A., Koocheki, A. & Nassiri-Mahallati, M. 2010. Nitrogen use efficiency of wheat as affected by preceding crop, application rate of nitrogen and crop residues. *Australian Journal of Crop Science* **4**(5), 363–368.

Ruža, A., Kreita, Dz., Krotovs, M., Maļecka, S., Stramkale, V. 2003. Nitrogen fertilizer use efficiency in winter wheat trials. *Environment. Technology. Resources* **1**, 232–237.

Ruža, A., Kreita, Dz., Katamadze, M., Skrabule, I., Vaivode, A. & Maļecka, S. 2013. The impact of nitrogen fertilizer norm on the indicators of nutrient use in spring barley. In *Proceeding of the Scientific and Practical Conference. Agricultural Science for Successful Farming.* Latvia University of Agriculture, Jelgava, Latvia, pp. 56–60 (in Latvian).

Todeschini, M.H., Milioni, A.S., Trevizan, D.M., Bornhofen, E., Finatto, T., Strock, L. & Benin, G. 2016. Nitrogen use efficiency in modern wheat cultivars. *Soil and Plant Nutrition* **75**(3), 351–361.

Wanic, M., Denert, M. & Treder, K. 2018. Effect of forecrops on the yield and quality of common wheat and spelt wheat grain. *Journal of Elementology* **24**(1), 369–383.

Agronomy Research **17**(2), 593–607, 2019
https://doi.org/10.15159/AR.19.067

Estonian dairy farms' technical efficiency and factors predicting it

H. Luik-Lindsaar*, R. Põldaru and J. Roots

Estonian University of Life Sciences, Institute of Economics and Social Sciences, Fr.R. Kreutzwaldi 1A, EE51006 Tartu, Estonia
*Correspondence: helis.luik@emu.ee

Abstract. Milk production is a complex process whose efficiency depends directly on the input-output ratio and indirectly on the decisions made at farm and animal level. Decisions made about farm hygiene, dairy cows' milk yield, cows' age at first calving etc. affect farms' efficiency. The aim of this study is to provide an understanding of the factors that affect dairy farms' technical efficiency. A two-stage approach was used in this study, consisting of a data envelopment analysis (DEA) in the first stage, and classification and regression tree (CART) in the second stage. DEA determined technical efficiency scores (TE), and CART enabled to detect the main factors that influenced efficiency in dairy farms. The analysis studied at the Estonian national level FADN dataset and Estonian Livestock Performance Recording data. 147 Estonian dairy farms were included in this analysis, all of which are specialized in dairy production. DEA results demonstrated that more than half of the farms (55%) were operating efficiently or rather efficiently (TE $\geq$ 0.900). CART results revealed that the main variables determining efficiency are milk yield per cow's lifetime (kg day^{-1}), feed costs (€ kg milk^{-1}), and somatic cell count (SCC; 10^3 ml^{-1}). Milk yield per cow's lifetime is a complicated factor as it is influenced by a lot of components (e.g. milk yield, number of lactations, age at first calving, and calving interval), but if it is known at farm level, it is also a useful variable for predicting efficiency. Feed costs per milk kg is an economic variable, i.e. lower costs are related with higher efficiency. Better hygiene (lower SCC) is also related with higher efficiency. The analysis showed that integrating farm accounts data, herd-level genetic information, and milk quality attributes enables to use more specific factors to explain the variation of TE between dairy farms.

Key words: data envelopment analysis, classification and regression tree, dairy farms' efficiency.

INTRODUCTION

Dairy milk production is one of the most important sectors in the agricultural economy of the Baltic region, and this is also the case in Estonia. In recent years, milk production accounted for approximately 1/3 of the value of agricultural output (Estonian Statistics, 2018). Consequently, it is obvious to investigate the efficiency of Estonian dairy farms.

Since 2004, Estonia is a member of the European Union. The enlargement of the EU has brought a lot of changes for all Eastern European countries at political, economic, and technical levels. All these changes have affected agricultural production, and therefore also milk production. Dairy milk production has undergone a considerable

modernization within a very short period: cowsheds have been renovated or new ones built, new milking technologies have been brought into use, new full-ratio feed mixtures are used, production intensity and the size of farms have increased, etc. New technologies set requirements for a better management, and we can conclude that today's dairy farm managers are more aware of processes (milk production, feed production), and process management than ever before. All the above-mentioned changes have an impact on dairy farms' productivity and efficiency.

The following changes in dairy production volume and quality have occurred within ten years after the accession of Estonia into the EU (2004–2014): milk yield per cow has increased from 5.6 to 8.4 tonnes (+ 50%); milk production has increased from 652 to 805 thousand tonnes (+ 23%); the number of dairy cows has decreased from 115.6 to 95.6 thousand (- 18%); the number of dairy farmers (milk quota owners) has decreased from 2467 to 709 (- 71.3%); the average somatic cell count has decreased from 385 to 327 thousand ml^{-1}; the share of Estonian Holstein (EHF) cows has increased by 6% pp from 73% to 79%; culling rate has increased from 27% to 31%; the average number of lactations per dairy cow's lifetime has decreased from 3.1 to 2.5; the average age at first calving has decreased from 28.9 to 26.9 months; the average breeding value for milk has increased from 74 to 102 (Estonian Statistics; Estonian Livestock Performance Recording Ltd. 2018). Some of the changes are caused by political decisions, e.g. the decrease in the number of cows and dairy farmers is the result of favouring production in larger dairy farms. The increased milk yield is the result of better housing conditions and improved feeding, including an increase in the proportion of maize silage in the feed ration by rationalizing maize cultivation (Põldaru & Roots, 2014). The decreased SCC is an indicator of better hygiene and better keeping. The higher share of EHF is a minor contributor to an increased average milk yield. Higher milk yield, on the other hand, has resulted in fewer lactations and an increased culling rate. Despite these negative consequences, farmers are still interested in a higher milk yield. This is due to economic reasons, seeing as higher production results in a higher revenue.

It has not been studied whether such managerial decisions increase or decrease farms' efficiency. Knowing the contributing factors of efficiency helps to improve farms' technical efficiency. The managers of dairy farms should pay attention to the main factors that influence efficiency. If these factors are considered, the efficiency of the whole sector can be improved.

To calculate the efficiency and to determine the factors that predict it, we decided to use a two-step approach – the nonparametric DEA model in the first stage to calculate the efficiency scores, and CART in the second stage to determine the variables for predicting efficiency. There are only a few studies that have combined DEA with CART to analyse efficiency and predictors (Emrouznejad & Anouze, 2010; Keizer & Emvalomatis, 2014). Rahimi & Behmanesh (2012) used DEA and regression trees to analyse poultry meat industries in Iran. Usually, the regression tree approach is used to predict the occurrence of an event based on some crucial factors. Piwczynski et al. (2013) used classification trees to analyse the effect of indicators affecting calving ease and stillbirths. Topal et al. (2010) analysed the factors that affect cattle birth weight using the regression tree approach. Scollo et al. (2017) and Grümpel et al. (2018) used regression trees to predict tail biting risk in pig farms. These previous researches are targeted at specific problem solving in agriculture.

The aim of this research is to evaluate efficiency and to determine the factors related to technical efficiency. It can be assumed that changes in Estonian dairy production affect efficiency either positively (e.g. increased milk yield) or negatively (e.g. decreased number of lactations). It is important to identify the impact of these factors.

Improving the efficiency and competitiveness of dairy farms and Estonian agriculture should be a priority in Estonian agricultural policy.

MATERIALS AND METHODS

Data

This study used the Estonian National level FADN dataset and data from Estonian Livestock Performance Recording. There were 179 farms specialized in milk production in FADN and the number of herds under milk recording was 833 in 2012. After integrating datasets and removing outliers, 147 farms remained for the analysis.

Data from FADN was used in the DEA analysis to calculate efficiency scores. Two output and six input variables were used. The output variables in the DEA analysis were: sales revenue of milk and dairy products; sales revenue of animals and other agricultural products. The input variables were: the number of dairy cows; the size of land; labour hours; feed costs; other production costs; costs of the capital. The selected output and input variables are also common in other studies dealing with dairy farms' efficiency (Davidova & Latruffe, 2007; Rasmussen, 2010; Latruffe et al., 2012; Keizer & Emvalomatis, 2014).

The descriptive statistics of the DEA model variables show that there is a large gap between the minimum and maximum values (Table 1). On the one hand, this gap is related to the farm size. Estonian dairy production is described by dualistic production, in that there are a lot of small farms producing a smaller part of the total milk production. It is clear that the main dairy milk production comes from the large farms. There are relatively few average-sized farms. This is due to political reasons. After the EU accession, subsidies favoured investing into large cowsheds rather than small or average ones.

Table 1. Descriptive statistics of DEA model outputs and inputs

Outputs and inputs	Unit	Min	Max	Mean	St. Dev.	Median
Sales revenue of milk and dairy products (y_1)	thousand euros	4.2	4,051.6	470.0	693.9	157.9
Sales revenue of animals and other agricultural products (y_2)	thousand euros	1.7	6,377.6	226.5	581.5	53.4
Dairy cows (x_1)	number	6	1,643	210	284	87
Agricultural area (x_2)	ha	27	5,729	693	893	269
Labour (x_3)	hours	2,000	254,376	29,611	38,759	10,800
Feed costs (x_4)	thousand euros	4.9	3,027.5	314.3	455.1	93.4
Other production costs (x_5)	thousand euros	4.9	5,327.3	305.7	559.1	9.5
Costs of the capital (x_6)	thousand euros	4.5	2,217.6	208.2	307.7	78.2

Data from Estonian Livestock Performance Recording and FADN is used to analyse the predictors for the efficiency score. There is one target value and thirteen predicting variables in CART. The target value is the efficiency score from the DEA analysis from the first stage. The following variables are chosen as predictors: milk yield per cow's lifetime; milk yield per cow per year; milk solids; relative breeding value for milk (dRBV milk); share of own feed; feed costs per milk kg; age at first calving; somatic cell count; culling rate; productive period; number of cows; share of EHF; age of manager.

The descriptive statistics of CART predictors show differences in farm production (milk yield and variables connected with it); farm hygiene (SCC); managerial decisions (share of own feed, age at first calving, number of cows, share of EHF) (Table 2). All these variables predict farms' technical efficiency. Most of the variables are changeable and depend on the farmer's decision, and therefore it is essential to determine the important ones.

Table 2. Descriptive statistics of CART target value and predictors

Variables in CART	Unit	Min	Max	Mean	St. Dev.	Median
Efficiency	score	0.549	1	0.879	0.118	0.918
Milk yield per cow's lifetime	kg day^{-1}	4.9	15.7	11	2.2	11
Milk yield	kg cow $year^{-1}$	4,225	9,953	7,323	1,431.5	7,275
Milk solids	kg cow $year^{-1}$	314.3	753.4	545.8	101.1	550.7
Drbv milk	points	-18.7	7.6	-2.2	4.7	-1.7
Share of own feed	%	18.4	100	67.2	18.7	69.6
Feed costs per milk kg	€ kg^{-1}	0.1	0.4	0.2	0.1	0.2
Age at first calving	day	698	1,305	879.2	115.5	849
Somatic cell count	10^3 ml^{-1}	97	918	348.2	148.3	313
Culling rate	%	3.8	59.5	27	10.8	26.3
Productive period	months	10.2	86	44.2	14.2	41.3
Cows	number	6.7	1,638.1	209.8	283.7	83.6
Share of EHF	%	0	100	72.9	35.6	93
Age of manager	years	20	79	51.6	11.7	52

Farm size varied a lot in this analysis: 78 farms had fewer than 100 dairy cows; 35 farms had 100–300 dairy cows, and 34 farms had more than 300 dairy cows. Production technology naturally differs in smaller and larger farms. The number of cows in the barn determines the technology used. Luik & Viira (2016) analysed Estonian dairy farms and pointed out that the main factor in the choice of technology is the farm size (number of cows). New cowsheds are modern and allow producing high quality milk. The high variability of min and max values of SCC might be the result of the technology used. Smaller producers still use the bucket and pipeline milking technology which may cause hygiene problems. The variables representing milk yield values also differ severalfold. The min and max values for milk yield per cow's lifetime differs three times, with the max value showing the potential to strive for.

Culling rate is in correlation with the productive period. A lower productive period indicates a higher culling rate. Grandl et al. (2019) concluded that increasing the productive period is a potential way to improve profitability. Additionally, they found that a longer productive period helps to reduce the climate impact, which is related to

the topic of decreasing greenhouse gas (GHG) emissions. Ariva et al. (2015) analysed Estonian GHG emissions in milk production and found that if milk yield per dairy cow increases, GHG emissions per kg of milk decrease. Analysing the efficiency and taking into account negative outcomes is also a very important subject and future field of study in Estonia.

Methods

The input-oriented variable returns to scale model (VRS) are used in the DEA to calculate technical efficiency. The analysed dairy farms are referred to as decision making units (DMUs). Homogeneous production inputs (e.g. the number of dairy cows) and outputs (e.g. milk production) are data in the DEA model. The DEA evaluates the input-output ratio for every DMU and compares it with other DMUs on a relative scale. The DEA constructs a best practice frontier by measuring the data of different DMUs and comparing the best DMUs to others. Companies that are on the best practice frontier are defined as technically efficient, whereas those deviating from the frontier are defined as technically inefficient.

Efficiency scores were calculated for each DMU (Formula 1). We used the VRS input-oriented model where inputs are minimised and outputs are kept at their current levels:

$\theta^* = \min \theta$

subject to

$$\sum_{j=1}^{n} \lambda_j x_{ij} \leq \theta x_{i0} \quad i = 1, 2, \dots, m;$$

$$\sum_{j=1}^{n} \lambda_j y_{rj} \geq y_{r0} \qquad r = 1, 2, \dots, s; \tag{1}$$

$$\sum_{j=1}^{n} \lambda_j = 1$$

$$\lambda_j \geq 0 \qquad j = 1, 2, \dots, n.$$

where *DMUo* represents one of the *n* DMUs under evaluation, and x_{io} and y_{ro} are the *i*th input and *r*th output for *DMUo*, respectively. If $\theta^* = 1$, the current input levels cannot be reduced (proportionally), indicating that *DMUo* is on the frontier. Otherwise, if $\theta^* < 1$, *DMUo* is dominated by the frontier (Zhu, 2009).

In the second stage we used the decision tree methodology for predicting target variables, based on the classification and regression trees (CART) algorithm by Breiman et al. (1984) and using a tree-like graph. CART is a nonparametric technique in which you can choose from a wide range of variables that interact and find out which are most important in determining the outcome or target variable to be explained (Yohanne & Hoddinott, 1999).

The CART decision tree is a binary recursive partitioning procedure including continuous and categorical (nominal) variables as targets and predictors (Steinberg, 2009). Classification trees are used if the target variable is categorical, whereas if the target variable is continuous or ordinal, regression trees are appropriate (Loh, 2011).

Regression tree models produce a numeric set of outcomes calculated mathematically by examining the relationships between target and predictor variables to determine their mathematical relationship (Kuhn et al., 2013). A key advantage of the recursive binary tree is its interpretability (Hastie et al., 2017).

The tree building process begins by partitioning a sample (all observations), called root node, into two subnodes or child nodes by certain rules, unless it is a terminal node (Yohanne & Hoddinott, 1999; Lemon et al., 2003; Hastie et al., 2017; Yang et al., 2017). Terminal nodes are nodes that cannot split further (Lemon et al., 2003). The splitting process is applied recursively on the data in each child node (Loh, 2011). Recursive splitting is used to grow the tree from the root node until a split node cannot yield sufficient reduction in deviation (Yang et al., 2017). For constructing a regression tree, CART uses the sum of squared residuals as impurity function (Loh, 2008; Hastie et al., 2017). A regression tree model gives the predicted values of target variables (efficiency) in each node (Loh, 2008).

The purpose of the CART analysis is to work out rules which break up the impure heterogeneous root node into binary nodes or groups which are more homogeneous than the root node (Yohanne & Hoddinott, 1999; Hastie et al., 2017).

CART algorithm is used to determine the effect of different variables on farm efficiency.

RESULTS AND DISCUSSION

The DEA benchmarking analysis revealed that 43 farms (29%) are operating in the best way. Their technical efficiency score is equal to 1.000 (TE = 1.000). Those farms have the optimal input-output usage and they act as a reference group to others.

Overall, 81 farms (55%) are operating mostly efficiently or efficiently (TE $\geq$ 0.900), 27 farms (18%) are operating with a lower efficiency (TE 0.810–0.890), and 39 farms (27%) have the lowest efficiency (TE $\leq$ 0.800).

We can interpret the DEA results as follows: the farms with a technical efficiency equal to 0.900 use 10% more inputs than needed. Those farms could reduce their input by 10% and still produce the same level of output, indicates a comparison with the reference farms. We refer to the group of farms, whose technical efficiency is higher than 0.900, as the efficient group. The next group of farmers (TE 0.810–0.890) could reduce input by 10–20% and produce the same level of output. This group's efficiency level is average. The farms whose efficiency score was lower than 0.800 could reduce input by more than 20%. This group of farmers is inefficient.

The analysis of efficiency groups showed that there are some remarkable differences between efficient and inefficient farms (Table 3). A higher revenue of milk and other products per dairy cow characterise efficient farms. The group of efficient farms uses less labour and agricultural area per dairy cow. A smaller agricultural area per dairy cow refers to intensive production, and the share of grassland out of the total agricultural land is lower in efficient farms. Cabrera et al. (2010) and Keizer & Emvalomatis (2014) found positive relationships between intensive dairy farming and efficiency.

Table 3. The average values of DEA model outputs and inputs and CART variables in three different efficiency groups

DEA model variables per dairy cow	Unit	TE ≥ 0.900	TE 0.810–0.890	TE ≤ 0.800
Sales revenue of milk and dairy products	€ cow^{-1}	2,136	1,792	1,609
Sales revenue of animals and other agricultural products	€ cow^{-1}	991	843	589
Land	ha cow^{-1}	3.5	4.1	4.5
Labour	hours cow^{-1}	159	154	171
Feed costs	€ cow^{-1}	1,351	1,208	1,317
Other production costs	€ cow^{-1}	1,292	1,278	1,147
Costs of the capital	€ cow^{-1}	1,035	924	868
Variables in CART				
Milk yield per cow's lifetime	kg day^{-1}	11.7	11.0	9.6
Milk production	kg cow year^{-1}	7,877	6,997	6,398
Milk solids	kg cow year^{-1}	584	525	481
Drbv milk	points	-1.4	-2.5	-3.8
Share of own feed	%	62	73	73
Feed costs	€ kg^{-1}	0.171	0.174	0.207
Age at first calving	day	857	880	927
Somatic cell count	10^3 ml^{-1}	312	366	411
Culling rate	%	27	28	26
Productive period	months	42.4	46.1	46.5
Dairy cows	number	235	153	196
Share of EHF	%	79	68	62
Age of manager	years	49.5	54.5	53.9
Other relevant variables				
Milk price	€ kg^{-1}	0.291	0.288	0.285
Share of milk marketed	%	94	92	91
Share of grassland	%	68	71	72
Farms	number	81	27	39

Higher feed, capital and other production costs per dairy cow apparently lead to higher milk production in efficient farms. Despite higher feed costs per dairy cow, efficient farms have the lowest feed cost per kg of milk. Larger farms (e.g. by the number of dairy cows and the size of land) tend to be more efficient, and therefore, lower unit costs come from the scale effect. Tauer & Mishra (2006) also found that farm size has a positive effect on efficiency, and that larger farms are more cost-efficient. The higher capital cost per dairy cow also refers to higher investments in modern technology which give larger farms the advantage to earn a higher sales revenue and produce higher quality milk (higher milk price, lower SCC). Lawson et al. (2004a) found that higher efficiency is associated with a lower frequency of milk fever (lower SCC). On the one hand, milk fever treatment is the largest source of treatment costs. On the other hand, milk fever is also the biggest source of milk losses (Hadrich et al., 2018). Milk fever treatment costs increase the total costs, and milk losses in turn decrease the milk revenue. Therefore, it

is crucial to keep the SCC as low as possible and to avoid mastitis, especially chronic mastitis. Furthermore, Archer et al. (2013) found that higher SCC in the first lactation is related to lower lifetime milk yield. This means that preventive activities are essential since they help to reduce SCC and avoid milk losses, helping to increase lifetime milk yield in the long-term.

Studies have shown that younger farmers are more efficient (Lawson et al., 2004b), which is also the case in our study. Younger managers are more willing to take risks and invest in capital, and therefore, their farms are more efficient.

Milk yield breeding value is an economic trait that has always been important for farmers. Efficient farms have a higher relative breeding value for milk (dRBV). Luik-Lindsaar et al. (2018) analysed the total effect that relative breeding value had on dairy farms' efficiency and concluded that higher values have a positive effect on efficiency.

Efficient farms have the lowest age at first calving (857 days, i.e. approximately 28.6 months), which is far from the optimal 22–26 months (Froidmont et al., 2013). The average age at first calving in inefficient farms is considerably higher, namely 927 days (approximately 30.9 months). Therefore, all dairy farmers could potentially improve their farms' efficiency by decreasing the age at first calving to 22–26 months.

Intensive production has resulted in some negative results in efficient farms. They have high culling rates (27%), and the productive period (42.4 months) is lowest in efficient farms. These negative results suggest a negative effect on efficiency, but higher production compensates that, and according to our results, the efficient farms remain efficient despite these problems. Culling rate should be lower in order to reach a higher level of efficiency, but it still remains in the optimal 25–27% range (De Vries, 2017).

An analysis of the studied farms' average efficiency scores across counties reveals that the most efficient dairy farms are located in Central Estonia and around it (Fig. 1). Efficiency is higher in the dark grey areas and lower in the light grey areas. There are several reasons for that. Firstly, these are the areas with the best soil conditions (higher bonitation index), which enables to grow high-quality feed and therefore produce more milk. Secondly, there are historical reasons that go back to the period of Soviet Union during which large collective farms were located in those areas (Viira et al., 2009; Viira et al., 2013). After the collapse of the Soviet Union, when Estonia regained its independence, agriculture went through a number of changes. The 1990s were characterized by rapid and profound economic and legal reforms, including the privatization of agriculture and rural entrepreneurship. These resulted in considerable regional, economic and social disparities in Estonia, which have persisted for the following 30 years (Põder et al., 2017). Privatization provided an opportunity to take over the capital of collective farms and start developing it further. Despite the low producer prices of milk at the beginning of 1990 (Viira et al., 2015), some managers were able to keep companies running. Seeing as the development of animal husbandry companies is a long-time process, consistent development has ensured the success of privatized farms.

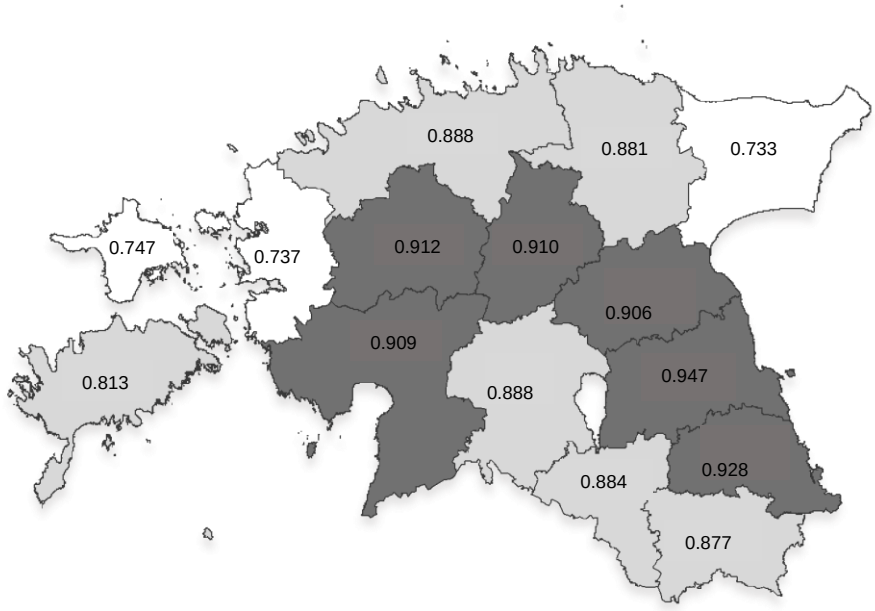

Figure 1. Dairy farms' average technical efficiency by county.

The more in-depth analysis is based on CART, using a regression tree. The target value is the efficiency score, and the chosen thirteen variables predict efficiency.

The result of the CART is a regression tree with several nodes and terminal nodes. This regression tree has ten terminal nodes (red nodes in Fig. 2). Eight predictors out of thirteen are presented in the tree. The information about the relative importance of variables indicates that the most important factor is milk yield per cow's lifetime (Fig. 3). Taking into account only these variables presented in the regression tree, the relative importance for milk yield per cow's lifetime is 100%. The next important variables are feed costs per kg milk (34%), somatic cell count (29%), and productive period (23%).

Each terminal node has information about the average efficiency in the group and the number of farms in the group. Each farmer belongs to some terminal node. According to the previous efficiency grouping, we can say that there are four terminal nodes with a high efficiency, two terminal nodes with an average efficiency, and four terminal nodes indicating inefficient farmers.

We can interpret every single node; all terminal nodes have their own rules. The root node shows that the most important variable for predicting technical efficiency is milk yield per cow's lifetime. The second most important variable is feed costs per kg of milk. In other words, if the farm's milk yield per cow's lifetime is lower than or equal to 11.47 (LIFETMILK < = 11.47) and feed costs per kg of milk are lower than or equal to 0.12 (FEED€KG <= 0.12), the farm is predicted to be highly efficient. There are 7 farms that meet these conditions, and their average efficiency is 0.990 (Terminal Node 1). The rules below are given according to the efficiency groups.

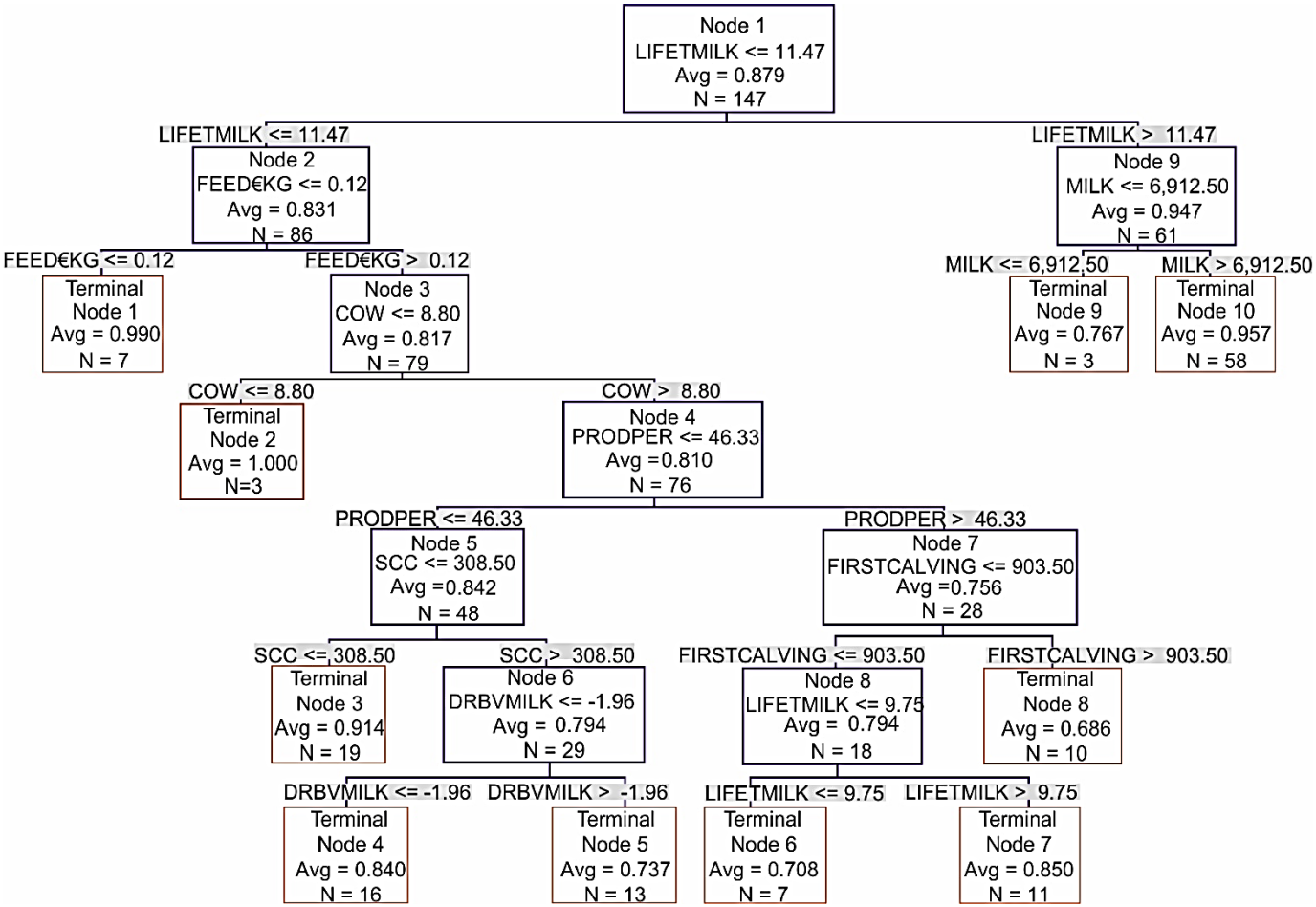

Figure 2. CART regression tree.

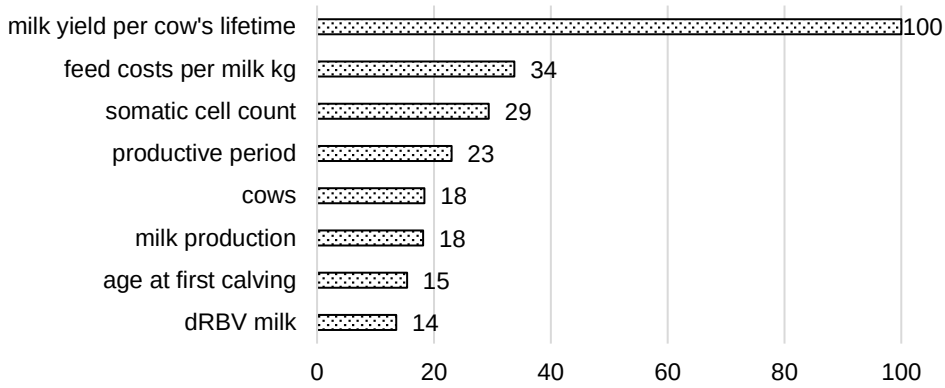

Figure 3. Relative importance (scale from 0 to 100%) of predictor variables in the Regression Tree Analysis.

Rules for high efficiency farms (TE ≥ 0.900):

- Milk yield per cow's lifetime, kg day^{-1} is lower than or equal to 11.47 kg, feed costs per kg milk is higher than 0.12 € kg^{-1}, and the number of cows is lower than or equal to 8.8 (TE = 1.000; 3 cases). (Terminal Node 2)
- Milk yield per cow's lifetime, kg day^{-1} is lower than or equal to 11.47 kg, and feed costs per kg milk is lower than or equal to 0.12 € kg^{-1} (TE = 0.990; 7 cases). (Terminal Node 1)
- Milk yield per cow's lifetime, kg day^{-1} is lower than or equal to 11.47 kg, feed costs per kg milk is higher than 0.12 € kg^{-1}, the productive period is lower than or equal to 46.33 months, and somatic cell count is lower than 308.50 (TE = 0.914; 19 cases). (Terminal Node 3)
- Milk yield per cow's lifetime, kg day^{-1} is higher than 11.47 kg, and milk yield per cow per year is higher than 6,912.50 kg (TE = 0.957; 58 cases). (Terminal Node 10)

Rules for average efficiency farms (TE 0.800–0.900):

- Milk yield per cow's lifetime, kg day^{-1} is lower than or equal to 11.47 kg, feed costs per kg milk is higher than 0.12 € kg^{-1}, the number of cows is higher than 8.8, the productive period is lower than or equal to 46.33 months, somatic cell count is higher than 308.50, and the dRBV is lower than or equal to - 1.96 (TE = 0.840; 16 cases). (Terminal Node 4)
- Milk yield per cow's lifetime, kg day^{-1} is lower than or equal to 11.47 kg, feed costs per kg milk is higher than 0.12 € kg^{-1}, the number of cows is higher than 8.8, the productive period is higher than 46.33 months, the age at first calving is lower than or equal to 903.50 days, and milk yield per cow's lifetime, kg day^{-1} is higher than 9.75 and lower or equal to 11.47 (TE = 0.850; 11 cases). (Terminal Node 7)

Rules for inefficient farms (TE ≤ 0.800):

- Milk yield per cow's lifetime, kg day^{-1} is higher than 11.47 kg, and milk yield per cow per year is lower than or equal to 6,912.50 kg (TE = 0.767; 3 cases). (Terminal Node 9)
- Milk yield per cow's lifetime, kg day^{-1} is lower than or equal to 11.47 kg, feed costs per kg milk is higher than 0.12 € kg^{-1}, the number of cows is higher than 8.8, the productive period is lower than or equal to 46.33 months, somatic cell count is higher than 308.50, and the dRBV is higher than - 1.96 (TE = 0.737; 13 cases). (Terminal Node 5)
- Milk yield per cow's lifetime, kg day^{-1} is lower than or equal to 11.47 kg, feed costs per kg milk is higher than 0.12 € kg^{-1}, the number of cows is higher than 8.8, the productive period is higher than 46.33 months, the age at first calving is lower than or equal to 903.50 days, and milk yield per cow's lifetime, kg day-^{1} is lower than or equal to 9.75 kg (TE = 0.708; 7 cases). (Terminal Node 6)
- Milk yield per cow's lifetime, kg day^{-1} is lower than or equal to 11.47 kg, feed costs per kg milk is higher than 0.12 € kg^{-1}, the number of cows is higher than 8.8, the productive period is higher than 46.33 months, and the age at first calving is higher than 903.50 days (TE = 0.686; 10 cases). (Terminal Node 8)

When analysing and comparing information in the terminal nodes, it appears that 39% (58 farms) are operating efficiently (TE = 0.957). If milk yield per cow's lifetime is higher than 11.47 kg, but at the same time, milk yield per cow per year is lower than 6,912.5 kg, the farm is predicted to be inefficient (TE = 0.767). Higher milk yield is one of the predicting variables for higher efficiency. It is also a reflection of intensive production which is found to affect efficiency in a positive way (Cabrera et al., 2010; Keizer & Emvalomatis, 2014)

It should be highlighted that a higher score of SCC predicts inefficiency. Comparing the Terminal Nodes 3, 4 and 5, it appears that the first four predictors are the same, but the fifth is different and it divides farms according to the score of SCC. The farms whose SCC is lower than 308.5 are efficient (TE = 0.914), and those whose SCC is higher than 308.5 are divided into two groups according to the dRBV. It appears that these groups' efficiency is considerably lower (TE = 0.840; TE = 0.737). The SCC is a crucial factor in predicting efficiency. Luik-Lindsaar et al. (2018) also found that a higher score of SCC has a negative impact on efficiency.

The age at first calving is another crucial factor for predicting efficiency. The Terminal Nodes 6, 7 and 8 belong to the same bundle of nodes, with the first four predictors being the same, but age at first calving dividing the farms into two groups. Farms where the age at first calving was higher than 903.5 (approx. 30.1 months) tend to be the most inefficient (TE = 0.686). According to Froidmont et al. (2013) the age at first calving should be 4–8 months less to reach the optimal level in this group of farms.

The regression tree analysis shows that milk yield per cow's lifetime, feed costs, SCC, productive period, the number of cows, milk yield, age at first calving, and dRBV are all predictors of efficiency.

CONCLUSIONS

Combining the DEA with the regression tree approach offers an opportunity to predict dairy farms' technical efficiency. This analysis shows that integrating farm accounts data and other specific herd-level variables enables using a more in-depth analysis.

Milk yield per cow's lifetime is a good starting point to predict dairy farms' efficiency. Milk yield per cow's lifetime contains information such as a cow's average yield, the age at first calving, calving interval, lactation curve, age when culled, etc. The analysis indicated that if milk yield per cow's lifetime is higher than 11.47 kg, the farm is more likely to be efficient.

A lower feed costs per kg milk predicts higher efficiency. A higher score of SCC predicts lower efficiency. Higher SCC indicates poor hygiene and farm management. The preventive activities before milking are essential to increase efficiency. A lower score of SCC, however, refers to a higher quality of milk, which means that a higher share of milk is marketed, and milk price could be higher compared to farms with a high SCC. Therefore, the prevention of mastitis is an important factor to increase milk revenue and decrease treatments costs.

A higher age at first calving predicts lower efficiency. It largely depends on managerial decisions, therefore, the key to increasing a farm's efficiency is in decreasing the age at first calving to the optimal level.

Farms whose efficiency is higher, have a higher dRBV for milk, and younger managers. The fact that younger managers are more efficient can be explained by their higher rate of investments into modern technology, which helps to produce high-quality milk. Small farms and farms located in outlying regions are less efficient. It is a challenge for politicians to decide whether it is rational and essential to offer state support to farmers whose efficiency is lower in order to improve their performance.

This research provides valuable information about predicting variables of efficiency. The predictors help dairy farm managers to assess whether they are efficient, as well as to set the right production goals to make their farms more efficient.

REFERENCES

Archer, S.C., Mc Coy, F., Wapenaar, W. & Green, M.J. 2013. Association between somatic cell count early in the first lactation and the longevity of Irish dairy cows. *Journal of Dairy Science* **5**, 2939–2950.

Ariva, J., Viira, A-H., Põldaru, R. & Roots, J. 2015. Medium-run projections for greenhouse gas emissions arising from agriculture: the case of milk production in Estonia. *Agricultural and Food Science* **24**, 300–312.

Breiman, L., Friedman, J., Olshen, R. & Stone, C. 1984. *Classification and Regression Trees*. New York. Chapman &Hall, 358 pp.

Cabrera, V.E., Solis, D. & del Corral, J. 2010. Determinants of technical efficiency among dairy farms in Wisconsin. *Journal of Dairy Science* **93**, 387–393.

Davidova, S. & Latruffe, L. 2007. Relationships between technical efficiency and financial management for Czech Republic farms. *Journal of Agricultural Economics* **58**, 269–288.

De Vries, A. 2017. Economic trade-offs between genetic improvement and longevity in dairy cattle. *Journal of Dairy Science* **5**, 4184–4192.

Emrouznejad, A. & Anouze, A.L. 2010. Data envelopment analysis with classification and regression tree – A case of banking efficiency. *Expert Systems* **27**, 231–246.

Estonian Livestock Performance Recording Ltd. 2018. Results of Animal Recording in Estonia 2017. Eesti Põllumajandusloomade Jõudluskontrolli AS, Tartu, Estonia.

Estonian Statistics. 2018. *www.stat.ee* Accessed 10.12.2018.

Froidmont, E., Mayeres, P., Picron, P., Turlot, A., Planchon, V. & Stilmant, D. 2013. Association between age at first calving, year and season of first calving and milk production in Holstein cows. *Animal* **7**, 665–672.

Grandl, F., Furger, M., Kreuzer, M. & Zehetmeier, M. 2019. Impact of longevity on greenhouse gas emissions and profitability of individual dairy cows analysed with different system boundaries. *Animal* **13**, 198–208.

Grümpel, A., Krieter, J., Veit, C. & Dippel, S. 2018. Factors influencing the risk for tail lesions in weaner pigs (*Sus scrofa*). *Livestock science* **216**, 219–226.

Hadrich, J.C., Wolf, C.A., Lombard, J. & Dolak, T.M. 2018. Estimating milk yield and value losses from increased somatic cell count on US dairy farms. *Journal of Dairy Science* **4**, 3588–3596.

Hastie, T., Tibshirani, R. & Friedman, J. 2017. *The Elements of Statistical Learning. Data Mining, Inference, and Prediction.* Second Edition. Springer. 745 p.

Keizer, T.H. & Emvalomatis, G. 2014. Differences in TFP growth among groups of dairy farms in the Netherlands. NJAS. *Wageningen Journal of Life Sciences* **70**, 33–38.

Kuhn, L., Page, K., Ward, J. & Worrall-Carter, L. 2014. The process and utility of classification and regression tree methodology in nursing research. *Journal of Advanced Nursing* **70**, 1276–1286.

Latruffe, L., Fogarasi, J. & Desjeux, Y. 2012. Efficiency, productivity and technology comparison for farms in Central and Western Europe: The case of field crop and dairy farming in Hungary and France. *Economic Systems* **36**, 264–278.

Lawson, L.G., Agger, J.F., Lund, M. & Coelli, T. 2004a. Lameness, metabolic and digestive disorders, and technical efficiency in Danish dairy herds: a stochastic frontier production-function approach. *Livestock Production Science* **91**, 157–172.

Lawson, L.G., Bruun, J., Coelli, T., Agger, J.F. & Lund, M. 2004b. Relationships of efficiency to reproductive disorders in Danish milk production: a stochastic frontier analysis. *Journal of Dairy Science* **87**, 212–224.

Lemon, S.C., Roy, J., Clark, M.A., Friedmann, P.D. & Rakowski, W. 2003. Classification and regression tree analysis in public health: methodological review and comparison with logistic regression. *Annals of Behavioral Medicine* **26**, 172–181.

Loh, W.Y. 2008. *Classification and Regression Tree Methods.* In: Encyclopedia of Statistics in Quality and Realibility. Eds:Ruggeri, Kenett and Faltin. Wiley, 315–323.

Loh, W.Y. 2011. Classification and regression trees. *WIREs Data Mining Knowl Discov* **1**, 14–23.

Luik, H. & Viira, A-H. 2016. Feeding, milking and manure systems in Estonian dairy barns. *Agraarteadus* **2**, 92–107 (in Estonian).

Luik-Lindsaar, H., Viira, A.-H., Viinalass, H., Kaart, T. & Värnik, R. 2018. How do herd's genetic level and milk quality affect performance of dairy farms? *Czech Journal of Animal Science* **63**, 379–388.

Piwczynski, D., Nogalski, Z. & Sitowska, B. 2013. Statistical modeling of calving ease and stillbirths in dairy cattle using the classification tree technique. *Livestock Science* **154**, 19–27.

Põder, A., Viira, A-H. & Värnik, R. 2017. Firm entries and exits in Estonian urban municipalities, urban hinterlands and rural peripheries 2005–2012. *Journal of Baltic Studies* **48**, 285–307.

Põldaru, R. & Roots, J. 2014. Using a nonlinear stochastic model to schedule silage maize harvesting on Estonian farms. *Computers and Electronics in Agriculture* **107**, 89–96.

Rahimi, I. & Behmanesh, R. 2012. Improve poultry farm efficiency in Iran: using combination neural networks, decision trees, and data envelopment analysis (DEA). *International Journal of Applied Operational Research* **2**, 69–84.

Rasmussen, S. 2010. Scale efficiency in Danish agriculture: An input distance-function approach. *European Review of Agricultural Economics* **37**, 335–367.

Scollo, A., Gottardo, F., Contiero, B. & Edwards, S.A. 2017. A cross-sectional study for predicting tail biting risk in pig farms using classification and regression tree analysis. *Preventive Veterinary Medicine* **146**, 114–20.

Steinberg, D. 2009. *The Top Ten Algorithms in Data Mining*. Ed. Wu, X & Kumar, V. Chapman & Hall, CRC Press, 208 pp.

Tauer, L.W. & Mishra, A.K. 2006. Dairy farm cost efficiency. *Journal of Dairy Science* **89**, 4937–4943.

Topal, M., Aksakal, V., Bayram, B. & Yağanoğlu, A.M. 2010. An analysis of the factors affecting birth weight and actual milk yield in Swedish red cattle using regression tree analysis. *The Journal of Animal & Plant Sciences* **20**, 63–69.

Viira, A-H., Põder, A. & Värnik, R. 2009. 20 years of transition – institutional reforms and the adaptation of production in Estonian agriculture. *Agrarwirtschaft* **58**, 286–295.

Viira, A-H., Põder, A. & Värnik, R. 2013. The determinants of farm growth, decline and exit in Estonia. *German Journal of Agricultural Economics* **62**, 52–64.

Viira, A-H., Omel, R., Värnik, R., Luik, H., Maasing, B. & Põldaru, R. 2015. Competitiveness of Estonian dairy sector from 1994−2014. *Journal of Agricultural Science* **26**, 84–105.

Yang, L., Liu, S., Tsoka, S. & Papageorgiou, L.G. 2017. A regression tree approach using mathematical programming. *Expert Systems With Applications* **78**, 347–357.

Yohanne, Y. & Hoddinott, J. 1999. *Classification and Regression Trees: An Introduction.* Technical Guide #3. International Food Policy Research Institute. Washington, USA. 30 pp.

Zhu, J. 2009. *Quantitative Model for Performance Evaluating and Benchmarking*. Springer, 327 pp.

Agronomy Research **17**(2), 608–620, 2019
https://doi.org/10.15159/AR.19.099

Formation of photosynthetic and grain yield of spring barley (*Hordeum vulgare* L.) depend on varietal characteristics and plant growth regulators

A. Panfilova*, M. Korkhova, V. Gamayunova, M. Fedorchuk, A. Drobitko, N. Nikonchuk and O. Kovalenko

Mykolayiv National Agrarian University, Faculty of Agricultural technologies, 73 Karpenko street, UA54021 Mykolayiv, Ukraine
*Correspondence: panfilovaantonina@ukr.net

Abstract. The aim of the study was to determine the efficiency of the barley treatment crops with modern retrograde preparations on the background of the mineral fertilizers introduction into the photosynthetic activity of crops and grain yield. The experiments were carried out in 2013 -2017 on the southern black soil in the conditions of the Ukrainian Steppe. On the basis of the study results, it was determined that the introduction of irrigated fertilizer barley in a dose of $N_{30}P_{30}$ (background) under pre-sowing cultivation and the application of extra-root crop supplements at the phases beginning of the barley outflow straw into the tube and the organoleptic fermentation of Organic D2 and natural microbial complex Escort - Bio creates favorable conditions for the formation at the optimal levels of photosynthetic parameters and grain yield. Thus, on average, over the years of research and by factor variety, grain yield on these experimental variants was 3.37–3.41 t ha^{-1}, which exceeded its level on uncontrolled control by 0.71–0.75 t ha^{-1} or 26.7–28.2%. Based on the study results, the use of modern regenerating agents against the background of mineral fertilizers can be recommended as an expedient and effective measure of spring barley raising the productivity.

Key words: spring barley, variety, plant nutrition, leaf area, photosynthetic potential, pure photosynthesis productivity.

INTRODUCTION

Grain crops have a long history of using by people. Cereals are the main food and they are important sources of nutrients in both developed and developing countries. World cereal consumption in 2015–2017 was 2.6 billion tons (FAO). Global consumption of cereals is projected to increase to 2.9 bln tons in 2027, driven mainly by higher feed use (+167 Mt) followed by food use (+151 Mt). Developing countries will account for 84% of projected increase in overall consumption, but contrary to global outlook, the absolute increase in food use (+148 Mt) for developing countries will exceed the growth of feed use (+132 Mt). Conversely, for developed countries, feed use (+36 Mt) will grow more than food use (+3 Mt). Cereal products are the important source of energy, carbohydrates, proteins and fiber, and they also contain a variety of trace elements and vitamins (McKevith, 2004; Ashikari et al., 2005; Hake, 2008; Hirano et al., 2014).

Historically, barley (*Hordeum vulgare* L.) was a common crop grown in far agricultural areas, but it was neglected by breeders of Europe during the period of intensive crop development (Šterna et al., 2017). During in recent years grain barley production has decreased from 65.7 million tons in 2008 to 58.7 million tons in 2017, ie 10.7%. This was primarily due to the low demand for barley and price policy (Eurostat regional yearbook, 2017). The increased interest in barley, as a grain culture which can be used in the food industry, arose after studies run by Wood (2004) and Anonymous (2005). Grain of spring barley is widely used for food, technical and nutritional purposes, including brewing, in the production of pearl barley and cereals, but its main amount is used for feed purposes (Yarchuk et al., 2015).

The growing needs of modern agrarian production determine the need to find new ways and means for increasing of the productivity of agricultural crops and the quality of their products. The formation of yields is influenced by environmental conditions and the availability of resources, the most important of which are nutrients, water and light (Kren et al., 2015; Korchova et al., 2018). Growth regulators are important components of modern plant growing technologies (Komarova, 1998; Henselová et al., 2001).

Interest in this group of compounds is due to a wide range of their effects on plants, the ability to directly regulate specific stages of ontogenesis with the aim of mobilizing the potential of the plant organism and more efficient implementation of the genetic program (Khan & Ansari Samiullah, 1998; Malinauskaitė & Jakienė, 2005). Stimulators-native phytohormones and their synthetic analogues are the most used group of growth regulators (Laichicxi et al., 2002; Gavelienė et al., 2007). With the help of these compounds it can be influenced on the intensity and direction of the physiological processes in the plant organism, including the photosynthetic processes (Xinping et al., 2002; Angela, 2004).

Photosynthesis is a major source of dry matter and crop yields. Improvement of photosynthesis of leaves occurred with the withdrawal of high-yielding crop varieties (Jiang et al., 2002).

Numerous studies of scientists in the world found that the use of complex organo-mineral fertilizers, composite growth bioregulators, inoculants, nanoparticles, biogenic elements contributes to the regulation of growth and development processes of plants, their resistance to stress through increased plant immunity, activation of biological processes, synthesis of organic substances, increasing the area of the leaf surface, improving the net productivity of photosynthesis and yields of crops (Wakchaure et al., 2016; Pestovsky & Martinez-Antonio, 2017; Piskaeva et al., 2017; Klein & Guimarães, 2018; Singh et al., 2018). However, today, the market presents a very wide range of preparations, which complicates the choice, and scientific evidence of the impact of those preparations on the productivity of spring barley remains unimportant in the world scientific literature.

Taking into account the acuteness of the problem, the aim of the study was to determine the impact of modern certified drugs, in particular organo-mineral fertilizers Organic D2 and natural microbial complex Escort-bio, on the productivity of barley of spring varieties Adapt, Stalker and Aeneas, which involves the partial replacement of mineral fertilizers and chemical pesticides in order to increase the net productivity of photosynthesis, the yield and quality of the grain and the creation of the most favourable conditions for the restoration of soil fertility. The relevance of this study increases with

the globalization of the influence of anthropo-technological load on the natural environment and the growth of the rate of depletion of natural ecosystems.

MATERIALS AND METHODS

Experimental researches were carried out during 2013–2017 years in the conditions of the educational-scientific-practical center of the Mykolaiv National Agrarian University.

The soil of experimental sites was represented by the southern, resiliently weakly sunny, heavy-sooty black soilon the loesses. The reaction of the soil solution was neutral (pH 6.8–7.2). The content of humus in the 0–30 cm layer was 123–125 g kg^{-1}. The arable layer of soil contained moving forms of nutrients on average: nitrates (by Grandval Liagou - this method is based on interactions between nitrates and disulpfo-phenolic acid from which trinitrophenol (picric acid) is formed. In alkaline environment it gives us yellow coloring due to formation of potassium trinitrophenolate (or natrium, depending from alkali used) in quantity equivalent to nitrates content) as 15–25 mg kg^{-1}, mobile phosphorus (by Machigin - this method is based on extraction of mobile phosphorus and potassium compounds from the soils with 1% ammonium carbonate solution, pH 9.0, at 25 ± 2 °C) as 41–46 mg kg^{-1}, exchangeable potassium (on a flame photometer) as 389–425 mg $kg^{-1}$of soil.

The territory of the farm locates in the third agro-climatic region and belongs to the subzone of the southern steppe of Ukraine. The climate here is temperate-continental, warm, dry, with unstable snow cover. Weather conditions by hydrothermal indices during the research years varied, which gave an opportunity to obtain objective results (Fig. 1).

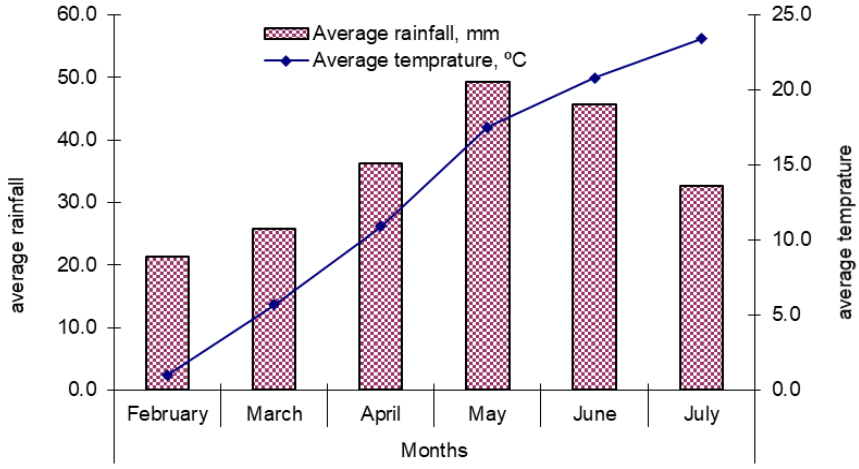

Figure 1. Average weather data during the 2013–2017 crop year.

The amount of precipitation for the vegetation period of spring barley on the average over the years of research (2013–2017) is 210.9 mm, which is within the normal range, but the average monthly rates have significant deviations from the norm. Thus, the smallest amount of precipitation (21.4 mm) fell in February, which is 31.6% less than

the norm (31.3 mm). The farthest from the norm for the years of research was April, with the average rainfall of 36.3 mm, which is 72.9% more than the average yearly norm (21.0 mm). The largest amount of precipitation (49.2 mm) dropped in May, representing 23.3% of the total for the entire period of vegetation of barley.

The temperature conditions for the growing season of barley in 2013–2017 were within the normal range, except for the average monthly temperature of March, which for the average in 5 years was 15.8% higher than the norm (4.8 °C).

The object of research was spring barley – varieties Adapt, Stalker and Aeneas. The technology of their cultivation, with the exception of the investigated factors, was generally accepted to the existing zonal recommendations for the Southern Steppe of Ukraine. Weather conditions in the years of research varied, in particular, in 2015 and 2016 during the vegetation the considerably more rainfall dropped. In general, they were typical for the southern steppe region of Ukraine.

The total area of the experimental plot was 80 m^2, the accounting one was 36 m^2, the repetition was three times. Scheme of the experiment included the following options:

Factor A – variety: 1. Adapt; 2. Stalker; 3. Aeneas.

Factor B – plantnutrition: 1. Control (without fertilizers); 2. $N_{30}P_{30}$ – under pre-sowing cultivation – background; 3. Background + Urea K1 (1 L ha^{-1}); 4. Background + Urea K2 (1 L ha^{-1}); 5. Background + Escort-bio (0.5 L ha^{-1}); 6. Background + Urea K1 + Urea K2 (0.5 L ha^{-1}); 7. Background + Organic D2 (1 L ha^{-1}). The standard working solution was 200 L ha^{-1}. The fertilization of crops by fertilizers was carried out at the beginning of the phases of the spring barley stooling and earing.

Preparations to be used for foliar application of barley crops were listed in the listof pesticides and agrochemicals authorized for use in Ukraine. Preparations of Urea K1 and Urea K2 are registered as fertilizers containing respectively N as 11–13%, P_2O_5 as 0.1–0.3%, K_2O as 0.05–0.15%, micronutrients as 0.1%, succinic acid as 0.1% and N as 9–11%, P_2O_5 as 0.5–0.7%, K_2O as 0.05–0.15%, sodium humate as 3 g L^{-1}, potassium humate as 1 g L^{-1}, trace elements as 1 g L^{-1}. Organic D2 is organo-mineral fertilizer containing N as 2.0–3.0%, P_2O_5 as 1.7–2.8%, K_2O as 1.3–2.0%, total calcium as 2.0–6.0%, organic matter as 65–70% (in terms of carbon). Escort-bio is a natural microbial complex that contains strains of microorganisms of genera Azotobacter, Pseudomonas, Rhizobium, Lactobacillus, Bacillus, and biologically active substances produced by them.

In the process of research, the method of the State Variety Testing of Agricultural Cultures was used (Volkodav et al., 2001). To determine phytometric indices (mass of dry and raw matter of plants, leaf area), plants were taken by frame method from 1 m^2 in three non-adjoining repeats in stages of growth and development. During the growing season, the area of the leaf surface of the plants was determined by the method of carving, the net productivity of photosynthesis (NFP) as the growth of the mass of dry matter per unit time per unit leaf area, the index of the leaf surface (PI) – as the ratio of the total leaf area to unit area of plantings. The crop structure was analyzed by the sheaves, which were taken before harvesting from the sites of 1 m^2. The yield was determined by the method of continuous harvesting of each registration area (Sampo – 130 combine harvester).

Variant placing in the experiments was random; repetition was three times. The results of the research were processed using the method of multivariate disperse analysis.

RESULTS AND DISCUSSION

The overground mass plays an important role in the life of plants as it mobilizes carbohydrates and nitrogen-containing substances to form the productive part of the crop. Particularly important role of the overground mass of plants is diverted to the south of Ukraine, where until the period of grain filling a significant part of the leaf apparatus (Panfilova et al., 2019).

Mineral fertilizers, including increasing doses of nitrogen fertilizers, contribute to the growth of the overground mass of plants and the increase in grain yield (Novotna et al., 2015; Povilaitis et al., 2018). One of the ways to increase the effectiveness of using mineral fertilizers for reducing their norms is the use of growth-stimulating preparations. The use of growth-stimulating preparations causes changes in the leaf apparatus of crops, in particular, it leads to a significant increasing in the number of leaves per plant, the mass of raw and dry matter of leaves, which is a typical reaction of the plant organism to the action of growth-stimulating preparations and it is confirmed in literary sources (Khan & Ansari, 1998; Fauate et al., 2007). On average, over the years of research, somewhat larger amounts of crude and dry earth masses have accumulated by plants of the Aeneas variety (Table 1).

Thus, on the control version of the experiment of the plants raw biomass of the Aeneas variety, in the stooling phase it was accumulated 896 g m^{-2}, and in the earing phase it was accumulated 1,692 g m^{-2}, which was at 28–57 g m^{-2}or 1.7–6.8% more compared to the raw mass of plants of the Adapt variety and at 15–48 g m^{-2}or 0.9–5.7% more than the Stalker variety. The same trend was observed in other variants of the experiment.

It should be noted that the application of foliar nutrition of plants during the period of vegetation with modern growth-regulating preparations Organic D2 and Escort - bio in the background of the application of a moderate dose of mineral fertilizers contributed to the accumulation of somewhat larger amounts of crude overground mass of plants of the studied varieties of spring barley. Thus, on average, over the years of research and by variety factor, at the end of the stooling phase it was formed 1,799–1,851 g m^{-2}, and in the earing phase it was formed 2,665–2,706 g m^{-2}, which respectively 938–990 and 987–1,028 g m^{-2}, or 52.1–53.5 and 37.0–38.0% exceeded the parameters of the control variant.

The dynamics of accumulation of dry matter during the growing of spring barley in our studies had practically the same tendencies that were found during the formation of the crude overground mass. In the tillering phase, the process of accumulation of dry matter by plants was slow, and the difference between the studied variants was only 9–11 g m^{-2}depending on the type of studied variety. However, already from the stooling phase it was seen a significant difference depending on the nutrition of plants and varieties by 40.6–59.8; 43.3–62.2 and 35.4–55.5% with the advantage of the background + Escort - bio.

And in the research of other scientists application of fertilizers in different ways influenced on the accumulation of dry mass of plants. Thus, an increase in the fertilizer dose up to 300 mg N per pot contributed to a decrease in the specified index in spring barley plants (Kostadinova et al., 2016).

Table 1. The growth of crude and dry overground mass of spring barley plants depending on the variety features and nutrition optimization (average for 2013–2017), g m^{-2}

Nutrition variant	Crude overground mass			Dry mass of plants		
	Phase of plant development					
	tillering	plant stooling	earing	tillering	plant stooling	earing
variety Adapt						
Control	307	839	1,664	65	177	566
$N_{30}P_{30}$ (background)	344	1,383	2,040	74	298	706
Background + Urea K1		1,607	2,475		360	867
Background + Urea K2		1,655	2,517		371	890
Background + Escort-bio		1,816	2,678		440	971
Background + Urea K1 + Urea K2		1,722	2,584		403	929
Background + Organic D2		1,773	2,639		413	953
variety Stalker						
Control	313	848	1,677	64	160	575
$N_{30}P_{30}$ (background)	351	1,436	2,057	75	282	717
Background + Urea K1		1,644	2,506		333	896
Background + Urea K2		1,679	2,548		344	916
Background + Escort-bio		1,847	2,704		423	1,002
Background + Urea K1 + Urea K2		1,761	2,601		367	945
Background + Organic D2		1,799	2,662		406	979
variety Aeneas						
Control	304	896	1,692	62	210	553
$N_{30}P_{30}$ (background)	342	1,360	2,086	71	325	727
Background + Urea K1		1,630	2,530		400	924
Background + Urea K2		1,651	2,574		420	947
Background + Escort-bio		1,889	2,737		472	1,045
Background + Urea K1 + Urea K2		1,768	2,633		437	982
Background + Organic D2		1,824	2,695		456	1,011
$LSD_{0.5}$ 2013: A		12	13		13	7
B		8	7		9	10
2014: A		5	5		16	16
B		3	7		9	9
2015: A		10	11		10	15
B		7	8		9	11
2016: A		15	13		21	9
B		11	12		17	10
2017: A		2	6		24	19
B		7	7		9	13

Photosynthesis is the basis of production and, at least, 90% of the grain crop is determined by it (Shao et al., 2005; Makino, 2011). In the process of photosynthesis the simple substances are formed into energy–rich complex and diverse in chemical composition organic compounds. The intensity of the accumulation of organic matter depends on the size of the leaf surface, which is determined by the biometric parameters of the plants and it significantly depends on the mode of their nutrition, as well as the

duration of the leaves activity (Malkina & Eremenko, 2016). The area of the leaf surface plays an important role in the analysis of plant growth processes and the formation of grain productivity (Sharma et al., 2003; Guendouz et al., 2016).

In modern agriculture, various plant growth regulators have been widely used, which influence on the intensity of photosynthetic processes. So, in studies of Ukrainian scientists (Gritsaenko et al., 2008) it was established that the treatment of plants with growth regulators increased the net productivity of photosynthesis, it increased the content of photosynthetic pigments in the chloroplasts.

Our research found that the use of foliar fertilization of spring barley crops contributed to an increase in the area of the plants leaf surface from the tillering phase to earing phase, after which in all years of the research a significant decrease was observed in this indicator related to the culture biology, namely, the fading of the leaf apparatus and the outflow of nutrients from the leaves to the generative organs, although the processes of plant development were still ongoing. Thus, on average, over the years of research, during the entire vegetation season in fertilized plants, the area of the leaf surface was greater than the area of untreated ones (Table 2).

So, for the growth of spring barley of the variety Adapt from the tillering phase and to the earing phase in the variants with a moderate dose of mineral fertilizers the index area of the leaf surface increased up to 3.29 m^2 m^{-2}, and for cultivating varieties Stalker and Aeneas it increased up to 3.49–3.71 m^2 m^{-2}.

Foliar nutrition of crops in the main periods of vegetation of spring barley plants with modern growth-regulating drugs in combination with the main application of $N_{30}P_{30}$ provided growth of the index of the leaf surface of plants of the Adapt in the earing phase up to 18.5–28.8%, while the specified index of Stalker and Aeneas varieties increased respectively up to 20.8–30.1 and 20.6–28.1% depending on the plant nutrition.

It should be noted that on average, over the years of research and in terms of nutrition, the index of the leaf surface of plants of spring barley of the variety Aeneas was slightly higher compared to other studied varieties: in the stooling phase it was higher at 3.3–7.1%, and in the earing phase it was higher at 5.3–10.0%.

According to the results of our researches, the work of the plant apparatus during vegetation was determined by the net productivity of photosynthesis (CRF). We determined that this index depended on the studied factors such as biological characteristics of the studied varieties of spring barley, the background of nutrition, and on the phases of plant growth and development. Thus, on average, over the years of research, in the experimental variants, where only the background fertilizer $N_{30}P_{30}$, in the Adapt and Stalker varieties was introduced in the interphase period of tillering - stooling it was 5.19–5.82 g m^{-2} per day, in the interphase period of stooling - earing it was 12.24–12.27 g m^{-2} per day. For the growing of spring barley of the variety Aeneas the specified values were slightly higher compared to other studied varieties, respectively, 6.16 and 13.14 g m^{-2}per day.

The largest net photosynthesis performance was determined in the background application of $N_{30}P_{30}$ and subsequent fertilization of the crops by Escort Bio. Thus, on average, over the years of research, in the interphase period of tilerring - earing, the net productivity of photosynthesis of the Adapt variety was 12.00 g m^{-2}per day, while the

Stalker and Aeneas varieties it was respectively 11.93 and 12.15 g m^{-2}per day, which exceeded control by 25.9; 26.2 and 34.1% respectively.

Table 2. Photosynthetic activity of spring barley crops depending on varietal characteristics and optimization of nutrition (average for 2013–2017)

Nutrition variant	Leaf index, m^2 m^{-2}			The net productivity of photosynthesis, G m^{-2}per day		
	Phase of plant development			Interphase periods		
	tillering	plant stooling	earing	tillering - stooling	stooling - earing	tillering -earing
variety Adapt						
Control	1.10	2.44	2.72	3.48	11.06	8.89
$N_{30}P_{30}$ (background)	1.21	3.01	3.29	5.82	12.27	9.60
Background + Urea K1		3.07	3.34	7.39	14.54	11.79
Background + Urea K2		3.12	3.40	7.54	14.68	12.01
Background + Escort-bio		3.51	3.82	8.52	13.11	12.00
Background + Urea K1 + Urea K2		3.30	3.62	8.01	13.81	11.96
Background + Organic D2		3.44	3.73	8.07	13.69	11,98
variety Stalker						
Control	1.14	2.59	2.81	2.89	11.31	8.80
$N_{30}P_{30}$ (background)	1.26	3.16	3.49	5.19	12.24	9.65
Background + Urea K1		3.22	3.55	6.37	15.15	11.54
Background + Urea K2		3.27	3.61	6.56	15.23	11.69
Background + Escort-bio		3.62	4.02	7.90	14.11	11.93
Background + Urea K1 + Urea K2		3.43	3.79	6.92	14.45	11.62
Background + Organic D2		3.55	3.92	7.59	14.24	11.80
variety Aeneas						
Control	1.17	2.69	3.00	4.27	11.07	8.01
$N_{30}P_{30}$ (background)	1.31	3.26	3.71	6.16	13.14	8.98
Background + Urea K1		3.32	3.78	7.82	13.78	10.74
Background + Urea K2		3.36	3.83	8.21	13.68	11.63
Background + Escort-bio		3.74	4.17	8.68	13.64	12.15
Background + Urea K1 + Urea K2		3.55	3.98	8.27	13.39	11.77
Background + Organic D2		3.67	4.11	8.50	13.42	11.87

It should be noted that on average, over the years of research and on the factor of plant nutrition, somewhat higher indicators of pure productivity of photosynthesis were for the cultivation of the Adapt variety. Thus, in the inter-phase period of tillering - earing, the net productivity of the photosynthesis of this variety exceeded this indicator in the varieties Stalker and Aeneas at 0.18–0.48 g m^{-2} per day or 1.6–4.5%.

Consequently, the increasing of growth processes in spring barley plants caused by the influence of modern organo-mineral and mineral fertilizers was resulted in the formation of a larger overground mass of plants, a more powerful leaf apparatus and increased the net productivity of photosynthesis. Such anatomical and morphological changes had a positive effect on the productivity of spring barley varieties (Table 3).

Table 3. Performance of spring barley, depending on varietal characteristics and optimization of nutrition, average for 2013–2017

Variety	Nutrition variant	Number of grains in the ear, pc.	Weight of corn grain, g	Grain yield, t ha^{-1}
Adapt	Control	20.0	0.915	2.56
	$N_{30}P_{30}$ (background)	20.7	1.001	2.91
	Background + Urea K1	20.9	1.024	3.05
	Background + Urea K2	21.0	1.033	3.11
	Background + Escort-bio	21.6	1.077	3.25
	Background + Urea K1 + Urea K2	21.2	1.046	3.17
	Background + Organic D2	21.4	1.061	3.22
Stalker	Control	20.5	0.950	2.63
	$N_{30}P_{30}$ (background)	21.4	1.026	3.02
	Background + Urea K1	21.6	1.051	3.19
	Background + Urea K2	21.8	1.060	3.23
	Background + Escort-bio	22.3	1.097	3.37
	Background + Urea K1 + Urea K2	21.9	1.074	3.29
	Background + Organic D2	22.1	1.084	3.33
Aeneas	Control	21.0	0.970	2.80
	$N_{30}P_{30}$ (background)	21.8	1.047	3.24
	Background + Urea K1	22.0	1.069	3.38
	Background + Urea K2	22.2	1.078	3.44
	Background + Escort-bio	22.6	1.113	3.61
	Background + Urea K1 + Urea K2	22.3	1.091	3.52
	Background + Organic D2	22.4	1.098	3.56
$LSD_{0.5}$ 2013:	A	2	0.010	0.08
	B	1	0.008	0.11
2014:	A	4	0.017	0.10
	B	2	0.013	0.13
2015:	A	8	0.023	0.09
	B	2	0.019	0.14
2016:	A	7	0.36	0.08
	B	4	0.032	0.10
2017:	A	2	0.002	0.11
	B	1	0.003	0.13

It is known that the structural elements such as the amount of grains in the ear and the mass of grains from the ear are the main components of grain crops. Formation of their level and variability on a huge selection of varieties and breeding lines, for many years, in a controlled environment is of great interest to the technology of breeding process. First of all, genotypes that stably form high structural elements of the crop, which in the future are used to create new varieties (Gusenkova & Tishchenko, 2018) can be chosen in the huge biological diversity of the investigated material. The variety combines in the genotype the maximum number of features and properties that contribute to obtaining a high level of harvest of appropriate quality. The list of these features was determined by the agroecological conditions and factors affecting agroecenos during the vegetation (Hudzenko et al., 2017). On average, over the years of our research, the nutrition variants to some extent affected on the number of grains in the ear of spring barley. Thus, introduction of pre-sowing cultivation of mineral

fertilizers in a dose of $N_{30}P_{30}$ contributed to the increase of the specified figure by 3.4–4.2% depending on the type of variety. The application of mineral fertilizers of extra-root nutritions during the growing season with modern preparations Organic D2 and Escort - bio contributed to an increase in the number of grains in the ear from 6.5 to 7.4% in the Adapt variety, it was from 7.2 to 8.1% in the Stalker variety and it was from 6.3 to 7.1% for the Aeneas variety.

Immediately after the transition of plants from vegetative development to generative one, a gradual implementation of the biopotential of an important element of yield is started as the number of grains in the ear, on which the varietal features have a significant impact (Solonechnuy, 2018). In our studies, somewhat larger amounts of grains in the ear were created during the years of research of the plants of the Aeneas variety. So, on average, over the years of research on the nutrition factor, they formed 22.0 pcs., which exceeded other studied varieties by 1.4–4.8%.

We found that on average over the years of research, varieties and variants of nutrition have affected on the mass of grain from one ear. So, for the introduction of the background recommended dose of mineral fertilizers for spring barley of the variety Adapt the weight of grain from the ear in comparison with unfertilized control increased by 9.4%, while in the Stalker variety it was increased by 8.00%, and in the Aeneas variety it was increased by 7.9%. Conducting of foliar nutrition on the background of mineral fertilizers increased the specified index of yield structure, respectively, by 11.9–17.7; 10.6–15.5 and 10.2–14.7% for control.

Yield is a major parameter of research in agriculture and the environment (Iizumi et al., 2014). Resource-saving technologies, which increase the yield of grain crops up to 10–15%, can contribute to the increase in yields (Dwyer et al., 1995; Markov et al., 2011). Combined use of organic and mineral fertilizers in combination with humic substances in studies by Indian scientists increased grain yield of wheat by 27% and it had beneficial effect on the nutrients and organic carbon content in the soil (Manzoor et al., 2014; Bharali et al., 2017).

In our studies, the growth of grain yield of spring barley of varieties Adapt and Stalker for the introduction of $N_{30}P_{30}$ to control was 0.35–0.39 t ha^{-1} or 13.7–14.8%. The application of growth-regulating drugs on the background of the application of $N_{30}P_{30}$ provided for an increase in the grain yield of spring barley, respectively, from 0.49 to 0.69 and 0.56 to 0.74 t ha^{-1} or 19.1 to 27.0 and 21.3 to 28.1% depending on the drug.

Extra-root fertilization of Aeneas spring barley crops also positively affected on grain yields. Thus, on average, over the years of research, specified agricultural method contributed to an increase in yields by 0.58–0.81 t ha^{-1} or by 20.7–28.9% compared to the control.

The yields of the studied varieties naturally grew on the variants of extra-root nutrition against the background of mineral fertilizers. At the same time, more significant increments of grain were formed in the variants of carrying on their background the fertilization of crops with the preparations Organic D2 and Escort - bio. Their application contributed to the growth of grain yield of spring barley of the variety Adapt at 0.66–0.69 t ha^{-1} or 25.8–27.0%, the growth of yield of the Stalker variety was at 0.70–0.74 t ha^{-1} or 26, 6 to 28.1%, while the growth of yield of the Aeneas variety was 0.76–0.81 t ha^{-1} or 27.1–29.9% respectively.

Grain yields are the result of the interaction of genetic features of plants, agrotechnological and climatic conditions of cultivation (Diacono et al., 2012). On

average, over the years of research, the Aeneas variety was superior to the Adapt and Stalker varieties, with the best indicators of the structure of spring barley and grain yield. Thus, on average, over the years of research and on the factor of nutrition, the grain yield of spring barley of the variety Aeneas compared to other studied varieties was formed higher by 0.21–0.32 t ha^{-1} or 6.3–9.5%.

CONCLUSION

In the conditions of southern Ukraine, on the average, during years of research, the application of mineral fertilizers at a dose of $N_{30}P_{30}$ under pre-sowing cultivation and the application of extra-root crop cultivation at the beginning of the stooling and earing phases with fertilizers Organic D2 and Escort-bio contributed to the accumulation of somewhat more crude and dry overground mass of the studied varieties plants of spring barley and the formation of their higher photosynthetic rates.

Nutrition with Escort-Bio and Organic D2 supplies the highest indicators of yield structure, at the same time, the essential influence of the investigated factor was on the mass of grain from one ear. It has been established that significantly higher yield of barley grain for these varieties of food provides the cultivation of the Aeneas variety - 3.56–3.61 t ha^{-1}.

REFERENCES

Angela, C. 2004. Dyphenylurea derivatives: Structure-activity relationship in plants. *ActaNatur. Aten.-Parm*. **40**(3–4), 85–89.

Anonymous. 2005. FDA allows barley products to claim reduction in risk of coronary heart disease. FDA news release, 23 December. http://www.fda.gov/NewsEvents/Newsroom/PressAnnouncements/ 2005/ ucm108543.htm

Ashikari, M., Sakakibara, H., Lin, S., Yamamoto, T., Takashi, T., Nishimura, A., Angeles, ER., Qian, Q., Kitano, H. & Matsuoka, M. 2005. Cytokininoxidaseregulates rice grain production. *Science*. **309**, 741–745.

Bharali, A., Baruah, KK. & Bhattacharyya, P. 2017. Integrated nutrient management in wheat grown in a northeast India soil: Impacts on soil organic carbon fractions in relation to grain yield. *Soil & tillage research*. **168**, 81–91.

Diacono, M., Castrignano, A., Troccoli, A., De Benedetto, D., Basso, B. & Rubino, P. 2012. Spatial and temporal variability of wheat grain yield and quality in a Mediterranean environment: A multivariate geostatistical approach. *Field Crops Research*. **131**, 49–62.

Dwyer, L.M., Stewart, D.W., Gregorich, E., Anderson, A.M. 1995. Quantifying the nonlinearity in chlorophyll meter response to corn leaf nitrogen concentration. *Canadian J Plant Sci*. **75**(1), 179–182. DOI: 10.4141/cjps95-030

Gavelienė, V., Novicienė, L. & Kazlauskienė, D. 2007. Effect of auxin physiological analogues on rape growth and reproductive development. *Bot. Lithuan*. **13**(2), 101–107.

Gritsaenko, Z.M., Ponomarenko, S.P., Karpenko, V.P. & Montju, I.B. 2008. Biologically active speech in Roslynnitstv. *Nichlava*, 352 pp. (in Ukrainian).

Guendouz, A., Semcheddine, N., Moumeni, L. & Hafsi, M. 2016. The effect of supplementary irrigation on leaf area, specific leaf weight, grain yield and water use efficiency in durum wheat (Triticum durum Desf.) cultivars. *Ekin Journal of Crop Breeding and Genetics*. **2**(1), 82–89.

Gusenkova, O. & Tishchenko, V. 2018. The balance of signs of productivity and quality of winter wheat grain, depending on the year of cultivation and sowing lines. *Ştiinţa agricolă*. **1**, 10–16 (in Russian).

Eurostat regional yearbook. doi: 10.2785/220518 https://ec.europa.eu/eurostat/statistics-explained/index.php/Eurostat_regional_yearbook

Fauate, A., Fauate, M., Ayub, R.A. & Barbosa, M.M. 2007. Aplicacão de GA4,7+BA (promalina) afetando o crescimento, desenvolvimento e qualidade do caqui (Diospyros kaki L.) cv. *Fuyu. Rev. Ceres*. **54**, 226–250.

Hake, S. 2008. Inflorescence architecture: the transition from branches to flowers. *Curr. Biol*. **18**, 1106–1108.

Henselová, M., Vizárová, G. & Macháčková, I. 2001. The effect of growth regulator Rastim 39 DKV on the level of endogenous phytohormones in tomato (Solanum lycopersicum L.). *RostlinnáVýroba*. **47**(9), 411–417.

Hirano, H.Y., Tanaka, W. & Toriba, T. 2014. Grass flower development. In Flower Development: Methods and Protocols; Humana Press: New York, NY, USA, 57–84.

Hudzenko, V.M., Vasylkivskyi, S.P., Demydov, O.A., Polishchuk, T.P. & Babiy, O.O. 2017. Spring barley breeding for increase in productive and adaptive capacities. *Selektsia i nasinnitstvo*. **111**, 51–61.

Jiang, H., Wang, X.H., Deng, Q.Y., Yuan, L.P. & Xu, D.Q. 2002. Comparison of some photosynthetic characters between two hybrid rice combinations differing in yield potential. *Photosynthetica*. **40**, 133–137.

Khan, N.A. & Ansari Samiullah, H.R. 1998. Effect of gibberellic acid spray during ontogeny of mustard on growth, nutrient uptake and yield characteristics. *J. Agron. Crop Sci*. **181**(1), 61–63.

Klein, J. & Guimarães, V.F. 2018. Evaluation of the agronomic efficiency of liquid and peat inoculants of Azospirillumbrasilense strains in wheat culture, associated with nitrogen fertilization. *Journal of Food, Agriculture & Environment.* **16** (1), 41–48. DOI: 10.1234/4.2018.5480

Komarova, V. 1998. The influence of growth regulator crossing on young apple trees photosynthesis activity under soil drought: Abstr. 11 th Congress of the Federation of European Societies of Plant Physiology, Varna, 7–11 Sept. *Bulg. J. Plant Physiol. Spec*. issue. 308.

Korchova, M.M., Panfilova, A.V., Kovalenko, O.A., Fedorchuk, M.I., Chernova, A.V., Khonenko, L.G. & Markova, N.V. 2018. Water supply of soft winter wheat under dependent of it sorts features and sowing terms and their influence on grain yields in the conditions of the Southern Step of Ukraine. Ukrainian Journal of Ecology, 8(2), 33–38. doi:10.15421/2018_306 (in Ukrainian).

Kostadinova, S., Panayotova, G. & Kuzmanova, L. 2016. Effect nitrogen on the translocation of dry mass and nitrogen in barley. *Scientific Papers. Series A. Agronomy*. Vol. **LIX**: 327–331.

Kren, J., Klem, K., Svobodova, I., Misa, P. & Lukas, V. 2015. Influence of sowing, nitrogen nutrition and weather conditions on stand structure and yield of spring barley. *Cereal research communications*. **43**(2), 326–335. DOI: 10.1556/CRC.2014.0036.

Laichicxi, M., Mercea, M., Gheorghe, I., Grozav, M., Neamtiu, I., Dorosencu, M. & Foarce, A. 2002. Preliminary research on the bioactive effect of 2-hidroye thy ldimethylammonium-4-aminobenzoate. *Proc. Rom. Acad*. **4**(3), 177–179.

Iizumi, T., Yokozawa, M., Sakurai, G., Travasso, M.I., Romanenkov, V., Oettli, P., Newby, T., Ishigooka, Y. & Furuya, J. 2014. Historical changes in global yields. *Global Ecology and Biogeography*. **23**, 346–357.

Makino, A. 2011. Photosynthesis, grain yield, and nitrogen utilization in rice and wheat. *Plant Physiol*. **155**, 125–129.

Malinauskaitė, R. & Jakienė, E. 2005. BSB grupėsstilitųįtakaraudonžiedžiošalavijoaugimui. *Vagos*. **67**, 25–30.

Malkina, V. & Eremenko, O. 2016. Method of determining the area of oil flax (Linumu sitatissimum L.) based on the processing and analysis of images. *Ştiinţa agricolă*. **2**, 36–40 (in Russian).

Manzoor, A., Khattak, R.A. & Dost, M. 2014. Humic acid and micronutrient effects on wheat yield and nutrients uptake in salt affected soils. *International journal of agriculture & biology*. **16**, 991–995.

Markov, I., Dmitryshak, M. & Mokrienko, V. 2011. Yar barley Modern technologies of agroindustrial complex. Growing major agricultural crops. Kyiv: Publishing House "Impers-Media" Ltd., pp 32–55 (in Ukrainian).

McKevith, B. 2004. Nutritional aspects of cereals. *British Nutrition Foundation Nutrition Bulletin*. **29**, 111–142.

Novotna, K., Rajsnerova, P., Vesela, B. & Klem, K. 2015. Interactive effects of elevated CO2 concentration, drought and nitrogen nutrition on yield and grain quality of spring barley and winter wheat. 4th Annual Global Change – A Complex Challenge. Brno, Czech Republic. Mar. 23–24. 2015, pp 106–109.

Panfilova, A., Korkhova, M., Gamayunova, V., Drobitko, A., Nikonchuk, N. & Markova, N. 2019. Formation of photosynthetic and grain yield of soft winter wheat (Triticum aestivum L.) depending on varietal characteristics and optimization of nutrition. *Research Journal of Pharmaceutical, Biological and Chemical Sciences*. **10**(2), 78–85.

Pestovsky, Y.S. & Martinez-Antonio, A. 2017. The use of nanoparticles and nanoformulations in agriculture. *Journal of nanoscience and nanotechnology*. **17**(12), 8699–8730. DOI: 10.1166/jnn.2017.15041

Piskaeva, A.I., Babich, O.O. & Dolganyuk, V.F. 2017. Analysis of influence of biohumus on the basis of consortium of effective microorganism son the productivity of winter wheat. *Foods and rawmaterial*. **5**(1), 90–99. DOI: 10.21179/2308-4057-2017-1-90-99.

Povilaitis, V., Lazauskas, S., Antanaitis, S., Feiziene, D., Feiza, V. & Tilvikiene, V. 2018. Relationship between spring barley productivity and growing management in Lithuania's lowland. Acta Agriculturae Scandinavica, Section B – *Soil & Plant Science*. **l. 68**, 86–95. DOI: 10.1080/09064710.2017.1367834

Sharma, S., Sain, R.S. & Sharma, R.K. 2003. The genetic control of the flag leaf length in normal and late sown durum wheat. *Journal of Agricultural Science*. **141**, 323–331.

Shao, H.B., Liang, Z.S., Shao, M.A., Sun, S.M. & Hu, Z.M. 2005. Investigation on dynamic changes of photosynthetic traits of 10 wheat (Triticum aestivum L.) genotypes during two vegetative-growth stages at water deficits. *Biointerfaces*. **43**, 221–227.

Singh, G., Sharma, G., Sanchita Kalra, P., Batish, D.R. & Verma, V. 2018. Role of alkyl silatranes as plant growthregulators: comparative substitution effect on root and shoot development of wheat and maize. *Journal of the science of food and agriculture* **98**(13), 5129–5133. DOI: 10.1002/jsfa.9052

Solonechnuy, P. 2018. The level of manifestation and correlation of quantitative traits of spring barley varieties. *Ştiinţa agricolă*. **1,** 23 – 27 (in Russian).

Šterna, V., Zute, S., Jansone, I. & Kantane, I. 2017. Chemical composition of covered and naked spring barley varieties and their potential for food production. Pol. J. Food Nutr. Sci. 67(2), 151–158. DOI: 10.1515/pjfns-2016-00Volkodav, V.V. 2001. The method of state variety testing of agricultural crops. Issue 2nd (grains, cereals and legumes). K., 65 pp. (in Ukrainian).

Wood, P.J. 2004. Relationships between solution properties of cereal b-glucans and physiological effects a review. *Trends Food Sci. Tech*. **13**, 313–320.

Xinping, C., Hongyu, Y., Rongzhi, C., Lili, Z., Bo, D., Qingmei, W. & Guangeun, H. 2002. Isolation and characterization of triacontanolregulated genes in rice (Oryza sativa L.): Possible role of triacontanol as a plant growth stimulator. *Plant Cell Physiol*. **43**(8), 869–876.

Yarchuk, I.I., Bozhko, V.Y. & Moroz, O.O. 2015. Winter barley cold-resistance and productivity depending on sowing terms and rates. *Bulletin of Poltava State Agrarian Academy*. **3**, 54–57 (in Ukrainian).

Agronomy Research **17**(2), 621–634, 2019
https://doi.org/10.15159/AR.19.079

Variety, seeding rate and disease control affect faba bean yield components

I. Plūduma-Pauniņa[1,2,*], Z. Gaile[1], B. Bankina[1] and R. Balodis[1]

[1]Latvia University of Life Sciences and Technologies, Faculty of Agriculture, Institute of Soil and Plant Science, Liela street 2, LV-3001 Jelgava, Latvia
[2]Latvia University of Agriculture, Faculty of Agriculture, Research and Study Farm "Pēterlauki", Platone parish, LV-3021, Latvia
[*]Correspondence: ievapluuduma@inbox.lv

Abstract. Faba beans (*Vicia faba* L.) have been grown since 8000 years B.C. in the Middle East. Despite their long growing history in the world, there are only few researches carried out in Baltic region in last decades about variety, seeding rate and disease control effect on faba beans' growth, development and yield formation. Research was carried out at the Latvia University of Life Sciences and Technologies during 2015–2017. Three factors were researched: A – variety ('Laura', 'Boxer', 'Isabell'), B – seeding rate (30, 40 and 50 germinate able seeds m^{-2}), C – treatment with fungicide (with and without application of fungicide Signum (1 kg ha^{-1})). Meteorological conditions were diverse and sometimes caused stress for crop, but in general they favoured faba beans' growth and development. High average yield of the field beans was obtained during all three trial years, however, yield differed significantly among them. Sowing time was constantly quite early, germination took longer time as expected due to the low air temperature, but later, temperature and humidity level improved and conditions were suitable for plant growth and development with some exceptions during flowering and pod filling. Number of productive stems per 1 m^2 was significantly affected only by seeding rate. Plant height in trial site was affected by variety ($p < 0.001$), fungicide application ($p = 0.008$) and meteorological conditions ($p < 0.001$) of the year. Number of pods per plant differed depending on trial year ($p < 0.001$). Number of seeds per plant had a close positive correlation with number of pods per plant. Whereas number of seeds per pod was a relatively stable and typical characteristic for variety. We can observe correlation between faba bean yield and number of productive stems per 1 m^2 at harvest, plant height, number of pods and seeds per plant.

Key words: field beans, agrotechnology, phenology, yield components.

INTRODUCTION

Faba beans (*Vicia faba* L.) is the third most important legume plant in the world after soy beans (*Glycine max* L.) and peas (*Pisum sativum* L.) (Singh et al., 2013). In Latvia, faba beans, known also as field, broad and horse beans, have been grown for ages, but nowadays, commercially mainly *Vicia faba* var. *minor* is grown for animal feed mostly.

Faba beans are known for their high value for green forage, they improve soil fertility and leave good effect on after-crops (Sahile et al., 2008).

During last 10 years, faba bean sowing area has grown more than 50 times in Latvia, reaching 42.3 thousand ha in 2017, which is about 3.3% from all agricultural land in the country. Despite important agronomical impact of faba beans, farmers' growing interest about this crop can be mostly explained by European Union greening requirements.

The last major study about several aspects of faba beans' growing in Latvia was performed in 1960-ties (Holms, 1967). Since then, there have not been plenty of studies about faba bean in Baltic countries or even in Northern Europe. Several various studies about variety and seeding rate impact on faba bean yield can be found (Skjelvag, 1981; Lopez-Bellido et al., 2005; Patrick & Stoddard, 2010; Flores et al., 2013), some studies about severity of diseases (Villegas-Fernandez et al., 2009; Bankina et al., 2016), but additional studies are necessary. Our research about faba beans is the first so extensive study of last decades in Latvia. The aim of this paper was to estimate how variety, seeding rate and disease control in different years affect development and yield components of faba bean.

MATERIALS AND METHODS

Research was carried out from 2015 until 2017, at Latvia University of Life Sciences and Technologies Research and Study farm "Pēterlauki" (56º32'31.2"N 23º42'57.6"E). Researched factors all three years were: variety (three different faba bean varieties – 'Laura', 'Boxer', 'Isabell'), seeding rate (three different seeding rates – 30, 40 and 50 germinate able seeds per m^2) and fungicide application (without fungicide and with fungicide Signum (boscalid, 267.0 g kg^{-1}, pyraclostrobin, 67.0 g kg^{-1}) application). Each year 18 variants in 4 replications were sown.

Faba bean sowing dates, depending on each year meteorological conditions, were 26 March 2015, 05 April 2016 and 04 April 2017. Traditional soil tillage was used – mould-board ploughing in the previous autumn and soil cultivation before sowing. Each trial year pesticides were used according to the rules of good agricultural practice. Fungicide Signum was used at GS 61–65 based on trial scheme. Used materials and methods in detail are described in our previous paper (Plūduma-Pauniņa et al., 2018).

During vegetation, main phenological observations were performed. Severity of diseases on leaves and pods (0–9 point scale) was assessed after emerging of first symptoms (not analysed in this paper). Plant height (in cm) was measured after flowering (GS 69). Sample sheet (10 plants) was taken from each plot shortly before harvesting (GS 88). Number of pods and seeds per plant and seeds per pod was detected from sample sheets. Number of productive stems per 1 m^2 was detected after harvesting using 0.5 m^2 frame. Yield (t ha^{-1}) was directly harvested from each plot and converted to standard moisture level (14%) and 100% purity.

For data mathematical processing three- and four-factor analysis of variance, correlation and regression was used together with Bonferroni test for comparison of factors' means. Variants are considered significantly different when $p \leq 0.05$. SPSS 15 and MS Excel softwares were used.

Agrometeorological information was recorded daily by an automatic weather station located near to the experimental field. Meteorological conditions were slightly different each year. In 2015, air temperature was low after sowing, therefore crop germination took longer time, but later temperature and humidity level was suitable for plant growth. During the second part of vegetation season, significant drought and high

air temperatures were observed and cause stress during flowering and pod filling. In 2016, vegetation season was warm and with sufficient moisture level. At the end of the season, overly high moisture level delayed beans' harvest. In last trial year (2017), vegetation season started with a bit cold weather, therefore germination took longer time than in 2016. At the same time, precipitation amount was less, thus faba beans' emergence was faster than in 2015. Further, vegetation period also was mostly cool with a high amount of precipitation, which favoured high yield formation, but delayed harvest for about half a month. For characterisation of faba beans' development, average air temperature, sum of active temperatures (above +5 °C), and sum of precipitation were used (see Results and Discussion section).

RESULTS AND DISCUSSION

Phenology. Plant growth and development is determined by heredity and environmental conditions. Knowing how environmental factors affect crop at each stage of development, we can analyse used management and decide how to improve plant growth, formation of yield and its quality. As meteorological conditions were different in each trial year, we could observe their strong effect on the length of faba bean growth stages (Fig. 1), and adverse effects were observed at some stages of development.

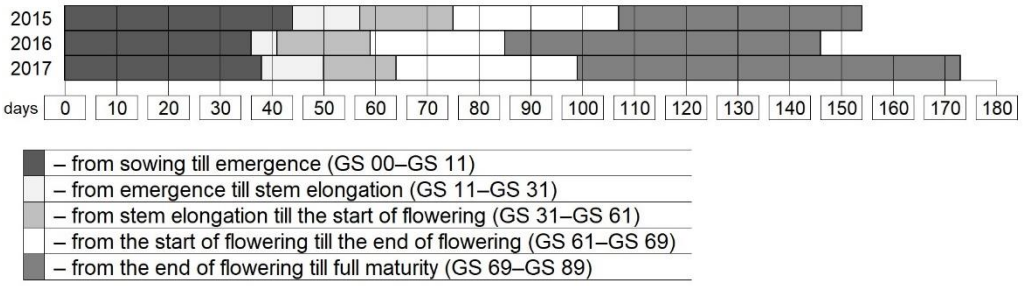

Figure 1. Length of faba beans' growth stages in days depending on trial year.

At the end of March 2015, soil temperature and moisture level was suitable for faba bean sowing. After sowing, meteorological conditions changed – air temperature decreased, so soil was not warm enough (average air temperature was 7.5 °C from sowing till emergence), and precipitation level at the same time was high (95.8 mm). For faba bean emergence 44 days were needed. During emergence, sum of active temperatures (262.6 °C; above +5 °C) were calculated. In 2016, the late March and early April was warmer than the long-term average data, so faba beans were sown in first decade of April. Despite suitable moisture level (52.8 mm; long term average 60.4 mm) and quite high air temperature (average 10.5 °C; long term average 8.6 °C) in April, 36 days were needed for faba beans' emergence this year (during this time sum of active temperatures was 313.2 °C). In 2017, conditions were also suitable for faba bean sowing in first decade of April, but after sowing air temperature dropped significantly (average air temperature 5.8 °C) and precipitation level was low (27.4 mm), so faba beans emerged 38 days after sowing (sum of active temperature was 236.0 °C).

Various number of days from field bean sowing time till emergence have been observed in other studies. For example, in trial conducted in Malaysia, in warm climate, (Zabawi & Dennett, 2010) water deficiency prolonged faba bean emergence for 4–7 days, while in 100% water supply plants emerged 10 days after sowing. In another study in Australia, with suitable weather conditions, faba beans emerged 20 days after sowing (McDonald et al., 1994). In Latvia, however, field beans can emerge in 20 days, if they are sown in late April – early May, and suitable weather conditions occur (Holms, 1967).

In 2016, period from emergence to stem elongation was the shortest (5 days), if compared with the same period in 2015 (13 days) or in 2017 (12 days). The cause was insufficient amount of precipitation (in the second and third decade of May precipitation amount was 1.4 mm; long term average precipitation amount in this period is 35.7 mm) and unusually high air temperature during the second half of May (average 18.8 °C; long term average temperature at the same time 12.6 °C).

We can describe the meteorological conditions between emergence and the start of flowering as appropriate for flowering and high yield formation during all trial years. Although the flowering times depending on variety tend to differ, still significant differences in the start of flowering among varieties were not observed during all years (all varieties started to flower in the same day or with one day difference in all the trial years). Slight tendency was observed – field beans sown in plots using lower seeding rate (30 germinate able seeds m^{-2}) start to flower first, but this observation was not typical enough.

On average, field beans flower 25–30 days. It is also observed in field and container experiment from Norway, where length of flowering period varied from 2 to 8 weeks. On average for both used varieties in these experiments, it was about 4 weeks – 28 days (Skjelvag, 1981). In 2015, flowering time was 32 days, in 2016 – 26 days, but in 2017 – 35 days in our trials. In 2015, there was high average air temperature during faba bean flowering period (16.4 °C) and reduced precipitation amount at the second and third decade of June (in all flowering period precipitation amount was 47.2 mm; while in June, during the early and full flowering it was only 15.7 mm), but it did not affect faba bean flowering and yield formation as much as drought observed later during pod filling. Studies in Malaysia showed that at 20% moisture availability flowering can be delayed by 35 days (Zabawi & Dennett, 2010). Meanwhile, the end of June and early July characterized with high average air temperature (16.4 °C) and high precipitation level (59.8 mm, most of precipitation was in third decade of June, at the end of flowering) in 2016. It was the reason why faba beans' flowering time was shorter than in other two trial years. However, faba beans can tolerate temporary flooding (Girma & Haile, 2014), thus this factor did not significantly affect their further development. The same tendency was observed in our trial, when after hard rainfall on first decade of July (totally per decade 39 mm, while on 7 July, heavy rainstorm was observed: 22 mm; long term average precipitation amount per this decade is 27.3 mm), half of our field bean trial flooded for about a week. This temporary flooding did not affect faba beans' further development or yield formation. In 2017, average air temperature during flowering period was lower (15.6 °C), but precipitation amount was the highest from all trial years (during the whole flowering period – 84.4 mm; while in June, during the early and full flowering it was half of this amount – 41.0 mm).

Precipitation level during the vegetation period (from sowing to harvest) of faba beans of 2015 was the lowest from all three trial years (233.9 mm; while in 2016 – 317.6 mm and in 2017 – 280.8 mm) and average air temperature was 13.1 °C. The length of faba beans' vegetation season in 2015 was 154 days. In addition, sum of active temperatures was calculated for the period from 1 April till the 31 August to show differences of three trial years. In 2015, sum of active temperatures (above +5 °C) was 2,044 °C. In 2016, vegetation season was 146 days long. This vegetation season characterizes with the highest average air temperature (15.4 °C), and also sum of active temperatures was higher than in previous year (2,244 °C). In its turn, plant growth and development was faster than in other two trial years. Vegetation period of 2017 was 173 days long. Average air temperature during vegetation period was the lowest per trial period – 13.0 °C and sum of active temperatures (1 April – 31 August) was 1,938 °C. Last trial year was cooler than the previous two and this is demonstrated also by average air temperature in period 1 April – 31 August: 13.6 °C in 2015, 14.8 °C in 2016 and 13.0 °C in 2017; in addition, rain was observed regularly, weather was often cloudy, and constant rainfalls were observed at the beginning and middle of August and at the beginning of September in 2017. Such conditions with moderate temperatures and sufficient precipitation level firstly favoured formation of high yield and yield components (see description hereinafter), but secondly delayed faba bean maturity for half a month.

According the results of studies conducted in foreign countries and the experience of field beans' growers from Latvia, the length of vegetation period of faba beans can be different. Two Latvian growers reported 117 and 118 days long faba beans' vegetation period; in both situations, faba beans were sown on 1 May, and they used variety 'Fuego' which can be characterized with early maturity. For comparison, in Australia, the average vegetation period for field beans was 90 days (Loss & Siddique, 1997), in studies in Egypt – 105 days (Badr et al., 2013). In a three-year study in Spain, with one variety and five sowing dates, the vegetation period averaged between 87 days (sowing at the end of April / early May), 99 days (sowing in late March / early April), 124 days (sowing in mid-February), 161 days (sowing in mid-December) and 209 days (sowing in late October / early November) (Villacampa et al., 2009). In a study conducted in Iran, choosing the sowing time of 30 March, which is the closest sowing time to that used in our study, the average vegetation period of the four varieties was 94 days (Ajam Norouzi & Vazin, 2011). Length of vegetation period may differ between varieties. In Ajam Norouzi & Vazin (2011) trial, where four different varieties were used, vegetation period was 95.0^{a}; $94.7^{a,b}$; 93.7^{b}; and 92.2^{c} days long (different small letters in superscript show significant difference between the length of vegetation periods of used varieties at confidence level $p = 0.05$). In our trial, we did not observe significant differences of vegetation period length between used varieties, the main influencing factor was conditions of the year.

Plant height. Plant height was measured right after flowering in all trial years. Plant height differed significantly between years and was affected by variety and fungicide application.

On average per three trial years, variety 'Laura' was characterized with the shortest plants (92.0 cm on average). Average plant height of varieties 'Boxer' (97.7 cm) and 'Isabell' (96.6 cm) was similar ($p = 0.609$), but significantly higher ($p < 0.001$), if compared with that of 'Laura'. In 2015, variety 'Isabell' was highest (91.1 cm), while in

2016, the highest was variety 'Boxer' (102.8 cm). In 2017, variety 'Isabell' showed the highest plants (103.8 cm), but its plant height did not differ significantly from variety 'Boxer' (102.5 cm; $p = 0.596$).

Although the sowing rate did not have a significant effect ($p = 0.083$) on the plant height, we observed that use of higher seeding rate increases plant height in all trial years. This tendency coincides with the data obtained in Pakistan, where 60 plants per m^2 of field beans ensured significantly higher plants, but plant height gradually reduced by decreasing the seeding density to 45, 30 and 15 plants per m^2, and the shortest plants were observed at the lowest seeding rate (Khalil et al., 2010). Experiments in vegetation containers also showed the same results – use of higher plant density in two-year experiment resulted with higher plants (Al-Suhaibani et al., 2013). The obtained results can be explained by the fact that plant competition begins for light and space at higher plant density (Turk & Tawaha, 2002; Derogar & Mojaddam, 2014).

This could be the reason of observed positive correlation between plant height and yield. If we look at all researched factors together, in 37% of cases, when plant height increased, we obtained higher faba bean yield ($r = 0.607 > r_{0.01} = 0.364$). Meanwhile, analysing only the variants where fungicide was applied, positive correlation tightens and in that case percentage grows up to 52% ($r = 0.721 > r_{0.01} = 0.487$; Fig. 2). Fungicide application increased plant height ($p = 0.008$).

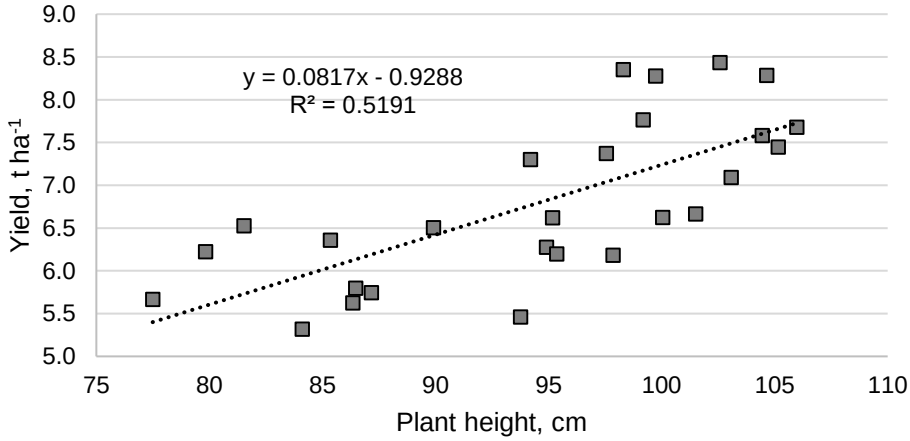

Figure 2. Correlation between faba bean plant height and yield if fungicide was applied ($p = 0.013$).

Plant height was affected significantly by conditions in trial year. In 2015, average plant height was 87.1 cm, in 2016, – 97.8 cm, but in last year (2017) – 101.5 cm. It can be explained by different meteorological conditions in each trail year. In 2015, during all vegetation season precipitation amount was the lowest between all trial years (as mentioned before: 2015 – 233.9 mm; 2016 – 317.6 mm; 2017 – 280.8 mm). Still the study of Mwanamwenge et al. (1999) showed that water shortage did not significantly affect plant height, but another study of Zabawi & Dennett (2010) showed a significant effect of water supply on plant height. At 100% of the water supply, field beans reached

plant height 250 cm, while at 20% of the water supply, they were only 120 cm high. At 40, 60 and 80% of water supply, the plant height varied around 150 cm.

Productive stems. The branching capacity of field beans depends on the conditions of the variety and the environment. The branching is associated with the length of the vegetation period – the longer the vegetation period, the higher number of new stems can be formed.

Study results from China showed that winter field beans have a strong branching capacity (up to 25 stems for one plant) when they are sown early; branching is medium (up to 10 stems) when they are sown late. In the spring sown field beans, however, only 2 to 3 stems are formed (Yu & Zhang, 1979). In addition, winter field beans branch mostly until the winter period (46–74% of cases), during winter they branch in 13–33% of cases, whereas after winter plants branch up to 24% of cases (Wu & Jing, 1988).

Although it is believed that branching is not widespread in conditions of Latvia and is seldom observed, plants in this study branched quite a lot. Some individual plants had up to 4 productive stems. Since the field beans in Latvia are sown in spring and the duration of plant growth and development is shorter, if compared with winter field beans, their branching capacity is significantly less than the results of studies performed in other countries show. However, field beans branching possibility slightly increased the number of productive stems per 1 m^2 at harvesting time.

Number of productive stems in this trial was significantly affected only by seeding rate ($p = 0.01$) – higher seeding rate provided more productive stems during harvest ($r = 0.605 > r_{0.01} = 0.364$; Fig. 3) which is logically, because seeding rate is the initial cause of plant density at harvest.

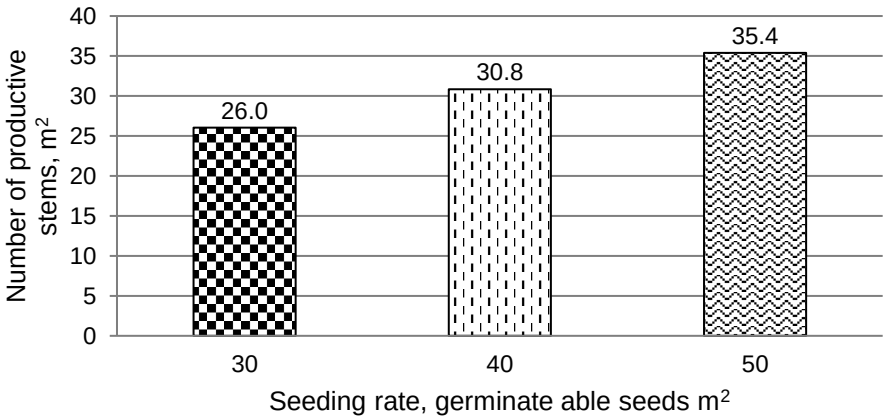

Figure 3. Number of faba beans' productive stems at harvest depending on seeding rate.

Despite the fact that significant difference in number of productive stems ($p = 0.073$) was not observed between varieties, higher number was provided by variety 'Laura' (32.0) in all trial years, while variety 'Boxer' provided 31.4 and variety 'Isabell' – 28.9 productive stems per 1 m^2. This proves information mentioned earlier, that number of productive stems and branching depends also on variety.

In this trial we observed positive correlation between faba bean yield and number of productive stems. It tightens with fungicide application (38% of cases faba beans with higher number of productive stems will provide higher seed yield; $r = 0.616 > r_{0.01} = 0.487$).

Insignificant tendency was observed that in variant, where fungicide was applied, number of productive stems decreased (on average with fungicide application – 30.5 productive stems per 1 m^2; without fungicide application – 31.0 productive stems per 1 m^2). Fungicide application also slightly prolonged the length of beans' vegetation period, but this lengthening was not so important to cause simultaneous branching of beans. In 2017, when the longest vegetation period of faba beans was observed (Fig. 1), number of productive stems per 1 m^2 was higher than in previous years due to slightly more intensive branching.

Pods per plant. Number of pods per plant can be influenced by the interaction of meteorological conditions and crop growing technology factors (such as seeding rate) (Lopez-Bellido et al., 2005). In our trial, this indicator was significantly ($p < 0.001$) affected by each year's meteorological conditions, seeding rate and fungicide application. Used variety had impact on number of pods per plant each year, but it differed between years; three-year average data did not show significant differences depending on variety (Table 1). On average, the highest number of pods per plant was observed in last trial year (2017). This could be explained with longest vegetation period (length of flowering was 35 days, while in 2015 – 32 days and in 2016 – 26 days; length of period from the end of flowering till full maturity was 74 days in 2017; 47 days in 2015; 61 day in 2016), thus plants had opportunity to produce more flowers that was pollinated and to form more pods per plant.

Table 1. Number of pods per plant depending on researched factors

Factors	Year			Average
	2015	2016	2017	
Variety ($p = 0.05$)				
'Laura'	12.00^{a}	14.15^{b}	21.11^{a}	15.76^{A}
'Boxer'	$10.95^{a,b}$	$14.70^{a,b}$	$19.25^{a,b}$	14.97^{A}
'Isabell'	10.53^{b}	16.01^{a}	18.05^{b}	14.86^{A}
Seeding rate (germinate able seeds m^{-2}) ($p = 0.001$)				
30	13.52^{a}	17.17^{a}	20.97^{a}	17.22^{A}
40	10.90^{b}	14.18^{b}	20.14^{a}	15.08^{B}
50	9.06^{c}	13.52^{b}	17.30^{b}	13.29^{C}
Fungicide application ($p = 0.001$)				
F0	11.10^{a}	11.96^{b}	18.94^{a}	14.00^{B}
F1	11.23^{a}	17.95^{a}	20.00^{a}	16.39^{A}
Average	11.16^{C}	14.95^{B}	19.47^{A}	×

F0 – without fungicide application; F1 – with fungicide application; Significantly different means are labelled with different letters in superscript: ^{A,B,C} – significant difference for average number of pods per plant of three trial years and means of factors' gradations; ^{a,b,c} – significant difference in a specific trial year.

Although on average variety did not affect number of pods per plant significantly, in each year separately there were significant differences of this indicator between varieties. In 2015 ($p = 0.045$) and 2017 ($p = 0.001$), highest number of pods per plant was obtained by variety 'Laura', while in 2016, by variety 'Isabell' ($p = 0.006$). Variety 'Boxer' did not differ significantly from other two varieties by number of pods per plant in each trial year. Badr et al. (2013) after two-year study showed that significant difference in number of pods per plant (respectively – 18.3 and 11.9 pods per plant) can be observed between varieties.

Seeding rate effect on number of pods per plant each year was the same – higher seeding rate decreased number of pods per plant. The highest number of pods per plant was obtained using 30 germinate able seeds m^{-2} (on average 17.22 pods), while use of 40 and 50 germinate able seeds m^{-2} gave respectively 15.08 and 13.29 pods per plant. Coelho & Pinto (1989) and Tuttobene & Vagliasindi (1995) reported similar results – high plant densities prompt greater competition for plant, causing abscission of flowers and decreasing number of pods per plant.

Looking on each trial year separately, fungicide application showed significant ($p < 0.001$) impact on number of pods per plant only in 2016. The cause of such fungicide application efficiency was fairly high spread of diseases (caused by *Alternaria* spp. and *Botrytis* spp.) in 2016 if compared to other trial years. Despite that, each year we could observe a tendency that fungicide application increases number of pods per plant. Positive effect of fungicide application on number of pods per plant was also obtained in various foreign studies (El-Sayed et al., 2011; Emeran et al., 2011; El-Hai, 2015).

Between the number of pods per plant and seed yield positive correlation was observed. Using all trial data, results showed that in 30% of cases plants with higher number of pods per plant will provide higher seed yield ($r = 0.545 > r_{0.01} = 0.364$). Based on the tight positive correlation between the number of pods per plant and number of seeds per plant ($r = 0.964 > r_{0.01} = 0.364$; Fig. 4), also number of seeds per plant positively correlated with yield (R^2=28%; $r = 0.531 > r_{0.01} = 0.364$).

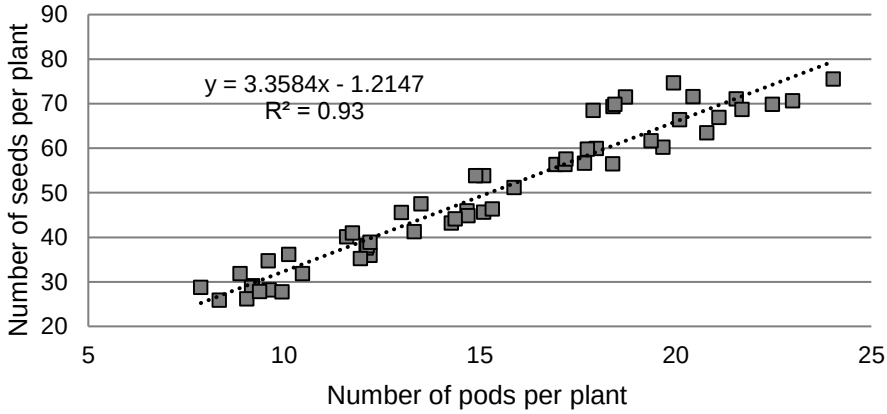

Figure 4. Correlation between faba beans' number of pods and seeds per plant ($p < 0.0001$).

Also in two year trial in Australia (Loss & Siddique, 1997), faba bean seed yield correlated with number of pods per plant. In their study, average number of pods per plant was affected by variety and sowing time. For earlier sown plants number of pods per plant was higher (average 19.9 pods per plant) than for later sown (average 10.2 pods per plant) because of the length of vegetation period (Loss & Siddique, 1997).

Seeds per plant. Together with number of pods, number of seeds per plant was determined by sample branches. In our trial, number of seeds per plant was significantly ($p < 0.001$) affected by meteorological conditions of trial year and seeding rate (Table 2).

Meteorological conditions during faba beans vegetation period (especially during flowering and pod filling stage) had the most impact on number of seeds per plant. From the end of flowering until full faba bean maturity in 2015 average air temperature was 17.6 °C, precipitation amount – 45.8 mm, while in 2016, average air temperature was 19.3 °C, precipitation amount – 180.4 mm, and in 2017, average air temperature was 15.9 °C, precipitation amount – 135.4 mm. In 2015, number of seeds per plant was the lowest in all three years (36.12 seeds). Pod filling phase (end of July and start of August) characterized with high average air temperature and significant drought, if compared to other trial years. Lack of moisture together with high air temperature affected pod formation and later pod filling with seeds. In 2016, average air temperature during pod filling stage was also high (higher than in 2015), but this stage characterizes with regular and excessive moisture level. Number of seeds per plant was higher than in 2015, but lower than in 2017. Pod filling stage characterized with moderate average air temperature and with sufficient precipitation level during the last trial year. Because of constant rainfalls in the August and early September, vegetation season of field beans prolonged, so pod filling phase also was longer.

Table 2. Number of seeds per plant depending on trial year and seeding rate

Factors	Year			Average
	2015	2016	2017	
Seeding rate ($p = 0.001$)				
30	43.73^{a}	54.97^{a}	70.70^{a}	56.47^{A}
40	35.41^{b}	44.60^{b}	67.78^{a}	49.26^{B}
50	29.20^{c}	43.16^{b}	58.80^{b}	43.72^{C}
Average	36.12^{C}	47.58^{B}	65.76^{A}	×

Significantly different means are labelled with different letters in superscript: ^{A,B,C} – significant difference for average number of seeds per plant of three trial years and means of factors' gradations; ^{a,b,c} – significant difference in a specific trial year.

Each trial year, with the increase of seeding rate the number of seeds per plant decreased. In 2015, significant differences was observed between variants with different seeding rates ($p = 0.01$). In 2016, only variant with lowest seeding rate (30 germinate able seeds m^{-2}) significantly differed ($p < 0.001$) from two others. In 2017, contrariwise only variant where the highest seeding rate (50 germinate able seeds m^{-2}) was used differed significantly ($p = 0.004$) from two others (Table 2). Our results coincide with the results obtained by other scientists – that with an increase of seeding rate the productivity of the individual plant decreases (Holms, 1967; Sharaan et al., 2002; Bakry et al., 2011; Barker & Dennett, 2013).

Fungicide application significantly affected number of seeds per plant only in 2016 ($p < 0.001$) because of the spread of diseases, while in 2015 ($p = 0.711$) and 2017 ($p = 0.068$), difference between variants was not significant.

The highest number of seeds per plant was provided by variety 'Isabell' in all trial years (53.4 seeds), the lowest – by variety 'Boxer' (47.9 seeds), leaving variety 'Laura' in the middle (48.3 seeds). In 2015, we did not observe significant difference between all varieties ($p = 0.289$) according this parameter. The same tendency was observed in 2017 ($p = 0.217$). In 2016, variety 'Isabell' with 54.5 seeds per plant differed significantly ($p < 0.001$), while between varieties 'Laura' (42.4 seeds) and 'Boxer' (45.8 seeds) differences was not considerable ($p = 0.329$). Variety effect on number of seeds

per plant can be explained based on seed size. Varieties with smaller seeds produce more seeds per plant, if compared with variety with larger seeds (Holms, 1967).

Seeds per pod. Number of seeds per pod is a typical and fairly stable indicator for faba beans. Several foreign studies have shown that on average 3 seeds per pod was noted for *Vicia faba* var. *minor* (Husain et al., 1988; Sharaan et al., 2002; Turk & Tawaha, 2002).

During the trial period, number of seeds per pod was affected significantly by variety ($p < 0.001$), fungicide application ($p = 0.023$) and trial year ($p < 0.001$). The highest ($p < 0.001$) average number of seeds per pod was observed for variety 'Isabell' (on average 3.6) in all years. The last trial year (2017) was characterized by moderate temperatures, enough precipitation, and prolonged vegetation period of beans, and in result most seeds per pod were observed for all varieties (Fig. 5). The fact that the number of seeds per pod is influenced by the variety has also been demonstrated in the above-mentioned Egyptian study (Sharaan et al., 2002).

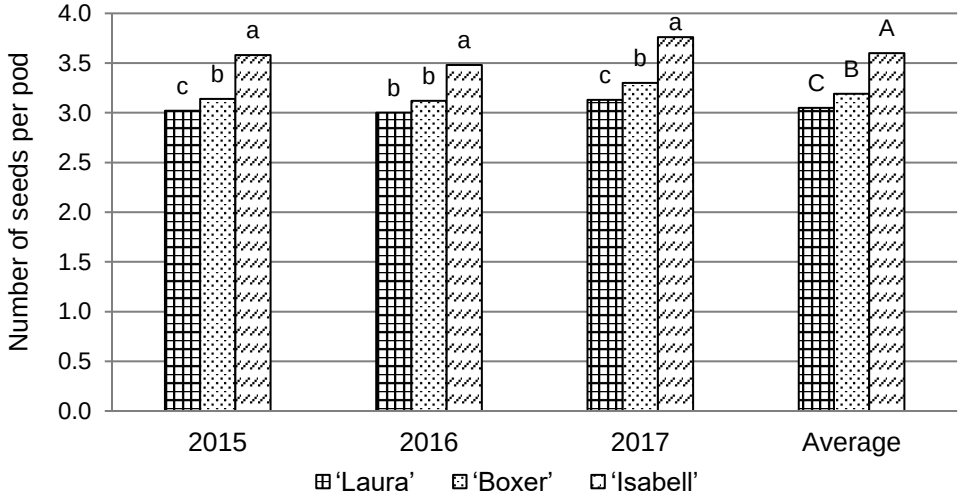

Figure 5. Number of seeds per pod depending on variety and trial year: ^{A,B,C} – significant difference on average per three trial years; ^{a,b,c} – significant difference between varieties in specific year.

The average data of three years show significant influence of fungicide application on number of seeds per pod, but in two out of three years this effect was not significant (2015 – $p = 0.333$; 2017 – $p = 0.487$). Only in 2016, fungicide application caused significant ($p = 0.046$) increase in number of seeds per pod (with fungicide application average number of seeds per pod was 3.25, while without fungicide application – 3.15). Similarly as the number of pods and seeds per plant, the number of seeds per pod in this year was influenced significantly by fungicide application based on the spread of the diseases. Despite that, in all trial years the observed tendency was the same – application of fungicide increased average number of seeds per pod.

Meanwhile, seeding rate did not affect this indicator ($p = 0.830$). The tendency in this trial showed, that by increasing seeding rate, number of seeds per pod decreases.

The same tendency was observed in studies in Jordan, based on different sowing rates (50, 75 and 100 germinating seeds per 1 m^2). Increase of seeding rate causes gradual decrease of the number of seeds per pod. In the case of 50 germinate able seeds per m^2 on average 3.4 seeds per pod were noted, however, when using higher seeding rates, this indicator decreased (respectively – 2.5 and 2.1 seeds per pod) (Turk & Tawaha, 2002).

Yield and thousand seed weight (TSW). Faba bean yield was high (on average 5.89–7.38 t ha^{-1} depending on the year) and affected significantly ($p < 0.001$) by all researched factors. The highest yield was provided by variety 'Boxer' using higher seeding rate (50 germinate able seeds per m^2) and in variant with fungicide application.

TSW, as a stable indicator related closely to variety and also yield, and was affected by all researched factors. Higher TSW was provided by variety with the highest yield – 'Boxer', using fungicide and higher seeding rate.

Detailed faba bean yield and thousand seed weight in this trial was described in our previous paper (Plūduma-Pauniņa et al., 2018), published in journal *Agronomy Research*.

CONCLUSIONS

Meteorological conditions affected the growth and development of faba beans significantly; drought during flowering and pod filling in 2015 decreased number of pods and seeds per plant and seeds per pod, as well as yield significantly.

Meteorological conditions of the trial year and variety affected plant height significantly. Positive correlation between faba bean plant height and yield was observed.

Number of productive stems was significantly affected only by seeding rate – its value was higher by increasing seeding rate.

Number of pods and seeds per plant was affected by all researched factors. They were significantly higher using lower seeding rate and when fungicide was applied. Positive correlation between both these yield components and yield was observed.

Number of seeds per pod is a typical and relatively stable indicator for the variety. Its value was significantly influenced by the variety and slightly increased when fungicide was applied.

Faba beans' yield and TSW was significantly affected by all researched factors – variety, seeding rate, fungicide application and year as a factor. Highest yield was provided by variety 'Boxer' when higher seeding rates and fungicide was used.

ACKNOWLEDGEMENTS. Research was carried out by the financial support of RSF "Pēterlauki" of LLU.

REFERENCES

Ajam Norouzi, H. & Vazin, F. 2011. Prediction of Flowering Occurrence in Faba Bean (*Vicia faba* L.). *Notulae Botanicae Horti Agrobotanici Cluj-Napoca* **39**(1), 198–207.

Al-Suhaibani, N., El-Hendawy, S. & Schmidhalter, U. 2013. Influence of varied plant density on growth, yield and economic return of drip irrigated faba bean (*Vicia faba* L.). *Turkish Journal of Field Crops* **18**(2), 185–197.

Badr, E.A., Wali, A.M. & Amin, G.A. 2013. Effect of Sowing Dates and Biofertilizer on Growth Attributes, Yield and its Components of Two Faba Bean (*Vicia faba* L.) Cultivars. *World Applied Sciences Journal* **28**(4), 494–498.

Bakry, B.A., Elewa, T.A., El karamany, M.F., Zeidan, M.S. & Tawfik, M.M. 2011. Effect of row spacing on yield and its components of some faba bean varieties under newly reclaimed sandy soil condition. *World Journal of Agricultural Sciences* **7**(1), 68–72.

Bankina, B., Bimšteine, G., Roga, A., Fridmanis, D. 2016. Leaf diseases – an emerging problem in the sowings of faba bean in Latvia. In *ESA 14 – Growing Landscapes – Cultivating Innovative Agricultural Systems: Conference*, Edinburgh, UK, pp. 15–16.

Barker, S. & Dennett, M.D. 2013. Effect of density, cultivar and irrigation on spring sown monocrops and intercrops of wheat (*Triticum aestivum* L.) and faba beans (*Vicia faba* L.). *Europ. J. Agronomy* **51**, 108–116.

Coelho, J.C. & Pinto, P.A. 1989. Plant density effects on growth and development of winter faba bean (*Vicia faba* var. *minor*). *Fabis Newslett*. **25**, 26–30.

Derogar, N. & Mojaddam, M. 2014. Effect of plant density on grain yield and yield components in faba bean. *International Journal of Plant, Animal and Enviromental Sciences* **4**(2), 92–96.

El-Hai, K.M.A. 2015. Controlling of Alternaria leaf spot disease on faba using some growth substances. *Asian Journal of Plant Pathology* **9**(3), 124–134.

El-Sayed, A.S., El-Shennawy, R.Z. & Ismail, A.I. 2011. Fungicidal management of chocolate spot of faba bean and assessment of yield losses due to the disease. *Annals of Agricultural Science* **56**, 27–35.

Emeran, A.A., Sillero, J. C., Fernandez – Aparicio, M. & Rubiales, D. 2011. Chemical control of faba bean rust (*Uromyces viciae – fabae*). *Crop Protection* **30**, 907–912.

Flores, F., Hybl, M., Knudsen, J.C., Marget, P., Muel, F., Nadal, S., Narits, L., Raffiot, B., Sass, O., Solis, I., Winkler, J., Stoddard, F.L. & Rubiales, D. 2013. Adaption of spring faba bean types across European climates. *Field Crops Research* **145**, 1–9.

Girma, F. & Haile, D. 2014. Effects of supplemental irrigation on physiological parameters and yield of faba bean (*Vicia faba* L.) varieties in the highlands of Bale, Ethiopia. *Journal of Agronomy* **13**, 29–34.

Holms, I. 1967. *Research on Field Beans Agrotechnology in Latvia SSR*: Theses for Earning the Degree of Candidate of Agriculture Sciences. Latvia Academy of Agriculture, Faculty of Agronomy. 269 p. (In Latvian).

Husain, M.M., Hill, G.D. & Gallagher, J.N. 1988. The response of fied beans (*Vicia faba* L.) to irrigation and sowing date. 1. Yield and yield components. *Journal of Agricultural Science* **111**, 221–232.

Khalil, S.K., Wahab, A., Rehman, A., Muhammad, F., Wahab, S., Khan, A.Z., Zubair, M., Shan, M.K., Khalil, I.H. & Amin, A.R. 2010. Density and planting date influence phenological development assimilate partitioning and dry matter production of faba bean. *Pak. J. Bot*. **42**(6), 3831–3838.

Lopez-Bellido, F.J., Lopez-Bellido, L., Lopez-Bellido, R.J. 2005. Competition, growth and yield of faba beans (*Vicia faba* L.). *European Journal of Agronomy* **23**, 359–378.

Loss, S.P. & Siddique, K.H.M. 1997. Adaptation of faba bean (*Vicia faba* L.) to dryland Mediterranean-type environments. I. Seed yield and yield components. *Field Crops Research* **52**, 17–28.

McDonald, G.K., Adisarwanto, T. & Knight, R. 1994. Effect of time of sowing on flowering in faba bean (*Vicia faba*). *Australian Journal of Experimental Agriculture* **34**, 395–400.

Patrick, J.W. & Stoddard, F.L. 2010. Physiology of flowering and grain filling in faba bean. *Field Crops Research* **115**, 234–242.

Plūduma-Pauniņa, I., Gaile, Z., Bankina, B. & Balodis, R. 2018. Field Bean (*Vicia faba* L.) Yield and Quality Depending on Some Agrotechnical Aspects. *Agronomy Research* **16**(1), 212–220.

Sahile, S., Fininsa, C., Sakhuja, P.K. & Ahmed, S. 2008. Effect of mixed cropping and fungicides on chocolate spot (*Botrytis fabae*) of faba bean (*Vicia faba*) in Ethiopia. *Crop Protection* **27**, 275–282.

Sharaan, A.N., Megawer, E.A., Saber, H.A. & Hemida, Z.A. 2002. Seed yield, yield components and quality characters as affected by cultivars, sowing dates and planting distances in faba bean. *Field Crops Research* **87**, 1–16.

Singh, A.K., Bharati, R.C., Manibhushan, N.C. & Pedpati, A. 2013. An assessement of faba bean (*Vicia faba* L.) current status and future prospect. *African Journal of Agricultural Research* **8**(55), 6634–6641.

Skjelvag, A.O. 1981. Effects of climatic factors on the growth and development of the field bean (*Vicia faba* L. var. *minor*). II. Phenological development in outdoor experiments. *Acta Agriculture Scandinavica* **31**. 372–381.

Turk, M.A. & Tawaha, A.M. 2002. Impact of seeding rate, seeding date, rate and method of phosphorus application in faba bean (*Vicia faba* L. *minor*) in the absence of moisture stress. *Biotechnologie, Agronomie, Societe et Environnement* **6**(3), 171–178.

Tuttobene, R. & Vagliasindi, C. 1995. Effects of plant density on flowering characteristics, growth and yield in 'Sikelia' a new faba bean genotipe (*Vicia faba* L.) recently released. In *Proceeding of the Second European Conference on Grain Legumes*. Copenhagen, Denmark, pp. 172.

Villacampa, Y., Confalone, A., Cortes, M., Ruiz-Nogueira, B. & Sau, F. 2009. Modelling the effect of temperature and photoperiod on the faba bean (*Vicia faba* L.). *WIT Transactions on Ecology and the Environment* **122**, 53–60.

Villegas-Fernandez, A.M., Sillero, J.C., Emeran, A.A., Winkler, J., Raffiot, B., Tay, J., Flores, F. & Rubiales, D. 2009. Identification and multi-environment validation of resistance to *Botrytis fabae* in *Vicia faba*. *Field Crops Research* **114**, 84–90.

Wu, Y. & Jing, H. 1988. Research on branching and ripe branches in faba bean. *Journal of Shanghai Agricultural College* **5**, 273–277.

Yu, S. & Zhang, D. 1979. Research on cultivation biology in faba bean. *Jiangsu Agricultural Science* **6**, 24–31.

Zabawi, A.G.M. & Dennett, M.D.D. 2010. Responses of faba bean (*Vicia faba*) to different levels of plant available water: I. Phenology, growth and biomass partitioning. *Journal of Tropical Agriculture and Food Science* **38**, 11–19.

INSTRUCTIONS TO AUTHORS

Papers must be in English (British spelling). English will be revised by a proofreader, but authors are strongly urged to have their manuscripts reviewed linguistically prior to submission. Contributions should be sent electronically. Papers are considered by referees before acceptance. The manuscript should follow the instructions below.

Structure: Title, Authors (initials & surname; an asterisk indicates the corresponding author), Authors' affiliation with postal address (each on a separate line) and e-mail of the corresponding author, Abstract (up to 250 words), Key words (not repeating words in the title), Introduction, Materials and methods, Results and discussion, Conclusions, Acknowledgements (optional), References.

Layout, page size and font

- Use preferably the latest version of **Microsoft Word**, doc., docx. format.
- Set page size to **ISO B5 (17.6 x 25 cm)**, all **margins at 2 cm**. All text, tables, and figures must fit within the text margins.
- Use single line spacing and **justify the text**. Do not use page numbering. Use **indent 0.8 cm** (do not use tab or spaces instead).
- Use font Times New Roman, point size for the title of article **14 (Bold)**, author's names 12, core text 11; Abstract, Key words, Acknowledgements, References, tables, and figure captions 10.
- Use *italics* for Latin biological names, mathematical variables and statistical terms.
- Use single ('…') instead of double quotation marks ("…").

Tables

- All tables must be referred to in the text (Table 1; Tables 1, 3; Tables 2–3).
- Use font Times New Roman, regular, 10 pt. Insert tables by Word's 'Insert' menu.
- Do not use vertical lines as dividers; only horizontal lines (1/2 pt) are allowed. Primary column and row headings should start with an initial capital.

Figures

- All figures must be referred to in the text (Fig. 1; Fig. 1 A; Figs 1, 3; Figs 1–3). Use only black and white or greyscale for figures. Avoid 3D charts, background shading, gridlines and excessive symbols. Use font **Arial, 10 pt** within the figures. Make sure that thickness of the lines is greater than 0.3 pt.
- Do not put caption in the frame of the figure.
- The preferred graphic format is Excel object; for diagrams and charts EPS; for half-tones please use TIFF. MS Office files are also acceptable. Please include these files in your submission.
- Check and double-check spelling in figures and graphs. Proof-readers may not be able to change mistakes in a different program.

References

- **Within the text**

In case of two authors, use '&', if more than two authors, provide first author 'et al.':

Smith & Jones (1996); (Smith & Jones, 1996);

Brown et al. (1997); (Brown et al., 1997)

When referring to more than one publication, arrange them by following keys: 1. year of publication (ascending), 2. alphabetical order for the same year of publication:

(Smith & Jones, 1996; Brown et al., 1997; Adams, 1998; Smith, 1998)

- **For whole books**

Name(s) and initials of the author(s). Year of publication. *Title of the book* (*in italics*). Publisher, place of publication, number of pages.

Shiyatov, S.G. 1986. *Dendrochronology of the upper timberline in the Urals*. Nauka, Moscow, 350 pp. (in Russian).

- **For articles in a journal**

Name(s) and initials of the author(s). Year of publication. Title of the article. *Abbreviated journal title* (*in italic*) volume (in bold), page numbers.

Titles of papers published in languages other than English, should be replaced by an English translation, with an explanatory note at the end, e.g., (in Russian, English abstr.).

Karube, I. & Tamiyra, M.Y. 1987. Biosensors for environmental control. *Pure Appl. Chem.* **59**, 545–554.

Frey, R. 1958. Zur Kenntnis der Diptera brachycera p.p. der Kapverdischen Inseln. *Commentat.Biol*. **18**(4), 1–61.

Danielyan, S.G. & Nabaldiyan, K.M. 1971. The causal agents of meloids in bees. *Veterinariya* **8**, 64–65 (in Russian).

- **For articles in collections:**

Name(s) and initials of the author(s). Year of publication. Title of the article. Name(s) and initials of the editor(s) (preceded by In:) *Title of the collection (in italics)*, publisher, place of publication, page numbers.

Yurtsev, B.A., Tolmachev, A.I. & Rebristaya, O.V. 1978. The floristic delimitation and subdivisions of the Arctic. In: Yurtsev, B. A. (ed.) *The Arctic Floristic Region*. Nauka, Leningrad, pp. 9–104 (in Russian).

- **For conference proceedings:**

Name(s) and initials of the author(s). Year of publication. Name(s) and initials of the editor(s) (preceded by In:) *Proceedings name (in italics)*, publisher, place of publishing, page numbers.

Ritchie, M.E. & Olff, H. 1999. Herbivore diversity and plant dynamics: compensatory and additive effects. In: Olff, H., Brown, V.K. & Drent R.H. (eds) *Herbivores between plants and predators. Proc. Int. Conf. The 38th Symposium of the British Ecological Society*, Blackwell Science, Oxford, UK, pp. 175–204.

.....……

Please note

- Use '.' (not ',') for decimal point: 0.6 ± 0.2; Use ',' for thousands – 1,230.4;
- Use '–' (not '-') and without space: pp. 27–36, 1998–2000, 4–6 min, 3–5 kg
- With spaces: 5 h, 5 kg, 5 m, 5 °C, C : D = 0.6 ± 0.2; $p < 0.001$
- Without space: 55°, 5% (not 55 °, 5 %)
- Use 'kg ha^{-1}' (not 'kg/ha');
- Use degree sign ' ° ' : 5 °C (not 5 ^{O}C).